SECTION 5.8: METEOROLOGY		
File name: 599270_ESK_TSSR 5.8 Meteorology Rev 0c		
Author's declaration:	I declare that appropriate diligence and quality assurance was applied in the compilation of this report. As such I am confident in the results here described and the conclusions drawn. Name: **Dr L W Burger**	Date: **12/03/2026**
Peer Reviewer:	I declare that this report has undergone independent peer review by myself, that comments were addressed to my satisfaction, and that as such, it is considered fit for publication. Name: **Prof C de W Rautenbach**	Date: **12/03/2026**
Project Manager Authorisation:	SRK Consulting - Certified Electronic Signature srk consulting 599270/46091/Report 1243-6350-5664-HOLD-12/03/2026 This signature has been printed digitally. The Author has given permission for its use for this document. The details are stored in the SRK Signature Database Name: **D Holmes**	Date: **12/03/2026**
Project Partner Authorisation:	SRK Consulting - Certified Electronic Signature srk consulting 599270/46091/Report 503-1340-6453-ENGE-12/03/2026 This signature has been printed digitally. The Author has given permission for its use for this document. The details are stored in the SRK Signature Database Name: **B Engelsman**	Date: **12/03/2026**
Eskom NSS Technical Lead Acceptance:	Name: **A Kilian**	Date: **2026-06-26**
Eskom NSS Employer's Agent Acceptance:	Name: **F van Mosseveld**	Date: **2026-06-29**

© Eskom 2026/Rev 0c

PRINTED VERSIONS OF THIS DOCUMENT ARE NOT CONTROLLED

AMENDMENT RECORD			
Rev	**Draft**	**Date**	**Description**
0		April 2015	New section. Thyspunt Site Safety Report compiled in support of Eskom's Nuclear Installation Site Licence for the Thyspunt site and submitted to the NNR.
0a		December 2024	Section updated to address NNR comments.
0b		March 2026	Footer revised to be consistent with other TSSR sections.
0c		June 2026	Minor editorial corrections made and cross reference links corrected.

© Eskom 2026/Rev 0c

PRINTED VERSIONS OF THIS DOCUMENT ARE NOT CONTROLLED

Executive Summary

This section of this Site Safety Report (SSR) presents an evaluation of the prevailing meteorological, corrosion and climatological characteristics for the Thyspunt site, with specific attention also to the extreme values of meteorological variables such as rainfall, air temperature and wind speed, and rare meteorological phenomena that occur infrequently. Future projections of these parameters due to climate change are also considered.

These characteristics have been investigated in support of the identification of hazards from important external phenomena as per RG-0011 (National Nuclear Regulator, 2016a), specifically meteorology, to the nuclear installation(s) on the site.

The following meteorological parameters were identified for onsite monitoring and inclusion in this SSR:

- wind speed and direction;
- ambient dry-bulb air temperature[1] at two vertical levels and temperature difference between two vertical levels;
- precipitation;
- relative humidity;
- ambient pressure;
- solar radiation;
- atmospheric stability[2];
- evapotranspiration rate[3];
- corrosivity[4].

[1] The dry-bulb temperature is the temperature of air measured by a thermometer freely exposed to the air but shielded from radiation from the sun. "Dry-bulb" is included because the air temperature is indicated by a thermometer not affected by the moisture of the air. The dry-bulb temperature is the temperature that is usually thought of as “air temperature”, and it is the true thermodynamic temperature. Whereas a normal, dry-bulb thermometer measures the temperature of ambient air, the wet-bulb temperature is the temperature of a surface from which water has evaporated into a stream of ambient air. It is the lowest temperature to which an object can be cooled solely by the evaporation of water.

[2] Atmospheric stability refers to the ability of the atmosphere to be turbulent. The effect of atmospheric stability is noted by wind gustiness and the dispersion of smoke. Stability is a characteristic of how the atmospheric layer above the earth’s surface reacts to small disturbances. If the disturbance is damped, the system is said to be stable; the air becomes, or is, laminar (non-turbulent, smooth, non-stormy). If the disturbance causes an amplifying response (irregular motions or regular oscillations, i.e. turbulent), the system is unstable. Neutral air has no tendency to change (disturbances neither amplify nor dampen).

[3] Evapotranspiration is the process by which water is transferred from the land to the atmosphere by evaporation from the soil and other surfaces and by transpiration from plants.

[4] Corrosivity of the atmosphere is the ability of the atmosphere to cause corrosion in a given corrosion system.

© Eskom 2026/Rev 0c

PRINTED VERSIONS OF THIS DOCUMENT ARE NOT CONTROLLED

The analysis of historical records addresses the following meteorological parameters, some of which are rare and extreme:

- hail;
- frost;
- fog;
- lightning;
- tornadoes;
- snow, avalanches, ice, ice cover and blizzards;
- thunder;
- extreme weather (wind speed, rainfall and temperature).
- tornado/tropical cyclones.

Meteorological parameters are monitored at the Thyspunt site using an automatic weather station (Thyspunt Weather Station (WS)) measuring dry-bulb temperature at two vertical levels, wind speed, solar radiation, relative humidity, atmospheric pressure, rainfall, visibility and lightning events. Additional meteorological history was also obtained from the South African Weather Services (SAWS) reports, and monitoring data from SAWS. The closest SAWS weather stations include Cape St Francis (9.3 km east-southeast) and Humansdorp (17.3 km north-northeast). Only precipitation is measured at Humansdorp. Additional regional weather stations include Jeffreys Bay (28 km northeast), Patensie (48 km north-northeast), Kariega (formerly known as Uitenhage) (78 km northeast) and Gqeberha (formerly known as Port Elizabeth) (93 km northeast). Only precipitation is measured at Jeffreys Bay, whilst precipitation, air temperature, ambient pressure, wind speed/direction, and relative humidity are measured at the other locations. In addition to the Thyspunt WS meteorological measurements, detailed statistical analysis also included the measurements made at the weather station at Cape St. Francis due to its proximity and the length of historical data of 39 years. Similarly, albeit limited to precipitation observations, annual rainfall (146 years) at Humansdorp was included for reference.

The Thyspunt WS was commissioned on 10 January 2008 and monitoring continued until 4 October 2013. The Thyspunt WS was re-established four years later, on 29 September 2017, using re-calibrated instruments and where necessary (i.e. operated outside specifications after 4 October 2013), replaced with new instruments and equipment. Data gathering stopped on 31 March 2019 following an Eskom Stop Work Order of 6 February 2019, which took effect from 1 April 2019. Albeit outside the contract period, monitoring at the Thyspunt WS continued until 3 June 2020 which was also considered for inclusion in the dataset for analyses. However, the data were deemed valid only for the period up to 30 September 2019. Although the total length of the

© Eskom 2026/Rev 0c

PRINTED VERSIONS OF THIS DOCUMENT ARE NOT CONTROLLED

meteorological database is approximately seven years[5], the four-year gap between the two campaigns does not allow the establishment of rainfall trends for this period. In general, the longer the observation period, typically 20 and more years, but not less than 10 years, the smaller the error in calculating the average annual precipitation and short-term extremes rain events. Furthermore, to allow seasonal and consecutive annual temporal trends, only six full years were available in the dataset. Other meteorological parameters are not as significantly affected by the missing data period.

Eskom Standard 238-52 – Meteorological Requirements for Nuclear Installations (Eskom, 2022a) and the analytical procedures provided in the IAEA Specific Safety Guide No. SSG-18 (International Atomic Energy Agency, 2011) were used as a basis for conducting the meteorological analyses.

Corrosivity[6] was determined using measurements of sulfate and chloride deposition rates at the site following the measurement methods specified in the International Organisation for Standardisation (ISO) 9225[7] on corrosion of metals and alloys-corrosivity of atmospheres (International Organisation for Standardisation, 2012c). This included three measurement campaigns, namely, from May 2008 to January 2009, October 2012 to September 2013, and October 2017 to March 2019. As per ISO 9225, the minimum measurement period is one year in order to cover seasonal variations and because the classification system is based on yearly average values. Since two of the campaigns include a minimum of two full years' measurement (October 2012 to September 2013, and 2018), the collective timeframes satisfy the monitoring requirements to establish the atmospheric corrosivity of the study area.

Summaries of meteorological parameters are provided in ***Table 5.8.A*** and ***Table 5.8.B***. ***Table 5.8.A*** includes the analyses of climate change projections published by the SAWS and the 5th Assessment Report of the Intergovernmental Panel on Climate Change (IPCC) (ARP5) (Intergovernmental Panel on Climate Change, 2013), as well as detailed analyses of downscaled global climate model simulations for the site, which were performed by the Council for Scientific and Industrial Research (CSIR).

[5] Although the total length of the meteorological database is approximately seven years, only the following calendar years included measurements of one-year durations: 2008, 2009, 2010, 2011, 2012 and 2018. Measurements during 2017 started in September 2017, and measurements during 2019 were only until September 2019. Only 8 months measurements were available during 2013. Therefore, only six calendar years available for rainfall analysis.

[6] Corrosivity of atmosphere is the ability of the atmosphere to cause corrosion in a given corrosion system

[7] The methods for estimation of the atmospheric corrosivity given in ISO 9223 (International Organisation for Standardisation, 2012a) are based on the measurement methods described in ISO 9225. ISO 9224 (International Organisation for Standardisation, 2012b), which is to be used in conjunction with ISO 9223, specifies the guiding values of corrosion attack for metals and alloys exposed to natural outdoor atmospheres for exposures greater than one year.

© Eskom 2026/Rev 0c

PRINTED VERSIONS OF THIS DOCUMENT ARE NOT CONTROLLED

Table 5.8.A
Site Specific Parameters Part 1

Meteorological Parameter		Baseline	Climate Change Projections	
			Near-Horizon (2050)	Far Horizon (2100)
Annual Average Wind Speed (m/s) at Thyspunt WS (***on page 5.8-56***)		5.4 ± 0.01	4.9 -0.5+1.5	5.4 -1.0+1.0
Annual Average Wind Speed (m/s) at Cape St Francis WS (***on page 5.8-53***)		6.0± 0.01	5.5 -0.5+1.5	6.0 -1.0+1.0
Hourly Maximum Wind Speed (1) [m/s] (Thyspunt WS 8 m above site ground level) **Return Periods Wind Speed** [m/s] (2) (Cape St Francis WS 10 m above site ground level) (***on page 5.8-165***)	Extreme Observed & Projected Thyspunt WS (***on page 5.8-56***)	19.6 ± 0.0	19.1 -0.5+1.5	19.6 -1.0+1.0
	Extreme Observed & Projected Cape St Francis WS (***on page 5.8-53***)	23.2 ± 0.0	22.7 -0.5+1.5	23.2 -1.0+1.0
	10 Year Return	22.0 ± 1.2	21.4 ± 1.2	22.0 ± 1.2
	100 Year Return	24.7 ± 2.1	24.0 ± 2.1	24.7 ± 2.1
	1 000 Year Return	27.3 ± 3.1	26.6 ± 3.1	27.3 ± 3.1
	10 000 Year Return	29.9 ± 4.1	29.2 ± 4.1	29.9 ± 4.1
	100 000 Year Return	32.6 ± 5.1	31.7 ± 5.1	32.6 ± 5.1
	1 000 000 Year Return	35.2 ± 6.1	34.3 ± 6.1	35.2 ± 6.1
	10 000 000 Year Return	37.9 ± 7.0	36.9 ± 7.0	37.9 ± 7.0
	100 000 000 Year Return	40.5 ± 8.0	39.5 ± 8.0	40.5 ± 8.0
Wind peaks (gusts) (3) [m/s] (Thyspunt WS 8 m above site ground level)	Extreme Observed & Projected Thyspunt WS (***on page 5.8-65***)	32.2 ± 0.0	31.7 -0.5+1.5	32.2 -1.0+1.0
	Extreme Observed & Projected Cape St Francis (***on page 5.8-66***)	45.8± 0.0	45.3 -0.5+1.5	45.8 -1.0+1.0
	10 Year Return	38.1 ± 3.5	37.6 ± 3.5	38.1 ± 3.5

© Eskom 2026/Rev 0c

PRINTED VERSIONS OF THIS DOCUMENT ARE NOT CONTROLLED

Meteorological Parameter		Baseline	Climate Change Projections	
			Near-Horizon (2050)	Far Horizon (2100)
Return Period Gusts [m/s] [(2)] (Cape St Francis WS 10 m above site ground level) (***on page 5.8-166***)	100 Year Return	44.3 ± 6.2	43.7 ± 6.2	44.3 ± 6.2
	1 000 Year Return	50.2 ± 8.8	49.6 ± 8.8	50.2 ± 8.8
	10 000 Year Return	56.2 ± 11.4	55.5 ± 11.4	56.2 ± 11.4
	100 000 Year Return	62.2 ± 14.1	61.4 ± 14.1	62.2 ± 14.1
	1 000 000 Year Return	68.2 ± 16.7	67.3 ± 16.7	68.2 ± 16.7
	10 000 000 Year Return	74.2 ± 19.3	73.2 ± 19.3	74.2 ± 19.3
	100 000 000 Year Return	80.2 ± 22.0	79.1 ± 22.0	80.2 ± 22.0
Ambient temperature [°C] (Thyspunt WS 2 m above site ground level) **Return Periods Dry Bulb Temperature** [m/s] [(4)] (Cape St Francis WS 10 m above site ground level) (***on page 5.8-165***)	Average daily maximum dry bulb temperature (***on page 5.8-73***)	20.8 ± 0.1	22.5 0.0+0.0	24.1 -0.04+0.2
	- coincident wet bulb temperature [(5)]	18.2 ± 0.2	19.4 1.0+1.8	20.1 1.0+2.3
	Average daily maximum wet bulb temperature [(5)] (***on page 5.8-73***)	16.7 ± 0.1	17.3 0.0+0.5	17.9 0.0+0.9
	Extreme Observed Thyspunt WS (***on page 5.8-74***) & Projected dry-bulb maximum	38.2 ± 0.0	39.7 -0.5+0.5	41.7 -1.5+0.5
	Extreme Observed Cape St Francis WS (***on page 5.8-74***) & Projected dry-bulb maximum	38.5 ± 0.0	40.0 -0.5+0.5	42.0 -1.5+0.5
	10 Year Return	37.0 ± 1.8	42.8 ± 2.9	45.6 ± 3.1
	100 Year Return	42.4 ± 3.1	48.1 ± 4.3	50.9 ± 4.5
	1 000 Year Return	47.7 ± 4.5	53.4 ± 5.7	56.2 ± 5.9
	10 000 Year Return	53.0 ± 5.9	58.7 ± 7.2	61.5 ± 7.4
	100 000 Year Return	58.3 ± 7.4	64.0 ± 8.7	66.9 ± 8.9
	1 000 000 Year Return	63.7 ± 8.9	69.3 ± 10.2	72.2 ± 10.4

© Eskom 2026/Rev 0c

PRINTED VERSIONS OF THIS DOCUMENT ARE NOT CONTROLLED

Meteorological Parameter		Baseline	Climate Change Projections	
			Near-Horizon (2050)	Far Horizon (2100)
	10 000 000 Year Return	69.0 ± 10.4	74.6 ± 11.6	77.5 ± 11.9
	100 000 000 Year Return	74.3 ± 11.9	80.0 ± 13.1	82.8 ± 13.4
	Maximum temperature of 3-hour duration [6] (***on page 5.8-84***)	37.0 Corresponding Wet Bulb Temperature 19.7 ± 1.8	38.7 0.0+0.0	40.3 -0.04+0.2
	Maximum temperature of 6-hour duration [6] (***on page 5.8-84***)	33.1 Corresponding Wet Bulb Temperature 18.8 ± 0.9	34.8 0.0+0.0	36.4 -0.04+0.2
	Maximum temperature of 7-day duration [6] (***on page 5.8-84***)	19.3 Corresponding Wet Bulb Temperature 16.8 ± 0.1	21.0 0.0+0.0	22.6 -0.04+0.2
	Average daily minimum dry bulb temperature (***on page 5.8-73***)	14.4 ± 0.1	16.1 0.0+0.0	17.7 -0.04+0.2
	- coincident wet bulb temperature [5]	11.8 ± 0.1	12.2 -0.1+0.2	12.6 -0.3+0.4
	Average daily minimum wet bulb temperature [5] (***on page 5.8-75***)	12.6 ± 0.1	13.0 0.0+0.3	13.5 0.0+0.6
	Extreme Observed Thyspunt WS (***on page 5.8-74***) & Projected dry-bulb minimum	6.7	9.2 -1.5+0.5	9.2 -0.5+1.5

© Eskom 2026/Rev 0c

PRINTED VERSIONS OF THIS DOCUMENT ARE NOT CONTROLLED

Meteorological Parameter		Baseline	Climate Change Projections	
			Near-Horizon (2050)	Far Horizon (2100)
	Extreme Observed Cape St Francis (***on page 5.8-74***) & Projected dry-bulb minimum	4.9	7.4 -1.5+0.5	7.4 -0.5+1.5
	10 Year Return	5.0 ± 0.7	6.0 ± 1.1	5.7 ± 1.2
	100 Year Return	3.2 ± 1.2	1.6 ± 1.6	3.8 ± 1.7
	1 000 Year Return	1.3 ± 1.7	-0.2 ± 2.1	2.0 ± 2.2
	10 000 Year Return	-0.5 ± 2.2	-2.0 ± 2.6	0.2 ± 2.7
	100 000 Year Return	-2.3 ± 2.7	-3.8 ± 3.1	-1.6 ± 3.2
	1 000 000 Year Return	-4.1 ± 3.2	-5.6 ± 3.6	-3.4 ± 3.7
	10 000 000 Year Return	-5.9 ± 3.7	-7.5 ± 4.1	-5.2 ± 4.2
	100 000 000 Year Return	-7.7 ± 4.2	-9.3 ± 4.7	-7.0 ± 4.7
	Minimum temperature of 3-hour duration [6] (***on page 5.8-84***)	7.2 Corresponding Wet Bulb Temperature 5.4 ± 0.3	8.9 0.0+0.0	10.5 -0.04+0.2
	Minimum temperature of 6-hour duration [6] (***on page 5.8-84***)	7.7 Corresponding Wet Bulb Temperature 6.0 ± 0.2	9.4 0.0+0.0	11.0 -0.04+0.2
	Minimum temperature of 7-day duration [6] (***on page 5.8-84***)	15.5 Corresponding Wet Bulb Temperature 13.3 ± 0.1	17.2 0.0+0.0	18.8 -0.04+0.2

© Eskom 2026/Rev 0c

PRINTED VERSIONS OF THIS DOCUMENT ARE NOT CONTROLLED

Meteorological Parameter		Baseline	Climate Change Projections	
			Near-Horizon (2050)	Far Horizon (2100)
Rainfall [mm] (0.7 m above site ground level)	Average Annual Total Thyspunt WS (***on page 5.8-88***)	774.4	777.5 -22.73+18.76	762.5 -32.33+6.4
	Average Annual Total Cape St Francis WS (***on page 5.8-88***)	619.5	622.6 -22.73+18.76	607.6 -32.33+6.4
	Extreme Annual Total	972.0	975.1 +18.76 -22.73	960.1 -32.33 +6.4
	Annual Re-occurrences (***on page 5.8-150***)*:*			
	10 Year Return	858.7 ± 84.8	861.8 ± 84.8	846.8 ± 84.8
	100 Year Return	1187.9 ± 147.1	1191.0 ± 147.1	1176.0 ± 147.1
	1 000 Year Return	1511.2 ± 212.2	1514.2 ± 212.2	1499.2 ± 212.2
	10 000 Year Return	1833.8 ± 278.4	1836.9 ± 278.4	1821.9 ± 278.4
	100 000 Year Return	2156.4 ± 345.0	2159.5 ± 345.0	2144.5 ± 345.0
	1 000 000 Year Return	2479.0 ± 412.0	2482.1 ± 412.0	2467.0 ± 412.0
	10 000 000 Year Return	2801.6 ± 479.0	2804.7 ± 479.0	2789.6 ± 479.0
	100 000 000 Year Return	3124.2 ± 546.2	3127.2 ± 546.2	3112.2 ± 546.2
	Extreme 24-hour Storm Thyspunt WS (***on page 5.8-88***)	113.5	124.9 -0.0+11.4	Assume same as Near-Horizon
	Extreme 24-hour Storm Cape St Francis WS (***on page 5.8-88***)	157.8	173.8 -0.0+15.8	Assume same as Near-Horizon
	24-Hour Re-occurrences (***on page 5.8-150***)*:*			
	10 Year Return	99.0 ± 20.8	108.9 ± 20.8	99.0 ± 20.8
	100 Year Return	151.4 ± 38.8	166.6 ± 38.8	151.4 ± 38.8
	1 000 Year Return	202.9 ± 56.8	223.2 ± 56.8	202.9 ± 56.8

© Eskom 2026/Rev 0c

PRINTED VERSIONS OF THIS DOCUMENT ARE NOT CONTROLLED

Meteorological Parameter		Baseline	Climate Change Projections	
			Near-Horizon (2050)	Far Horizon (2100)
	10 000 Year Return	254.3 ± 74.9	279.7 ± 74.9	254.3 ± 74.9
	100 000 Year Return	305.6 ± 93.0	336.2 ± 93.0	305.6 ± 93.0
	1 000 000 Year Return	357.0 ± 111.1	392.7 ± 111.1	357.0 ± 111.1
	10 000 000 Year Return	408.4 ± 129.2	449.2 ± 129.2	408.4 ± 129.2
	100 000 000 Year Return	459.7 ± 147.3	505.7 ± 147.3	459.7 ± 147.3
	Extreme 1-hour Storm	51.9	57.1 0.0+5.2	Assume same as Near-Horizon
Mean Sea Level Atmospheric pressure [hPa]	Daily Minimum (***on page 5.8-100***)	999.1 ± 0.2	Not available (7)	Not available (7)
	Daily Maximum (***on page 5.8-100***)	1037.4 ± 0.2	Not available (7)	Not available (7)
	Extreme Lower (Hourly) (***on page 5.8-100***)	994.1 ± 0.2	Not available (7)	Not available (7)
	Average Annual (***on page 5.8-100***)	1016.3 ± 0.2	Not available (7)	Not available (7)
	Extreme Upper (Hourly) (***on page 5.8-100***)	1040.6 ± 0.2	Not available (7)	Not available (7)

Notes:

(1) Thyspunt WS included 7 years of measurements. The maximum wind speeds were on average 20% lower at the Thyspunt WS than the observations at the Cape St Francis WS (highest wind speed 23.2 m/s)

(2) Extreme analyses were completed using the measurements from the Cape St Francis WS since the database included 19 years of data compared to the 7 years of measurements at the Thyspunt WS. These extremes are biased by the 20% on average higher wind speed observations than at the Thyspunt WS and are likely conservative projections.

(3) Thyspunt WS included 7 years of measurements. The maximum wind speeds were on average 20% lower at the Thyspunt WS than the observations at the Cape St Francis WS (highest gust of 45.8 m/s).

(4) Extreme analyses were completed using the measurements from the Cape St Francis WS since the database included 19 years of data compared to the 7 years of measurements at the Thyspunt WS. The maximum dry bulb temperature extremes are slightly different, i.e. 38.2 °C at Thyspunt WS compared to 38.5°C at the Cape St Francis WS. The minimum dry bulb temperature extremes are more significantly different, i.e. 6.7 °C at Thyspunt WS compared to 4.9 °C at the Cape St Francis WS. The lower temperatures at the Cape St Francis WS therefore provides a more conservative estimate of the minimum temperature return periods.

© Eskom 2026/Rev 0c

PRINTED VERSIONS OF THIS DOCUMENT ARE NOT CONTROLLED

Meteorological Parameter	Baseline	Climate Change Projections	
		Near-Horizon (2050)	Far Horizon (2100)
(5) Wet-bulb temperature projections are not part of the primary meteorological variables provided by the climate change model used in the analyses. The projections provided in the table are based on using the daily minimum, average and maximum temperature projected increases and assuming ±25% variation in the corresponding moisture content. (6) Temperatures of 3-hour, 6- hour and 7-day durations assumed projected temperature increases as per the climate change model. (7) Global climate projections from the ARP5 indicate relatively small changes in the projected mean sea-level atmospheric pressure over South Africa (max seasonal increase of 0.5 hPa in summer and reduction of 0.5 hPa in winter for the far horizon).			

© Eskom 2026/Rev 0c

PRINTED VERSIONS OF THIS DOCUMENT ARE NOT CONTROLLED

Table 5.8.B
Site Specific Parameters Part 2

Meteorological Parameter			Value			
Tornadoes	Tornado Probability (EF - Enhanced Fujita Scale)	Based on 116-year database 1905 - 2020 (***on page 5.8-144***)	All[2]	6.8×10^{-6} per year per km²		
			EF0	1.3×10^{-6} per year per km²		
			EF1	2.1×10^{-6} per year per km²		
			EF2	6.6×10^{-7} per year per km²		
			EF3	$<1.0 \times 10^{-8}$ per year per km²		
			EF4	$<1.0 \times 10^{-8}$ per year per km²		
			EF5	$<1.0 \times 10^{-9}$ per year per km²		
		Based on 25-year database 1996 - 2020 [1] (***on page 5.8-144***)	All[2]	3.2×10^{-6} per year per km²		
			EF0	4.0×10^{-5} per year per km²		
			EF1	2.3×10^{-6} per year per km²		
			EF2 [3]	6.6×10^{-7} per year per km²		
			EF3[3]	$<1.0 \times 10^{-8}$ per year per km²		
			EF4[3]	$<1.0 \times 10^{-8}$ per year per km²		
			EF5[3]	$<1.0 \times 10^{-9}$ per year per km²		
	10^{-7} per year wind speed: - maximum wind speed (***on page 5.8-146***) - maximum translational (***on page 5.8-146***) - maximum rotational (***on page 5.8-146***)		75.0 m/s 15.0 m/s 60.0 m/s			
			Lower Quartile	Upper Quartile	Median	Average
	Path Width [m] (*on page 5.8-145*):					
	EF0 tornado (40% to 64% probability)		22.9	68.6	45.7	54.9
	EF1 tornado (36% to 48% probability)		68.6	182.9	91.4	163.8
	EF2 tornado (0% to 4% probability)		137.2	402.3	228.6	344.1
	EF3 tornado (0% to 4% probability)		339.5	1005.8	548.6	736.3
	Path Length [km] (*on page 5.8-145*):					
	EF0 tornado (40% to 64% probability)		0.29	2.7	0.8	2.27
	EF1 tornado (36% to 48% probability)		1.77	9.33	4.4	7.1
	EF2 tornado (0% to 4% probability)		4.53	19.25	10	14.3
	EF3 tornado (0% to 4% probability)		12.38	36.34	23	29.1

© Eskom 2026/Rev 0c

PRINTED VERSIONS OF THIS DOCUMENT ARE NOT CONTROLLED

Meteorological Parameter		Value	
	Pressure drop for 10^{-7} per year wind speed (***on page 5.8-146***)	40 hPa	
	Maximum rate of pressure drop for 10^{-7} per year wind speed (***on page 5.8-146***)	13 hPa/s	
Atmospheric Turbulence (Sigma-Theta Method) (***on page 5.8-107***)	Convective (A)	3.33%	
	Unstable (B)	1.84%	
	Moderately Unstable (C)	4.88%	
	Neutral (D)	40.89%	
	Moderately Stable (E)	46.14%	
	Stable (F)	2.92%	
	Very Stable (G)	0.01%	
Prolonged Inversions ***(on page 5.8-104***)	Likelihood	Annual	30%
		Summer	19%
		Winter	44%
Snowfall (3) (***on page 5.8-98***)	Average	0.0 mm/h	
	Maximum load	0.0 N/m³	
Lightning (***on page 5.8-148***)	Flashes/year/km²	1.0 flash/year/km² (range 0.02 to 1.0)	
	Average strokes per flash	5	
	Maximum strokes per flash	16	
	Average peak current	25 kA	
	Highest peak current	166 kA	
Thunder (***on page 5.8-98***)	Average number of days with thunder	7.2 days/year	
Hail (***on page 5.8-98***)	Average number of days with hail	0.8 days/year	
Frost (***on page 5.8-98***)	Average number of days with frost	0 days/year	
Fog (***on page 5.8-98***)	Average number of days with fog	25.4 days/year (Thyspunt WS) 24.3 days/year (Cape St Francis WS)	
Relative humidity (***on page 5.8-98***)	Summer (relative humidity at 37 ºC, dry bulb)	17.6% (Thyspunt WS) 14.7% (Cape St. Francis WS)	
	Winter (relative humidity at -25 ºC, dry bulb)	78.8% at 6.6 °C (Thyspunt WS) 81.0% at 4.9 °C (Cape St. Francis WS) Assume 100% at -25ºC	
Solar Radiation	Lowest daily total (***on page 5.8-102***)	8.4 MJ/m².day (June)	
	Highest daily total (***on page 5.8-102***)	26.3 MJ/m².day (January)	

© Eskom 2026/Rev 0c

PRINTED VERSIONS OF THIS DOCUMENT ARE NOT CONTROLLED

Meteorological Parameter		Value	
Penman-Monteith Evapotranspiration (***on page 5.8-118***)	Monthly Total Minimum	84.8 mm (June)	
	Monthly Total Minimum	146.1 mm (January)	
Corrosivity (***on page 5.8-130***)	Rate in 1st year	Carbon steel	68.0 (50.6-81.6) µm/year
		Zinc	2.8 (2.2-3.4) µm/year
		Copper	1.8 (1.5;1.9) µm/year
		Aluminium	1.0 (0.7;1.2) µm/year
	Average rate over 20 years	Carbon steel	8.8 to 11.1 µm/year
		Zinc	1.3 to 1.6 µm/year
		Copper	0.4 to 0.5 µm/year
		Aluminium	0.3 to 0.4 µm/year

Notes:

(1) Tornado activity has increased since 1987 within an 80 km radius from the site. Whilst climate change may have contributed to increases in tornado frequencies, it may also simply be that the reporting of tornadoes has increased due to population spread as well as the associated damage to property.

(2) The “All” tornado entry combines all frequencies from EF0 to EF4 in the table.

(3) No tornadoes of strength higher than EF2 were observed during the last 34 years of reporting and therefore assumed the same values as for the long-term analysis.

(4) This reflects current observation; however extreme minimum temperatures (excluding climate change projections) indicate temperatures well below freeze point for water and may result in the occurrence of snow at the site.

© Eskom 2026/Rev 0c

PRINTED VERSIONS OF THIS DOCUMENT ARE NOT CONTROLLED

CONTENTS

5.8 METEOROLOGY 5.8-27
5.8.1 Introduction 5.8-27
5.8.2 Purpose and Scope 5.8-29
5.8.3 Regulatory Framework 5.8-30
5.8.4 Requirement Documents and Guides 5.8-30
5.8.5 Evaluation Approach 5.8-33
5.8.5.1 Meteorological Data Analysis 5.8-33
5.8.5.2 Meteorological Measurement 5.8-34
5.8.5.3 Onsite Meteorological Instrumentation 5.8-36
5.8.5.4 Instrument Accuracy 5.8-39
5.8.5.5 Macro and Micro Siting of Instrumentation 5.8-42
5.8.5.6 Length of Monitoring 5.8-44
5.8.6 Meteorological Parameters 5.8-48
5.8.7 Atmospheric Dispersion Modelling 5.8-167
5.8.8 Monitoring Programme 5.8-220
5.8.9 Management of Uncertainties 5.8-223
5.8.10 Management System 5.8-236
5.8.11 Potential Impact on the Nuclear Installation Design and Operation 5.8-250
5.8.12 Conclusions 5.8-251
5.8.13 References 5.8-263

© Eskom 2026/Rev 0c

PRINTED VERSIONS OF THIS DOCUMENT ARE NOT CONTROLLED

TABLES

Table 5.8.1 Meteorological Stations and Measurements 5.8-37

Table 5.8.2 Instrument Accuracies and Resolutions 5.8-40

Table 5.8.3 Wind Speed [m/s] as Function of Time of Day at the Cape St. Francis WS and Thyspunt WS 5.8-56

Table 5.8.4 Wind Speed and Direction Categorisation at the Cape St. Francis WS (June 2004 to December 2023) 5.8-58

Table 5.8.5 Wind Speed and Direction Categorisation at the Thyspunt WS (January 2008 to October 2013 and June 2017 to September 2019)..... 5.8-59

Table 5.8.6 Average and Maximum Hourly Wind Speed per Direction at the Cape St. Francis WS (June 2004 to December 2023)..... 5.8-60

Table 5.8.7 Average and Maximum Hourly Wind Speed per Direction at the Thyspunt WS (January 2008 to October 2013 and June 2017 to September 2019) 5.8-61

Table 5.8.8 Sustained Wind Speeds at the Cape St. Francis and the Thyspunt WS5.8-62

Table 5.8.9 Seasonal Wind Direction Occurrence at the Thyspunt WS (January 2008 to October 2013 and June 2017 to September 2019)..... 5.8-65

Table 5.8.10 Seasonal Wind Direction Occurrence at the Cape St. Francis WS (June 2004 to December 2023) 5.8-66

Table 5.8.11 Average Wind Speed per Month at the Cape St. Francis WS (June 2004 to December 2023) 5.8-67

Table 5.8.12 Maximum Wind Speed per Month at the Cape St. Francis WS (June 2004 to December 2023) 5.8-68

Table 5.8.13 Average Wind Speed per Month at the Thyspunt WS (January 2008 to October 2013 and June 2017 to September 2019)..... 5.8-69

Table 5.8.14 Maximum Wind Speed per Month at the Thyspunt WS (January 2008 to October 2013 and June 2017 to September 2019)..... 5.8-70

Table 5.8.15 Monthly Maximum Hourly Average and Wind Gusts [m/s] at the Cape St. Francis WS and the Thyspunt WS..... 5.8-71

Table 5.8.16 Gusts Above 20 m/s Directional Occurrence and Maximum Gusts at the Cape St. Francis WS and the Thyspunt WS 5.8-71

Table 5.8.17 Ambient Air Dry Bulb Temperature [°C] at the Thyspunt WS (January 2008 to October 2013 and June 2017 to September 2019)..... 5.8-78

Table 5.8.18 Ambient Air Dry Bulb Temperature [°C] at the Cape St. Francis WS (June 2004 to December 2023) 5.8-79

© Eskom 2026/Rev 0c

PRINTED VERSIONS OF THIS DOCUMENT ARE NOT CONTROLLED

Table 5.8.19 Ambient Air Wet Bulb Temperature [°C] at the Thyspunt WS (January 2008 to October 2013 and June 2017 to September 2019 ..... 5.8-80

Table 5.8.20 Ambient Air Wet Bulb Temperature [°C] at the Cape St. Francis WS (June 2004 to December 2023) 5.8-81

Table 5.8.21 Ambient Air Dewpoint Temperature [°C] at the Thyspunt WS (January 2008 to October 2013 and June 2017 to September 2019)5.8-82

Table 5.8.22 Ambient Air Dewpoint Temperature [°C] at the Cape St. Francis WS (June 2004 to December 2023) 5.8-83

Table 5.8.23 Maximum and Minimum Ambient Air Dry Bulb Temperature and Corresponding Wet bulb Temperature for Sustained 3 and 6 Hours, and 7 Days..... 5.8-84

Table 5.8.24 Summary of Long-Term Mean Annual Precipitation (MAP) at Nearest Weather Stations in Comparison with Thyspunt WS 5.8-85

Table 5.8.25 Average, Highest and Lowest Monthly Rainfall for Cape St. Francis WS, Humansdorp WS and Thyspunt WS 5.8-90

Table 5.8.26 Maximum 24-hour Rainfall [mm] for the Cape St. Francis, Thyspunt WS and the Humansdorp WS..... 5.8-92

Table 5.8.27 Highest 1 hour Rainfall (mm) for the Cape St. Francis WS and the Thyspunt WS 5.8-92

Table 5.8.28 SAWS and WMO Adopted SPI Values 5.8-94

Table 5.8.29 Average Number of Days with Thunder, Hail, Snow and Fog at Cape St. Francis (1881-1984) and Fog Estimate at Thyspunt WS (2008-2013 & 2017-2019) 5.8-98

Table 5.8.30 Daily Average, Daily Maximum and Minimum Relative Humidity (%) for the Cape St. Francis WS and the Thyspunt WS 5.8-99

Table 5.8.31 Daily Average, Daily Maximum and Minimum Barometric Pressure (hPa) for the Cape St. Francis WS and the Thyspunt WS 5.8-100

Table 5.8.32 Hourly Maximum and Minimum Barometric Pressure [hPa] for the Cape St. Francis WS and the Thyspunt WS 5.8-101

Table 5.8.33 Daily Average, Daily Maximum and Minimum Mean Sea Level Barometric Pressure [hPa] for the Cape St. Francis WS and the Thyspunt WS5.8-101

Table 5.8.34 Hourly Maximum and Minimum Mean Sea Level Barometric Pressure [hPa] for the Cape St. Francis WS and the Thyspunt WS 5.8-102

Table 5.8.35 Solar Radiation at the Thyspunt WS (2008-2013 & 2017-2019) Compared with Schulze's Atlas for the Thyspunt Region 5.8-103

Table 5.8.36 Joint Frequency Distribution of Pasquill-Gifford Stability Classes with Wind Direction: Thyspunt WS (Delta-T Method [8m/2m] – (Eskom, 2022a))5.8-

© Eskom 2026/Rev 0c

PRINTED VERSIONS OF THIS DOCUMENT ARE NOT CONTROLLED

106

Table 5.8.37 Joint Frequency Distribution of Pasquill-Gifford Stability Classes with Wind Direction: Thyspunt WS (Sigma-Theta Method [9 m] – (Eskom, 2022a)) 5.8-107

Table 5.8.38 Joint Frequency Distribution of Pasquill-Gifford Stability Classes with Wind Direction: Thyspunt WS (SRDT Method – (United States Environmental Protection Agency, 2000)) 5.8-108

Table 5.8.39 Joint Frequency Distribution of Pasquill-Gifford Stability Classes with Wind Direction: Thyspunt WS (Richardson Number Method – (Stull, 1997))5.8-109

Table 5.8.40 Joint Frequency Distribution of Pasquill-Gifford Stability Class A with Wind Direction and Wind Speed: Thyspunt WS (Sigma-Theta Method [9 m] – (Eskom, 2022a)) 5.8-110

Table 5.8.41 Joint Frequency Distribution of Pasquill-Gifford Stability Class B with Wind Direction and Wind Speed: Thyspunt WS (Sigma-Theta Method [9 m] – (Eskom, 2022a)) 5.8-111

Table 5.8.42 Joint Frequency Distribution of Pasquill-Gifford Stability Class C with Wind Direction and Wind Speed: Thyspunt WS (Sigma-Theta Method [9 m] – (Eskom, 2022a)) 5.8-112

Table 5.8.43 Joint Frequency Distribution of Pasquill-Gifford Stability Class D with Wind Direction and Wind Speed: Thyspunt WS (Sigma-Theta Method [9 m] – (Eskom, 2022a)) 5.8-113

Table 5.8.44 Joint Frequency Distribution of Pasquill-Gifford Stability Class E with Wind Direction and Wind Speed: Thyspunt WS (Sigma-Theta Method [9 m] – (Eskom, 2022a)) 5.8-114

Table 5.8.45 Joint Frequency Distribution of Pasquill-Gifford Stability Class F with Wind Direction and Wind Speed: Thyspunt WS (Sigma-Theta Method [9 m] – (Eskom, 2022a)) 5.8-115

Table 5.8.46 Joint Frequency Distribution of Pasquill-Gifford Stability Class G with Wind Direction and Wind Speed: Thyspunt WS (Sigma-Theta Method [9 m] – (Eskom, 2022a)) 5.8-116

Table 5.8.47 Monthly Total Potential Evapotranspiration Rates 5.8-118

Table 5.8.48 Classification of Marine Atmospheres Based on the Per Cent Mass Loss 5.8-125

Table 5.8.49 Average Marine Corrosivity at Thyspunt and Surrounding Coast (Gross & Nixon, 1993) 5.8-125

Table 5.8.50 ISO 9223:2012 Categories of Corrosivity of the Atmosphere.. 5.8-127

Table 5.8.51 ISO 9223:2012 Corrosion Rates, r_{corr}, for the First Year of Exposure for the

© Eskom 2026/Rev 0c

PRINTED VERSIONS OF THIS DOCUMENT ARE NOT CONTROLLED

Different Corrosivity Categories 5.8-127

Table 5.8.52 Constants for Dose-Response Function to Estimate Corrosion Attack Rates (ISO 9223:2012) 5.8-130

Table 5.8.53 ISO 9224:2012 Calculated Corrosion Rate Values for Various Metals and Exposure Periods 5.8-130

Table 5.8.54 Constant (*b*) for Attack Depth Function (ISO 9224:2012)..... 5.8-131

Table 5.8.55 EF-Scale Wind Speed Ranges Derived from Fujita-Scale Wind Speed Ranges (McDonald & Mehta, 2006)..... 5.8-137

Table 5.8.56 Summary of Tornado Phenomena Recorded Around Thyspunt Area (1905-2020) ((Goliger, et al., 1997) (SAWS, 2024d)*)* 5.8-140

Table 5.8.57 Tornado Path Length and Width Correlated to Enhanced-Fujita Scales (Elsner, et al., 2014) 5.8-145

Table 5.8.58 Calculated Tornado Path Areas (1905-2020)..... 5.8-145

Table 5.8.59 Expected Annual Total Rainfall in Return Periods of 10 to 100 000 000 Years at the Site (38 Years) Based on Cape St. Francis WS Observations 5.8-150

Table 5.8.60 Expected Maximum 24-hour Total Rainfall in Return Periods of 10 to 100 000 000 Years at the Site (38 Years) Based on Cape St. Francis WS Observations..... 5.8-150

Table 5.8.61 Expected Annual Total Rainfall in Return Periods Including Climate Change Projections at the Site 5.8-154

Table 5.8.62 Expected Maximum 24-hour Total Rainfall in Return Periods Including Climate Change Projections at the Site 5.8-155

Table 5.8.63 Expected Minimum and Maximum Hourly Average Temperature (°C) in Return Periods of 10 to 100 000 000 Years at the Site (19 Years)5.8-156

Table 5.8.64 Expected Minimum Hourly Average Temperatures Including Climate Change Projections at the Site 5.8-159

Table 5.8.65 Expected Maximum Hourly Average Temperatures Including Climate Change Projections at the Site 5.8-160

Table 5.8.66 Extreme Highest Hourly Average Wind Speed and Wind Gust [m/s] Estimated for the Site..... 5.8-161

Table 5.8.67 Expected Maximum Hourly Average Wind Speeds Including Climate Change Projections at the Site 5.8-165

Table 5.8.68 Expected Wind Gust Speeds Including Climate Change Projections at the Site..... 5.8-166

Table 5.8.69 Dispersion Factors (s/m³) based on 2nd Highest Hourly, 3-Hourly, 8-Hourly and 24-hourly Average Predictions at 800 m, 3 km and 8 km Downwind of

© Eskom 2026/Rev 0c

PRINTED VERSIONS OF THIS DOCUMENT ARE NOT CONTROLLED

the Nuclear Installation(s) for Different Wind Directions..... 5.8-199

Table 5.8.70 Dispersion Factors (s/m³) based on Highest Averages of 3-Daily, Monthly, Annual and 95th Percentile Predictions at 800 m, 3 km and 8 km Downwind of the Nuclear Installation(s) for Different Wind Directions..... 5.8-200

Table 5.8.71 Fallout Factors (1/m²-deposition period) based on 2nd Highest Hour, 3-Hour, 8-Hour and 24-hour Total Deposition Predictions at 800 m, 3 km and 8 km Downwind of the Nuclear Installation(s) for Different Wind Directions 5.8-210

Table 5.8.72 Fallout Factors (1/m²- deposition period) based on Hourly, 3-Day, Month, Annual and 95th Percentile Total Deposition Predictions at 800 m, 3 km and 8 km Downwind of the Nuclear Installation(s) for Different Wind Directions..... 5.8-211

Table 5.8.73 Comparison of Atmospheric Stability Classification Schemes for the Site (1997-2023) 5.8-224

Table 5.8.74 Fractional Climate Change Projections for Rainfall, Temperature and Wind Speed 5.8-233

Table 5.8.75 Climate Change Projections for Rainfall, Temperature and Wind Speed (Thyspunt WS and Cape St Francis Baselines)..... 5.8-234

Table 5.8.76 Regulatory Compliance Matrix 5.8-238

Table 5.8.77 Summary of Activities, Links and Quality Requirements..... 5.8-248

Table 5.8.78 Site Specific Parameters Part 1 ..... 5.8-253

Table 5.8.79 Site Specific Parameters Part 2 ..... 5.8-260

© Eskom 2026/Rev 0c

PRINTED VERSIONS OF THIS DOCUMENT ARE NOT CONTROLLED

FIGURES

Figure 5.8.1 Locations of the Eskom Historical Monitoring Points, SAWS WS and the Thyspunt WS 5.8-35

Figure 5.8.2 Topography of the 40 km by 40 km Study Area 5.8-43

Figure 5.8.3 Comparison of SAWS Cape St. Francis WS and Thyspunt WS for 2008-2013 data period 5.8-51

Figure 5.8.4 Comparison of SAWS Cape St. Francis WS and Thyspunt WS for 2017-2019 data period 5.8-52

Figure 5.8.5 Comparison of Cape St. Francis WS and Thyspunt WS Day- and Night-time Wind Roses (2008 to 2013) 5.8-54

Figure 5.8.6 Comparison Cape St. Francis WS and Thyspunt WS Day- and Night-time Wind Roses (2017 to 2019) 5.8-55

Figure 5.8.7 Comparison of Seasonal Wind Roses for Cape St. Francis WS and Thyspunt WS (2008 to 2013) 5.8-63

Figure 5.8.8 Comparison of Seasonal Wind Roses for Cape St. Francis WS and Thyspunt WS (2017 to 2019) 5.8-64

Figure 5.8.9 Mean Annual Precipitation for South Africa (Schulze, 1997) 5.8-87

Figure 5.8.10 Annual Rainfall Totals at the Cape St. Francis WS 5.8-89

Figure 5.8.11 Monthly Rainfall Data at Cape St. Francis WS, Humansdorp WS and Thyspunt WS 5.8-91

Figure 5.8.12 Dry and Wet Rainfall Periods Observed at Cape St. Francis WS5.8-95

Figure 5.8.13 Dry and Wet Rainfall Periods at the Cape St. Francis WS..... 5.8-96

Figure 5.8.14 Average Durations (Hours) of Dust Conditions per Day Per Month5.8-121

Figure 5.8.15 Corrosion Monitoring Locations Using Coupon-Based Method (August 1987 to August 1989) (Gross & Nixon, 1993) 5.8-124

Figure 5.8.16 Calculated Corrosion Attack Depths as a Function of Time Using the ISO 9224:2012 Methodology 5.8-133

Figure 5.8.17 Occurrence of Tornadoes for Period from 1905 to 2020..... 5.8-141

Figure 5.8.18 Average Annual Rate of Occurrence of F1 Tornadoes (1905 to 2020) 5.8-142

Figure 5.8.19 Average Annual Rate of Occurrence of F2 Tornadoes (1905 to 2020) 5.8-142

Figure 5.8.20 Average Annual Rate of Occurrence of F3 Tornadoes (1905 to 2020) 5.8-143

Figure 5.8.21 Average Annual Rate of Occurrence of F4 Tornadoes (1905 to 2020)

© Eskom 2026/Rev 0c

PRINTED VERSIONS OF THIS DOCUMENT ARE NOT CONTROLLED

..... 5.8-143

Figure 5.8.22 Average Annual Ground Flash Density (flashes/km²) for 2006 to 2018 (Gijben, 2021) 5.8-148

Figure 5.8.23 Map of Fundamental Value of Basic 3-s Gust Wind Speed (50 Year Return Period) (South African National Standards, 2019) 5.8-162

Figure 5.8.24 The Predicted 2nd Highest Hourly Average Ground Level Concentration Dispersion Factor (א/Q) (s/m³) for a 5 km by 5 km area..... 5.8-171

Figure 5.8.25 The Predicted 2nd Highest Hourly Average Ground Level Concentration Dispersion Factor (א/Q) (s/m³) for a 40 km by 40 km area..... 5.8-172

Figure 5.8.26 The Predicted 95th Percentile Ground Level Concentration Dispersion Factor (א/Q) (s/m³) for a 5 km by 5 km area..... 5.8-173

Figure 5.8.27 The Predicted 95th Percentile Ground Level Concentration Dispersion Factor (א/Q) (s/m³) for a 40 km by 40 km area..... 5.8-174

Figure 5.8.28 The Predicted 2nd Highest 3-Hourly Average Ground Level Concentration Dispersion Factor (א/Q) (s/m³) for a 5 km by 5 km area..... 5.8-175

Figure 5.8.29 The Predicted 2nd Highest 3-Hourly Average Ground Level Concentration Dispersion Factor (א/Q) (s/m³) for a 40 km by 40 km area..... 5.8-176

Figure 5.8.30 The Predicted 2nd Highest 8-Hourly Average Ground Level Concentration Dispersion Factor (א/Q) (s/m³) for a 5 km by 5 km area..... 5.8-177

Figure 5.8.31 The Predicted 2nd Highest 8-Hourly Average Ground Level Concentration Dispersion Factor (א/Q) (s/m³) for a 40 km by 40 km area..... 5.8-178

Figure 5.8.32 The Predicted 2nd Highest 24-Hourly Average Ground Level Concentration Dispersion Factor (א/Q) (s/m³) for a 5 km by 5 km area..... 5.8-179

Figure 5.8.33 The Predicted 2nd Highest 24-Hourly Average Ground Level Concentration Dispersion Factor (א/Q) (s/m³) for a 40 km by 40 km area..... 5.8-180

Figure 5.8.34 The Predicted Highest Monthly Average Ground Level Concentration Dispersion Factor (א/Q) (s/m³) for a 5 km by 5 km area..... 5.8-181

Figure 5.8.35 The Predicted Highest Monthly Average Ground Level Concentration Dispersion Factor (א/Q) (s/m³) for a 40 km by 40 km area..... 5.8-182

Figure 5.8.36 The Predicted Highest Annual Average Ground Level Concentration Dispersion Factor (א/Q) (s/m³) for a 5 km by 5 km area..... 5.8-183

Figure 5.8.37 The Predicted Highest Annual Average Ground Level Concentration Dispersion Factor (א/Q) (s/m³) for a 40 km by 40 km area..... 5.8-184

Figure 5.8.38 The Predicted 2nd Highest Hourly Total Deposition Dispersion Factor (*D/Q*) (1/m²- hour) for a 5 km by 5 km area..... 5.8-185

Figure 5.8.39 The Predicted 2nd Highest Hourly Total Deposition Dispersion Factor (*D/Q*) (1/m²- hour) for a 40 km by 40 km area..... 5.8-186

© Eskom 2026/Rev 0c

PRINTED VERSIONS OF THIS DOCUMENT ARE NOT CONTROLLED

Figure 5.8.40 The Predicted 95th Percentile Hourly Total Deposition Factor (*D/Q*) (1/m²-hour) for a 5 km by 5 km area 5.8-187

Figure 5.8.41 The Predicted 95th Percentile Hourly Total Deposition Factor (*D/Q*) (1/m²-hour) for a 40 km by 40 km area 5.8-188

Figure 5.8.42 The Predicted 2nd Highest 3-Hour Total Deposition Factor (*D/Q*) (1/m²- 3 hours) for a 5 km by 5 km area 5.8-189

Figure 5.8.43 The Predicted 2nd Highest 3-Hour Total Deposition Factor (*D/Q*) (1/m²- 3 hours) for a 40 km by 40 km area 5.8-190

Figure 5.8.44 The Predicted 2nd Highest 8-Hour Total Deposition Factor (*D/Q*) (1/m²- 8 hours) for a 5 km by 5 km area 5.8-191

Figure 5.8.45 The Predicted 2nd Highest 8-Hour Total Deposition Factor (*D/Q*) (1/m²- 8 hours) for a 40 km by 40 km area 5.8-192

Figure 5.8.46 The Predicted 2nd Highest 24-Hour Total Deposition Factor (*D/Q*) (1/m²-24 hours) for a 5 km by 5 km area 5.8-193

Figure 5.8.47 The Predicted 2nd Highest 24-Hour Total Deposition Factor (*D/Q*) (1/m²-24-hours) for a 40 km by 40 km area 5.8-194

Figure 5.8.48 The Predicted Highest Monthly Total Deposition Factor (*D/Q*) (1/m²-month) for a 5 km by 5 km area 5.8-195

Figure 5.8.49 The Predicted Highest Monthly Total Deposition Factor (*D/Q*) (1/m²-month) for a 40 km by 40 km area 5.8-196

Figure 5.8.50 The Predicted Highest Annual Total Deposition Factor (D/Q) (1/m²-year) for a 5 km by 5 km area 5.8-197

Figure 5.8.51 The Predicted Highest Annual Total Deposition Factor (*D/Q*) (1/m²- year) for a 40 km by 40 km area 5.8-198

Figure 5.8.52 Dispersion Factors (א/Q) (s/m³) based on the 2nd Highest Hourly Average Predictions at 800 m, 3 km and 8 km Downwind of the Nuclear Installation(s) for Different Wind Directions 5.8-201

Figure 5.8.53 Dispersion Factors (א/Q) (s/m³) based on the Highest 3-Hourly Average Predictions at 800 m, 3 km and 8 km Downwind of the Nuclear Installation(s) for Different Wind Directions 5.8-202

Figure 5.8.54 Dispersion Factors (א/Q) (s/m³) based on the Highest 8-Hourly Average Predictions at 800 m, 3 km and 8 km Downwind of the Nuclear Installation(s) for Different Wind Directions 5.8-203

Figure 5.8.55 Dispersion Factors (א/Q) (s/m³) based on the Highest 24-Hourly Average Predictions at 800 m, 3 km and 8 km Downwind of the Nuclear Installation(s) for Different Wind Directions 5.8-204

Figure 5.8.56 Dispersion Factors (א/Q) (s/m³) based on the Highest 3-Daily Average Predictions at 800 m, 3 km and 8 km Downwind of the Nuclear

© Eskom 2026/Rev 0c

PRINTED VERSIONS OF THIS DOCUMENT ARE NOT CONTROLLED

Installation(s) for Different Wind Directions 5.8-205

Figure 5.8.57 Dispersion Factors (א/Q) (s/m³) based on the Highest Monthly Average Predictions at 800 m, 3 km and 8 km Downwind of the Nuclear Installation(s) for Different Wind Directions 5.8-206

Figure 5.8.58 Dispersion Factors (א/Q) (s/m³) based on the Highest Annual Average Predictions at 800 m, 3 km and 8 km Downwind of the Nuclear Installation(s) for Different Wind Directions 5.8-207

Figure 5.8.59 Dispersion Factors (א/Q) (s/m³) Based on the 95th Percentile of the Hourly Average Predictions at 800 m, 3 km and 8 km Downwind of the Nuclear Installation(s) for Different Wind Directions 5.8-208

Figure 5.8.60 Dispersion Factors (א/Q) (s/m³) Based on Concentration Predictions at Various Downwind Distances and Averaging Periods 5.8-209

Figure 5.8.61 Fallout Factors (D/Q) (1/m²- hour) based on the 2nd Highest Hourly Total Predictions at 800 m, 3 km and 8 km Downwind of the Nuclear Installation(s) for Different Wind Directions 5.8-212

Figure 5.8.62 Fallout Factors (*D/Q*) (1/m²- 3 hours) based on the Highest 3-Hourly Total Predictions at 800 m, 3 km and 8 km Downwind of the Nuclear Installation(s) for Different Wind Directions 5.8-213

Figure 5.8.63 Fallout Factors (*D/Q*) (1/m²- 8 hours) based on the Highest 8-Hourly Total Predictions at 800 m, 3 km and 8 km Downwind of the Nuclear Installation(s) for Different Wind Directions 5.8-214

Figure 5.8.64 Fallout Factors (*D/Q*) (1/m²- 24 hours) based on the Highest 24-Hourly Total Predictions at 800 m, 3 km and 8 km Downwind of the Nuclear Installation(s) for Different Wind Directions 5.8-215

Figure 5.8.65 Dispersion Factors (D/Q) (1/m²- 3 days) based on the Highest 3-Daily Average Predictions at 800 m, 3 km and 8 km Downwind of the Nuclear Installation(s) for Different Wind Directions 5.8-216

Figure 5.8.66 Fallout Factors (*D/Q*) (1/m²- month) based on the Highest Monthly Total Predictions at 800 m, 3 km and 8 km Downwind of the Nuclear Installation(s) for Different Wind Directions 5.8-217

Figure 5.8.67 Fallout Factors (*D/Q*) (1/m²- year) based on the Highest Annual Total Predictions at 800 m, 3 km and 8 km Downwind of the Nuclear Installation(s) for Different Wind Directions 5.8-218

Figure 5.8.68 Fallout Factors (*D/Q*) (1/m²- hour) Based on the 95th Percentile of the Hourly Total Predictions at 800 m, 3 km and 8 km Downwind of the Nuclear Installation(s) for Different Wind Directions 5.8-219

Figure 5.8.69 Fallout Factors (D/Q) (1/m²- deposition period) for Deposition Predictions at Various Downwind Distances and Averaging Periods 5.8-220

© Eskom 2026/Rev 0c

PRINTED VERSIONS OF THIS DOCUMENT ARE NOT CONTROLLED

APPENDICES

Appendix 5.8.A: Thyspunt Weather Station Location 5.8-273
Appendix 5.8.B: Distribution of Extreme Values 5.8-310
Appendix 5.8.C: Evapotranspiration Rate Estimation 5.8-336
Appendix 5.8.D: Instrument Specifications 5.8-348
Appendix 5.8.E: Second Edition of the ISO Corrosion Standard 5.8-356
Appendix 5.8.F: Calibration Certificates 5.8-357
Appendix 5.8.G: Data Collection and Validation Procedure 5.8-358
Appendix 5.8.H: Particle Size Distribution 5.8-362
Appendix 5.8.I: Reportable Meteorological Incidents 5.8-366
Appendix 5.8.J to 5.8.T 5.8-369

© Eskom 2026/Rev 0c

PRINTED VERSIONS OF THIS DOCUMENT ARE NOT CONTROLLED

5.8 METEOROLOGY

The meteorological[8] and climatological[9] characteristics for the Thyspunt site (the site) have been investigated in support of the identification of external meteorological events[10] and potential hazards to the nuclear installation(s) on the site. This section of this Site Safety Report (SSR) presents the approach to evaluation of these site characteristics, with specific attention to the extreme values of meteorological variables such as air temperature and wind speed and rare meteorological phenomena that occur infrequently[11] (International Atomic Energy Agency, 2019).

5.8.1 Introduction

The approach to be followed during the evaluation of the site for locating the new nuclear installation(s) has been provided in ***Chapter 4*** (Site Investigation Approach) and in the meteorology section of the SSR Technical Specification for Site Safety Reports (Eskom, 2022c). The most important requirement for completing the meteorology section is the provision of sufficient data to perform the analyses required for this section, which include historical data and reports, and on-site meteorological parameter measurements. The information must serve to confirm that the site is suitable for its intended use and to provide the site characteristics in a manner that is fit for use in the Safety Analysis Report (SAR) that will demonstrate the adequacy of the design of the nuclear installation(s) to protect public health, safety, plant security and provide environmental protection.

The key meteorological aspects have been identified as follows:

[8] Meteorology is the scientific study of the earth's atmosphere and how it causes changes in weather conditions at a location. Meteorology includes different times and distance scales. Thes scales are categorised into microscale, mesoscale, and synoptic scale. Microscale meteorology describes the smallest and shortest event; events that only last seconds or minutes, and only in areas less than 2 km. Mesoscale meteorology occur up to several hours and roughly 1 000 km. These events include thunderstorms, sea breezes, severe local storms, tornado events, and low-level jet streams. Synoptic scale meteorology the study of weather events from 1 000 to 2 500 km at a certain point in time.

[9] Climatological characteristics include the conditions of the atmosphere at a particular location over a long period of time; and it is the long-term summation of the atmospheric elements (and their variations) that, over short time periods, constitute weather. These elements are solar radiation, temperature, humidity, precipitation (type, frequency, and amount), atmospheric pressure, and wind (speed and direction).

[10] Events originating outside the nuclear installation(s) with the potential to cause adverse conditions or even damage to safety important structures, systems or components (Eskom, 2022b).

[11] In RG 0011, clause 7.1 General approach for External Events (National Nuclear Regulator, 2016a), the assessment of hazards associated with external natural and human-induced events alternatively uses the terms "external phenomena" and "severe events". In the meteorology section of the TSSR, this includes, extreme meteorological events, such as extreme winds and heavy rains that are often short-lived, as well as rare, but severe meteorological phenomena such as cyclones, tornadoes, severe thunderstorms, hail, etc. An extreme weather event is rare at a particular place and time of year, with unusual characteristics in terms of magnitude, location, timing, or extent.

© Eskom 2026/Rev 0c

PRINTED VERSIONS OF THIS DOCUMENT ARE NOT CONTROLLED

- wind field parameters, including average and extreme wind speeds, average and extreme wind gusts, wind directions and turbulence (derived from the standard deviation of wind direction) - These parameters are necessary to calculate the atmospheric dispersion of air emissions from the nuclear installation(s), under normal operating conditions and upset or accidental releases. Wind speed data are also required to estimate extreme oceanographic events, such as extreme storm surges. The extremes of wind speeds, including tornadoes and cyclones, are also required to establish the adequacy of the nuclear installation design.
- air temperature, including dry- and wet-bulb temperatures - The nuclear installation design should accommodate the effects of temperature extremes, including both very high and low temperatures.
- rainfall, including the amount, type and durations are important to design surface water holding and drainage systems;
- snow - This is an important parameter in regions where snow may represent a significant load factor in the design of plant structures.
- lightning - Lightning transients exhibit extremely high voltages, currents and current rise rates and knowledge of lightning expected at the site is required for the design of insulators to minimise damage.
- blizzards, dust and sandstorms, drought, icing and hail – These rare meteorological phenomena are included owing to their possible impact on plant safety.
- solar radiation - The measurement of the solar radiation is required to determine the development of the day-time atmospheric structure and evapotranspiration[12] rates.
- barometric pressure - required to estimate extreme oceanographic events;
- corrosivity potential - required to enable the selection of appropriate construction and fabrication material - It is also required to assist with the selection of protective coating systems, if implemented.

The onsite Thyspunt Weather Station (WS) was commissioned on 10 January 2008 and monitoring included two campaigns: 10 January 2008 to 4 October 2013 and 29 September 2017 to 31 March 2019. Data gathering stopped on 31 March 2019 following an Eskom Stop Work Order of 6 February 2019, which took effect from 1 April 2019. Albeit outside the

[12] Evapotranspiration is the process by which water is transferred from the land to the atmosphere by evaporation from the soil and other surfaces and by transpiration from plants.

© Eskom 2026/Rev 0c

PRINTED VERSIONS OF THIS DOCUMENT ARE NOT CONTROLLED

contract period, monitoring at the Thyspunt WS continued until 3 June 2020; however, the data were deemed valid only for the period up to September 2019. Although the total length of the meteorological database is approximately seven years[13], the four-year gap between the two campaigns does not allow the establishment of rainfall trends for this period. In general, the longer the observation period, typically 20 and more years, but not less than 10 years[14] (Smithers & Schulze, 2000), the smaller the error in calculating the average annual precipitation and short-term extremes rain events. Furthermore, to allow seasonal and consecutive annual temporal trends, only six full years were available in the dataset[15]. Other meteorological parameters are not as significantly affected by the missing data period.

Long-term rainfall observed at Cape St. Francis, Humansdorp and Gqeberha (formerly known as Port Elizabeth) accumulated over longer periods improve the accuracy of estimating extreme weather conditions. Additional information was therefore also obtained from the SAWS reports, and monitoring data from SAWS.

5.8.2 Purpose and Scope

The purpose of the meteorological investigation of the site is to:

- provide baseline information for site evaluation and this SSR that will be updated over the life cycle of the nuclear installation(s);
- confirm the suitability of the site through the identification of external meteorological events and potential hazards for the nuclear installation(s);
- develop the atmospheric structure (including wind and turbulent fields) to enable atmospheric dispersion predictions necessary for the assessment of potential radiological impact to the public and the environment in ***Chapter 7*** (Potential Radiological Impact on the Public and the Environment, PRIPE) and the evaluation of the feasibility of the emergency planning in ***Chapter 8*** (Emergency Planning);
- define the local air quality with specific reference to corrosion potential.

[13] 2008, 2009, 2010, 2011, 2012, 2013 (8 months), September 2017 to September 2018, September 2018 to September 2019.

[14] As discussed in (Smithers & Schulze, 2000), the reliability of design rainfall values increases with longer records and records lengths less than 10 years are generally not suitable for design rainfall estimation.

[15] 2008, 2009, 2010, 2011, 2012, and albeit not calendar years, September 2017 to September 2018, and September 2018 to September 2019.

© Eskom 2026/Rev 0c

PRINTED VERSIONS OF THIS DOCUMENT ARE NOT CONTROLLED

The results of the meteorological analysis also provide input into the:

- selection of appropriate dispersion models for the site and the assessment of the atmospheric dispersion of radionuclides to the environment;
- demonstration of compliance with the National Nuclear Regulator's (NNR's) licensing requirements for operating a nuclear installation in terms of radiological protection to ensure public health and safety;
- establishment of limits for nuclear installation design performance.

These additional functions, however, require additional data and detail that depend on the nuclear installation design.

5.8.3 Regulatory Framework

The overall legal and regulatory basis for this SSR is outlined in ***Chapter 2*** (Legal and Regulatory Basis) of this SSR. The main national regulations specifically relevant to a meteorological investigation for site evaluation are the Regulations on Siting of New Nuclear Installations (Department of Energy, 2011). These require the SSR to present the characteristics of the proposed site, which include *inter alia*:

- [Regulation 4(5)] Natural phenomena and potential man-made hazards must be appropriately accounted for in the design of the new nuclear installation(s), and that adequate emergency plans and nuclear security measures can be developed.
- [Regulation 5(3)] The characteristics of the site relevant to the design assessment, risk and dose calculations, including *inter alia*:
  - [Regulation 5(3)(a)] external events (and in this case, of meteorological origin); and
  - [Regulation 5(3)(b)] meteorological data.

5.8.4 Requirement Documents and Guides

The Regulation is complemented by the following NNR documents[16]:

[16] This document incorporates guidelines and safety requirements of the International Atomic Energy Agency and United States Nuclear Regulatory Commission as listed, but some references are not cited again herein. Whilst not all the listed references are used in the sections, these are included since they were used in the development of the Technical Specification.

© Eskom 2026/Rev 0c

PRINTED VERSIONS OF THIS DOCUMENT ARE NOT CONTROLLED

- Interim Guidance for the Siting of Nuclear Facilities, Regulatory Guide RG-0011, Rev 0 – Sections 7.2.2 and 8.3 (National Nuclear Regulator, 2016a)
- Consideration of External Events for New Nuclear Installations, Position Paper PP-0014, Rev 0 – Sections 11.3, 11.4, 11.5 and 11.9 (National Nuclear Regulator, 2012a);
- Emergency Planning Technical Basis for New Nuclear Installations, Position Paper PP-0015, Rev 0 – Sections 7.3.2.3 and 7.3.4 (National Nuclear Regulator, 2012b);
- Guidance on the Verification and Validation of Evaluation and Calculation Models used in Safety and Design Analyses, Regulatory Guide RG-0016, Rev 0 (National Nuclear Regulator, 2016b);
- Quality and Safety Management Requirements for Nuclear Installations. Requirement Document No. RD-0034 (National Nuclear Regulator, 2008).
- Emergency Prepared and Response Requirements. Requirement Document No. RD-014 (National Nuclear Regulator, 2005).
- Demonstration of compliance with the NNR requirements has also been performed following the available NNR guidelines and internationally accepted safety standards and supporting documents, US regulatory guidance and Eskom standards as follows:
  - International Atomic Energy Agency (IAEA) Safety Requirement No. SSR-1 on Site Evaluation for Nuclear Installations (International Atomic Energy Agency, 2019);
  - IAEA Specific Safety Guide No. SSG-18 on Meteorological and Hydrological Hazards in Site Evaluation for Nuclear Installations (International Atomic Energy Agency, 2011);
  - IAEA Safety Guide No. NS-G-3.2 on Dispersion of Radioactive Material in Air and Water and Consideration of Population Distribution in Site Evaluation for Nuclear Power Plants (International Atomic Energy Agency, 2002);
  - IAEA Specific Safety Guide No. SSG-68 on Design of Nuclear Installations Against External Events Excluding Earthquakes (International Atomic Energy Agency, 2021);
  - IAEA Safety Report Series No. 19. on Generic Models for Use in Assessing the Impact of Discharge of Radioactive Substances to the Environment (International Atomic Energy Agency, 2001);

© Eskom 2026/Rev 0c

PRINTED VERSIONS OF THIS DOCUMENT ARE NOT CONTROLLED

- United States Nuclear Regulatory Commission (US NRC) NUREG 0800 (Parts 2.3.1 to 2.3.4.) (United States Nuclear Regulatory Commission, 2007a);
- US NRC Regulatory Guide 1.145 on Atmospheric Dispersion Models for Potential Accident Consequence Assessments at Nuclear Power Plants (United States Nuclear Regulatory Commission, 1983);
- US NRC Regulatory Guide No. 1.76 on Design Basis Tornado and Tornado Missiles for Nuclear Power Plants (United States Nuclear Regulatory Commission, 2007b);
- US NRC Regulatory Guide No. 1.23 on Meteorological Monitoring Programs for Nuclear Power Plants (United States Nuclear Regulatory Commission, 2007c);
- American Nuclear Society – Determining Meteorological Information at Nuclear Facilities, American Nuclear Society, ANSI/ANS-3.11-2015 (American National Standard, 2015);
- EPA-454/R-99-005 on Meteorological Monitoring Guidance for Regulatory Modelling Applications (United States Environmental Protection Agency, 2000);
- ISO 9223 on Corrosion of Metals and Alloys-Corrosivity of Atmospheres – Classification (International Organisation for Standardisation, 2012a);
- Eskom Standard 238-52 – Meteorological Requirements for Nuclear Installations (Eskom, 2022a)[17].

Regulatory Guide 1.23 Rev 1 (United States Nuclear Regulatory Commission, 2007c) was used as reference for the specification of meteorological instruments and operation of the weather station since the start of the monitoring programme at the site. This guide reflects the regulatory requirements and best practices, using guidance provided in ANSI/ANS-3.11-2005 *"Determining Meteorological Information at Nuclear Facilities*. Although the latter standard has subsequently been revised to ANSI/ANS-311-2015 (American National Standard, 2015), the meteorological monitoring specification in the current campaign still conforms to the listed criteria.

[17] This section of this SSR identifies the criteria for establishing and implementing an onsite meteorological measurements programme that aims to demonstrate compliance with the National Nuclear Regulator (NNR) requirements for collection of basic meteorological data. At the time of writing, no specific NNR requirements for the collection of basic meteorological data have been provided. In the interim, the Eskom Standard 238-52 – Radiation Protection: Meteorological Requirements (***Eskom, 2017***) will be followed.

© Eskom 2026/Rev 0c

PRINTED VERSIONS OF THIS DOCUMENT ARE NOT CONTROLLED

5.8.5 Evaluation Approach

This subsection provides the background to the meteorological information on which the analyses are based. This includes information on both on- and off-site meteorological data.

5.8.5.1 Meteorological Data Analysis

The following steps have been identified (Eskom, 2022c) to evaluate the meteorological characteristics of the site:

- identification of key meteorological parameters required to characterise events that are likely to occur within the site (both rare and extreme);
- desk study evaluation of existing meteorological information including key historical data, analyses, reports and related information;
- analysis of monitored onsite meteorological data;
- identification, quantification and management of uncertainties;
- identification of any further work required prior to or during construction and operation of the nuclear installation(s).

The analytical procedures provided in the IAEA Specific Safety Guide No. SSG-18 (International Atomic Energy Agency, 2011) were used as a basis for conducting the meteorological analyses. The main tasks in the meteorological analysis included the following:

- to assess the meteorological and climatological characteristics for the region around the site;
- to describe the basic meteorological parameters, regional orography[18] and phenomena including wind speed and direction, air temperature, precipitation, humidity, solar radiation, atmospheric stability parameters, prolonged inversions and dispersion potential;
- to determine extreme values of meteorological variables (e.g. wind speed, precipitation, snow and temperature);
- to determine the potential frequency and severity of lightning;
- to determine the potential occurrence of tornadoes in the region;

[18] Orography is the study of the topographic relief of mountains, and can more broadly include hills, and any part of a region's elevated terrain.

© Eskom 2026/Rev 0c

PRINTED VERSIONS OF THIS DOCUMENT ARE NOT CONTROLLED

- to determine the potential for tropical cyclones, hurricanes and hurricane force winds;
- to establish a monitoring programme for meteorological measurements; and
- to determine uncertainties in the measurements and to take them into account in the evaluation of statistical results.

The monitoring requirements (and any potentially additional requirements) will continue throughout the nuclear installation operation and up until decommissioning (International Atomic Energy Agency, 2002) and (Eskom, 2022a).

5.8.5.2 Meteorological Measurement

The site was investigated with regard to the meteorological characteristics that could be significant to safety in respect of external meteorological events. The following are addressed in the subsections:

- the available data prior to site investigations;
- the meteorological measurements performed (and on-going) for the purpose of this SSR;
- the meteorological stations;
- data resources;
- the evaluation techniques used;
- the methods for analysis of data.

5.8.5.2.1 Availability of Data

At present there are no long-term local meteorological data for the site, apart from the results from the seven year's on-site meteorological measurements (more detailed discussion in the next subsection). Historically, Eskom Holdings (further referred to as Eskom) collected meteorological data at four sites in the vicinity of the site (Cadman & Peerce, 1987; Peerce, 1988a; Peerce, 1988b; Tosen, et al., 1987a; Tosen, et al., 1987b), namely De Hoek, Thyspunt, Klippepunt, and Brakkeduine (see ***Figure 5.8.1***). The monitoring occurred at these sites between December 1986 and September 1988. Unfortunately, vandalism of equipment resulted in limited data recovery. The most appropriate data set was recovered from January 1987 to September 1988.

© Eskom 2026/Rev 0c

PRINTED VERSIONS OF THIS DOCUMENT ARE NOT CONTROLLED

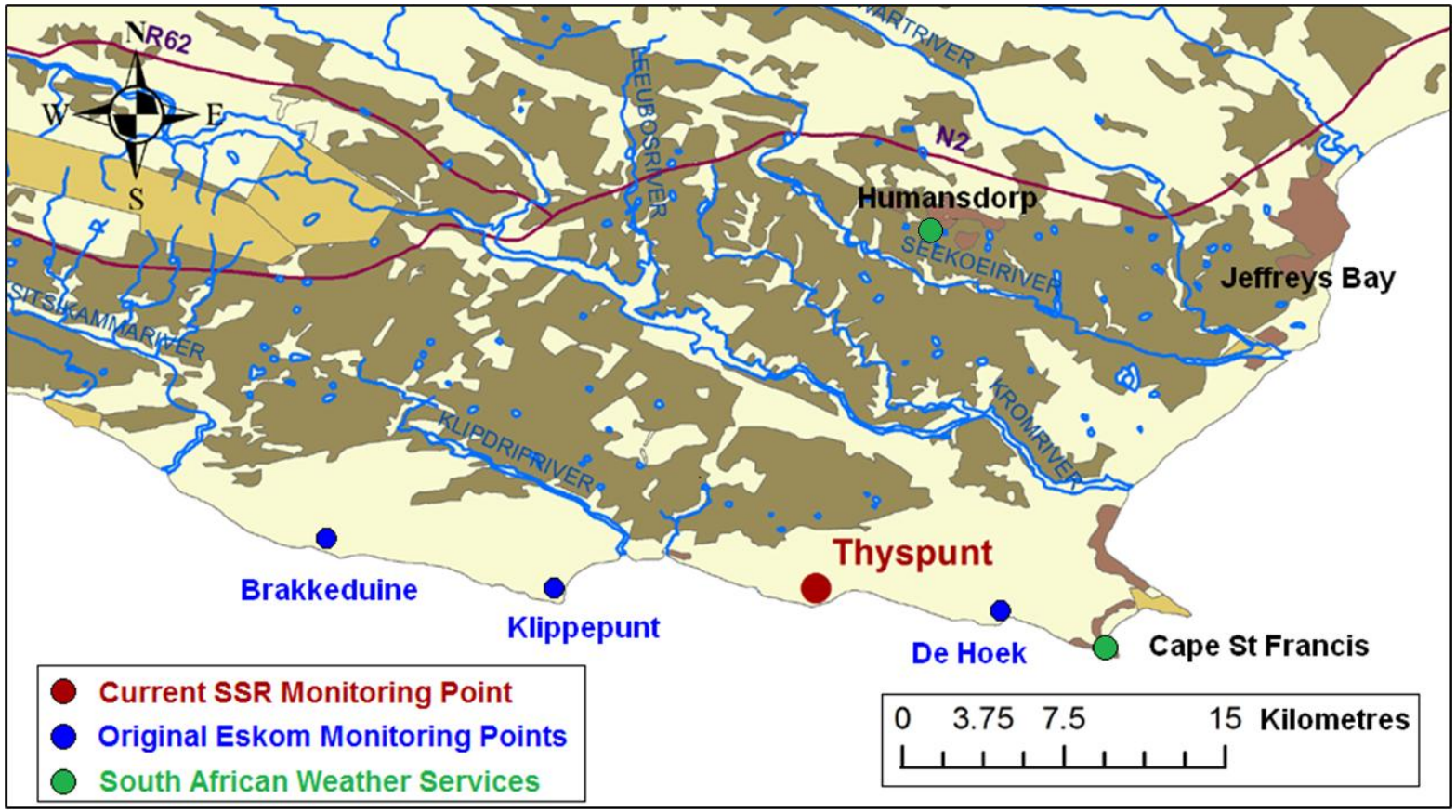


Figure 5.8.1
Locations of the Eskom Historical Monitoring Points, SAWS WS and the Thyspunt WS

© Eskom 2026/Rev 0c

PRINTED VERSIONS OF THIS DOCUMENT ARE NOT CONTROLLED

The IAEA (International Atomic Energy Agency, 2019) considers it acceptable to collect meteorological information from nearby weather stations that would allow the establishment of historical trends. SAWS weather stations included in a 100 km radius from the site are summarised in ***Table 5.8.1***. Although several stations are included in the table, only Cape St Francis and Humansdorp, were considered to best represent the meteorological conditions for the site. The other sites are far removed and represent meteorological conditions that do not apply to the study area.

Long-term meteorological data have been collected by the SAWS at Cape St. Francis [redacted], approximately 9.3 km east-southeast of the site at a height of 9 m above mean sea level (m amsl) (***Figure 5.8.1***). The parameters measured at this station include the wind vector (speed and direction), ambient temperature, relative humidity, atmospheric pressure and rainfall. Wind speed and direction measurements at the Cape St Francis WS are made at approximately 10 m above ground level. Due to the proximity and location at the coast, the atmospheric conditions are expected to be similar to those at the site. This assumption is verified through comparisons of observations of meteorological parameters from the two weather stations.

In addition to the meteorological observations at the Cape St. Francis WS, long term rainfall data have been collected at the Humansdorp WS, approximately 17.3 km north-northeast of the site [redacted] and 109 m amsl) (***Figure 5.8.1***).

5.8.5.3 Onsite Meteorological Instrumentation

The Thyspunt WS is established at [redacted] and an altitude of 51 m amsl, which is approximately 730 m west of the current site centroid [redacted] and 28 m amsl) and about 760 m from the high tide mark. Parameters measured at this weather station include wind speed and direction at 9 m above ground level, dry-bulb temperature at 2 m and 8 m above ground level, solar radiation, relative humidity, atmospheric pressure, rainfall, visibility and lightning events.

The Thyspunt WS was commissioned on 10 January 2008 and monitoring continued until 20 September 2013. The Thyspunt WS was re-commissioned four years later, on 29 September 2017, using re-calibrated instruments and where required (i.e. operated outside specifications), replaced with new instruments and equipment. Data gathering stopped on 31 March 2019 following an Eskom Stop Work Order of 6 February 2019, which took effect from 1 April 2019.

© Eskom 2026/Rev 0c

PRINTED VERSIONS OF THIS DOCUMENT ARE NOT CONTROLLED

Table 5.8.1
Meteorological Stations and Measurements

Station	Distance from Site	Meteorological Parameters Measured	Availability
Brakkeduine (1)	23 km west	Wind Speed and Direction	January 1987 to September 1988
Klippepunt (1)	12 km west	Wind Speed and Direction	January 1987 to September 1988
De Hoek (1)	8 km east	Wind Speed and Direction	January 1987 to September 1988
Thyspunt (1)	On-site	Wind Speed and Direction	January 1987 to September 1988
Thyspunt WS	On-site	Precipitation, Air temperature, Ambient pressure, Wind Speed/Direction, Relative Humidity, Solar radiation	10 January 2008 to 20 September 2013 29 September 2017 to 30 September 2019 (5)
Cape St. Francis (0017582 7) (2)	9.3 km east-southeast	Precipitation	January 1881 to December 2003
Cape St. Francis (0017582A1) (2)	9.3 km east-southeast	Precipitation, Air temperature, Ambient pressure, Wind Speed/Direction, Relative Humidity	15 June 2004 to 31 December 2023
Humansdorp (0017452 7)	17.3 km north-northeast	Precipitation	1878 - 2022
Jeffreys Bay (4) (0017723 1)	28 km northeast	Precipitation	1879 - 2023
Emerald Hill (3) (4) (0035060)	93 km northeast	Precipitation	118 years
Gqeberha (4) (0035209)	95 km east-northeast	Wind Speed/Direction, Relative Humidity, Air temperature, Ambient pressure, Wind	January 1970 to August 1992
Gqeberha4) (0035179 5)	95 km east-northeast	Wind Speed/Direction, Relative Humidity, Air temperature, Ambient pressure, Wind	August 1992 to December 2023
Patensie (4) (0033556 5)	48 km north-northeast	Precipitation, Air temperature, Ambient pressure, Wind Speed/Direction, Relative Humidity	
Patensie (4) (0033526 3)	48 km north-northeast	Precipitation	
Kariega (4) (0034763 X)	78 km northeast	Precipitation, Air temperature, Ambient pressure, Wind Speed/Direction, Relative Humidity	
Kariega (4) (0034767 7)	78 km northeast	Precipitation	

Notes:
(1) Eskom monthly reports (Cadman & Peerce, 1987; Peerce, 1988a; Peerce, 1988b; Tosen, et al., 1987a; Tosen, et al., 1987b).
(2) The original Cape St. Francis (0017562 7) station was replaced end of December 2003 by an automatic weather station (0017582A1).
(3) Emerald Hill (Gqeberha) was discontinued.
(4) Data from this weather station were not used in the analyses.

© Eskom 2026/Rev 0c

PRINTED VERSIONS OF THIS DOCUMENT ARE NOT CONTROLLED

Station	Distance from Site	Meteorological Parameters Measured	Availability
(5) Data gathering stopped on 31 March 2019 following an Eskom Stop Work Order, however the data were deemed valid for the period up to 30 September 2019			

An automatic data logger is used to record meteorological data. The data are stored as 10-minute averages in electronic format (Eskom, 2022c; International Atomic Energy Agency, 2002; International Atomic Energy Agency, 2011). The following information is recorded:

- location, date and time;
- horizontal wind direction (degrees) and wind speed (m/s) (including wind gusts) at 9 m;
- standard deviation of wind direction (degrees) in horizontal plane ('sigma theta') at 9 m;
- ambient dry-bulb air temperature[19] (°C) at 2 m and 8 m;
- ambient temperature gradients (lapse rates) between levels 2 m and 8 m (°C);
- atmospheric moisture (per cent);
- precipitation (mm);
- solar radiation (kW/m²);
- barometric pressure (hPa);
- visibility (km);
- lightning events (counts).

The data can be retrieved remotely via telephone dial-up modem or downloaded onsite, using a data transfer connection cable and personal computer.

Evapotranspiration and atmospheric stability are derived from these parameters, as discussed in ***Subsections 5.8.5.1.10*** and ***5.8.5.1.9***, respectively.

Corrosivity of the local atmosphere was measured using the ISO 9223 International Standard (International Organisation for Standardisation, 2012a) methodology including the periods from May 2008 to January 2009,

[19] The dry-bulb temperature is the temperature of air measured by a thermometer freely exposed to the air but shielded from radiation from the sun. "Dry-bulb" is included because the air temperature is indicated by a thermometer not affected by the moisture of the air. The dry-bulb temperature is the temperature that is usually thought of as "air temperature", and it is the true thermodynamic temperature. Whereas a normal, dry-bulb thermometer measures the temperature of ambient air, the wet-bulb temperature is the temperature of a surface from which water has evaporated into a stream of ambient air. It is the lowest temperature to which an object can be cooled solely by the evaporation of water.

© Eskom 2026/Rev 0c

PRINTED VERSIONS OF THIS DOCUMENT ARE NOT CONTROLLED

October 2012 to September 2013, and October 2017 to March 2019 (Burger, 2019). The ISO Standard 9223 methodology utilises the measured temperature and relative humidity from the local weather station together with the deposition rate of sulfur dioxide and airborne salinity to determine the corrosivity rate.

Measurement of meteorological parameters at higher levels will be initiated at least one year prior to the start of the nuclear installation construction (United States Nuclear Regulatory Commission, 2007c).

5.8.5.4 Instrument Accuracy

As part of the management of uncertainties (see ***Subsection 5.8.9***) all instrumentation is within the accuracy specifications contained in the SSR Technical Specification (Eskom, 2022c). The required instrument accuracies, ranges and measurement resolutions of the instrumentation included on the Thyspunt WS are summarised in ***Table 5.8.2*** (Eskom, 2022c; American National Standard, 2015). These accuracies equal or better the requirements of the US NRC (United States Nuclear Regulatory Commission, 2007c). The technical specifications of the meteorological instrumentation for the Thyspunt WS are given in ***Appendix 5.8.D***.

The meteorological instrumentation is checked on a monthly basis as part of the maintenance programme described in ***Subsection 5.8.8***. More specific maintenance such as sensor calibration, sensor performance testing and sensor component replacement are done on a bi-annual basis (United States Nuclear Regulatory Commission, 2007c).

Validation of the data includes the following steps:

- identify period during which instrument calibration activity occurred and remove data during this period since it would include data generated by the calibration process (when applicable);
- check that all data are within valid ranges. Two range checks are:
  - instrument ranges;
  - ranges based on actual extreme observations;
- check that the readings from the instruments are not fixed on a value for extended periods and that no sudden jumps occurred.

If any of these conditions are not met, the data are automatically flagged. Flagged data are subsequently checked by the data analyst and replaced by a missing parameter identifier (“-9999”) if they are suspected to be invalid. These data validation checks would identify instrument malfunction. The necessary actions to rectify any issues are initiated and executed as soon as possible, to minimise data loss.

© Eskom 2026/Rev 0c

PRINTED VERSIONS OF THIS DOCUMENT ARE NOT CONTROLLED

Table 5.8.2
Instrument Accuracies and Resolutions

Measurement Parameter	Thyspunt WS Instrument Specification		ANSI/ANS-3.11-2015 (*American National Standard, 2015*)	
	System Accuracy and Range	**Measurement Resolution**	**Required Accuracy and Range**	**Required Measurement Resolution**
Wind speed	± 0.2 m/s with starting threshold of less than 0.4 m/s Range 0 to 50 m/s	0.1 m/s	±0.2 m/s or 5% of observed wind speed starting threshold < 0.45 m/s (1)	0.1 m/s
Wind direction	± 3° of azimuth, with starting threshold of less than 0.5 m/s Range 0 to 360 m/s	1°	± 5° of azimuth, with starting threshold of less than 0.5 m/s	1°
Sigma theta	Degrees azimuth	0.1	Not applicable	0.1
True North	± 3°	1°	None stated	None stated
Ambient Air Temperature	± 0.5 °C Range -50 to +50 °C	0.1 °C	±0.5 °C	0.1 °C
Solar Radiation	±5%, linearity 1% max up to 3 000 W/m², stability <±2% per year, operating temperature of -20 to +65°C and minimum response time of 10 µS Range 400-1 100 nanometre	0.1 W/m²	5% of observed	±1 W/m²
Relative Humidity	±2 % at 20 °C:, stability: better than ±1 % per year and response time of 10 seconds (without filter) Range 0 to 100%	0.1%	±4%	0.1%
Precipitation	2% up to 25 mm/hr 3% up to 50 mm/hr	0.1 mm	±10% for a volume equivalent to 2.54 mm of precipitation at a rate < 50 mm/hr	0.25 mm
Atmospheric Pressure	±0.5 hPa (mbar) at -50 to +60°C Range 600 to 1 100 hPa (mbar)	0.1 hPa	±3 hPa	0.1 hPa
Time	±5 min	1 min	±5 min	1 min

Note

(1) The starting threshold defines calm wind conditions. This includes any speed below the starting threshold of the wind speed or direction sensor; or any wind speed below that which is appropriate for input into atmospheric dispersion models, whichever is greater. In the United States of America, calm is typically defined as any speed less than 1 mph, i.e. 0.45 m/s.

© Eskom 2026/Rev 0c

PRINTED VERSIONS OF THIS DOCUMENT ARE NOT CONTROLLED

The first monitoring campaign included the period from 2008 to 2013. For the individual years of 2008, 2010, 2011 and 2012 the data validity was on average 99.9 per cent, whereas valid data for 2009 and 2013 were on average 96.47 per cent and 98.98 per cent respectively. The 2013 monitoring period included 1 January 2013 to 4 October 2013. The second monitoring campaign included the period from 29 September 2017 to 30 September 2019. Valid data for the second monitoring campaign for 2017 were 99.60 per cent and 100 per cent for 2018 and 2019. The seven full years of monitoring include: 2008, 2009, 2010, 2011, 2012, September 2017 to September 2018, September 2018 to September 2019. Only 8 months monitoring occurred in 2013.

The overall availability of the meteorological parameters for the two monitoring campaigns (Eskom, 2023a) is given below:

- horizontal wind speed, direction and standard deviation of wind direction:
  - 2009 to 2013 : 99.84 per cent
  - 2017 to 2019 : 99.91 per cent
- ambient air temperature:
  - 2009 to 2013
    - 2 m : 99.84 per cent
    - 8 m : not measured
  - 2017 to 2019
    - 2 m : 99.91 per cent
    - 8 m : 99.90per cent
- vertical temperature difference:
  - 2009 to 2013 : not measured
  - 2017 to 2019 : 99.90 per cent
- barometric pressure:
  - 2009 to 2013 : 99.84 per cent
  - 2017 to 2019 : 99.91 per cent
- relative humidity :
  - 2009 to 2013 : 99.84 per cent
  - 2017 to 2019 : 99.91 per cent
- solar radiation:
  - 2009 to 2013 : 99.84 per cent

© Eskom 2026/Rev 0c

PRINTED VERSIONS OF THIS DOCUMENT ARE NOT CONTROLLED

- 2017 to 2019 : 99.91 per cent

- Rainfall[20]:
  - 2009 to 2013 : 99.84 per cent
  - 2017 to 2019 : 99.91 per cent
- Visibility:
  - 2009 to 2013 : no measurement
  - 2017 to 2019 : 99.91 per cent
- lightning events:
  - 2009 to 2013 : no measurement
  - 2017 to 2019 : 99.91 per cent

Instrument calibrations were performed by an ISO 17025 (International Organisation of Standardisation, 2017) accredited laboratory on a biannual basis (***Appendix 5.8.F***).

5.8.5.5 Macro and Micro Siting of Instrumentation

The most important consideration in siting of meteorological observation instrumentation is spatial and temporal "representativeness" for the intended application (American National Standard, 2015). Local topographical characteristics and surface features can influence atmospheric transport and dispersion and must be considered when planning or evaluating a meteorological monitoring programme. As shown in ***Figure 5.8.2***, the major topographical features run parallel along a northwest to southeast vector. The site is characterised by undulating hills with elevations reaching up to 150 m amsl[21], 4.6 km north from the centroid (28 m amsl). Within a radius of 1 km from the centroid, the dunes run more parallel to the coastline and rise to maximum heights of about 98 m towards the north, approximately 24 m towards the east and 65 m amsl towards the west. Further north (20 km from centroid), the topography rises to about 230 m amsl.

The atmospheric structure located near the ocean can be influenced by sea and land breezes and long-range transport of stable plumes over water. A feature of shoreline sites is the potential formation of a thermal internal boundary layer (TIBL) at the coastline, which deepens with increasing

[20] Although the total length of the meteorological database is approximately seven years, the four-year gap between the 2008-2013 and 2017-2019 campaigns does not allow the establishment of a complete rainfall trend for the 2008-2019 period. Furthermore, the following calendar years include measurements of one-year durations: 2008, 2009, 2010, 2011, 2012 and 2018, whereas the measurements during 2017 started in September 2017, and measurements during 2019 were only until September 2019. Only 8 months measurements were available during 2013.

[21] amsl – standard reference to "above mean sea level"

© Eskom 2026/Rev 0c

PRINTED VERSIONS OF THIS DOCUMENT ARE NOT CONTROLLED

distance away from the water body. The ANSI/ANS -3.11-2015 standard (American National Standard, 2015) recommends that at least one measurement level shall be located within the TIBL.

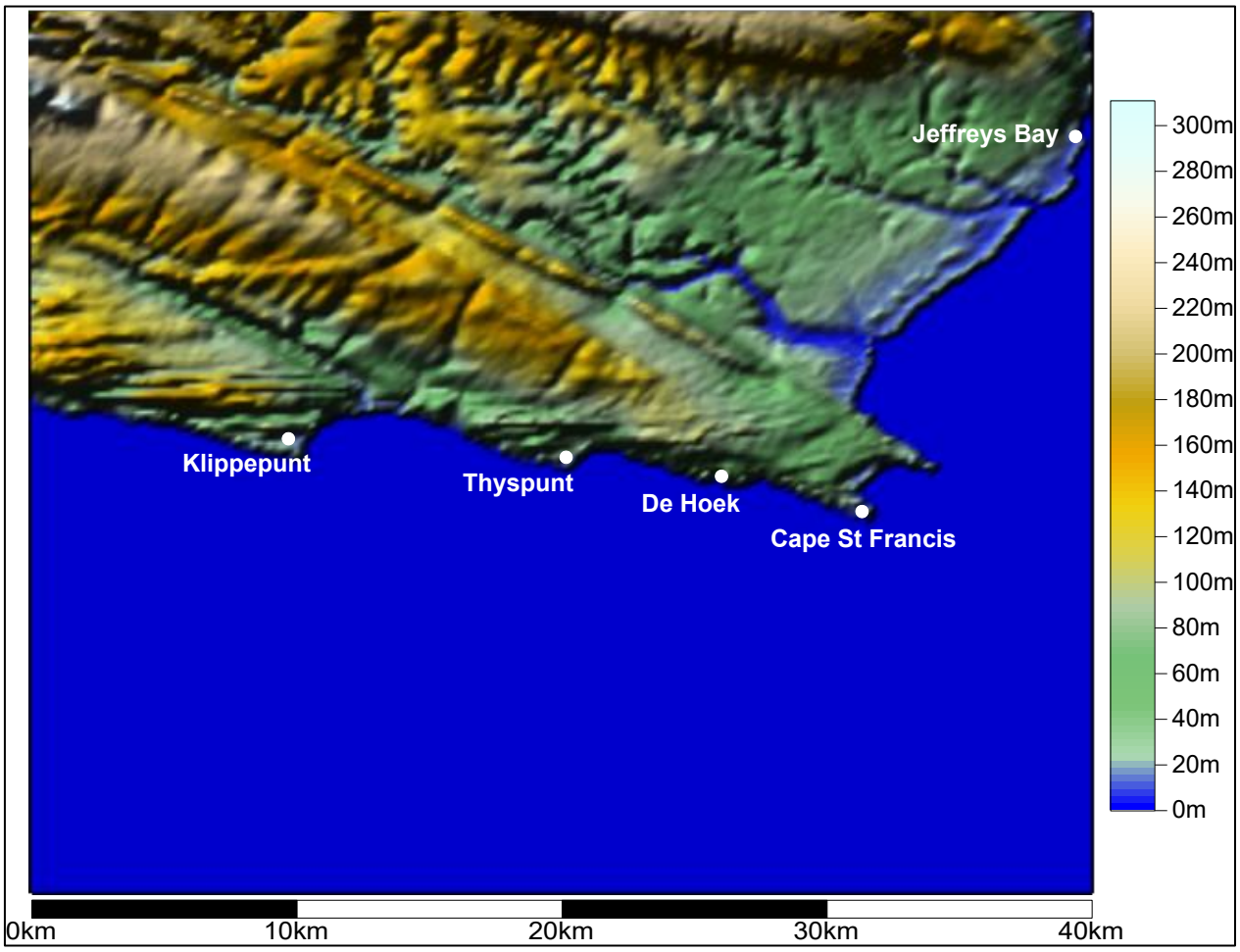


Figure 5.8.2
Topography of the 40 km by 40 km Study Area

The selection of a suitable location for the mast and all instrumentation took several factors into account to ensure the quality of the measurements. Guided by ANSI/ANS-3.11 (American National Standard, 2015) considerations in the siting of meteorological observation instrumentation, the following micro-siting measures were applied in the installation of the instruments to prevent local effects from unduly altering the values of the meteorological parameters to be measured:

- wind speed and direction measurements are at approximately 10 m above ground level;

© Eskom 2026/Rev 0c

PRINTED VERSIONS OF THIS DOCUMENT ARE NOT CONTROLLED

- the nearby buildings and other structures at the site do not influence the wind readings;
- the measurement locations are away from any dunes, trees or other vegetation that could influence the wind readings;
- the meteorological mast is located on an elevation which would represent as closely as possible the same meteorological characteristics as the surface layer into which any airborne material will be released.

Meteorological monitoring programmes in complex terrain may require supplemental masts and towers to characterise dispersion in the region of transport. The number and nature of supplemental masts depends on the relevant atmospheric features within the domain of interest. ANSI/ANS-3.11 (American National Standard, 2015) recommends that airflow studies be conducted to assist with siting of masts. Although the dunes create several shallow valleys, these are relatively local and variation in altitude is relatively gradual with a maximum gradient of 3.9 per cent to the south, 3.1 per cent to the east, 3.0 per cent to the west and 2.6 per cent north from centroid. As a result, wind field simulations (***Appendix 5.8.A***) indicate that a single well-exposed weather station would suffice to establish the prevailing wind field across the local region. The mast and instruments were placed on a concrete slab of approximately 7 m x 10 m, with the base of the mast at a height of 51 m amsl. The closest dune higher than this is towards the west, 70 m amsl, at a distance of approximately 520 m. The location is approximately 760 m from the closest shoreline and well located to observe the TIBL.

5.8.5.6 Length of Monitoring

The length of monitoring (monitoring timeframes) includes the prevailing (near-current) meteorology as well as long-term historical records. The latter information is specifically needed to improve the accuracy of predicting extreme values for wind speeds, dry bulb temperature and rainfall rates.

Measured data from the instruments at the Thyspunt WS are logged on a Campbell CR1000 logger, from where the data are downloaded remotely via a modem and mobile phone connection. As a backup option, the data may also be downloaded locally via cable onto a portable computer. The data logger was initially (10 January 2008 to 29 July 2009) programmed to sample all meteorological parameters once every 10 seconds, and to provide the average of these over a 60-minute period, which was stored in the data logger memory. The 60-minute period coincided with the start of every hour of the day. From 30 July 2009 the sampling resolution was increased to one second intervals, with 10- minute averages stored in the

© Eskom 2026/Rev 0c

PRINTED VERSIONS OF THIS DOCUMENT ARE NOT CONTROLLED

data logger. Wind speed gusts are also recorded and represent the highest wind speed observed in an hour (10 January 2008 to 29 July 2009) or 10-minute (30 July 2009 to 4 October 2013 and 29 September 2017 to 30 September 2019) averaging period, based on a 10 or one second sampling interval, respectively.

All parameters are provided as 10-minute averages or totals (i.e. solar radiation and rainfall) using 360 readings per sampling period. The recorded logger date and time coincided with the start of every 10-minute monitoring period.

The following statistical analyses are followed on the validated meteorological data (note “mean”, as used in this context and throughout the report is understood to be “arithmetic mean”, which is the same as “average”):

- short-term wind gusts, hourly average values for all meteorological parameters, and averages of daily maximums and minimums for rainfall, relative humidity and ambient dry-bulb temperature - These values are reported per month to illustrate the seasonal behaviour. Extreme values (minimums and maximums) are also determined per month for rainfall (highest 1- and 24-hour totals), dry bulb temperatures (hourly averages) and wind speed (hourly averages and gusts). The total monitoring time includes the period from 10 January 2008 to 4 October 2013 and 29 September to 30 September 2019, i.e. a total of 67704 valid hours.
- a joint frequency distribution of hourly average wind speed and wind direction data - The prevailing wind field is best described through a joint frequency which is normally displayed in tabular form and wind roses[22]. The total monitoring time includes the period from 10 January 2008 to 4 October 2013 and 29 September to 30 September 2019, i.e. a total of 67704 valid hours.
- atmospheric stability classification - The atmospheric stability is typically classified into one of seven categories ranging from very stable to convective conditions. The classification is determined through the rate of temperature increase (stable) or decrease (unstable) with height above ground level (International Atomic Energy Agency, 2002) (“delta-T” method). The temperature difference between the two temperature instruments at 2 m and 8 m,

[22] A wind rose comprises 16 spokes which represent the directions from which winds blew during the period. The colours/shades of grey or box width reflect the different categories of wind speeds, the box closest to the inner circle, for example, represents winds of 1 m/s to 2 m/s. The dotted circles provide information regarding the frequency of occurrence of wind speed and direction categories. For the wind roses provided in this analysis, each dotted circle represents 5 per cent frequency of occurrence. The figure given in the centre of the circle describes the frequency with which calms occurred, i.e. periods during which the wind speed was below 1 m/s.

© Eskom 2026/Rev 0c

PRINTED VERSIONS OF THIS DOCUMENT ARE NOT CONTROLLED

provide the temperature gradient and are provided as hourly averages. The fluctuations in wind direction are also used to provide a measure of atmospheric turbulence (International Atomic Energy Agency, 2002). These are provided as the standard deviations of wind direction ('sigma-theta' method) and are calculated using the 1-second wind direction readings at 9 m and are provided as hourly averages. The total monitoring time includes the period from 10 January 2008 to 4 October 2013 and 29 September to 30 September 2019, i.e. a total of 67704 valid hours for the sigma theta method and 17526 valid hours for the delta-T method.

- hourly-totalled solar radiation levels - Solar radiation levels, in combination with the hourly average wind speed, ambient air temperature and atmospheric stability allow a full description of the atmospheric structure (International Atomic Energy Agency, 2002) suitable for use in the atmospheric dispersion model. The effects of both routine air discharges and accidental air releases from the nuclear installation(s) are calculated using the dispersion on an hourly average basis, using the hourly averages of wind speed, wind direction, dry bulb temperature, relative humidity and the hourly totals for solar radiation and rainfall. These dispersion calculations are then used to estimate exposures for longer periods, for example, 2-hourly, 8-hourly, 24-hourly, 3-daily, monthly and annually. The total monitoring time includes the period from 10 January 2008 to 4 October 2013 and 29 September to 30 September 2019, i.e. a total of 67704 valid hours.
- extreme value analyses of long-term meteorological parameter values are based on the methodologies given in (International Atomic Energy Agency, 2011).

The accuracy of estimated statistical parameters improves with longer term monitoring. The World Meteorology Organisation (WMO) states that the optimal length of record for predictive use of normals[23] varies with element, geography and secular trend (World Meteorological Organisation, 2011). The WMO further states that, in general, the most recent 5- to 10-year period of record has as much predictive value as a 30-year record (World Meteorological Organisation, 2011). For elements that show a substantial underlying trend (such as average temperature), predictive accuracy is improved by updating the averages and period averages frequently (World Meteorological Organisation, 2011). The Thyspunt WS meteorological data covered a period of approximately 7 years. The analyses of these data are

[23] Under the WMO Technical Regulations, climatological standard normals are averages of climatological data computed for the following consecutive periods of 30 years: 1 January 1901 to 31 December 1930, 1 January 1931 to 31 December 1960, and so forth (World Meteorological Organisation, 2011). The latest normal covers the period 1 January 1991 to 31 December 2010.

© Eskom 2026/Rev 0c

PRINTED VERSIONS OF THIS DOCUMENT ARE NOT CONTROLLED

therefore considered adequate to draw basic statistical conclusions. Extrapolating extreme meteorological parameters from observations, however, typically requires more years of data (ideally 30 years and more). Therefore, the extreme rainfall analyses were conducted using the observations made at the Cape St Francis WS that included a 19-year data period from 2005 to 2023, which albeit not 30 years, proves to be a better option than the Thyspunt WS observations of 7 years. A comparison of rainfall at Thyspunt WS and Cape St Francis WS for coinciding monitoring periods assist with the validity of assuming equivalence.

Corrosion monitoring was first initiated by Eskom in 1987. This monitoring campaign continued from August 1987 to August 1989 and was done at four sites, namely Brakkeduine (August 1987 to August 1989), De Hoek (August 1987 to August 1989); Klippepunt (August 1987 to November 1988) and the site (August 1987 to August 1989). Subsequent corrosion monitoring at the site included three periods from May 2008 to January 2009, October 2012 to September 2013, and October 2017 to March 2019 (Burger, 2022). The total monitoring time includes the period May 2008 to January 2009, October 2012 to September 2013 and October 2017 to March 2019, i.e. a total of 36 months.

As per ISO 9225 Sulfation Plate Method (International Organisation for Standardisation, 2012c), average gas concentrations can be calculated using diffusive sampling devices. As per the ISO 9225 Standard, standardised corrosivity estimation is based on information on levels of the dominating environmental parameters: the temperature-humidity complex, and pollution with SO_2 and airborne chlorides (International Organisation for Standardisation, 2012c). According to the ISO 9225 Standard, the period of measurement is preferably one year in order to cover seasonal variations of relative humidity, temperature and pollution concentrations, and because the classification system is based on yearly average values (International Organisation for Standardisation, 2012c). Since the completed monitoring periods include four years and six months continuous monitoring (October 2017 to April 2022), as well as a full year from April 2008 to April 2009, and an eleven-month period from October 2012 to September 2013, the monitoring campaigns are considered adequate to conclude corrosion rates with current conditions. As per the International Standard, annual corrosion rates based on these measurements may be used to project up to 20 years (International Organisation for Standardisation, 2012b). The International Standard also indicate that for some engineering applications, more general guiding corrosion values defined in intervals of average corrosion rates for corrosivity categories may be used. Average corrosion rates of up to 10 years are considered to correspond to the initial period of exposure. Average corrosion rates for periods longer than 10 years are considered steady-state corrosion rates, but that the uncertainty level for guiding

© Eskom 2026/Rev 0c

PRINTED VERSIONS OF THIS DOCUMENT ARE NOT CONTROLLED

corrosion values defined as averages for initial and steady-state periods is high. Changes in the affecting parameters, namely relative humidity, temperature and pollution concentrations, may affect the corrosion rate. This could be as a result of natural variations in the climate, projected climate change and/or the increase or decrease in air pollution levels. Although these parameters are not expected to vary significantly over the near future, continued corrosion monitoring should identify changes in the rates.

5.8.6 Meteorological Parameters

The following meteorological parameters were identified for onsite monitoring and inclusion in this SSR:

- wind speed and direction;
- ambient dry-bulb air temperature[24] at two vertical levels and temperature difference between two vertical levels;
- precipitation;
- relative humidity;
- ambient pressure;
- solar radiation;
- atmospheric stability[25] (derived temperature gradient and from the standard deviation of horizontal wind direction, or ‘sigma theta’, wind speed and solar radiation);
- evapotranspiration rate [26] (derived from the ambient air temperature, wind speed, solar radiation and relative humidity);
- corrosivity[27].

[24] The dry-bulb temperature is the temperature of air measured by a thermometer freely exposed to the air but shielded from radiation from the sun. "Dry-bulb" is included because the air temperature is indicated by a thermometer not affected by the moisture of the air. The dry-bulb temperature is the temperature that is usually thought of as “air temperature”, and it is the true thermodynamic temperature. Whereas a normal, dry-bulb thermometer measures the temperature of ambient air, the wet-bulb temperature is the temperature of a surface from which water has evaporated into a stream of ambient air. It is the lowest temperature to which an object can be cooled solely by the evaporation of water.

[25] Atmospheric stability refers to the ability of the atmosphere to be turbulent. The effect of atmospheric stability is noted by wind gustiness and the dispersion of smoke. Stability is a characteristic of how the atmospheric layer above the earth’s surface reacts to small disturbances. If the disturbance is damped, the system is said to be stable; the air becomes, or is, laminar (non-turbulent, smooth, non-stormy). If the disturbance causes an amplifying response (irregular motions or regular oscillations, i.e. turbulent), the system is unstable. Neutral air has no tendency to change (disturbances neither amplify nor dampen).

[26] Evapotranspiration is the process by which water is transferred from the land to the atmosphere by evaporation from the soil and other surfaces and by transpiration from plants.

[27] Corrosivity of the atmosphere is the ability of the atmosphere to cause corrosion in a given corrosion system.

© Eskom 2026/Rev 0c

PRINTED VERSIONS OF THIS DOCUMENT ARE NOT CONTROLLED

Also, details of the following regional meteorological parameters have been obtained from the SAWS:

- hail;
- frost;
- fog;
- lightning;
- tornadoes;
- extreme weather (wind speed, rainfall and temperature);
- snow, avalanches, ice, ice cover and blizzards;
- thunder.

In addition, and in line with the international recommendations (International Atomic Energy Agency, 2011) the severe and rare phenomena at the proposed site were identified using historical records compiled by the SAWS, and include:

- lightning;
- extreme winds;
- tornado/tropical cyclones;
- extreme meteorological variability.

5.8.6.1 Site Meteorological Parameters

This section addresses the measurement and evaluation of the site meteorological characteristics, augmented where necessary due to limited data recordings by observations made at SAWS stations, which involve slightly longer monitoring periods.

5.8.6.1.1 Wind Speed and Direction

The atmospheric dispersion of air emissions from the site is largely a function of the wind speed and direction. The wind speed influences both the distance of downward transport and the rate of dilution. The generation of mechanical turbulence is similarly a function of the wind speed, and the wind direction determines the advection[28] path.

[28] Advection is the process of transport of an atmospheric property solely by the mass motion (velocity field) of the atmosphere. It also includes the rate of change of the value of the advected property at a given point.

© Eskom 2026/Rev 0c

PRINTED VERSIONS OF THIS DOCUMENT ARE NOT CONTROLLED

(a) Prevailing Wind Patterns

Summary reports of historical meteorological data for the period 1987 to 1989 at De Hoek, Thyspunt/Tony's Bay, Klippepunt, and Brakkeduine (as shown in ***Figure 5.8.1***) were published by Eskom (Cadman & Peerce, 1987; Peerce, 1988a; Peerce, 1988b; Tosen, et al., 1987a; Tosen, et al., 1987b). The most dominant wind direction observed during the 1987 monitoring period was from the west-northwest to northwest at all monitoring locations. More frequent stronger winds were concurrently also recorded from these wind directions. The locations towards the west of site, i.e. Brakkeduine and Klippepunt, were characterised by winds of more northerly direction than at Thyspunt and De Hoek. The Thyspunt monitoring location was at 15 m amsl and close to the shoreline (250 m) which may explain the increased frequency of southwesterly wind directions that was observed during the 1988 campaign, specifically June 1988 and August 1988. Significant frequency of west-southwesterly winds was also observed at this location during the 1989 period. A very low frequency (less than 2 per cent) of calm wind conditions occurred at these locations. Mild wind speeds occurred from the northeast, albeit infrequent. The wind speed tended to increase to mid-afternoon as the instability is highest at around 14h00.

The offshore flow, i.e. northerly winds, are characterised by low wind speeds (less than 3 m/s) indicating the occurrence of land breezes. Off-shore wind flows occurred about 30 per cent of the time at all the meteorological locations. The occurrence of onshore flow, i.e. southerly winds, is negligible at all locations.

The more recent wind speed and direction observations that were made for the periods 2008-2013 (***Figure 5.8.3***) and 2017-2019 (***Figure 5.8.4***) at both the SAWS weather station at Cape St. Francis (SAWS, 2024a) and the onsite Thyspunt WS (Eskom, 2023a) clearly illustrate the dominance of westerly and easterly wind directions in the wind roses. The east-west bimodal wind direction is more pronounced at the Cape St. Francis WS, than at the Thyspunt WS. Furthermore, the maximum wind speed at the Cape St. Francis WS is slightly higher than at the Thyspunt WS, i.e. 23.2 m/s versus 19.6 m/s for the 2008-2013 period, and 20.6 m/s versus 16.6 m/s for the 2008-2013 period. This is most likely due to the location of the Cape St. Francis WS which observes conditions more closely to those prevailing over the ocean compared to the Thyspunt WS that is further inland and therefore observes prevailing conditions more closely to the centroid.

© Eskom 2026/Rev 0c

PRINTED VERSIONS OF THIS DOCUMENT ARE NOT CONTROLLED

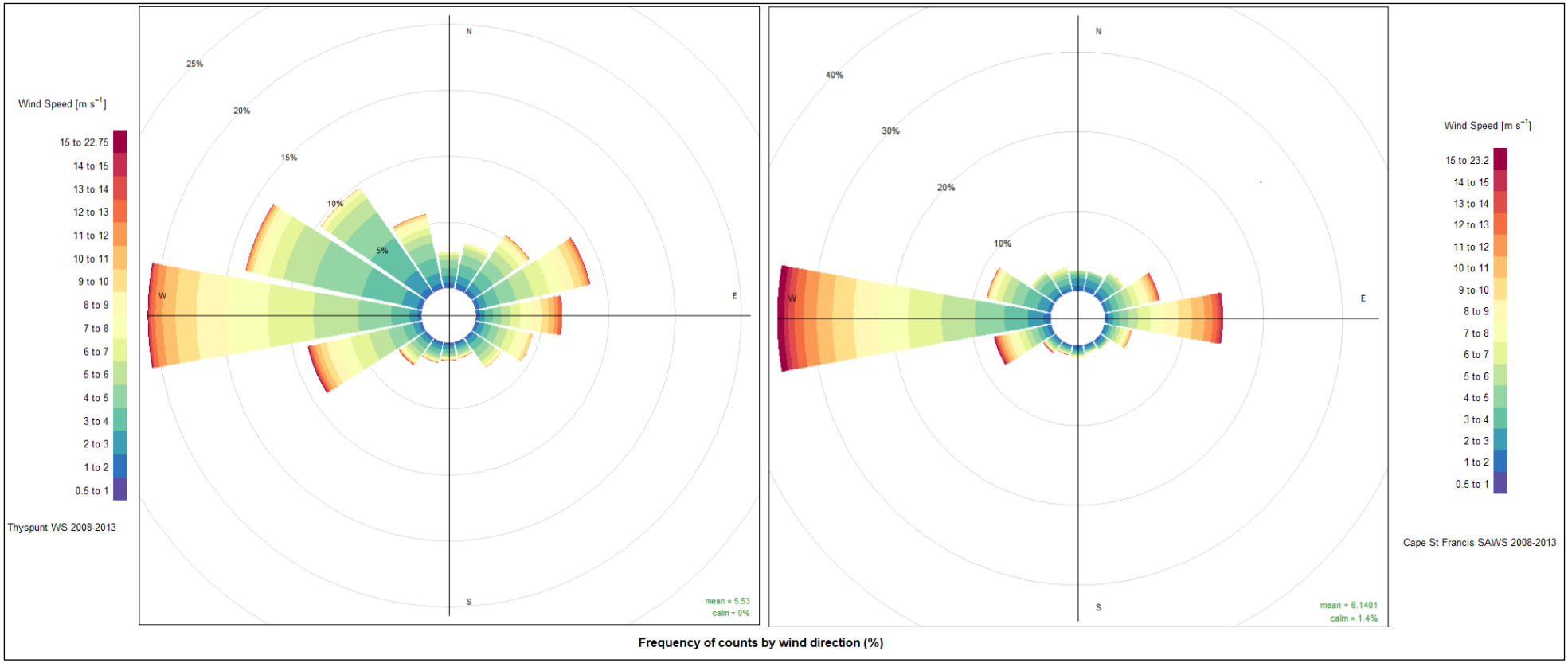


Figure 5.8.3
Comparison of SAWS Cape St. Francis WS and Thyspunt WS for 2008-2013 data period

© Eskom 2026/Rev 0c

PRINTED VERSIONS OF THIS DOCUMENT ARE NOT CONTROLLED

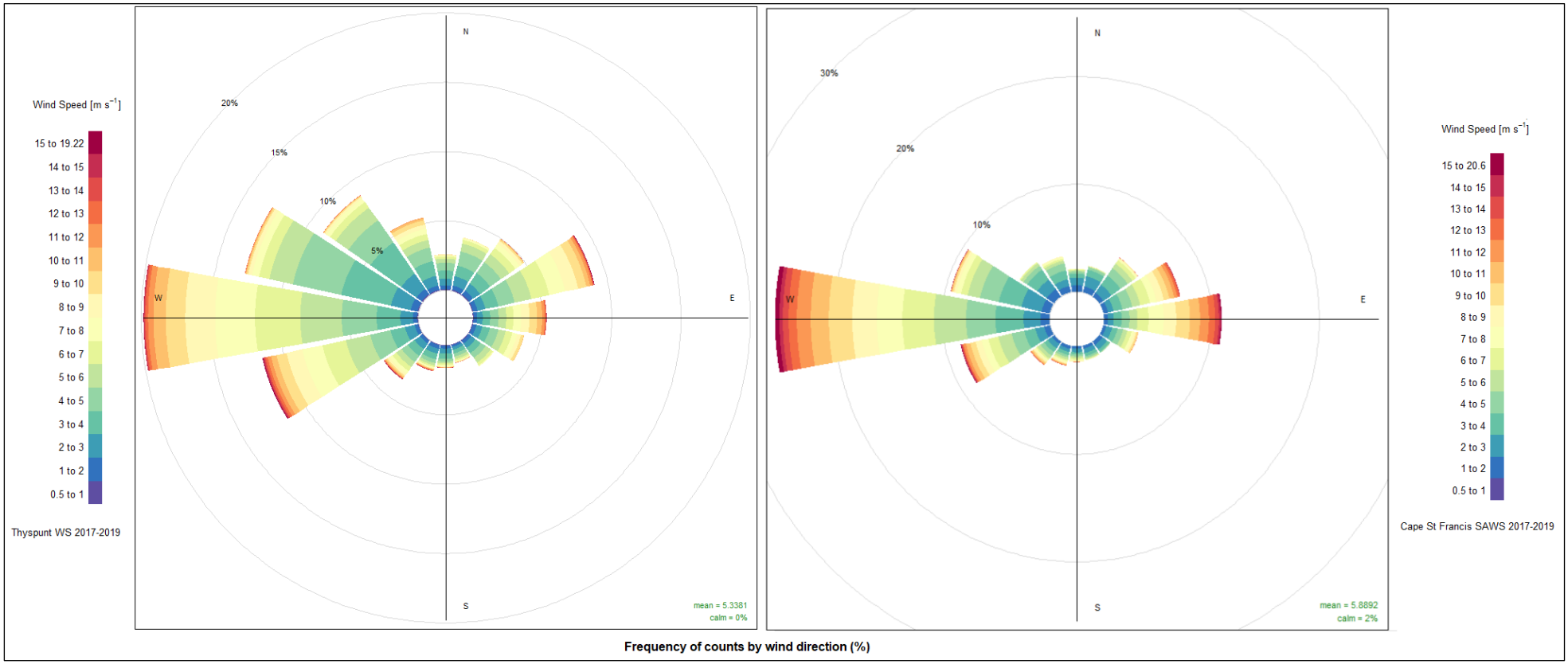


Figure 5.8.4
Comparison of SAWS Cape St. Francis WS and Thyspunt WS for 2017-2019 data period

© Eskom 2026/Rev 0c

PRINTED VERSIONS OF THIS DOCUMENT ARE NOT CONTROLLED

The difference was even more noticeable during the night-time hours as shown in ***Figure 5.8.5*** for the 2008-2013 period, and ***Figure 5.8.6*** for the 2017-2019 period. The prevailing night-time wind direction at the Thyspunt WS during the 2008-2013 period was from the west-northwest, rather than westerly winds observed at the Cape St. Francis WS for the same period. Although the 2017-2019 period also observed frequent west-northwest at the Thyspunt WS, westerly winds were slightly more dominant. The frequency of the easterly night-time wind direction at the Thyspunt WS for both periods was also less pronounced with more east-northeasterly winds reported. Easterly winds were however more frequent than the east-northeasterly winds at the Cape St. Francis WS.

Compared with the Thyspunt WS, the Cape St. Francis WS data observed lower prevalence of land-sea breeze circulation flows, i.e. winds between the northern and southern sectors. As the air over land cools down during the night, it is expected that a sea breeze that may have been present during the day would disappear and result in the development of an onshore land breeze. However, the observations at both Cape St. Francis and the Thyspunt WS indicate increased offshore flows at night, with less evidence of onshore winds.

The wind speeds at both the Cape St. Francis WS and Thyspunt WS tended to increase towards mid-afternoon as the instability is highest at around 14h00 to 15h00 (***Table 5.8.3***).

The observation at the Cape St. Francis WS for the period 2004 to 2023 indicate annual average wind speeds varying between 5.5 m/s (2018) and 6.4 m/s (2019) with an average of 6.0 m/s, with most of these occurring from the west (32,40 per cent), followed by easterly winds (13.93 per cent) (***Table 5.8.4***). The highest hourly average wind speed was 23.2 m/s from the west (***Table 5.8.6***).

© Eskom 2026/Rev 0c

PRINTED VERSIONS OF THIS DOCUMENT ARE NOT CONTROLLED

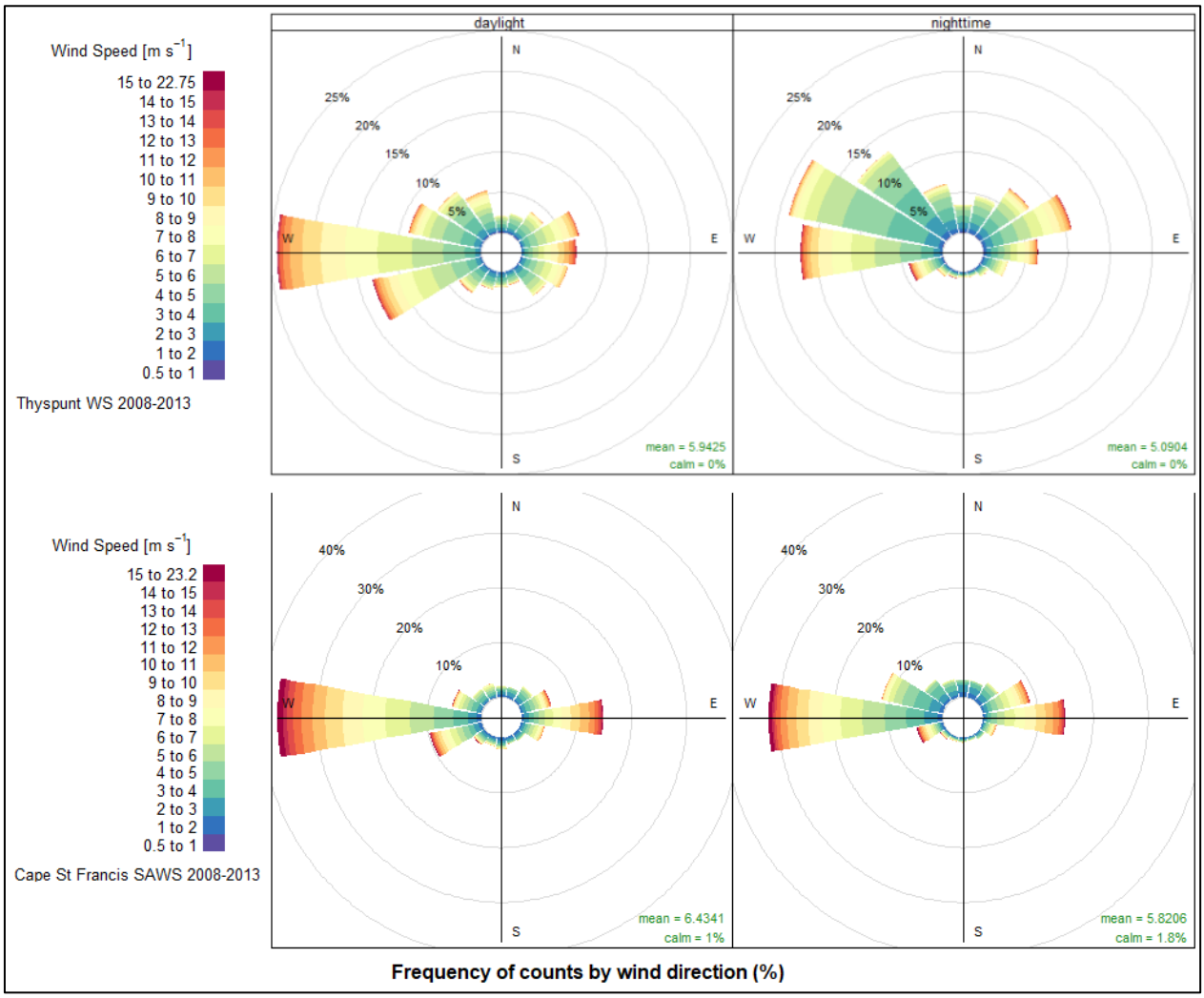


Figure 5.8.5
Comparison of Cape St. Francis WS and Thyspunt WS Day- and Night-time Wind Roses (2008 to 2013)

© Eskom 2026/Rev 0c

PRINTED VERSIONS OF THIS DOCUMENT ARE NOT CONTROLLED

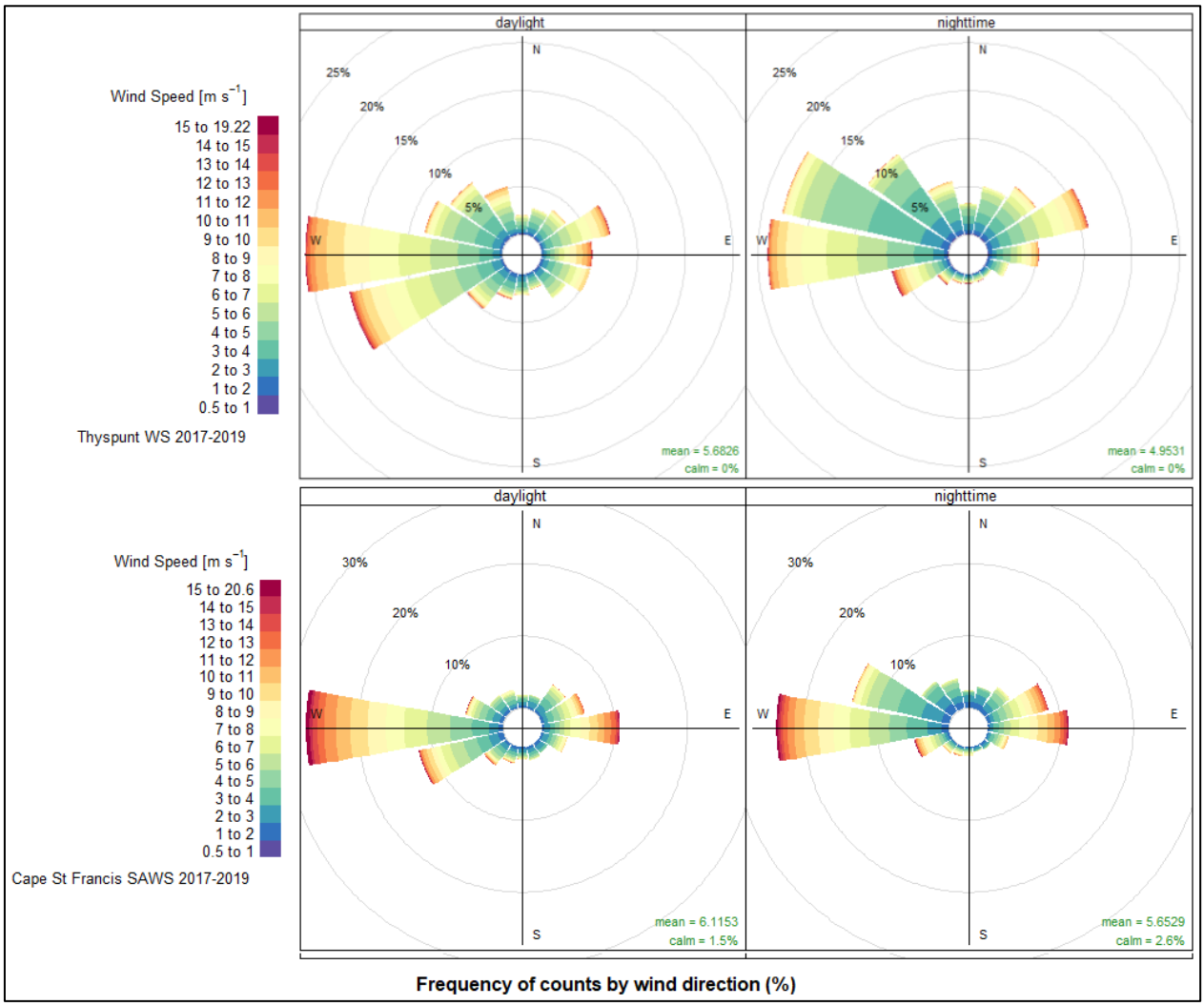


Figure 5.8.6
Comparison Cape St. Francis WS and Thyspunt WS Day- and Night-time Wind Roses (2017 to 2019)

© Eskom 2026/Rev 0c

PRINTED VERSIONS OF THIS DOCUMENT ARE NOT CONTROLLED

Table 5.8.3
Wind Speed [m/s] as Function of Time of Day at the Cape St. Francis WS and Thyspunt WS

Hour of Day	Cape St. Francis WS (2004-2023)		Thyspunt WS (2008-2013 & 2017-2019)	
	Average	95th Percentile	Average	95th Percentile
01h00	5.5	11.5	4.9	8.9
02h00	5.5	11.4	4.8	8.9
03h00	5.5	11.5	4.9	8.9
04h00	5.4	11.5	4.9	9.0
05h00	5.4	11.6	4.9	9.0
06h00	5.4	11.6	4.9	9.1
07h00	5.4	11.4	4.9	9.2
08h00	5.5	11.7	5.0	9.2
09h00	5.6	11.6	5.2	9.4
10h00	5.8	12.0	5.4	9.8
11h00	6.0	12.2	5.7	10.1
12h00	6.3	12.4	6.0	10.3
13h00	6.5	12.6	6.3	10.6
14h00	6.7	12.7	6.5	10.8
15h00	6.8	12.8	6.5	10.9
16h00	6.8	12.7	6.4	10.9
17h00	6.7	12.7	6.2	11.0
18h00	6.6	12.6	5.9	10.8
19h00	6.4	12.5	5.6	10.3
20h00	6.2	12.3	5.3	10.1
21h00	6.0	12.2	5.2	9.9
22h00	5.9	12.0	5.1	9.6
23h00	5.7	11.8	5.0	9.4
24h00	5.6	11.6	4.9	9.2

The observation at the Thyspunt WS for the 2008 to 2013 and 2017 to 2019 periods indicate annual average wind speeds varying between 5.08 m/s (2019) and 5.64 m/s (2017) with an average of 5.44±0.1 m/s, with most of these occurring from the west (20.75 per cent), followed by west-northwesterly winds (13.76 per cent) and then east-northeasterly winds (9.56 per cent) (***Table 5.8.5***). The highest hourly average wind speed was 19.6 m/s which occurred from the south-southeast (***Table 5.8.7***).

As discussed earlier, the Eskom reports (Cadman & Peerce, 1987; Peerce, 1988a; Peerce, 1988b; Tosen, et al., 1987a; Tosen, et al., 1987b) indicate

© Eskom 2026/Rev 0c

PRINTED VERSIONS OF THIS DOCUMENT ARE NOT CONTROLLED

very few calm wind conditions, as recorded at both Cape St. Francis and at the Thyspunt WS. It should be noted that the threshold minimum wind speed of the anemometer at the Thyspunt WS is 0.4 m/s, whereas the same threshold at the Cape St. Francis WS is 1.0 m/s. The Cape St. Francis WS experienced 1.65 per cent calm wind conditions, i.e. wind speeds below 1.0 m/s (***Table 5.8.4***) and the Thyspunt WS experienced 0.37 per cent calm wind conditions, i.e. wind speeds below 0.4 m/s (***Table 5.8.5***).

The following seasonal frequencies of calm wind conditions were experienced (autumn, winter, spring, summer):

- Cape St. Francis WS (less than 1.0 m/s) – 3.9 per cent, 2.7 per cent, 2.9 per cent and 3.2 per cent;
- Thyspunt WS (less than 0.4 m/s) – 0.2 per cent, 0.1 per cent, 0.7 per cent and 0.2 per cent.

As shown in ***Table 5.8.6*** the highest hourly average wind, averaged per sector, at the Cape St. Francis WS occurred from the east with a wind speed of 7.6 m/s, followed by winds from the west with an average wind speed of 7.1 m/s. Northerly winds have the lowest average wind speed of 1.8 m/s. The highest wind speeds measured in each cardinal wind direction is also presented in ***Table 5.8.6***. The top hourly maximum wind speed per sector occurred from the west with a maximum hourly wind speed of 23.2 m/s followed by a west-southwest wind with an hourly maximum wind speed of 22.8 m/s.

Similarly, as shown in ***Table 5.8.7***, the highest hourly average wind, averaged per sector, at the Thyspunt WS occurred from the west and east with a wind speed of 6.7 m/s and 6.6 m/s respectively. Southerly winds have the lowest average wind speed of 3.8 m/s. The highest hourly maximum wind occurred from the south-southeastern sector with maximum wind speed of 19.6 m/s followed by the southern sector with maximum wind speed of 18.3 m/s (***Table 5.8.7***).

The persistence (continuous duration) of hourly average winds above 10 m/s, 12 m/s, 14 m/s and 16 m/s at the Cape St. Francis WS and Thyspunt WS are summarised in ***Table 5.8.8***. The longest duration of 10 m/s (and higher) wind speeds at the Cape St. Francis WS was 57 consecutive hours, 12 m/s (and higher) was for 45 hours, 14 m/s (and higher) was for 38 hours, and 16 m/s (and higher) was 20 hours. The corresponding longest durations at the Thyspunt WS were less, with 41 consecutive hours for a minimum wind speed of 10 m/s, 20 hours for 12 m/s (and higher), 18 hours for 14 m/s (and higher) and 5 hours for 16 m/s (and higher).

© Eskom 2026/Rev 0c

PRINTED VERSIONS OF THIS DOCUMENT ARE NOT CONTROLLED

Table 5.8.4
Wind Speed and Direction Categorisation at the Cape St. Francis WS (June 2004 to December 2023)

Wind Direction	Wind Speed [m/s] at 10 m level												Total (%)
	<0.5	0.5-1.0	1.0-2.0	2.0-3.0	3.0-4.0	4.0-5.0	5.0-6.0	6.0-8.0	8.0-10.0	10.0-13.0	13.0-18.0	>18.0	
N	1.65%	0.00%	0.60%	0.91%	0.50%	0.26%	0.16%	0.09%	0.01%	0.00%	0.00%	0.00%	4.16%
NNE	0.00%	0.00%	0.56%	0.91%	0.68%	0.27%	0.08%	0.04%	0.00%	0.00%	0.00%	0.00%	2.56%
NE	0.00%	0.00%	0.41%	0.83%	0.90%	0.75%	0.42%	0.39%	0.12%	0.03%	0.00%	0.00%	3.85%
ENE	0.00%	0.00%	0.29%	0.64%	0.85%	0.88%	0.87%	1.73%	1.24%	0.88%	0.17%	0.00%	7.56%
E	0.00%	0.00%	0.36%	0.75%	0.88%	1.06%	1.26%	3.21%	3.08%	2.73%	0.60%	0.00%	13.93%
ESE	0.00%	0.00%	0.26%	0.45%	0.48%	0.47%	0.51%	0.75%	0.33%	0.12%	0.00%	0.00%	3.38%
SE	0.00%	0.00%	0.32%	0.47%	0.30%	0.17%	0.09%	0.08%	0.04%	0.00%	0.00%	0.00%	1.47%
SSE	0.00%	0.00%	0.22%	0.33%	0.26%	0.17%	0.11%	0.13%	0.03%	0.01%	0.00%	0.00%	1.27%
S	0.00%	0.00%	0.27%	0.41%	0.31%	0.25%	0.18%	0.27%	0.12%	0.05%	0.01%	0.00%	1.87%
SSW	0.00%	0.00%	0.21%	0.29%	0.29%	0.22%	0.20%	0.27%	0.16%	0.10%	0.02%	0.00%	1.76%
SW	0.00%	0.00%	0.23%	0.39%	0.39%	0.40%	0.35%	0.45%	0.30%	0.26%	0.10%	0.01%	2.87%
WSW	0.00%	0.00%	0.42%	0.68%	0.82%	1.00%	1.07%	1.95%	1.50%	1.21%	0.45%	0.02%	9.12%
W	0.00%	0.00%	0.83%	1.96%	2.95%	3.69%	4.01%	7.32%	5.35%	4.50%	1.71%	0.09%	32.40%
WNW	0.00%	0.00%	0.43%	1.26%	1.82%	1.49%	1.03%	1.04%	0.37%	0.14%	0.03%	0.00%	7.61%
NW	0.00%	0.00%	0.39%	0.75%	1.18%	0.66%	0.26%	0.22%	0.02%	0.00%	0.00%	0.00%	3.49%
NNW	0.00%	0.00%	0.34%	0.52%	0.65%	0.47%	0.28%	0.38%	0.06%	0.01%	0.00%	0.00%	2.71%
TOTAL	1.65%	0.00%	6.13%	11.56%	13.27%	12.21%	10.86%	18.32%	12.73%	10.04%	3.11%	0.12%	100.00%

© Eskom 2026/Rev 0c

PRINTED VERSIONS OF THIS DOCUMENT ARE NOT CONTROLLED

Table 5.8.5
Wind Speed and Direction Categorisation at the Thyspunt WS (January 2008 to October 2013 and June 2017 to September 2019)

Wind Direction	Wind Speed [m/s] at 9 m level												Total (%)
	<0.5	0.5-1.0	1.0-2.0	2.0-3.0	3.0-4.0	4.0-5.0	5.0-6.0	6.0-8.0	8.0-10.0	10.0-13.0	13.0-18.0	>18.0	
N	0.02%	0.05%	0.32%	0.53%	0.66%	0.61%	0.34%	0.21%	0.04%	0.00%	0.00%	0.00%	2.79%
NNE	0.02%	0.06%	0.31%	0.61%	0.85%	0.85%	0.50%	0.32%	0.04%	0.00%	0.00%	0.00%	3.57%
NE	0.03%	0.07%	0.34%	0.64%	1.07%	1.11%	0.77%	0.92%	0.37%	0.09%	0.01%	0.00%	5.45%
ENE	0.03%	0.07%	0.31%	0.59%	0.99%	1.37%	1.44%	2.53%	1.57%	0.59%	0.07%	0.00%	9.56%
E	0.03%	0.05%	0.24%	0.37%	0.59%	0.66%	0.63%	1.45%	1.30%	0.80%	0.08%	0.00%	6.21%
ESE	0.02%	0.04%	0.21%	0.39%	0.50%	0.59%	0.67%	1.15%	0.54%	0.03%	0.00%	0.00%	4.14%
SE	0.02%	0.04%	0.19%	0.36%	0.48%	0.53%	0.41%	0.36%	0.05%	0.02%	0.00%	0.00%	2.47%
SSE	0.02%	0.04%	0.17%	0.23%	0.25%	0.24%	0.15%	0.15%	0.05%	0.03%	0.01%	0.00%	1.33%
S	0.02%	0.04%	0.16%	0.32%	0.33%	0.19%	0.11%	0.16%	0.07%	0.03%	0.01%	0.00%	1.44%
SSW	0.01%	0.05%	0.22%	0.33%	0.39%	0.22%	0.18%	0.16%	0.08%	0.04%	0.02%	0.00%	1.70%
SW	0.01%	0.04%	0.18%	0.41%	0.50%	0.50%	0.41%	0.45%	0.21%	0.12%	0.03%	0.00%	2.86%
WSW	0.02%	0.05%	0.24%	0.48%	0.87%	1.25%	1.66%	2.76%	1.46%	0.72%	0.17%	0.00%	9.69%
W	0.02%	0.04%	0.31%	0.79%	1.57%	2.46%	3.34%	6.59%	3.76%	1.65%	0.22%	0.00%	20.75%
WNW	0.04%	0.06%	0.37%	1.34%	3.48%	4.01%	2.16%	1.64%	0.47%	0.18%	0.02%	0.00%	13.76%
NW	0.03%	0.08%	0.44%	1.29%	2.85%	2.12%	1.18%	0.73%	0.15%	0.03%	0.00%	0.00%	8.90%
NNW	0.02%	0.07%	0.32%	0.71%	1.12%	1.02%	0.61%	0.88%	0.51%	0.12%	0.00%	0.00%	5.38%
TOTAL	0.37%	0.85%	4.33%	9.39%	16.51%	17.73%	14.56%	20.49%	10.67%	4.45%	0.64%	0.01%	100.00%

© Eskom 2026/Rev 0c

PRINTED VERSIONS OF THIS DOCUMENT ARE NOT CONTROLLED

Table 5.8.6
Average and Maximum Hourly Wind Speed per Direction at the Cape St. Francis WS (June 2004 to December 2023)

Sector-Averaged Hourly Wind Speed		Sector Maximum Hourly Wind Speed	
Wind Direction	**Wind Speed [m/s]**	**Wind Direction**	**Wind Speed (m/s)**
E	7.6	**W**	23.2
W	7.1	**WSW**	22.8
WSW	6.9	**E**	20.2
ENE	6.5	**SW**	20.0
SW	5.8	**SSW**	19.5
ESE	5.2	**S**	18.5
SSW	5.0	**WNW**	18.3
WNW	4.5	**ENE**	17.7
S	4.4	**SSE**	16.7
NE	4.0	**SE**	16.1
NNW	4.0	**NE**	14.9
SSE	3.7	**ESE**	14.4
NW	3.6	**NNW**	11.8
SE	3.3	**NW**	9.5
NNE	2.9	**NNE**	9.3
N	1.8	**N**	9.0

© Eskom 2026/Rev 0c

PRINTED VERSIONS OF THIS DOCUMENT ARE NOT CONTROLLED

Table 5.8.7
Average and Maximum Hourly Wind Speed per Direction at the Thyspunt WS (January 2008 to October 2013 and June 2017 to September 2019)

Sector-Averaged Hourly Wind Speed		Sector Maximum Hourly Wind Speed	
Wind Direction	**Wind Speed [m/s]**	**Wind Direction**	**Wind Speed (m/s)**
W	6.7	**SSE**	19.6
E	6.6	**S**	18.3
WSW	6.4	**SW**	18.2
ENE	6.1	**ENE**	17.9
ESE	5.4	**W**	17.9
NNW	5.0	**NE**	17.8
NE	4.8	**WSW**	17.6
SW	4.7	**E**	17.6
WNW	4.6	**SSW**	16.6
N	4.3	**WNW**	14.8
NNE	4.2	**NW**	13.8
NW	4.1	**SE**	12.2
SE	4.1	**NNW**	12.2
SSW	4.1	**ESE**	12.1
SSE	3.9	**N**	10.7
S	3.8	**NNE**	9.9

© Eskom 2026/Rev 0c

PRINTED VERSIONS OF THIS DOCUMENT ARE NOT CONTROLLED

Table 5.8.8
Sustained Wind Speeds at the Cape St. Francis and the Thyspunt WS

Month	Hourly Persistence (Continuous Duration)							
	Cape St. Francis WS (2004-2023)				Thyspunt WS (2008 – 2013 & 2017-2019)			
	10 m/s	12 m/s	14 m/s	16 m/s	10 m/s	12 m/s	14 m/s	16 m/s
January	32	19	9	5	14	8	7	2
February	49	38	10	2	13	6	1	0
March	29	16	8	7	11	8	2	0
April	39	35	26	20	28	7	1	0
May	51	27	25	11	24	10	4	0
June	57	45	38	20	41	20	18	4
July	42	30	22	12	33	17	11	5
August	52	40	25	12	31	15	5	0
September	39	22	22	8	21	16	14	3
October	48	27	18	8	21	18	6	3
November	48	24	12	2	17	10	3	0
December	36	31	10	3	18	6	3	0

Seasonal wind roses based on the wind data measured at the Cape St. Francis WS and the Thyspunt WS for the observational periods of January 2008 to October 2013 and June 2017 to September 2019 are compared in ***Figure 5.8.7*** and ***Figure 5.8.8***. The wind roses per season for the monitoring periods and two locations are similar. Spring and summer wind patterns are similar for both locations. An increased frequency of strong westerly winds was observed during spring and winter (***Tables 5.8.9*** and ***5.8.10***). Winter also had a significant increased frequency of west-northwest, northwest and north-northwest winds (***Tables 5.8.9*** and ***5.8.10***).

Overall, the most common summer winds were from the west with 20.28 per cent at Thyspunt WS (***Table 5.8.9***) and 30.67 per cent at Cape St. Francis (***Table 5.8.10***). The second most frequent winds during summer were from the east-northeast with 13.01 per cent at Thyspunt WS (***Table 5.8.9***) and from the east with 22.11 per cent at Cape St. Francis (***Table 5.8.10***).

Winter winds were also mostly prevalent from the west with 19.34 per cent at Thyspunt WS (***Table 5.8.9***) and 31.52 per cent at Cape St. Francis (***Table 5.8.10***). The second most frequent winds during winter were from the west-northwest with 16.61 per cent at Thyspunt WS (***Table 5.8.9***) and 12.33 per cent at Cape St. Francis (***Table 5.8.10***).

© Eskom 2026/Rev 0c

PRINTED VERSIONS OF THIS DOCUMENT ARE NOT CONTROLLED

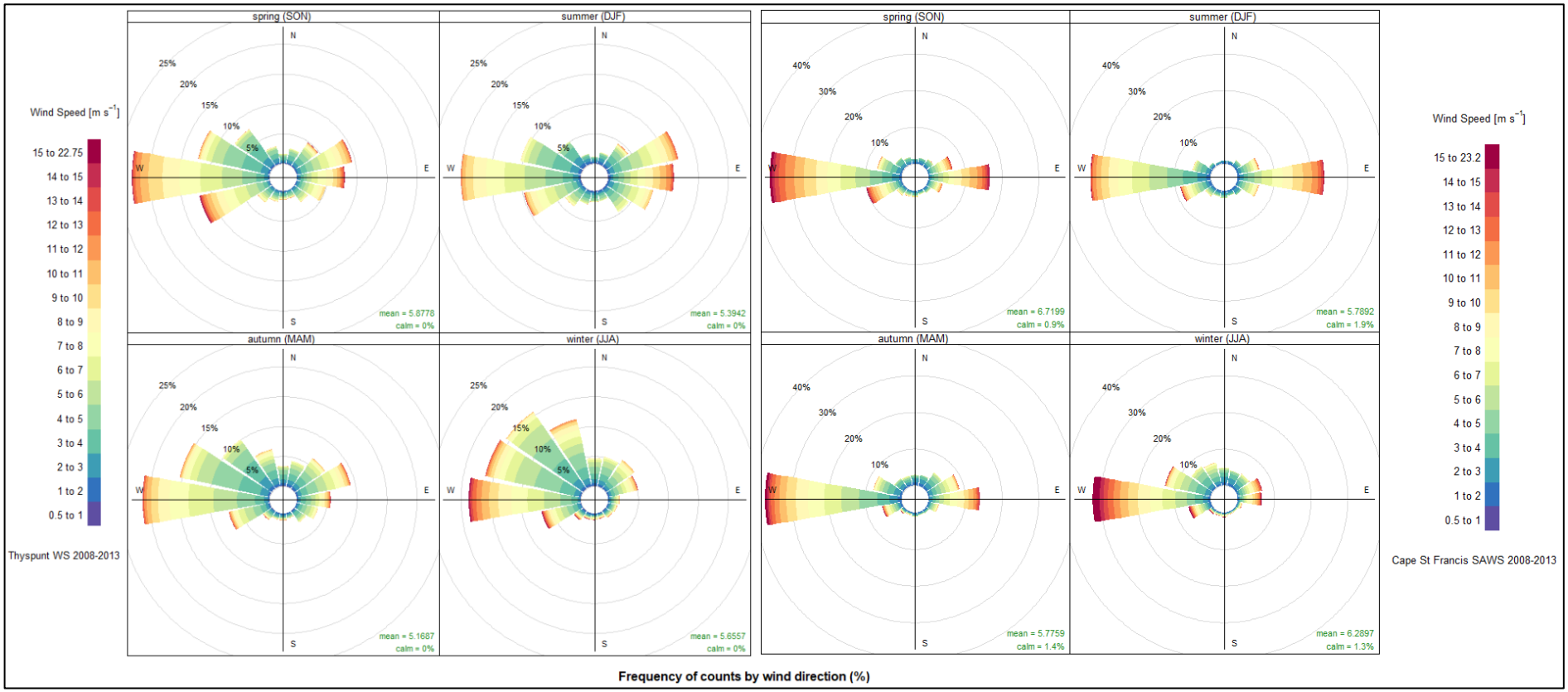


Figure 5.8.7
Comparison of Seasonal Wind Roses for Cape St. Francis WS and Thyspunt WS (2008 to 2013)

© Eskom 2026/Rev 0c

PRINTED VERSIONS OF THIS DOCUMENT ARE NOT CONTROLLED

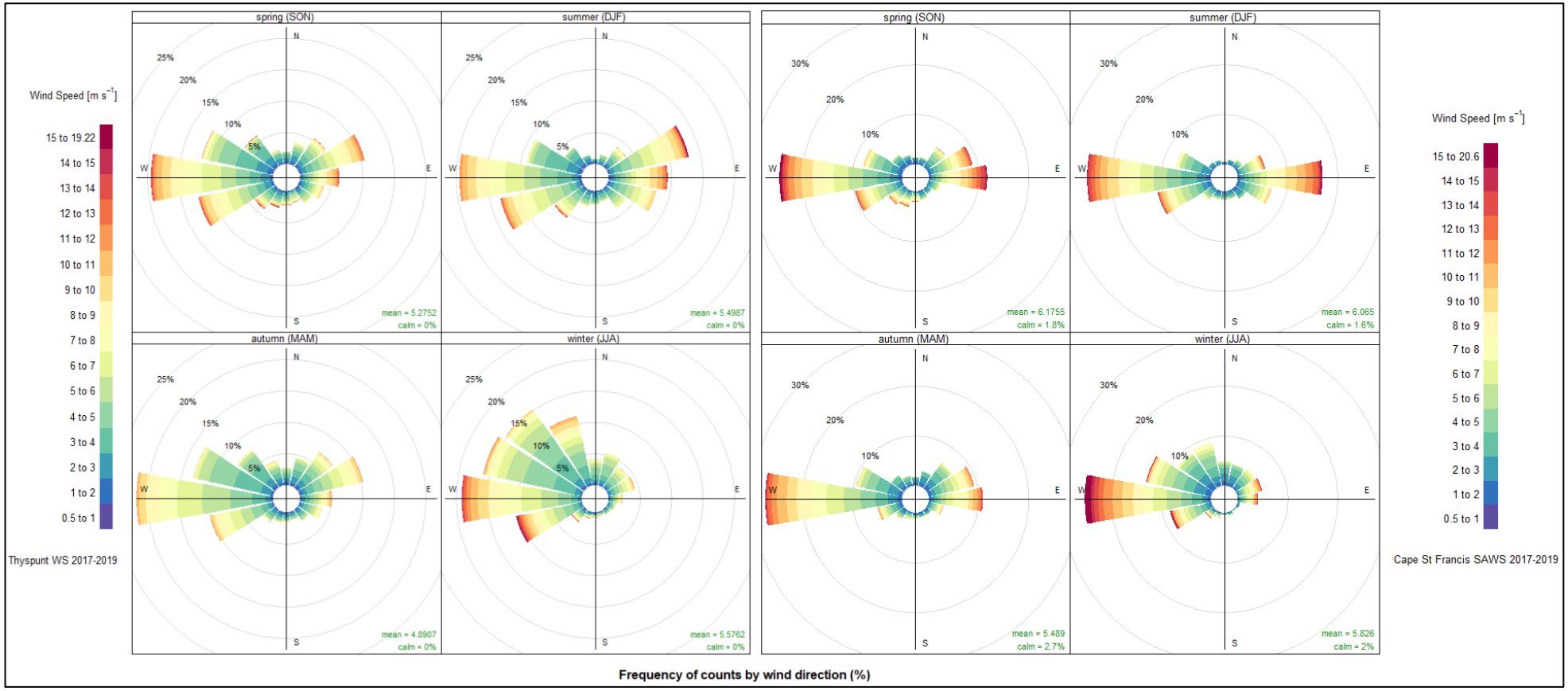


Figure 5.8.8
Comparison of Seasonal Wind Roses for Cape St. Francis WS and Thyspunt WS (2017 to 2019)

© Eskom 2026/Rev 0c

PRINTED VERSIONS OF THIS DOCUMENT ARE NOT CONTROLLED

Spring winds were also mostly prevalent from the west with 21.85 per cent at Thyspunt WS (***Table 5.8.9***) and 31.58 per cent at Cape St. Francis (***Table 5.8.10***). The second most frequent winds during spring were from the west-southwest with 12.46 per cent at Thyspunt WS (***Table 5.8.9***) and from the east 15.82 per cent at Cape St. Francis (***Table 5.8.10***).

Autumn winds were also mostly prevalent from the west with 21.67 per cent at Thyspunt WS (***Table 5.8.9***) and 35.87 per cent at Cape St. Francis (***Table 5.8.10***). The second most frequent winds during autumn were from the west-northwest with 15.23 per cent at Thyspunt WS (***Table 5.8.9***) and from the east 12.37 per cent at Cape St. Francis (***Table 5.8.10***).

Table 5.8.9
Seasonal Wind Direction Occurrence at the Thyspunt WS (January 2008 to October 2013 and June 2017 to September 2019)

Wind Direction	Frequency of Occurrence			
	Spring	Summer	Autumn	Winter
N	1.84%	1.06%	3.29%	4.65%
NNE	2.85%	1.78%	4.46%	4.94%
NE	5.21%	4.32%	6.83%	5.37%
ENE	10.24%	13.01%	10.47%	5.18%
E	7.52%	10.61%	5.34%	2.07%
ESE	4.51%	7.69%	3.46%	1.40%
SE	2.64%	4.27%	2.09%	1.12%
SSE	1.69%	1.66%	1.14%	0.89%
S	1.72%	1.92%	1.30%	0.92%
SSW	2.22%	2.35%	1.25%	1.10%
SW	3.45%	4.21%	1.92%	2.03%
WSW	12.46%	10.76%	7.70%	8.14%
W	21.85%	20.28%	21.67%	19.34%
WNW	12.44%	10.21%	15.23%	16.61%
NW	6.66%	4.30%	8.48%	15.19%
NNW	2.70%	1.57%	5.36%	11.06%
TOTAL	100%	100%	100%	100%

Monthly average and maximum wind speeds observed at the Cape St. Francis WS and at the Thyspunt WS are provided in ***Table 5.8.11*** and ***Table 5.8.12***, and ***Table 5.8.13*** and ***Table 5.8.14***, respectively. A summary of the highest hourly average and wind gusts recorded at the Cape St. Francis WS for the 2004 to 2023 period is provided in ***Table 5.8.15*** (SAWS, 2024a). The highest gust recorded at the Thyspunt WS was 37.9 m/s, which

© Eskom 2026/Rev 0c

PRINTED VERSIONS OF THIS DOCUMENT ARE NOT CONTROLLED

was recorded on 24 September 2019 at 07h00. The highest gust at the Cape St Francis WS on the same day and hour was 31.6 m/s. The highest gust at the Cape St. Francis WS was significantly higher, i.e. 45.8 m/s recorded on 18 August 2020 at 13h15. Unfortunately, this was outside the monitoring campaign for the Thyspunt WS for a comparison.

Table 5.8.10
Seasonal Wind Direction Occurrence at the Cape St. Francis WS (June 2004 to December 2023)

Wind Direction	Frequency of Occurrence			
	Spring	Summer	Autumn	Winter
N	3.17%	2.48%	4.70%	6.28%
NNE	1.66%	0.94%	3.29%	4.33%
NE	3.18%	2.09%	5.25%	4.88%
ENE	8.33%	6.99%	8.83%	6.11%
E	15.82%	22.11%	12.37%	5.47%
ESE	3.56%	6.14%	2.59%	1.24%
SE	1.68%	2.41%	1.14%	0.63%
SSE	1.52%	1.83%	1.06%	0.69%
S	2.43%	2.39%	1.58%	1.09%
SSW	2.57%	1.88%	1.26%	1.34%
SW	3.69%	3.28%	2.37%	2.15%
WSW	10.84%	10.33%	6.98%	8.28%
W	31.58%	30.67%	35.87%	31.52%
WNW	6.06%	4.73%	7.26%	12.33%
NW	2.41%	1.13%	2.99%	7.40%
NNW	1.48%	0.59%	2.46%	6.26%
TOTAL	100%	100%	100%	100%

Most of the gusts above 20 m/s at the Cape St. Francis WS occurred during westerly winds (51.55 per cent), followed by west-southwesterly (18.97 per cent), west-northwesterly winds (7.93 per cent) and easterly winds (6.72 per cent), as summarised in ***Table 5.8.16***.

Albeit a much shorter period (January 2008 to October 2013 and June 2017 to September 2019), the observations at the Thyspunt WS also indicate most of the gusts above 20 m/s to be westerly winds (50.62 per cent), followed by west-southwesterly (20.71 per cent), easterly winds (8.71 per cent) and west-northwesterly winds (6.49 per cent), as summarised in ***Table 5.8.16***.

© Eskom 2026/Rev 0c

PRINTED VERSIONS OF THIS DOCUMENT ARE NOT CONTROLLED

Table 5.8.11
Average Wind Speed per Month at the Cape St. Francis WS (June 2004 to December 2023)

Wind Direction	Wind Speed [m/s] at 10 m level per Month												Annual
	Jan	Feb	Mar	Apr	May	Jun	Jul	Aug	Sep	Oct	Nov	Dec	
N	0.6	0.6	1.0	1.4	2.1	2.9	2.7	2.4	1.5	1.0	0.9	0.7	1.8
NNE	2.3	2.1	2.4	2.7	2.9	3.3	3.1	3.1	2.9	2.7	2.5	2.5	2.9
NE	3.6	3.6	3.7	3.9	3.9	4.3	4.1	4.4	4.5	4.3	4.0	3.6	4.0
ENE	6.0	5.9	5.9	5.9	6.1	6.9	6.4	7.1	7.5	6.8	7.1	6.0	6.5
E	7.8	7.5	7.4	7.0	7.2	6.6	7.2	7.3	7.8	8.0	8.2	7.5	7.6
ESE	5.4	5.2	5.2	4.8	4.8	4.5	5.2	4.2	4.9	5.2	5.6	5.1	5.2
SE	3.1	2.8	2.9	3.2	4.6	4.5	3.6	3.2	3.3	4.0	3.0	3.1	3.3
SSE	3.5	3.0	3.6	3.9	3.6	3.6	4.2	4.2	4.0	4.1	3.7	3.6	3.7
S	4.0	3.7	4.1	4.3	3.9	5.3	5.3	5.5	4.0	4.9	4.6	3.8	4.4
SSW	3.9	3.5	4.9	5.7	5.7	5.7	6.8	5.1	5.6	4.9	5.1	4.2	5.0
SW	4.7	4.3	5.6	6.1	6.3	7.8	7.4	6.4	5.7	5.1	5.3	6.0	5.8
WSW	6.1	6.0	6.5	6.6	6.5	7.0	6.9	7.8	7.2	7.3	6.9	7.0	6.9
W	6.2	6.2	6.5	7.1	7.1	8.0	8.0	8.2	7.6	7.2	6.8	6.3	7.1
WNW	4.0	4.0	4.0	4.6	4.4	4.9	5.0	5.0	4.5	4.3	4.2	3.9	4.5
NW	2.8	2.7	2.9	3.0	3.5	4.0	4.0	3.8	3.3	3.2	3.1	2.9	3.6
NNW	2.5	2.7	2.8	3.0	4.1	4.7	4.6	4.0	3.2	2.9	2.6	2.5	4.0
Average	5.9	5.7	5.8	5.7	5.5	5.9	6.0	6.3	6.3	6.3	6.2	5.9	6.0

© Eskom 2026/Rev 0c

PRINTED VERSIONS OF THIS DOCUMENT ARE NOT CONTROLLED

Table 5.8.12
Maximum Wind Speed per Month at the Cape St. Francis WS (June 2004 to December 2023)

Wind Direction	Wind Speed [m/s] at 10 m level per Month												Annual
	Jan	Feb	Mar	Apr	May	Jun	Jul	Aug	Sep	Oct	Nov	Dec	
N	4.8	6.2	5.8	7.0	8.8	8.8	9.0	8.3	8.4	5.9	8.6	5.3	9.0
NNE	5.9	6.6	7.4	8.3	7.5	9.1	7.4	8.0	8.2	6.8	7.6	9.3	9.3
NE	10.5	14.0	9.5	10.9	10.5	14.9	11.1	12.9	14.0	10.6	12.2	9.9	14.9
ENE	15.6	14.4	16.2	14.2	15.0	15.7	16.2	15.6	16.4	17.7	15.8	14.3	17.7
E	16.8	16.4	16.3	15.5	14.8	17.4	20.2	15.4	17.2	18.0	16.3	16.5	20.2
ESE	11.3	11.7	11.2	11.1	12.8	14.4	12.6	8.9	12.0	12.1	13.9	12.7	14.4
SE	7.7	8.2	6.6	8.5	16.1	12.6	10.3	12.1	8.5	9.4	8.8	7.5	16.1
SSE	12.4	7.0	9.5	9.0	16.7	7.0	11.2	12.8	12.7	12.5	10.4	10.6	16.7
S	11.2	10.3	10.1	14.1	10.8	14.7	18.5	17.4	12.6	12.4	16.2	14.3	18.5
SSW	11.5	10.9	19.5	13.8	14.8	17.5	18.3	17.7	14.6	18.5	13.4	14.4	19.5
SW	12.1	12.4	19.5	16.1	16.3	19.9	19.3	20.0	14.6	17.7	14.6	16.2	20.0
WSW	18.8	16.4	17.3	17.1	22.8	19.0	19.9	19.5	15.9	18.3	16.2	19.7	22.8
W	16.7	16.6	16.7	18.1	19.5	23.2	21.2	21.1	18.8	19.3	17.5	18.1	23.2
WNW	15.4	10.8	9.7	14.0	12.1	18.3	15.8	15.6	14.9	13.0	10.9	15.9	18.3
NW	5.8	6.3	8.0	8.5	8.2	9.4	9.5	9.4	9.1	8.9	7.6	4.9	9.5
NNW	5.0	9.4	7.5	8.2	10.2	9.8	11.8	8.6	8.2	8.0	4.7	5.5	11.8
Maximum	18.8	16.6	19.5	18.1	22.8	23.2	21.2	21.1	18.8	19.3	17.5	19.7	23.2

© Eskom 2026/Rev 0c

PRINTED VERSIONS OF THIS DOCUMENT ARE NOT CONTROLLED

Table 5.8.13
Average Wind Speed per Month at the Thyspunt WS (January 2008 to October 2013 and June 2017 to September 2019)

Wind Direction	Wind Speed [m/s] at 9 m level per Month												Annual
	Jan	Feb	Mar	Apr	May	Jun	Jul	Aug	Sep	Oct	Nov	Dec	
N	2.4	2.7	3.1	3.8	3.7	4.4	4.2	4.0	3.7	3.1	2.8	2.7	3.8
NNE	2.9	3.2	3.5	4.1	3.9	4.4	4.3	4.2	3.9	3.3	3.5	3.5	3.9
NE	4.3	4.4	4.7	4.7	4.7	5.2	4.9	5.4	4.9	4.6	4.3	3.9	4.7
ENE	6.4	6.6	6.0	5.7	5.5	6.2	5.4	6.2	6.0	6.4	6.7	5.7	6.1
E	7.4	6.9	6.5	5.3	4.7	5.0	5.0	5.7	6.1	6.8	7.9	6.9	6.7
ESE	5.8	5.6	5.4	4.6	4.1	4.2	4.9	4.1	4.4	5.3	6.8	5.6	5.4
SE	4.4	4.3	4.2	3.9	3.5	3.7	5.1	3.8	3.8	4.3	4.6	4.5	4.3
SSE	4.0	3.4	4.1	3.3	3.0	4.8	5.7	5.7	3.8	5.1	4.4	3.3	4.2
S	3.6	3.1	3.8	4.3	4.3	4.4	5.6	4.5	4.4	4.7	4.4	3.3	4.1
SSW	3.8	3.5	4.0	3.7	3.0	4.2	5.7	4.2	4.6	4.9	4.0	3.7	4.1
SW	5.2	4.4	4.5	4.8	3.6	5.4	5.6	5.2	5.1	5.2	4.9	5.0	5.0
WSW	6.4	5.6	6.0	5.6	5.2	6.3	6.3	6.8	7.4	6.1	6.6	6.6	6.4
W	6.1	6.0	6.0	6.4	6.4	7.4	7.0	7.4	7.2	6.6	6.4	6.2	6.6
WNW	3.8	3.9	4.0	4.8	4.6	5.3	5.1	5.0	4.8	4.1	4.1	4.1	4.6
NW	3.1	3.2	3.4	3.8	4.0	4.7	4.7	4.3	4.1	3.5	3.6	3.3	4.1
NNW	2.8	3.0	3.3	4.4	4.9	5.6	5.6	4.9	4.0	3.2	2.7	2.5	4.8
Average	5.5	5.2	5.2	5.1	4.9	5.6	5.5	5.6	5.7	5.4	5.8	5.4	5.4

© Eskom 2026/Rev 0c

PRINTED VERSIONS OF THIS DOCUMENT ARE NOT CONTROLLED

Table 5.8.14
Maximum Wind Speed per Month at the Thyspunt WS (January 2008 to October 2013 and June 2017 to September 2019)

Wind Direction	Wind Speed [m/s] at 9 m level per Month												Annual
	Jan	Feb	Mar	Apr	May	Jun	Jul	Aug	Sep	Oct	Nov	Dec	
N	6.6	7.2	6.7	10.0	10.1	9.7	8.7	10.7	8.6	6.6	5.3	4.8	10.7
NNE	7.1	9.5	8.9	8.7	8.3	9.9	8.8	8.2	7.9	7.4	9.1	9.2	9.9
NE	11.8	12.4	10.7	12.0	10.4	12.6	10.6	11.9	11.7	17.8	10.4	10.3	17.8
ENE	16.6	14.8	13.8	13.9	11.8	14.6	17.0	11.6	12.7	17.9	12.6	14.9	17.9
E	14.6	13.5	14.4	11.7	9.5	10.9	16.4	11.3	12.0	17.6	13.8	12.4	17.6
ESE	10.6	11.4	10.2	8.1	8.9	11.4	12.1	7.5	9.1	9.7	10.8	11.3	12.1
SE	8.6	7.9	8.7	8.9	10.3	11.0	12.2	11.2	7.2	8.5	10.4	7.8	12.2
SSE	7.6	7.6	8.1	8.6	8.1	12.0	19.6	15.4	13.2	11.8	10.7	6.8	19.6
S	10.6	10.3	10.8	11.6	11.6	14.9	18.3	13.8	16.0	10.2	11.5	8.0	18.3
SSW	8.3	9.7	10.0	9.9	9.9	13.9	16.6	11.3	16.2	13.4	10.5	8.8	16.6
SW	15.4	10.1	10.7	14.1	11.0	14.2	18.2	12.5	12.4	15.2	11.7	16.2	18.2
WSW	14.1	13.3	13.5	13.2	14.7	16.9	16.3	15.9	17.6	14.9	15.2	16.6	17.6
W	12.3	11.9	12.6	13.1	15.1	17.9	16.1	16.4	16.2	14.0	14.6	12.5	17.9
WNW	8.9	8.8	9.4	11.7	12.3	14.8	12.7	13.6	12.5	13.2	11.1	9.1	14.8
NW	8.5	8.2	8.8	9.6	8.7	11.1	11.2	10.1	13.8	11.7	11.3	7.2	13.8
NNW	6.0	7.8	9.2	9.5	10.9	12.1	12.2	11.9	11.3	9.0	5.1	4.6	12.2
Maximum	16.6	14.8	14.4	14.1	15.1	17.9	19.6	16.4	17.6	17.9	15.2	16.6	19.6

© Eskom 2026/Rev 0c

PRINTED VERSIONS OF THIS DOCUMENT ARE NOT CONTROLLED

Table 5.8.15
Monthly Maximum Hourly Average and Wind Gusts [m/s] at the Cape St. Francis WS and the Thyspunt WS

Month	Cape St. Francis WS		Thyspunt WS	
	2004 – 2023		2004 – 2013 & 2017 – 2019	
	Max of Hour Average	Highest Gust	Max of Hour Average	Highest Gust
January	18.8	34.5	16.6	29.0
February	16.6	35.7	14.8	30.7
March	19.5	31.2	14.7	24.1
April	18.1	28.7	14.1	31.6
May	22.8	39.7	15.1	31.6
June	23.2	32.6	17.9	30.2
July	21.2	37.9	19.3	32.2
August	21.1	45.8	16.4	29.2
September	18.8	31.6	17.9	37.9
October	19.3	38.5	17.9	31.7
November	17.5	30.2	15.5	25.5
December	19.7	34.1	16.6	24.2
Annual	23.2	45.8	19.3	37.9

Table 5.8.16
Gusts Above 20 m/s Directional Occurrence and Maximum Gusts at the Cape St. Francis WS and the Thyspunt WS

Wind Direction	Cape St. Francis WS		Thyspunt WS	
	2004 – 2023		2004 – 2013 & 2017 – 2019	
	Frequency Distribution of Gust Above 20 m/s	Highest Gust [m/s]	Frequency Distribution of Gust Above 20 m/s	Highest Gust [m/s]
N	0.00%	19.3	0.08%	22.0
NNE	0.00%	17.8	0.08%	30.7
NE	0.17%	21.5	0.58%	26.9
ENE	3.28%	35.7	5.34%	31.6
E	6.72%	32.1	8.71%	28.2
ESE	0.52%	34.1	0.16%	20.6
SE	0.17%	25.6	0.33%	31.7
SSE	0.34%	22.8	0.49%	29.9
S	1.38%	26.7	1.15%	29.1
SSW	2.93%	39.7	1.23%	26.4
SW	5.69%	34.5	3.53%	30.6
WSW	18.97%	38.5	20.71%	32.2
W	51.55%	45.8	50.62%	31.9
WNW	7.93%	34.0	6.49%	26.4
NW	0.34%	21.9	0.33%	24.4
NNW	0.00%	19.6	0.16%	37.9

© Eskom 2026/Rev 0c

PRINTED VERSIONS OF THIS DOCUMENT ARE NOT CONTROLLED

Wind Direction	Cape St. Francis WS 2004 – 2023		Thyspunt WS 2004 – 2013 & 2017 – 2019	
	Frequency Distribution of Gust Above 20 m/s	Highest Gust [m/s]	Frequency Distribution of Gust Above 20 m/s	Highest Gust [m/s]
Total/Max	100%	45.8	100%	37.9

(b) Valley Flow and Land/Sea Breeze Interactions

The differential heating of slopes can potentially give rise to anabatic (up-valley) flow during the day and katabatic (down-valley) flow during the night. However, apart from very small micro-climates, the study area contains no significant valley flow scenarios. On the other hand, diurnal and nocturnal[29] land/sea breeze conditions are evident. The large heat capacity of oceans reduces water-surface temperature change to near-zero values during a diurnal/nocturnal cycle. The land surface, however, warms and cools more dramatically because of the small molecular conductivity and heat capacity in soil prevents the diurnal and nocturnal temperature signal from propagating rapidly away from the surface. As a result, the land is warmer than the water during the day and cooler at night. During the morning, when the nocturnal surface boundary layer has been eliminated, air begins to rise over the warm land near the shoreline, and cooler air from the water flows in to replace it. This is known as the sea-breeze. A return circulation (the anti-sea-breeze) brings the warmer air back out to sea where it descends toward the sea surface to close the circulation. At night, land surfaces usually cool faster than the neighbouring water bodies, reversing the temperature gradient that was present during the day. The result is a land breeze: cool air from land flows out to sea at low levels, warms, rises, and returns aloft toward land (anti-land-breeze) where it eventually descends to close the circulation (Stull, 1997).

Low to moderate wind regimes at the site largely reflect the land/sea breezes with increased frequency of westerlies (sea breeze) observed during the daytime and increased frequency of easterlies (land breeze) occurring during the night-time. These are discussed further in ***Appendix 5.8.A***.

5.8.6.1.2 Ambient Air Temperature

Temperature is a primary climatological parameter that is used as an index of the energy status of the environment. Similarly, monitoring levels for temperature differences are representative of and characterise the magnitude of atmospheric turbulence at potential release height(s) from the existing nuclear installation(s).

[29] Diurnal and nocturnal conditions in this context refer to the daily and nightly cycles or periodical occurrence of a meteorological parameter that occur every day, e.g. sun rise in the morning, reaching a peak at midday and setting in the evening.

© Eskom 2026/Rev 0c

PRINTED VERSIONS OF THIS DOCUMENT ARE NOT CONTROLLED

The reference height for ambient air temperature measurement is typically 2 m above ground level (American National Standard, 2015). The monitoring levels for air temperature at Thyspunt WS was initially only at 2 m (2009-2013), but from 2017 to 2019 a second temperature sensor was established at 8 m. The temperature at the Cape St. Francis WS is also located at 2 m above ground level.

Dry bulb air temperature[30] observations at the Thyspunt WS (January 2008 to October 2013 and June 2017 to September 2019) recorded the following:

- average of the daily maximums: 20.8 °C (average of monthly ADMxT in ***Table 5.8.17***);
- average of the daily minimums: 14.4 °C (average of monthly ADMnT in ***Table 5.8.17***);
- the months with the highest average daily maximum temperatures of 23.4 °C are January and February (highest monthly ADMxT in ***Table 5.8.17***);
- the month with the lowest average daily maximum temperature of 18.4 °C is August (lowest monthly ADMxT in ***Table 5.8.17***);
- the month with the highest average daily minimum temperature of 17.8 °C is January (highest monthly ADMnT in ***Table 5.8.17***);
- the month with the lowest average daily minimum temperature of 11.2 °C is August (lowest monthly ADMnT in ***Table 5.8.17***);
- the annual average temperature (average of hourly average temperatures) is 17.3 °C (average of average monthly temperatures is 17.4 °C (average of monthly ADT in ***Table 5.8.17***).

Dry bulb air temperature observations at the Cape St. Francis WS (June 2004 to December 2023) recorded the following:

- average of the daily maximums: 19.9 °C (average of monthly ADMxT in ***Table 5.8.18***);
- average of the daily minimum: 14.2 °C (average of monthly ADMxT in ***Table 5.8.18***);
- the month with the highest average daily maximum temperature of 22.9 °C is January (highest monthly ADMxT in ***Table 5.8.18***);

[30] The dry-bulb temperature is the temperature of air measured by a thermometer freely exposed to the air but shielded from radiation from the sun. It is the temperature that is usually thought of as “air temperature”, and it is the true thermodynamic temperature. "Dry-bulb" is included because the air temperature is indicated by a thermometer not affected by the moisture of the air.

© Eskom 2026/Rev 0c

PRINTED VERSIONS OF THIS DOCUMENT ARE NOT CONTROLLED

- the month with the lowest average daily maximum temperature of 17.6 °C is July (lowest monthly ADMxT in ***Table 5.8.18***);
- the month with the highest average daily minimum temperature of 17.9 °C is January (highest monthly ADMnT in ***Table 5.8.18***);
- the month with the lowest average daily minimum temperature of 10.6 °C is July (lowest monthly ADMnT in ***Table 5.8.18***);
- the annual average temperature (average of hourly average temperatures) is 17.3 °C (average of average monthly temperatures is 17.3 °C (average of monthly ADT in ***Table 5.8.18***).

The lowest and highest hourly average temperatures (TMn and TMx in ***Table 5.8.17***) recorded at the Thyspunt WS (2 m level) were 6.7 °C (August) and 38.2 °C (April). The extreme hourly temperatures (TMn and TMx in ***Table 5.8.18***) at the Cape St. Francis WS (2 m level) were 4.9 °C (21 June 2018) and 38.5 °C (28 March 2022) (Eskom, 2023a).

The average number of days which were above or below selected maximum and minimum temperatures are also provided in the ***Tables 5.8.17*** and ***5.8.18***. Days with maximum hourly temperatures above 30 °C and 35 °C and with minimum hourly temperatures below 10 °C and 5 °C were used in the analyses.

The Thyspunt WS recorded the highest average number of days with hourly temperatures above 35 °C of 0.3 days, and this was for April (A#DDMxT in ***Table 5.8.17***). The Cape St. Francis WS recorded the highest average number of days with hourly temperatures above 35 °C of 0.1 days, and this was for March, May and September (A#DDMxT in ***Table 5.8.18***).

The Thyspunt WS recorded the highest average number of days with hourly temperatures above 30 °C of 1.0 day each for March and May (A#DDMxT in ***Table 5.8.17***). The Cape St. Francis WS recorded the highest average number of days with hourly temperatures above 30 °C of 0.8 days, and this was for May (A#DDMxT in ***Table 5.8.18***).

The highest average number of days with temperatures below 10 °C were recorded at the Thyspunt WS, which was 8.3 days (August) (A#DDMxT in ***Table 5.8.17***). There were no measurements below 5 °C at the Thyspunt WS. The highest average number of days with temperatures below 10 °C and 5 °C recorded at the Cape St. Francis WS were 11.1 days (July) and 1.3 days (June), respectively (A#DDMxT in ***Table 5.8.18***).

© Eskom 2026/Rev 0c

PRINTED VERSIONS OF THIS DOCUMENT ARE NOT CONTROLLED

The corresponding wet-bulb temperature[31] statistics at the Thyspunt WS were estimated as follows (***Table 5.8.19***).:

- Average of the daily maximum: 16.7 °C (average of monthly ADMxT in ***Table 5.8.19***);
- Average of the daily minimum: 12.6 °C average of monthly ADMnT in ***Table 5.8.19***);
- the months with the highest average daily maximum temperature of 19.9 °C are January and February (highest monthly ADMxT in ***Table 5.8.19***);
- the month with the lowest average daily maximum temperature of 13.9 °C is July (Lowest monthly ADMxT in ***Table 5.8.19***);
- the month with the highest average daily minimum temperature of 16.4 °C is January (highest monthly ADMnT in ***Table 5.8.19***);
- the month with the lowest average daily minimum temperature of 9.0 °C is August (Lowest monthly ADMnT in ***Table 5.8.19***).

The lowest and highest hourly average wet-bulb temperatures were 3.5 °C (16 June 2019) and 23.8 °C (16 March 2019).

The wet-bulb temperature statistics at the Cape St. Francis WS were estimated as follows (***Table 5.8.20***):

- average of the daily maximum: 14.8 °C (average of monthly ADMxT in ***Table 5.8.20***);
- average of the daily minimum: 11.1 °C (average of monthly ADMnT in ***Table 5.8.20***);

[31] An equation for wet-bulb temperature as a function of air temperature and relative humidity at standard sea level pressure was derived by Stull (Stull, 2011):

$$T_W = T\ \text{atan}\left(0.151977\sqrt{RH\% + 8.313659}\right) + \text{atan}(T + RH\%) - \text{atan}(RH\% - 1.676331) + 0.00391838(RH\%)^{\frac{3}{2}}\text{atan}(0.023RH\%) - 4.686035$$

Where T_W = Wet-bulb temperature [°C]

T = Dry-bulb temperature [°C]

$RH\%$ = Relative humidity [per cent]

atan () = arctangent function [radians]

The errors between the equation estimate and the T_W values used to develop the equation had a mean error of -0.00528°C, a median error of 0.0268°C, and a mean absolute error of 0.288°C, and the fraction of variance (r^2) explained by the regression of 99.95 per cent.

To illustrate its usage, plugging $T = 20\ °C$ and $RH\% = 50\ per\ cent$ into the equation gives:

$$T_W = 20\,\text{atan}\left(0.151977\sqrt{50 + 8.313659}\right) + \text{atan}(20 + 50) - \text{atan}(50 - 1.676331) + 0.00391838(50)^{\frac{3}{2}}\text{atan}(0.023\ x\ 50) - 4.686035 = 13.7°C$$

© Eskom 2026/Rev 0c

PRINTED VERSIONS OF THIS DOCUMENT ARE NOT CONTROLLED

- the months with the highest average daily maximum wet-bulb temperature of 17.7 °C are January and February (highest monthly ADMxT in ***Table 5.8.20***);
- the months with the lowest average daily maximum wet-bulb temperature of 12.2 °C are July and August (lowest monthly ADMxT in ***Table 5.8.20***);
- the month with the highest average daily minimum wet-bulb temperature of 14.6 °C is January (highest monthly ADMnT in ***Table 5.8.20***);
- the month with the lowest average daily minimum wet-bulb temperature of 7.6 °C is July (lowest monthly ADMnT in ***Table 5.8.20***).

The lowest and highest hourly average wet-bulb temperatures were 3.1 °C (21 June 2017) and 24.4 °C (13 February 2021), respectively.

The corresponding dewpoint temperature [32] [33] statistics for the Thyspunt WS were estimated as follows (***Table 5.8.21***):

- average of the daily maximum: 15.5 °C (average of monthly ADMxT in ***Table 5.8.21***);

[32] The dewpoint is the temperature at which the air is saturated with respect to water vapour over a liquid surface. When the temperature is equal to the dewpoint then the relative humidity is 100 per cent. The three mechanisms for relative humidity to be 100 per cent are to (a) cool the air to the dewpoint, (b) evaporate moisture into the air until the air is saturated, or (c) lift the air until it cools to the dewpoint. Dew forms when the temperature becomes equal to the dewpoint. The favourable weather elements for dew include clear skies, light wind, adequate soil moisture, and low night-time dewpoint depressions.

When the dry-bulb temperatures drop below freezing and the temperature reaches the dewpoint temperature, the ice formed on the ground surface is termed frost. Frost can form in two ways, namely by deposition or freezing of dew. Depositional frost occurs when the dewpoint is below freezing. When this frost forms, the water vapour goes directly to the solid state. Frost that forms due to the freezing of liquid water (i.e. dew) is best referred to as frozen dew. Initially, both the dewpoint and temperature are above freezing when dew forms. Longwave radiational cooling gradually lowers the temperature to or below freezing during the night. Cold air advection can also initiate freezing (e.g. cold air moving through during the night after dew has formed). Once the temperature falls to freezing, the condensed dew droplets freeze.

[33] The dew point temperature (T_d) is calculated using the Magnus formula (Alduchov & Eskridge, 1996) :

$$T_d = \frac{b}{\left[\frac{a}{ln(RH\%/100) + \frac{aT}{b+T}} - 1\right]}$$

Where T_d = Dewpoint temperature [°C]
T = Dry-bulb temperature [°C]
$RH\%$ = Relative humidity [per cent
a = constant, 17.625 [unitless]
b = constant, 243.04 [°C]
ln () = natural logarithm [unitless]

The errors between the equation estimate and the T_d values used to develop the equation had a maximum relative error of less than 0.384 per cent over a temperature range of -40°C to 50°C. To illustrate its usage, plugging $T = 20\,°C$ and $RH\% = 50\ per\ cent$ into the equation gives:

$$T_d = \frac{243.04}{\left[\frac{17.625}{ln(50/100) + \frac{17.625T}{243.04+20}} - 1\right]} = 9.26\,°C$$

© Eskom 2026/Rev 0c

PRINTED VERSIONS OF THIS DOCUMENT ARE NOT CONTROLLED

- average of the daily minimum: 10.5 °C (average of monthly ADMnT in ***Table 5.8.21***);
- the months with the highest average daily maximum temperature of 19.0 °C are January and February (highest monthly ADMxT in ***Table 5.8.21***);
- the month with the lowest average daily maximum temperature of 12.1 °C is July (lowest monthly ADMxT in ***Table 5.8.21***);
- the month with the highest average daily minimum temperature of 15.5 °C is January (highest monthly ADMnT in ***Table 5.8.21***);
- the month with the lowest average daily minimum temperature of 5.5 °C is July (lowest monthly ADMnT in ***Table 5.8.21***).

The lowest and highest hourly average dewpoint temperatures were -6.5 °C (17 June 2017) and 23.1 °C (18 December 2018), respectively.

The corresponding dewpoint temperature statistics for the Cape St. Francis WS were estimated as follows (***Table 5.8.22***):

- average of the daily maximum: 13.8 °C (average of monthly ADMxT in ***Table 5.8.22***);
- average of the daily minimum: 9.8 °C (average of monthly ADMnT in ***Table 5.8.22***);
- the months with the highest average daily maximum temperature of 16.8 °C are January and February (highest monthly ADMxT in ***Table 5.8.22***);
- the month with the lowest average daily maximum temperature of 11.0 °C is July (lowest monthly ADMxT in ***Table 5.8.22***);
- the month with the highest average daily minimum temperature of 13.8 °C is January (highest monthly ADMnT in ***Table 5.8.22***);
- the month with the lowest average daily minimum temperature of 5.3 °C is July (lowest monthly ADMnT in ***Table 5.8.22***).

The lowest and highest hourly average dewpoint temperature were 0.0 °C (25 June 2020) and 23.5 °C (4 January 2016), respectively.

© Eskom 2026/Rev 0c

PRINTED VERSIONS OF THIS DOCUMENT ARE NOT CONTROLLED

Table 5.8.17
Ambient Air Dry Bulb Temperature [°C] at the Thyspunt WS (January 2008 to October 2013 and June 2017 to September 2019)

Month	Daily Average		95% Confidence Interval of Average	Daily Median	Percentiles		Maximums and Minimums						A#DDMxT		A#DDMnT	
	ADT	StdDev			25%	75%	MnADT	MxADT	TMn	TMx	ADMnT	ADMxT	>35.0	>30.0	<10.0	<5.0
1	20.5	1.3	±2.58	20.4	18.9	22.0	16.8	24.3	13.0	31.3	17.8	23.4	0.0	0.3	0.0	0.0
2	20.4	1.6	±3.04	20.3	18.7	21.8	16.0	26.4	13.5	32.4	17.6	23.4	0.0	0.9	0.0	0.0
3	19.8	1.7	±3.26	19.6	18.2	21.1	15.0	25.2	11.7	36.6	17.1	23.0	0.0	1.0	0.0	0.0
4	17.8	2.2	±4.35	17.7	15.8	19.4	11.7	25.3	8.3	38.2	14.8	21.3	0.3	0.9	0.1	0.0
5	17.0	2.4	±4.62	16.7	14.8	18.5	12.0	27.2	8.4	35.8	13.9	20.9	0.1	1.0	0.9	0.0
6	15.2	2.5	±4.98	14.8	12.7	16.9	10.0	24.7	7.1	31.2	11.8	19.1	0.0	0.4	5.1	0.0
7	15.1	3.0	±5.86	14.5	12.3	17.0	9.8	25.9	7.2	31.8	11.7	19.1	0.0	0.5	6.8	0.0
8	14.6	2.2	±4.35	14.3	12.3	16.4	9.8	22.6	6.7	31.3	11.2	18.4	0.0	0.3	8.3	0.0
9	15.4	2.2	±4.23	15.3	13.3	17.1	10.8	28.7	7.6	36.3	12.2	18.8	0.1	0.6	2.9	0.0
10	16.5	2.0	±3.98	16.2	14.7	17.9	12.9	25.9	9.4	34.7	13.6	19.5	0.0	0.7	0.4	0.0
11	17.3	1.6	±3.08	17.3	15.7	18.9	13.1	23.4	9.6	32.9	14.5	20.3	0.0	0.4	0.1	0.0
12	19.3	1.7	±3.30	19.1	17.6	20.9	15.7	23.6	11.2	34.0	16.5	22.1	0.0	0.3	0.0	0.0

ADT - Average daily temperature: average of the temperatures observed at 24 equidistant times in the course of a continuous 24-hour period (midnight to midnight).
StdDev – Standard deviation.
MnADT - Minimum of average daily temperature for a month: minimum of the average daily temperatures.
MxADT - Maximum of average daily temperature for a month: maximum of the average daily temperatures.
TMn - Minimum hourly temperature: minimum of the temperatures observed at 24 equidistant times in the course of a continuous 24-hour period.
TMx - Maximum hourly temperature: maximum of the temperatures observed at 24 equidistant times in the course of a continuous 24-hour period.
ADMxT - Average daily maximum temperature for a month: average of the daily maximum temperatures.
ADMnT - Average daily minimum temperature for a month: average of the daily minimum temperatures.
A#DDMxT - average number of days with maximum hourly temperature above.
A#DDMnT - average number of days with minimum hourly temperature below.

© Eskom 2026/Rev 0c

PRINTED VERSIONS OF THIS DOCUMENT ARE NOT CONTROLLED

Table 5.8.18
Ambient Air Dry Bulb Temperature [°C] at the Cape St. Francis WS (June 2004 to December 2023)

Month	Daily Average		95% Confidence Interval of Average	Daily Median	Percentiles		Maximums and Minimums						A#DDMxT		A#DDMnT	
	ADT	StdDev			25%	75%	MnADT	MxADT	TMn	TMx	ADMnT	ADMxT	>35.0	>30.0	<10.0	<5.0
1	20.4	1.5	±2.92	20.4	18.9	21.9	15.6	25.1	12.4	28.0	17.9	22.9	0.0	0.0	0.0	0.0
2	20.0	1.4	±2.80	20.0	18.5	21.5	15.2	24.7	11.6	31.5	17.4	22.6	0.0	0.1	0.0	0.0
3	19.2	1.5	±2.95	19.1	17.8	20.6	15.2	27.8	11.0	38.5	16.7	21.9	0.1	0.2	0.0	0.0
4	17.4	1.6	±3.11	17.4	16.0	18.9	12.4	22.7	8.7	34.7	14.8	20.1	0.0	0.2	0.3	0.0
5	16.6	1.9	±3.82	16.3	14.8	18.1	9.9	26.4	6.7	36.5	13.3	19.7	0.1	0.8	1.7	0.2
6	15.3	2.2	±4.26	15.0	13.2	17.0	10.8	24.1	4.9	32.3	11.0	18.2	0.0	0.4	8.1	1.3
7	14.7	2.1	±4.12	14.6	12.7	16.5	9.2	23.4	5.1	31.8	10.6	17.6	0.0	0.2	11.1	1.2
8	14.9	1.8	±3.54	14.9	13.2	16.6	9.2	23.9	5.0	33.7	11.3	18.0	0.0	0.6	9.1	0.1
9	15.6	1.4	±2.79	15.7	14.3	17.1	11.2	24.7	7.0	37.6	12.3	18.0	0.1	0.1	4.0	0.5
10	16.7	1.5	±3.03	16.7	15.3	18.0	12.0	26.0	8.5	33.5	13.7	18.4	0.0	0.1	1.9	1.0
11	17.8	1.5	±2.94	17.9	16.2	19.3	13.3	21.8	9.3	31.1	14.9	19.9	0.0	0.2	0.7	0.6
12	19.3	1.6	±3.22	19.4	17.8	20.9	14.1	24.1	12.0	27.9	16.7	21.7	0.0	0.0	0.2	0.2

ADT - Average daily temperature: average of the temperatures observed at 24 equidistant times in the course of a continuous 24-hour period (midnight to midnight).
StdDev – Standard deviation.
MnADT - Minimum of average daily temperature for a month: minimum of the average daily temperatures.
MxADT - Maximum of average daily temperature for a month: maximum of the average daily temperatures.
TMn - Minimum hourly temperature: minimum of the temperatures observed at 24 equidistant times in the course of a continuous 24-hour period.
TMx - Maximum hourly temperature: maximum of the temperatures observed at 24 equidistant times in the course of a continuous 24-hour period.
ADMxT - Average daily maximum temperature for a month: average of the daily maximum temperatures.
ADMnT - Average daily minimum temperature for a month: average of the daily minimum temperatures.
A#DDMxT - average number of days with maximum hourly temperature above.
A#DDMnT - average number of days with minimum hourly temperature below.

© Eskom 2026/Rev 0c

PRINTED VERSIONS OF THIS DOCUMENT ARE NOT CONTROLLED

Table 5.8.19
Ambient Air Wet Bulb Temperature [°C] at the Thyspunt WS (January 2008 to October 2013 and June 2017 to September 2019

Month	Daily Average		95% Confidence Interval of Average	Daily Median	Percentiles		Maximums and Minimums						A#DDMxT		A#DDMnT	
	ADT	StdDev			25%	75%	MnADT	MxADT	TMn	TMx	ADMnT	ADMxT	>35.0	>30.0	<10.0	<5.0
1	18.3	1.6	±3.20	18.5	17.1	19.7	13.8	22.4	11.4	23.5	16.4	19.9	0.0	0.0	0.0	0.0
2	18.3	1.6	±3.17	18.4	17.0	19.6	13.8	23.1	11.0	22.3	16.2	19.9	0.0	0.0	0.0	0.0
3	17.8	1.8	±3.51	17.9	16.5	19.2	11.4	21.7	12.6	23.8	15.7	19.5	0.0	0.0	0.4	0.0
4	15.2	2.0	±3.92	15.2	13.6	16.9	8.8	19.6	8.9	21.7	13.0	17.2	0.0	0.0	3.0	0.0
5	13.9	1.8	±3.43	14.1	12.4	15.5	8.3	18.1	7.0	20.5	11.6	16.0	0.0	0.0	5.0	0.1
6	11.7	1.7	±3.42	11.7	10.1	13.4	7.4	16.5	3.5	17.3	9.2	14.1	0.0	0.0	17.6	0.2
7	11.5	1.7	±3.40	11.6	9.8	13.4	6.9	15.3	4.9	18.2	9.1	13.9	0.0	0.0	17.6	0.4
8	11.6	1.9	±3.68	11.6	9.9	13.4	7.1	16.0	4.4	19.0	9.0	14.0	0.0	0.0	18.8	0.4
9	12.7	2.0	±3.89	12.7	10.9	14.4	8.2	17.7	6.4	20.1	10.2	14.7	0.0	0.0	12.4	0.0
10	14.2	2.0	±3.89	14.2	12.5	15.9	9.6	20.0	7.0	23.0	11.8	16.1	0.0	0.0	4.7	0.0
11	15.0	1.8	±3.55	15.0	13.5	16.5	10.2	19.7	6.5	21.4	12.8	16.7	0.0	0.0	2.3	0.0
12	17.0	1.9	±3.74	17.2	15.5	18.6	12.1	21.8	10.4	23.6	15.1	18.6	0.0	0.0	0.3	0.0

ADT - Average daily temperature: average of the temperatures observed at 24 equidistant times in the course of a continuous 24-hour period (midnight to midnight).
StdDev – Standard deviation.
MnADT - Minimum of average daily temperature for a month: minimum of the average daily temperatures.
MxADT - Maximum of average daily temperature for a month: maximum of the average daily temperatures.
TMn - Minimum hourly temperature: minimum of the temperatures observed at 24 equidistant times in the course of a continuous 24-hour period.
TMx - Maximum hourly temperature: maximum of the temperatures observed at 24 equidistant times in the course of a continuous 24-hour period.
ADMxT - Average daily maximum temperature for a month: average of the daily maximum temperatures.
ADMnT - Average daily minimum temperature for a month: average of the daily minimum temperatures.
A#DDMxT - average number of days with maximum hourly temperature above.
A#DDMnT - average number of days with minimum hourly temperature below.

© Eskom 2026/Rev 0c

PRINTED VERSIONS OF THIS DOCUMENT ARE NOT CONTROLLED

Table 5.8.20
Ambient Air Wet Bulb Temperature [°C] at the Cape St. Francis WS (June 2004 to December 2023)

Month	Daily Average		95% Confidence Interval of Average	Daily Median	Percentiles		Maximums and Minimums						A#DDMxT		A#DDMnT	
	ADT	StdDev			25%	75%	MnADT	MxADT	TMn	TMx	ADMnT	ADMxT	>35.0	>30.0	<10.0	<5.0
1	18.2	1.6	±3.15	18.2	16.9	19.6	14.0	23.3	10.4	24.3	14.6	17.7	0.0	0.0	3.3	3.3
2	18.1	1.5	±3.03	18.1	16.8	19.5	13.9	22.8	10.1	24.4	14.4	17.7	0.0	0.0	2.9	2.9
3	17.1	1.5	±3.03	17.1	15.9	18.5	12.3	21.2	9.6	22.7	13.4	16.7	0.0	0.0	3.5	3.4
4	15.2	1.7	±3.33	15.2	13.9	16.7	9.6	19.1	7.0	21.9	11.6	15.1	0.0	0.0	5.9	3.3
5	13.9	1.6	±3.10	14.0	12.6	15.5	7.3	17.6	4.0	19.9	10.1	14.2	0.0	0.0	10.6	3.5
6	12.2	1.6	±3.23	12.3	10.6	14.0	7.9	16.9	3.1	18.3	7.8	12.5	0.0	0.0	20.6	4.9
7	11.8	1.7	±3.33	11.9	10.1	13.7	6.7	15.4	3.3	18.0	7.6	12.2	0.0	0.0	22.8	5.5
8	12.2	1.8	±3.58	12.2	10.6	14.1	6.9	17.2	3.2	19.3	7.9	12.2	0.0	0.0	20.5	5.7
9	13.1	1.7	±3.28	13.2	11.7	14.7	8.5	17.7	4.6	19.8	8.8	12.6	0.0	0.0	15.0	4.8
10	14.4	1.8	±3.60	14.5	13.0	16.0	9.0	21.0	6.3	22.2	10.5	13.6	0.0	0.0	9.3	4.8
11	15.5	1.7	±3.31	15.4	14.1	16.9	10.9	20.8	7.8	21.7	12.0	15.3	0.0	0.0	4.4	3.1
12	17.0	1.8	±3.51	17.0	15.6	18.5	12.4	22.4	9.2	23.9	13.9	17.3	0.0	0.0	2.4	2.3

ADT - Average daily temperature: average of the temperatures observed at 24 equidistant times in the course of a continuous 24-hour period (midnight to midnight).
StdDev – Standard deviation.
MnADT - Minimum of average daily temperature for a month: minimum of the average daily temperatures.
MxADT - Maximum of average daily temperature for a month: maximum of the average daily temperatures.
TMn - Minimum hourly temperature: minimum of the temperatures observed at 24 equidistant times in the course of a continuous 24-hour period.
TMx - Maximum hourly temperature: maximum of the temperatures observed at 24 equidistant times in the course of a continuous 24-hour period.
ADMxT - Average daily maximum temperature for a month: average of the daily maximum temperatures.
ADMnT - Average daily minimum temperature for a month: average of the daily minimum temperatures.
A#DDMxT - average number of days with maximum hourly temperature above.
A#DDMnT - average number of days with minimum hourly temperature below.

© Eskom 2026/Rev 0c

PRINTED VERSIONS OF THIS DOCUMENT ARE NOT CONTROLLED

Table 5.8.21
Ambient Air Dewpoint Temperature [°C] at the Thyspunt WS (January 2008 to October 2013 and June 2017 to September 2019)

Month	Daily Average		95% Confidence Interval of Average	Daily Median	Percentiles		Maximums and Minimums						A#DDMxT		A#DDMnT	
	ADT	StdDev			25%	75%	MnADT	MxADT	TMn	TMx	ADMnT	ADMxT	>35.0	>30.0	<10.0	<5.0
1	17.3	2.0	±3.91	17.5	15.9	18.9	11.9	22.2	10.3	23.0	15.5	19.0	0.0	0.0	0.0	0.0
2	17.3	1.9	±3.72	17.6	15.9	18.9	11.7	21.8	7.7	20.6	15.2	19.0	0.0	0.0	0.6	0.0
3	16.8	2.1	±4.15	17.1	15.5	18.5	7.9	21.0	9.3	22.1	14.6	18.6	0.0	0.0	1.9	0.1
4	13.8	2.5	±4.90	14.0	11.9	15.9	6.8	19.2	5.3	20.7	11.0	16.0	0.0	0.0	10.1	1.0
5	12.0	2.6	±5.18	12.4	10.1	14.4	0.4	17.6	2.8	18.6	8.8	14.6	0.0	0.0	17.3	4.0
6	9.1	3.1	±5.98	9.5	7.1	11.8	-3.0	16.4	-6.5	16.3	5.7	12.3	0.0	0.0	24.4	10.0
7	8.9	2.7	±5.30	9.2	6.7	11.7	0.0	14.5	-5.0	17.1	5.5	12.1	0.0	0.0	24.4	11.0
8	9.6	2.8	±5.47	9.7	7.5	12.1	-1.9	15.7	-4.8	17.5	6.1	12.6	0.0	0.0	24.1	8.7
9	11.0	2.6	±5.02	11.2	9.0	13.2	3.9	17.1	-1.5	18.2	8.1	13.4	0.0	0.0	18.0	3.9
10	12.9	2.5	±4.92	12.9	10.9	15.0	6.7	18.1	2.5	19.0	10.2	15.1	0.0	0.0	9.4	1.0
11	13.7	2.2	±4.38	13.7	12.0	15.6	7.8	18.9	4.3	20.0	11.4	15.6	0.0	0.0	7.9	0.4
12	16.0	2.3	±4.49	16.2	14.4	17.8	9.8	21.5	8.7	23.1	14.0	17.6	0.0	0.0	2.6	0.0

ADT - Average daily temperature: average of the temperatures observed at 24 equidistant times in the course of a continuous 24-hour period (midnight to midnight).
StdDev – Standard deviation.
MnADT - Minimum of average daily temperature for a month: minimum of the average daily temperatures.
MxADT - Maximum of average daily temperature for a month: maximum of the average daily temperatures.
TMn - Minimum hourly temperature: minimum of the temperatures observed at 24 equidistant times in the course of a continuous 24-hour period.
TMx - Maximum hourly temperature: maximum of the temperatures observed at 24 equidistant times in the course of a continuous 24-hour period.
ADMxT - Average daily maximum temperature for a month: average of the daily maximum temperatures.
ADMnT - Average daily minimum temperature for a month: average of the daily minimum temperatures.
A#DDMxT - average number of days with maximum hourly temperature above.
A#DDMnT - average number of days with minimum hourly temperature below.

© Eskom 2026/Rev 0c

PRINTED VERSIONS OF THIS DOCUMENT ARE NOT CONTROLLED

Table 5.8.22
Ambient Air Dewpoint Temperature [°C] at the Cape St. Francis WS (June 2004 to December 2023)

Month	Daily Average		95% Confidence Interval of Average	Daily Median	Percentiles		Maximums and Minimums						A#DDMxT		A#DDMnT	
	ADT	StdDev			25%	75%	MnADT	MxADT	TMn	TMx	ADMnT	ADMxT	>35.0	>30.0	<10.0	<5.0
1	17.3	1.8	±3.61	17.4	15.9	18.9	11.8	22.7	9.3	23.5	13.8	16.8	0.0	0.0	3.4	3.3
2	17.2	1.8	±3.50	17.3	15.9	18.7	11.6	22.1	6.7	23.3	13.7	16.8	0.0	0.0	3.2	2.9
3	16.2	1.8	±3.56	16.3	14.9	17.7	9.3	20.7	6.3	22.3	12.6	15.9	0.0	0.0	5.0	3.4
4	14.2	2.0	±4.00	14.2	12.7	15.9	7.7	18.8	3.6	20.2	10.5	14.2	0.0	0.0	9.6	3.5
5	12.5	2.1	±4.13	12.7	11.1	14.5	5.4	17.3	0.1	18.5	8.5	13.1	0.0	0.0	17.6	5.6
6	10.2	2.5	±4.98	10.5	8.2	12.7	-0.1	16.6	0.0	17.3	5.4	11.3	0.0	0.0	25.4	11.6
7	9.9	2.5	±4.85	10.2	7.9	12.4	1.0	14.8	0.0	16.9	5.3	11.0	0.0	0.0	27.1	13.1
8	10.7	2.5	±4.88	10.7	8.8	13.0	-0.3	17.2	0.0	19.1	6.3	11.1	0.0	0.0	24.8	10.8
9	11.8	2.1	±4.20	11.9	10.1	13.7	5.1	17.5	0.0	19.5	7.6	11.7	0.0	0.0	20.0	7.0
10	13.3	2.3	±4.59	13.5	11.6	15.2	0.1	18.8	0.1	20.8	9.4	12.7	0.0	0.0	14.3	5.3
11	14.3	2.0	±4.01	14.4	12.7	16.0	8.0	20.5	0.5	21.1	11.0	14.3	0.0	0.0	7.9	3.2
12	16.0	2.1	±4.18	16.2	14.5	17.7	9.2	21.8	5.7	23.0	13.0	16.2	0.0	0.0	3.8	2.3

ADT - Average daily temperature: average of the temperatures observed at 24 equidistant times in the course of a continuous 24-hour period (midnight to midnight).
StdDev – Standard deviation.
MnADT - Minimum of average daily temperature for a month: minimum of the average daily temperatures.
MxADT - Maximum of average daily temperature for a month: maximum of the average daily temperatures.
TMn - Minimum hourly temperature: minimum of the temperatures observed at 24 equidistant times in the course of a continuous 24-hour period.
TMx - Maximum hourly temperature: maximum of the temperatures observed at 24 equidistant times in the course of a continuous 24-hour period.
ADMxT - Average daily maximum temperature for a month: average of the daily maximum temperatures.
ADMnT - Average daily minimum temperature for a month: average of the daily minimum temperatures.
A#DDMxT - average number of days with maximum hourly temperature above.
A#DDMnT - average number of days with minimum hourly temperature below.

© Eskom 2026/Rev 0c

PRINTED VERSIONS OF THIS DOCUMENT ARE NOT CONTROLLED

The temperature persistence (in hours) at the monitoring sites is summarised in ***Table 5.8.23***. The recorded 6-hour duration maximum hourly temperature at the Thyspunt WS was 33.1 °C. A lower maximum temperature for this duration was observed at the Cape St. Francis WS, i.e., 31.2 °C. The recorded 3-hour duration maximum hourly temperature at the Thyspunt WS and Cape St. Francis WS were 37.0 °C and 36.1 °C, respectively. The recorded 6-hour and 3-hour sustained minimum hourly temperatures at the Thyspunt WS were 7.7 °C and 7.2 °C, respectively. The minimum temperatures for the same durations at the Cape St. Francis WS were 6.5 °C and 6.5 °C, respectively.

Table 5.8.23
Maximum and Minimum Ambient Air Dry Bulb Temperature and Corresponding Wet bulb Temperature for Sustained 3 and 6 Hours, and 7 Days

Weather Station	Sustained Maximum Temperature [°C] for						Sustained Minimum Temperature [°C] for					
	7 days		6 hours		3 hours		7 days		6 hours		3 hours	
	DBT	WBT	DBT	WBT	DBT	WBT	DBT	WBT	DBT	WBT	DBT	WBT
Cape St. Francis SAWS (1)	20.8	18.2	31.2	16.2	36.1	18.1	15.0	12.9	6.5	4.3	6.5	4.8
Thyspunt WS (2)	19.3	16.8	33.1	18.8	37.0	19.7	15.5	13.3	7.7	6.0	7.2	5.4

Notes:
(1) The statistics included June 2004 to 31 December 2023 period.
(2) The statistics included January 2008 to October 2013 and June 2017 to September 2019 periods.

Albeit a relatively short monitoring period at the Thyspunt WS, the observed dry-bulb air temperatures did not drop below 6.7°C. The observed minimum dry-bulb air temperatures at the Cape St. Francis WS were lower but did not drop below 4.9°C. It is therefore expected that frost would be a rare occurrence at the site.

A measure of the vertical temperature difference (United States Nuclear Regulatory Commission, 2007c) allows the calculation of atmospheric turbulence, e.g. 'delta-T' method. This is discussed in ***Subsection 5.8.6.1.9***. The alternative method of using the direct measurement of wind fluctuations, i.e. the 'sigma-theta' method (International Atomic Energy Agency, 2002), is also discussed and compared in ***Subsection 5.8.6.1.9***.

5.8.6.1.3 Precipitation

Types of precipitation include hail, sleet, snow, rain, and drizzle. Frost and dew are not classified as precipitation because they form directly on solid surfaces. The formation of precipitation may occur at temperatures above or below freezing. Since the rainfall measurements are done automatically,

© Eskom 2026/Rev 0c

PRINTED VERSIONS OF THIS DOCUMENT ARE NOT CONTROLLED

it is not currently possible to determine the details of the type of precipitation. Instead, a constant precipitation type ('showers') most common to the area is used to evaluate the impact of precipitation on airborne concentrations of contaminants and on ground contamination. No records could be obtained that quantified the occurrence of freezing precipitation at the site. However, given the relatively high wet-bulb temperatures recorded at the site (lowest of 3.5 °C at the Thyspunt WS and 3.1 °C at the Cape St. Francis WS), the likelihood of freezing precipitation is expected to be low.

The site receives rainfall throughout the year with wetter months typically from April to November (Preston-Whyte & Tyson, 1988; Schulze, 1986) and drier months from December to March. Historically (Schulze, 1997), the Mean Annual Precipitation (MAP) was reported to be between 600.0 mm and 800.0 mm with some areas near the site experiencing up to 1 000 mm, as shown in ***Figure 5.8.9***. Due to the limited period of nine years of monitoring at the Thyspunt WS, reference and comparison to other weather stations in the vicinity of the site is therefore necessary (International Atomic Energy Agency, 2011) (***Table -5.8.24***).

Table 5.8.24
Summary of Long-Term Mean Annual Precipitation (MAP) at Nearest Weather Stations in Comparison with Thyspunt WS

Station	Years of Record	Distance from Site (km)	Elevation (m amsl)	MAP [mm]
Humansdorp [0017422 5]	146 (1878-2022)	17.3	109	678.8
Cape St. Francis(4) [0017582 07]	104 (1881-1984)	9.3	7	673.0
Cape St. Francis(4) [0017582 07]	19 (1985-2003)	9.3	7	660.9
Cape St. Francis(4) [0017582A1]	20 (2004(1)-2023)	9.3	7	595.0
Thyspunt	6 (2008-2013(2) & 2017-2019(3))	-	51	774.4

Notes:
(1) Partial year for 2004 (15 June to 31 December) and subsequently excluded
(2) Partial year for 2013 (1 January to 4 October)
(3) Partial year for 2017 (16 June to 31 December) and 2019 (1 January to 10 October)
(4) Combining all rainfall data from 1881 to 2023 recorded at Cape St. Francis, the MAP is calculated to be 619.5 mm

Based on 146 years of observations at the SAWS' Humansdorp WS (1878-2022) (SAWS, 2024b) (SAWS, 2024c), the MAP was estimated to be 678.8 mm. However, this site is approximately 17.3 km inland from Thyspunt and may not reflect identical rainfall conditions. The Cape St. Francis WS (SAWS, 2024c) is closer to Thyspunt (approximately 9.3 km

© Eskom 2026/Rev 0c

PRINTED VERSIONS OF THIS DOCUMENT ARE NOT CONTROLLED

east), however, this location is very close to the shoreline and may be influenced by this proximity.

Only monthly and annual rainfall statistical values for the period from 1881 to 1984 were available for the Cape St. Francis WS (Schulze, 1986). An MAP of 673.0 mm was given for this period. Twenty-four-hour historical rainfall at the Cape St. Francis WS was available for analysis for the period 1985 to 2023, however, the weather station was replaced during 2004 and ***Table -5.8.24*** includes separate MAP values for the two periods pre- and post-2004, i.e. 660.9 mm and 595.0 mm, respectively. Hourly rainfall data were only available from 2004 with the replacement of the weather station. The combined rainfall data for the period 1881 to 2023 provides an MAP of 619.5 mm. ***Figure 5.8.10*** summarises the 39-year (1985 to 2023) total annual precipitation (maximum 972.2 mm) recorded at the Cape St. Francis WS (SAWS, 2024b) (SAWS, 2024c). The rainfall for 2004 is excluded due to the changeover of weather stations that resulted in an incomplete monitoring period. Unfortunately, the Thyspunt WS data included only six full years from 2008 to 2012 (2013 not full year) and 2018 (2017 and 2019 not full years). The MAP for this period was calculated to be 774.4 mm, which is higher than the observed MAP for the Cape St. Francis WS and the Humansdorp WS. Above average annual rainfall was observed during 2011 and 2012 at the Thyspunt WS, which skewed the average over the period.

Monthly average, minimum and maximum rainfall results for Humansdorp, Cape St. Francis and Thyspunt are presented in ***Table 5.8.25***. The monthly average rainfall totals for these three weather stations are also given graphically in ***Figure 5.8.11***. Whereas monthly averages were similar for the three locations, some differences were observed when comparing Humansdorp and Cape St. Francis to Thyspunt for June and July. The average monthly rainfall observed at Cape St. Francis WS and the Thyspunt WS both peaked from May to August, whereas the observations at the Humansdorp WS peaked later, from August to October. A similar trend was observed with the highest monthly totals, with the peak for both Cape St. Francis WS and Thyspunt WS during July, and for the Humansdorp WS during October. The measurements of maximum 24-hour rainfall rates for the three weather station locations are provided in ***Table 5.8.26***. The maximum 24-hour rainfall events observed at the Humansdorp WS were mostly higher than the 24-hour observations made at the Cape St. Francis WS except for March. The maximum 24-hour at the Cape St Francis WS was 157.8 mm. Apart from July, most of the Thyspunt WS maximum 24-hour observations were slightly lower than or similar to the Humansdorp WS 24-hour maximum observations. The maximum 24-hour at the Thyspunt WS was 113.5 mm.

© Eskom 2026/Rev 0c

PRINTED VERSIONS OF THIS DOCUMENT ARE NOT CONTROLLED

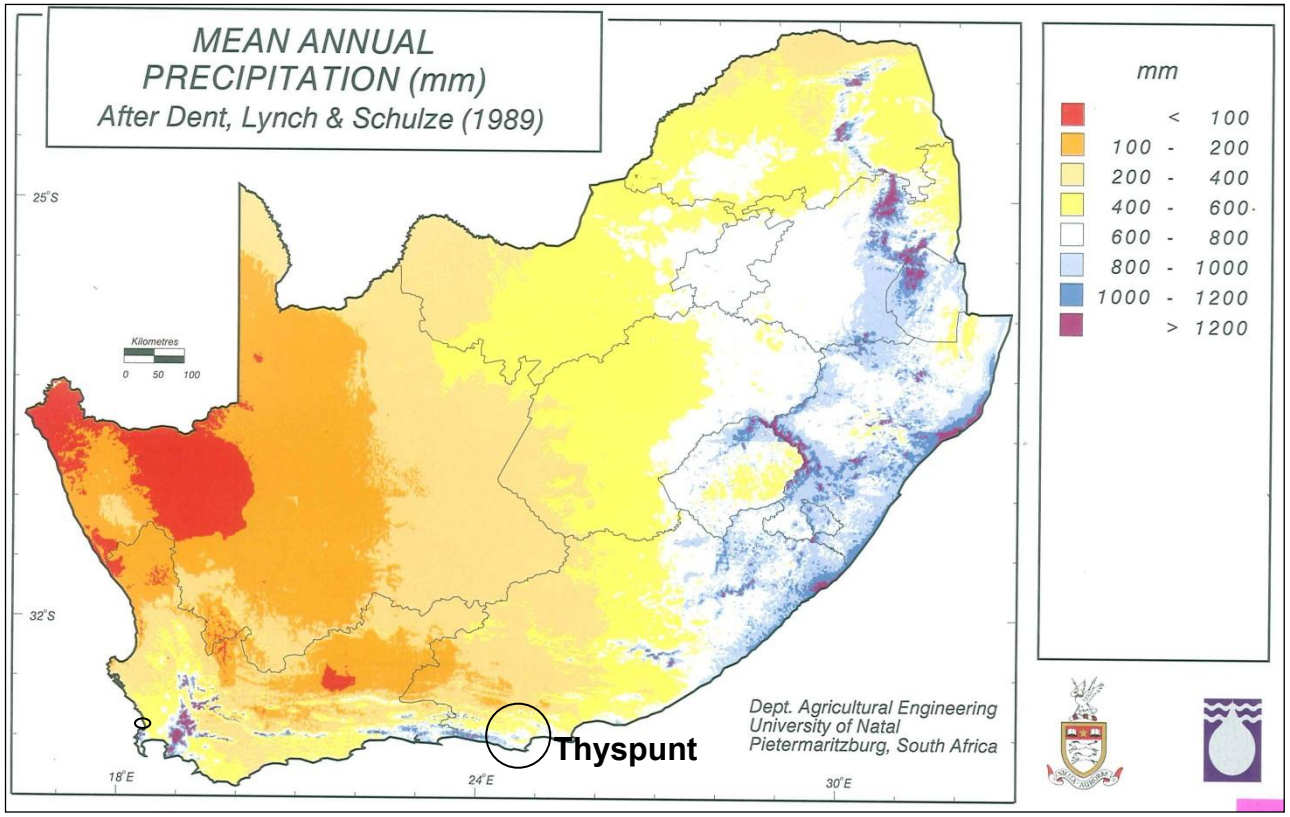


Figure 5.8.9
Mean Annual Precipitation for South Africa (Schulze, 1997)

© Eskom 2026/Rev 0c

PRINTED VERSIONS OF THIS DOCUMENT ARE NOT CONTROLLED

Hourly rainfall was available for the Cape St. Francis WS, but only from 2004 to 2023 (SAWS, 2024c). These highest 1-hour totals are provided in ***Table 5.8.27*** for Cape St. Francis and Thyspunt. Overall, the hourly totals observed at the Cape St. Francis WS were similar to those observed at the Thyspunt WS. Lower hourly totals at the Thyspunt WS were observed during the drier months of December and January. The highest hourly total observed at the Cape St. Francis WS was 37.4 mm (17 December 2022) and at the Thyspunt WS was 51.9 mm (17 March 2011).

© Eskom 2026/Rev 0c

PRINTED VERSIONS OF THIS DOCUMENT ARE NOT CONTROLLED

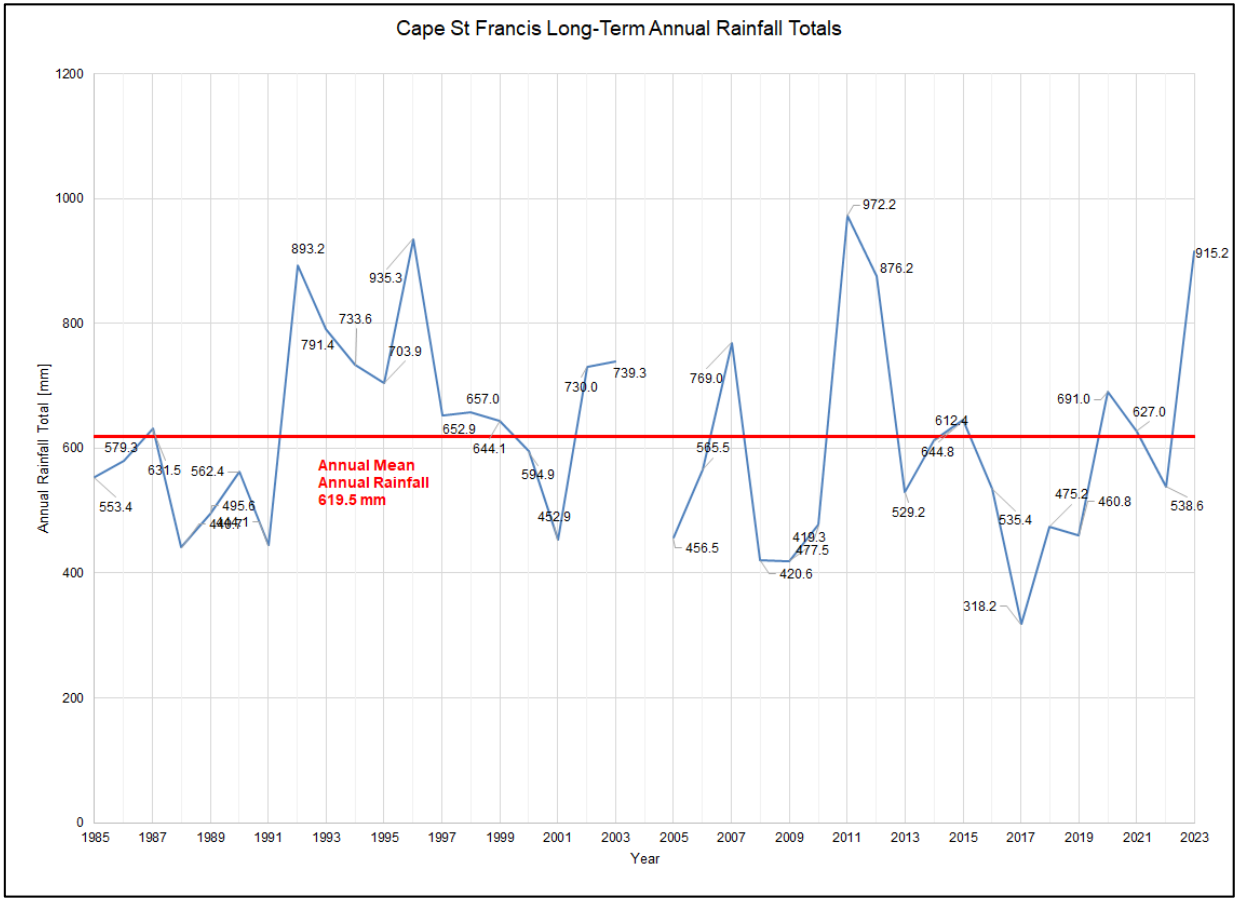


Figure 5.8.10
Annual Rainfall Totals at the Cape St. Francis WS

© Eskom 2026/Rev 0c

PRINTED VERSIONS OF THIS DOCUMENT ARE NOT CONTROLLED

Table 5.8.25
Average, Highest and Lowest Monthly Rainfall for Cape St. Francis WS, Humansdorp WS and Thyspunt WS

Month	Average Monthly [mm]				Highest Monthly [mm]				Lowest Monthly [mm]			
	Cape St. Francis		Humansdorp	Thyspunt	Cape St. Francis		Humansdorp	Thyspunt	Cape St. Francis		Humansdorp	Thyspunt
	(1)	(2)	(3)	(4)	(1)	(2)	(3)	(4)	(1)	(2)	(3)	(4)
January	31.1	21.1	39.9	24.8	104	70.2	176.1	48.2	0.0	4.4	2.8	11.0
February	34.1	25.7	42.5	41.8	188	49.4	217.0	77.3	3.0	7.4	1.8	18.6
March	45.6	49.2	57.9	48.4	257	173.4	250.3	169.7	1.0	0.4	1.4	0.5
April	55.5	46.3	53.7	53.2	173	104.4	193.3	101.3	1.0	8.2	2.3	7.9
May	67.7	55.2	53.8	68.3	251	209.2	261.2	245.5	0.1	7.0	0.5	20.7
June	69.4	66.2	48.8	106.7	215	212.2	270.2	199.7	0.0	15.8	0.8	29.2
July	72.3	78.8	50.0	98.0	198	224.2	238.3	353.2	6.0	2.4	4.9	10.8
August	76.1	82.7	60.2	77.8	185	213.0	465.0	192.4	0.0	9.4	0.3	10.5
September	64.7	43.7	59.8	52.6	366	121.2	341.5	122.4	3.4	11.2	6.0	1.1
October	64.2	52.5	65.1	86.8	209	167.6	487.7	208.6	7.0	8.4	2.4	34.4
November	50.4	41.5	57.7	57.6	188	117.2	263.5	121.6	1.0	3.8	4.8	23.4
December	37.3	32.4	41.4	31.9	176	138.0	244.3	81.0	4.0	0.4	2.5	6.5
Average	55.7	49.6	52.6	62.3	209	150.0	284.0	160.1	2.2	6.6	2.5	14.6
Highest	76.1	82.7	65.1	106.7	366	224.2	487.7	353.2	7.0	15.8	6.0	34.4
Lowest	31.1	21.1	39.9	24.8	104	49.4	176.1	48.2	0.0	0.4	0.3	0.5

Notes:
(1) The statistics included 1881 to 2003
(2) The statistics included the June 2004 to December 2023 data. Partial year for 2004 (15 June to 31 December) and subsequently excluded.
(3) The statistics included the May 1878 to December 2023 data.
(4) The statistics included the January 2008 to October 2013 and June 2017 to September 2019 data. Partial year for 2013 (1 January to 4 October). Partial year for 2017 (16 June to 31 December) and 2019 (1 January to 10 October).

© Eskom 2026/Rev 0c

PRINTED VERSIONS OF THIS DOCUMENT ARE NOT CONTROLLED

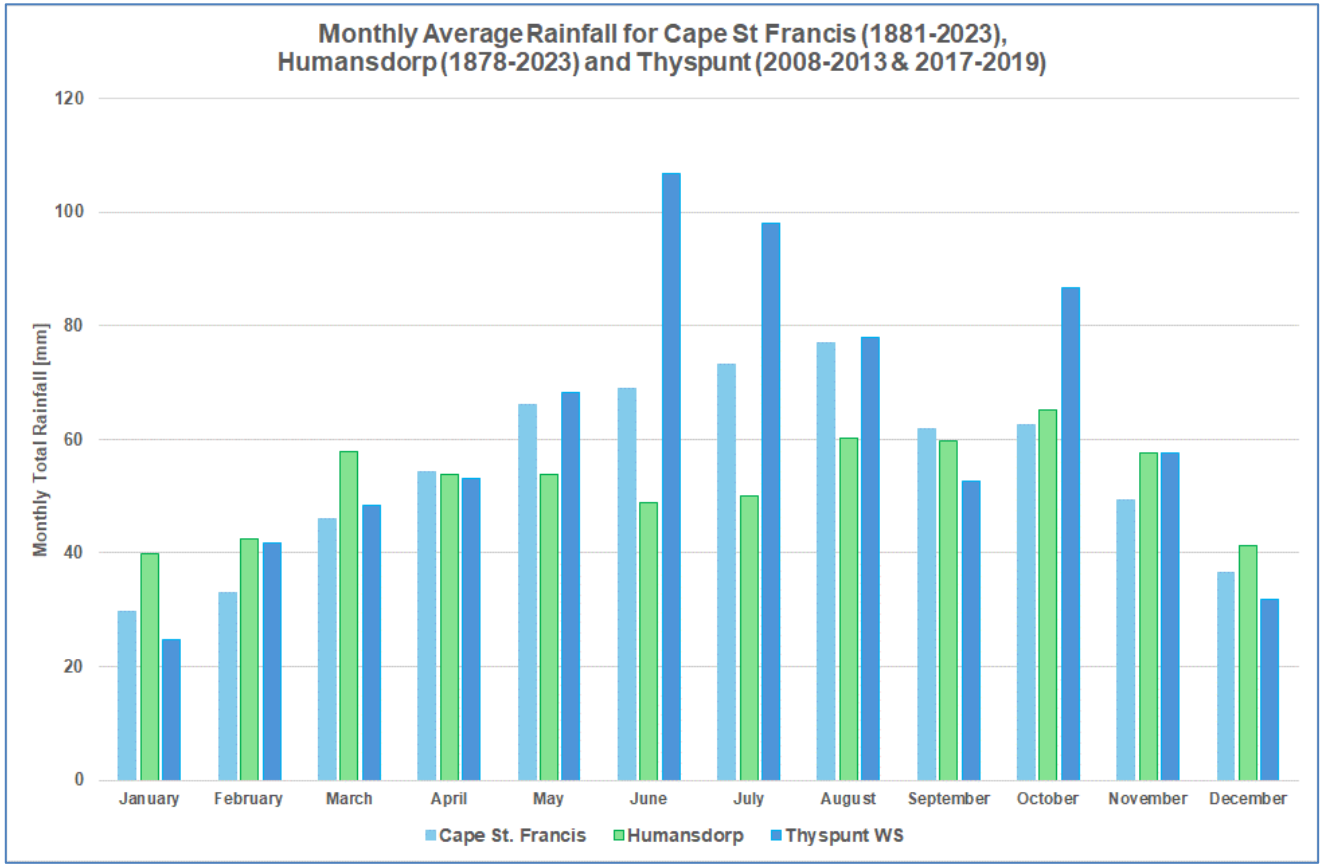


Figure 5.8.11
Monthly Rainfall Data at Cape St. Francis WS, Humansdorp WS and Thyspunt WS

© Eskom 2026/Rev 0c

PRINTED VERSIONS OF THIS DOCUMENT ARE NOT CONTROLLED

Table 5.8.26
Maximum 24-hour Rainfall [mm] for the Cape St. Francis, Thyspunt WS and the Humansdorp WS

Month	Cape St. Francis			Thyspunt WS	Humansdorp
	1881-1984 (1)	1985-2003 (2)	2004-2023 (2)	2008-2013 & 2017-2019 (3)	1878-2023 (2)
January	60.0	40.1	40.8	13.3	117.9
February	89.0	89.0	29.0	33.4	186.0
March	120.0	55.0	157.8	79.5	122.0
April	74.0	49.5	73.6	63.9	167.0
May	130.0	65.0	126.4	113.5	106.2
June	61.0	82.0	61.2	73.6	213.0
July	75.0	103.5	95.0	72.4	187.0
August	113.0	67.0	83.8	62.6	302.0
September	109.0	99.5	45.0	39.4	135.0
October	84.0	107.6	52.8	62.4	209.8
November	78.0	70.0	70.2	68.8	114.3
December	85.0	56.4	53.2	22.0	104.6
Annual	130.0	107.6	157.8	113.5	302.0

Notes:
(1) (Schulze, 1986)
(2) (SAWS, 2024b) (SAWS, 2024c)
(3) (Eskom, 2023a)

Table 5.8.27
Highest 1 hour Rainfall (mm) for the Cape St. Francis WS and the Thyspunt WS

Month	Cape St. Francis WS	Thyspunt WS
	2004-2023(1)	2008-2013 & 2017-2019 (2)
January	17.8	7.2
February	14.0	17.8
March	35.4	51.9
April	16.6	42.4
May	32.8	26.4
June	25.4	19.9
July	28.8	19.4
August	24.0	25.0
September	10.8	9.3
October	16.6	32.5
November	19.4	14.8
December	37.4	10.2

Notes:
(1) (SAWS, 2024c)
(2) (Eskom, 2023a)

© Eskom 2026/Rev 0c

PRINTED VERSIONS OF THIS DOCUMENT ARE NOT CONTROLLED

5.8.6.1.4 Droughts and Wet Years

The SAWS defines drought on the basis of two indices. The first index is based on the degree of dryness in comparison to normal or average amounts of rainfall for a particular area or place and the duration of the dry period. This is what is termed a meteorological drought, and the normal year would be calculated over a 30-year period.

Less than 75 per cent of normal rainfall is regarded as a severe meteorological drought but 80 per cent of normal rainfall will cause crop and water shortages. A wet year has 25 per cent more rainfall than the normal year (i.e. 125 per cent).

The drought and wet years as observed at the Cape St. Francis WS during the period 1985 to 2023 are provided in ***Figure 5.8.12***. During this period, six wet years (1992, 1993, 1996, 2011, 2012 and 2023) and seven drought years (1988, 1991, 2001, 2005, 2008, 2009 and 2017) were observed. Two years, 2007 and 2019 were on the cuff of being a wet and dry year, respectively. However, the disadvantage of this index is that it compares the rainfall deficit in the current month with rainfall for the same month in the history of the station and does not consider the cumulative effect of rainfall deficit.

The Standardised Precipitation Index (SPI) has been introduced in an attempt to alleviate this shortcoming and is based on the probability of rainfall for any time scale (or moving average window). The SPI calculation is based on the distribution of rainfall over long time periods (preferably more than 50 years). The long-term rainfall record is fitted to a probability distribution, which is then normalised so that the mean (average) SPI for any place and time period is zero. SPI values above zero indicate wetter periods and values less than 0 indicate drier periods.

The SPI values adopted at the SAWS (***Table 5.8.28***) are the same as those developed used by the World Meteorological Organization (WMO) (World Meteorological Organization, 2012). A drought event occurs any time the SPI is continuously negative and reaches an intensity of -1.0 or less. The event ends when the SPI becomes positive. Each drought event, therefore, has a duration defined by its beginning and end, and an intensity for each month that the event continues. The positive sum of the SPI for all the months within a drought event can be termed the drought's "magnitude".

© Eskom 2026/Rev 0c

PRINTED VERSIONS OF THIS DOCUMENT ARE NOT CONTROLLED

Table 5.8.28
SAWS and WMO Adopted SPI Values

SPI	Description
2.0 and more	Extremely wet
1.50 to 1.99	Very wet
1.00 to 1.49	Moderately wet
-0.99 to 0.99	Near normal
-1.00 to -1.49	Moderately dry
-1.50 to -1.99	Severely dry
-2.00 and less	Extremely dry

The timescales employed in the calculation reflect the impacts of drought on the needs of different water resources. Meteorological and soil moisture conditions (agriculture) respond to precipitation anomalies on relatively short timescales, for example 1-6 months, whereas streamflow, reservoirs, and groundwater respond to longer-term precipitation anomalies of the order of 6 months up to 24 months or longer.

The National Drought Mitigation Center-UNL developed the SPI Generator (NDMC, 2021), which allows the calculation of SPI for a given historical rainfall data set. Using the monthly rainfall totals for the 39-year period from 1985 to 2023, the 12-month timescale SPIs were calculated using the SPI Generator and summarised in ***Figure 5.8.13***. A 12-month SPI is a comparison of the precipitation for 12 consecutive months with that recorded in the same 12 consecutive months in all previous years of available data. Because these timescales are the cumulative result of shorter periods that may be above or below normal, the longer SPIs tend to gravitate toward zero unless a distinctive wet or dry trend is taking place.

During the 39-year historical period, five “extremely dry” years (1989, 2004, 2005, 2017 and 2018) were observed with two “extremely wet” years (1997 and 2012). “Near normal” rain years account for 33 per cent (13 years) of the historical period, followed by “very wet” years (18 per cent, i.e., 7 years), “severely dry” years and “extremely dry” years (14 per cent, i.e., 5 years), and “moderately dry” years (10 per cent, i.e., 4 years). “Moderately wet” and “extremely wet” years account for 8 per cent (3 years each) and 5 per cent (2 years), respectively.

© Eskom 2026/Rev 0c

PRINTED VERSIONS OF THIS DOCUMENT ARE NOT CONTROLLED

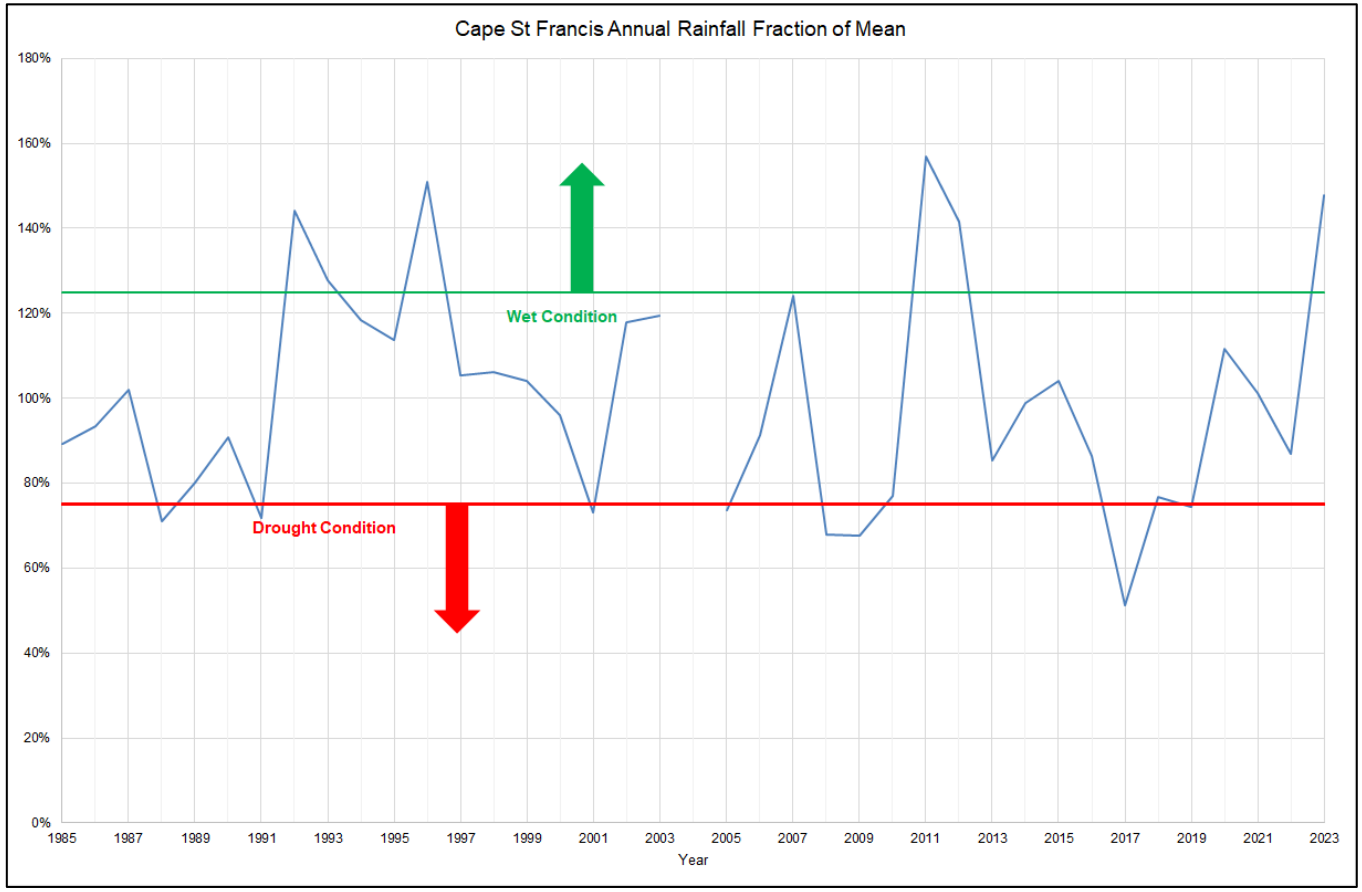


Figure 5.8.12
Dry and Wet Rainfall Periods Observed at Cape St. Francis WS

© Eskom 2026/Rev 0c

PRINTED VERSIONS OF THIS DOCUMENT ARE NOT CONTROLLED

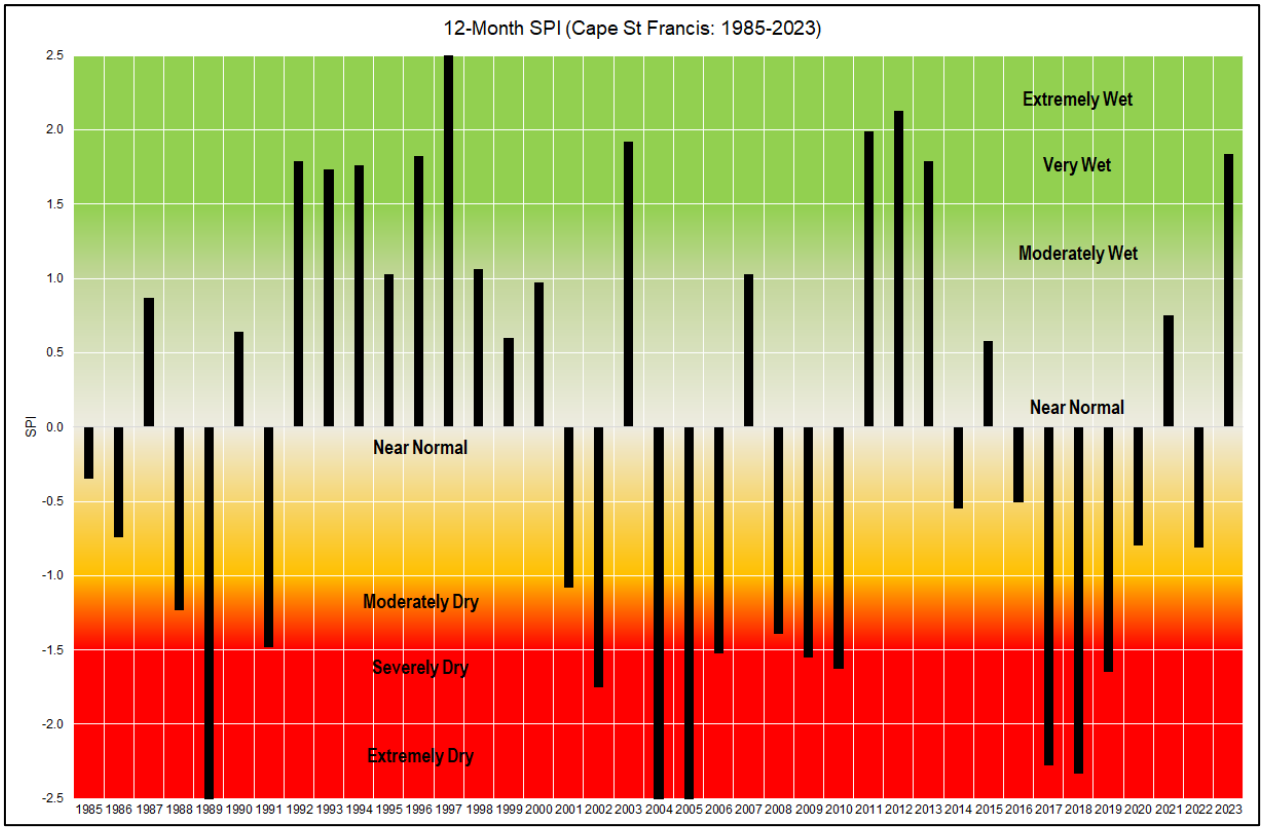


Figure 5.8.13
Dry and Wet Rainfall Periods at the Cape St. Francis WS

5.8.6.1.5 Thunder, Hail, Snow and Fog

SAWS climate data for Cape St. Francis (1881-1984) (Schulze, 1986) were used to determine the average number of days that thunder, hail, snow and fog occur. Whereas the occurrence of fog may be estimated from the measured dry- and calculated dew point temperatures, thunder, hail and snow must be physically observed (thunder and hail) or measured (snow). By pure definition of the dewpoint temperature, a fog event was estimated to have occurred at the Thyspunt WS when the dry-bulb and dew point temperatures are near equal[34] and no rainfall measured at the same time.

[34] To allow for uncertainty in the calculation of the dew point temperature from the dry-bulb temperature and the relative humidity, an allowance of 0.075°C was used, based on the median error of 0.384 per cent for the formula for the dewpoint temperature (see ***Section 5.8.6.1.2***).

© Eskom 2026/Rev 0c

PRINTED VERSIONS OF THIS DOCUMENT ARE NOT CONTROLLED

According to the SAWS, the observations for the period from 1985 to 2003 were unreliable and were not included in the analyses. Furthermore, since the changeover to an automatic weather station in 2004, these parameters could no longer be observed. The results of the data analysis are presented below and summarised in ***Table-5.8.29*** (Schulze, 1986) and the following are observed:

- thunder – The occurrence of thunder shows no particular preference towards a season or month.
- hail – Hail tends to mainly occur during the winter months of May, June, July and August.
- snow – No snow falls were recorded at Cape St. Francis for the period 1881 – 1984.
- avalanches – Since no snow has been recorded to date, there is no record of avalanches occurring at the site.
- blizzards – Since no snow has been recorded to date, there is no record of blizzards occurring at the site.
- ice and ice cover – Since the air and sea temperatures never reaches freezing point, no ice and ice covers have been reported.
- fog – Fog appears to occur more frequently during the summer months, with the highest frequency during March at Cape St Francis, but as calculated for Thyspunt WS, also during September.

© Eskom 2026/Rev 0c

PRINTED VERSIONS OF THIS DOCUMENT ARE NOT CONTROLLED

Table 5.8.29
Average Number of Days with Thunder, Hail, Snow and Fog at Cape St. Francis (1881-1984) and Fog Estimate at Thyspunt WS (2008-2013 & 2017-2019)

Month	Thunder	Hail	Snow	Fog	
				Cape St Francis	Thyspunt WS
January	0.6	0.0	0.0	2.0	3.0
February	0.7	0.0	0.0	4.0	2.5
March	1.0	0.0	0.0	4.8	3.1
April	0.8	0.0	0.0	2.8	2.0
May	0.7	0.2	0.0	1.1	0.5
June	0.3	0.1	0.0	0.2	0.4
July	0.3	0.2	0.0	0.5	0.6
August	0.4	0.2	0.0	0.8	3.6
September	0.5	0.0	0.0	1.0	3.9
October	0.8	0.1	0.0	2.4	3.3
November	0.6	0.0	0.0	2.1	1.0
December	0.5	0.0	0.0	2.6	1.5
Annual	7.2	0.8	0.0	24.3	25.4

5.8.6.1.6 Atmospheric Moisture

Measurements of relative humidity were performed for the period January 2008 to October 2013 and June 2017 to September 2019 at the Thyspunt WS. A summary of the monthly and annual statistics is provided in ***Table 5.8.30***. As a comparison, data from the SAWS weather station at Cape St. Francis for the period 2004 to 2023 are also included in the table.

The annual average relative humidity recorded was 76.9 per cent at the Thyspunt WS and 79.0 per cent at the Cape St. Francis WS.

The lowest daily average relative humidity recorded at the Thyspunt WS was during July (66.9 per cent) and during June at the Cape St. Francis WS (72.6 per cent). The highest daily average relative humidity at the Thyspunt WS and Cape St. Francis WS was recorded during February at both sites, i.e. 83.5 per cent and 84.1 per cent, respectively.

The relative humidity during summer at a dry bulb temperature of 37 ºC was 17.6 per cent at the Thyspunt WS and 14.7 per cent at the Cape St. Francis WS. At the coldest hourly temperature during winter 6.6 °C (Thyspunt WS) and 4.9 °C (Cape St. Francis WS), the relative humidity was 78.6 per cent at the Thyspunt WS and 81.0 per cent at the Cape St Francis WS.

© Eskom 2026/Rev 0c

PRINTED VERSIONS OF THIS DOCUMENT ARE NOT CONTROLLED

Table 5.8.30
Daily Average, Daily Maximum and Minimum Relative Humidity (%) for the Cape St. Francis WS and the Thyspunt WS

Month	Cape St. Francis WS 2004-2023			Thyspunt WS 2008-2013 & 2017-2019		
	Ave	Min	Max	Ave	Min	Max
January	83.2	69.7	94.7	83.1	64.3	97.7
February	84.1	64.5	94.9	83.5	65.9	99.1
March	83.3	66.6	95.0	83.2	62.6	96.6
April	82.1	63.3	94.7	79.3	57.1	95.2
May	78.8	59.0	93.7	74.9	49.9	93.1
June	72.6	46.1	91.5	70.7	41.1	93.8
July	75.5	49.5	93.9	66.9	40.3	91.3
August	77.8	54.7	95.6	74.8	50.3	98.5
September	77.9	58.7	95.5	77.7	47.9	99.9
October	75.9	63.4	97.5	74.4	54.8	98.4
November	77.2	64.0	93.1	72.8	58.3	95.4
December	80.0	64.5	95.1	82.0	64.1	96.4
Annual	79.0	46.1	97.5	76.9	40.3	99.9

5.8.6.1.7 Barometric Pressure

A summary of the barometric pressure measured at the Thyspunt WS (January 2008 to October 2013 and June 2017 to September 2019 October 1997 to September 2023) as well as at the Cape St. Francis WS (2005 to 2023) is provided in ***Table 5.8.31*** (daily average and average of daily maximum and minimum) and ***Table 5.8.32*** (maximum and minimum hourly). The corresponding mean sea level barometric pressure is provided in ***Table 5.8.33*** (daily average and average of daily maximum and minimum) and ***Table 5.8.34*** (maximum and minimum hourly).

Summer coastal lows are clearly observed with monthly average barometric pressures at the Thyspunt WS (***Table 5.8.31***) of 1006.8 hPa (January), 1007.0 hPa (February) and 1007.2 hPa (December), and mean sea level barometric pressures (***Table 5.8.33***) of 1013.0 hPa (January), 1013.2 hPa (February) and 1013.4 hPa (December). Conversely, winter stagnant high pressures are observed with monthly average barometric pressures at the Thyspunt WS (***Table 5.8.31***) of 1012.2 hPa (June), 1014.4 hPa (July) and 1012.2 hPa (August), and mean sea level barometric pressures (***Table 5.8.33***) of 1018.5 hPa (June), 1020.8 hPa (July) and 1018.5 hPa (August).

The lowest and highest daily barometric pressures measured at the Thyspunt WS were 992.9 hPa and 1030.8 hPa. The measured lowest and highest hourly barometric pressure at the Thyspunt WS were 992.9 hPa and 1030.8 hPa, with an annual average of 1010.0 hPa. The lowest and highest

© Eskom 2026/Rev 0c

PRINTED VERSIONS OF THIS DOCUMENT ARE NOT CONTROLLED

daily mean sea level barometric pressures measured at the Thyspunt WS were 999.1 hPa and 1037.4 hPa. The measured lowest and highest hourly mean sea level barometric pressure at the Thyspunt WS were 994.1 hPa and 1040.6 hPa, with an annual average of 1016.3 hPa.

For comparison, the mean sea level barometric pressures observed at the Cape St. Francis WS (***Table 5.8.33***) during the summer lows were 1014.4 hPa (January), 1014.4 hPa (February) and 1015.0 hPa (December). The winter stagnant high mean sea level barometric pressures observed at the Cape St. Francis WS (***Table 5.8.33***) were 1019.5 hPa (June), 1021.5 hPa (July) and 1019.5 hPa (August).

During spring and autumn, the pressures are similar with the lower mean sea level barometric pressures at the end of spring (monthly average 1015.0 hPa at Thyspunt WS and 1016.0 hPa at Cape St. Francis WS for November) and the start of autumn (monthly average of 1014.7 hPa at Thyspunt WS and 1015.8 hPa at Cape St. Francis WS for March). Conversely, barometric pressures are higher at the beginning of spring (monthly average of 1017.7 hPa at Thyspunt WS and 1019.5 hPa at Cape St. Francis WS for September) and the end of autumn (monthly average of 1016.2 hPa at Thyspunt WS and 1018.0 hPa at Cape St. Francis WS for May).

Table 5.8.31
Daily Average, Daily Maximum and Minimum Barometric Pressure (hPa) for the Cape St. Francis WS and the Thyspunt WS

Month	Cape St. Francis WS			Thyspunt WS		
	2004-2023			2008-2013 & 2017-2019		
	Ave	Min	Max	Ave	Min	Max
January	1013.3	1009.2	1017.7	1006.8	1002.8	1010.9
February	1013.3	1008.7	1018.1	1007.0	1002.6	1011.7
March	1014.7	1010.3	1019.5	1008.4	1004.2	1013.7
April	1016.9	1012.1	1021.7	1010.2	1005.9	1013.6
May	1016.9	1011.2	1023.1	1009.9	1005.9	1015.0
June	1018.6	1012.6	1025.3	1012.2	1007.0	1018.1
July	1020.4	1012.9	1027.2	1014.4	1006.8	1020.3
August	1018.6	1011.9	1024.0	1012.2	1005.9	1017.7
September	1018.3	1010.7	1034.3	1011.4	1005.1	1016.6
October	1017.1	1011.3	1022.6	1010.6	1005.3	1016.0
November	1015.0	1009.8	1019.8	1008.7	1003.7	1013.5
December	1013.8	1009.7	1018.3	1007.2	1003.9	1011.2
Annual	1016.2	1008.7	1034.3	1010.1	1002.6	1020.3

© Eskom 2026/Rev 0c

PRINTED VERSIONS OF THIS DOCUMENT ARE NOT CONTROLLED

Table 5.8.32
Hourly Maximum and Minimum Barometric Pressure [hPa] for the Cape St. Francis WS and the Thyspunt WS

Month	Cape St. Francis WS		Thyspunt WS	
	2004-2023		2008-2013 & 2017-2019	
	Min	Max	Min	Max
January	997.2	1027.2	991.3	1019.1
February	995.1	1027.9	991.0	1020.0
March	1001.8	1031.1	997.0	1024.0
April	996.9	1034.4	993.3	1026.0
May	995.7	1034.1	991.0	1024.4
June	994.3	1036.2	989.0	1028.2
July	995.1	1041.1	989.4	1032.3
August	994.0	1040.2	988.0	1034.0
September	999.0	1050.0	993.1	1030.0
October	996.6	1035.6	990.6	1028.1
November	996.9	1032.8	991.6	1023.4
December	996.0	1030.4	991.0	1021.3
Annual	994.0	1050.0	988.0	1034.0

Table 5.8.33
Daily Average, Daily Maximum and Minimum Mean Sea Level Barometric Pressure [hPa] for the Cape St. Francis WS and the Thyspunt WS

Month	Cape St. Francis WS			Thyspunt WS		
	2004-2023			2008-2013 & 2017-2019		
	Ave	Min	Max	Ave	Min	Max
January	1014.4	1010.2	1018.8	1013.0	1008.9	1010.9
February	1014.4	1010.3	1019.2	1013.2	1008.7	1011.7
March	1015.8	1011.4	1020.5	1014.7	1010.3	1013.7
April	1018.1	1013.7	1022.8	1016.5	1012.1	1013.6
May	1018.0	1012.3	1024.2	1016.2	1012.1	1015.0
June	1019.5	1012.0	1026.4	1018.5	1013.3	1018.1
July	1021.5	1014.0	1028.3	1020.8	1013.1	1020.3
August	1019.5	1013.0	1025.1	1018.5	1012.2	1017.7
September	1019.5	1011.8	1035.4	1017.7	1011.3	1016.6
October	1018.1	1012.4	1023.3	1016.9	1011.5	1016.0
November	1016.0	1010.9	1020.7	1015.0	1009.9	1013.5
December	1015.0	1010.7	1019.7	1013.4	1010.1	1011.2
Annual	1017.0	1010.2	1035.4	1015.7	1008.7	1020.3

© Eskom 2026/Rev 0c

PRINTED VERSIONS OF THIS DOCUMENT ARE NOT CONTROLLED

Table 5.8.34
Hourly Maximum and Minimum Mean Sea Level Barometric Pressure [hPa] for the Cape St. Francis WS and the Thyspunt WS

Month	Cape St. Francis WS		Thyspunt WS	
	2004-2023		2008-2013 & 2017-2019	
	Min	Max	Min	Max
January	1001.2	1028.3	997.3	1025.5
February	996.1	1029.0	996.9	1026.3
March	1002.8	1032.2	1003.1	1030.4
April	997.9	1035.5	999.4	1032.4
May	996.8	1035.2	997.1	1030.8
June	995.3	1037.3	995.1	1034.6
July	996.2	1042.2	995.5	1038.7
August	995.1	1041.3	994.1	1040.6
September	1000.0	1051.1	999.2	1036.5
October	1000.0	1036.7	996.6	1034.5
November	997.9	1033.9	997.8	1029.8
December	997.0	1031.5	997.1	1027.7
Annual	995.1	1051.1	994.1	1040.6

5.8.6.1.8 Solar Radiation

Systematic solar radiation measurements in southern Africa started in the 1950s (Clemence, 1992). Based on this work a solar radiation atlas for South Africa was developed (Schulze, 1997). According to this atlas, the site should typically experience solar radiation with:

- a maximum value of about 26 MJ/m^2.day in December and 25 MJ/m^2 for January and November;
- a minimum value of about 11 MJ/m^2.day in June.

The actual solar radiation readings at the Thyspunt WS for January 2008 to October 2013 and June 2017 to September 2019 October 1997 observed slightly lower values (Eskom, 2023a), as shown in ***Table 5.8.35***. In comparison, average daily total solar radiation measurement for December was 24 MJ/m^2.day and for January was 23.9 MJ/m^2.day and 9.2 MJ/m^2.day for June.

The highest daily solar radiation was recorded in November with 26.3 MJ/m^2.day and the lowest daily solar radiation of 8.4 MJ/m^2.day was during June.

© Eskom 2026/Rev 0c

PRINTED VERSIONS OF THIS DOCUMENT ARE NOT CONTROLLED

Table 5.8.35
Solar Radiation at the Thyspunt WS (2008-2013 & 2017-2019) Compared with Schulze's Atlas for the Thyspunt Region

Month	Average Daily Total ($MJ/m^2.day$)		Thyspunt WS	
	Schulze's Atlas[1]	Thyspunt WS	Highest Daily Total ($MJ/m^2.day$)	Lowest Daily Total ($MJ/m^2.day$)
January	25	23.9	25.1	22.9
February	23	21.2	23.6	19.2
March	20	18.3	20.2	16.9
April	17	14.0	15.5	12.3
May	13	11.0	11.7	10.1
June	11	9.2	9.8	8.4
July	13	10.3	11.2	9.0
August	15	13.4	14.6	12.1
September	20	17.3	18.7	15.1
October	23	20.0	21.2	17.4
November	25	23.6	26.3	21.2
December	26	24.0	25.7	20.8

Notes:
(1) (Schulze, 1997)

5.8.6.1.9 Atmospheric Stability

The atmospheric boundary layer includes the first few hundred metres of the atmosphere. This layer is directly affected by the earth's surface, either through the retardation of flow due to the frictional drag of the earth's surface, or as result of the heat and moisture exchanges that take place at the surface (Stull, 1997).

During the daytime, the atmospheric boundary layer is characterised by thermal turbulence due to the heating of the earth's surface and the extension of the mixing layer to the lowest elevated inversion. Radiative flux divergence during the night usually results in the establishment of ground-based inversions. Night-time is characterised by weak vertical mixing and the predominance of a stable layer. These conditions are normally associated with low wind speeds, hence less dilution potential (Stull, 1997).

The mixed layer ranges in depth from a few metres (i.e. stable or neutral layers) during night-time to the base of the lowest-level elevated inversion during unstable, day-time conditions. Elevated inversions may occur for a variety of reasons and on some occasions as many as five may occur in the first 1 000 m above the surface (Tyson , et al., 1976).

The southern and western coastal areas experience a persistent low-level subsidence inversion, termed the sub-escarpment layer, with its base at approximately 500 m and a thickness of about 600 m. This layer is due to

© Eskom 2026/Rev 0c

PRINTED VERSIONS OF THIS DOCUMENT ARE NOT CONTROLLED

the predominance of the South Atlantic High Pressure (HP) system, and represents the boundary between the dry, subsided upper air and the moist influx of maritime air. The height above ground surface of this layer is related to the thickness of the sea breeze system and the intensity of subsidence in the upper air. The strength of the inversion has been shown to vary between an average of 7°C in summer and 5.2°C in winter (Tyson , et al., 1976; Preston-Whyte, et al., 1977). The sub-escarpment inversion is stronger and occurs more frequently during the summer (51 per cent) due to the South Atlantic HP reaching its most easterly position during December (Tyson , et al., 1976).

Based on the temperature gradient between the 2 m and 8 m levels, it is estimated that surface inversions occurred for approximately 30 per cent over the year (Eskom, 2023a), with the most prevalent during winter months with a 51 per cent frequency of occurrence during June and 45 per cent during May and July (Eskom, 2023a). As expected, summer occurrences are significantly lower ranging from 17 per cent in December to 18 per cent in March (Eskom, 2023a).

Eskom Standard 238-52 (Eskom, 2022a) requires that the atmosphere be classified into one of seven atmospheric stability classes suggested by Pasquill in 1961 (Pasquill, 1961) and later modified by Gifford in 1962 (Gifford, 1961). The seven stability classes are described as follows:

A: Very unstable or convective conditions. Calm wind, clear skies and hot day-time conditions.

B: Moderately unstable. Clear skies, day-time conditions.

C: Unstable conditions. Moderate wind, slightly overcast day-time conditions.

D: Neutral atmospheres. Strong winds or cloudy days and nights.

E: Stable conditions. Moderate wind and slightly overcast night-time conditions.

F: Moderately stable conditions. Low winds, clear skies, cold night-time conditions.

G: Very stable conditions. Calm winds, clear skies, cold night-time conditions.

The frequencies of atmospheric stability classes were calculated according to the Eskom Standard 238-52 (Eskom, 2022a). Both the Thyspunt WS vertical temperature difference between levels 2 m and 8 m (‘delta-T method’) (2017 to 2019) and the standard deviations of the wind direction (‘sigma-theta method’) (2008-2013 & 2017-2019) were used to calculate the atmospheric stability classes.

© Eskom 2026/Rev 0c

PRINTED VERSIONS OF THIS DOCUMENT ARE NOT CONTROLLED

The results of the classification are summarised in ***Table 5.8.36*** (delta-T method) and ***Table 5.8.37*** (sigma-theta method). Using the delta-T method, the most prevalent atmospheric condition at the Thyspunt WS was observed to be very unstable (stability class A) with 55.97 per cent. However, using the sigma-theta method, the most prevalent atmospheric conditions at the Thyspunt WS was observed to be slightly stable (stability class E) with 46.14 per cent and neutral (stability class D) with 40.89 per cent.

The delta-T method for the Thyspunt WS resulted in very different classifications compared with the sigma-theta method. This is primarily due to the steep temperature gradient normally observed close to the ground – hence the requirement for temperature measurements at higher levels in the surface layer depth. The sigma-theta method is therefore more suitable for stability classification at the Thyspunt WS. The delta-T method is preferred for establishing the vertical atmospheric stability, but only if the two temperatures adequately represent the conditions in the surface layer. The two temperatures at 2 m and 8 m on the Thyspunt WS mast only observe a small part of the surface layer, i.e. the section with the steepest vertical temperature gradient. In this case, it is therefore more advisable to utilise the sigma-theta method, or the solar radiation/delta-T (SRDT) method as recommended by the US EPA (United States Environmental Protection Agency, 2000) and ANS (American National Standard, 2015). The SRDT method uses the surface layer wind speed (measured at or near 10 m) in combination with measurements of total solar radiation during the day and a low-level vertical temperature difference (delta-T) at night.

The atmospheric stability changes per hour of day depending on both the thermal (buoyant) production and mechanical turbulence (Stull, 1997). The ratio of the buoyant production to mechanical production of turbulence is expressed as a measure for dynamic stability through the Richardson (Ri) number (Stull, 1997). Several formulations exist for the Ri number, with the most common being flux-, gradient-, bulk- and surface-layer Ri number. The flux and gradient Ri number require both vertical temperature and wind speed gradient measurements, whereas with the bulk and surface-layer Ri number a finite difference approximation is used for the gradients. The bulk Ri number is calculated using wind speeds and temperatures at the two vertical levels, whereas only the wind speed at one height and the average temperature gradient between this height and the ground are required. Given the available measurements at the Thyspunt WS, the surface layer Ri number was calculated to classify atmospheric stability.

Although the SRDT and Ri number methods are not included in the Eskom Standard 238-52 (Eskom, 2022a), the stability classes calculated using these two methods are provided in ***Table 5.8.38*** (SRDT method) and ***Table 5.8.39*** (Ri number method) for comparative purposes.

© Eskom 2026/Rev 0c

PRINTED VERSIONS OF THIS DOCUMENT ARE NOT CONTROLLED

Table 5.8.36
Joint Frequency Distribution of Pasquill-Gifford Stability Classes with Wind Direction: Thyspunt WS
(Delta-T Method [8m/2m] – (Eskom, 2022a))

Wind Direction	Stability Classification							
	A	B	C	D	E	F	G	Total
N	0.52%	0.01%	0.00%	0.06%	0.12%	0.23%	1.73%	2.68%
NNE	0.59%	0.01%	0.00%	0.09%	0.28%	0.77%	1.95%	3.69%
NE	1.81%	0.05%	0.07%	0.41%	1.14%	0.92%	0.86%	5.27%
ENE	5.48%	0.23%	0.23%	1.18%	1.45%	0.46%	0.50%	9.53%
E	4.08%	0.13%	0.10%	0.43%	0.41%	0.14%	0.13%	5.41%
ESE	3.49%	0.03%	0.02%	0.12%	0.11%	0.03%	0.03%	3.84%
SE	2.06%	0.01%	0.01%	0.07%	0.06%	0.05%	0.00%	2.26%
SSE	1.15%	0.01%	0.02%	0.11%	0.10%	0.10%	0.05%	1.55%
S	1.34%	0.01%	0.00%	0.09%	0.12%	0.10%	0.02%	1.67%
SSW	1.55%	0.00%	0.00%	0.10%	0.17%	0.12%	0.04%	1.99%
SW	2.82%	0.03%	0.02%	0.14%	0.22%	0.12%	0.06%	3.42%
WSW	10.05%	0.12%	0.16%	0.59%	0.52%	0.23%	0.10%	11.77%
W	14.45%	0.64%	0.54%	2.08%	1.51%	0.61%	0.36%	20.18%
WNW	3.66%	0.23%	0.26%	1.36%	3.06%	2.70%	2.06%	13.34%
NW	1.91%	0.11%	0.10%	0.45%	1.29%	1.94%	2.42%	8.23%
NNW	1.00%	0.01%	0.02%	0.15%	0.72%	1.06%	2.20%	5.16%
Total	55.97%	1.65%	1.58%	7.41%	11.28%	9.58%	12.53%	100%

© Eskom 2026/Rev 0c

PRINTED VERSIONS OF THIS DOCUMENT ARE NOT CONTROLLED

Table 5.8.37
Joint Frequency Distribution of Pasquill-Gifford Stability Classes with Wind Direction: Thyspunt WS
(Sigma-Theta Method [9 m] – (Eskom, 2022a))

Wind Direction	Stability Classification							
	A	B	C	D	E	F	G	Total
N	0.26%	0.10%	0.33%	1.03%	1.07%	0.01%	0.00%	2.80%
NNE	0.27%	0.11%	0.24%	0.70%	2.23%	0.02%	0.00%	3.58%
NE	0.27%	0.16%	0.29%	1.34%	3.39%	0.01%	0.00%	5.46%
ENE	0.24%	0.13%	0.44%	3.26%	5.47%	0.03%	0.00%	9.57%
E	0.18%	0.15%	0.36%	3.34%	2.18%	0.00%	0.00%	6.21%
ESE	0.13%	0.09%	0.21%	1.00%	2.72%	0.00%	0.00%	4.14%
SE	0.13%	0.07%	0.19%	1.13%	0.95%	0.00%	0.00%	2.46%
SSE	0.11%	0.07%	0.20%	0.46%	0.49%	0.00%	0.00%	1.32%
S	0.11%	0.07%	0.26%	0.50%	0.50%	0.00%	0.00%	1.44%
SSW	0.14%	0.07%	0.26%	0.66%	0.56%	0.00%	0.00%	1.69%
SW	0.14%	0.07%	0.22%	1.13%	1.29%	0.00%	0.00%	2.85%
WSW	0.22%	0.12%	0.31%	3.78%	5.24%	0.01%	0.00%	9.69%
W	0.28%	0.17%	0.58%	16.95%	2.75%	0.02%	0.00%	20.76%
WNW	0.32%	0.17%	0.41%	3.75%	7.58%	1.52%	0.00%	13.76%
NW	0.31%	0.14%	0.28%	0.89%	6.34%	0.93%	0.00%	8.90%
NNW	0.22%	0.14%	0.29%	0.98%	3.40%	0.35%	0.00%	5.38%
Total	3.33%	1.84%	4.88%	40.89%	46.14%	2.92%	0.01%	100%

© Eskom 2026/Rev 0c

PRINTED VERSIONS OF THIS DOCUMENT ARE NOT CONTROLLED

Table 5.8.38
Joint Frequency Distribution of Pasquill-Gifford Stability Classes with Wind Direction: Thyspunt WS
(SRDT Method – (United States Environmental Protection Agency, 2000))

Wind Direction	Stability Classification							
	A	B	C	D	E	F	G	Total
N	0.00%	0.05%	0.17%	2.29%	0.09%	0.08%	0.00%	2.68%
NNE	0.00%	0.05%	0.28%	3.15%	0.12%	0.09%	0.00%	3.69%
NE	0.00%	0.09%	0.52%	4.44%	0.08%	0.13%	0.00%	5.27%
ENE	0.00%	0.14%	0.72%	8.55%	0.05%	0.07%	0.00%	9.53%
E	0.00%	0.12%	0.56%	4.67%	0.03%	0.03%	0.00%	5.41%
ESE	0.03%	0.23%	1.04%	2.51%	0.01%	0.01%	0.00%	3.84%
SE	0.03%	0.46%	1.01%	0.74%	0.01%	0.00%	0.00%	2.26%
SSE	0.02%	0.40%	0.33%	0.79%	0.01%	0.00%	0.00%	1.55%
S	0.02%	0.38%	0.41%	0.84%	0.00%	0.01%	0.00%	1.67%
SSW	0.01%	0.56%	0.57%	0.84%	0.00%	0.01%	0.00%	1.99%
SW	0.01%	0.47%	1.26%	1.66%	0.01%	0.00%	0.00%	3.42%
WSW	0.02%	0.31%	2.69%	8.71%	0.00%	0.03%	0.00%	11.77%
W	0.00%	0.05%	1.19%	18.88%	0.02%	0.04%	0.00%	20.18%
WNW	0.00%	0.04%	0.66%	12.46%	0.09%	0.08%	0.00%	13.34%
NW	0.00%	0.08%	0.45%	7.50%	0.07%	0.13%	0.00%	8.23%
NNW	0.00%	0.03%	0.26%	4.70%	0.07%	0.10%	0.00%	5.16%
Total	0.16%	3.48%	12.12%	82.72%	0.69%	0.82%	0.00%	100%

© Eskom 2026/Rev 0c

PRINTED VERSIONS OF THIS DOCUMENT ARE NOT CONTROLLED

Table 5.8.39
Joint Frequency Distribution of Pasquill-Gifford Stability Classes with Wind Direction: Thyspunt WS
(Richardson Number Method – (Stull, 1997))

Wind Direction	Stability Classification							
	A	B	C	D	E	F	G	Total
N	0.00%	0.00%	0.04%	0.56%	1.92%	0.15%	0.00%	2.68%
NNE	0.00%	0.00%	0.06%	0.72%	2.74%	0.18%	0.00%	3.69%
NE	0.01%	0.01%	0.11%	2.45%	2.51%	0.17%	0.00%	5.27%
ENE	0.01%	0.00%	0.02%	7.62%	1.75%	0.12%	0.00%	9.53%
E	0.03%	0.01%	0.03%	4.79%	0.49%	0.05%	0.00%	5.41%
ESE	0.03%	0.00%	0.07%	3.59%	0.12%	0.02%	0.00%	3.84%
SE	0.04%	0.02%	0.05%	2.04%	0.09%	0.00%	0.00%	2.26%
SSE	0.03%	0.00%	0.07%	1.23%	0.22%	0.01%	0.00%	1.55%
S	0.03%	0.00%	0.06%	1.36%	0.21%	0.01%	0.00%	1.67%
SSW	0.01%	0.01%	0.07%	1.61%	0.28%	0.01%	0.00%	1.99%
SW	0.02%	0.01%	0.07%	2.96%	0.36%	0.00%	0.00%	3.42%
WSW	0.02%	0.00%	0.06%	11.04%	0.60%	0.05%	0.00%	11.77%
W	0.02%	0.00%	0.02%	18.24%	1.81%	0.08%	0.00%	20.18%
WNW	0.01%	0.01%	0.04%	6.21%	6.90%	0.16%	0.00%	13.34%
NW	0.02%	0.00%	0.04%	2.76%	5.20%	0.21%	0.00%	8.23%
NNW	0.00%	0.00%	0.01%	1.27%	3.66%	0.21%	0.00%	5.16%
Total	0.31%	0.11%	0.84%	68.44%	28.85%	1.45%	0.00%	100%

© Eskom 2026/Rev 0c

PRINTED VERSIONS OF THIS DOCUMENT ARE NOT CONTROLLED

Table 5.8.40
Joint Frequency Distribution of Pasquill-Gifford Stability Class A with Wind Direction and Wind Speed: Thyspunt WS
(Sigma-Theta Method [9 m] – (Eskom, 2022a))

Wind Direction	Wind Speed [m/s] at 9 m level, Sigma-Theta Method											
	<0.5	0.5-1.0	1.0-2.0	2.0-3.0	3.0-4.0	4.0-5.0	5.0-6.0	6.0-8.0	8.0-10.0	10.0-13.0	13.0-18.0	>18.0
N	0.26%	0.68%	3.17%	2.10%	0.86%	0.43%	0.21%	0.17%	0.00%	0.00%	0.00%	0.00%
NNE	0.30%	1.24%	3.08%	2.10%	0.90%	0.21%	0.17%	0.17%	0.00%	0.00%	0.00%	0.00%
NE	0.47%	1.16%	2.65%	1.97%	0.98%	0.60%	0.13%	0.04%	0.00%	0.00%	0.00%	0.00%
ENE	0.30%	0.98%	2.61%	1.54%	0.98%	0.56%	0.21%	0.09%	0.00%	0.00%	0.00%	0.00%
E	0.26%	0.77%	1.80%	0.94%	1.03%	0.43%	0.13%	0.09%	0.00%	0.00%	0.00%	0.00%
ESE	0.26%	0.51%	1.76%	0.94%	0.30%	0.04%	0.04%	0.00%	0.00%	0.00%	0.00%	0.00%
SE	0.13%	0.68%	1.63%	0.94%	0.39%	0.09%	0.00%	0.00%	0.00%	0.00%	0.00%	0.00%
SSE	0.26%	0.34%	1.46%	0.90%	0.26%	0.00%	0.04%	0.04%	0.00%	0.00%	0.00%	0.00%
S	0.39%	0.68%	0.86%	0.81%	0.26%	0.17%	0.09%	0.00%	0.04%	0.00%	0.00%	0.00%
SSW	0.13%	0.81%	1.84%	0.73%	0.30%	0.13%	0.13%	0.00%	0.04%	0.00%	0.00%	0.00%
SW	0.13%	0.68%	1.46%	0.81%	0.51%	0.26%	0.21%	0.04%	0.04%	0.00%	0.00%	0.00%
WSW	0.30%	0.86%	2.31%	1.58%	1.07%	0.17%	0.13%	0.04%	0.09%	0.00%	0.00%	0.00%
W	0.26%	0.47%	3.21%	2.40%	1.16%	0.47%	0.26%	0.21%	0.00%	0.04%	0.00%	0.00%
WNW	0.34%	0.86%	3.34%	2.53%	0.98%	0.86%	0.47%	0.17%	0.09%	0.00%	0.00%	0.00%
NW	0.30%	1.03%	3.00%	3.00%	1.16%	0.47%	0.17%	0.13%	0.09%	0.00%	0.00%	0.00%
NNW	0.34%	1.16%	2.27%	1.58%	0.64%	0.21%	0.21%	0.21%	0.04%	0.00%	0.00%	0.00%
TOTAL	4.41%	12.93%	36.43%	24.87%	11.77%	5.09%	2.61%	1.41%	0.43%	0.04%	0.00%	0.00%

© Eskom 2026/Rev 0c

PRINTED VERSIONS OF THIS DOCUMENT ARE NOT CONTROLLED

Table 5.8.41
Joint Frequency Distribution of Pasquill-Gifford Stability Class B with Wind Direction and Wind Speed: Thyspunt WS
(Sigma-Theta Method [9 m] – (Eskom, 2022a))

Wind Direction	Wind Speed [m/s] at 9 m level, Sigma-Theta Method											
	<0.5	0.5-1.0	1.0-2.0	2.0-3.0	3.0-4.0	4.0-5.0	5.0-6.0	6.0-8.0	8.0-10.0	10.0-13.0	13.0-18.0	>18.0
N	0.08%	0.15%	1.55%	1.78%	0.93%	0.77%	0.23%	0.08%	0.00%	0.00%	0.00%	0.00%
NNE	0.08%	0.23%	1.47%	2.09%	1.16%	0.70%	0.23%	0.00%	0.00%	0.00%	0.00%	0.00%
NE	0.00%	0.39%	2.01%	2.78%	1.47%	1.08%	0.54%	0.23%	0.00%	0.00%	0.00%	0.00%
ENE	0.31%	0.31%	2.01%	1.55%	1.55%	0.93%	0.46%	0.15%	0.00%	0.00%	0.00%	0.00%
E	0.23%	0.70%	1.62%	1.85%	1.85%	1.16%	0.31%	0.31%	0.00%	0.00%	0.00%	0.00%
ESE	0.15%	0.23%	1.31%	1.85%	0.70%	0.31%	0.23%	0.15%	0.00%	0.00%	0.00%	0.00%
SE	0.31%	0.46%	1.24%	1.16%	0.31%	0.15%	0.08%	0.00%	0.08%	0.00%	0.00%	0.00%
SSE	0.00%	0.31%	1.85%	1.08%	0.39%	0.23%	0.00%	0.08%	0.00%	0.00%	0.00%	0.00%
S	0.08%	0.08%	1.00%	1.85%	0.54%	0.08%	0.00%	0.23%	0.00%	0.08%	0.00%	0.00%
SSW	0.08%	0.39%	1.62%	1.00%	0.62%	0.15%	0.08%	0.00%	0.00%	0.00%	0.00%	0.00%
SW	0.23%	0.62%	1.00%	0.85%	0.46%	0.54%	0.15%	0.08%	0.08%	0.00%	0.00%	0.00%
WSW	0.23%	0.62%	1.85%	1.93%	0.46%	0.70%	0.31%	0.23%	0.08%	0.08%	0.00%	0.00%
W	0.08%	0.31%	2.09%	1.78%	1.70%	1.55%	0.62%	0.46%	0.23%	0.39%	0.00%	0.00%
WNW	0.15%	0.39%	2.09%	3.01%	1.85%	1.08%	0.62%	0.08%	0.15%	0.00%	0.00%	0.00%
NW	0.15%	0.39%	1.85%	2.01%	1.55%	0.93%	0.31%	0.39%	0.00%	0.00%	0.00%	0.00%
NNW	0.00%	0.54%	2.01%	1.78%	1.31%	1.47%	0.23%	0.00%	0.08%	0.00%	0.00%	0.00%
TOTAL	2.16%	6.11%	26.58%	28.36%	16.85%	11.82%	4.40%	2.47%	0.70%	0.54%	0.00%	0.00%

© Eskom 2026/Rev 0c

PRINTED VERSIONS OF THIS DOCUMENT ARE NOT CONTROLLED

Table 5.8.42
Joint Frequency Distribution of Pasquill-Gifford Stability Class C with Wind Direction and Wind Speed: Thyspunt WS
(Sigma-Theta Method [9 m] – (Eskom, 2022a))

Wind Direction	Wind Speed [m/s] at 9 m level, Sigma-Theta Method											
	<0.5	0.5-1.0	1.0-2.0	2.0-3.0	3.0-4.0	4.0-5.0	5.0-6.0	6.0-8.0	8.0-10.0	10.0-13.0	13.0-18.0	>18.0
N	0.06%	0.23%	0.88%	1.61%	1.34%	0.99%	0.61%	0.70%	0.26%	0.03%	0.00%	0.00%
NNE	0.03%	0.12%	0.79%	1.64%	1.49%	0.55%	0.20%	0.09%	0.03%	0.00%	0.00%	0.00%
NE	0.06%	0.23%	0.96%	1.90%	1.52%	0.61%	0.44%	0.29%	0.03%	0.00%	0.00%	0.00%
ENE	0.09%	0.26%	1.05%	1.23%	2.42%	2.28%	1.14%	0.44%	0.00%	0.03%	0.00%	0.00%
E	0.12%	0.09%	0.93%	1.43%	1.52%	1.43%	1.02%	0.73%	0.06%	0.00%	0.00%	0.00%
ESE	0.00%	0.20%	0.93%	1.11%	1.05%	0.50%	0.18%	0.32%	0.00%	0.00%	0.00%	0.00%
SE	0.15%	0.09%	0.91%	1.34%	0.93%	0.32%	0.03%	0.06%	0.03%	0.00%	0.00%	0.00%
SSE	0.06%	0.20%	0.93%	1.40%	1.02%	0.32%	0.03%	0.00%	0.03%	0.00%	0.00%	0.00%
S	0.12%	0.06%	1.28%	2.10%	1.46%	0.12%	0.06%	0.06%	0.03%	0.00%	0.00%	0.00%
SSW	0.06%	0.12%	1.11%	2.25%	1.34%	0.09%	0.15%	0.18%	0.06%	0.03%	0.00%	0.00%
SW	0.09%	0.09%	0.93%	1.52%	1.23%	0.38%	0.12%	0.18%	0.03%	0.03%	0.03%	0.00%
WSW	0.03%	0.12%	0.88%	1.75%	1.64%	0.70%	0.41%	0.44%	0.18%	0.26%	0.03%	0.00%
W	0.03%	0.15%	1.14%	2.63%	2.74%	1.87%	1.20%	1.46%	0.38%	0.26%	0.12%	0.00%
WNW	0.09%	0.12%	0.93%	2.01%	2.34%	1.43%	1.05%	0.38%	0.12%	0.00%	0.00%	0.00%
NW	0.09%	0.26%	1.20%	1.37%	1.20%	0.61%	0.58%	0.44%	0.03%	0.00%	0.00%	0.00%
NNW	0.03%	0.18%	0.82%	1.52%	1.14%	0.85%	0.58%	0.55%	0.23%	0.09%	0.00%	0.00%
TOTAL	1.08%	2.51%	15.68%	26.80%	24.38%	13.05%	7.80%	6.31%	1.49%	0.73%	0.18%	0.00%

© Eskom 2026/Rev 0c

PRINTED VERSIONS OF THIS DOCUMENT ARE NOT CONTROLLED

Table 5.8.43
Joint Frequency Distribution of Pasquill-Gifford Stability Class D with Wind Direction and Wind Speed: Thyspunt WS
(Sigma-Theta Method [9 m] – (Eskom, 2022a))

Wind Direction	Wind Speed [m/s] at 9 m level, Sigma-Theta Method											
	<0.5	0.5-1.0	1.0-2.0	2.0-3.0	3.0-4.0	4.0-5.0	5.0-6.0	6.0-8.0	8.0-10.0	10.0-13.0	13.0-18.0	>18.0
N	0.01%	0.02%	0.21%	0.44%	0.50%	0.57%	0.37%	0.32%	0.07%	0.01%	0.00%	0.00%
NNE	0.01%	0.01%	0.18%	0.31%	0.47%	0.35%	0.21%	0.15%	0.02%	0.00%	0.00%	0.00%
NE	0.02%	0.03%	0.24%	0.42%	0.68%	0.66%	0.55%	0.53%	0.13%	0.02%	0.00%	0.00%
ENE	0.02%	0.03%	0.18%	0.45%	0.80%	1.09%	1.32%	2.36%	1.37%	0.33%	0.03%	0.00%
E	0.01%	0.01%	0.19%	0.27%	0.55%	0.60%	0.72%	2.04%	2.25%	1.41%	0.11%	0.00%
ESE	0.01%	0.02%	0.11%	0.33%	0.45%	0.41%	0.34%	0.54%	0.19%	0.03%	0.00%	0.00%
SE	0.01%	0.01%	0.14%	0.44%	0.80%	0.78%	0.45%	0.10%	0.01%	0.00%	0.00%	0.00%
SSE	0.00%	0.01%	0.10%	0.20%	0.32%	0.31%	0.11%	0.04%	0.02%	0.01%	0.00%	0.00%
S	0.00%	0.02%	0.09%	0.29%	0.43%	0.27%	0.07%	0.03%	0.01%	0.01%	0.00%	0.00%
SSW	0.00%	0.02%	0.13%	0.38%	0.58%	0.30%	0.11%	0.06%	0.02%	0.01%	0.00%	0.00%
SW	0.00%	0.01%	0.11%	0.50%	0.77%	0.74%	0.37%	0.15%	0.05%	0.04%	0.01%	0.00%
WSW	0.01%	0.01%	0.11%	0.44%	1.07%	1.55%	1.77%	2.65%	1.01%	0.50%	0.13%	0.00%
W	0.01%	0.02%	0.15%	0.81%	2.07%	4.10%	6.82%	14.45%	8.65%	3.84%	0.52%	0.00%
WNW	0.01%	0.02%	0.18%	0.68%	1.25%	1.81%	1.57%	2.29%	0.91%	0.41%	0.05%	0.00%
NW	0.00%	0.02%	0.19%	0.34%	0.57%	0.38%	0.26%	0.29%	0.09%	0.02%	0.00%	0.00%
NNW	0.01%	0.01%	0.18%	0.24%	0.44%	0.30%	0.30%	0.47%	0.36%	0.09%	0.00%	0.00%
TOTAL	0.15%	0.29%	2.52%	6.53%	11.75%	14.23%	15.35%	26.48%	15.15%	6.71%	0.84%	0.00%

© Eskom 2026/Rev 0c

PRINTED VERSIONS OF THIS DOCUMENT ARE NOT CONTROLLED

Table 5.8.44
Joint Frequency Distribution of Pasquill-Gifford Stability Class E with Wind Direction and Wind Speed: Thyspunt WS
(Sigma-Theta Method [9 m] – (Eskom, 2022a))

Wind Direction	Wind Speed [m/s] at 9 m level, Sigma-Theta Method											
	<0.5	0.5-1.0	1.0-2.0	2.0-3.0	3.0-4.0	4.0-5.0	5.0-6.0	6.0-8.0	8.0-10.0	10.0-13.0	13.0-18.0	>18.0
N	0.00%	0.01%	0.09%	0.29%	0.62%	0.59%	0.31%	0.08%	0.00%	0.00%	0.00%	0.00%
NNE	0.01%	0.01%	0.13%	0.63%	1.12%	1.40%	0.86%	0.55%	0.07%	0.00%	0.00%	0.00%
NE	0.01%	0.01%	0.15%	0.57%	1.44%	1.66%	1.12%	1.49%	0.69%	0.18%	0.02%	0.00%
ENE	0.00%	0.00%	0.13%	0.59%	1.05%	1.71%	1.81%	3.34%	2.20%	1.00%	0.12%	0.00%
E	0.01%	0.00%	0.08%	0.27%	0.51%	0.68%	0.60%	1.24%	0.81%	0.48%	0.08%	0.00%
ESE	0.01%	0.00%	0.07%	0.30%	0.53%	0.84%	1.11%	1.98%	1.01%	0.04%	0.00%	0.00%
SE	0.01%	0.00%	0.03%	0.14%	0.20%	0.41%	0.48%	0.68%	0.09%	0.03%	0.00%	0.00%
SSE	0.01%	0.01%	0.02%	0.05%	0.10%	0.20%	0.22%	0.27%	0.08%	0.06%	0.02%	0.01%
S	0.01%	0.00%	0.04%	0.10%	0.17%	0.17%	0.18%	0.31%	0.13%	0.06%	0.02%	0.00%
SSW	0.00%	0.00%	0.05%	0.04%	0.13%	0.18%	0.26%	0.28%	0.15%	0.08%	0.04%	0.00%
SW	0.00%	0.00%	0.04%	0.19%	0.23%	0.36%	0.53%	0.82%	0.39%	0.21%	0.05%	0.00%
WSW	0.00%	0.00%	0.08%	0.28%	0.68%	1.21%	1.95%	3.58%	2.24%	1.08%	0.26%	0.00%
W	0.01%	0.01%	0.12%	0.45%	1.10%	1.36%	1.00%	1.30%	0.44%	0.13%	0.02%	0.00%
WNW	0.01%	0.01%	0.19%	1.40%	4.54%	5.81%	2.93%	1.48%	0.20%	0.03%	0.00%	0.00%
NW	0.02%	0.02%	0.28%	1.38%	4.39%	3.88%	2.22%	1.26%	0.24%	0.04%	0.00%	0.00%
NNW	0.01%	0.02%	0.18%	0.73%	1.45%	1.63%	0.97%	1.41%	0.74%	0.17%	0.00%	0.00%
TOTAL	0.11%	0.12%	1.68%	7.41%	18.24%	22.07%	16.54%	20.08%	9.50%	3.62%	0.62%	0.02%

© Eskom 2026/Rev 0c

PRINTED VERSIONS OF THIS DOCUMENT ARE NOT CONTROLLED

Table 5.8.45
Joint Frequency Distribution of Pasquill-Gifford Stability Class F with Wind Direction and Wind Speed: Thyspunt WS
(Sigma-Theta Method [9 m] – (Eskom, 2022a))

Wind Direction	Wind Speed [m/s] at 9 m level, Sigma-Theta Method											
	<0.5	0.5-1.0	1.0-2.0	2.0-3.0	3.0-4.0	4.0-5.0	5.0-6.0	6.0-8.0	8.0-10.0	10.0-13.0	13.0-18.0	>18.0
N	0.05%	0.00%	0.00%	0.10%	0.05%	0.00%	0.00%	0.00%	0.00%	0.00%	0.00%	0.00%
NNE	0.00%	0.00%	0.00%	0.05%	0.39%	0.39%	0.00%	0.00%	0.00%	0.00%	0.00%	0.00%
NE	0.00%	0.00%	0.05%	0.05%	0.20%	0.20%	0.00%	0.00%	0.00%	0.00%	0.00%	0.00%
ENE	0.00%	0.00%	0.00%	0.34%	0.59%	0.20%	0.00%	0.00%	0.00%	0.00%	0.00%	0.00%
E	0.00%	0.00%	0.05%	0.00%	0.00%	0.00%	0.00%	0.00%	0.00%	0.00%	0.00%	0.00%
ESE	0.00%	0.00%	0.00%	0.00%	0.00%	0.00%	0.00%	0.00%	0.00%	0.00%	0.00%	0.00%
SE	0.00%	0.00%	0.00%	0.00%	0.00%	0.00%	0.00%	0.00%	0.00%	0.00%	0.00%	0.00%
SSE	0.00%	0.00%	0.00%	0.00%	0.05%	0.00%	0.00%	0.00%	0.00%	0.00%	0.00%	0.00%
S	0.00%	0.05%	0.00%	0.00%	0.00%	0.00%	0.00%	0.00%	0.00%	0.00%	0.00%	0.00%
SSW	0.00%	0.00%	0.05%	0.00%	0.05%	0.00%	0.00%	0.00%	0.00%	0.00%	0.00%	0.00%
SW	0.00%	0.00%	0.05%	0.05%	0.00%	0.00%	0.00%	0.00%	0.00%	0.00%	0.00%	0.00%
WSW	0.00%	0.05%	0.05%	0.05%	0.05%	0.00%	0.00%	0.00%	0.00%	0.00%	0.00%	0.00%
W	0.10%	0.00%	0.10%	0.15%	0.29%	0.10%	0.00%	0.00%	0.00%	0.00%	0.00%	0.00%
WNW	0.24%	0.05%	0.59%	6.59%	24.45%	16.84%	3.12%	0.15%	0.00%	0.00%	0.00%	0.00%
NW	0.05%	0.10%	1.22%	10.79%	16.06%	3.66%	0.15%	0.00%	0.00%	0.00%	0.00%	0.00%
NNW	0.00%	0.00%	0.10%	3.81%	5.61%	2.34%	0.20%	0.00%	0.00%	0.00%	0.00%	0.00%
TOTAL	0.44%	0.24%	2.24%	21.96%	47.78%	23.72%	3.47%	0.15%	0.00%	0.00%	0.00%	0.00%

© Eskom 2026/Rev 0c

PRINTED VERSIONS OF THIS DOCUMENT ARE NOT CONTROLLED

Table 5.8.46
Joint Frequency Distribution of Pasquill-Gifford Stability Class G with Wind Direction and Wind Speed: Thyspunt WS
(Sigma-Theta Method [9 m] – (Eskom, 2022a))

Wind Direction	Wind Speed [m/s] at 9 m level, Sigma-Theta Method											
	<0.5	0.5-1.0	1.0-2.0	2.0-3.0	3.0-4.0	4.0-5.0	5.0-6.0	6.0-8.0	8.0-10.0	10.0-13.0	13.0-18.0	>18.0
N	0.00%	0.00%	0.00%	0.00%	0.00%	0.00%	0.00%	0.00%	0.00%	0.00%	0.00%	0.00%
NNE	0.00%	0.00%	0.00%	0.00%	0.00%	0.00%	0.00%	0.00%	0.00%	0.00%	0.00%	0.00%
NE	20.00%	0.00%	0.00%	0.00%	0.00%	0.00%	0.00%	0.00%	0.00%	0.00%	0.00%	0.00%
ENE	0.00%	0.00%	0.00%	0.00%	0.00%	0.00%	0.00%	0.00%	0.00%	0.00%	0.00%	0.00%
E	0.00%	0.00%	0.00%	0.00%	0.00%	0.00%	0.00%	0.00%	0.00%	0.00%	0.00%	0.00%
ESE	0.00%	0.00%	0.00%	0.00%	0.00%	0.00%	0.00%	0.00%	0.00%	0.00%	0.00%	0.00%
SE	0.00%	0.00%	0.00%	0.00%	0.00%	0.00%	0.00%	0.00%	0.00%	0.00%	0.00%	0.00%
SSE	0.00%	0.00%	0.00%	0.00%	0.00%	0.00%	0.00%	0.00%	0.00%	0.00%	0.00%	0.00%
S	0.00%	0.00%	0.00%	0.00%	0.00%	0.00%	0.00%	0.00%	0.00%	0.00%	0.00%	0.00%
SSW	0.00%	0.00%	0.00%	0.00%	0.00%	0.00%	0.00%	0.00%	0.00%	0.00%	0.00%	0.00%
SW	0.00%	0.00%	0.00%	0.00%	0.00%	0.00%	0.00%	0.00%	0.00%	0.00%	0.00%	0.00%
WSW	20.00%	0.00%	0.00%	0.00%	0.00%	0.00%	0.00%	0.00%	0.00%	0.00%	0.00%	0.00%
W	0.00%	0.00%	0.00%	0.00%	0.00%	0.00%	0.00%	0.00%	0.00%	0.00%	0.00%	0.00%
WNW	0.00%	0.00%	0.00%	0.00%	40.00%	20.00%	0.00%	0.00%	0.00%	0.00%	0.00%	0.00%
NW	0.00%	0.00%	0.00%	0.00%	0.00%	0.00%	0.00%	0.00%	0.00%	0.00%	0.00%	0.00%
NNW	0.00%	0.00%	0.00%	0.00%	0.00%	0.00%	0.00%	0.00%	0.00%	0.00%	0.00%	0.00%
TOTAL	40.00%	0.00%	0.00%	0.00%	40.00%	20.00%	0.00%	0.00%	0.00%	0.00%	0.00%	0.00%

© Eskom 2026/Rev 0c

PRINTED VERSIONS OF THIS DOCUMENT ARE NOT CONTROLLED

The vertical component of dispersion is a function of the extent of thermal turbulence and the depth of the surface-mixing layer. Unfortunately, the mixing layer is not easily measured as this requires measurements up to 1 km to 2 km above surface. In the absence of upper air measurements, the mixing layer depths for the dispersion model were estimated using prognostic models that derive the depth from other parameters including solar radiation, wind speed, dry bulb temperature and atmospheric turbulence that are routinely measured (see (International Atomic Energy Agency, 2011)).

5.8.6.1.10 Evapotranspiration Rate

Evapotranspiration rates were calculated for the January 2008 to September 2013 and September 2017 to March 2019 monitoring periods at the Thyspunt WS using the Penman[35] and Penman-Monteith[36] methods for open water and crop evaporation (see ***Table 5.8.47***). These methods require data on dry bulb temperature, relative humidity, solar radiation and wind speed as discussed in ***Appendix 5.8.C***).

Estimates from the atlas of potential evapotranspiration rates[37] for South Africa (Schulze, 1997) have also been included (see ***Table 5.8.47***) to enable a comparison of these regional values with the calculated values using the site data. The evapotranspiration rates calculated using the Penman method is higher than both the Penman-Monteith method and the Schulze's estimates, but the same monthly trends and values are observed, with:

- the maximum evapotranspiration rates occur during January and December at the site;
- the minimum evapotranspiration rate occurs during June at the site.

As used in the Schulze atlas (Schulze, 1997) it is recommended to use the calculated Penman-Monteith values for the SSR.

[35] In 1948, Penman combined an energy balance with a mass transfer method and derived an equation to compute the evaporation from an open water surface from standard climatological records of sunshine, temperature, humidity and wind speed.

[36] The Penman method was further developed by many researchers and extended to cropped surfaces by introducing resistance factors. The Penman-Monteith equation is one such method and predicts the crop evapotranspiration at a location using daily average temperature, wind speed, relative humidity, and solar radiation.

[37] The rate of evapotranspiration from a hypothetical crop with an assumed crop height of 0.12 m, a fixed canopy resistance of 70.00 s/m and an albedo of 0.23, which would closely resemble evapotranspiration from an extensive surface of green grass of uniform height, actively growing, completely shading the ground and not short of water.

© Eskom 2026/Rev 0c

PRINTED VERSIONS OF THIS DOCUMENT ARE NOT CONTROLLED

Table 5.8.47
Monthly Total Potential Evapotranspiration Rates

Month	Schulze's Atlas[1]	Thyspunt WS [2] (2008-2013 & 2017-2019)	
	[mm]	[mm]	
	Penman-Monteith	Penman-Monteith	Penman
January	140	146.1	212.7
February	120	119.9	171.2
March	110	114.2	162.5
April	90	95.0	129.6
May	80	90.2	116.4
June	65	84.8	107.4
July	70	88.4	112.6
August	80	95.4	131.0
September	95	101.1	145.9
October	115	111.4	166.6
November	120	127.8	192.6
December	140	142.5	208.3

Notes:
(1) (Schulze, 1997)
(2) (Eskom, 2023a)

The high evaporation rates observed during the summer months (***Table 5.8.47***) are further exacerbated through the coincidence of the summer dry season. Windy conditions during the summer are therefore more conducive to episodes of windblown dust than during the winter.

5.8.6.1.11 Corrosivity

(a) Abrasive Effects by Sand and Dust

Since strong winds are evident at the site, large exposed sandy areas could be prone to the development of windblown dust. They occur when wind forces exceed the threshold value at which loose sand and dust are removed from a dry surface and become airborne. The term 'dust storm' is most often used when fine particles are blown long distances, whereas the term 'sandstorm' is more likely to be used when, in addition to fine particles obscuring visibility, a considerable amount of larger sand particles become airborne and are mobilised, but closer to the surface. The vegetation found on the site, however, acts as a natural mitigation measure. Dust mobilisation occurs only for wind velocities higher than a threshold value and is not linearly dependent on the wind friction and velocity. Typically, wind speeds that exceed 5.4 m/s near the surface (United States Environmental Protection Agency , 1992) could initiate dust mobilisation from disturbed land surfaces. The IAEA (International Atomic Energy Agency, 2011) suggests 5.8 m/s for this threshold. An alternative form to describe the

© Eskom 2026/Rev 0c

PRINTED VERSIONS OF THIS DOCUMENT ARE NOT CONTROLLED

mobilisation threshold is by using a threshold friction velocity. The threshold friction velocity, defined as the minimum friction velocity required for the initiation of particle motion, is dependent on the size of the erodible particles and the effect of the wind shear stress on the surface. The threshold friction velocity decreases with a decrease in the particle diameter, for particles with diameters >60 µm. Particles with a diameter <60 µm result in increasingly high threshold friction velocities, due to the increasingly strong cohesion forces linking such particles to each other (Marticorena & Bergametti, 1995). Thyspunt is characterised by aeolian sands with particle size ranging from 283µm to 496µm (***Appendix 5.8.H***). The friction velocity is therefore estimated to be about 0.3 m/s to 0.4 m/s (Marticorena & Bergametti, 1995).

(Hsu, 1977) established a relationship for the friction velocity in terms of wind speeds measured at 2 m above the surface:

$$u_* = au_{2m}$$

where the constant *a* varies between 0.037 to 0.099, as shown below:

Tidal flat	a = 0.037
Beaches	a = 0.044
Low dune field (<50cm)	a = 0.048
Dune (scarp)	a = 0.050
Swale	a = 0.058
Dune top (<45 m)	a = 0.070
Dune lee	a = 0.099

Assuming the constant representing dunes of 0.050, the threshold velocity is estimated at 6.0 m/s at 2 m measurement height or 7.5 m/s by extrapolating to 9 m height.

According to the IAEA (International Atomic Energy Agency, 2011), the frequency of dust storms and sandstorms can be identified through hourly weather observations when visibility is 10 kilometres or less, the wind speed exceeds a threshold value (i.e. 7.5 m/s), and relative humidity is below a threshold value (i.e. less than 70 per cent) (International Atomic Energy Agency, 2011).

On analysis of the Thyspunt WS data (January 2008 to September 2013 and September 2017 to March 2019), the highest number of hours of windblown dust occurred during the summer months, with September and

© Eskom 2026/Rev 0c

PRINTED VERSIONS OF THIS DOCUMENT ARE NOT CONTROLLED

November experiencing the highest occurrence. The lowest dust conditions occurred during March. These results are represented in ***Figure 5.8.14***.

The IAEA (2011) further proposes that appropriate values of dust or sand concentration should be computed on the basis of empirical relationships using visibility observations. The need to understand the relationship between visibility and dust concentration as part of wind erosion research has long been recognised (e.g. (Chepil & Woodruff, 1957; Patterson & Gillette, 1977; Ette & Olorode, 1988; Ackerman & Cox, 1989). In a relatively recent study by Baddock *et al* (Baddock, et al., 2014), several empirical correlations were analysed and that led to a new correlation that was based on an outcome of an ongoing, long term, synergistic dust monitoring programme in rural New South Wales, Australia. The general form of these correlations is as follows:

$$C_{VTSD} = bVis^{n}$$

Where C_{VTSD} is the total suspended dust concentration (mg/m³), Vis is the visibility (km) and *b* and *n* are experimentally derived constants. Baddock *et al* (Baddock, et al., 2014) derived the following values for the constants:

$$b = 4.050 \text{ and } n = -1.016$$

As recommended by the IAEA (International Atomic Energy Agency, 2011), the results of the assessment are to be expressed as total dust or sand loading (mg-h/m³), duration (h), and average dust or sand loading (mg/m³) for the historic dust storm or sandstorm that had the largest calculated time integrated dust or sand loading. The dust loadings were calculated using the IAEA (International Atomic Energy Agency, 2011) methodology and the concentrations estimated as indicated in the above equation.

The highest dust loading during the monitoring period occurred from 01h00 to 21h00 on 27 August 2018. The time integrated dust loading for this period was calculated to be 22.3 mg-h/m³ and the duration, 21 hours. The average dust concentration during this period was 0.964 mg/m³. The average wind speed for the 21-hour period was 9.6 m/s (hourly average minimum of 7.5 m/s and maximum of 12.7 m/s) which occurred from the southwest (202.4°), with maximum gusts up to 22.8 m/s.

Based on the observed frequency of dust events (***Figure 5.8.14***), June, August, September and November are the months most likely to experience dust storms, whereas March is the month least likely to experience dust storms. The summer season is likely to have between 7 and 10 days of dust events in total.

© Eskom 2026/Rev 0c

PRINTED VERSIONS OF THIS DOCUMENT ARE NOT CONTROLLED

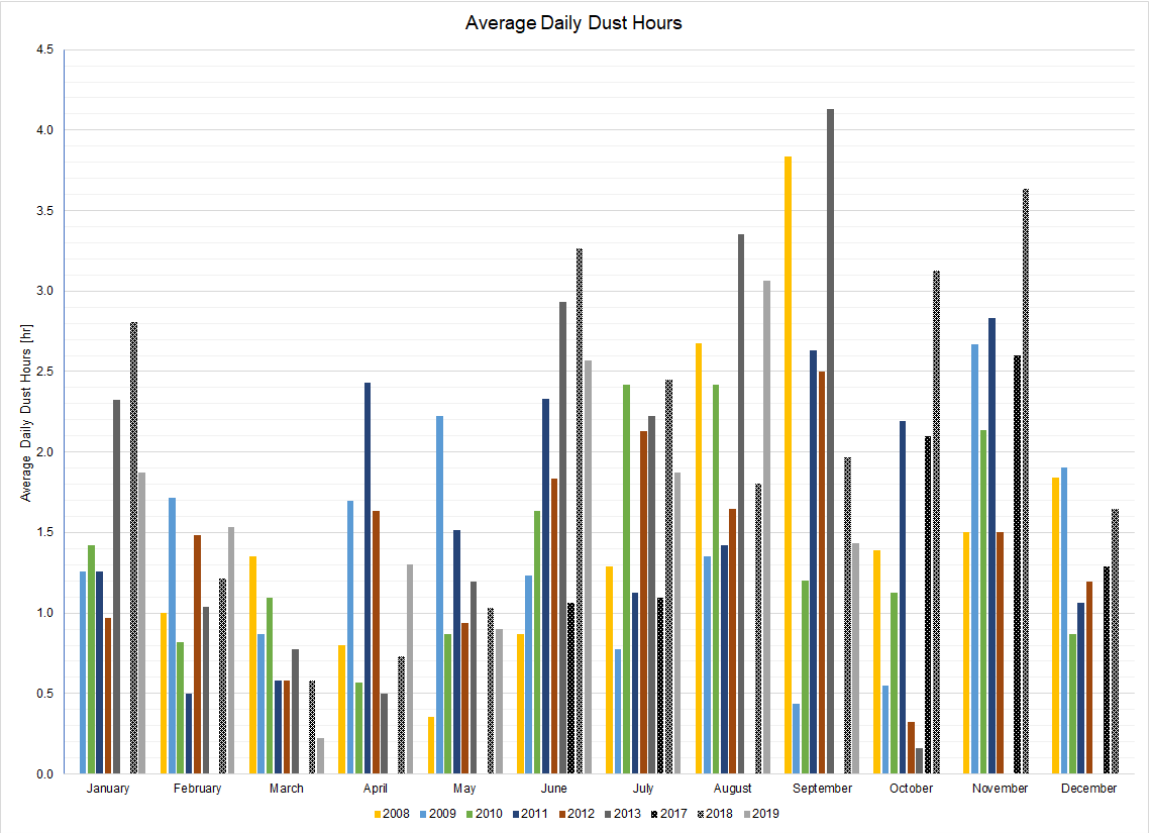


Figure 5.8.14
Average Durations (Hours) of Dust Conditions per Day Per Month

© Eskom 2026/Rev 0c

PRINTED VERSIONS OF THIS DOCUMENT ARE NOT CONTROLLED

(b) Freeze-Thaw

There are two ways that the phenomenon of freeze-thaw occurs in nature. The first is through the repeated cycle of melting and freezing of water on the natural cracks and grooves of rocks, or concrete building structures. The second phenomenon occurs when the surface layer of rock or concrete is baked by direct sunlight causing the top layer to expand and contract repeatedly, causing distress and eventually, cracks. Both phenomena require extreme daily temperature variations. Concrete can better withstand the effects of both phenomena with the addition of additives. Freeze-thaw occurs when concrete (or rocks) is saturated with water and the temperature drops, freezing the water molecules. The frozen water expands by nine per cent of its original volume. Whilst there are many theories (Guo, et al., 2022) as to the damage mechanisms in concrete, the simple view is that the increase in volume produces increased pressure in the pores of the concrete. Tiny cracks will form where this pressure exceeds the tensile strength of the concrete. Increased frequency of freeze-thaw cycles will result in more stress on the concrete structure. However, besides the frequency of freeze–thaw cycles, the frost intensity should also play an important role. The frost intensity describes how long and to what extent the temperature falls below the 0°C transition. According to Walder and Hallet (Walder & Hallet , 1985), most of the damage potential can be assumed for a temperature of -10°C.

However, this temperature range has not been observed at the Thyspunt site with the recorded lowest hourly average of 4.9°C (Cape St. Francis WS) and 6.7 °C (Thyspunt WS). The 10 000-year return period projects a temperature below 0°C, i.e. -0.5°C. The projected 100 000 000-year return period estimate reached -7.7°C. The possibility of freeze-thaw from frozen water in the pores is therefore not likely at the site; estimated to be 1 in 10 000 years chance, and hence freezing thaw phenomenon is not an issue. Additionally, regarding the possibility of ice occurring in the sea surrounding the site, the lowest seawater temperature measured in all the data sets described in ***Section 5.9*** is 7.9°C. On this basis ice is not anticipated to form in the sea at the site.

(c) Atmospheric Corrosion

Metal components exposed to weather elements and sea mist will inevitably experience damage due to atmospheric corrosion. The severity of the corrosion and the rate at which corrosion will take place are dependant primarily upon the properties of the surface formed electrolytes, which in turn are dependent upon factors such as the humidity and pollution levels in the atmosphere.

© Eskom 2026/Rev 0c

PRINTED VERSIONS OF THIS DOCUMENT ARE NOT CONTROLLED

Three relatively common methods to assess the corrosivity of a particular atmosphere include:

- The coupon-based method (CLIMAT). This method involves the exposure of metallic coupons which may include steel, zinc, copper and aluminium to the environment and classifying the resultant corrosion. Flat panels exposed on exposure racks are a common coupon-type device for atmospheric corrosivity measurements (ISO Standard 9226, (International Organisation of Standardisation, 2012d)). ISO 9226 also provides the open helix specimens as an alternative. The 'wire-on-bolt'[38] is a slight modification of this version. Various other specimen configurations may also be used, including stressed U-bend or C-ring specimens for stress corrosion cracking studies.
- Different from the coupon method, the exposure programme provides actual corrosion rates of materials. The corrosion rates are calculated from the weight loss because of corrosion over the test period. The test period is however considerably longer than for the CLIMAT testing, with panels being removed for evaluation only once a year. Typically, a number of test panels for each material would be exposed so that as the panels are removed, the corrosion rates for exposure times of one year, two years, three years etc. can be determined. This provides information as to whether the corrosion rate of a material increases or decreases with time.
- The third method (ISO Standard 9223, (International Organisation for Standardisation, 2012a)) involves measuring meteorological parameters (temperature and relative humidity) and the deposition rate of sulfur dioxide and airborne salinity and classifying the atmosphere according to standardised measurements.

Four campaigns of corrosion monitoring have been completed. The first campaign employed the coupon-based and exposure methods (August 1987 to August 1989) (Gross & Nixon, 1993), with the second, third and fourth campaigns based on the monitoring of sulfur dioxide fallout, airborne salinity and meteorological parameters. The second campaign occurred during the period 18 April 2008 to 26 January 2009, the third campaign from 11 October 2012 to 11 September 2013 and the fourth campaign from 11 October 2017 to 12 March 2022 (Burger, 2019). The results from these campaigns are discussed below.

[38] With the 'wire on bolt' technique, the CLIMAT unit consists of three bolts of different materials around which are wound aluminium wires of known mass. The bolt materials used are nylon, steel and copper to determine the atmospheric, marine and industrial corrosivities, respectively.

© Eskom 2026/Rev 0c

PRINTED VERSIONS OF THIS DOCUMENT ARE NOT CONTROLLED

(i) Coupon-Based Corrosion Monitoring

Two CLIMAT units were placed at four sites at and near Thyspunt (Gross & Nixon, 1993), namely Brakkeduine (August 1987 to August 1989), De Hoek (August 1987 to August 1989); Klippepunt (August 1987 to November 1988) and Thyspunt (August 1987 to August 1989). The locations of these sites are shown in ***Figure 5.8.15***.

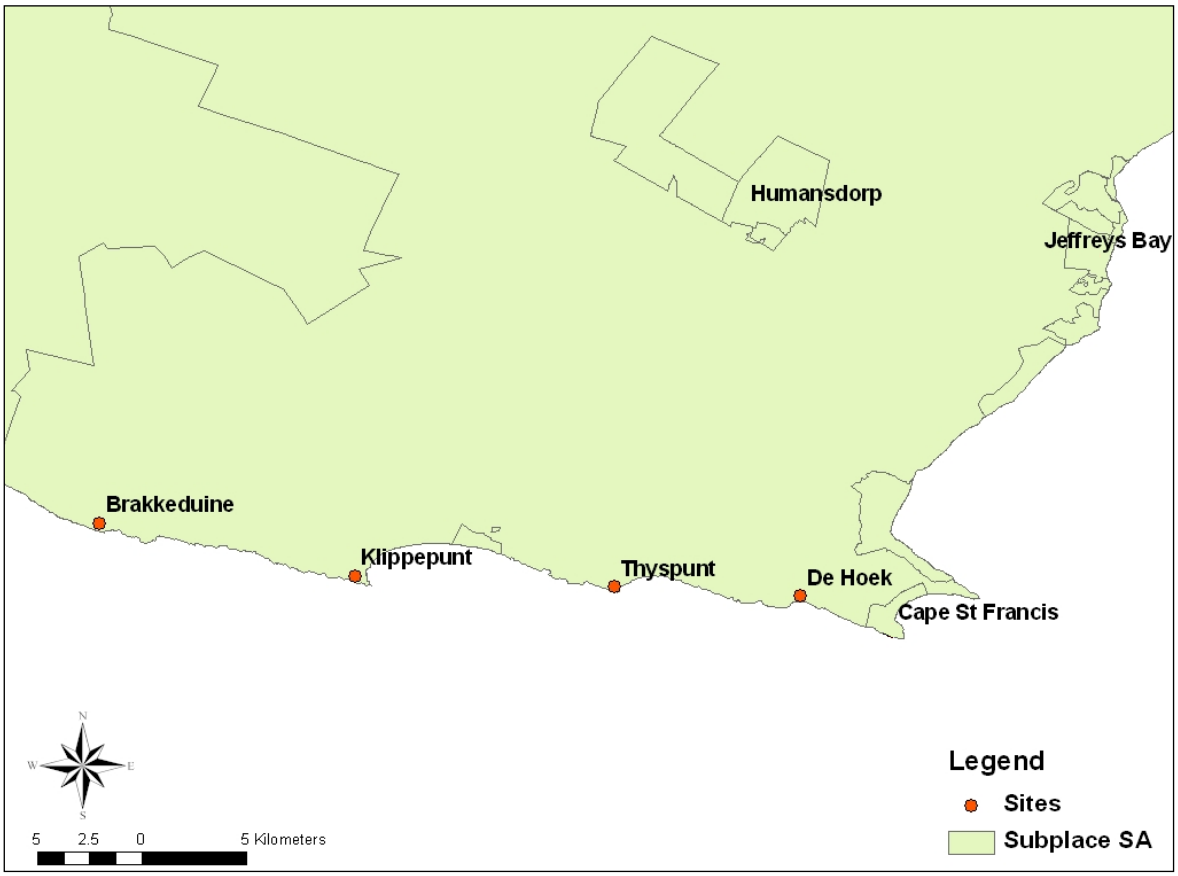


Figure 5.8.15
Corrosion Monitoring Locations Using Coupon-Based Method (August 1987 to August 1989) (Gross & Nixon, 1993)

The coupons were exposed for approximately 90 days where after the weight loss of the coupons was measured and from this the corrosivity was calculated. Three units were erected on wooden poles, at varying distance from the sea (100 m, 500 m and 1 000 m), at each of these four sites. Marine and atmospheric corrosivity were determined. The industrial corrosivity was not determined, since the sites are situated in rural areas with no industrial activities. The marine corrosion was expected to be the controlling form of corrosion (Gross & Nixon, 1993).

© Eskom 2026/Rev 0c

PRINTED VERSIONS OF THIS DOCUMENT ARE NOT CONTROLLED

The corrosivity[39] is expressed in terms of degrees of severity and is divided into five levels depending upon the average per cent mass loss measured. The definitions of these levels are provided in ***Table 5.8.48***. The *Negligible* range would indicate that the corrosion rates are very low and only minimal corrosion protection would be required. The corrosion would become significant in the *Moderate* range increasing up to the *Very Severe* range where corrosion would be expected to be a major problem requiring comprehensive corrosion protection.

Table 5.8.48
Classification of Marine Atmospheres Based on the Per Cent Mass Loss

Classification	% Mass Loss	Significance
Negligible (N)	0% to 2%	Average Habitable Area
Moderate (M)	2% to 5%	Seaside
Moderately Severe (MS)	5% to 10%	Seaside and Exposed
Severe (S)	10% to 20%	Very Exposed
Very Severe (VS)	above 20%	Very Exposed, Wind and Sand Swept

Averages of the marine corrosivity values at the four sites at 100 m, 500 m and 1 000 m from the high tide mark over the respective test periods are summarised ***Table 5.8.49*** (Gross & Nixon, 1993). At 100 m from the high tide mark all the sites, except the Thyspunt site showed corrosivity in the *Very Severe* range. As the distance from the sea increased, so the corrosivity tended to decrease at all sites. Brakkeduine showed the most dramatic effect in this regard although corrosivity at 1 000 m was still in the *Severe* range.

Table 5.8.49
Average Marine Corrosivity at Thyspunt and Surrounding Coast (Gross & Nixon, 1993)

Site	Distance from high tide mark			Period
	100 m	500m	1000m	
Brakkeduine	31.7%	15.5%	13.9%	August 1987 to August 1989
De Hoek	35.2%	33.0%	24.4%	August 1987 to August 1989
Klippepunt	30.8%	21.5%	12.3%	August 1987 to November 1988
Thyspunt	18.7%	17.7%	13.9%	August 1987 to August 1989
Average	29.1%	21.9%	16.1%	

Note: Samples were located on 3-month, back-to-back cycles for the indicated periods

[39] Corrosivity of atmosphere is the ability of the atmosphere to cause corrosion in a given corrosion system

© Eskom 2026/Rev 0c

PRINTED VERSIONS OF THIS DOCUMENT ARE NOT CONTROLLED

The site was least affected by the increase in distance from the sea. The corrosivity at all positions at the De Hoek site remained in the *Very Severe* range.

(ii) Measurement of Pollutants Corrosion Monitoring

The more recent corrosion tests were completed based on the ISO 9223 International Standard (International Organisation for Standardisation, 2012a) methodology including the periods from 18 April 2008 to 26 January 2009, from 11 October 2012 to 11 September 2013 and from 11 October 2017 to 12 March 2019 (Burger, 2019).

Marine atmospheric corrosion is primarily catalysed by moisture and oxygen but is accentuated by contaminants such as sulfur compounds and salt spray. The prediction of atmospheric corrosion rates therefore contains a term for 'time of wetness', which is a function of the ambient air temperature and relative humidity, and the quantity of pollutants in the air, specifically sulfur dioxide and sodium chloride. The ISO 9223 International Standard (International Organisation for Standardisation, 2012a) specifies the key factors in the atmospheric corrosion of metals and alloys and provides the methods for determining these.

The International Standard provides a corrosion classification scheme that can directly be used for technical and economic analyses of corrosion damage and for the rational choice of protection measures. According to this classification scheme, corrosion rates (r_{corr}) are provided (***Table 5.8.51***) corresponding to the six categories (*C1* to *C5* and *CX*), ranging from very low to very high and extreme (***Table 5.8.50***).

As per the ISO 9223 International Standard these corrosion rates may also be estimated from a combination of the annual average temperature, relative humidity, and sulfur dioxide[40] and chloride deposition rates.

[40] The sulfur dioxide deposition rate is calculated from the measured air concentration according to the method provided in the International Standard (ISO 9225 (International Organisation for Standardisation, 2012c)).

© Eskom 2026/Rev 0c

PRINTED VERSIONS OF THIS DOCUMENT ARE NOT CONTROLLED

Table 5.8.50
ISO 9223:2012 Categories of Corrosivity of the Atmosphere

Category	Corrosivity	Typical Environment Examples
C1	Very low	Dry or cold zone, atmospheric environment with very low pollution and time of wetness, e.g. certain deserts, Central Arctic/Antarctica
C2	Low	Temperate zone, atmospheric environment with low pollution (annual average sulfur dioxide less than 5 µg/m³), e.g. rural areas, small towns Dry or cold zone, atmospheric environment with short time of wetness, e.g. deserts, subarctic areas
C3	Medium	Temperate zone, atmospheric environment with medium pollution (annual average sulfur dioxide 5 µg/m³ to 30 µg/m³) or some effect of chlorides, e.g. urban areas, coastal areas with low deposition of chlorides Subtropical and tropical zone, atmosphere with low pollution
C4	High	Temperate zone, atmospheric environment with high pollution (annual average sulfur dioxide 30 µg/m³ to 90 µg/m³) or substantial effect of chlorides, e.g. polluted urban areas, industrial areas, coastal areas without spray of salt water or, exposure to strong effect of de-icing salts. Subtropical and tropical zone, atmosphere with medium pollution
C5	Very high	Temperate and subtropical zone, atmospheric environment with very high pollution (annual average sulfur dioxide 90 µg/m³ to 250 µg/m³) and/or significant effect of chlorides, e.g. industrial areas, coastal areas, sheltered positions on coastline
CX	Extreme	Subtropical and tropical zone (very high time of wetness), atmospheric environment with very high sulfur dioxide pollution (annual average higher than 250 µg/m³) including accompanying and production factors and/or strong effect of chlorides, e.g. extreme industrial areas, coastal and offshore areas, occasional contact with salt spray.

Table 5.8.51
ISO 9223:2012 Corrosion Rates, r_{corr}, for the First Year of Exposure for the Different Corrosivity Categories

Corrosivity category	Corrosion rates of metals r_{corr}				
	Unit	Carbon steel	Zinc	Copper	Aluminium
C1	g/m²-annum	$r_{corr} \leq 10$	$r_{corr} \leq 0.7$	$r_{corr} \leq 0.9$	negligible
	µm/annum	$r_{corr} \leq 1.3$	$r_{corr} \leq 0.1$	$r_{corr} \leq 0.1$	—
C2	g/m²-annum	$10 < r_{corr} \leq 200$	$0.7 < r_{corr} \leq 5$	$0.9 < r_{corr} \leq 5$	$r_{corr} \leq 0.6$
	µm/annum	$1.3 < r_{corr} \leq 25$	$0.1 < r_{corr} \leq 0.7$	$0.1 < r_{corr} \leq 0.6$	—
C3	g/m²-annum	$200 < r_{corr} \leq 400$	$5 < r_{corr} \leq 15$	$5 < r_{corr} \leq 12$	$0.6 < r_{corr} \leq 2$
	µm/annum	$25 < r_{corr} \leq 50$	$0.7 < r_{corr} \leq 2.1$	$0.6 < r_{corr} \leq 1.3$	—
C4	g/m²-annum	$400 < r_{corr} \leq 650$	$15 < r_{corr} \leq 30$	$12 < r_{corr} \leq 25$	$2 < r_{corr} \leq 5$
	µm/annum	$50 < r_{corr} \leq 80$	$2.1 < r_{corr} \leq 4.2$	$1.3 < r_{corr} \leq 2.8$	—
C5	g/m²-annum	$650 < r_{corr} \leq 1\,500$	$30 < r_{corr} \leq 60$	$25 < r_{corr} \leq 50$	$5 < r_{corr} \leq 10$
	µm/annum	$80 < r_{corr} \leq 200$	$4.2 < r_{corr} \leq 8.4$	$2.8 < r_{corr} \leq 5.6$	—
CX	g/m²-annum	$1\,500 < r_{corr} \leq 5\,500$	$60 < r_{corr} \leq 180$	$50 < r_{corr} \leq 90$	$r_{corr} > 10$

© Eskom 2026/Rev 0c

PRINTED VERSIONS OF THIS DOCUMENT ARE NOT CONTROLLED

Corrosivity category	Corrosion rates of metals r_{corr}				
	Unit	Carbon steel	Zinc	Copper	Aluminium
	µm/annum	$200 < r_{corr} \leq 700$	$8,4 < r_{corr} \leq 25$	$5,6 < r_{corr} \leq 10$	—

Notes

- The classification criterion is based on the methods of determination of corrosion rates of standard specimens for the evaluation of corrosivity (see ISO 9226).
- The corrosion rates, expressed in grams per square metre per year [g/(m²-annum)], are recalculated in micrometres per year(µm/annum) and rounded.
- The standard metallic materials are characterised in ISO 9226.
- Aluminium experiences uniform and localised corrosion. The corrosion rates shown in this table are calculated as uniform corrosion. Maximum pit depth or number of pits can be a better indicator of potential damage. It depends on the final application. Uniform corrosion and localised corrosion cannot be evaluated after the first year of exposure due to passivation effects and decreasing corrosion rates.
- Corrosion rates exceeding the upper limits in category C5 are considered extreme. Corrosivity category CX refers to specific marine and marine/industrial environments

Sulfur Dioxide Deposition

Sulfate ions are formed in the surface moisture layer by the oxidation of sulfur dioxide and their formation is considered to be the main corrosion accelerating effect from sulfur dioxide. Sulfur dioxide may be expressed either in terms of a deposition rate or an airborne concentration. The method of determining the deposition rate in this instance followed the ISO 9225 Sulfation Plate Method (International Organisation for Standardisation, 2012c).

The average sulfate deposition rate observed for the period 18 April 2008 to 26 January 2009 was 0.121 mg/m²-day, with monthly deposition rates ranging from 0.076 mg/m²-day to 0.289 mg/m²-day. The average sulfate deposition rate observed during the 11 October 2012 to 11 September 2013 campaign was 0.636 mg/m²-day and ranged from 0.114 mg/m²-day to 2.563 mg/m²-day per month. The average sulfate deposition rate observed during the 11 October 2017 to 12 March 2019 campaign was 0.443 mg/m²-day and ranged from 0.040 mg/m²-day to 3.648 mg/m²-day per month (Burger, 2019).

Chlorine Deposition

Airborne salinity was evaluated and recorded in accordance with ISO 9225 (International Organisation for Standardisation, 2012c). The average chloride deposition rate observed for the period 18 April 2008 to 26 January 2009 was 216.7 mg/m²-day, with monthly deposition rates ranging from 22.7 mg/m²-day to 613 mg/m²-day. The average chloride deposition rate observed during the 11 October 2012 to 11 September 2013 campaign was 188.5 mg/m²-day and ranged from 106.1 mg/m²-day to 380.2 mg/m²-day per month. The average chloride deposition rate observed

© Eskom 2026/Rev 0c

PRINTED VERSIONS OF THIS DOCUMENT ARE NOT CONTROLLED

during the 11 October 2017 to 12 March 2019 campaign was 119.7 mg/m²-day and ranged from 52.6 mg/m²-day to 222.6 mg/m²-day per month (Burger, 2019).

(iii) Atmospheric Corrosivity Dose Response Functions

In the International Standard (ISO 9223:2012, (International Organisation for Standardisation, 2012a)), the corrosion rate for steel, zinc, copper and aluminium is calculated using dose-response functions. Dose-response functions for these standard metals are given, describing the corrosion attack after the first year of exposure in open air as a function of sulfur dioxide dry deposition, chloride dry deposition, temperature and relative humidity. The functions are based on results of worldwide corrosion field exposures and cover climatic earth conditions and pollution situations within the scope of the Standard. The general form of the dose-response function is as follows:

$$r_{corr} = c_1 P_d^{c_2} \exp(c_3 RH + c_4[T - 10]) + c_5 S_d^{c_6} \exp(c_7 RH + c_8 T)$$

where:

r_{corr} = first-year corrosion rate of metal, expressed in µm/annum

RH = annual average relative humidity, expressed as a percentage [%]

T = annual average temperature, expressed in degrees Celsius [°C]

P_d = annual average SO_2 deposition, expressed in mg/m²-day

S_d = annual average chloride deposition, expressed in mg/m²-day

$c_1 \; to \; c_8$ = are constants as defined in ***Table 5.8.52***.

© Eskom 2026/Rev 0c

PRINTED VERSIONS OF THIS DOCUMENT ARE NOT CONTROLLED

Table 5.8.52
Constants for Dose-Response Function to Estimate Corrosion Attack Rates (ISO 9223:2012)

Constant		Steel	Zinc	Copper	Aluminium
c1		1.77	0.0129	0.0053	0.004
c2		0.52	0.44	0.26	0.73
c3		0.020	0.046	0.059	0.025
c4	*T≤10*	0.150	0.038	0.126	0.004
	T>10	-0.054	-0.071	-0.080	-0.043
c5		0.013	0.017	0.010	0.0018
c6		0.62	0.57	0.27	0.60
c7		0.033	0.008	0.036	0.020
c8		0.040	0.085	0.049	0.094

A summary of the calculated corrosion rates for carbon steel, zinc, copper and aluminium using the above relationship is provided in ***Table 5.8.53***. Estimated levels of uncertainty for assessment of the corrosivity category based on the dose-response function according to ISO 9223 for carbon steel, zinc and copper are -33 per cent to +50 per cent and -50 per cent to 100 per cent for aluminium (International Organisation for Standardisation, 2012a). The estimated corrosion rate range based on these levels of uncertainty is also included in the table. The annual average relative humidity and temperature used in the relationship were 77.5 per cent and 16.7°C, respectively. Annual average sulfur dioxide and chloride deposition rates of 1.08 mg/m²-day and 277.3 mg/m²-day respectively were used. Considering the levels of uncertainty of the estimation method, the site is considered to have a high (C4) to very high (C5) corrosion potential (***Table 5.8.53***).

Table 5.8.53
ISO 9224:2012 Calculated Corrosion Rate Values for Various Metals and Exposure Periods

Metal	Corrosion Rate [µm/annum]		Corrosivity category (from *Table 5.8.51*)
	First Year	20-Year Average	
Carbon Steel	68.0 (50.6;81.6) (1)	8.8 to 11.1 (2)	C5 (C4 to C5) (1)
Zinc	2.8 (2.2;3.4) (1)	1.3 to 1.6 (2)	C4 (C4 to C4) (1)
Copper	1.8 (1.5;1.9) (1)	0.4 to 0.5 (2)	C4 (C4 to C4) (1)
Aluminium	1.0 (0.7;1.2) (1)	0.3 to 0.4 (2)	(3)

© Eskom 2026/Rev 0c

PRINTED VERSIONS OF THIS DOCUMENT ARE NOT CONTROLLED

Metal	Corrosion Rate [µm/annum]		Corrosivity category (from ***Table 5.8.51***)
	First Year	20-Year Average	

Notes
(1) Values in brackets represent level of uncertainty.
(2) Range as calculated using the average and conservative constants as presented in ***Table 5.8.52***.
(3) Aluminium is not categorised by penetration rate (µg/m²) in ***Table 5.8.51*** because aluminium alloys corrode by a pitting mechanism. The corrosion category was therefore not established.

The International Standard (ISO 9224:2012 (International Organisation for Standardisation, 2012b)), provides a relationship that can be used to indicate that the total attack, *D*, expressed either as mass loss per unit area or penetration depth, is given as:

$$D = r_{corr} t^b$$

where

D = total attack, expressed as penetration depth [µm]

r_{corr} = first-year corrosion rate of metal, expressed in µm/annum

t = exposure time, expressed in years

b = metal-environment-specific time exponent (***Table 5.8.54***)

Table 5.8.54
Constant (*b*) for Attack Depth Function (ISO 9224:2012)

Applicable Estimate	Steel	Zinc	Copper	Aluminium
Average Estimate	0.523	0.813	0.667	0.728
Conservative Estimate	0.575	0.873	0.726	0.807

The attack depth was calculated using the onsite parameters and the average estimate is illustrated in ***Figure 5.8.16*** for the first 20 years of exposure. The corrosivity at the site, based on the marine and atmospheric corrosion calculations, is considered to vary between severe and very severe. The change in corrosivity as a function of distance from the sea was discussed in the Coupon-based Corrosion Monitoring section (***Subsection 5.8.6.1.11(c)(i)***). From the average rate of change, based on coupon results at 100 m and 1000 m from the high tide mark for Thyspunt (***Table 5.8.49***), the corrosion rates closer to the sea can be extrapolated. Given that the corrosion was measured at the Thyspunt WS which is approximately 760 m from the hightide mark, applicable ratio for extrapolation is estimated to be 1.16 at 100 m. For example, using the values in ***Table 5.8.54***, the extrapolated average rates for carbon steel at 100 m from the high tide mark is estimated to be approximately 79 µg/year.

© Eskom 2026/Rev 0c

PRINTED VERSIONS OF THIS DOCUMENT ARE NOT CONTROLLED

5.8.6.2 Extreme, Severe and Rare Phenomena

5.8.6.2.1 Severe and Rare Phenomena

The IAEA standards state that rare meteorological phenomena (International Atomic Energy Agency, 2011) occur infrequently. Thus, at any station, the instruments used for routine measurements would rarely register characteristics of these phenomena. Rare meteorological phenomena, which are highly complex, are usually scaled in terms of their intensity. These intensity values may be expressed in terms of either a qualitative characteristic such as damage or a quantitative physical parameter such as wind speed.

The paucity of detailed studies on severe storm and climate hazards at Thyspunt has made it difficult to analyse and synthesise information for the purposes of quantifying the frequency of occurrence. As a result, for the purpose of this SSR, it was necessary to use information from weather observations made by the SAWS at Cape St. Francis. Although it is not possible to quantify an uncertainty in this approach, it is expected that similar weather patterns would be exhibited. This is expected because of the proximity of the site and the Cape St. Francis WS and because these locations are affected by the same synoptic scale systems (Preston-Whyte & Tyson, 1988).

© Eskom 2026/Rev 0c

PRINTED VERSIONS OF THIS DOCUMENT ARE NOT CONTROLLED

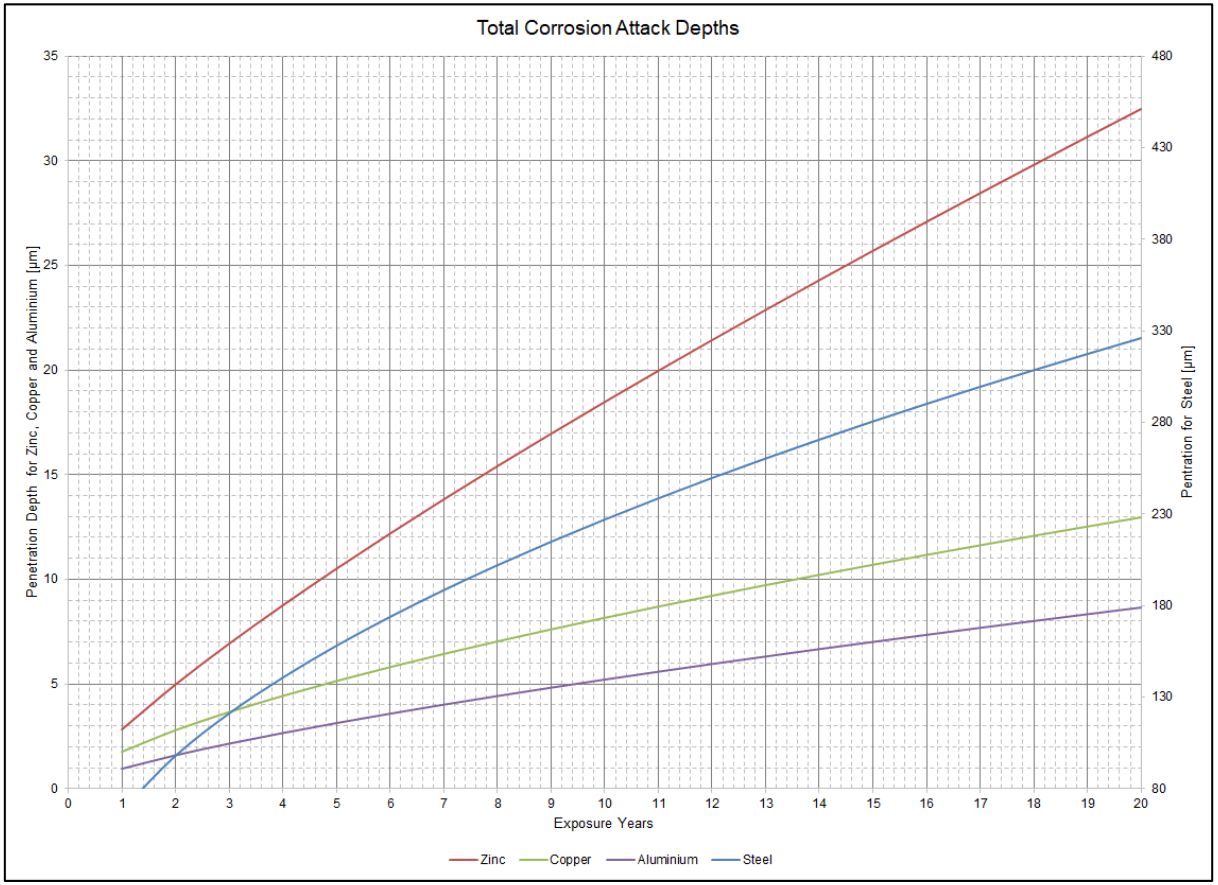


Figure 5.8.16
Calculated Corrosion Attack Depths as a Function of Time Using the ISO 9224:2012 Methodology

© Eskom 2026/Rev 0c

PRINTED VERSIONS OF THIS DOCUMENT ARE NOT CONTROLLED

(a) Severe Weather

The southern and southwestern coast of South Africa is subject to large synoptic scale systems that drive the local weather conditions in any given area. As described in the South African Weather Bureau Report WB40 (Schulze, 1986), these local weather conditions are normally characterised by low level stratus clouds and not by towering convective storms that produce hail and thunder showers. Severe weather is more closely associated with severe wind conditions. Four main wind producing systems have been identified (Preston-Whyte & Tyson, 1988):

- coastal low buster;
- cut-off lows;
- shallow southeasterlies;
- mid-latitude lows.

The last two systems are the most significant in terms of wind speed. Winds in these systems can produce speeds at ground level between 25 m/s (90 km/h) and 40 m/s (144 km/h) (Goliger & Retief, 2002), which can cause considerable damage to buildings that are not designed to withstand these conditions[41].

The site can potentially experience severe weather in the form of thunderstorms, hail, hurricane force winds and possibly tornadoes. Many of the severe storms occurring in the Eastern Cape are compound, producing various combinations of hail, wind, tornado, lightning and flash flooding. Damaging winds associated with severe thunderstorms include tornadoes, downbursts (macrobursts or microbursts)[42], straight-line winds[43], gust fronts and derechoes[44]. Historical records, covering a period of about 160 years of severe weather events in the region (radius of 100 km), lists 20 gale force or severe wind events and 3 tornadoes up to 2023 (SAWS, 1991) (SAWS, 2024d) (SAWS, 2020). The same record also lists 6 severe rain and 32 flood events. ***Appendix 5.8.I*** summarises the most severe of these events, also

[41] A typical example of such winds is the famous 'Cape Doctor'. Its average duration is between 1 and 2 days (1–2), although often several coastal lows form one after the other, and the total duration (including the periods of calm) appears to be 5–7 days. It is estimated that in total, about 30 events of 1- to 2-day duration occur along the coast. (Goliger & Retief, 2002)

[42] A downburst is created by an area of significantly rain-cooled air that, after hitting ground level, spreads out in all directions producing strong winds. Microbursts and macrobursts are downbursts at very small and larger scales, respectively. Most downbursts are less than 4 km in extent: these are called microbursts. Downbursts larger than 4 km in extent are sometimes called macrobursts (Eskom, 2023a).

[43] Straight-line winds are common with the gust front of a thunderstorm or originate with a downburst from a thunderstorm. If these winds meet or exceed 93 km/h then the storm is classified as severe (Eskom, 2023a).

[44] The term 'derecho' is used to describe larger scale straight-line winds advancing very quickly ahead of a well organised, long-lasting squall line or a large-scale multiple cell storm (International Atomic Energy Agency, 2011).

© Eskom 2026/Rev 0c

PRINTED VERSIONS OF THIS DOCUMENT ARE NOT CONTROLLED

including extreme cold and hot, dense fog, snow, frost, hail and fires (SAWS, 1991). These are discussed below.

(b) Tropical Cyclones

Nuclear power plants must be designed so that they remain in a safe condition under extreme meteorological events, including those that could result in the most extreme wind events (cyclones/hurricanes[45] and tornadoes) that could reasonably be predicted to occur at the site. The maximum probable wind speed at the site must therefore be considered in determining the acceptability of the site for a nuclear installation(s). Furthermore, site parameters must be established such that potential threats from such strong winds will pose no undue risk to the proposed and existing nuclear installation(s).

It is important to note the difference between a hurricane and hurricane force winds. The latter refers to a wind speed scale described by the Beaufort Scale as winds with speeds above 118 km/h (32.8 m/s). This wind speed (as a gust) has been exceeded on 16 days (2008 and 2007) over the 20-year monitoring period at the Cape St. Francis WS. The highest gust of 45.8 m/s occurred on 18 August 2020. The Thyspunt WS, albeit less than 9 years of data, recorded one hurricane force wind (37.9 m/s) on 2 September 2013.

The Thyspunt region is not on a hurricane (tropical cyclone) track or adjacent to a warm ocean. Therefore, it is not expected that the site will experience a cyclone, or at least there is a very low probability. Tropical cyclones are generated in areas where the ocean surface temperature is greater than 27°C and between latitudes 5°S to 30°S. The site is located south of 33°S and is therefore not subject to tropical cyclones. It is not clear how climate change will affect the occurrence of cyclones and it has not been presented in the 5th Assessment Report of the Intergovernmental Panel on Climate Change (IPCC) (Intergovernmental Panel on Climate Change, 2013).

To ensure the safety of nuclear installation(s) in the event of a hurricane strike, NRC regulations (United States Nuclear Regulatory Commission, 2011) require that nuclear installation(s) designs consider the impact of hurricane-generated missiles, in addition to the direct action of the hurricane wind. The two basic approaches used to characterise hurricane-generated missiles are (United States Nuclear Regulatory Commission, 2010):

[45] Depending on its location and strength, a tropical cyclone is referred to by different names, including hurricane, typhoon, tropical storm, cyclonic storm, tropical depression, or simply cyclone. A hurricane is a tropical cyclone that occurs in the Atlantic Ocean and northeastern Pacific Ocean, and a typhoon occurs in the northwestern Pacific Ocean; in the south Pacific or Indian Ocean, comparable storms are referred to simply as "tropical cyclones" or "severe cyclonic storms".

© Eskom 2026/Rev 0c

PRINTED VERSIONS OF THIS DOCUMENT ARE NOT CONTROLLED

(1) A standard spectrum of hurricane missiles – protection from a spectrum of missiles (ranging from a massive missile that deforms on impact to a rigid penetrating missile) provides assurance that the necessary structures, systems, and components will be available to mitigate the potential effects of a hurricane on plant safety. Given that the design basis hurricane windspeed has a very low frequency of occurrence to be credible, the representative missiles must be common items around the plant site and must have a reasonable probability of becoming airborne within the hurricane wind field.

(2) A site-specific probabilistic assessment of the hurricane hazard – no definitive guidance has been developed for use in applying hazard probability methods to characterise site dependent hurricane-generated missiles. Damage to safety-related structures by hurricanes or other wind generated missiles implies that a sequence of random events has occurred. That event sequence typically includes an occurrence of a hurricane in the plant vicinity, existence, and availability of missiles in the area, injection of missiles into the wind field, suspension and flight of those missiles, impact of the missiles on safety-related structures, and resulting damage to critical equipment.

(3) To ensure the safety of nuclear power plants in the event of a tornado or hurricane strike in the Unites States the NRC regulations require that nuclear power plant designs consider the impact of tornado or hurricane-generated missiles in addition to the direct action of the wind (United States Nuclear Regulatory Commission, 2007b; United States Nuclear Regulatory Commission, 2011). As per these NRC regulations, the wind speeds used to determine the wind gust are nominal 3-second peak-gust values corresponding to an exceedance frequency of 10^{-7} per year measured at an approximate height of 10 m above ground level in flat open terrain. From an analysis of wind gusts observed at the 10 m level of the Cape St. Francis WS for the period 2004 to 2023, the wind gust corresponding to an exceedance frequency of 10^{-7} per year is estimated to be between 74.2 m/s and 92.3 m/s (see ***Subsection 5.8.6.2.2***).

(c) Tornadoes

Tornadoes[46] are amongst the most violent and destructive of all extreme weather phenomena. Tornadoes in South Africa are typically associated with very hot air masses and severe thunderstorms (Goliger, et al., 1997). There are several different methods of classifying tornadoes. Historically, South Africa used the 'Fujita-Pearson scale classification' (Goliger, et al., 1997) to record tornado occurrences. This system classifies tornadoes in

[46] A tornado, from the Latin tornare ('to turn'), is a violent rotating column of air extending from a thunderstorm.

© Eskom 2026/Rev 0c

PRINTED VERSIONS OF THIS DOCUMENT ARE NOT CONTROLLED

six intensities, ranging from F0 (no damage) to F5 (incredible damage). The intensity is based on the apparent damage to structures, the extent of the path and other descriptors from which wind speeds are then inferred. About 65 per cent of the South African tornadoes (Goliger, et al., 1997) are classified as F0 or F1 (light damage), while more than 90 per cent are classified as F0, F1 or F2 (considerable damage, with maximum wind speeds of up to 70 m/s). Only about 8 per cent of the documented tornadoes were F3, i.e. severe damage, with maximum wind speeds of up to 90 m/s. The tornado which occurred in Mount Ayliff (Eastern Cape Province) in January 1999 was seemingly the most severe ever reported in South Africa, with a classification of F4. The Fujita Scale has been replaced in some countries by the updated Enhanced Fujita Scale (EF-Scale). As with the Fujita Scale, the EF-Scale is still a set of wind estimates (not measurements) based on damage. It uses three-second gusts estimated at the point of damage based on a judgment of 8 levels of damage to a set of 28 indicators ranging from damage to small barns and farm outbuildings (indicator 1) to destruction of soft-wood trees (indictor 28). These estimates vary with height and exposure. The EF-Scale more accurately matches wind speeds to the severity of damage, as opposed to the Fujita scale that classifies only on a scale of damage. The EF-Scale was formulated due to research which suggested that the wind speeds required to inflict damage by intense tornadoes on the Fujita Scale are greatly overestimated. A process of expert elicitation with top engineers and meteorologists developed a correlation between the original Fujita Scale and the EF-Scale wind speeds for the historical Fujita Scale database to be preserved. By correlating the Fujita Scale wind speeds with the EF-Scale wind speeds, a tornado rated according to the Fujita Scale will have the same “F-Number” in the EF-Scale, e.g. F3 translates into EF3, although the wind speed ranges are different. The wind speeds based on the equivalent EF-Scale are summarised in ***Table 5.8.55*** (McDonald & Mehta, 2006).

Table 5.8.55
EF-Scale Wind Speed Ranges Derived from Fujita-Scale Wind Speed Ranges (McDonald & Mehta, 2006)

Enhanced Fujita Scale (Fujita Scale)	3-Second Gust Estimate	Fujita-Scale Description
EF0 (F0)	105 to 137 km/hr 29 to 38 m/s	Light damage. Some damage to chimneys; branches broken off trees; shallow-rooted trees pushed over; sign boards damaged.

© Eskom 2026/Rev 0c

PRINTED VERSIONS OF THIS DOCUMENT ARE NOT CONTROLLED

Enhanced Fujita Scale (Fujita Scale)	3-Second Gust Estimate	Fujita-Scale Description
EF1 (F1)	138 to 177 km/hr 39 to 49 m/s	Moderate damage. The lower limit is the beginning of hurricane wind speed; peels surface off roofs; mobile homes pushed off foundations or overturned; moving vehicles pushed off the roads; attached garages may be destroyed.
EF2 (F2)	178 to 217 km/hr 50 to 60 m/s	Significant damage. Roofs torn off frame houses; mobile homes demolished; boxcars overturned; large trees snapped or uprooted; high-rise windows broken and blown in; light-object missiles generated
EF3 (F3)	218 to 269 km/hr 61 to 75 m/s	Severe damage. Roofs and some walls torn off well-constructed houses; trains overturned; most trees in forests uprooted; heavy cars lifted off the ground and thrown.
EF4 (F4)	270 to 322 km/hr 76 to 89 m/s	Devastating damage. Well-constructed houses levelled; structures with weak foundations blown away some distance; cars thrown, and large missiles generated.
EF5 (F5)	>322 km/hr >89 m/s	Incredible damage. Strong frame houses lifted off foundations and carried considerable distances to disintegrate; automobile-sized missiles fly through the air farther than 100 metres; trees debarked; steel-reinforced concrete structures badly damaged and skyscrapers toppled

On the basis of the available tornado occurrences from 1905 to 2023 (Goliger, et al., 1997) (SAWS, 2024d) an estimate of tornado frequency for the site was made by spatial analyses of location and corresponding intensities of all tornado recordings listed by the SAWS as well as those in ***Table 5.8.56***. The table includes tornadoes witnessed up to a maximum distance of about 300 km from the site, which corresponds to the Thyspunt region used in the Seismic Study. One occurrence of a waterspout was witnessed, albeit along the coast at Herold's Bay, which is approximately 215 km west of the site. Similar to a tornado on land, a waterspout is a rotating column of air that occurs over a body of water, usually appearing as a funnel-shaped cloud in contact with the water and a cumuliform cloud. These may occur as a weak vortex known as a "fair weather" or "non-tornadic" waterspout, which is more common than a classic tornado occurring over water rather than land. The reporting at Herold's Bay did not qualify whether it was of the former or later type. The rarity of waterspouts off the coast near the site, is likely because these occur mostly in tropical and subtropical areas.

The likelihood of a tornado striking a specific region can be expressed in terms of the number of tornadoes over a given period of time reported within

© Eskom 2026/Rev 0c

PRINTED VERSIONS OF THIS DOCUMENT ARE NOT CONTROLLED

a specific unit area (Goliger, et al., 1997). The frequency of tornadoes listed for this area is 23 over a period of 116 years (***Table 5.8.56***), therefore a frequency of about 0.20 per year. Six occurrences were within a distance of less than 100 km, whilst 11 occurred further than 200 km from the site. Six occurrences occurred between 100 km and 200 km from the site. Most tornado occurrences (74 per cent) therefore occurred beyond 100km from the site.

Using the distances from the site to the reported locations of the tornadoes (***Table 5.8.56***), and calculating the area included by these radiuses, the average tornado strike frequency (irrespective of the severity) was calculated to be $5.0x10^{-6}$ per year per km², with a minimum estimate of $4.0x10^{-6}$ per year per km² and a maximum estimate of $1.0x10^{-5}$ per year per km². This confirms the result obtained by Goliger *et al* (Goliger, et al., 1997), as displayed in (***Figure 5.8.17***), which indicates that the frequency is 10^{-5} or less per year per km².

Using the estimated probabilities for the various tornado severities, discussed above, it is estimated that the frequencies are $1.6x10^{-6}$ per year per km² for F0, $2.9x10^{-6}$ per year per km² for F1, $5.0x10^{-7}$ per year per km² for F2, and $3.8x10^{-8}$ per year per km² for F3. Over the 116 years included in the analysis, three F4 tornadoes have been recorded in South Africa (Welkom, Free State – 20 March 1990, Mount Ayliff, Eastern Cape – 18 January 1999, and Duduza, Gauteng – 2 October 2011), indicating a probability of an order lower than F3 tornado intensity, with 26 occurrences. Conservatively, a frequency of $3.8x10^{-9}$ per year per km² may be assumed for F4 and F5.

From ***Table 5.8.56*** it is evident that tornado activity has increased since 1996 albeit only up to F1 scale. Twelve tornadoes were reported during the 74 years from 1907 to 1980 and 11 tornadoes during the 25 years from 1996 to 2020. Whilst climate change may have contributed to increases in tornado frequencies, it may also simply be that the reporting of tornadoes has increased due to population spread as well as the associated damage to property. Nevertheless, considering the past 25 years' tornado history in ***Table 5.8.56***, the number of tornadoes were 11 and therefore the probability of a tornado increases to 0.44 per year. The average tornado strike frequency estimate would then increase to $2.3x10^{-5}$ per year per km², and the frequencies per severity increase to $4.8x10^{-6}$ per year per km² for F0 and $3.2x10^{-6}$ per year per km² for F1.

© Eskom 2026/Rev 0c

PRINTED VERSIONS OF THIS DOCUMENT ARE NOT CONTROLLED

Table 5.8.56
Summary of Tornado Phenomena Recorded Around Thyspunt Area (1905-2020) ((Goliger, et al., 1997) (SAWS, 2024d))

Location	Date	F-Scale	Distance from Site (km)
Graaff-Reinet	8 January 1907	F1	215
Jansenville	8 January 1907	F1	137
Fort Cox	30 May 1916	F3	266
Bedford	11 February 1953	F1	210
Port Elizabeth	16 March 1956	F2	74
Fort Beaufort	17 January 1958	F0	236
Uitenhage	25 January 1959	F0	76
Patensie	8 February 1961	F1	48
Paterson	1 February 1962	F1	142
Oudtshoorn	4 May 1975	F1	241
Port Elizabeth	10 October 1978	F1	74
Grahamstown	26 December 1980	F1	194
Fort Beaufort	5 January 1996	F1	236
Port Elizabeth	2 November 2000	F1	74
Jansenville	2 February 2005	F1	137
George (1)	24 December 2007	F? (2)	207
Port Elizabeth (1)	12 October 2012	(3)	74
Calitzdorp (1)	9 January 2014	F? (2)	290
Mossel bay (1)	10 December 2014	F? (2)	238
Plettenberg bay (1)	5 March 2015	F? (2)	124
Adelaide (1)	24 January 2017	(3)	220
Sedgefield (1)	23 September 2019	F?	178
Herold's Bay(1)	9 October 2019	WS	215

Notes
(1) Not included in SAWS database but listed in https://sawx.co.za/resources/history-tornadoes-south-africa/.
(2) Listed in as a tornado but the F Scale is unknown (https://sawx.co.za/resources/history-tornadoes-south-africa/)
(3) Listed in as a possible tornado but the F Scale is unknown (https://sawx.co.za/resources/history-tornadoes-south-africa/)

In the second approach, all recorded tornadoes were included in the analysis and a spatial interpolation applied to estimate the frequency over South Africa, as per Goliger *et al* (Goliger, et al., 1997). The locations of these tornadoes and Fujita-Scales for the period 1905 to 2020 are shown in ***Figure 5.8.17***. The inter-distance between all tornadoes were used to establish optimal spatial clusters that would be representative of tornado bins. A large cluster would incorporate more tornado occurrences; however, the larger area would reduce the frequency spatially (i.e. per km²).

© Eskom 2026/Rev 0c

PRINTED VERSIONS OF THIS DOCUMENT ARE NOT CONTROLLED

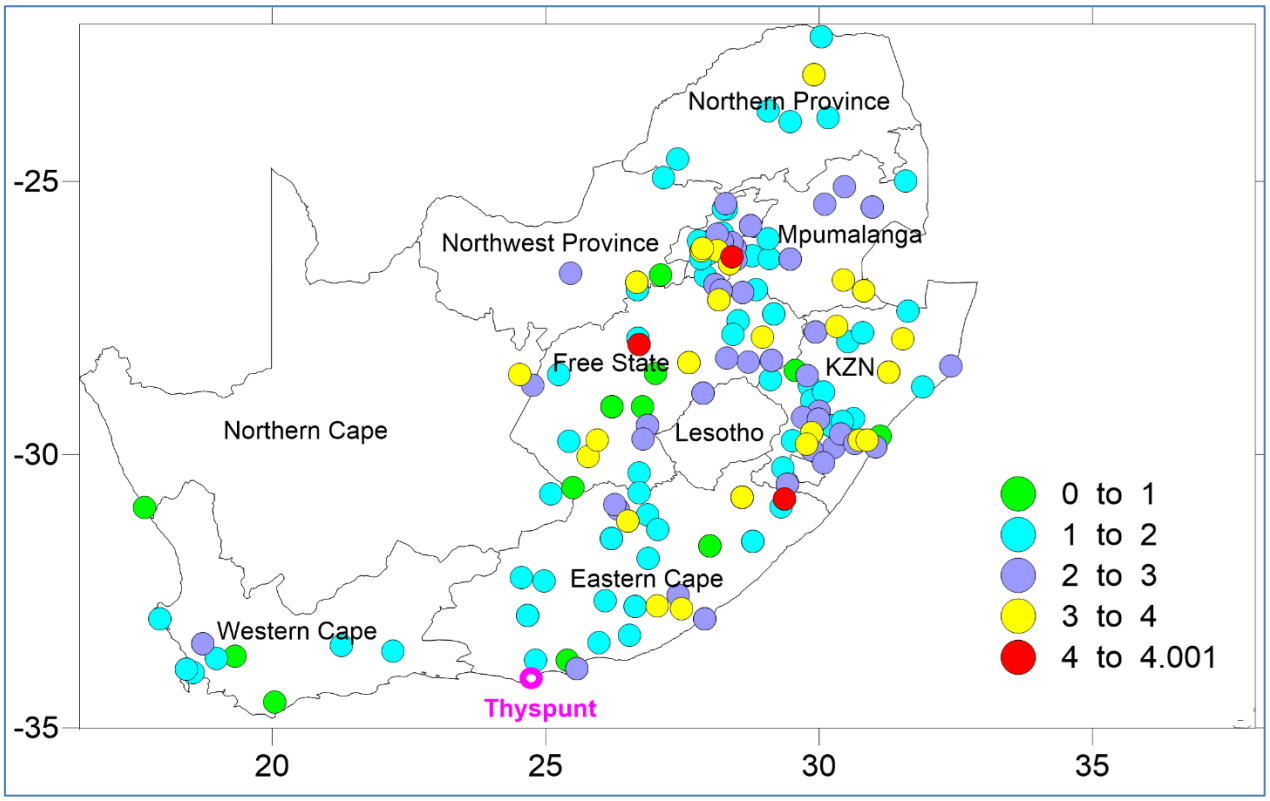


Figure 5.8.17
Occurrence of Tornadoes for Period from 1905 to 2020

A smaller cluster would have a lower number of tornadoes; however, the smaller area may increase the spatial value. Based on an analysis of the 222 tornadoes, it was calculated that by grouping tornadoes into regions represented by circles with a radius of 120 km, the tornado frequency per km² estimate would reach a maximum. The number of tornadoes per cluster and per Fujita-Scale was therefore determined for the 116-year period and these totals divided by the cluster area (i.e. area of circle with radius 120 km = 45 239 km²). The resulting tornado frequency distributions for South Africa for the four Fujita Scales are shown in ***Figure 5.8.18*** to ***Figure 5.8.21***.

© Eskom 2026/Rev 0c

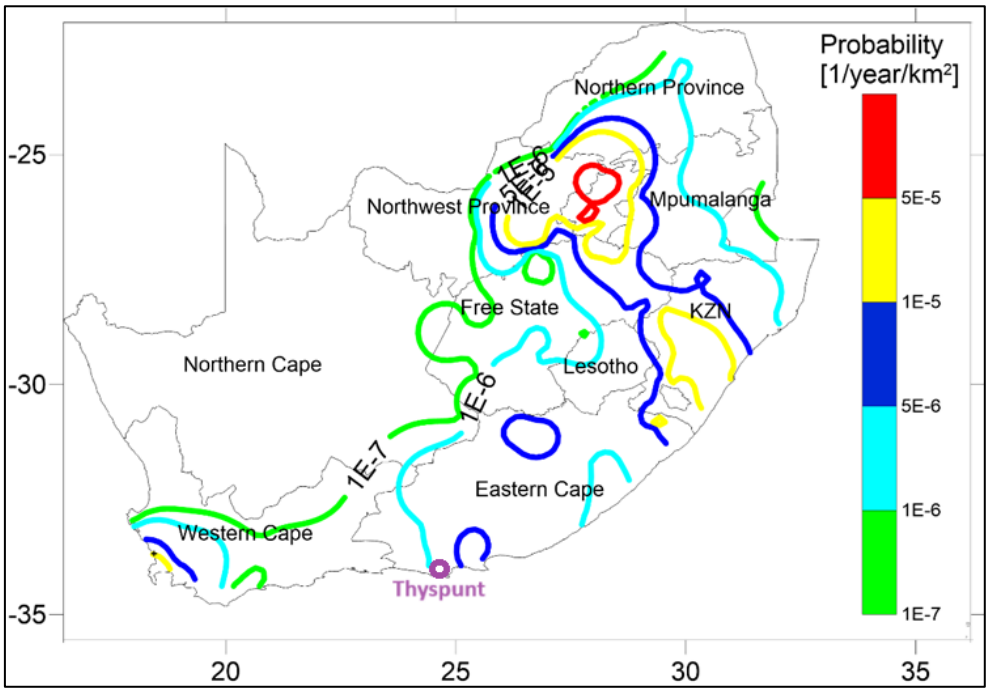


Figure 5.8.18
Average Annual Rate of Occurrence of F1 Tornadoes (1905 to 2020)

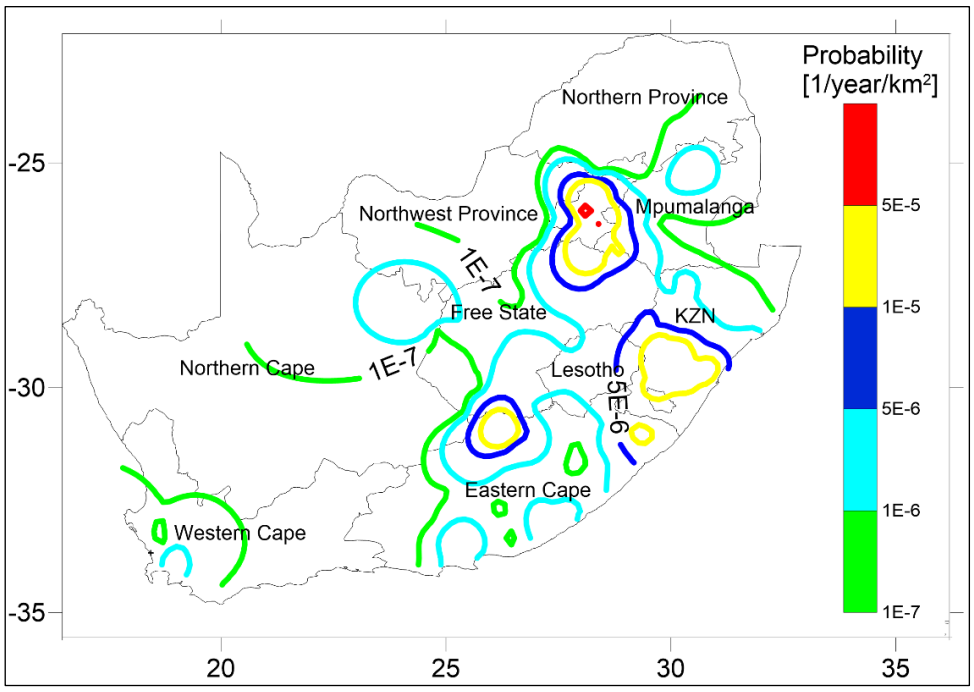


Figure 5.8.19
Average Annual Rate of Occurrence of F2 Tornadoes (1905 to 2020)

© Eskom 2026/Rev 0c

PRINTED VERSIONS OF THIS DOCUMENT ARE NOT CONTROLLED

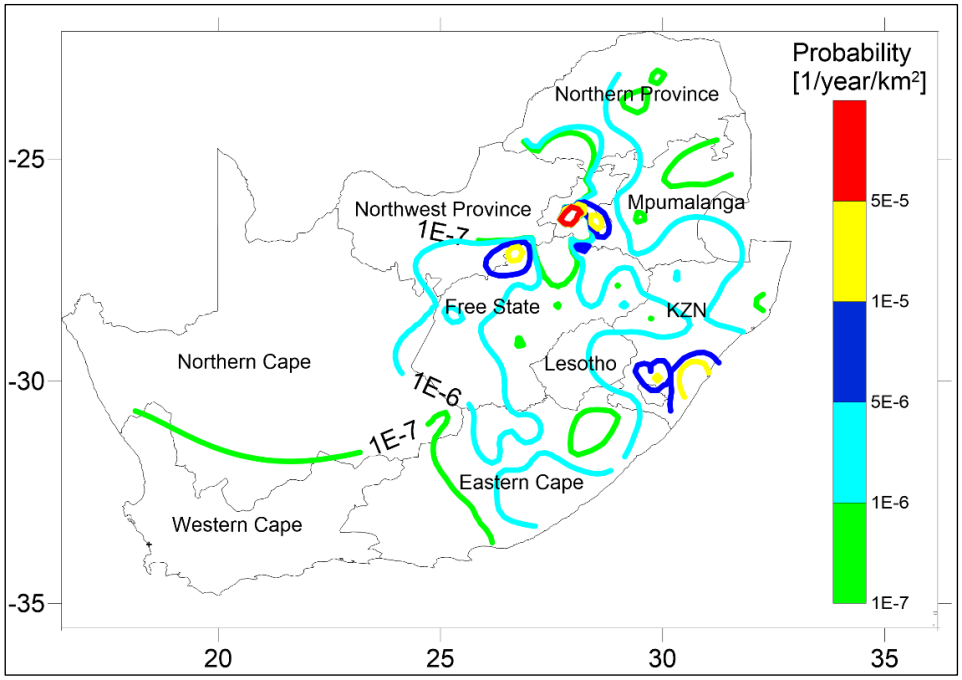


Figure 5.8.20
Average Annual Rate of Occurrence of F3 Tornadoes (1905 to 2020)

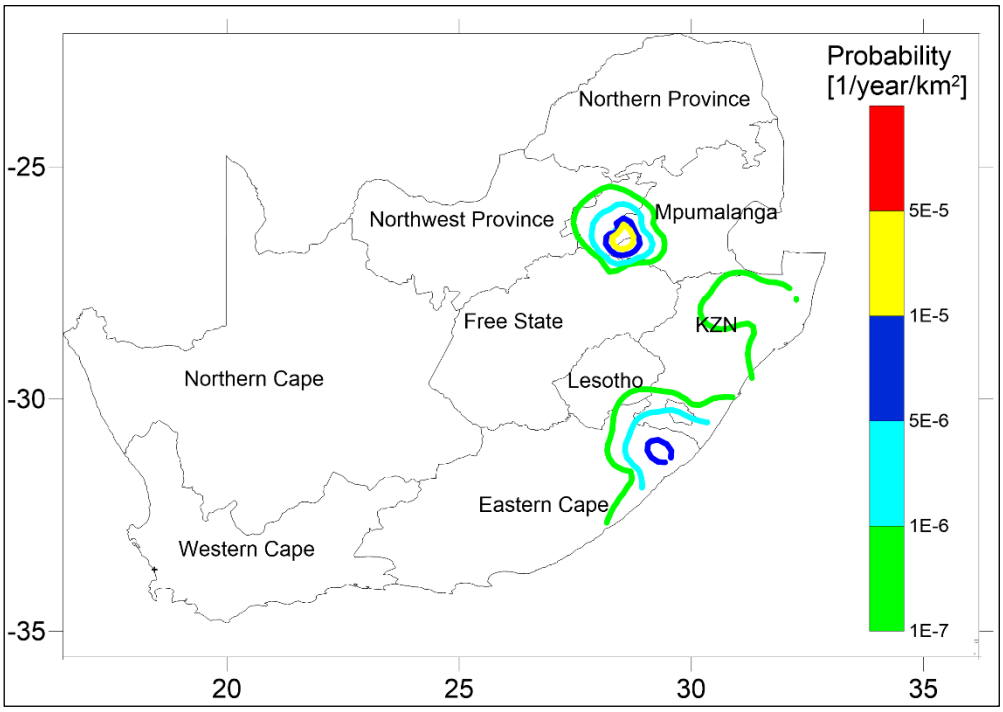


Figure 5.8.21
Average Annual Rate of Occurrence of F4 Tornadoes (1905 to 2020)

© Eskom 2026/Rev 0c

PRINTED VERSIONS OF THIS DOCUMENT ARE NOT CONTROLLED

Using the calculated probabilities for the various tornado severities, discussed above, it is estimated that the average tornado strike frequency for the site (irrespective of the severity) was calculated to be $6.8x10^{-6}$ per year per km². The frequencies per severity are $1.3x10^{-6}$ per year per km² for F0, $2.1x10^{-6}$ per year per km² for F1, $6.6x10^{-7}$ per year per km² for F2, and less than $1.0x10^{-8}$ per year per km² for F3. Based on the scarcity of F4 tornadoes in South Africa, a probability of an order lower than F3 tornado intensity may be assumed. Although no F5 tornadoes have been witnessed in South Africa since 1905, a frequency less than $1.0x10^{9}$ per year per km² may therefore be assumed for F5.

Adjusting these results to account for the observed recent increases in tornado observations over the past 25 years, the average tornado strike frequency estimate increases to $3.2x10^{-5}$ per year per km², and the frequencies per severity increase to $4.0x10^{-6}$ per year per km² for F0 and $2.3x10^{-6}$ per year per km² for F1, but no F2, F3 and F4 tornadoes were observed. As previously discussed, a frequency less than $1.0x10^{8}$ per year per km² may be assumed for F3 and F4, and less than $1.0x10^{9}$ per year per km² for F5.

As concluded by Goliger *et al* (Goliger, et al., 1997), it is extremely difficult to obtain direct and reliable wind speed records from a tornado, and this necessitated the use of indirect methods of estimating the tornado wind speeds, such as those used in the EF-Scale. According to the above analysis, EF2 tornadoes at the site have an expected probability that is above 10^{-7} per year and EF3 tornadoes well below 10^{-7} per year. Using the EF-Scale, the estimated maximum tornado wind speeds are estimated to be 61 m/s to 75 m/s (***Table 5.8.55***) (McDonald & Mehta, 2006).

As an alternative, the frequency may be based on the affected area of the tornado path assuming uniformly distributed strikes within the area of interest (i.e. 300 m radius) used above. This approach requires knowledge of tornado path length and width, and for the current purposes used the path length and widths which are associated with the Enhanced-Fujita Scale as determined by and summarised in (***Table 5.8.57***).

Using the number of recorded tornadoes of 23 in the area of interest over a period of 116 years, total area in the tornado path is calculated as 40.375 km² (***Table 5.8.58***).

© Eskom 2026/Rev 0c

PRINTED VERSIONS OF THIS DOCUMENT ARE NOT CONTROLLED

Table 5.8.57
Tornado Path Length and Width Correlated to Enhanced-Fujita Scales (Elsner, et al., 2014)

Scale	Path Length [km]				Path Width [m]			
	Range		Median	Average	Range		Median	Average
	Lower Quartile	Upper Quartile			Lower Quartile	Upper Quartile		
EF0	0.29	2.7	0.8	2.27	22.9	68.6	45.7	54.9
EF1	1.77	9.33	4.4	7.1	68.6	182.9	91.4	163.8
EF2	4.53	19.25	10	14.3	137.2	402.3	228.6	344.1
EF3	12.38	36.34	23	29.1	339.5	1005.8	548.6	736.3
EF4	17.07	64.63	35	52.6	603.5	1207	804.7	997.9
EF5	45.51	65.93	59	72	1207	1609.3	1920.2	1635.8

Table 5.8.58
Calculated Tornado Path Areas (1905-2020)

Scale	Tornado Path								
	Length [km]	Width [m]	Area [km²]	Number Recorded		Total Area [km²]		Total Length [km]	
				1905 - 2020	1987-2020	1905 - 2020	1987-2020	1905 - 2020	1987-2020
F0	2.27	54.9	0.1	10	7	1.246	0.872	22.7	15.9
F1	7.1	163.8	1.2	11	4	12.793	4.652	78.1	28.4
F2	14.29	344.1	4.9	1	0	4.917	0.000	14.3	0
F3	29.09	736.3	21.4	1	0	21.419	0.000	29.1	0
F4	52.55	997.9	52.4	0	0	0.000	0.000	0	0
F5	71.95	1635.8	117.7	0	0	0.000	0.000	0	0
TOTAL				23	11	40.375	5.524	144.2	44.3

As per (Ramsdell, J. V.,Jr; Rishel, J. P., 2007), the annual strike frequency would then be:

$$P_p = \frac{A_t}{NA_r}$$

Where, A_t is the total tornado path area in the region of interest, A_r, and N is the number of years of record of tornado strikes. The inherent assumption is that tornado strikes within the area of interest A_r are uniformly distributed. With $A_t = 40.3752$ km², $A_r = 282743.3$ km² ($A_r = \pi R^2 = \pi\, 300^2 = 282743.3$), and $N = 116$, the annual strike frequency is calculated to be 1.2x10^{-6}. Alternatively, if only half of the area is considered to be land-based, the annual strike frequency is calculated to be 2.5x10^{-6}. If the tornado

© Eskom 2026/Rev 0c

PRINTED VERSIONS OF THIS DOCUMENT ARE NOT CONTROLLED

numbers for the latest 34 years are used, the annual strike frequency is calculated to be 7.8x10^{-7} (full area) and 1.6x10^{-6} (half area).

To estimate the additional probability of a tornado striking a large structure, it is necessary to determine a characteristic dimension of the structure and the expected length of the tornados. The additional annual strike frequency is given by (Ramsdell, J. V.,Jr; Rishel, J. P., 2007)

$$P_{ps} = \frac{w_s L_t}{N A_r}$$

Where the impacted area is the product of a characteristic dimension of the structure w_s and the total length of the tornado paths, L_t. Assuming for illustrative purposes, $w_s = 1\,000$ m, the additional annual strike frequency based on the 116 years' data is calculated to be 4.4x10^{-6} (8.8x10^{-6} half area) and the total annual strike frequency therefore 5.6x10^{-6} (1.1x10^{-5} half area). The additional annual strike frequency based on the 25 years' data is calculated to be 6.3x10^{-6} (1.3x10^{-5} half area) and the total annual strike frequency therefore 7.0x10^{-6} (1.4x10^{-5} half area). It is noted that these calculated probabilities are very similar to the values obtained with the previous two methods, i.e. for the 116-year database, 5.0x10^{-5} per year per km² and 6.8x10^{-6} per year per km², respectively.

The pressure drop and rate of pressure drop estimates are taken from the methodology given in the US NRC Guide for Design-Basis Tornado and Tornado Missiles for Nuclear Power (United States Nuclear Regulatory Commission, 2007b). The US NRC Guide defines the tornado maximum rotational wind speed as the difference between the maximum tornado wind speed and the translational speed. The tornado translational speed for the tornado is one fifth of the maximum tornado wind speed. As discussed above, using the EF-Scale, the estimated maximum tornado wind speeds for the site are estimated to be 61 m/s to 75 m/s (***Table 5.8.55***) (McDonald & Mehta, 2006). Using the US NRC Guide (United States Nuclear Regulatory Commission, 2007b) the maximum rotational wind speed is estimated to be 57 m/s and the translational wind speed estimated to be 14 m/s (Table 1 in the US NRC Guide). For the current purposes, since the maximum tornado wind speeds is estimated to be 75 m/s wind speed[47], the maximum rotational speed is assumed to be 60 m/s and the translational wind speed 15 m/s. The characteristic pressure drop for these conditions is 40 hPa and the rate of pressure drop to be 13 hPa/s.

[47] Using the EF-Scale, the estimated maximum tornado wind speeds for EF3 are estimated to be 61 m/s to 75 m/s (Table 5.8.55) (McDonald & Mehta, 2006). The maximum is assumed.

© Eskom 2026/Rev 0c

PRINTED VERSIONS OF THIS DOCUMENT ARE NOT CONTROLLED

(d) Severe thunderstorms

Given the low likelihood of tornadoes in the region, as discussed in the previous section, the majority of severe thunderstorms are therefore most probably non-tornadic. Downbursts and straight-line winds, as opposed to tornadic winds, would mostly be accountable for damage to property and livelihoods at the site. A downburst is an exceptionally energetic downdraft that exits at the base of a thunderstorm and spreads out at the earth's surface as strong and gusty horizontal winds that may cause property damage (Greer, 1996). Winds may reach 280 km/h in exceptionally powerful events (Geer, 1996). Gust fronts, straight-line winds and derechoes develop along the leading edge or outflow boundary of an advancing thunderstorm. Straight-line winds, usually blowing from one direction, as distinct from rotational winds in tornadoes, develop in association with gust fronts and may cause considerable damage, with winds of up to 160 km/h. The highest wind speed (gust) on record based on the Cape St. Francis WS was 45.8 m/s (165 km/h) (***Table 5.8.15***). The highest recorded at the Thyspunt site was 32.2 m/s (116 km/h) (***Table 5.8.15***).

As given in ***Subsection 5.8.6.1.5***, it is estimated, based on observations at Cape St. Francis, that the number of thunder days at the site is 7.2 per year. There appears to be no preference to a specific season or month; however, the likelihood is lowest during June and July.

(e) Hail

The average number of days with hail at the site is estimated to be 0.8 per year (***Subsection 5.8.6.1.5*** and (Schulze, 1986)).

(f) Lightning

Lightning data have been collected in the vicinity of the site, and the SAWS provided valid data for the period July 2007 to December 2008 (Mzukisi & Mkhwanazi, 2010). The number of strikes recorded during this period was 211. The average number of strokes per flash was 5 with a maximum of 16. The area included in the observation was approximately 15.8 km by 15.9 km. The site therefore experiences less than 1 lightning flash per year per km². The highest peak cloud to ground current recorded during the period was 166 kA with an average of 25 kA.

A Lightning Detection Network (LDN) was set up in 2006 by the SAWS in South Africa. The annual average lightning stroke/flash ratio was found to be 2.4 (Gijben, 2021). The annual CG flash density for South Africa according to the LDN observations for the period 2006 to 2018 is shown in

© Eskom 2026/Rev 0c

PRINTED VERSIONS OF THIS DOCUMENT ARE NOT CONTROLLED

Figure 5.8.22 (Gijben, 2021). From this observation, the cloud to ground flash density confirms the lightning density to be less than 1 lightning flash per year per km².

Lightning activities were also measured at the Thyspunt WS from June 2017 to October 2019. The average annual number of lightning strokes measured at the Thyspunt WS was 179 887 strokes. The number of flashes has been estimated assuming a minimum of 2.5 strokes per flash (Gijben, 2021) as the Upper Estimate (14 710 flashes), 25 strokes per flash as the Lower Estimate (1 765 flashes) (Gill, 2009) and 13.75 strokes per flash (mid value) as the Middle Estimate (7 881 flashes)[48]. The flash density for the monitoring period is therefore estimated to be between 0.4 and 3.3 flashes per km², with a mid-value of 1.8 flashes per km², which is slightly higher than the SAWS observations.

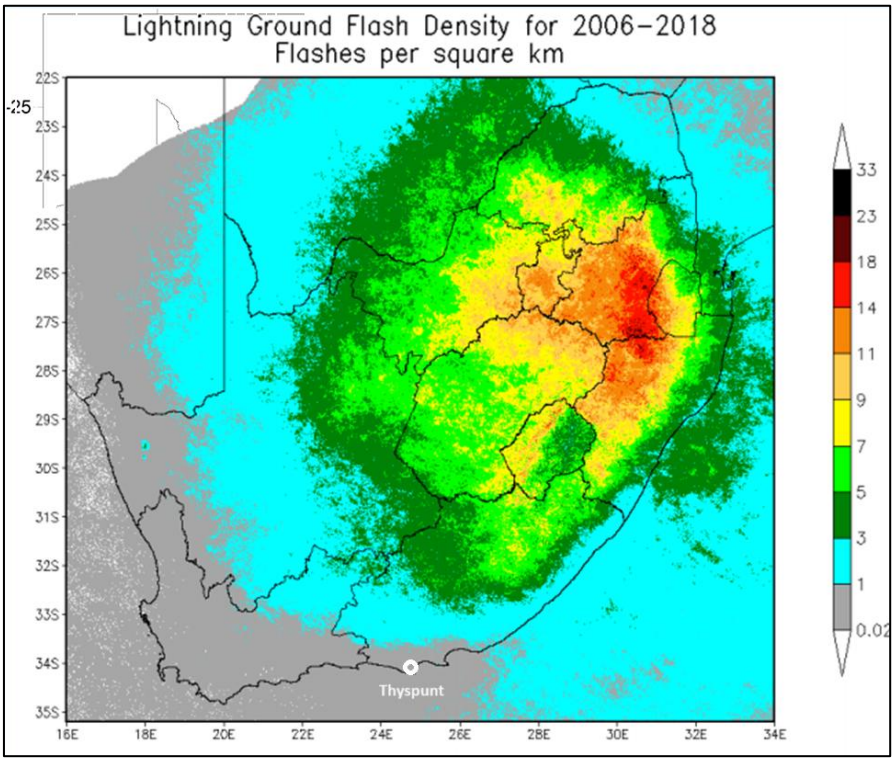


Figure 5.8.22
Average Annual Ground Flash Density (flashes/km²) for 2006 to 2018 (Gijben, 2021)

[48] A flash consists of one or perhaps as many as 25 return strokes (Rakov, 2007; Gill, 2009). International studies done on stroke multiplicity in cloud to ground (CG) lightning flashes found that the average negative stroke multiplicity is 4.6, 6.4, 3.4 and 4.5 for Florida, New Mexico, Sweden and Sri-Lanka respectively (Rakov & Huffines, 2003). Similar CG stroke multiplicity of 4.2 was found in South Africa by (Schonland, 1956)and 3.5 by (Malan,, 1956).

© Eskom 2026/Rev 0c

PRINTED VERSIONS OF THIS DOCUMENT ARE NOT CONTROLLED

5.8.6.2.2 Extreme Meteorological Variables

Extreme values of meteorological variables (International Atomic Energy Agency, 2019), such as air temperature and wind speed need to be considered in the development of the nuclear installation(s). These variables are measured routinely over a network of fixed stations. These measurements are normalised e.g. data collected on wind speed are normalised to given heights. The extreme values, associated with the annual probabilities of being exceeded, have been derived from the measurements. The following three extreme variables are considered of importance for the nuclear installation(s) on the site:

- extreme rainfall;
- extreme air ambient temperature;
- extreme wind.

Since the meteorological data collected at the Thyspunt WS covers a period of less than 9 years, it was decided to instead analyse the longer-term extreme observations from the Cape St. Francis WS. Annual and 24-hour total rainfall data for a 39-year the period (1985 to 2023, excluding 2004) were available for analyses, whereas wind speed and temperature data were available for a shorter, 20-year period (2004 to 2023). Although not ideal for extrapolating to the required return periods, these data are considered passable to provide estimates of the extreme values for rainfall, temperature and wind speed. The confidence in the statistically expected extremes and return periods improve with the timeframe of the data record; this is addressed further in the section on uncertainty.

Extreme value analysis was performed by fitting an extreme distribution (i.e. Gumbel) using Method of Moments, Method of L-Moments, Method of Maximum Likelihood, Gumbel's Fitting Method and the Method of Least Squares (see ***Appendix 5.8.B***). The highest peaks (e.g. wind gust, extreme minimum and maximum temperatures) per year were used in the analysis. The uncertainty was calculated using a Jackknife resampling method. The Jackknife samples are computed by leaving out one observation from the set of observations at a time. Each Jackknife sample is then used to evaluate the average and standard deviation of the estimate. For each annual probability of exceedance, the 95 per cent confidence interval is calculated assuming a normal distribution, i.e. 1.96 × standard deviation.

(a) Extreme Rainfall

Rainfall has been measured at the site during the two monitoring periods 2008 to 2013 and 2017 to 2019. However, 2013, 2017 and 2019 were

© Eskom 2026/Rev 0c

PRINTED VERSIONS OF THIS DOCUMENT ARE NOT CONTROLLED

incomplete years and therefore only 6 years are available[49] to support long-term projections. Instead, the extreme analysis was based on the Cape St. Francis WS rainfall data for the 1985-2023 period (***Subsection 5.8.6.1.3***).

The highest hourly, 24-hourly, monthly and annual precipitation were 37.4 mm, 157.8 mm, 366.0 mm and 972.2 mm, respectively. Extreme value analyses were performed on the observed annual and 24-hour totals for the 38-year period (1985-2023, missing 2004). The statistical approach which was followed in the analyses is discussed in ***Appendix 5.8.B***. Extreme values for probabilities ranging from "1-in-10" to "1-in-100 000 000" (or $1x10^{-1}$ to $1x10^{-8}$ or return periods of 10 to 100 000 000 years) were calculated by fitting observed rainfall totals to a Gumbel distribution function. The results from the analysis for annual totals and 24-hour storms are given in ***Table 5.8.59*** and ***Table 5.8.60***, respectively.

Table 5.8.59
Expected Annual Total Rainfall in Return Periods of 10 to 100 000 000 Years at the Site (38 Years) Based on Cape St. Francis WS Observations

Return Periods	Annual Total Rainfall (mm)	
	Annual	95th Confidence Interval
10	858.7	± 84.8
100	1187.9	± 147.1
1 000	1511.2	± 212.2
10 000	1833.8	± 278.4
100 000	2156.4	± 345.0
1 000 000	2479.0	± 412.0
10 000 000	2801.6	± 479.0
100 000 000	3124.2	± 546.2

Table 5.8.60
Expected Maximum 24-hour Total Rainfall in Return Periods of 10 to 100 000 000 Years at the Site (38 Years) Based on Cape St. Francis WS Observations

Return Periods	24-Hour Storm (mm)	
	Annual	95th Confidence Interval
10	99.0	± 20.8
100	151.4	± 38.8
1 000	202.9	± 56.8

[49] Although the total length of the meteorological database is approximately seven years, only the following calendar years included measurements of one-year durations: 2008, 2009, 2010, 2011, 2012 and 2018. Measurements during 2017 started in September 2017, and measurements during 2019 were only until September 2019. Only 8 months measurements were available during 2013. Therefore, only six calendar years available for rainfall analysis.

© Eskom 2026/Rev 0c

PRINTED VERSIONS OF THIS DOCUMENT ARE NOT CONTROLLED

Return Periods	24-Hour Storm (mm)	
	Annual	95th Confidence Interval
10 000	254.3	± 74.9
100 000	305.6	± 93.0
1 000 000	357.0	± 111.1
10 000 000	408.4	± 129.2
100 000 000	459.7	± 147.3

According to the latest climate change projections (5th Assessment Report the IPCC (Intergovernmental Panel on Climate Change, 2013) (ARP5), both increases and decreases in heavy precipitation are predicted over southern Africa, depending on the region and precipitation statistical parameter examined. Changes in wet-day intensity and in the fraction of days with rainfall higher than 20 mm are expressed in units of standard deviations. Accordingly, the projections show a decrease of up to 0.4 standard deviations for the former and a decrease up to 0.6 for the latter for the site. Changes in percentages of days with precipitation above the 95 per cent quantile are projected to be reduced by up to 1 per cent in the Western Cape in both the near-future (typically 2050) and far-future (typically 2100). Downscaled climate change models have been prepared for South Africa by SAWS (South African Weather Service, 2017) and the Council for Scientific and Industrial Research (CSIR) (Engelbrecht, et al., 2019) and (CSIR, 2019)). The CSIR (CSIR, 2019) study, which provided projections for near (2021-2050) and far (2071-2099) horizons, were used in current analyses.

In order to accommodate the uncertainties in future greenhouse gas (GHG – most importantly, carbon dioxide (CO_2), methane (CH_4) and nitrous oxide (N_2O)) emission scenarios, a standard set of scenarios were used in ARP5 to ensure that the starting conditions, historical data, and projections employed by the different groups are complementary, comparable and consistent across the various branches of climate science. These scenarios are called Representative Concentration Pathways (RCPs) that describe alternative assumptions about selected approximate total radiative forcing values for the year 2100 relative to 1750 (Intergovernmental Panel on Climate Change, 2013). RCPs are scenarios depicting the evolution of emissions and concentrations of the most important GHGs, aerosols, chemically active gases and those related to changes in land use and land cover resulting in specified levels of radiative forcing. For each category of emissions, an RCP contains a set of starting values and the estimated emissions up to 2100, based on assumptions about economic activity, energy sources, population growth and other socio-economic factors. There are four pathways, namely RCP8.5, RCP6, RCP4.5 and RCP2.6, with each numerical referring to the radiative forcing in W/m². Therefore RCP8.5 implies radiative forcing higher than 8.5 W/m² by 2100, whereas radiative forcing stabilises at approximately 6 W/m², 4.5 W/m³ and 2.6 W/m³ after

© Eskom 2026/Rev 0c

PRINTED VERSIONS OF THIS DOCUMENT ARE NOT CONTROLLED

2100 in the RCP6, RCP4.5 and RCP2.6 pathways, respectively. The worse-case pathway is RCP 8.5, which is representative of scenarios in the literature that lead to high GHG levels (Riahi, et al., 2007).

Based on the downscaled simulations performed by the CSIR (CSIR, 2019), the projected annual total rainfall changes, at 8 km resolution, for the Thyspunt site for the RCP8.5 scenario are as follows:

- near-horizon (2021-2050) : +3.08 (+18.76; -22.73) mm;
- far-horizon (2071-2099) : -11.95 (-32.33; +6.4) mm.

The values in brackets represent the 10th and 90th percentiles, respectively. Based on these projections, it is therefore estimated that the extreme observed annual total rainfalls would be:

- near-horizon (2021-2050) : 975.1 (+18.76; -22.73) mm;
- far-horizon (2071-2099) : 960.1 (-32.33; +6.40) mm.

It should be noted, however, that these projections were based on a simulated baseline for the 1960-1990 period and provided an annual average rainfall for the region of 1027.30 (988.01;1058.17) mm (CSIR, 2019), which is higher than the actual measurement at the Cape St. Francis and Thyspunt WSs. As an alternative, the fractional changes, normalised with these baseline rainfall totals could have been used, i.e.

- near-horizon (2021-2050) : 974.9 (+17.75; -21.51) mm;
- far-horizon (2071-2099) : 960.6 (-30.59; +6.05) mm.

The two approaches result in similar projections.

The projected changes in annual total rainfall due to climate change factors for the near-horizon and far-horizon were used in the extreme estimates, as provided in ***Table 5.8.61***. The near-horizon estimates are therefore slightly higher and the far-horizon lower than the extremes calculated for the present baseline. As a conservative estimate, the near-horizon extremes may be adopted for the far-horizon projections.

The CSIR (CSIR, 2019) results also provided projected changes in the average number of extreme rainfall days. An extreme rainfall event is defined as 20 mm of rain occurring within 24 hours over an area of 64 km².

- near-horizon (2021-2050) : -0.30 (-0.14,-0.03) days;
- far-horizon (2071-2099) : -2.14 (-3.16,-2.04) days.

© Eskom 2026/Rev 0c

PRINTED VERSIONS OF THIS DOCUMENT ARE NOT CONTROLLED

These projections are also reflected in the (Engelbrecht, et al., 2019) results indicating a decrease in the number of extreme rainfall events. In a 2011 perspective on climate change and the South African water sector, (Schulze, 2011) concluded that for short duration rainfall events (i.e. 5 minutes to 24 hours) design rainfall for a given location can be estimated as (*Figure 7.1.5* in (Schulze, 2011)):

- Overall, across South Africa an increase up to 10 per cent in short duration design rainfalls may be expected by the intermediate future, but with patches south of 32 °S and north of 27 °S where the models show no discernible change from the present.
- Of note is the high projected change in short duration design rainfall in the area transitional between the summer and winter rainfall areas, where increases of up to 40 per cent are projected.

For the site particularly, the average ratio of changes for short duration design rainfall (all return periods) were estimated by Schulze (Schulze, 2011) to have a unitless ratio of change between 1.0 and 1.1 for the near future (2046-2065) and no change from the baseline for the far future (2081-2100) scenarios. As discussed in (McBride, et al., 2022), with the projected surface temperatures increasing due to climate change, the water content of the atmosphere could potentially increase due to the increases in the water-holding capacity of the atmosphere. The increase in water content equate to approximately 7 per cent per degree Celsius of warming (assuming constant relative humidity). With more moisture available, the nature of rainfall events may become more intense with increased rainfall rates. Therefore, the intensity of extreme precipitation events may increase, even in areas where average precipitation is projected to decrease, as indicated by the CSIR (CSIR, 2019) projections for the site. This was investigated through the analysis of the historical daily time series of 70 rainfall stations in South Africa, over the period 1921 to 2020. The analysis period was divided into two equal historical periods of 50 years for comparison. The changes in the probability of receiving more than 50 mm per day, 75 mm per day and 115 mm per day in the region of the site showed an increase in their 1:50- and 1:100-year return period values of between 25 per cent and 50 percent. The lowering of return values was also observed ranging from 70 per cent to 80 per cent. In other words, a 10-year event in the first half of the data changed to a 7- to 8-year return event in the second dataset. However, these findings were based on historical trends and may not necessarily reflect the future projections, which according to the CSIR model (CSIR, 2019) indicate less intense extremes along the southwest and west coasts of South Africa, with little projected change along the southern coast, which includes the Thyspunt site (Lennard, et al., 2016). This finding was also supported by (Tim, et al., 2023).

© Eskom 2026/Rev 0c

PRINTED VERSIONS OF THIS DOCUMENT ARE NOT CONTROLLED

Table 5.8.61
Expected Annual Total Rainfall in Return Periods Including Climate Change Projections at the Site

Return Periods	Annual Total Rainfall (mm)					
	Present		Near-Horizon (2050)		Far Horizon (2100)	
	Extreme	95% Confidence Interval	Extreme	95 % Confidence Interval	Extreme	95% Confidence Interval
10	858.7	± 84.8	861.8	± 84.8	846.8	± 84.8
100	1187.9	± 147.1	1191.0	± 147.1	1176.0	± 147.1
1 000	1511.2	± 212.2	1514.2	± 212.2	1499.2	± 212.2
10 000	1833.8	± 278.4	1836.9	± 278.4	1821.9	± 278.4
100 000	2156.4	± 345.0	2159.5	± 345.0	2144.5	± 345.0
1 000 000	2479.0	± 412.0	2482.1	± 412.0	2467.0	± 412.0
10 000 000	2801.6	± 479.0	2804.7	± 479.0	2789.6	± 479.0
100 000 000	3124.2	± 546.2	3127.2	± 546.2	3112.2	± 546.2

© Eskom 2026/Rev 0c

PRINTED VERSIONS OF THIS DOCUMENT ARE NOT CONTROLLED

Table 5.8.62
Expected Maximum 24-hour Total Rainfall in Return Periods Including Climate Change Projections at the Site

Return Periods	24-HourStorm (mm)					
	Present		Near-Horizon (2050)		Far Horizon (2100)	
	Extreme	95% Confidence Interval	Extreme	95 % Confidence Interval	Extreme	95% Confidence Interval
10	99.0	± 20.8	108.9	± 20.8	108.9	± 20.8
100	151.4	± 38.8	166.6	± 38.8	166.6	± 38.8
1 000	202.9	± 56.8	223.2	± 56.8	223.2	± 56.8
10 000	254.3	± 74.9	279.7	± 74.9	279.7	± 74.9
100 000	305.6	± 93.0	336.2	± 93.0	336.2	± 93.0
1 000 000	357.0	± 111.1	392.7	± 111.1	392.7	± 111.1
10 000 000	408.4	± 129.2	449.2	± 129.2	449.2	± 129.2
100 000 000	459.7	± 147.3	505.7	± 147.3	505.7	± 147.3

© Eskom 2026/Rev 0c

PRINTED VERSIONS OF THIS DOCUMENT ARE NOT CONTROLLED

Since the climate change projections indicate no change or perhaps a decrease in the number of extreme rainfall events and rates, it would be reasonable to assume the same extreme values estimated in ***Table 5.8.60*** for projected 24-hour storm events. However, due to the uncertainties associated with climate change projections, it may be more prudent to adopt the more conservative approach of assuming a 10 per cent increase, as per the projections of Schulze (Schulze, 2011). It should be kept in mind that this increase was projected for the near-future scenario only and not the far-future scenario, for which the projection shows no increase. Therefore, assuming the more conservative approach, the projected extreme 24-hour storm events are provided in ***Table 5.8.62*** with the far-future assuming the same as the near-future.

(b) Extreme Ambient Air Temperature

Extreme ambient air temperature measurements at the standard height of 2 m were available at the Cape St. Francis WS for a period of 19 years (2005[50] to 2023) (Eskom, 2023a). These data were used instead of the onsite Thyspunt WS due to the inadequate length of the monitoring period.

The expected extreme ambient air temperatures for this station are summarised in ***Table 5.8.63***. Details of the methodology for calculating the return period temperatures are provided in ***Appendix 5.8.B***.

Table 5.8.63
Expected Minimum and Maximum Hourly Average Temperature (°C) in Return Periods of 10 to 100 000 000 Years at the Site (19 Years)

Return Period	Minimum Hourly Average Temperature (°C)		Maximum Hourly Average Temperature (°C)	
	Minimum	95th Confidence Interval	Maximum	95th Confidence Interval
10	5.0	± 0.7	37.0	± 1.8
100	3.2	± 1.2	42.4	± 3.1
1 000	1.3	± 1.7	47.7	± 4.5
10 000	-0.5	± 2.2	53.0	± 5.9
100 000	-2.3	± 2.7	58.3	± 7.4
1 000 000	-4.1	± 3.2	63.7	± 8.9
10 000 000	-5.9	± 3.7	69.0	± 10.4
100 000 000	-7.7	± 4.2	74.3	± 11.9

The IAEA (International Atomic Energy Agency, 2011) considers the temperature increase by 2100 relative to 2000 to be 1.8–4.0°C (best estimate) and 1.1–6.4°C (including the likely uncertainty range for each of the scenarios considered owing to different responses of the climate models

[50] Since 2004 did not include a full year's data, it was excluded from the extreme analysis.

© Eskom 2026/Rev 0c

PRINTED VERSIONS OF THIS DOCUMENT ARE NOT CONTROLLED

(***Subsection 5.8.9.2***)). The projections from the CSIR downscaled models, (Engelbrecht, et al., 2019) and (CSIR, 2019), provided the following minimum, average and maximum daily temperature changes averaged over the Thyspunt site for the RCP8.5 scenario:

- Annual average temperature change (°C) (CSIR, 2019):
    - near-horizon (2021-2050) : +1.68 (+1.65; +1.68) °C;
    - far-horizon (2071-2099) : +3.28 (+3.24; +3.47) °C;
- Annual average minimum temperature change (°C) (Engelbrecht, et al., 2019):
    - near-horizon (2021-2050) : +2.50 (+1.00; +3.00) °C;
    - far-horizon (2071-2099) : +2.50 (+2.00; +4.00) °C;
- Annual average maximum temperature change (°C) (Engelbrecht, et al., 2019):
    - near-horizon (2021-2050) : +1.50 (+1.00; +2.00) °C;
    - far-horizon (2071-2099) : +3.50 (+2.00; +4.00) °C.

The values in brackets represent the 5th and 95th percentiles (this corresponds to the 90 per cent confidence interval). The simulated baseline temperature for the 1960-1990 period for the region is 17.14 (17.03;17.45) °C (CSIR, 2019), which is very similar to the annual average observed at the Thyspunt and Cape St. Francis WSs, i.e. 17.4 and 17.3 respectively.

The *Special Report on Managing the Risks of Extreme Events and Disasters to Advance Climate Change Adaptation* (SREX) (Intergovernmental Panel on Climate Change, 2012) has been jointly coordinated by Working Groups I (WGI) and II (WGII) of the IPCC. The SREX report focuses on the relationship between climate change and extreme weather and climate events, the impacts of such events, and the strategies to manage the associated risks. A changing climate leads to changes in the frequency, intensity, spatial extent, duration, and timing of extreme weather and climate events. The SREX report approaches the topic by assessing the scientific literature on issues that range from the relationship between climate change and extreme weather and climate events (‘climate extremes’) to the implications of these events for society and sustainable development. Projections of extremes in any of the meteorological parameters are difficult to determine. Based on the SREX report, the approach to adjusting maximum temperature extremes for climate change is to apply a reduction in the return period of the predicted extreme value. So, a 10-fold reduction would average that an extreme value calculated for a 1 000-year return

© Eskom 2026/Rev 0c

PRINTED VERSIONS OF THIS DOCUMENT ARE NOT CONTROLLED

period (unadjusted for climate change) would instead be for a 100-year return period. Based on this approach, and based on the ARP5 results, which indicate that a 20-year return period would reduce to a 3-year return period and for the near-future, and a 2-year return period for a far future projection. The return periods for the extreme hourly maximum temperatures should be reduced by approximately 7-fold for the near-future and 10-fold for the far-future projections. As a conservative estimate, the hourly minimum temperature extremes will assume the unadjusted projections, but with adjusted 95 per cent confidence interval. The expected extreme temperature ranges due to these temperature increase predictions are included in ***Table 5.8.64*** and ***Table 5.8.65***.

© Eskom 2026/Rev 0c

PRINTED VERSIONS OF THIS DOCUMENT ARE NOT CONTROLLED

Table 5.8.64
Expected Minimum Hourly Average Temperatures Including Climate Change Projections at the Site

Return Periods	Hourly Minimum Temperatures [°C]					
	Present		Near-Horizon (2050)		Far Horizon (2100)	
	Extreme	95% Confidence Interval	Extreme	95 % Confidence Interval	Extreme	95% Confidence Interval
10	5.0	± 0.7	6.0	± 1.1	5.7	± 1.2
100	3.2	± 1.2	4.1	± 1.6	3.8	± 1.7
1 000	1.3	± 1.7	2.3	± 2.1	2.0	± 2.2
10 000	-0.5	± 2.2	0.5	± 2.6	0.2	± 2.7
100 000	-2.3	± 2.7	-1.3	± 3.1	-1.6	± 3.2
1 000 000	-4.1	± 3.2	-3.1	± 3.6	-3.4	± 3.7
10 000 000	-5.9	± 3.7	-5.0	± 4.1	-5.2	± 4.2
100 000 000	-7.7	± 4.2	-6.8	± 4.7	-7.0	± 4.7

© Eskom 2026/Rev 0c

PRINTED VERSIONS OF THIS DOCUMENT ARE NOT CONTROLLED

Table 5.8.65
Expected Maximum Hourly Average Temperatures Including Climate Change Projections at the Site

Return Periods	Hourly Maximum Temperatures [°C]					
	Present		Near-Horizon (2050)		Far Horizon (2100)	
	Extreme	95% Confidence Interval	Extreme	95 % Confidence Interval	Extreme	95% Confidence Interval
10	37.0	± 1.8	42.8	± 2.9	45.6	± 3.1
100	42.4	± 3.1	48.1	± 4.3	50.9	± 4.5
1 000	47.7	± 4.5	53.4	± 5.7	56.2	± 5.9
10 000	53.0	± 5.9	58.7	± 7.2	61.5	± 7.4
100 000	58.3	± 7.4	64.0	± 8.7	66.9	± 8.9
1 000 000	63.7	± 8.9	69.3	± 10.2	72.2	± 10.4
10 000 000	69.0	± 10.4	74.6	± 11.6	77.5	± 11.9
100 000 000	74.3	± 11.9	80.0	± 13.1	82.8	± 13.4

© Eskom 2026/Rev 0c

PRINTED VERSIONS OF THIS DOCUMENT ARE NOT CONTROLLED

(c) Extreme Wind Speed

Operating experience of nuclear installations globally has shown that extreme winds mainly affect the power supply and availability of the electricity grid. However, sometimes damage is sustained to the switchyards. Recorded accidents typically evolve into turbine trip and loss of off-site power. In a few cases, the pressure differential creates some false signals to nuclear installation instrumentation. At sites close to the marine environment, heavy salt sprays from the sea in the form of a precipitation during the most violent phases created electrical shorts in exposed electrical equipment (bushings and switchgears) and, later, deep corrosion and malfunctions (International Atomic Energy Agency, 2021). As a result of the high occurrence of strong wind speeds, such incidents may be likely to occur at the site.

Wind speed measurements at the standard height of 10 m were available at the Cape St. Francis WS for a period of 19 years (2005 to 2023) (Eskom, 2023a). These data were used instead of the onsite Thyspunt WS due to the inadequate length of the monitoring period. From the analysis of the wind speed data (***Subsection 5.8.6.1.1***) the highest gust and hourly wind speeds were 48.5 and 23.2 m/s, respectively. Extreme value analyses were performed on the observed maximum hourly and gusts for this 19-year period (***Appendix 5.8.B***). The expected extreme wind speeds for the site are summarised in ***Table 5.8.66***.

Table 5.8.66
Extreme Highest Hourly Average Wind Speed and Wind Gust [m/s] Estimated for the Site

Return Period	Maximum Hourly Average Wind Speed [m/s]		Wind Gust (m/s)	
	Average	95th Confidence Interval	Average	95th Confidence Interval
10	22.0	± 1.2	38.1	± 3.5
100	24.7	± 2.1	44.3	± 6.2
1 000	27.3	± 3.1	50.2	± 8.8
10 000	29.9	± 4.1	56.2	± 11.4
100 000	32.6	± 5.1	62.2	± 14.1
1 000 000	35.2	± 6.1	68.2	± 16.7
10 000 000	37.9	± 7.0	74.2	± 19.3
100 000 000	40.5	± 8.0	80.2	± 22.0

When compared with the observed maximum wind gust of 45.8 m/s recorded at Cape St Francis WS (***Subsection 5.8.6.1.1***), the observed event indicates wind conditions equivalent to a 100-year return period. Although this is the correct conclusion from the extreme analysis, the limitation of using only 19 years of wind data needs to be recognised. The

© Eskom 2026/Rev 0c

PRINTED VERSIONS OF THIS DOCUMENT ARE NOT CONTROLLED

45.8 m/s gust is approximately 19% higher than the next highest gust of 38.5 m/s. All other subsequent gusts differ by 2 per cent on average. The extreme analysis could therefore have been biased towards the rest of the observed wind speeds.

The South African National Standards (SANS) issued a national design code for wind loadings on buildings and structures, SANS 10160-Part 3 (South African National Standards, 2019), which provides regional basic 3-second wind speeds for a 50-year return period. ***Figure 5.8.23*** (South African National Standards, 2019) illustrates the map contained in the national design code of the SANS standard.

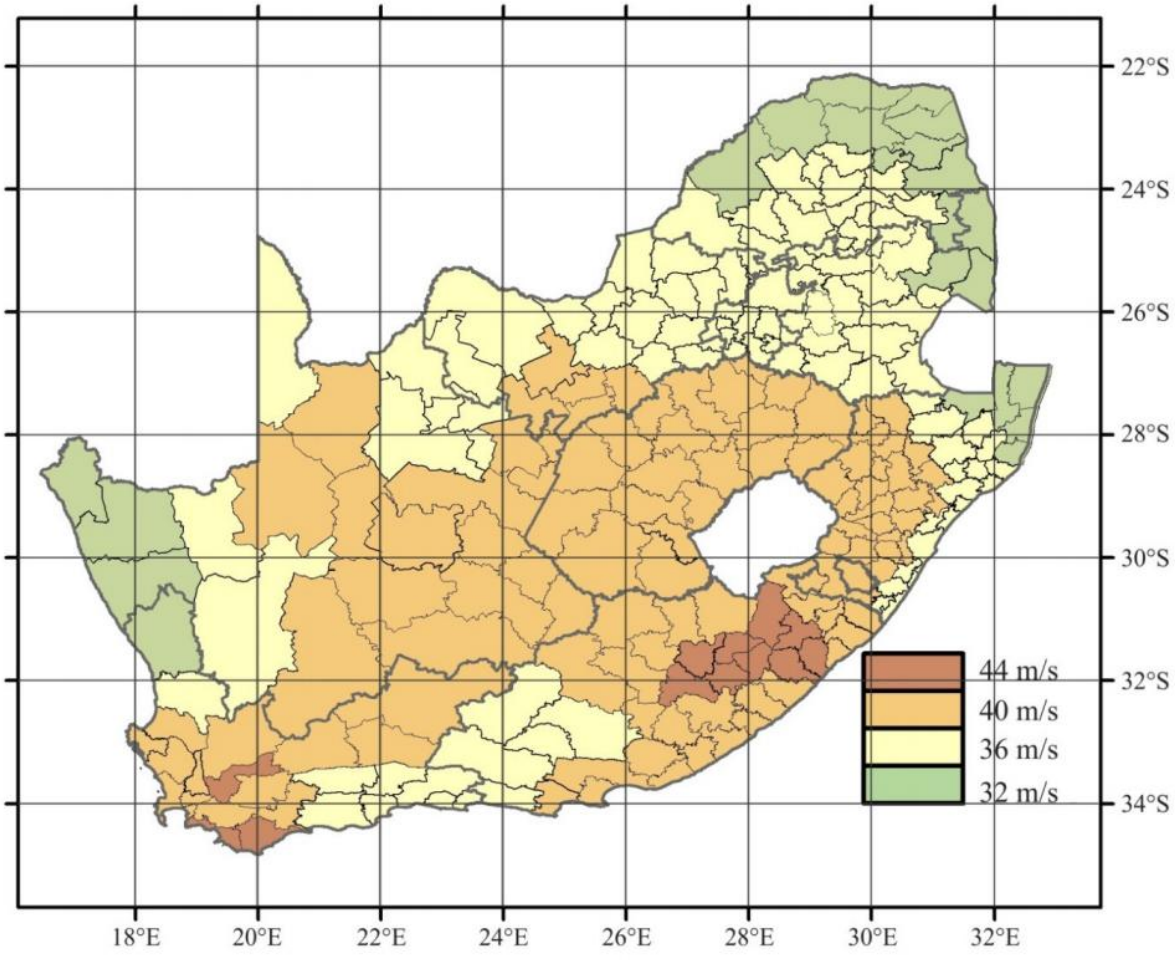


Figure 5.8.23
Map of Fundamental Value of Basic 3-s Gust Wind Speed (50 Year Return Period) (South African National Standards, 2019)

© Eskom 2026/Rev 0c

PRINTED VERSIONS OF THIS DOCUMENT ARE NOT CONTROLLED

According to this code, the 50-year return period regional basic wind speed 3-s gust is 40 m/s. Although not given in ***Table 5.8.66***, the calculated 50-year return 3-s gust for the site is calculated to be 42.4 (±5.4) m/s (Method of Maximum Likelihood). These values are very similar. It is stated in the NNR position paper (NNR PP-0014) on hazards from important external phenomena that should be considered in assessing sites, that the extreme value cannot be lower than the value provided by the national design code for the same region.

Extreme winds are often considered in the context of the extreme phenomena with which they are associated such as cyclones, thunderstorm downbursts, and tornadoes. Changes in wind extremes may arise from changes in the intensity or location of their associated phenomena (e.g. a change in local convective activity) or from other changes in the climate system such as the movement of large-scale circulation patterns. The SREX report (Intergovernmental Panel on Climate Change, 2012) states that there is evidence to suggest an increase in extreme winds from tropical cyclones in the future. Furthermore, an increase in atmospheric GHG concentrations may cause some of the atmospheric conditions conducive to tornadoes such as atmospheric instability to increase due to increasing temperature and humidity, while others such as vertical shear to decrease due to a reduced pole-to-equator temperature gradient, but the literature on these phenomena is extremely limited. There is thus low confidence in projections of changes in such small-scale systems because of limited studies, inability of climate models to resolve these phenomena and possible competing factors affecting future changes. Confidence in the extreme wind changes is therefore lower in the regions most influenced by these phenomena irrespective of whether there is high agreement between simulation models on the direction (i.e., increase or decrease) of the wind speed change. Based on the downscaled CSIR simulations extracted in (Engelbrecht, et al., 2019), the annual average wind speed change from the baseline wind speed (indicated by the range 5 m/s to 6 m/s) over the Thyspunt site for the RCP8.5 scenario is as follows:

- near-horizon (2021-2050) : -0.5 (-1.0; +1.0) m/s;
- far-horizon (2071-2099) : 0.0 (-1.0; +1.0) m/s.

The values in brackets represent the 5th and 95th percentiles (90 per cent confidence interval). The annual average wind speed observed at the Thyspunt WS was 5.4 m/s (see ***Subsection 5.8.6.1.1.(a)***), which is within the range of baseline wind speed. The projections show a slight reduction in the near-future scenario and unchanged in the far-future scenario.

Future gust projections could not be extracted from these sources. It is stated in the SREX report that changes in extremes may be directly related

© Eskom 2026/Rev 0c

PRINTED VERSIONS OF THIS DOCUMENT ARE NOT CONTROLLED

to changes in average climate, because average future conditions in some variables are projected to lie within the tails of present-day condition probability distributions. It was therefore assumed that the predicted extreme winds in ***Table 5.8.66*** will similarly remain relatively unchanged from the current observations, as per the projections for the annual average wind speed. The predicted extreme winds for the two projection horizons and return periods are summarised in ***Table 5.8.67*** for the maximum hourly average wind speeds and in ***Table 5.8.68*** for gusts.

The confidence intervals were assumed to remain the same as for the original extreme value analysis. As a conservative approach, the extreme wind speeds for the baseline should be adopted instead of the projected reduction.

Wind direction changes were not provided as part of the downscaled model outputs. Instead, the study by (Herbst & Rautenbach, 2015) which attempted to quantify the projected changes in seasonal daily average wind speeds and directions for South Africa around the mid-21st century (2051-2075) was consulted. The following seasonal changes were projected:

- March-April-May an easterly wind shift;
- June-July-August a southerly wind shift;
- September-October-November a southeasterly wind shift;
- December-January-February an easterly wind shift.

© Eskom 2026/Rev 0c

PRINTED VERSIONS OF THIS DOCUMENT ARE NOT CONTROLLED

Table 5.8.67
Expected Maximum Hourly Average Wind Speeds Including Climate Change Projections at the Site

Return Periods	Maximum Hourly Average Wind Speed [m/s]					
	Present		Near-Horizon (2050)		Far Horizon (2100)	
	Extreme	95% Confidence Interval	Extreme	95 % Confidence Interval	Extreme	95% Confidence Interval
10	22.0	± 1.2	21.4	± 1.2	22.0	± 1.2
100	24.7	± 2.1	24.0	± 2.1	24.7	± 2.1
1 000	27.3	± 3.1	26.6	± 3.1	27.3	± 3.1
10 000	29.9	± 4.1	29.2	± 4.1	29.9	± 4.1
100 000	32.6	± 5.1	31.7	± 5.1	32.6	± 5.1
1 000 000	35.2	± 6.1	34.3	± 6.1	35.2	± 6.1
10 000 000	37.9	± 7.0	36.9	± 7.0	37.9	± 7.0
100 000 000	40.5	± 8.0	39.5	± 8.0	40.5	± 8.0

© Eskom 2026/Rev 0c

PRINTED VERSIONS OF THIS DOCUMENT ARE NOT CONTROLLED

Table 5.8.68
Expected Wind Gust Speeds Including Climate Change Projections at the Site

Return Periods	Maximum Gust [m/s]					
	Present		Near-Horizon (2050)		Far Horizon (2100)	
	Extreme	95% Confidence Interval	Extreme	95 % Confidence Interval	Extreme	95% Confidence Interval
10	38.1	± 3.5	37.6	± 3.5	38.1	± 3.5
100	44.3	± 6.2	43.7	± 6.2	44.3	± 6.2
1 000	50.2	± 8.8	49.6	± 8.8	50.2	± 8.8
10 000	56.2	± 11.4	55.5	± 11.4	56.2	± 11.4
100 000	62.2	± 14.1	61.4	± 14.1	62.2	± 14.1
1 000 000	68.2	± 16.7	67.3	± 16.7	68.2	± 16.7
10 000 000	74.2	± 19.3	73.2	± 19.3	74.2	± 19.3
100 000 000	80.2	± 22.0	79.1	± 22.0	80.2	± 22.0

© Eskom 2026/Rev 0c

PRINTED VERSIONS OF THIS DOCUMENT ARE NOT CONTROLLED

5.8.7 Atmospheric Dispersion Modelling

5.8.7.1 Dispersion Model

The IAEA recognises Gaussian-plume models (International Atomic Energy Agency, 2001) to be well suited for use in radiological assessment activities and specifically near-field (typically <50 km) applications where the steady-state meteorology assumption is most likely to apply.

Perhaps the most widely used Gaussian dispersion model internationally that requires stability classes as input (in addition to wind speed, wind direction, and air temperature) has been the US Environmental Protection Agency (US EPA) AERMET/AERMOD model suite (Cimorelli, et al., 2004). It is stated in *Section 1* of RG-0016 that *"All calculation models and/or evaluation models used in safety analyses are designed, developed, verified and validated, implemented, used and controlled in accordance with recognised nuclear industry standards and/or practices."*

The details of the model selection, validation and verification is provided in the Validation and Verification Report (V&V Report) (Burger, 2024). In the V&V Report, it was concluded that the US EPA AERMOD atmospheric model satisfies the requirements for simulation of atmospheric dispersion from nuclear installations for the purposes of this SSR[51].

AERMET is a meteorological pre-processor for AERMOD. Input data can come from hourly cloud cover observations, surface meteorological observations and twice-a-day upper air soundings. As applied in this instance, onsite hourly average wind speed, wind direction, standard-deviation of wind direction, dry bulb temperature and solar radiation were used to prepare the input parameters required for input into the model. The input files are contained in ***Appendix 5.8.N*** (surface meteorological data) and ***Appendix 5.8.O*** (profile data).

AERMAP is a terrain pre-processor designed to simplify and standardise the input of terrain data for AERMOD. Input data include receptor terrain elevation data. The model input file is provided in ***Appendix 5.8.P.*** The model results are expressed as concentrations (normally at ground level) and deposition rates over different periods of exposure.

[51] The atmospheric dispersion simulations were performed with the following *BREEZE AERMOD* version 11:
- *AERMOD* was run with the US EPA executable version 23132 (US EPA Release on 23 October 2023)
- US EPA Regulatory Mode selected
- *AERMET* version 18081.

© Eskom 2026/Rev 0c

PRINTED VERSIONS OF THIS DOCUMENT ARE NOT CONTROLLED

5.8.7.2 Dispersion Factor

The dispersion factor was calculated using the AERMOD model and provided as the effluent concentration (χ) and deposition (D) normalised by the source strength (Q). This was calculated using hourly averaged meteorological data obtained from the site for a five-year period 2009 to 2012 and 2018 since the year 2013 did not contain complete year's data.

To simulate worst-case postulated accidents, the following assumptions were made:

- there is no building wake effect;
- the effective release is from 1.5 m above ground level[52];
- exit gas velocity assumed 0 m/s[53];
- stack diameter of 2 m;
- exit gas temperature assumed 298 K[54];
- the receptor height is 1.5m;
- modelling domain includes an area of 40 km by 40 km, with the nuclear installation(s) located at the centre of the modelling domain;
- the grid resolutions:
  - 100 m by 100 m for a 5 km by 5 km domain;
  - 200 m by 200 m for 40 km by 40 km domain.

The hourly average meteorological surface and tower data are used to simulate a release event and the concentrations/depositions for that hour are calculated at each of the regular grid locations (receptors). The concentrations/depositions for each of the simulation hours are individually compared at a receptor and the 99.9th (2nd highest) and 95th percentile concentrations/depositions stored for the preparation of the spatial and directional plots given below.

[52] The design of the nuclear installation has not yet been selected and in the absence of a selected plant design, Eskom has given priority to completing this SSR for the site using a plant parameter envelope (Eskom, 2022b). Although the heights of release points have not been established, typical release heights may vary from 0 m to about 100 m above ground level (agl). To calculate the most conservative ground level concentration, a release close to ground level is assumed.

[53] Plume rise depends on the volumetric flow rate (exit gas velocity) and exit gas temperature. An exit gas velocity of zero result in no plume rise due to plume momentum.

[54] Plume rise depends on the volumetric flow rate and exit gas temperature. An exit gas temperature corresponding to an average ambient air temperature of 298 K will result in insignificant plume rise due to plume buoyancy.

© Eskom 2026/Rev 0c

PRINTED VERSIONS OF THIS DOCUMENT ARE NOT CONTROLLED

The normalised deposition rate includes rain washout as well as dry deposition.

The figures below represent the following dispersion factors:

- concentration:
  - 2nd highest hourly average:
    - 5 km by 5 km : ***Figure 5.8.24***
    - 40 km by 40 km : ***Figure 5.8.25***
  - 95th percentile hourly average:
    - 5 km by 5 km : ***Figure 5.8.26***
    - 40 km by 40 km : ***Figure 5.8.27***
  - 2nd Highest 3-hourly average:
    - 5 km by 5 km : ***Figure 5.8.28***
    - 40 km by 40 km : ***Figure 5.8.29***
  - 2nd Highest 8-hourly average:
    - 5 km by 5 km : ***Figure 5.8.30***
    - 40 km by 40 km : ***Figure 5.8.31***
  - 2nd Highest 24-hourly (daily) average:
    - 5 km by 5 km : ***Figure 5.8.32***
    - 40 km by 40 km : ***Figure 5.8.33***
  - Highest monthly average:
    - 5 km by 5 km : ***Figure 5.8.34***
    - 40 km by 40 km : ***Figure 5.8.35***
  - Highest Annual average:
    - 5 km by 5 km : ***Figure 5.8.36***
    - 40 km by 40 km : ***Figure 5.8.37***
- deposition:
  - 2nd highest hourly total:
    - 5 km by 5 km : ***Figure 5.8.38***
    - 40 km by 40 km : ***Figure 5.8.39***
  - 95th percentile hourly total:
    - 5 km by 5 km : ***Figure 5.8.40***

© Eskom 2026/Rev 0c

PRINTED VERSIONS OF THIS DOCUMENT ARE NOT CONTROLLED

- 40 km by 40 km : ***Figure 5.8.41***

- 2nd Highest 3-hour total:
  - 5 km by 5 km : ***Figure 5.8.42***
  - 40 km by 40 km : ***Figure 5.8.43***
- 2nd Highest 8-hour total:
  - 5 km by 5 km : ***Figure 5.8.44***
  - 40 km by 40 km : ***Figure 5.8.45***
- 2nd Highest 24-hour total:
  - 5 km by 5 km : ***Figure 5.8.46***
  - 40 km by 40 km : ***Figure 5.8.47***
- Highest monthly total:
  - 5 km by 5 km : ***Figure 5.8.48***
  - 40 km by 40 km : ***Figure 5.8.49***
- Highest annual total:
  - 5 km by 5 km : ***Figure 5.8.50***
  - 40 km by 40 km : ***Figure 5.8.51***

Figure 5.8.52 to ***Figure 5.8.59*** are summaries of the χ/Q values of the 2nd highest hourly, 3-hourly, 8-hourly, 24-hourly, and highest monthly and annual averages, grouped into the 16 cardinal wind directions at 800 m, 3 km and 8 km, downwind of the nuclear installation(s).

The data used to develop these figures are summarised in ***Table 5.8.69*** and ***Table 5.8.70***.

Similarly, ***Figure 5.8.61*** to ***Figure 5.8.68*** are summaries of the D/Q values of the 2nd highest hour, 3-hour, 8-hour, 24-hour and highest month and annual totals, grouped into the 16 cardinal wind directions at 800 m, 3 km and 8 km, downwind of the nuclear installation(s). Please note that the deposition rate is the total over the respective period.

The data used to develop these figures are summarised in ***Table 5.8.71*** and ***Table 5.8.72***.

© Eskom 2026/Rev 0c

PRINTED VERSIONS OF THIS DOCUMENT ARE NOT CONTROLLED

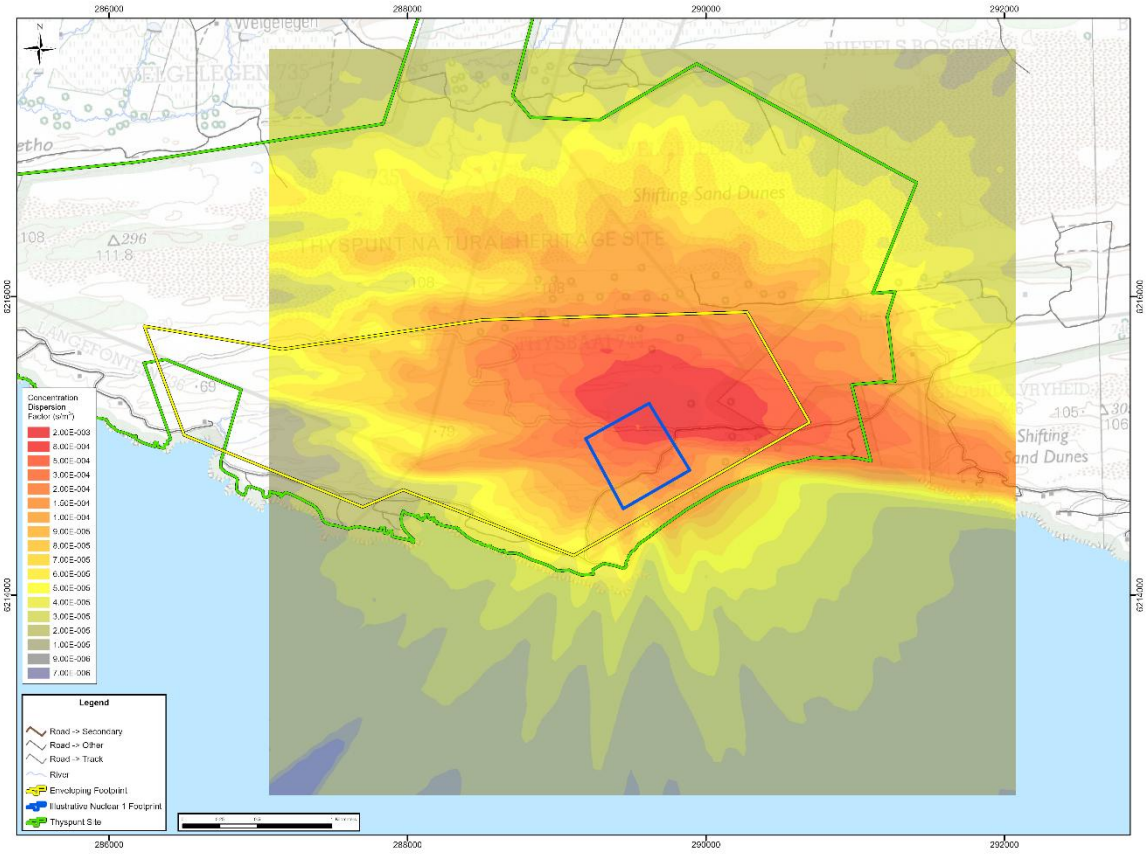


Figure 5.8.24
The Predicted 2nd Highest Hourly Average Ground Level Concentration Dispersion Factor (χ/Q) (s/m³) for a 5 km by 5 km area

© Eskom 2026/Rev 0c

PRINTED VERSIONS OF THIS DOCUMENT ARE NOT CONTROLLED

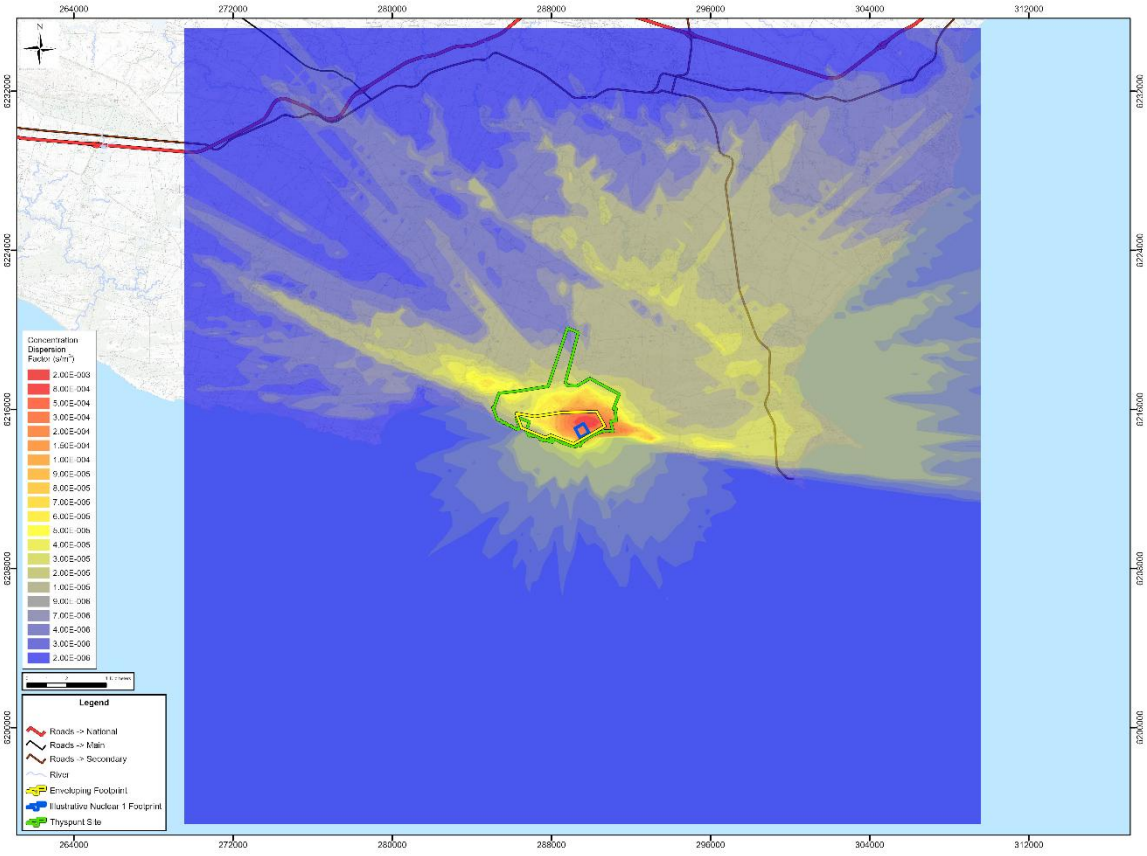


Figure 5.8.25
The Predicted 2nd Highest Hourly Average Ground Level Concentration Dispersion Factor (χ/Q) (s/m³) for a 40 km by 40 km area

© Eskom 2026/Rev 0c

PRINTED VERSIONS OF THIS DOCUMENT ARE NOT CONTROLLED

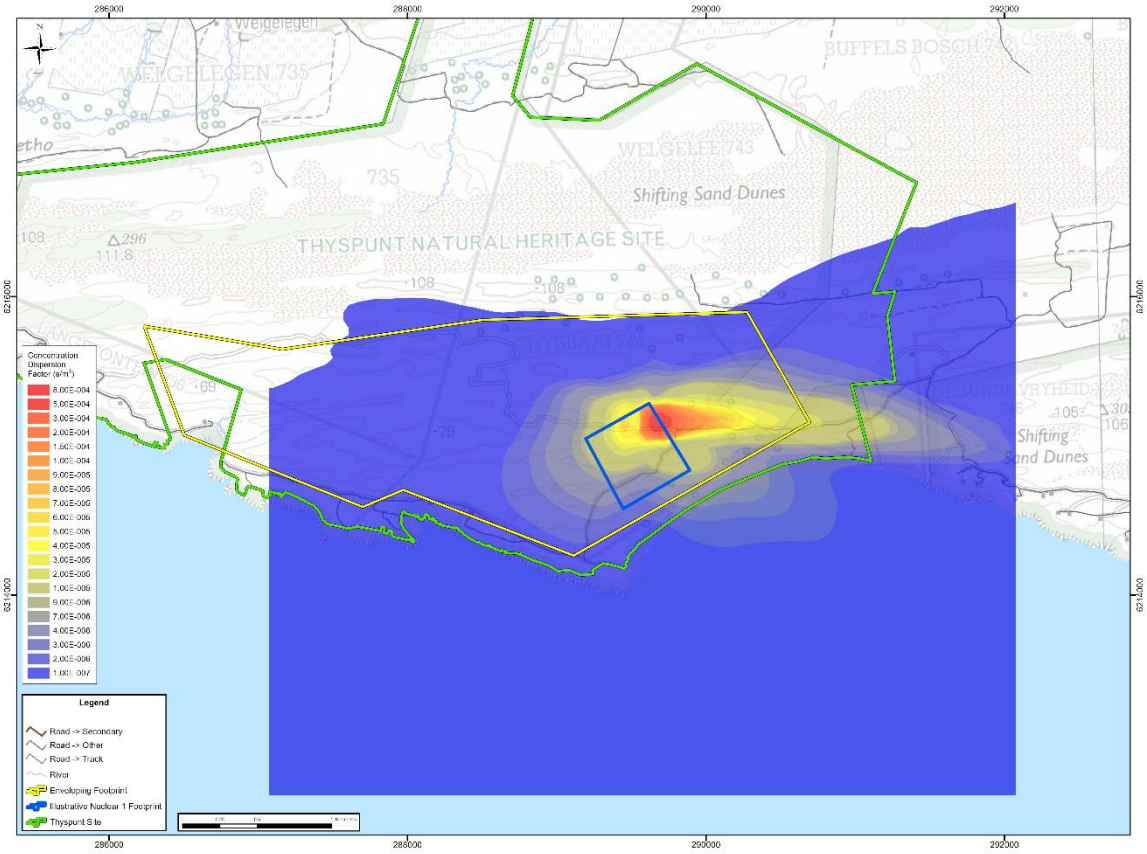


Figure 5.8.26
The Predicted 95th Percentile Ground Level Concentration Dispersion Factor (χ/Q) (s/m³) for a 5 km by 5 km area

© Eskom 2026/Rev 0c

PRINTED VERSIONS OF THIS DOCUMENT ARE NOT CONTROLLED

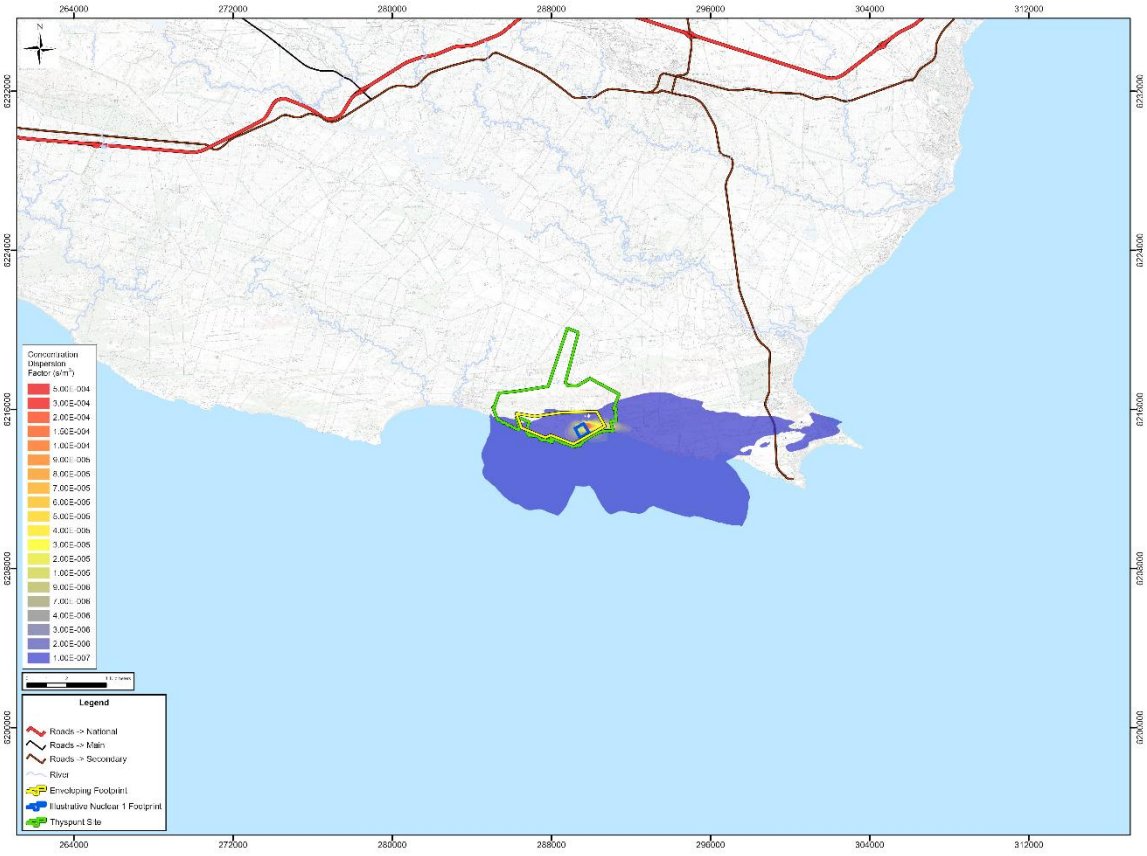


Figure 5.8.27
The Predicted 95th Percentile Ground Level Concentration Dispersion Factor (χ/Q) (s/m³) for a 40 km by 40 km area

© Eskom 2026/Rev 0c

PRINTED VERSIONS OF THIS DOCUMENT ARE NOT CONTROLLED

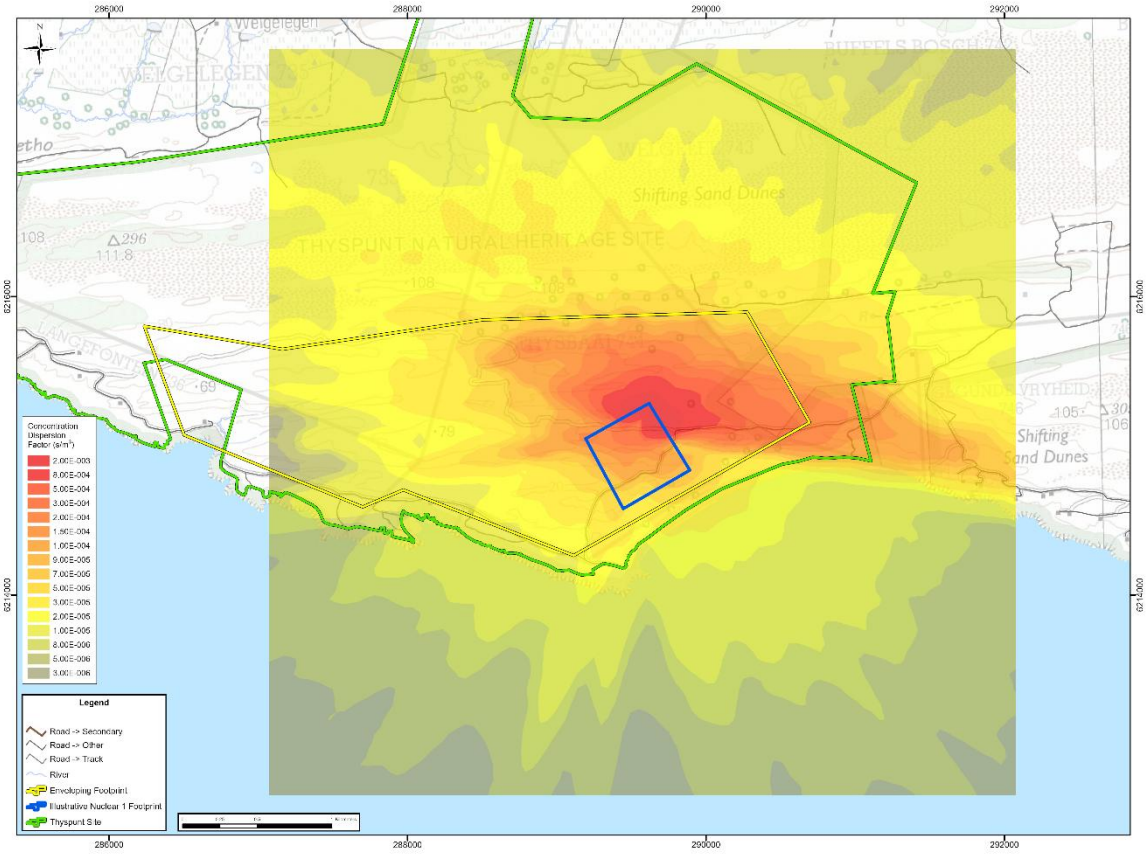


Figure 5.8.28
The Predicted 2nd Highest 3-Hourly Average Ground Level Concentration Dispersion Factor (χ/Q) (s/m³) for a 5 km by 5 km area

© Eskom 2026/Rev 0c

PRINTED VERSIONS OF THIS DOCUMENT ARE NOT CONTROLLED

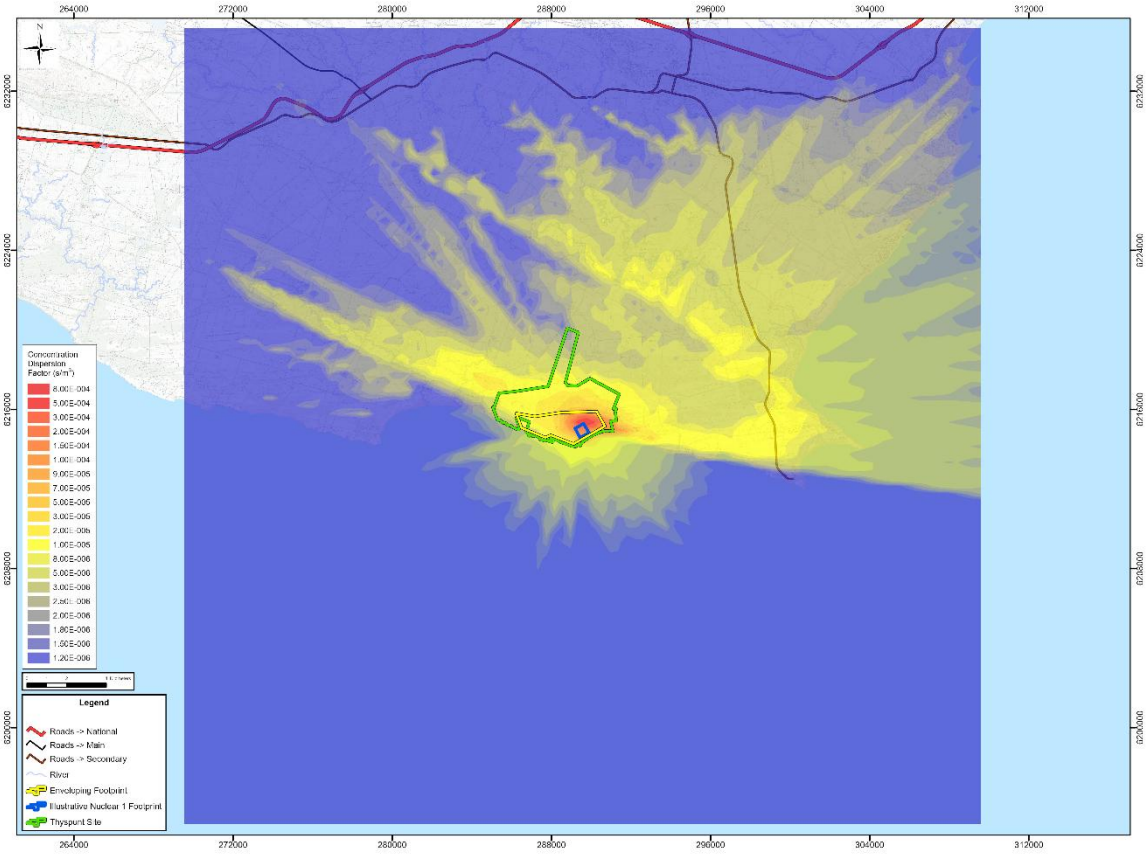


Figure 5.8.29
The Predicted 2nd Highest 3-Hourly Average Ground Level Concentration Dispersion Factor (χ/Q) (s/m³) for a 40 km by 40 km area

© Eskom 2026/Rev 0c

PRINTED VERSIONS OF THIS DOCUMENT ARE NOT CONTROLLED

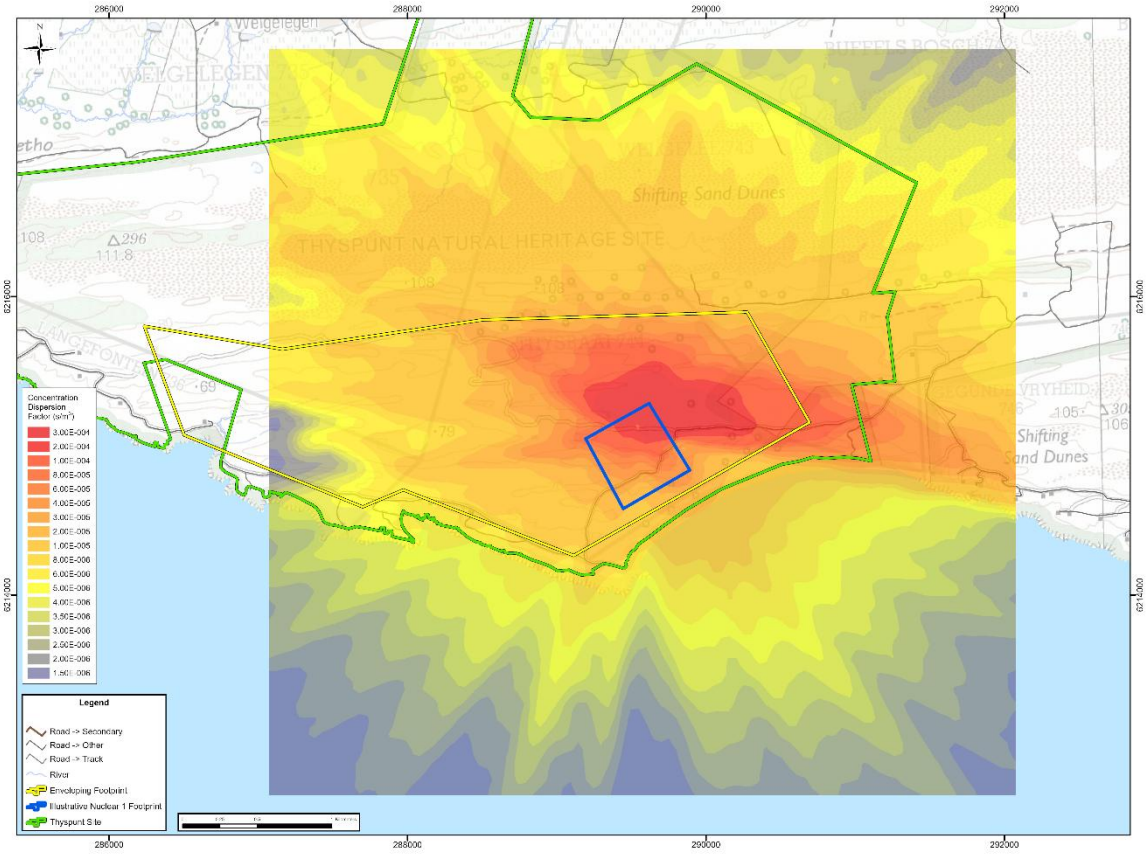


Figure 5.8.30
The Predicted 2nd Highest 8-Hourly Average Ground Level Concentration Dispersion Factor (χ/Q) (s/m³) for a 5 km by 5 km area

© Eskom 2026/Rev 0c

PRINTED VERSIONS OF THIS DOCUMENT ARE NOT CONTROLLED

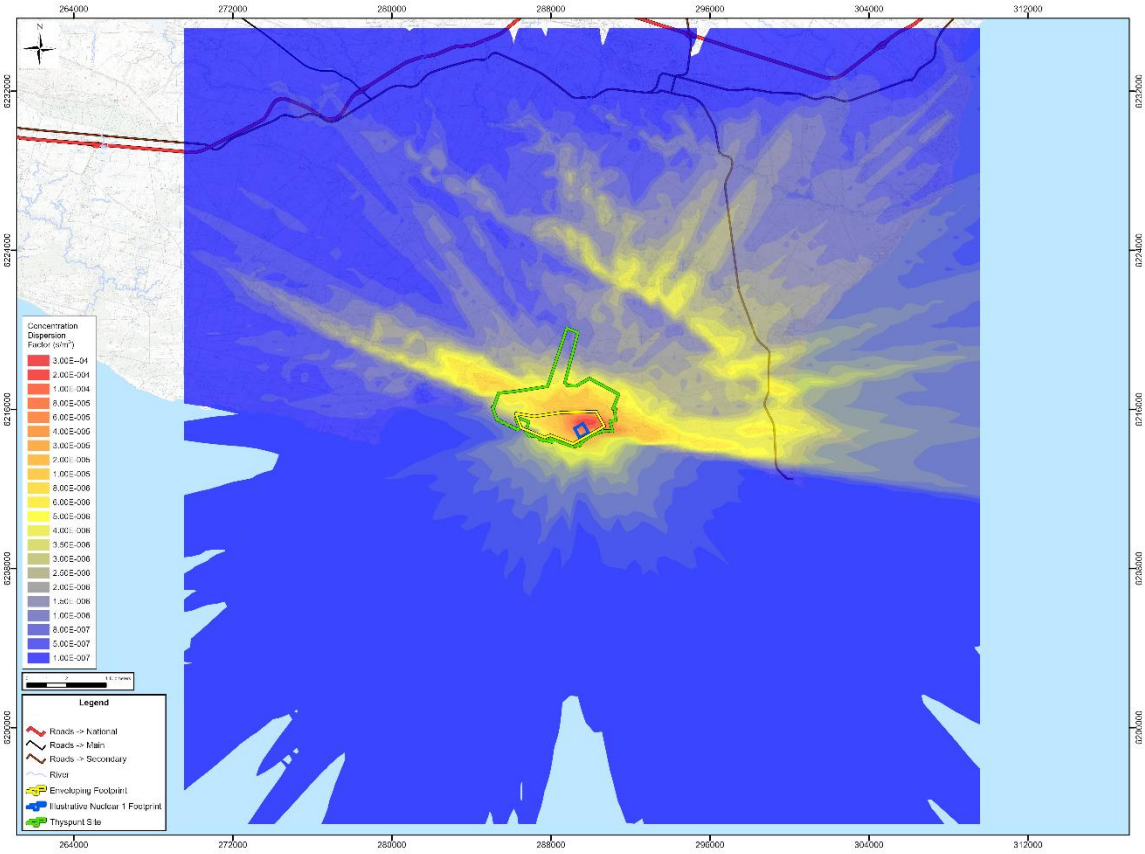


Figure 5.8.31
The Predicted 2nd Highest 8-Hourly Average Ground Level Concentration Dispersion Factor (χ/Q) (s/m³) for a 40 km by 40 km area

© Eskom 2026/Rev 0c

PRINTED VERSIONS OF THIS DOCUMENT ARE NOT CONTROLLED

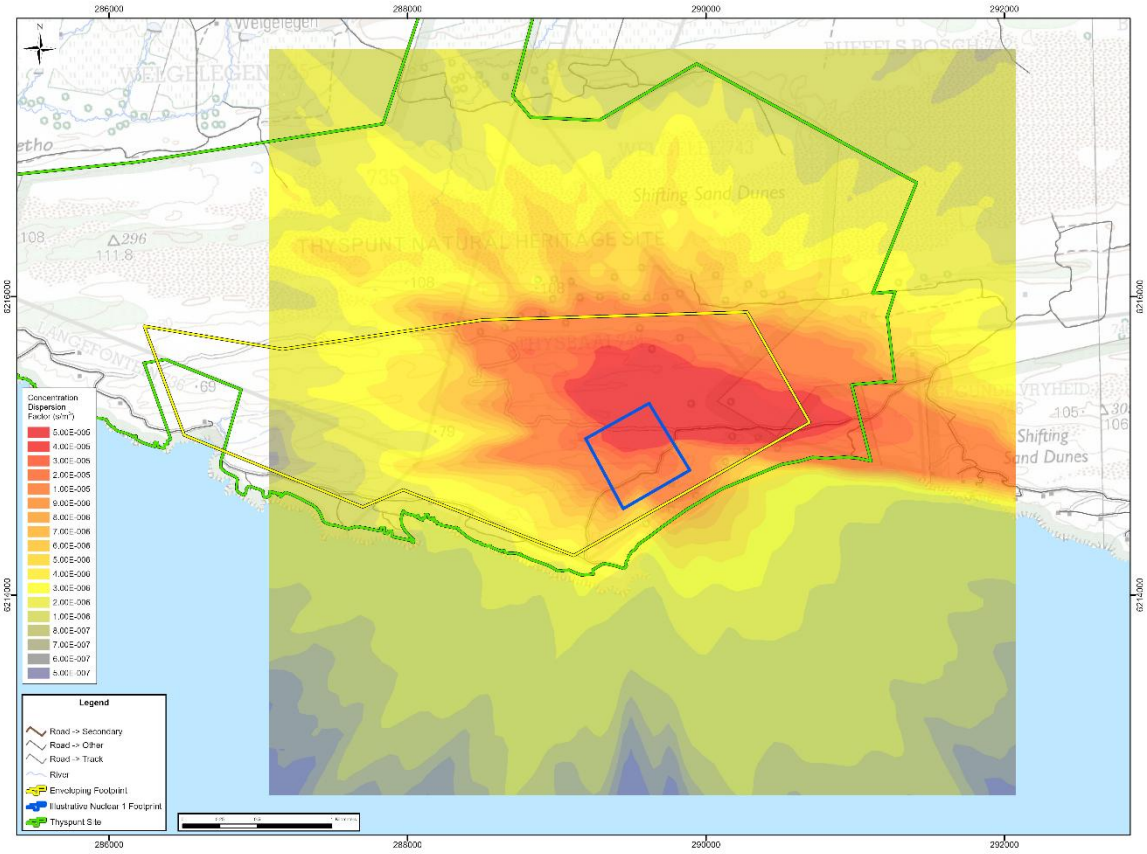


Figure 5.8.32
The Predicted 2nd Highest 24-Hourly Average Ground Level Concentration Dispersion Factor (χ/Q) (s/m³) for a 5 km by 5 km area

© Eskom 2026/Rev 0c

PRINTED VERSIONS OF THIS DOCUMENT ARE NOT CONTROLLED

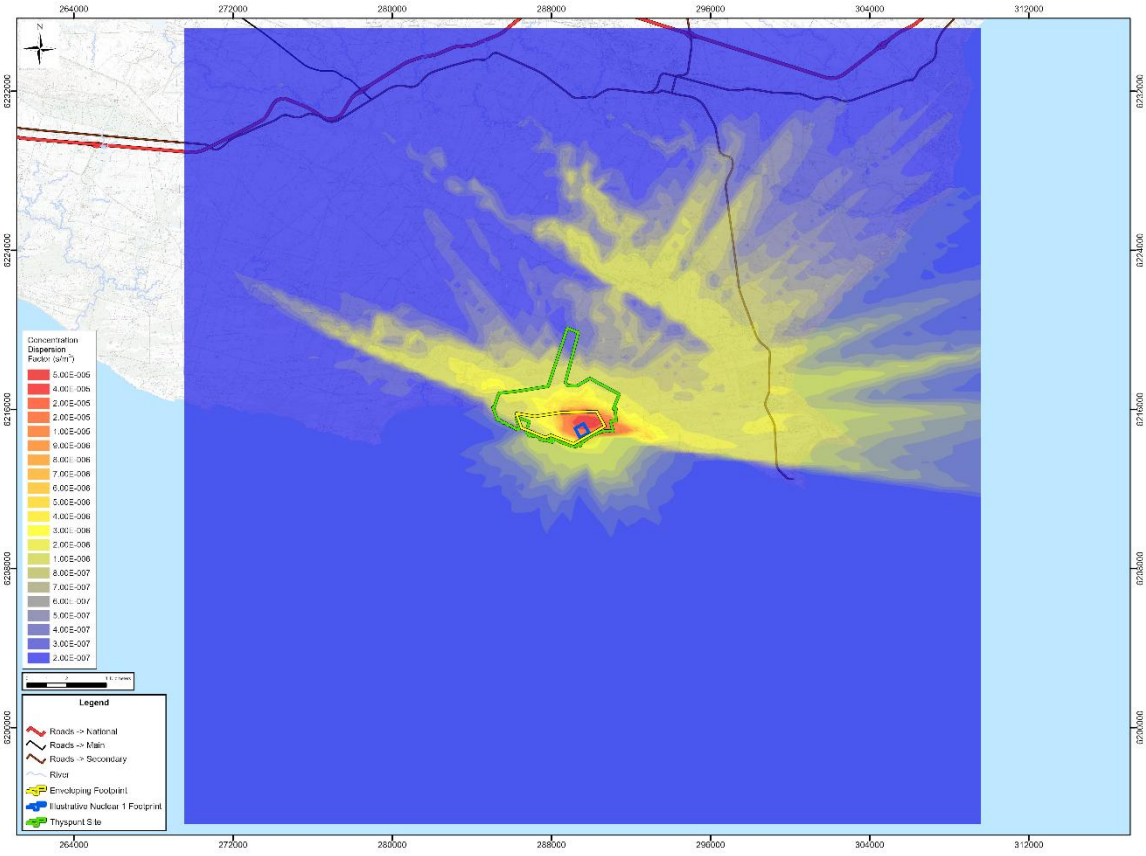


Figure 5.8.33
The Predicted 2nd Highest 24-Hourly Average Ground Level Concentration Dispersion Factor (χ/Q) (s/m³) for a 40 km by 40 km area

© Eskom 2026/Rev 0c

PRINTED VERSIONS OF THIS DOCUMENT ARE NOT CONTROLLED

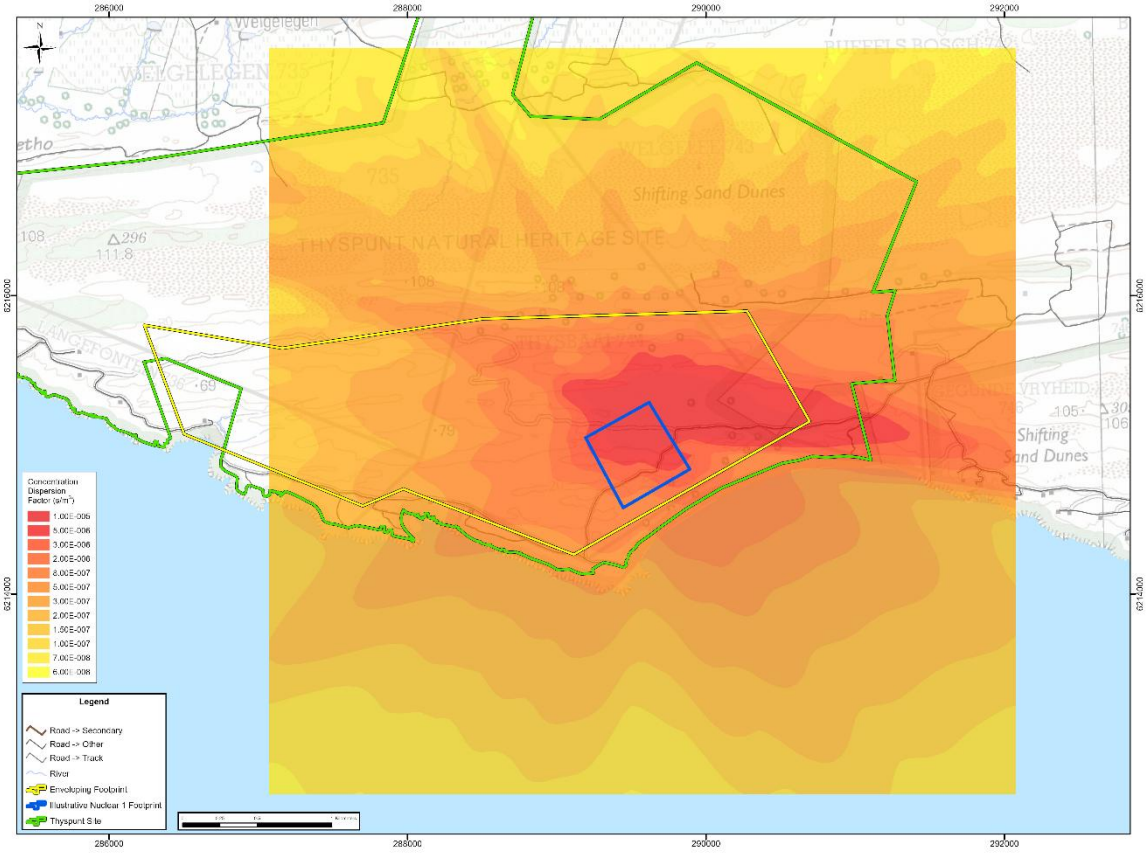


Figure 5.8.34
The Predicted Highest Monthly Average Ground Level Concentration Dispersion Factor (χ/Q) (s/m³) for a 5 km by 5 km area

© Eskom 2026/Rev 0c

PRINTED VERSIONS OF THIS DOCUMENT ARE NOT CONTROLLED

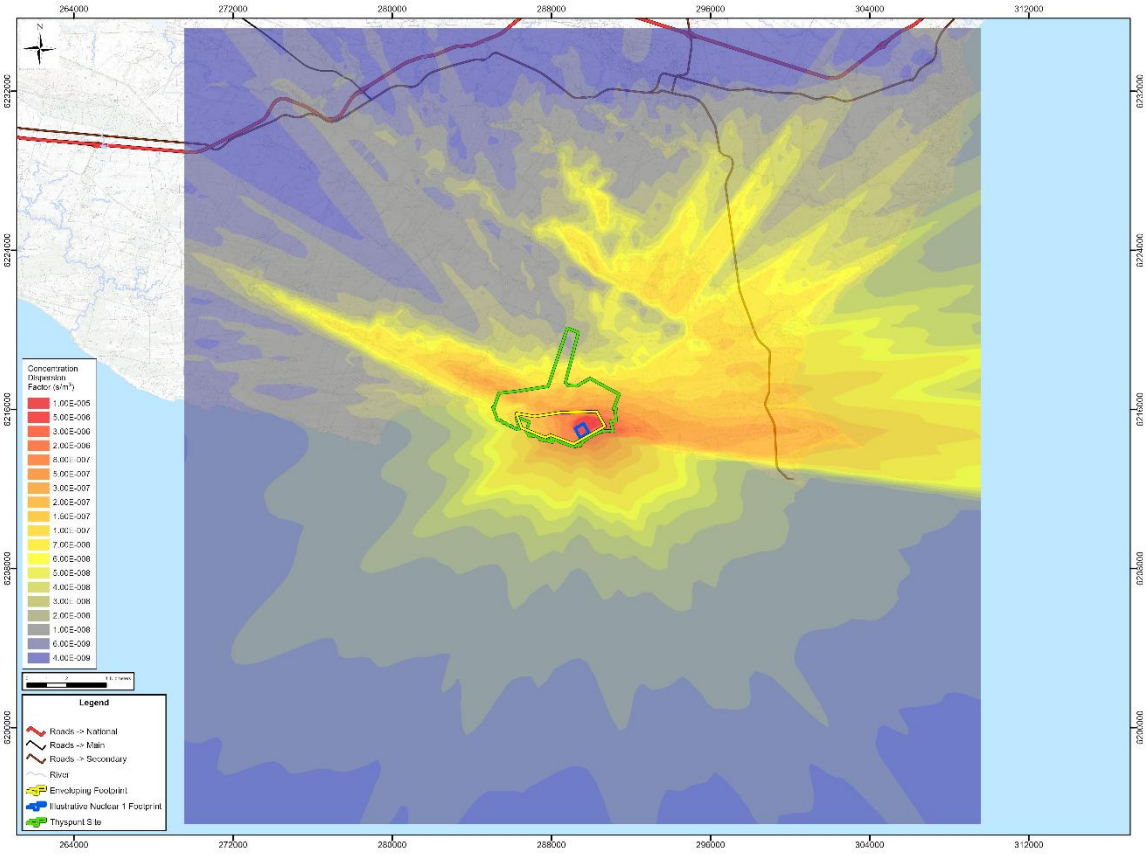


Figure 5.8.35
The Predicted Highest Monthly Average Ground Level Concentration Dispersion Factor (χ/Q) (s/m³) for a 40 km by 40 km area

© Eskom 2026/Rev 0c

PRINTED VERSIONS OF THIS DOCUMENT ARE NOT CONTROLLED

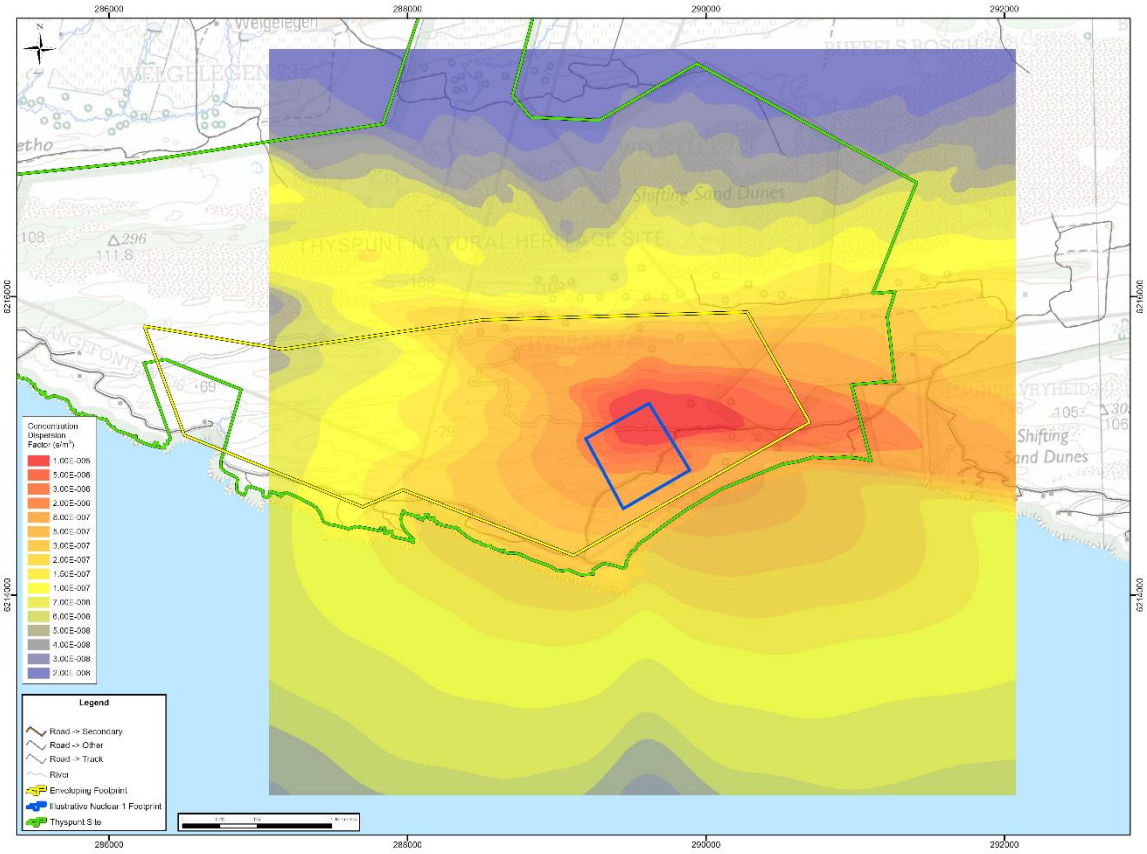


Figure 5.8.36
The Predicted Highest Annual Average Ground Level Concentration Dispersion Factor (χ/Q) (s/m³) for a 5 km by 5 km area

© Eskom 2026/Rev 0c

PRINTED VERSIONS OF THIS DOCUMENT ARE NOT CONTROLLED

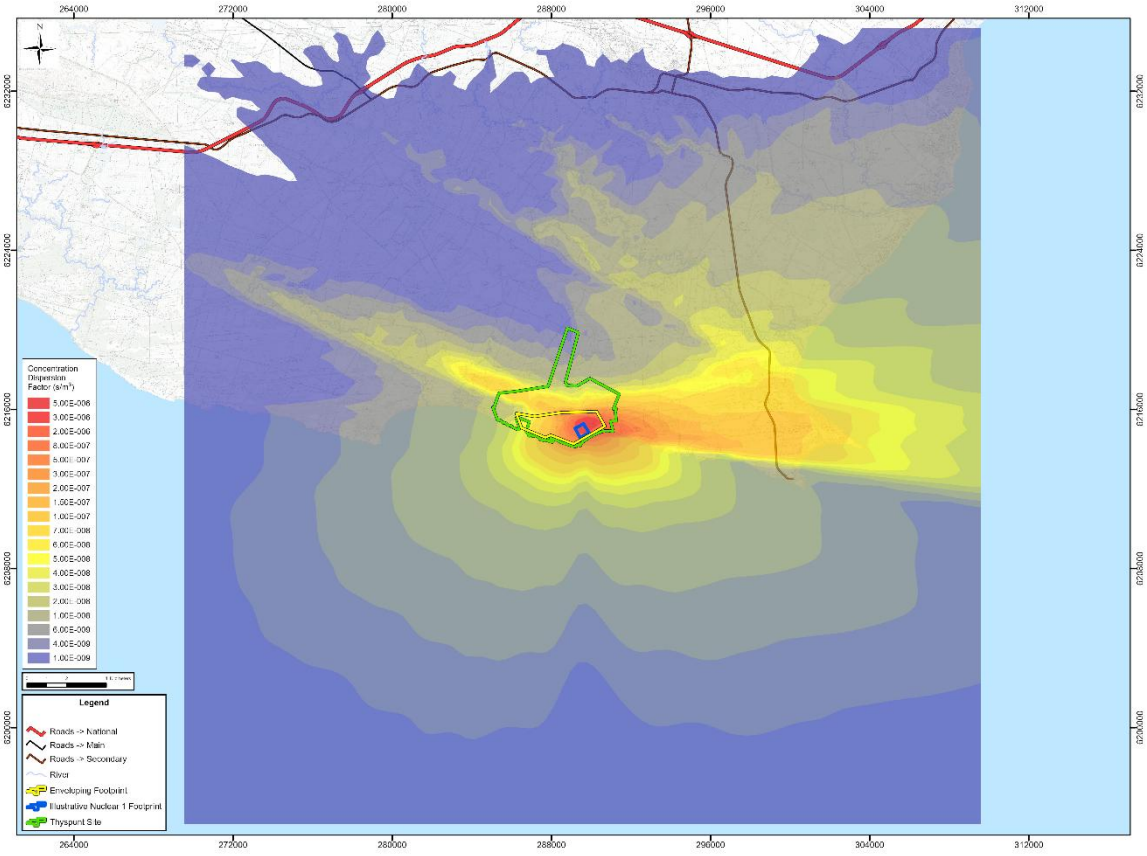


Figure 5.8.37
The Predicted Highest Annual Average Ground Level Concentration Dispersion Factor (χ/Q) (s/m³) for a 40 km by 40 km area

© Eskom 2026/Rev 0c

PRINTED VERSIONS OF THIS DOCUMENT ARE NOT CONTROLLED

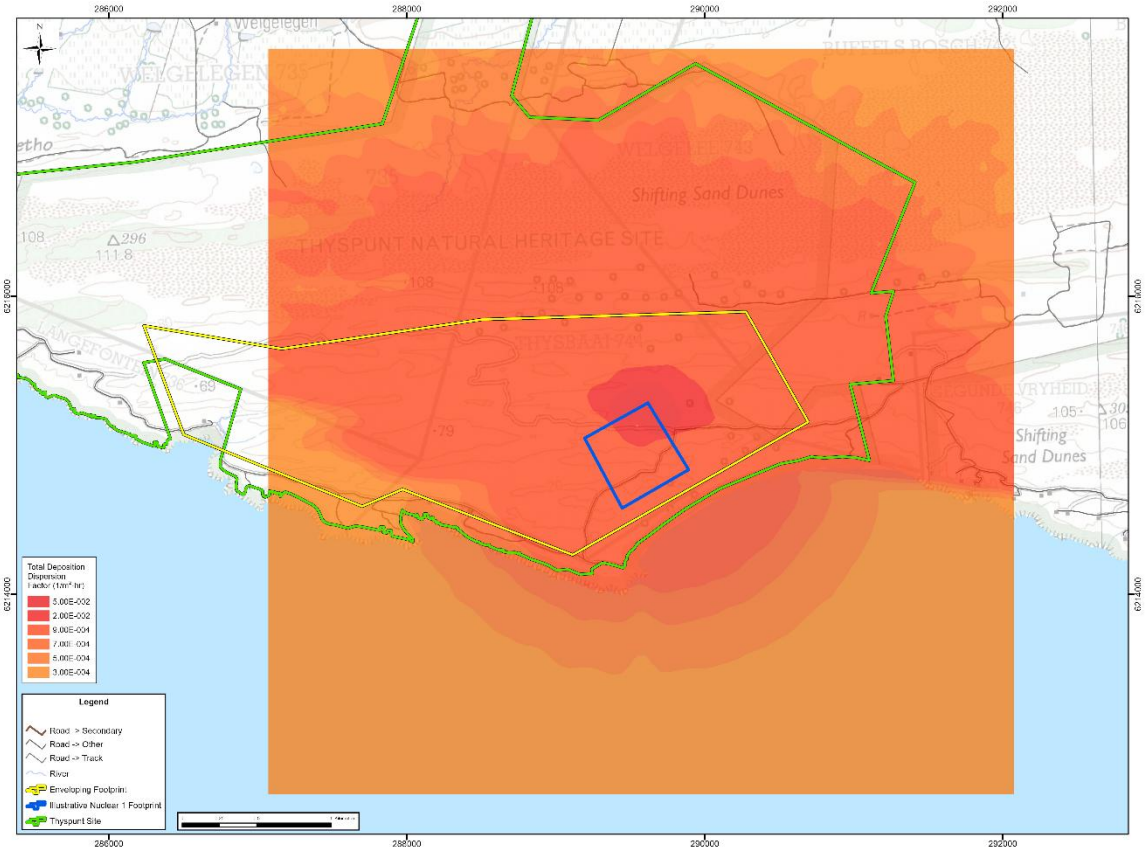


Figure 5.8.38
The Predicted 2nd Highest Hourly Total Deposition Dispersion Factor (*D/Q*) (1/m²- hour) for a 5 km by 5 km area

© Eskom 2026/Rev 0c

PRINTED VERSIONS OF THIS DOCUMENT ARE NOT CONTROLLED

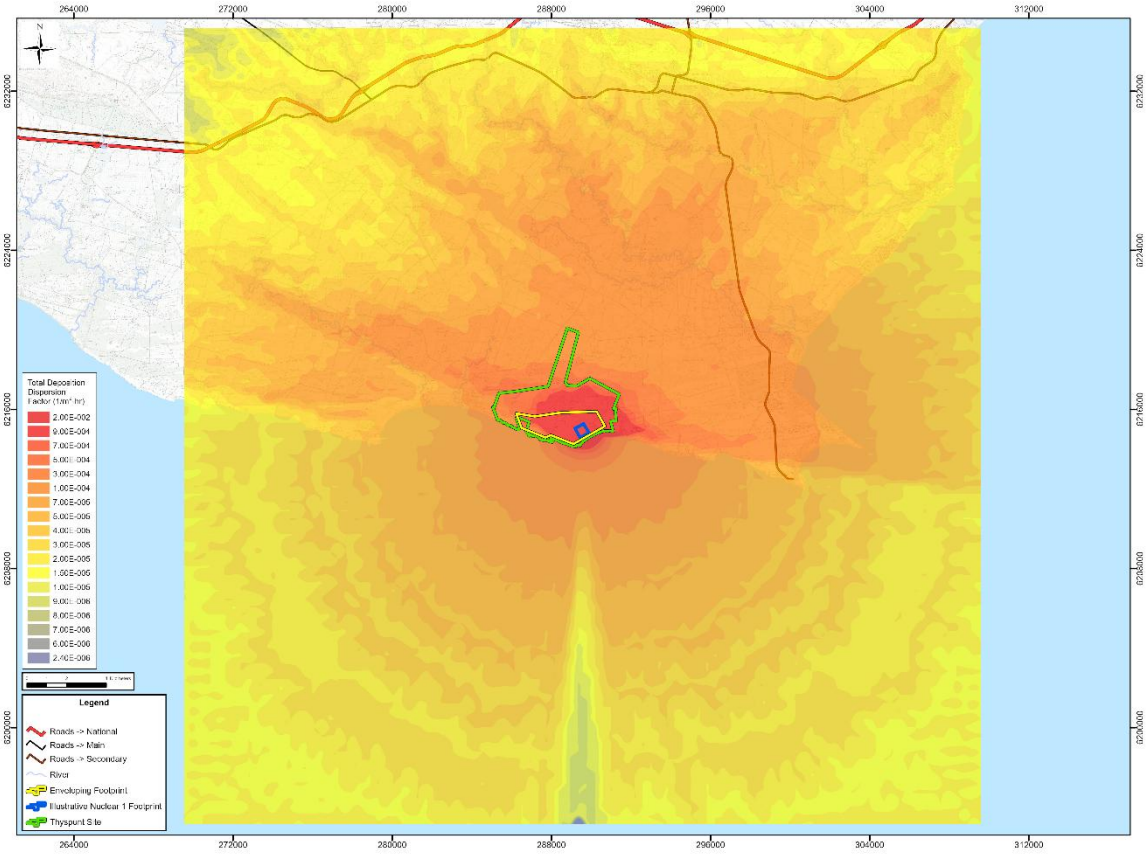


Figure 5.8.39
The Predicted 2nd Highest Hourly Total Deposition Dispersion Factor (*D/Q*) (1/m²- hour) for a 40 km by 40 km area

© Eskom 2026/Rev 0c

PRINTED VERSIONS OF THIS DOCUMENT ARE NOT CONTROLLED

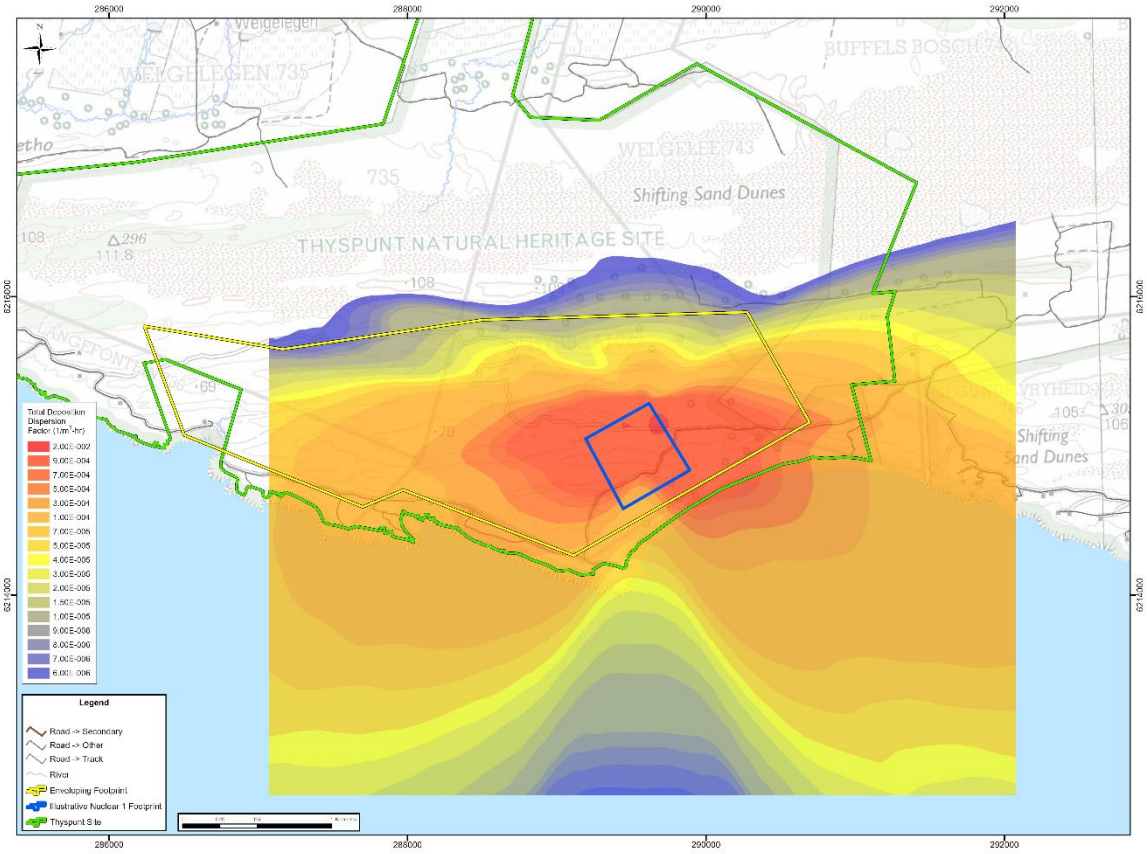


Figure 5.8.40
The Predicted 95th Percentile Hourly Total Deposition Factor (*D/Q*) (1/m²- hour) for a 5 km by 5 km area

© Eskom 2026/Rev 0c

PRINTED VERSIONS OF THIS DOCUMENT ARE NOT CONTROLLED

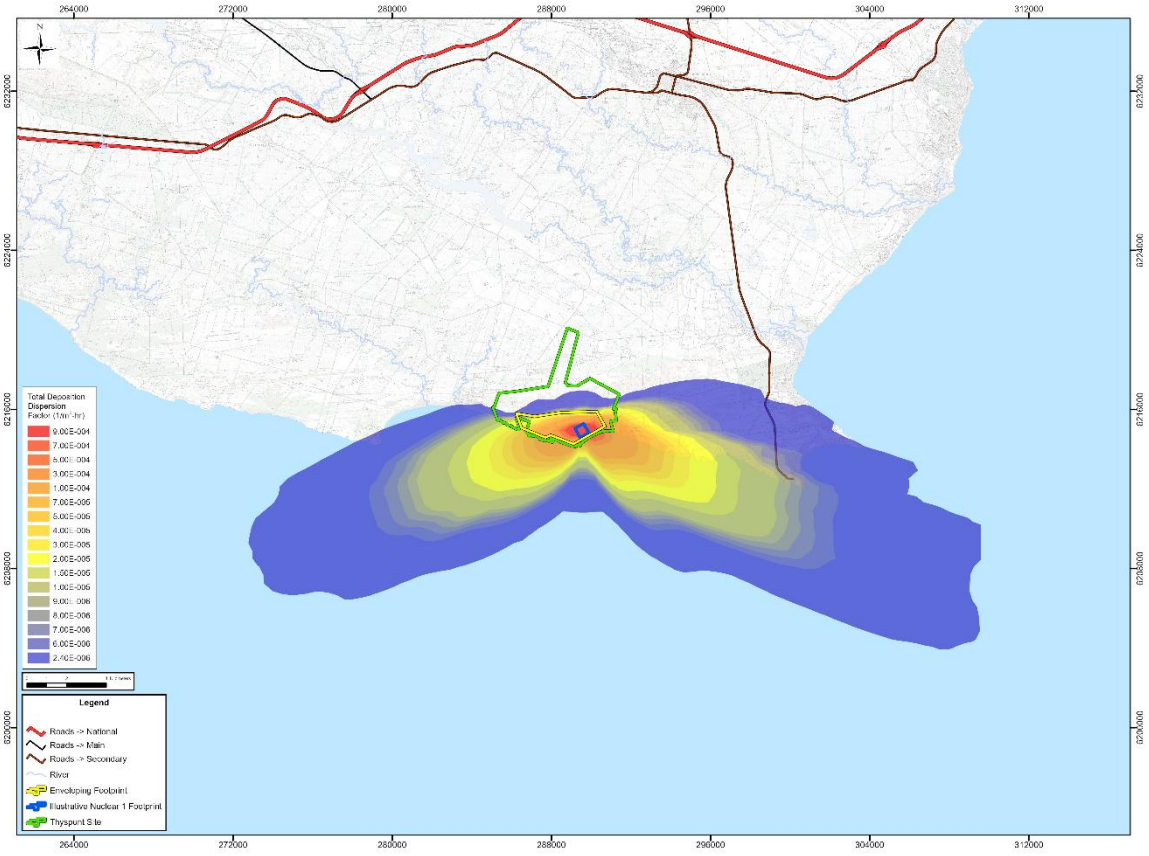


Figure 5.8.41
The Predicted 95th Percentile Hourly Total Deposition Factor (*D/Q*) (1/m²- hour) for a 40 km by 40 km area

© Eskom 2026/Rev 0c

PRINTED VERSIONS OF THIS DOCUMENT ARE NOT CONTROLLED

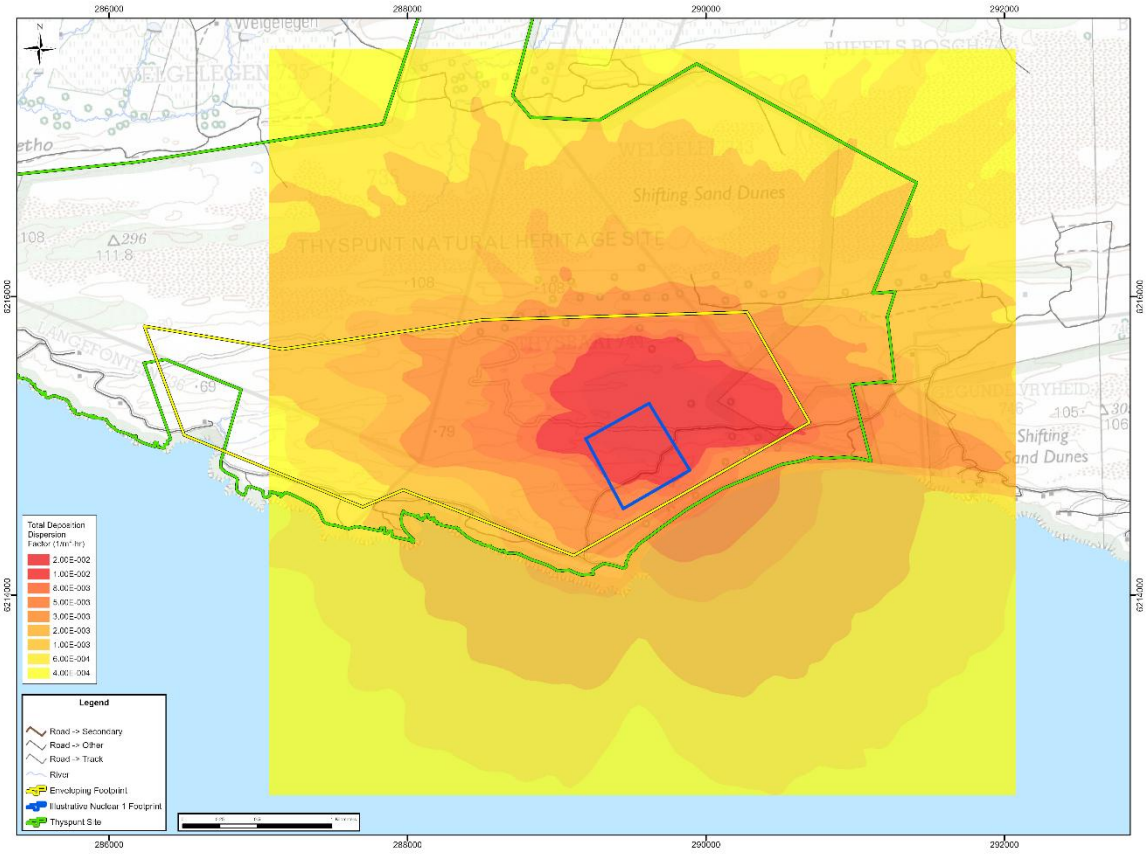


Figure 5.8.42
The Predicted 2nd Highest 3-Hour Total Deposition Factor (*D/Q*) (1/m²-3 hours) for a 5 km by 5 km area

© Eskom 2026/Rev 0c

PRINTED VERSIONS OF THIS DOCUMENT ARE NOT CONTROLLED

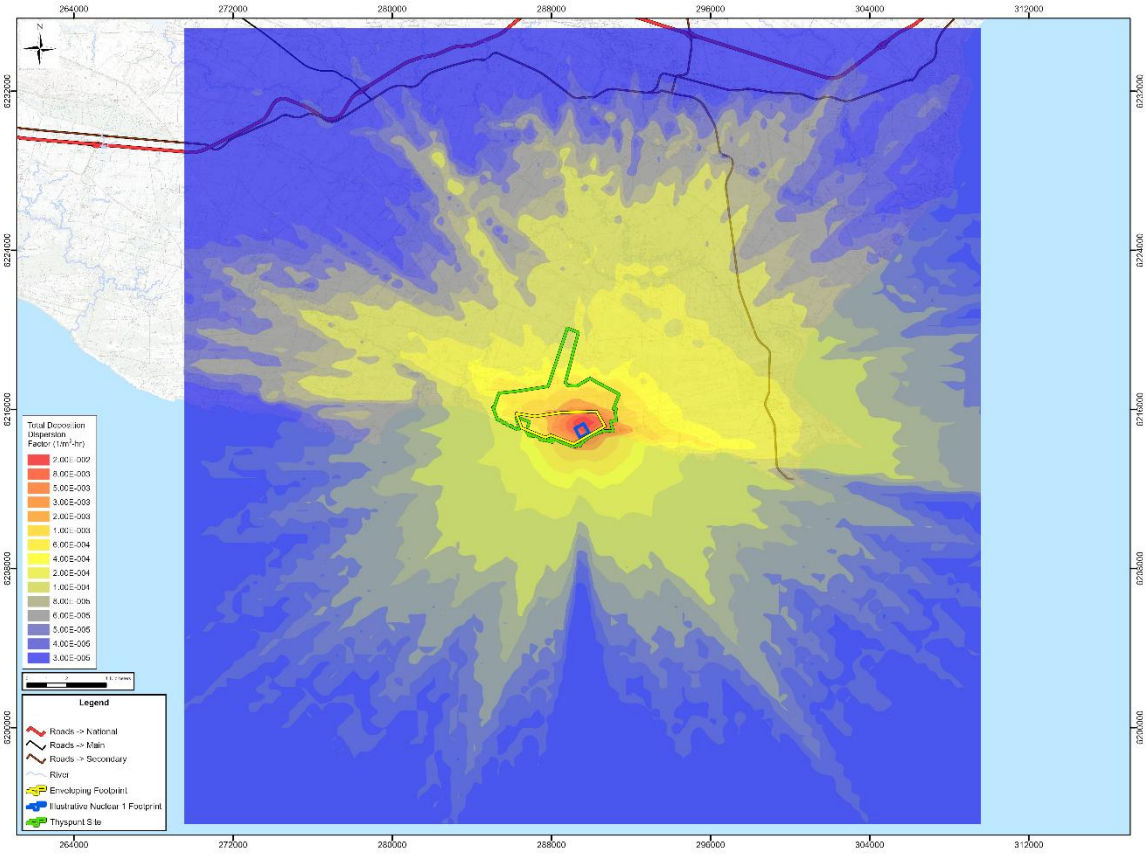


Figure 5.8.43
The Predicted 2nd Highest 3-Hour Total Deposition Factor (*D/Q*) (1/m²-3 hours) for a 40 km by 40 km area

© Eskom 2026/Rev 0c

PRINTED VERSIONS OF THIS DOCUMENT ARE NOT CONTROLLED

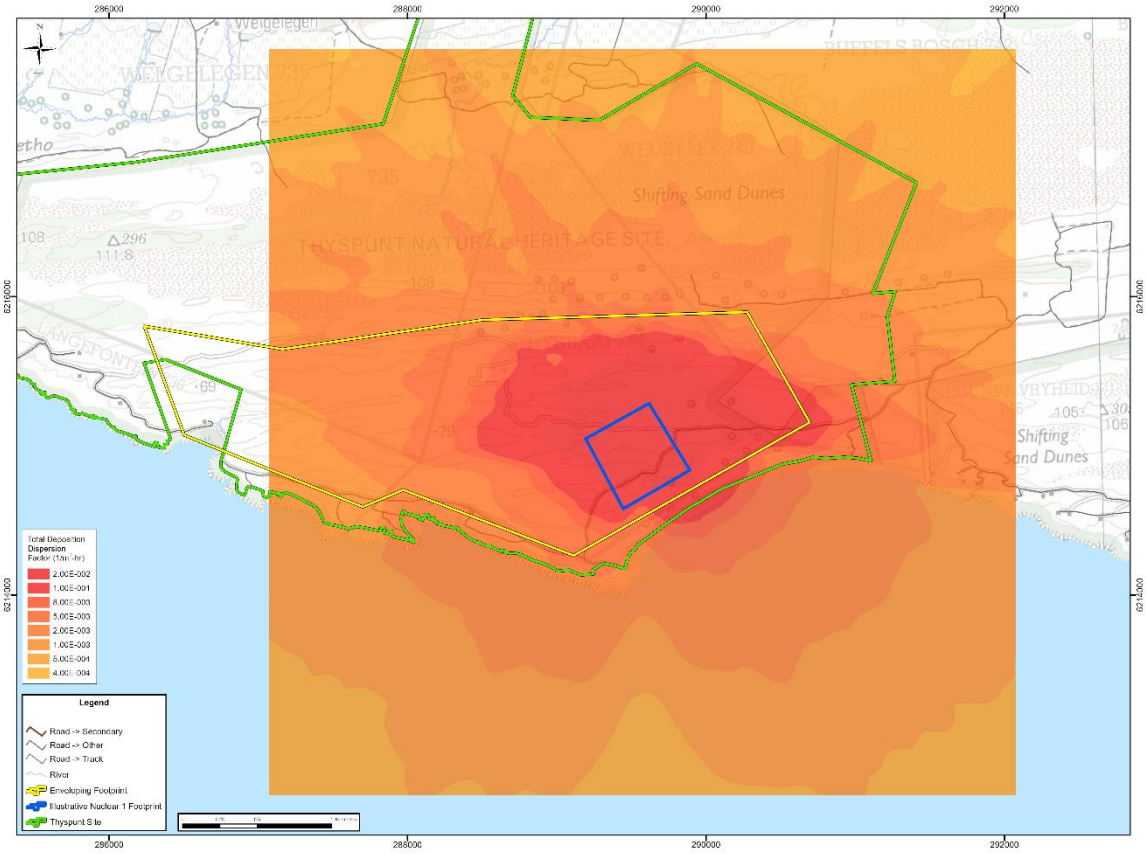


Figure 5.8.44
The Predicted 2nd Highest 8-Hour Total Deposition Factor (*D/Q*) (1/m²-8 hours) for a 5 km by 5 km area

© Eskom 2026/Rev 0c

PRINTED VERSIONS OF THIS DOCUMENT ARE NOT CONTROLLED

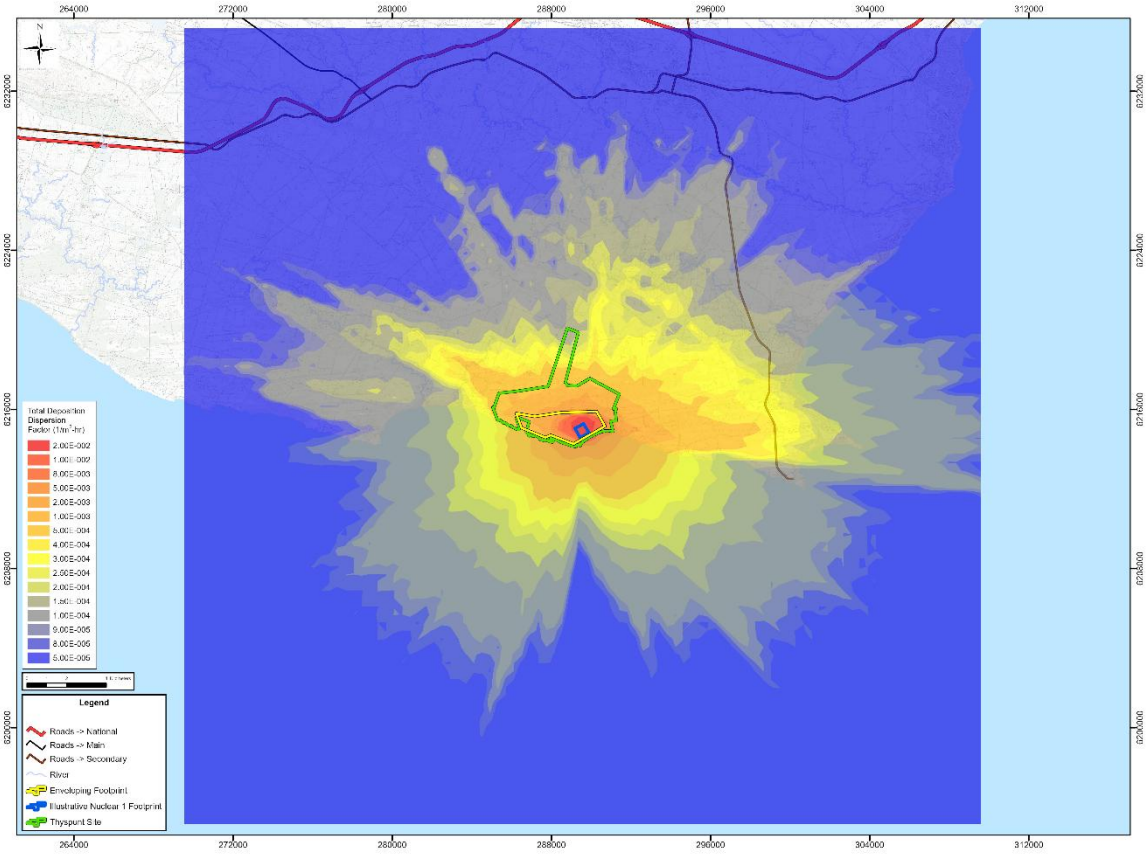


Figure 5.8.45
The Predicted 2nd Highest 8-Hour Total Deposition Factor (*D/Q*) (1/m²-8 hours) for a 40 km by 40 km area

© Eskom 2026/Rev 0c

PRINTED VERSIONS OF THIS DOCUMENT ARE NOT CONTROLLED

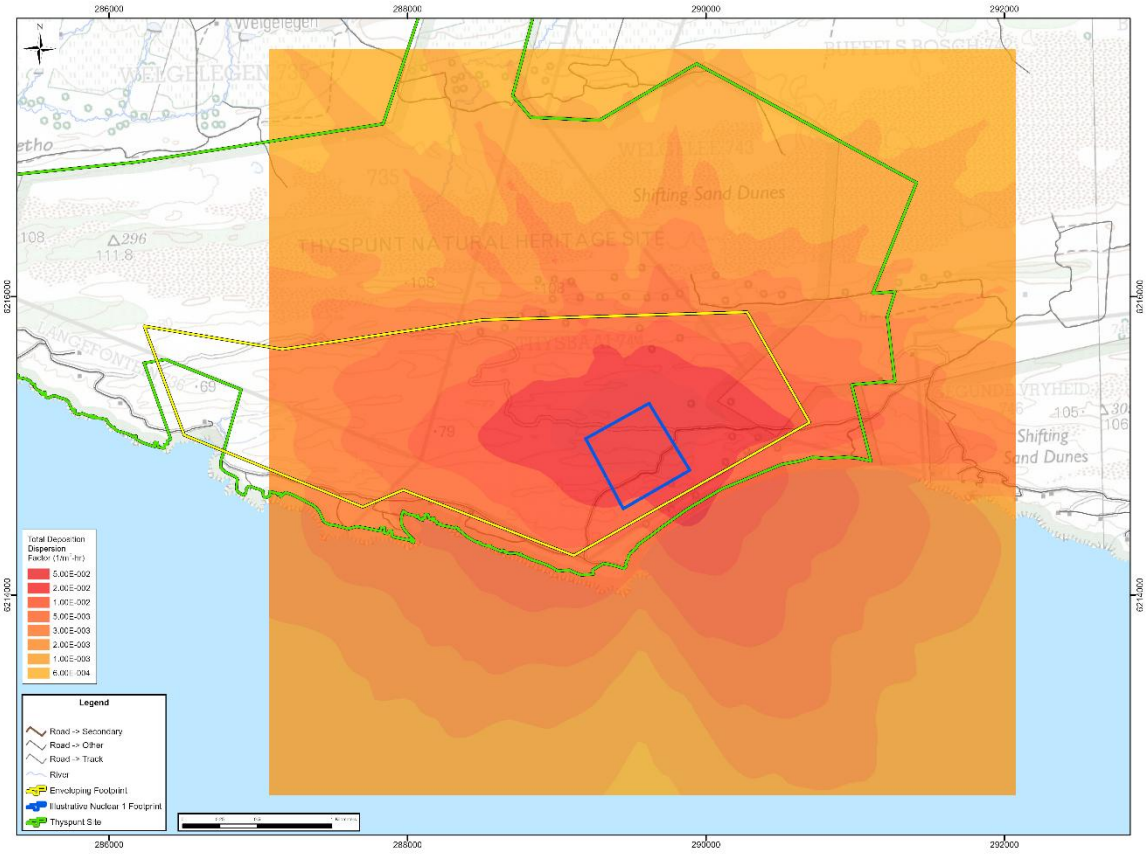


Figure 5.8.46
The Predicted 2nd Highest 24-Hour Total Deposition Factor (*D/Q*) (1/m²- 24 hours) for a 5 km by 5 km area

© Eskom 2026/Rev 0c

PRINTED VERSIONS OF THIS DOCUMENT ARE NOT CONTROLLED

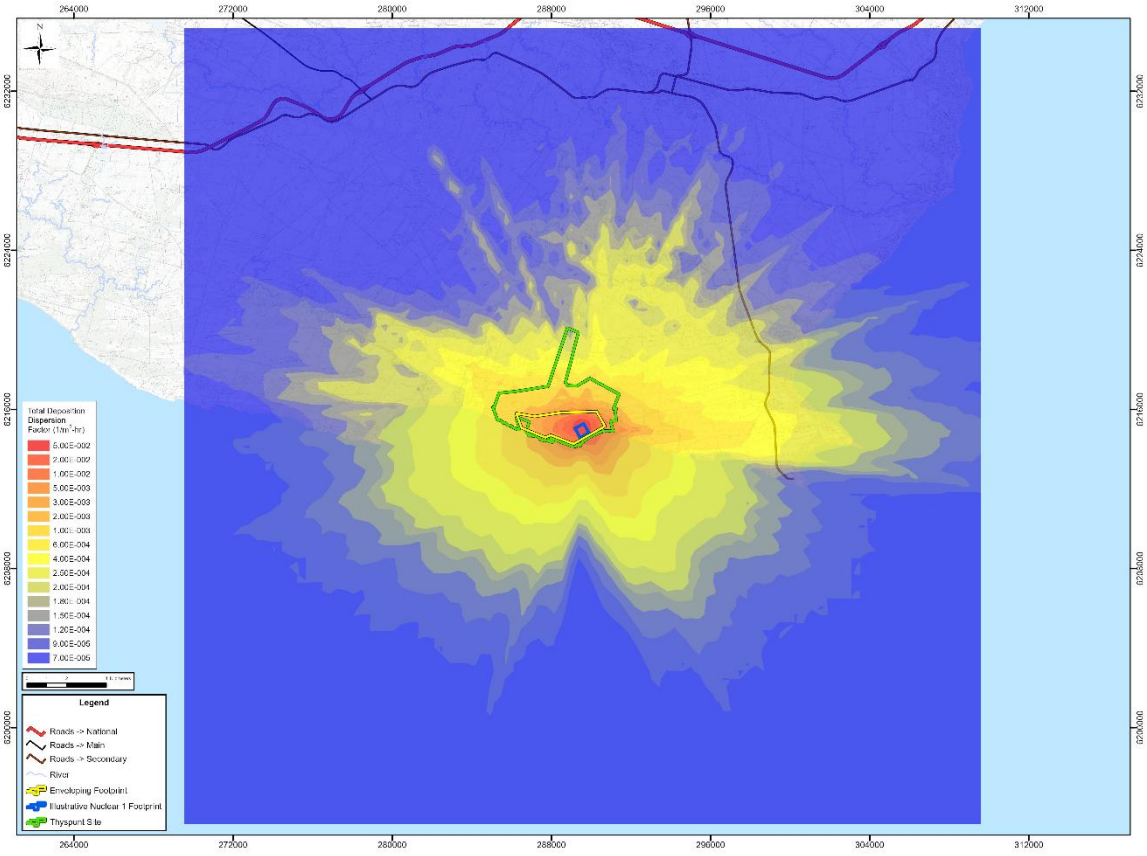


Figure 5.8.47
The Predicted 2nd Highest 24-Hour Total Deposition Factor (*D/Q*) (1/m²-24-hours) for a 40 km by 40 km area

© Eskom 2026/Rev 0c

PRINTED VERSIONS OF THIS DOCUMENT ARE NOT CONTROLLED

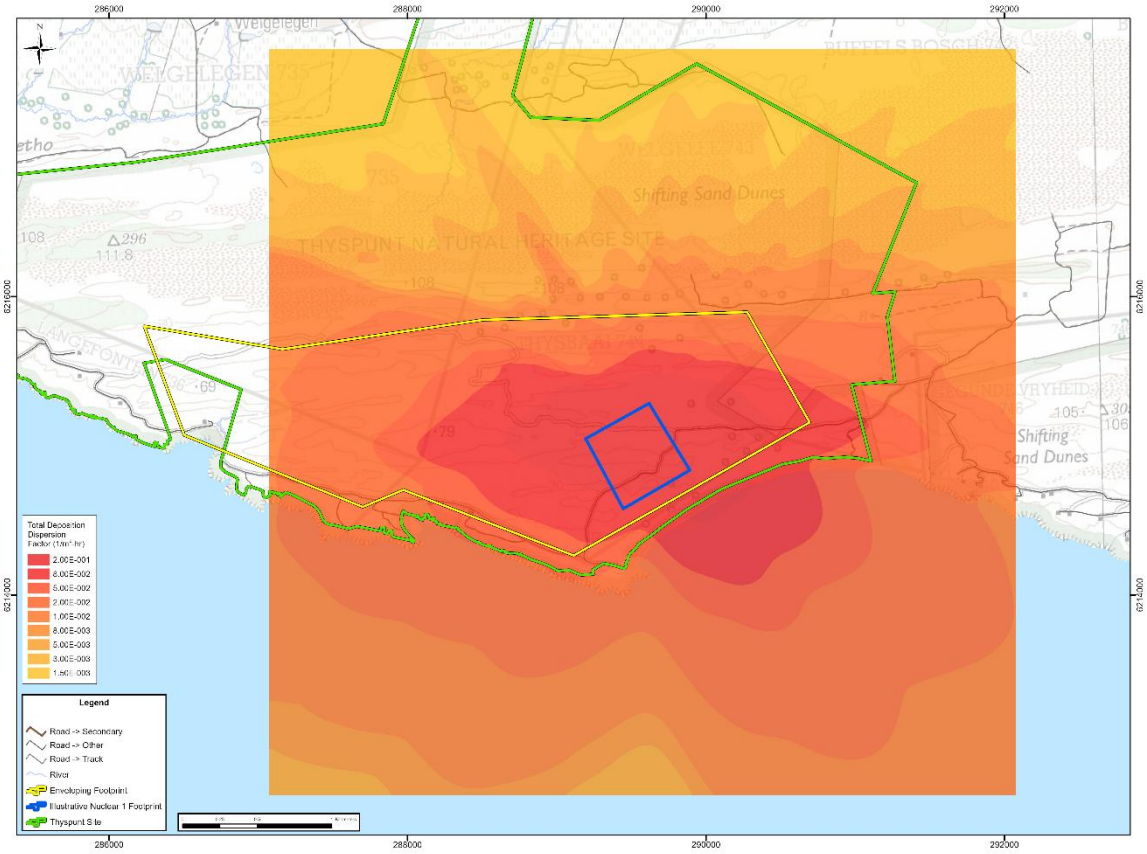


Figure 5.8.48
The Predicted Highest Monthly Total Deposition Factor (*D/Q*) (1/m²-month) for a 5 km by 5 km area

© Eskom 2026/Rev 0c

PRINTED VERSIONS OF THIS DOCUMENT ARE NOT CONTROLLED

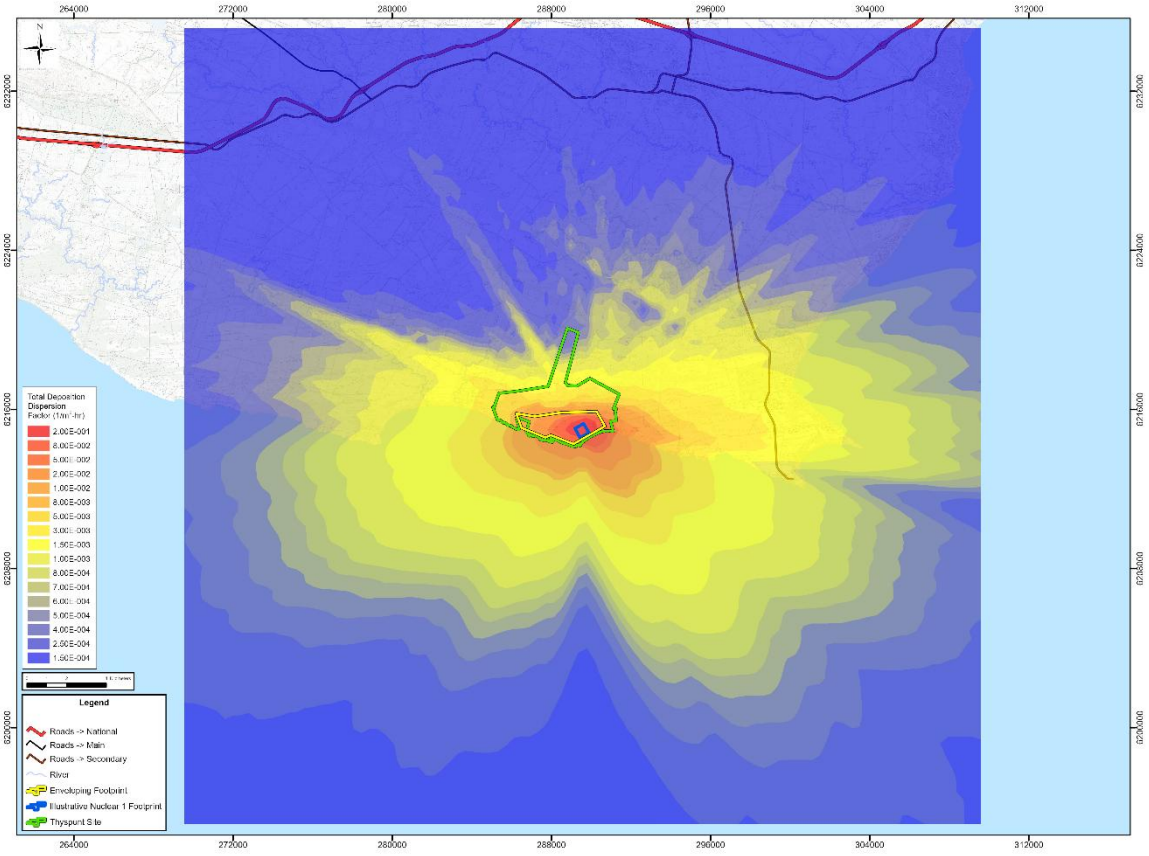


Figure 5.8.49
The Predicted Highest Monthly Total Deposition Factor (*D/Q*) (1/m²-month) for a 40 km by 40 km area

© Eskom 2026/Rev 0c

PRINTED VERSIONS OF THIS DOCUMENT ARE NOT CONTROLLED

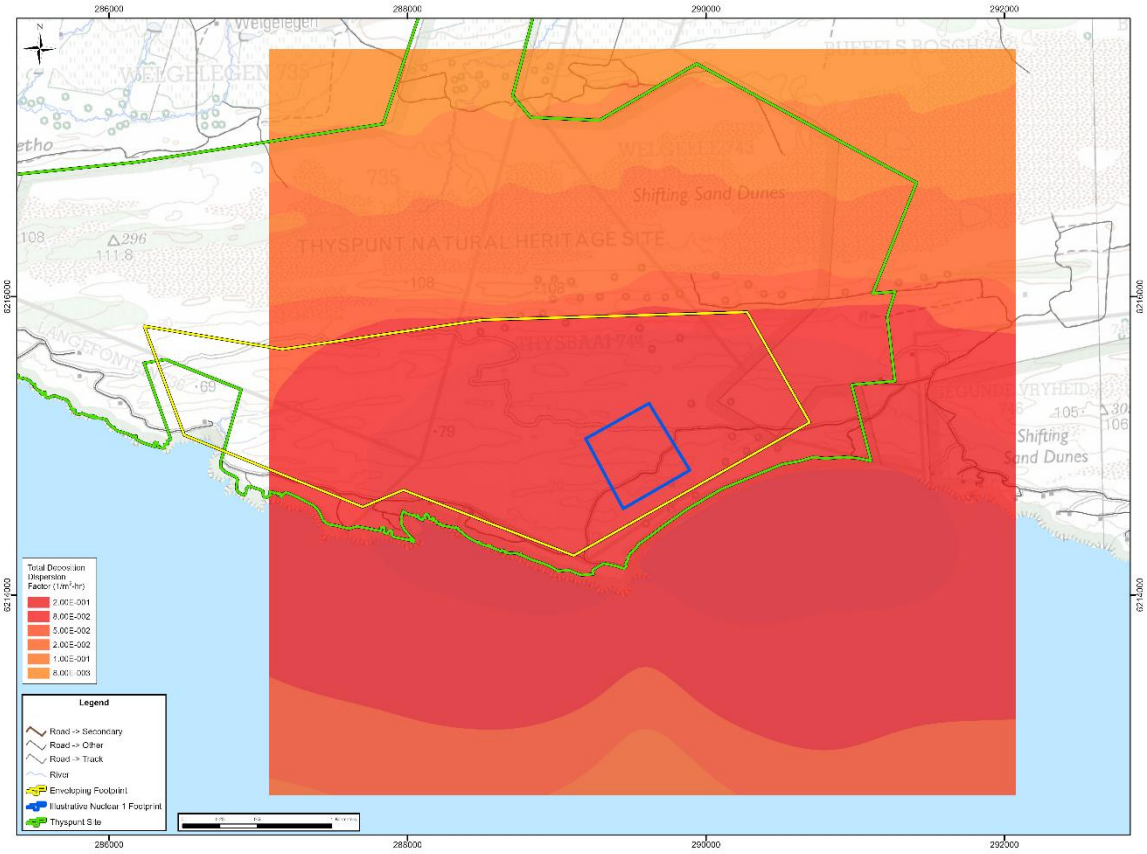


Figure 5.8.50
The Predicted Highest Annual Total Deposition Factor (D/Q) (1/m²-year) for a 5 km by 5 km area

© Eskom 2026/Rev 0c

PRINTED VERSIONS OF THIS DOCUMENT ARE NOT CONTROLLED

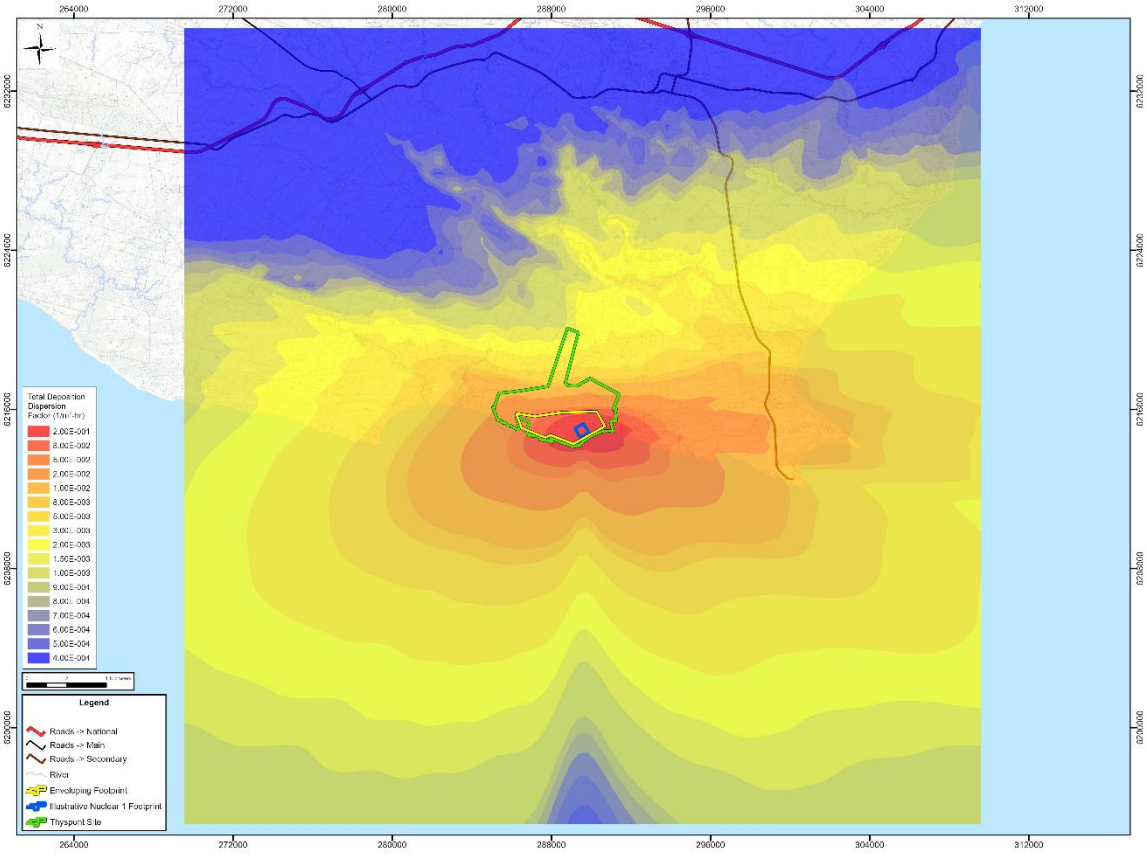


Figure 5.8.51
The Predicted Highest Annual Total Deposition Factor (*D/Q*) (1/m²-year) for a 40 km by 40 km area

© Eskom 2026/Rev 0c

PRINTED VERSIONS OF THIS DOCUMENT ARE NOT CONTROLLED

Table 5.8.69
Dispersion Factors (s/m³) based on 2nd Highest Hourly, 3-Hourly, 8-Hourly and 24-hourly Average Predictions at 800 m, 3 km and 8 km Downwind of the Nuclear Installation(s) for Different Wind Directions

Distance (m)	Highest Hourly			Highest 3-Hourly			Highest 8-Hourly			Highest 24-Hourly		
	800	3000	8000	800	3000	8000	800	3000	8000	800	3000	8000
N	1.82E-04	2.40E-05	2.81E-05	8.89E-05	4.95E-06	7.06E-06	6.71E-05	1.11E-05	1.51E-05	1.87E-05	1.78E-06	2.36E-06
NNE	3.18E-04	2.43E-05	3.54E-05	1.16E-04	9.04E-06	6.65E-06	1.52E-04	1.19E-05	1.76E-05	2.17E-05	1.57E-06	2.22E-06
NE	4.44E-04	2.83E-05	4.35E-05	1.77E-04	1.36E-05	6.65E-06	9.18E-05	1.36E-05	1.77E-05	2.34E-05	2.00E-06	2.22E-06
ENE	6.71E-04	2.98E-05	4.62E-05	3.39E-04	1.62E-05	8.50E-06	3.39E-04	1.63E-05	2.26E-05	4.50E-05	2.82E-06	2.96E-06
E	9.11E-04	1.49E-04	4.10E-05	5.59E-04	2.25E-05	8.51E-06	5.59E-04	5.79E-05	1.92E-05	8.68E-05	8.49E-06	2.86E-06
ESE	2.49E-04	7.46E-05	1.13E-05	8.35E-05	1.72E-05	2.13E-06	8.35E-05	2.67E-05	3.78E-06	1.83E-05	5.76E-06	7.32E-07
SE	8.81E-05	1.50E-05	3.52E-06	4.76E-05	7.29E-06	1.23E-06	3.73E-05	7.29E-06	3.25E-06	7.60E-06	1.09E-06	4.12E-07
SSE	9.67E-05	1.46E-05	3.52E-06	3.84E-05	5.14E-06	9.52E-07	3.64E-05	5.71E-06	2.41E-06	9.21E-06	9.84E-07	3.24E-07
S	9.44E-05	1.46E-05	3.42E-06	3.30E-05	1.95E-06	6.01E-07	2.65E-05	5.17E-06	1.59E-06	4.85E-06	6.58E-07	2.01E-07
SSW	1.07E-04	1.34E-05	3.48E-06	4.28E-05	5.21E-06	7.20E-07	4.02E-05	6.99E-06	1.63E-06	6.51E-06	9.86E-07	2.46E-07
SW	9.96E-05	1.44E-05	3.69E-06	3.99E-05	5.46E-06	6.49E-07	3.48E-05	5.46E-06	1.41E-06	7.05E-06	9.10E-07	2.29E-07
WSW	2.37E-04	1.46E-05	3.53E-06	1.27E-04	6.45E-06	7.72E-07	1.27E-04	7.84E-06	1.86E-06	1.64E-05	1.19E-06	2.60E-07
W	1.91E-04	5.13E-05	3.24E-06	1.03E-04	6.92E-06	7.60E-07	1.03E-04	1.77E-05	1.67E-06	1.41E-05	2.34E-06	2.56E-07
WNW	3.40E-04	6.41E-05	3.63E-05	1.79E-04	2.95E-05	6.57E-06	1.42E-04	2.79E-05	1.65E-05	3.05E-05	4.39E-06	2.19E-06
NW	4.28E-04	5.78E-05	1.18E-05	2.23E-04	2.61E-05	2.58E-06	1.21E-04	1.77E-05	5.99E-06	4.09E-05	3.51E-06	8.02E-07
NNW	3.11E-04	2.71E-05	8.08E-06	1.43E-04	1.07E-05	1.63E-06	1.14E-04	2.56E-05	3.41E-06	2.60E-05	3.64E-06	5.52E-07

© Eskom 2026/Rev 0c

PRINTED VERSIONS OF THIS DOCUMENT ARE NOT CONTROLLED

Table 5.8.70
Dispersion Factors (s/m³) based on Highest Averages of 3-Daily, Monthly, Annual and 95th Percentile Predictions at 800 m, 3 km and 8 km Downwind of the Nuclear Installation(s) for Different Wind Directions

Distance (m)	Highest 3-Daily			Highest Monthly			Highest Annual			95th Percentile		
	800	3000	8000	800	3000	8000	800	3000	8000	800	3000	8000
N	1.55E-05	1.48E-06	1.96E-06	7.12E-07	7.89E-08	1.19E-07	1.70E-07	1.42E-08	2.46E-08	6.11E-08	5.65E-09	2.09E-08
NNE	1.80E-05	1.31E-06	1.84E-06	1.85E-06	1.05E-07	1.38E-07	5.47E-07	2.06E-08	2.71E-08	3.73E-07	5.63E-09	2.15E-08
NE	1.94E-05	1.66E-06	1.84E-06	3.16E-06	1.71E-07	1.84E-07	1.13E-06	5.36E-08	4.47E-08	1.35E-06	5.35E-08	4.19E-08
ENE	3.73E-05	2.34E-06	2.46E-06	6.92E-06	4.16E-07	2.11E-07	4.37E-06	2.34E-07	8.55E-08	1.05E-05	4.01E-07	6.07E-08
E	7.21E-05	7.05E-06	2.37E-06	1.63E-05	1.24E-06	4.23E-07	7.79E-06	7.36E-07	1.52E-07	4.00E-05	9.76E-07	1.63E-07
ESE	1.52E-05	4.78E-06	6.08E-07	2.05E-06	4.82E-07	6.26E-08	1.29E-06	2.59E-07	3.14E-08	6.36E-06	6.28E-07	1.30E-07
SE	6.31E-06	9.03E-07	3.42E-07	1.58E-06	1.74E-07	3.36E-08	9.21E-07	1.02E-07	2.03E-08	4.52E-06	5.73E-07	1.09E-07
SSE	7.64E-06	8.17E-07	2.69E-07	1.68E-06	1.63E-07	3.21E-08	7.67E-07	6.78E-08	1.40E-08	3.63E-06	2.49E-07	4.91E-08
S	4.03E-06	5.46E-07	1.67E-07	8.47E-07	9.54E-08	2.29E-08	3.96E-07	4.34E-08	1.05E-08	1.47E-06	1.01E-07	2.78E-08
SSW	5.40E-06	8.19E-07	2.04E-07	1.23E-06	1.19E-07	2.73E-08	7.30E-07	6.08E-08	1.28E-08	3.33E-06	2.15E-07	4.39E-08
SW	5.85E-06	7.56E-07	1.90E-07	1.43E-06	1.89E-07	4.08E-08	7.21E-07	7.10E-08	1.45E-08	3.25E-06	2.84E-07	5.90E-08
WSW	1.36E-05	9.88E-07	2.16E-07	2.01E-06	2.01E-07	4.35E-08	8.83E-07	7.66E-08	1.52E-08	3.85E-06	3.03E-07	6.26E-08
W	1.17E-05	1.94E-06	2.13E-07	1.41E-06	1.68E-07	3.35E-08	5.32E-07	5.85E-08	1.29E-08	2.24E-06	2.09E-07	4.32E-08
WNW	2.53E-05	3.64E-06	1.82E-06	3.22E-06	3.28E-07	1.55E-07	8.98E-07	1.01E-07	3.89E-08	1.47E-06	4.97E-08	3.83E-08
NW	3.40E-05	2.91E-06	6.65E-07	2.28E-06	2.66E-07	4.26E-08	9.68E-07	8.51E-08	1.14E-08	8.47E-07	2.87E-08	4.10E-09
NNW	2.16E-05	3.02E-06	4.59E-07	9.78E-07	1.53E-07	2.55E-08	3.26E-07	2.02E-08	4.90E-09	2.26E-07	8.90E-09	2.42E-09

© Eskom 2026/Rev 0c

PRINTED VERSIONS OF THIS DOCUMENT ARE NOT CONTROLLED

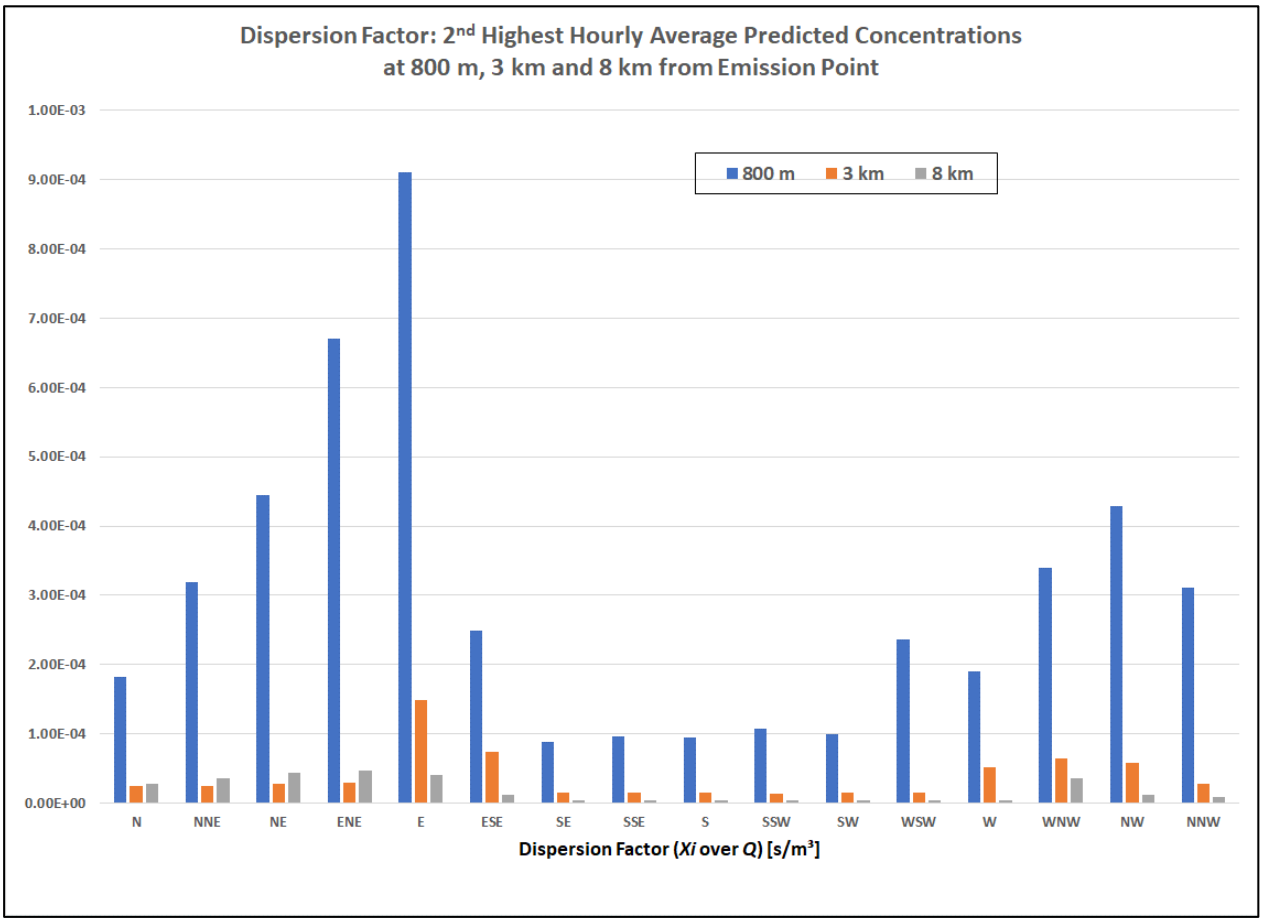


Figure 5.8.52
Dispersion Factors (χ/Q) (s/m³) based on the 2nd Highest Hourly Average Predictions at 800 m, 3 km and 8 km Downwind of the Nuclear Installation(s) for Different Wind Directions

© Eskom 2026/Rev 0c

PRINTED VERSIONS OF THIS DOCUMENT ARE NOT CONTROLLED

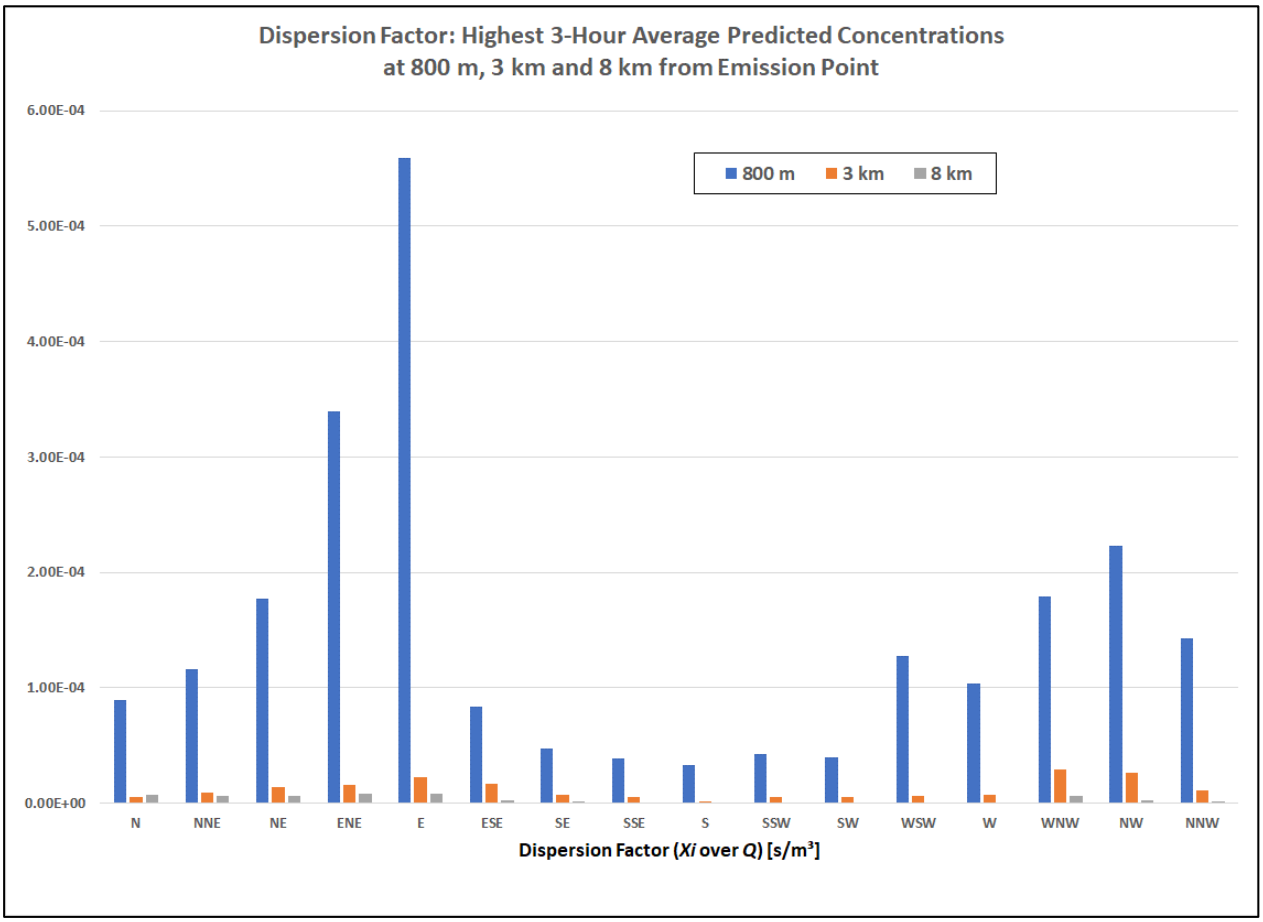


Figure 5.8.53
Dispersion Factors (χ/Q) (s/m³) based on the Highest 3-Hourly Average Predictions at 800 m, 3 km and 8 km Downwind of the Nuclear Installation(s) for Different Wind Directions

© Eskom 2026/Rev 0c

PRINTED VERSIONS OF THIS DOCUMENT ARE NOT CONTROLLED

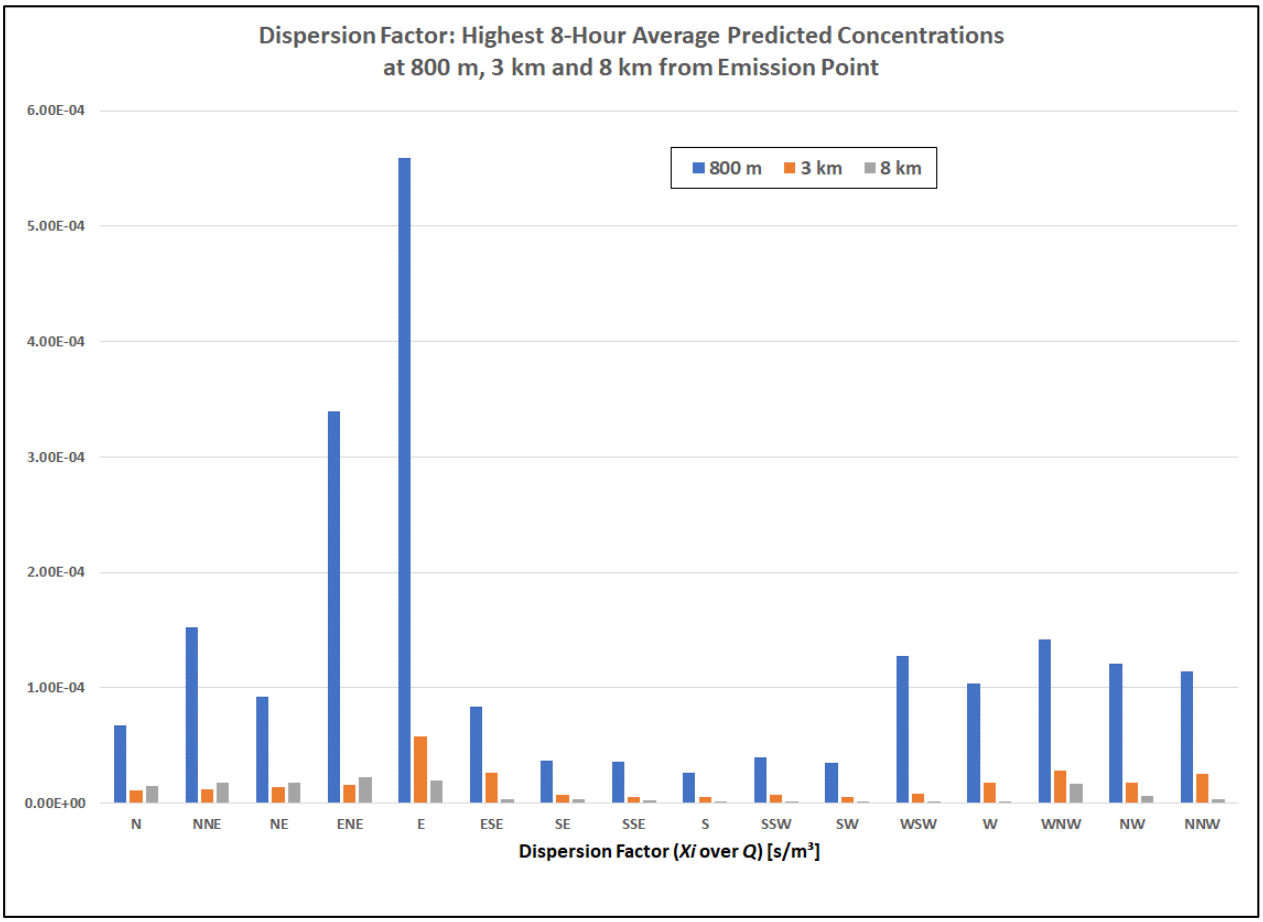


Figure 5.8.54
Dispersion Factors (χ/Q) (s/m³) based on the Highest 8-Hourly Average Predictions at 800 m, 3 km and 8 km Downwind of the Nuclear Installation(s) for Different Wind Directions

© Eskom 2026/Rev 0c

PRINTED VERSIONS OF THIS DOCUMENT ARE NOT CONTROLLED

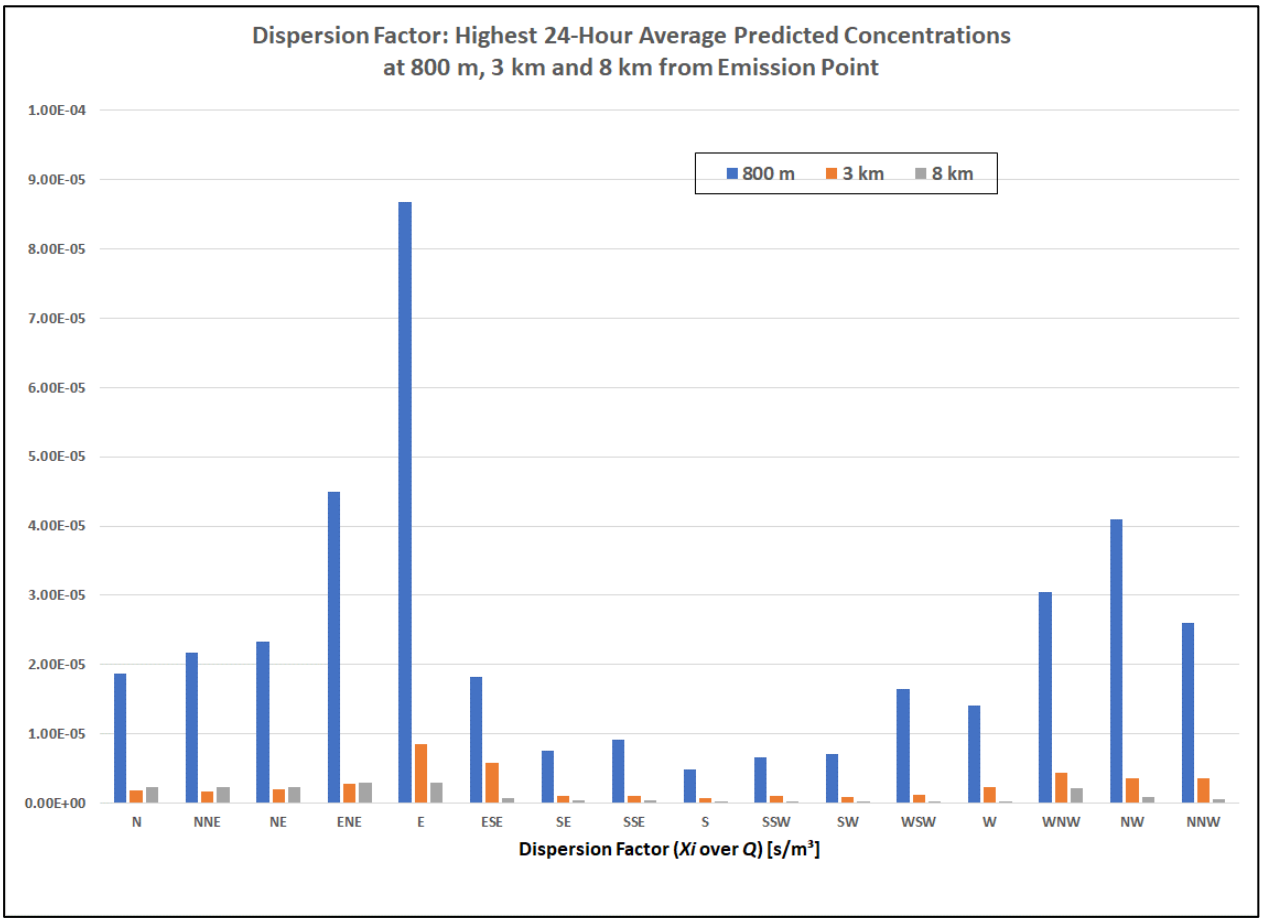


Figure 5.8.55
Dispersion Factors (χ/Q) (s/m³) based on the Highest 24-Hourly Average Predictions at 800 m, 3 km and 8 km Downwind of the Nuclear Installation(s) for Different Wind Directions

© Eskom 2026/Rev 0c

PRINTED VERSIONS OF THIS DOCUMENT ARE NOT CONTROLLED

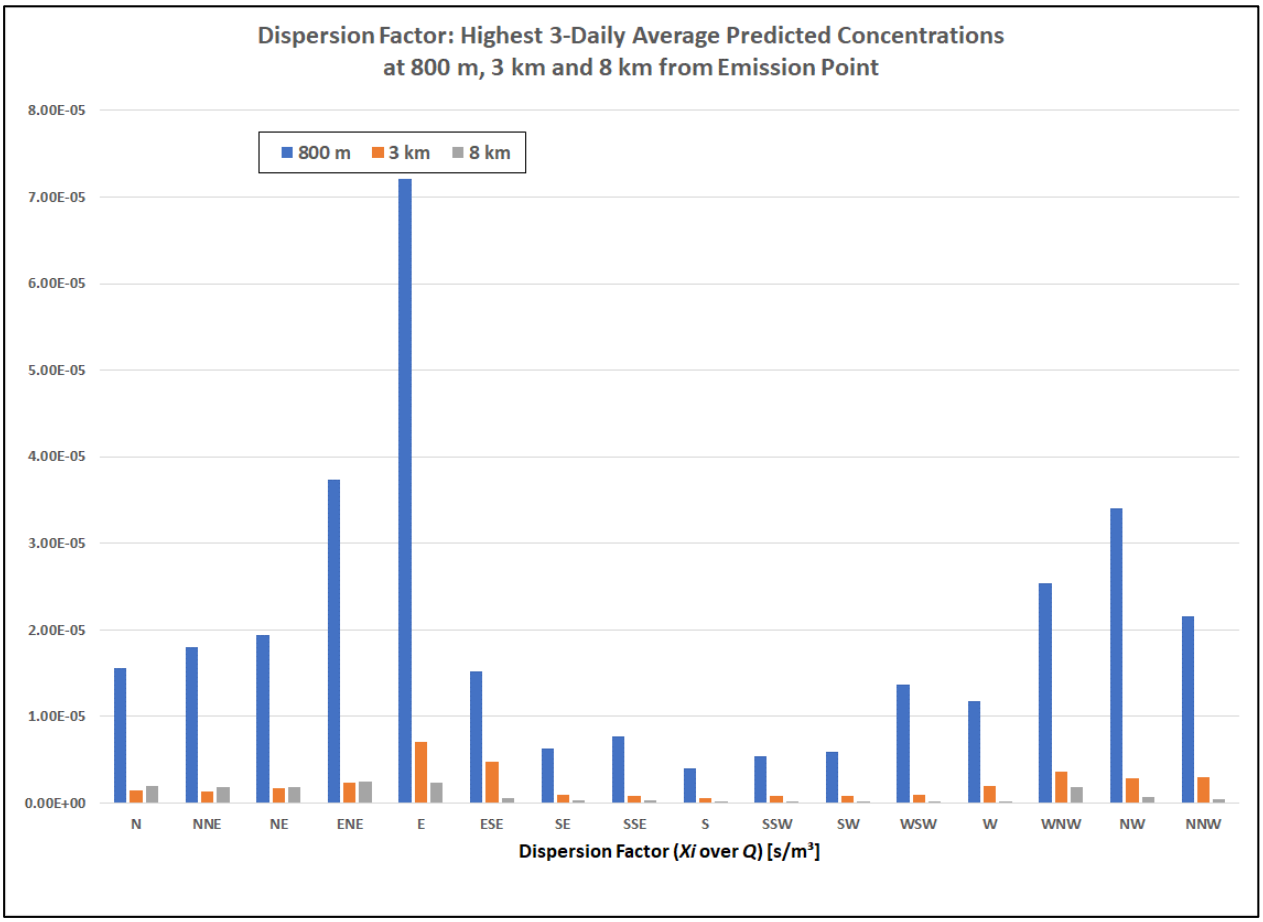


Figure 5.8.56
Dispersion Factors (χ/Q) (s/m³) based on the Highest 3-Daily Average Predictions at 800 m, 3 km and 8 km Downwind of the Nuclear Installation(s) for Different Wind Directions

© Eskom 2026/Rev 0c

PRINTED VERSIONS OF THIS DOCUMENT ARE NOT CONTROLLED

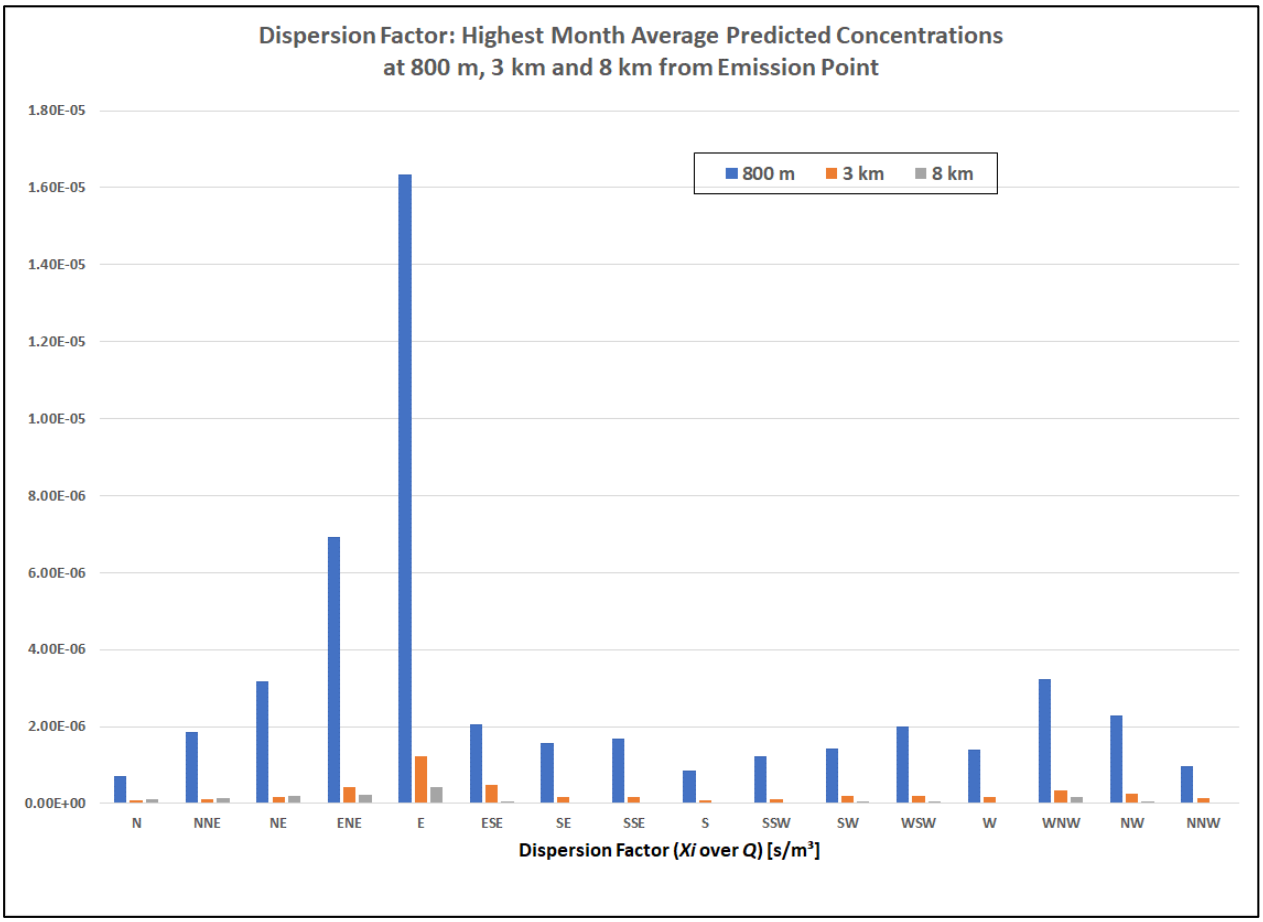


Figure 5.8.57
Dispersion Factors (χ/Q) (s/m³) based on the Highest Monthly Average Predictions at 800 m, 3 km and 8 km Downwind of the Nuclear Installation(s) for Different Wind Directions

© Eskom 2026/Rev 0c

PRINTED VERSIONS OF THIS DOCUMENT ARE NOT CONTROLLED

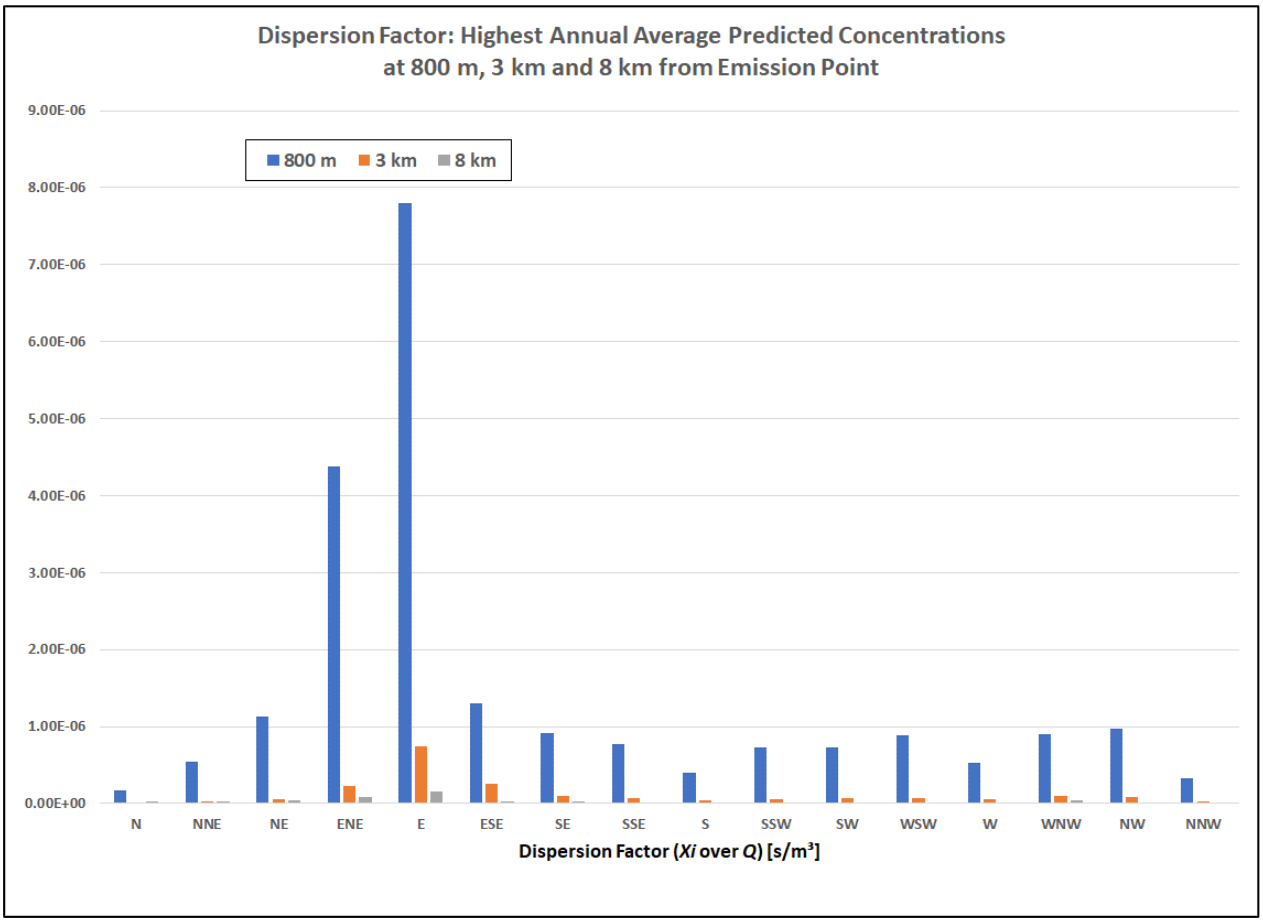


Figure 5.8.58
Dispersion Factors (χ/Q) (s/m³) based on the Highest Annual Average Predictions at 800 m, 3 km and 8 km Downwind of the Nuclear Installation(s) for Different Wind Directions

© Eskom 2026/Rev 0c

PRINTED VERSIONS OF THIS DOCUMENT ARE NOT CONTROLLED

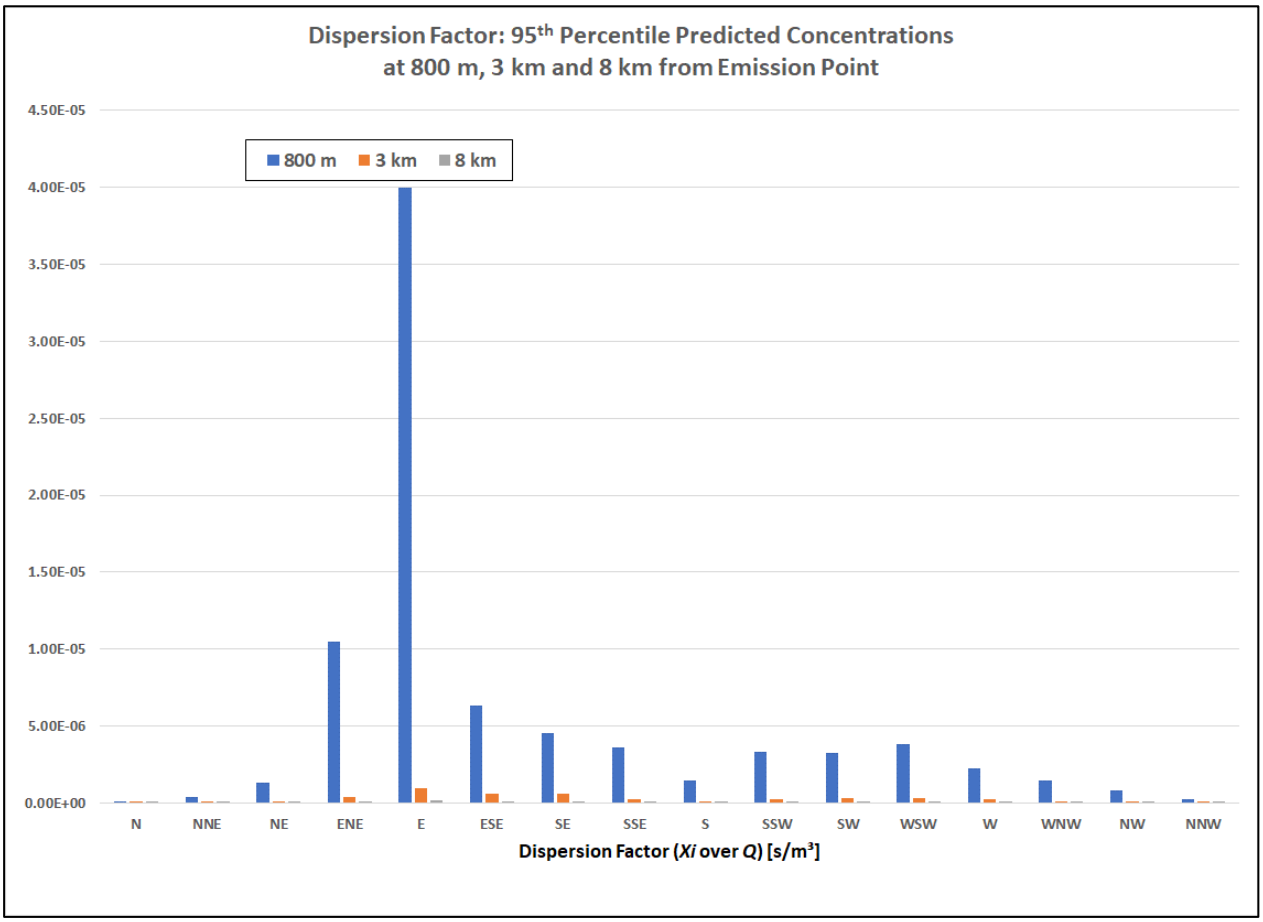


Figure 5.8.59
Dispersion Factors (χ/Q) (s/m³) Based on the 95th Percentile of the Hourly Average Predictions at 800 m, 3 km and 8 km Downwind of the Nuclear Installation(s) for Different Wind Directions

Figure 5.8.60 is a summary of the χ/Q values for different downwind distances and averaging periods.

Figure 5.8.61 to ***Figure 5.8.68*** summarise the D/Q values given as the total deposition over the period of interest (i.e. 1-hour, 3-hour, 8-hour, 1-day, 3-days, month, year and 95th percentile) for different downwind distances and averaging periods.

Figure 5.8.69 is a summary of the D/Q values given as the total deposition over the period of interest (i.e. 1-hour, 1-day, month, year) for different downwind distances and averaging periods.

© Eskom 2026/Rev 0c

PRINTED VERSIONS OF THIS DOCUMENT ARE NOT CONTROLLED

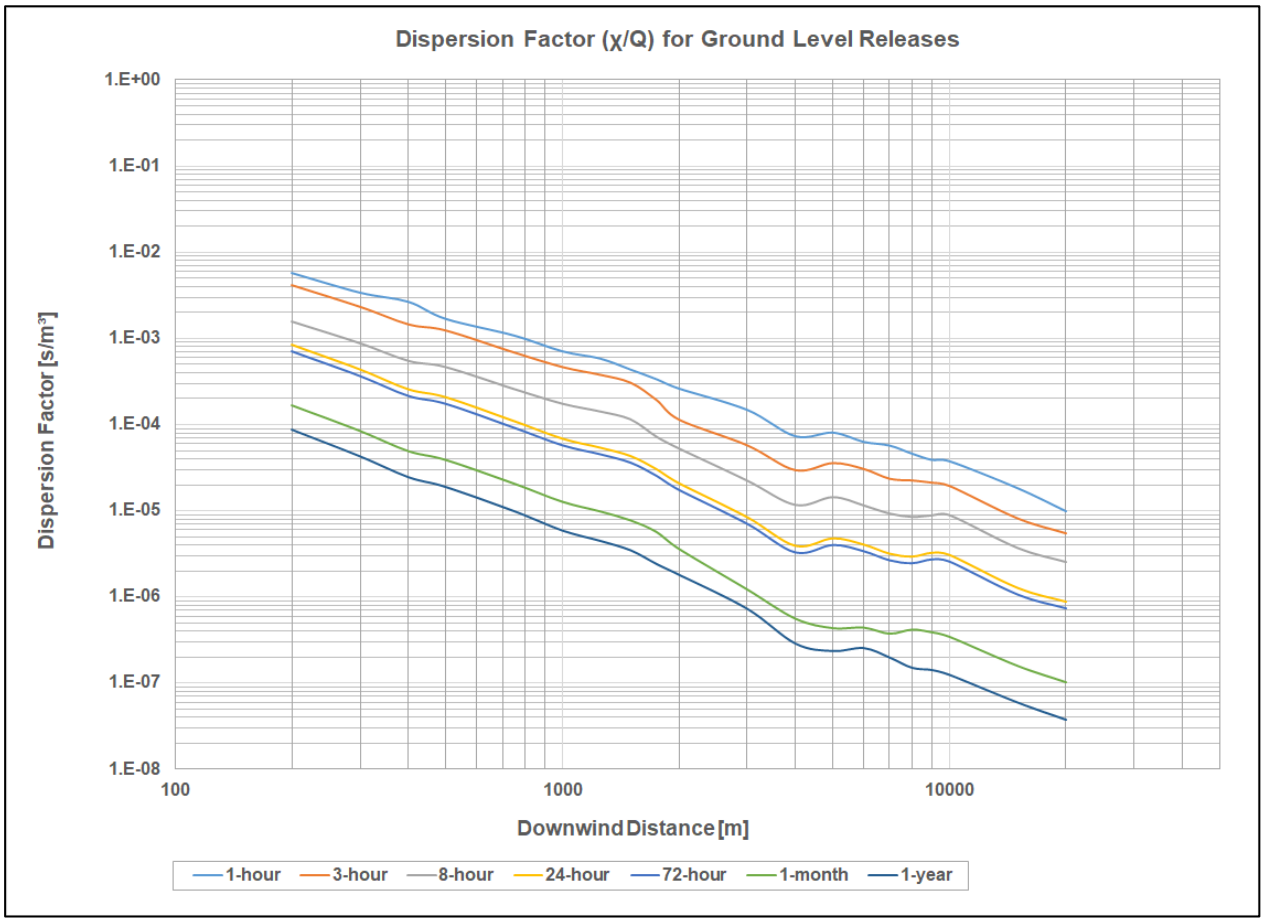


Figure 5.8.60
Dispersion Factors (χ/Q) (s/m³) Based on Concentration Predictions at Various Downwind Distances and Averaging Periods

© Eskom 2026/Rev 0c

PRINTED VERSIONS OF THIS DOCUMENT ARE NOT CONTROLLED

Table 5.8.71
Fallout Factors (1/m²-deposition period) based on 2nd Highest Hour, 3-Hour, 8-Hour and 24-hour Total Deposition Predictions at 800 m, 3 km and 8 km Downwind of the Nuclear Installation(s) for Different Wind Directions

Distance (m)	Highest Hourly (1/m²- hour)			Highest 3-Hourly (1/m²- 3 hours)			Highest 8-Hourly (1/m²- 8 hours)			Highest 24-Hourly (1/m²- 24 hours)		
	800	3000	8000	800	3000	8000	800	3000	8000	800	3000	8000
N	3.66E-03	4.50E-04	2.50E-04	5.39E-03	8.90E-04	4.00E-04	9.11E-03	9.00E-04	5.50E-04	1.18E-02	1.04E-03	5.50E-04
NNE	5.54E-03	4.40E-04	2.70E-04	7.98E-03	6.50E-04	3.60E-04	8.73E-03	9.80E-04	3.60E-04	9.91E-03	1.10E-03	3.70E-04
NE	7.28E-03	5.40E-04	2.10E-04	8.58E-03	8.70E-04	2.90E-04	1.08E-02	1.36E-03	4.10E-04	1.47E-02	1.37E-03	4.10E-04
ENE	1.04E-02	5.30E-04	3.40E-04	1.64E-02	9.10E-04	4.30E-04	1.64E-02	1.27E-03	4.30E-04	2.08E-02	1.79E-03	6.00E-04
E	9.16E-03	1.38E-03	3.20E-04	2.17E-02	2.38E-03	5.90E-04	2.44E-02	3.23E-03	7.10E-04	3.04E-02	3.30E-03	7.70E-04
ESE	2.44E-03	4.40E-04	8.00E-05	5.35E-03	8.20E-04	1.80E-04	1.17E-02	1.25E-03	2.40E-04	2.00E-02	1.84E-03	3.00E-04
SE	1.70E-03	2.10E-04	8.00E-05	4.92E-03	5.70E-04	1.80E-04	1.03E-02	1.11E-03	2.30E-04	2.06E-02	1.77E-03	2.90E-04
SSE	1.95E-03	2.10E-04	8.00E-05	5.31E-03	5.80E-04	1.30E-04	1.08E-02	1.01E-03	1.70E-04	2.38E-02	2.07E-03	3.40E-04
S	1.62E-03	2.10E-04	8.00E-05	3.59E-03	4.00E-04	1.00E-04	7.59E-03	8.30E-04	1.60E-04	1.16E-02	8.50E-04	1.70E-04
SSW	1.85E-03	2.20E-04	8.00E-05	4.84E-03	5.30E-04	1.60E-04	1.11E-02	9.90E-04	2.40E-04	1.97E-02	1.49E-03	2.50E-04
SW	1.63E-03	2.20E-04	8.00E-05	4.23E-03	5.50E-04	1.60E-04	9.36E-03	1.07E-03	2.00E-04	1.83E-02	1.75E-03	2.70E-04
WSW	4.36E-03	2.10E-04	8.00E-05	9.10E-03	5.90E-04	1.40E-04	1.49E-02	1.02E-03	2.20E-04	3.24E-02	2.16E-03	3.60E-04
W	4.28E-03	8.50E-04	8.00E-05	1.02E-02	1.00E-03	1.10E-04	1.69E-02	1.66E-03	1.90E-04	3.63E-02	2.72E-03	3.70E-04
WNW	6.18E-03	8.60E-04	3.00E-04	1.15E-02	1.37E-03	3.80E-04	1.44E-02	1.78E-03	6.60E-04	2.40E-02	2.51E-03	6.70E-04
NW	7.45E-03	7.80E-04	1.60E-04	1.16E-02	9.90E-04	2.00E-04	1.64E-02	1.20E-03	2.10E-04	1.70E-02	1.41E-03	2.50E-04
NNW	5.68E-03	5.10E-04	1.30E-04	8.57E-03	1.39E-03	1.80E-04	1.22E-02	1.63E-03	3.60E-04	1.44E-02	1.81E-03	3.80E-04

© Eskom 2026/Rev 0c

PRINTED VERSIONS OF THIS DOCUMENT ARE NOT CONTROLLED

Table 5.8.72
Fallout Factors (1/m²- deposition period) based on Hourly, 3-Day, Month, Annual and 95th Percentile Total Deposition Predictions at 800 m, 3 km and 8 km Downwind of the Nuclear Installation(s) for Different Wind Directions

Distance (m)	Highest 3-Daily (1/m²- 3 days)			Highest Monthly (1/m²- month)			Highest Annual (1/m²- year)			95th Percentile (1/m²- hour)		
	800	3000	8000	800	3000	8000	800	3000	8000	800	3000	8000
N	2.93E-02	2.59E-03	1.37E-03	1.74E-02	1.58E-03	8.80E-04	7.50E-02	5.41E-03	3.84E-03	1.15E-05	7.30E-07	7.28E-07
NNE	2.47E-02	2.74E-03	9.21E-04	3.56E-02	1.93E-03	8.30E-04	1.91E-01	7.30E-03	4.01E-03	2.15E-05	7.55E-07	7.45E-07
NE	3.67E-02	3.41E-03	1.02E-03	6.22E-02	3.76E-03	1.39E-03	3.15E-01	1.60E-02	6.03E-03	1.77E-05	1.44E-06	7.64E-07
ENE	5.19E-02	4.46E-03	1.49E-03	1.51E-01	9.54E-03	2.56E-03	1.14E+00	6.30E-02	1.71E-02	4.57E-04	2.25E-05	3.09E-06
E	7.57E-02	8.22E-03	1.92E-03	2.39E-01	2.24E-02	3.94E-03	1.90E+00	1.66E-01	2.73E-02	1.18E-03	9.85E-05	1.24E-05
ESE	4.99E-02	4.58E-03	7.47E-04	2.69E-01	1.83E-02	2.76E-03	1.66E+00	1.24E-01	1.93E-02	1.23E-03	1.06E-04	1.80E-05
SE	5.12E-02	4.41E-03	7.22E-04	2.28E-01	1.72E-02	2.48E-03	1.26E+00	1.05E-01	1.60E-02	6.99E-04	8.23E-05	1.39E-05
SSE	5.94E-02	5.16E-03	8.47E-04	2.43E-01	1.65E-02	2.45E-03	9.86E-01	6.15E-02	9.49E-03	8.35E-04	3.42E-05	3.21E-06
S	2.88E-02	2.12E-03	4.23E-04	8.00E-02	5.49E-03	1.02E-03	3.97E-01	2.99E-02	5.58E-03	1.04E-04	4.81E-06	7.74E-07
SSW	4.92E-02	3.71E-03	6.23E-04	1.22E-01	8.66E-03	1.28E-03	8.39E-01	5.41E-02	8.61E-03	6.32E-04	2.25E-05	2.09E-06
SW	4.55E-02	4.36E-03	6.72E-04	1.33E-01	1.16E-02	1.76E-03	9.78E-01	8.05E-02	1.22E-02	5.93E-04	6.80E-05	9.47E-06
WSW	8.08E-02	5.38E-03	8.97E-04	2.30E-01	1.56E-02	2.31E-03	1.29E+00	9.19E-02	1.39E-02	1.18E-03	7.95E-05	1.24E-05
W	9.03E-02	6.77E-03	9.21E-04	2.62E-01	1.40E-02	2.31E-03	1.17E+00	7.24E-02	1.19E-02	7.85E-04	6.27E-05	9.97E-06
WNW	5.97E-02	6.25E-03	1.67E-03	1.40E-01	1.21E-02	2.12E-03	5.32E-01	4.53E-02	6.77E-03	1.52E-04	3.75E-06	9.57E-07
NW	4.24E-02	3.51E-03	6.23E-04	4.31E-02	3.10E-03	5.30E-04	2.66E-01	1.78E-02	2.26E-03	1.36E-05	1.03E-06	1.96E-07
NNW	3.60E-02	4.51E-03	9.46E-04	2.73E-02	2.78E-03	5.50E-04	1.35E-01	6.70E-03	1.17E-03	1.82E-05	8.28E-07	1.30E-07

© Eskom 2026/Rev 0c

PRINTED VERSIONS OF THIS DOCUMENT ARE NOT CONTROLLED

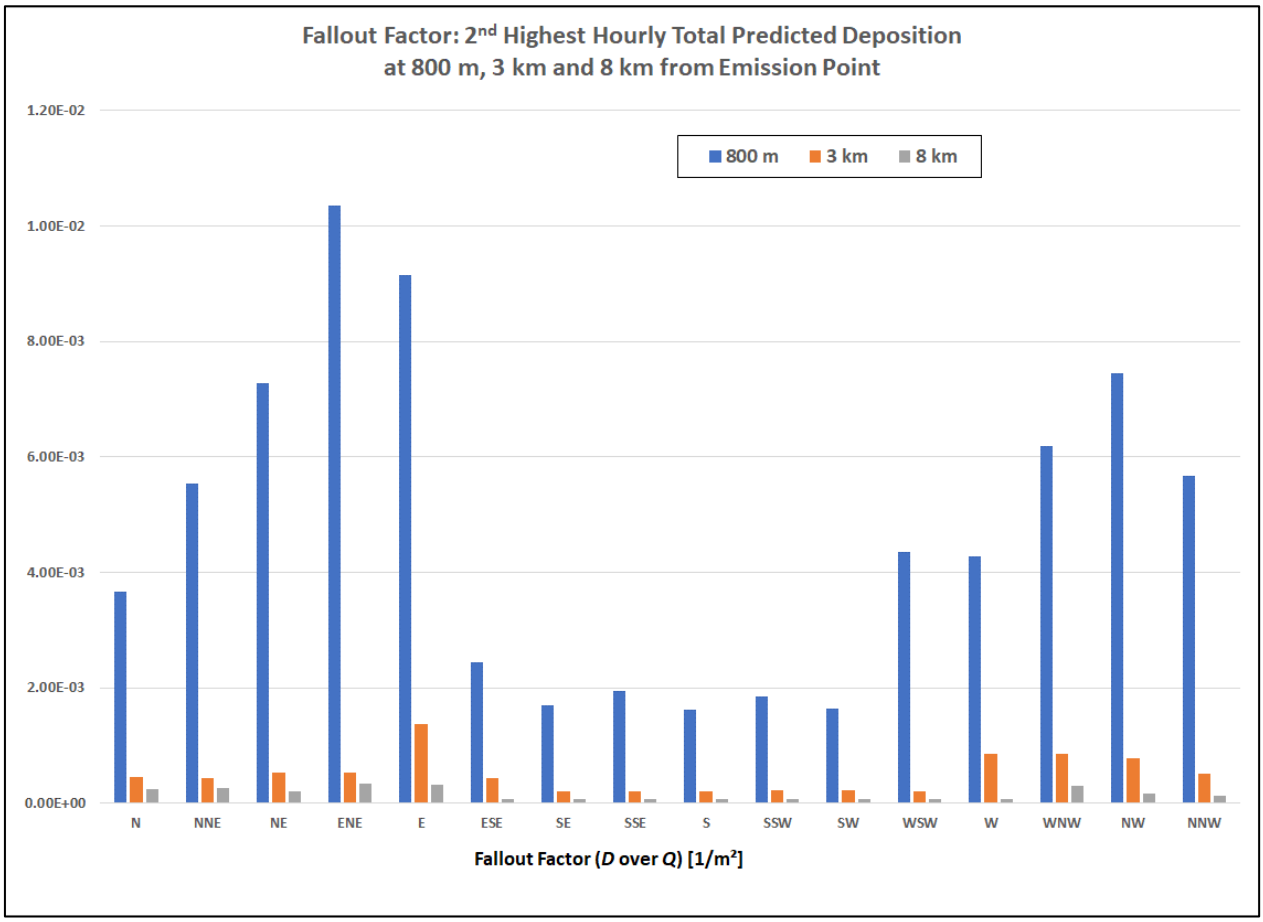


Figure 5.8.61
Fallout Factors (D/Q) (1/m²- hour) based on the 2nd Highest Hourly Total Predictions at 800 m, 3 km and 8 km Downwind of the Nuclear Installation(s) for Different Wind Directions

© Eskom 2026/Rev 0c

PRINTED VERSIONS OF THIS DOCUMENT ARE NOT CONTROLLED

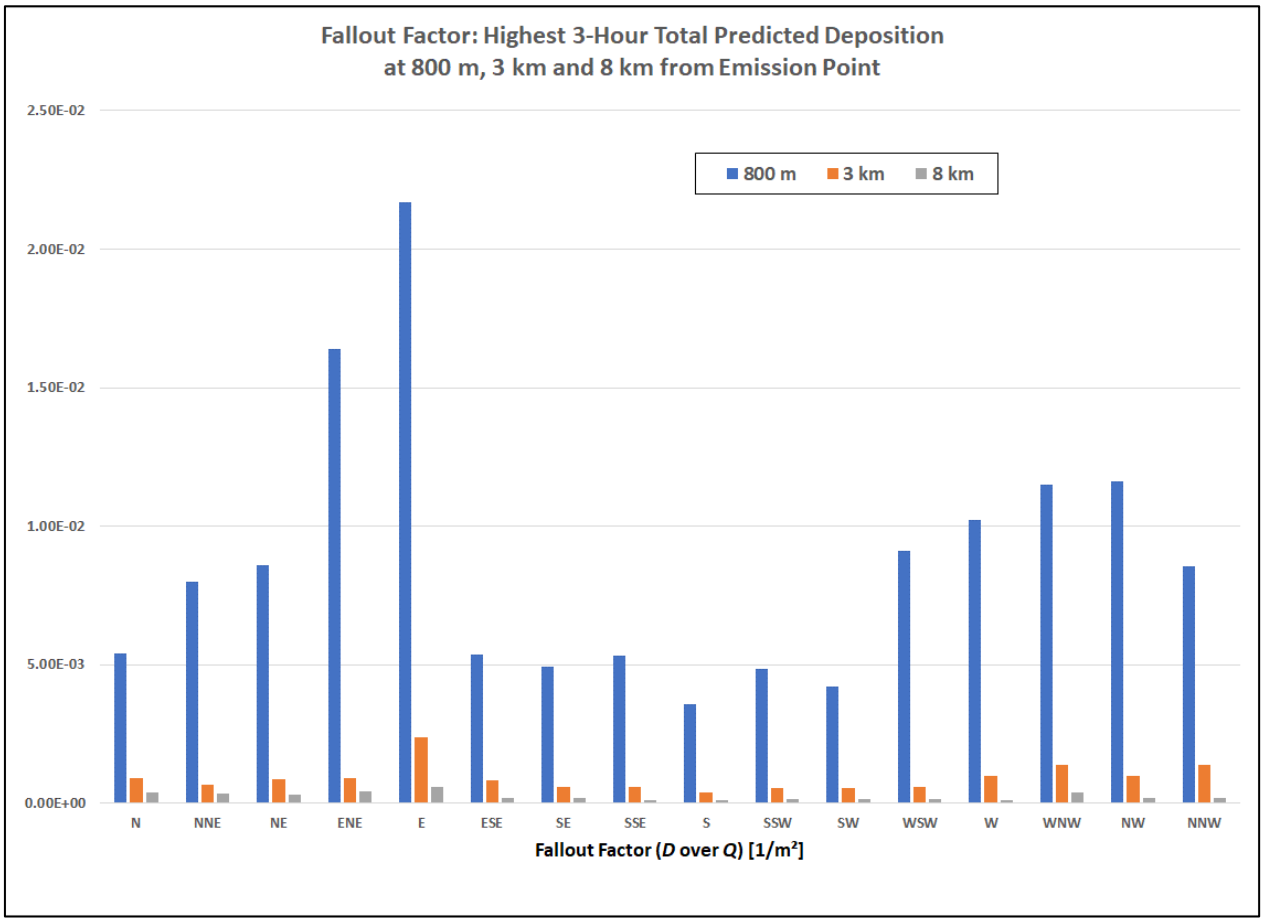


Figure 5.8.62
Fallout Factors (*D/Q*) (1/m²- 3 hours) based on the Highest 3-Hourly Total Predictions at 800 m, 3 km and 8 km Downwind of the Nuclear Installation(s) for Different Wind Directions

© Eskom 2026/Rev 0c

PRINTED VERSIONS OF THIS DOCUMENT ARE NOT CONTROLLED

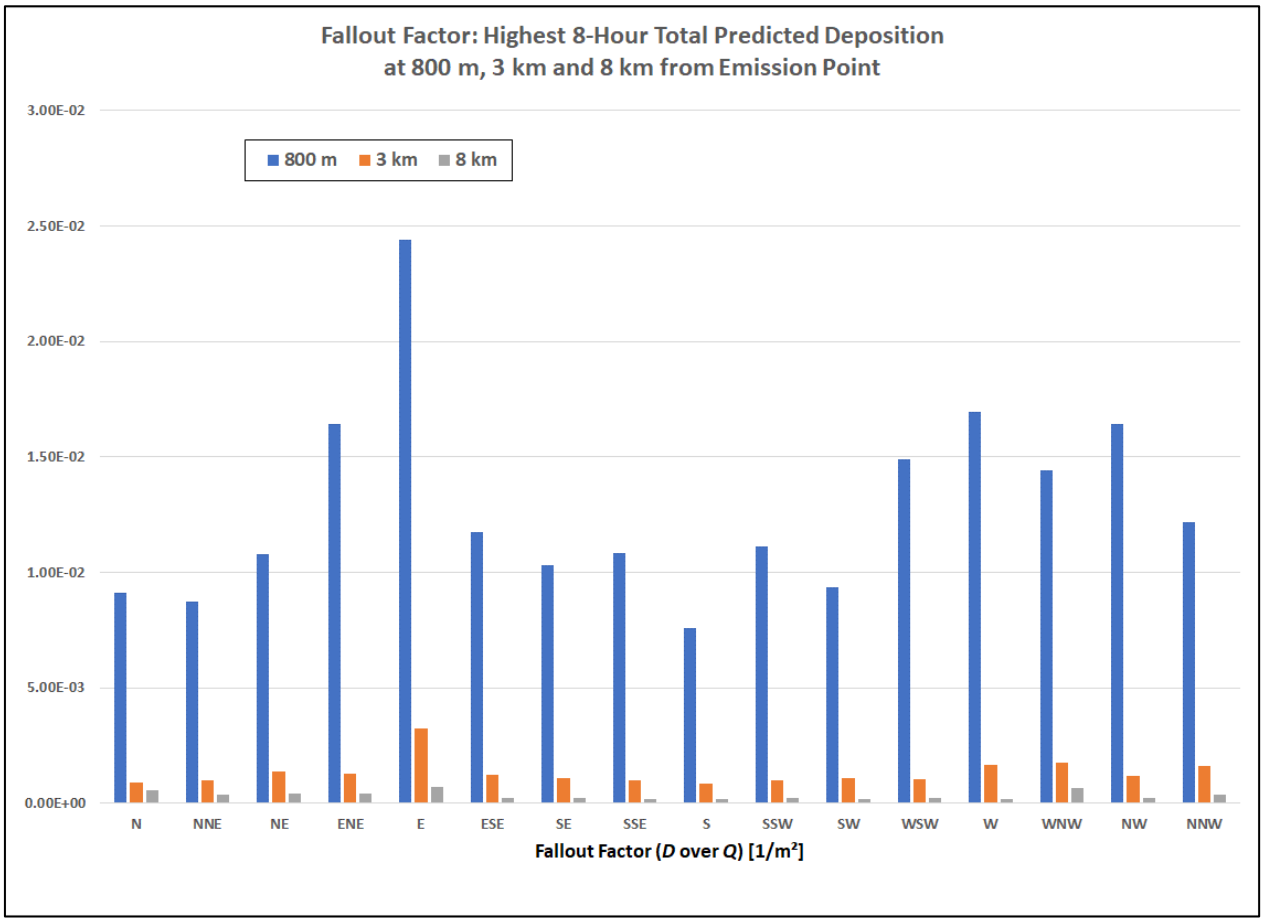


Figure 5.8.63
Fallout Factors (*D/Q*) (1/m²- 8 hours) based on the Highest 8-Hourly Total Predictions at 800 m, 3 km and 8 km Downwind of the Nuclear Installation(s) for Different Wind Directions

© Eskom 2026/Rev 0c

PRINTED VERSIONS OF THIS DOCUMENT ARE NOT CONTROLLED

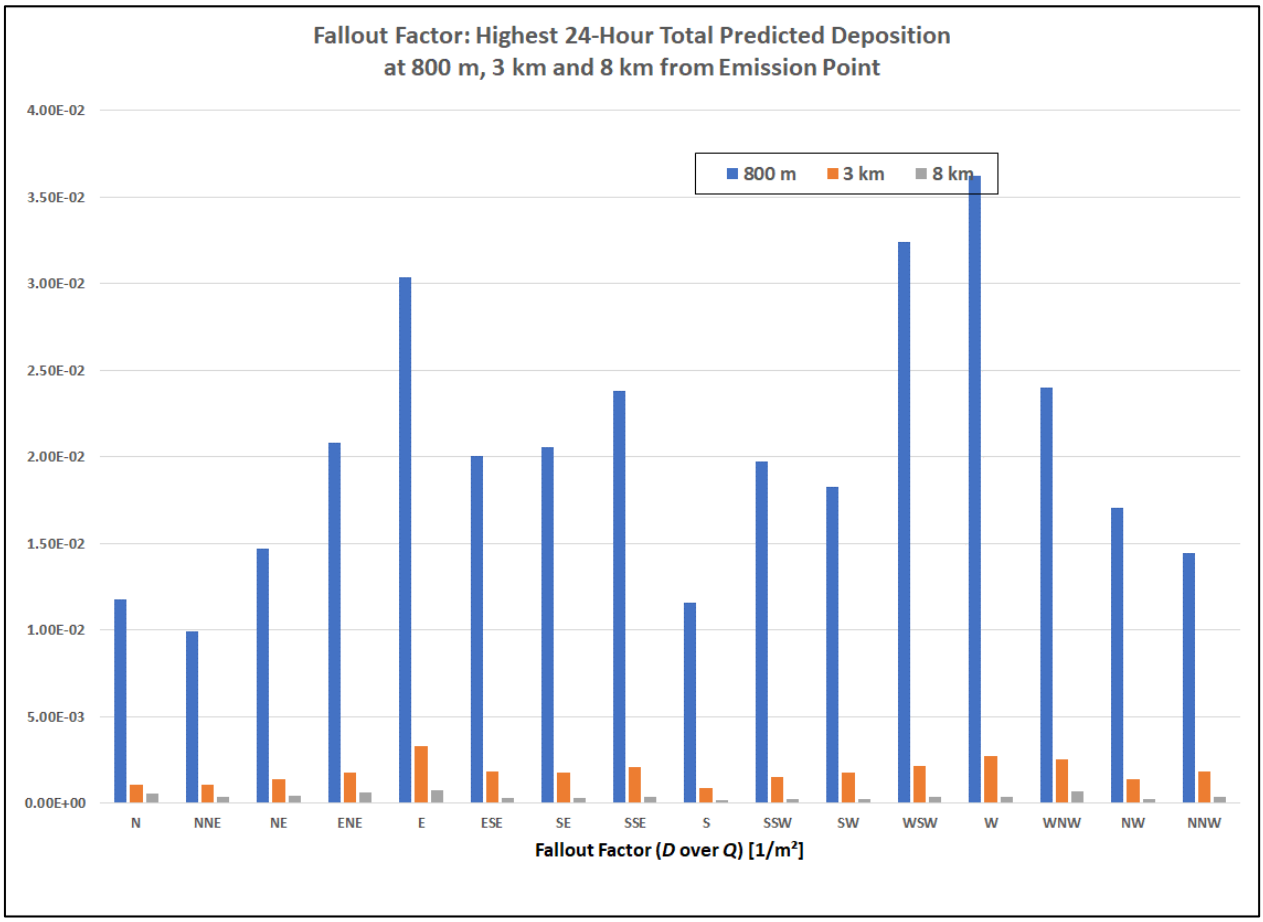


Figure 5.8.64
Fallout Factors (*D/Q*) (1/m²- 24 hours) based on the Highest 24-Hourly Total Predictions at 800 m, 3 km and 8 km Downwind of the Nuclear Installation(s) for Different Wind Directions

© Eskom 2026/Rev 0c

PRINTED VERSIONS OF THIS DOCUMENT ARE NOT CONTROLLED

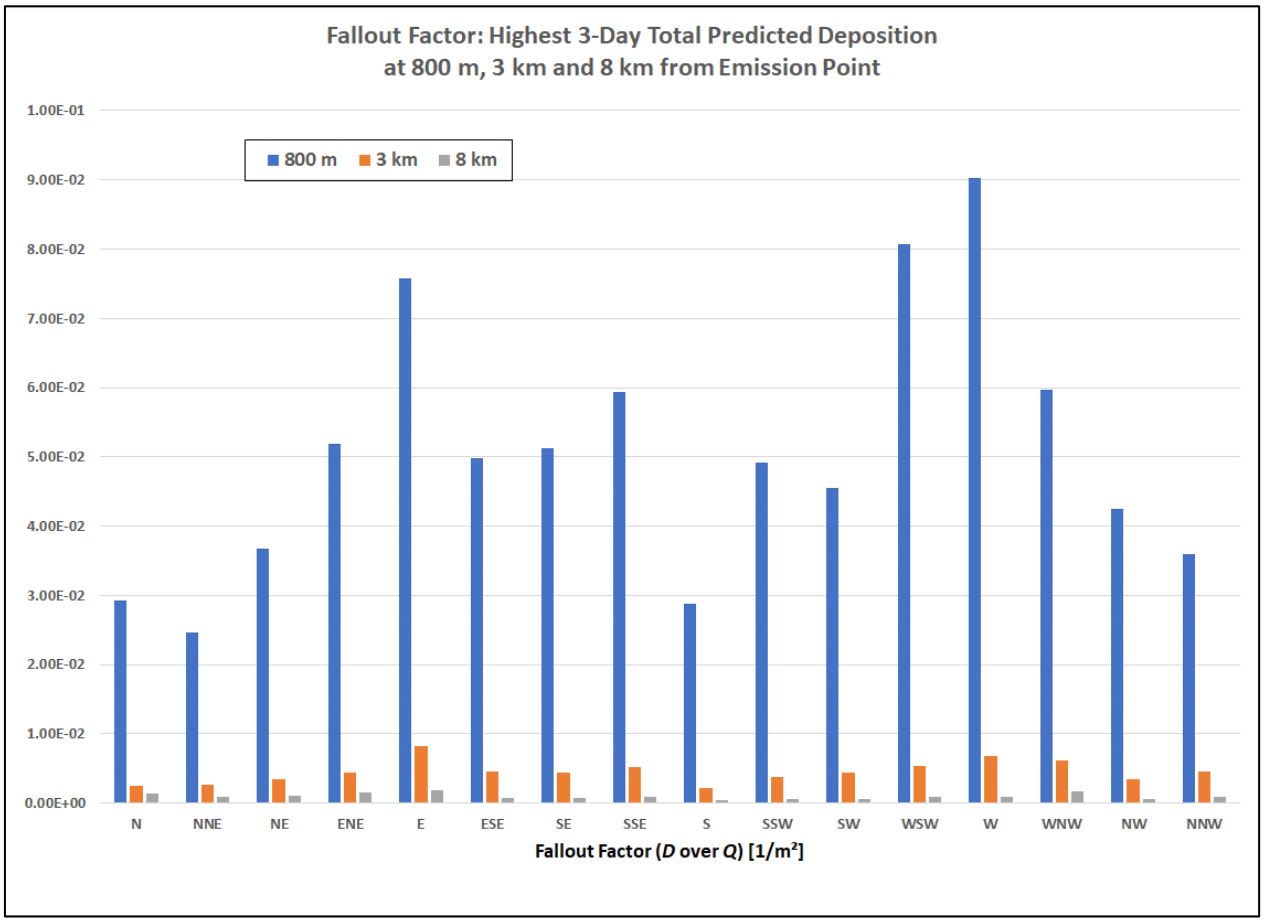


Figure 5.8.65
Dispersion Factors (D/Q) (1/m²- 3 days) based on the Highest 3-Daily Average Predictions at 800 m, 3 km and 8 km Downwind of the Nuclear Installation(s) for Different Wind Directions

© Eskom 2026/Rev 0c

PRINTED VERSIONS OF THIS DOCUMENT ARE NOT CONTROLLED

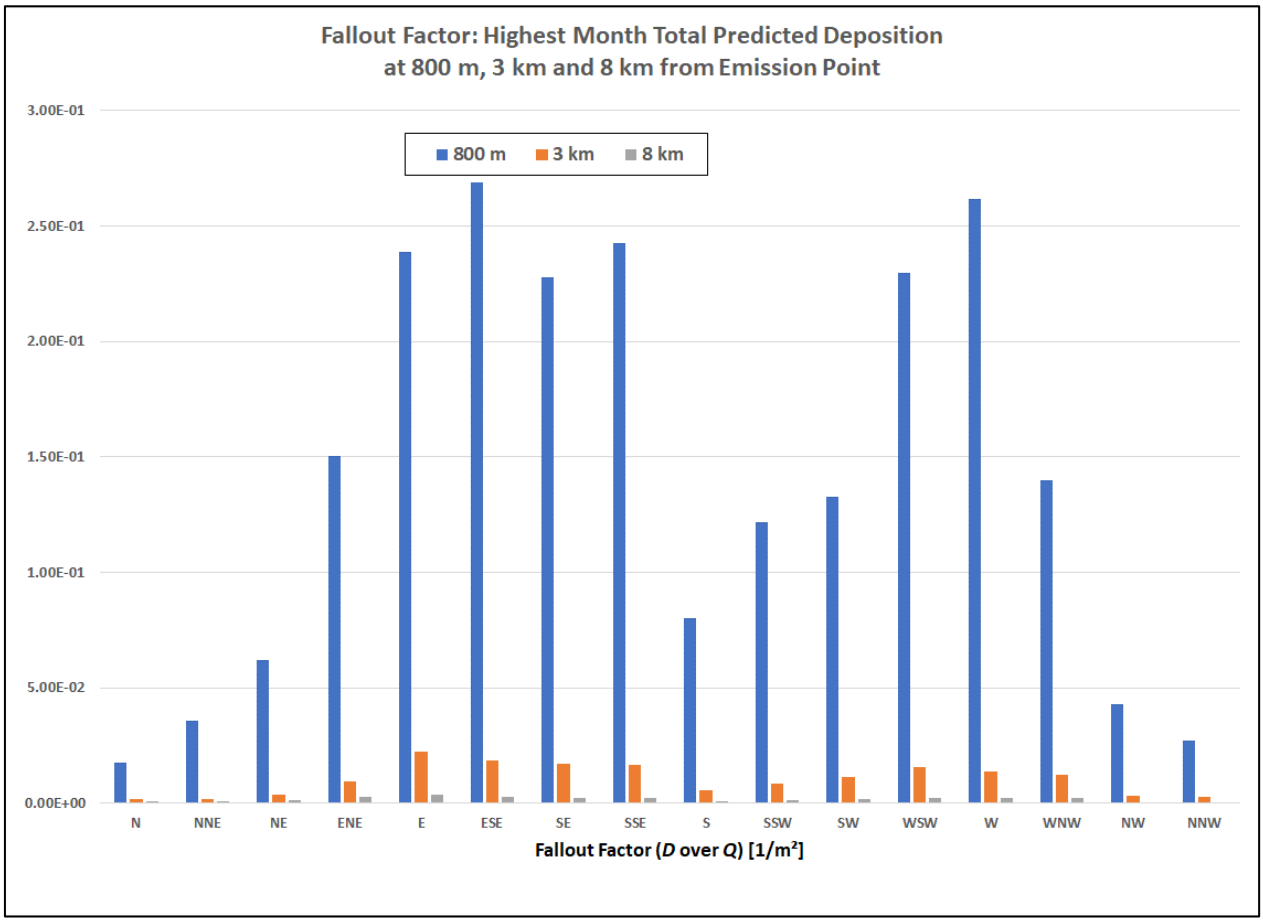


Figure 5.8.66
Fallout Factors (*D/Q*) (1/m²- month) based on the Highest Monthly Total Predictions at 800 m, 3 km and 8 km Downwind of the Nuclear Installation(s) for Different Wind Directions

© Eskom 2026/Rev 0c

PRINTED VERSIONS OF THIS DOCUMENT ARE NOT CONTROLLED

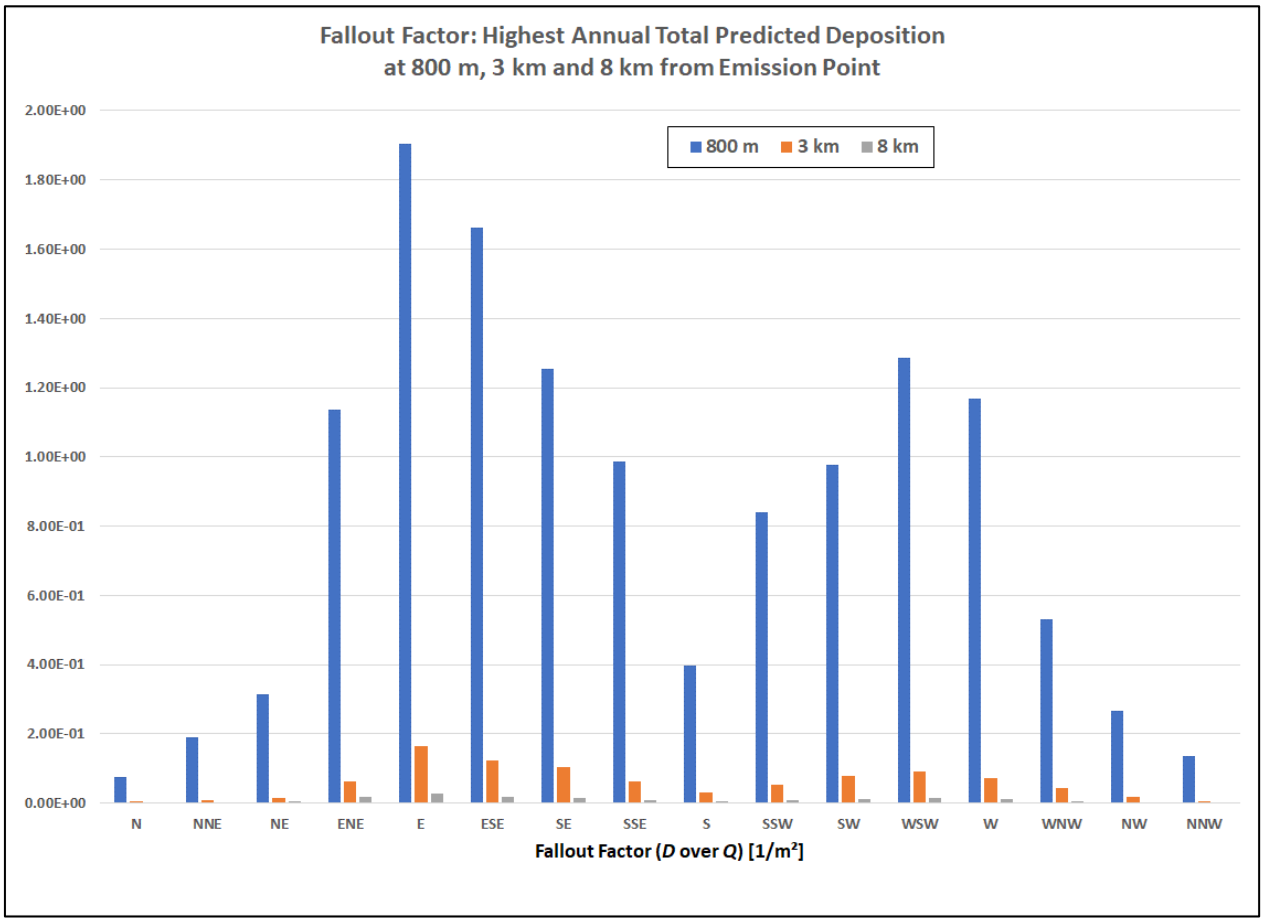


Figure 5.8.67
Fallout Factors (*D/Q*) (1/m²- year) based on the Highest Annual Total Predictions at 800 m, 3 km and 8 km Downwind of the Nuclear Installation(s) for Different Wind Directions

© Eskom 2026/Rev 0c

PRINTED VERSIONS OF THIS DOCUMENT ARE NOT CONTROLLED

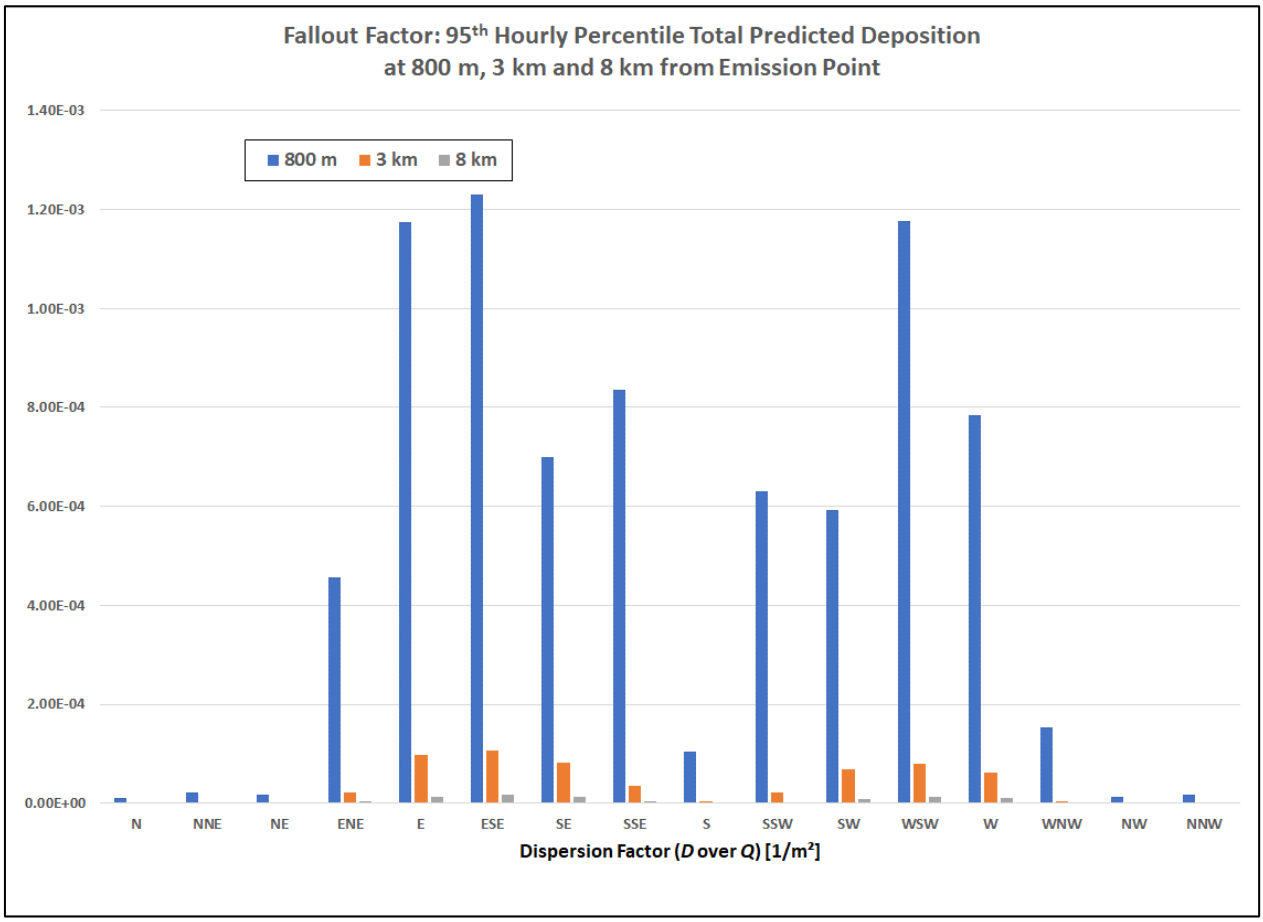


Figure 5.8.68
Fallout Factors (*D/Q*) (1/m²- hour) Based on the 95th Percentile of the Hourly Total Predictions at 800 m, 3 km and 8 km Downwind of the Nuclear Installation(s) for Different Wind Directions

© Eskom 2026/Rev 0c

PRINTED VERSIONS OF THIS DOCUMENT ARE NOT CONTROLLED

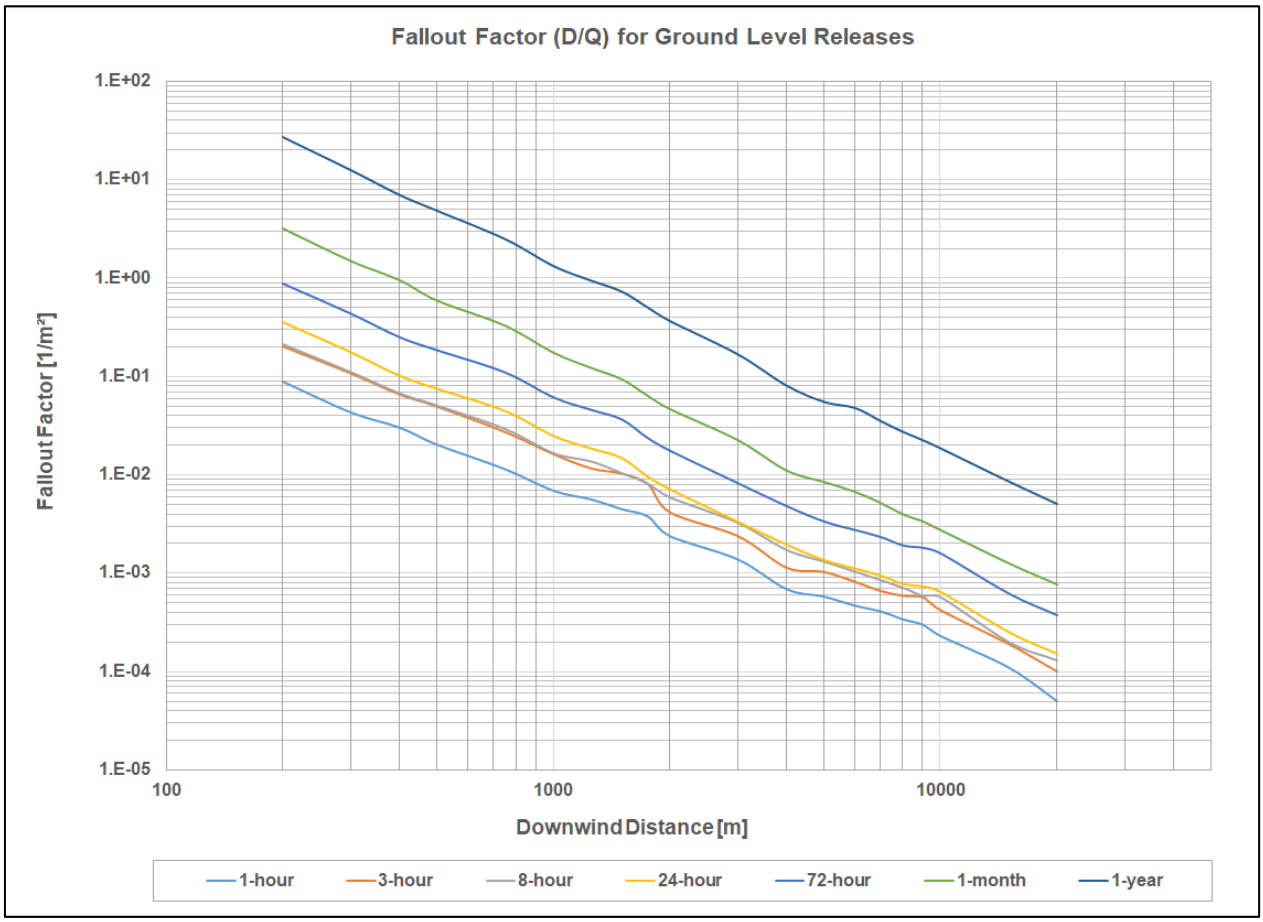


Figure 5.8.69
Fallout Factors (D/Q) (1/m²- deposition period) for Deposition Predictions at Various Downwind Distances and Averaging Periods

5.8.8 Monitoring Programme

Meteorological parameters were monitored to characterise the atmospheric conditions at the proposed site and to enable, *inter alia*, an assessment of the magnitude and recurrence probability of external meteorological events. The analysis made use of both on- and off-site monitoring data; the latter mainly due to the relatively short duration of on-site information to enable long term analysis.

5.8.8.1 On-Site Monitoring

International standards for nuclear installation site applications (International Atomic Energy Agency, 2011) and (United States Nuclear

© Eskom 2026/Rev 0c

PRINTED VERSIONS OF THIS DOCUMENT ARE NOT CONTROLLED

Regulatory Commission, 2007c) require consideration of the meteorological characteristics of the site that are necessary for safety analysis or that may have an impact on plant design. They also require the evaluation of atmospheric dispersion characteristics and the establishment of dispersion parameters, as atmospheric dispersion estimates are significant inputs to safety assessment (see ***Subsection 5.8.3***). These assessments are needed for design and licensing purposes (International Atomic Energy Agency, 2011).

For these reasons, a meteorological monitoring programme has been implemented and will be continued at the site and the region in order to evaluate regional and site-specific meteorological parameters during the nuclear installation lifetime.

5.8.8.1.1 Prior to Nuclear Installation Operation

The historical meteorological data are planned to be continuously compared with on-site data collected after the new nuclear installation(s) are designed and constructed (but before operation), to assist with confirmation of the acceptability of the as built plant and confirm assumptions made in the calculation models (International Atomic Energy Agency, 2002) and (United States Environmental Protection Agency, 2000)). The meteorological parameters included in the monitoring programme are:

- wind direction (degrees) and derived standard deviation of wind direction (degrees);
- wind speed (m/s) including wind gusts (m/s);
- ambient temperature (°C) (including temperature differences between height levels (°C);
- relative humidity (per cent);
- precipitation (mm);
- solar radiation (kW/m²);
- barometric pressure (hPa).

The instrument specifications, tower height, instrument placements at different heights on the tower, sampling intervals and averaging periods, data recording and storage will be as per ANSI/ANS-3.11 Standard (American National Standard, 2015) and Eskom Standard 238-52 (Eskom, 2022a) for meteorological requirements for nuclear installations. Evapotranspiration and atmospheric stabilities are derived from these parameters, as discussed in ***Subsection 5.8.6.1.8*** and ***Subsection 5.8.6.1.9***, respectively.

© Eskom 2026/Rev 0c

PRINTED VERSIONS OF THIS DOCUMENT ARE NOT CONTROLLED

Corrosion monitoring will also be repeated to build up a longer history. Although the existing observations are adequate to determine the current corrosivity at the site, a long-term history will identify any changes that might occur.

5.8.8.1.2 During Nuclear Installation, Operation and Decommissioning

All meteorological data parameters, as listed in the previous section, will continuously be collected and evaluated to:

- confirm the design bases for the nuclear installation(s);
- enable calculations of atmospheric dispersion and statistical analyses;
- demonstrate the on-going feasibility of the emergency plan;
- meet the requirements for a safe nuclear installation operation.

More specifically, the programme will be developed to provide the relevant meteorological information needed for the following assessments (United States Nuclear Regulatory Commission, 2007c; Eskom, 2022a; National Nuclear Regulator, 2016a):

- an assessment of the annual radiation dose to the public resulting from the routine discharges to demonstrate compliance with regulatory requirements;
- an assessment of atmospheric dispersion immediately following an accidental release of airborne radioactive materials to provide input to the evaluation of the consequences of radioactive releases to the atmosphere and to aid in the implementation of emergency response decisions in accordance with the NNR requirements;
- a periodic assessment of natural phenomena being experienced or projected beyond usual levels (e.g. high winds) for the purposes of emergency planning;
- a periodic assessment of the potential dispersion of radioactive materials from, and the radiological consequences of, a spectrum of accidents to aid in evaluating the environmental risk posed by the nuclear installation(s).

Periodic assessment of meteorological instruments and information requirements will identify the need for new or enhanced instrumentation, for example, on-line real-time atmospheric dispersion modelling for use during emergency conditions.

© Eskom 2026/Rev 0c

PRINTED VERSIONS OF THIS DOCUMENT ARE NOT CONTROLLED

While the nuclear facility is being decommissioned, the continued need for onsite meteorological data should be evaluated based on the potential impacts of the remaining hazard footprint (American National Standard, 2015).

5.8.8.2 Off-Site Monitoring

Whilst still building up a history of on-site meteorological data, long-term data from weather stations in the vicinity of the site will be analysed to support estimating extreme weather conditions. These include data from the Cape St. Francis WS.

5.8.9 Management of Uncertainties

5.8.9.1 Measurement and Analyses

The uncertainties associated with the establishment of a meteorological baseline for the site will be introduced through the following activities:

- observation of meteorological parameters:
  - onsite measurements;
  - use of other sources (e.g. SAWS);
- data analyses:
  - statistical methods;
  - derived meteorological parameters;
  - atmospheric dispersion calculations.

The factors that influence the uncertainty of data from the onsite monitoring station include:

- sufficient instrumentation to monitor relevant parameters;
- instrumentation accuracy;
- location (macro and micro);
- timeframe of monitoring database.

Instrumentation has been provided to monitor the main meteorological parameters that can be measured without observation i.e. not including mist, fog, cloud cover, cloud type. These parameters include the wind vector, ambient air, dry bulb temperature, relative humidity, atmospheric pressure, solar radiation and precipitation. Other meteorological parameters can be

© Eskom 2026/Rev 0c

PRINTED VERSIONS OF THIS DOCUMENT ARE NOT CONTROLLED

derived from these and typically include atmospheric stability, wet-bulb temperature, dew point and evapotranspiration.

The methodologies used to derive the latter parameters are based on first principles (e.g. wet-bulb temperature and dew point) and empirical correlations (e.g. atmospheric turbulence and evapotranspiration). The uncertainties associated with parameters obtained from empirical correlations are expected to be greater than those from first principles, because the former methods are derived from experimentation with inherent uncertainties, whereas the latter are inter-related meteorological relationships. Atmospheric stability classes are estimated using either the vertical temperature gradient ('delta-T') or from a measure of the change in wind direction ('sigma theta'). Whilst both methods aim to define the same atmospheric stability classes, different results were shown to be obtained at the Thyspunt WS (see ***Tables 5.8.36*** and ***5.8.37***). A comparison of the two methods provided in the Eskom Standard 238-52 (Eskom, 2022a), as well as the SRDT and Ri number methods is given in ***Tables 5.8.73***. The delta-T method refers to the vertical temperature difference between 8 m and 2 m measurement levels, and the sigma-theta method refers to the standard deviation of the wind direction at the 9 m wind measurement level. The SRDT method employs wind speed at 9 m, simple knowledge of the temperature gradient at night, i.e. positive or negative gradient, and the solar radiation during the day. The Ri number method employs the wind speed at 9 m and the two temperatures at 2 m and 8 m.

Table 5.8.73
Comparison of Atmospheric Stability Classification Schemes for the Site (1997-2023)

Stability Class	Atmospheric Stability Frequency of Occurrence			
	Delta-T Method [8m/2m] Vertical Stability	Sigma-Theta Method Horizontal [9m] Stability	SRDT Method (Wind Speed [9m], Temperature Gradient [8m/2m], Solar Radiation)	Ri Method (Wind Speed [9m], Temperature [2m] and Temperature [8 m])
A	55.97%	3.85%	0.16%	0.31%
B	1.65%	1.83%	3.48%	0.11%
C	1.58%	4.85%	12.12%	0.84%
D	7.41%	40.67%	82.72%	68.44%
E	11.28%	45.89%	0.69%	28.85%
F	9.58%	2.90%	0.82%	1.45%
G	12.53%	0.01%	0.00%	0.00%

In comparison, the delta-T method is significantly dissimilar to the sigma-theta, SRDT and Ri number methods. According to the classification results, there is a significant bias towards very unstable and stable conditions (classes A and G) with the delta-T method, i.e. 55.97 and 12.53 per cent

© Eskom 2026/Rev 0c

PRINTED VERSIONS OF THIS DOCUMENT ARE NOT CONTROLLED

compared with 3.85 and 0.01 per cent with the sigma-theta method, 0.16 and 0.00 per cent with the SRDT method, and 0.31 and 0.00 per cent with the Ri number method. The sigma-theta method produced mostly neutral and slightly stable conditions (classes D and E) which is expected given the prevalence of well-defined, strong wind speeds that characterise these atmospheric conditions (Pasquill, 1961). Although the SRDT and Ri number methods similarly produced mostly class D, the former is biased more towards class C, with the latter similar to the sigma-theta method, i.e. class E. Furthermore, as shown in ***Table 5.8.36***, according to the delta-T method, very stable conditions (class G) were observed during winds originating from the WNW, NW, and NNW wind directions. E and F-class stabilities were observed predominantly from WNW, followed by NW. Unstable and neutral conditions (classes A to D) occurred most frequently from W, with some observations also made for winds from WSW for very unstable conditions (class A). The sigma-theta method exhibited similar stability-wind direction preferences for stability classes B to F; however, the D-class frequency dominated the distribution significantly more than with the delta-T method, i.e. 16.86 per cent compared with 2.06 per cent. Similarly, E-class stability using the sigma-theta method observed 5.48 per cent with winds from the ENE direction, with only 1.51 per cent using the delta-T method. Given that a typical temperature change in the vertical in the surface layer follows a power law profile, with a steep gradient close to ground level, the stability classification based on the delta-T method is sensitive to the location of the temperature measurements.

The estimation of atmospheric turbulence is very important for the calculation of atmospheric dispersion. The Eskom Standard 238-52 (Eskom, 2022a) specifies the use of delta-T and sigma theta methods for establishing the stability classes. With the uncertainty in using the delta-T method the classification based on the sigma-theta method is recommended.

There will always be some error in any mathematical model, but it is desirable to structure the model in such a way to minimise the total error. Essentially, the dispersion model represents the most likely outcome of an ensemble of experimental results. The total uncertainty can be thought of as the sum of three components: the uncertainty due to errors in the model physics; the uncertainty due to data errors; and the uncertainty due to stochastic processes (turbulence) in the atmosphere.

The stochastic uncertainty includes all errors or uncertainties in data such as source variability, observed concentrations, and meteorological data. Even if the field instrument accuracy is excellent, there can still be large uncertainties due to unrepresentative placement of the instrument (or taking of a sample for analysis). Model evaluation studies suggest that the data

© Eskom 2026/Rev 0c

PRINTED VERSIONS OF THIS DOCUMENT ARE NOT CONTROLLED

input error term is often a major contributor to total uncertainty. Even in the best tracer studies, the atmospheric emission rates are known only with an accuracy of ±5 per cent, which translates directly into a minimum error of that magnitude in the model predictions. It is also well known that wind direction errors are the major cause of poor agreement, especially for relatively short-term predictions (minutes to hourly) and long downwind distances. All of the above factors contribute to the inaccuracies not even associated with the mathematical models themselves.

The AERMOD model has been shown to be an improvement on the older generation dispersion models that utilise discrete diffusion parameters (e.g. Pasquill-Gifford), especially short-term predictions (Hanna, et al., 1999; Perry, et al., 2004). However, the range of uncertainty of the model predictions is still regarded to be within a factor of two (Perry, et al., 2004). The accuracy improves with fairly strong wind speeds and during neutral atmospheric conditions (Perry, et al., 2004). Vamsidhar *et al* (Vamsidhar , et al., 2010) presented a comprehensive review of the uncertainty and sensitivity analyses associated with prediction of ground level pollutant concentrations using the US EPA's AERMOD equations for point sources. Both stable and unstable (convective) boundary layer conditions were studied. The parameters considered for these analyses included emission rate, stack exit velocity, stack exit temperature, wind speed, lateral dispersion parameter, vertical dispersion parameter, weighting coefficients for both updraft and downdraft, total horizontal distribution function, cloud cover, ambient temperature, and surface roughness length. A roughness length of 0.36 m was estimated using the average vegetation height[55]. The corresponding probability distribution functions, depending on the measured or practical values, are assigned to perform uncertainty and sensitivity analyses in both unstable and stable atmospheric cases. The results for uncertainty in predicting ground level concentrations at different downwind distances during unstable conditions varied between 67 per cent and 75 per cent, while they ranged between 40 per cent and 47 per cent in stable boundary layer. The sensitivity analysis showed that vertical dispersion parameter and total horizontal distribution function have contributed to 82 per cent and 15 per cent variance, respectively, in predicting concentrations in the unstable boundary layer. In the stable boundary layer, vertical dispersion parameter and total horizontal distribution function have contributed about 10 per cent and 75 per cent to variance, respectively, in

[55] The aerodynamic roughness length is a theoretical height that must be determined from the wind speed profile. In the absence of wind speed measurements at several height levels an estimate of the roughness length can be made using the nature and heights of surrounding obstacles. There has been some success at relating this height to the arrangement, spacing, and physical height of individual roughness elements such as vegetation or houses. As an approximation, the roughness length is approximately one-tenth of the height of the surface roughness elements. The average height of the vegetation in the surrounding area ranges between 2 m and 4 m, and the roughness length is therefore assumed to be 0.36 m.

© Eskom 2026/Rev 0c

PRINTED VERSIONS OF THIS DOCUMENT ARE NOT CONTROLLED

predicting concentrations. Wind speed had a negative contribution to variance and the other parameters had a negligent or zero contribution to variance.

Table 5.8.2 provides the required accuracies of the measuring instruments. These accuracies equal or better the requirements of ANSI/ANS-311-2015 (ANS 2015) and (Eskom, 2022a), and have been maintained through the adopted quality assurance programme of calibration and maintenance. The instrument uncertainties were calculated using the methodology contained in *Guidelines for Evaluating and Expressing the Uncertainty of NIST Measurement Results* published by the United States Department of Commerce, Technology Administration National Institute of Standards and Technology (NIST) (Barry & Kuyatt, 1994). The calculated expanded uncertainties associated with the meteorological instrumentation are as follows:

Wind direction (0 to 360)	: 1 degree
Wind direction (True North)	: 5 degrees
Wind speed (200 to 6200 rpm)	: 6 rev. per minute
Wind speed (starting threshold)	: 100 µNewton-metre
Barometric pressure (800 to 1100 hPa)	: 1 hPa
Temperature (0°C to 40°C)	: 0.2 °C
Solar Irradiance (0 to 1200 W/m²)	: 60 W/m²
Rain gauge (2.5 to 5 millilitres)	: 0.1 millilitres
Humidity (11 to 75 per cent)	: 4 per cent

These uncertainties are being managed through bi-annual calibration checks on all meteorological monitoring instrumentation.

Both short- and long-term analyses are required from the meteorological data collected on site. Short-term analyses would typically include hourly average dispersion calculations, whereas long-term analyses would be required to establish extremes and rare phenomena. The monitoring data collected with the Thyspunt WS (2008 to 2013 and 2017 to 2019) and the

© Eskom 2026/Rev 0c

PRINTED VERSIONS OF THIS DOCUMENT ARE NOT CONTROLLED

Cape St. Francis WS (1881-2003 for rainfall only, and 2004 – 2023 for all parameters) have provided adequate information to determine both average and extreme observations; however, the accuracy of forecasting future extreme meteorological events would only improve with increased historical information. The IAEA recommends (International Atomic Energy Agency, 2011) that the long-term data used to evaluate extreme values of meteorological variables should cover a period proportionate with the return period used for assessing the corresponding design basis, i.e. not greater than four times the duration of the sample. Notwithstanding the above recommendation, wind gusts, extreme minimum and maximum temperatures and rainfall rates, for return years of up to 100 000 000 have been calculated (see ***Subsection 5.8.6.2.2***), as required by the Technical Specification for this section (Eskom, 2022c). Rainfall extremes are based on measured data sets covering a period of 39 years (1985 to 2023, with incomplete data for 2004), and wind speed and temperature a period of 19 years (2004 to 2023), which implies that values for return periods more than 100 years need to be interpreted with caution. This is demonstrated by the increasing 95th confidence interval estimates for increasing return years in ***Subsection 5.8.6.2.2***. The conservative approach would be to apply the upper estimate of the interval, rather than the average.

5.8.9.2 Uncertainties due to Climate Change

Climate change is a key area of uncertainty that will affect the meteorology of the site. The key aspects here are greater variations in extreme temperature, wind speed and rainfall events. All key climate indicators reflect trends consistent with a warming climate, including land and ocean temperatures, sea level and greenhouse gas (GHG) concentrations in the atmosphere, which all surpassed the records set just in the preceding year. The following global changes have been observed:

- from 1880 to 2012, globally averaged surface temperature increased by 0.85°C;
- the past 5 years are collectively the warmest years in modern record;
- Northern Hemisphere (NH): 2016 warmest year with +1.27°C;
- Southern Hemisphere (SH): 2016 warmest year with +0.71°C;
- the global mean sea level rose by 0.19 m between 1901 and 2010;
- the upper few metres of the ocean are warming - Data from the US National Oceanic and Atmospheric Administration (NOAA) show an increase of *c.* 0.13°C per decade over the past 100 years.
- the greatest ocean warming is occurring in the SH and contributing to the subsurface melting of Antarctic ice shelves.

© Eskom 2026/Rev 0c

PRINTED VERSIONS OF THIS DOCUMENT ARE NOT CONTROLLED

Assessments of historical trends of measured surface temperature in South Africa have all shown a general upward trend, in both average and extreme values, over recent decades (Kruger & Nxumalo, 2016). In addition, some regional differences in trends have been identified. However, these observations indicate that South Africa is warming at a slower rate than most other continental parts of the world, i.e. mostly less than 0.1°C per decade. This may be due to the buffering effect of the surrounding oceans. Using a data homogenisation procedure enabled the combination of stations from different time series from which trend analysis could be applied, to a common analysis period back to around 1931. The analyses show the general warming trend with a general increase in extreme warm events, and a general decrease in extreme cold events across South Africa. The analysis of seasonal trends shows that, while there are noteworthy differences on a regional basis, austral summer shows on average the strongest warming, followed by autumn, winter and spring. However, the central interior shows non-significant or similar trends when compared to the other parts of South Africa. There is no countrywide acceleration in the warming trends, but some regional consistencies in the temporal changes in trends could be determined, i.e. increases in trends in the central interior and decreases in trends along most of the coastal region.

A rainfall trend analysis for South Africa was completed by Kruger and Nxumalo (Kruger & Nxumalo, 2017) through optimizing district rainfall and individual rainfall station data sets for the longest possible period of analysis (i.e. 1921–2015). Two interlinked data sets were used for the trend analyses, namely, daily time series of 60 individual rainfall stations and the daily district rainfall of 88 of 94 rainfall districts. In general, the results show an increase in rainfall for most rainfall stations in the southern interior of South Africa, and indications of decreases in rainfall in the far northern and northeastern parts. The increase in the annual rainfall in the south is reflected in the seasonal trends, where summer rainfall shows a similar increase, but also extends into the central interior. For other seasons, most of the country shows no significant historical trend changes in annual total rainfall. Decreases in rainfall from wet spells were noted in most places over the east and northeast, while the southern and eastern parts along the escarpment experienced shorter annual dry spells. From the extreme rainfall analyses, an increase in daily rainfall extremes in the southern to western interior is apparent, but apart from summer rainfall regions, the other areas do not show spatially coherent statistically significant results. Mixed indications were observed in the updated analysis of the trends in extreme rainfall for South Africa (1931 to 2019) (SAWS, 2024c). The annual maximum daily and five-daily rainfalls show significant increases in the central and southern interior, whereas trends in the intensity of rainfall on rainy days show mixed signals, but there are clear decreases in the far northeastern interior and increases in the central and southeastern parts. In

© Eskom 2026/Rev 0c

PRINTED VERSIONS OF THIS DOCUMENT ARE NOT CONTROLLED

the case of the 25 mm rainfall threshold, increases are apparent over the central and southern interior and spreading eastwards, while decreases are only apparent in the far north.

In the research article by (Wright & Grab, 2017) of wind speed characteristics and implications for wind power generation in the Northern, Western and Eastern Cape provinces, data from 19 weather stations with high-resolution wind records between 1995 and 2014 were evaluated. The closest weather stations in the analysis to the Thyspunt study area were at Plettenberg Bay (coastal) and Uitenhage (coastal hinterland). Although a 20-year period is insufficient to establish conclusive changes in wind associated with climate change, the record is nevertheless able to provide tentative comparison of the data sets and indicate average wind speed variance and trends over the last 20 years for these two stations. The most significant findings were:

- The average rate of decrease across the two stations over the 20-year period equates to -3.25 per cent (Plettenberg Bay) and -1.53 per cent (Uitenhage).
- Spring and summer had the largest decline in wind speeds for Plettenberg Bay and Uitenhage.
- Whilst winter winds were also declining at Plettenberg Bay, an increase was observed at Uitenhage.
- Winds during autumn observed increases at both Plettenberg Bay and Uitenhage.

It is noted that these observed reductions in wind speed are also reflected in the downscaled model projections discussed in ***Subsection 5.8.6.2.2(c)***, albeit only for the near-horizon projection (-9.2 per cent). The far-horizon projection shows no change in the average wind speed. Medium confidence is assumed.

Climate change over southern Africa may be anticipated to be closely linked to changes in the dynamics of the regional Hadley cell (Seidel, et al., 2008). High- and low-pressure systems are projected to change in response to the expansion of the Hadley cell in a warmer world. Over southern Africa, the strengthening and expanding subtropical high-pressure belt is, under climate change, projected to contribute to the southward displacement (or blocking) of frontal systems bringing rainfall over southern Africa. As per AR5, the mean sea level pressure is therefore projected to decrease.

As discussed in ***Subsection 5.8.2.6.6***, the IPCC has prepared four scenarios that assume the stabilisation of anthropogenic forcing of the climate system at different levels. The treatment of climate change for the

© Eskom 2026/Rev 0c

PRINTED VERSIONS OF THIS DOCUMENT ARE NOT CONTROLLED

study area is based on downscaled model simulations completed by the CSIR (Engelbrecht, et al., 2019; CSIR, 2019) and the SAWS (South African Weather Service, 2017) for South Africa for two RCPs, namely RCP4.5 and RCP8.5. The CSIR data consisted of two data sets and reports for the two future horizons of 2021-2050 and 2070-2099 (Engelbrecht, et al., 2019) and (CSIR, 2019). The two data sets were provided on a 50 km downscaled to a 8 km model grid resolution, respectively. The SAWS simulations were also for two future horizons, i.e. 2036-2065 and 2066-2095, and covered a 0.44° (approximately 45 km) spatial resolution. Where the required information could not be obtained from these downscaled models, the analysis was supplemented with information extracted from the ARP5. Although the downscaled simulations included both gradual climate change (GCC) and extreme weather events (EWE), the latter treatments were only focussed on extreme rainfall days, hot and heatwave days (Engelbrecht, et al., 2019). No attempt was made in the downscaled models to forecast extreme temperatures, wind gusts and rainfall events. Instead, the SREX reports (Intergovernmental Panel on Climate Change, 2012) treatment of risks of extreme events was consulted in combination with the downscaled CSIR results. The projections based on RCP8.5 were adopted for inclusion in this SSR due to the uncertainty on whether any of the mitigation emissions would be achieved.

Wind direction changes were not provided as part of the downscaled model outputs. Instead, the study by Herbst and Rautenbach (Herbst & Rautenbach, 2015), which attempted to quantify the projected changes in seasonal daily average wind speeds and directions for South Africa around the mid-21st century (2051-2075), was consulted. Small scale rare weather events such as thunder, lightning and hail events have not been simulated in any of the global climate models (GCMs). Projections of extremes in any of the meteorological parameters are difficult to determine. Extreme rainfall events are mostly caused by intense thunderstorms, which are often also the cause of lightning, hail, damaging winds and flash floods. That is, the climate change projections analysed with these models are indicative that decreases in these hazardous rainfall events are plausible over the study area. The more conservative approach would therefore be to assume the historical statistics rather than to reduce any frequencies of these events. Similarly, none of the models simulate the occurrence of tornadoes.

Based on the SREX report (Intergovernmental Panel on Climate Change, 2012), the approach to adjusting temperature extremes for climate change is to apply a reduction in the return period of the predicted extreme value. For wind speeds and rainfall, it is recommended to adopt the projected changes in the GCC.

© Eskom 2026/Rev 0c

PRINTED VERSIONS OF THIS DOCUMENT ARE NOT CONTROLLED

In summary, the projected fractional changes in rainfall, temperature and wind speed due to climate change are given in ***Table 5.8.74***. The absolute values for these meteorological parameters are summarised in ***Table 5.8.75***.

© Eskom 2026/Rev 0c

PRINTED VERSIONS OF THIS DOCUMENT ARE NOT CONTROLLED

Table 5.8.74
Fractional Climate Change Projections for Rainfall, Temperature and Wind Speed

Parameter	Period	Baseline		Statistic	Horizon Projected Fractional Change (per cent)	
		Thyspunt	Cape St Francis		Near-Horizon	Far-Horizon
Rainfall	Annual Average	774.0 mm	619.5 mm	90th Percentile	1.82%	-3.18%
				Average	0.30%	-1.18%
				10th Percentile	-2.21%	0.63%
	24-Hour Maximum	113.5 mm	157.8 mm	90th Percentile	10.0%	0.00%
				Average	10.0%	0.00%
				10th Percentile	10.0%	0.00%
Temperature	Average Min Daily	14.4 °C	14.2 °C	90th Percentile	7.58%	15.15%
				Average	18.94%	18.94%
				10th Percentile	22.73%	30.30%
	Average Daily	17.4 °C	17.4 °C	90th Percentile	9.63%	18.90%
				Average	9.80%	19.14%
				10th Percentile	9.80%	20.25%
	Average Max Daily	20.8 °C	19.9 °C	90th Percentile	4.93%	9.85%
				Average	7.39%	17.24%
				10th Percentile	9.85%	19.70%
Wind Speed	Annual Average	5.4 m/s	6.0 m/s	90th Percentile	18.38%	18.38%
				Average	-9.19%	0.00%
				10th Percentile	-18.38%	-18.38%
	Peak Hourly Maximum	19.6 m/s	23.2 m/s	90th Percentile	5.10%	5.10%
				Average	-2.55%	0.00%
				10th Percentile	-5.10%	-5.10%
	Gust	32.2 m/s	45.8 m/s	90th Percentile	3.11%	3.11%
				Average	-1.55%	0.00%
				10th Percentile	-3.11%	-3.11%

© Eskom 2026/Rev 0c

PRINTED VERSIONS OF THIS DOCUMENT ARE NOT CONTROLLED

Table 5.8.75
Climate Change Projections for Rainfall, Temperature and Wind Speed (Thyspunt WS and Cape St Francis Baselines)

Weather Station	Meteorological Parameter	Period	Baseline	Statistic	Horizon Projected Absolute Values	
					Near-Horizon	Far-Horizon
Thyspunt WS	Rainfall	Annual Average	774.0 mm	90th Percentile	790.41	740.25
				Average	776.32	764.87
				10th Percentile	759.22	769.74
		24-Hour Maximum	113.5 mm	90th Percentile	136.20	113.50
				Average	124.85	113.50
				10th Percentile	124.85	113.50
	Temperature	Min Daily	14.4 °C	90th Percentile	15.4	16.4
				Average	16.9	16.9
				10th Percentile	17.4	18.4
		Average Daily	17.4 °C	90th Percentile	19.0	20.6
				Average	19.0	20.6
				10th Percentile	19.0	20.8
		Max Daily	20.8 °C	90th Percentile	21.8	22.8
				Average	22.3	24.3
				10th Percentile	22.8	24.8
	Wind Speed	Hour Average	5.4 m/s	90th Percentile	6.4	6.4
				Average	4.9	5.4
				10th Percentile	4.4	4.4
		Peak Hourly Maximum	19.6 m/s	90th Percentile	20.6	20.6
				Average	19.1	19.6
				10th Percentile	18.6	18.6
		Gust	32.2 m/s	90th Percentile	33.2	33.2
				Average	31.7	32.2

© Eskom 2026/Rev 0c

PRINTED VERSIONS OF THIS DOCUMENT ARE NOT CONTROLLED

Weather Station	Meteorological Parameter	Period	Baseline	Statistic	Horizon Projected Absolute Values	
					Near-Horizon	Far-Horizon
				10th Percentile	31.2	31.2
Cape St Francis	Rainfall	Annual Average	619.5 mm	90th Percentile	632.63	592.49
				Mean	621.36	612.19
				10th Percentile	607.67	616.09
		24-Hour Maximum	158.0 mm	90th Percentile	189.60	158.00
				Mean	173.80	158.00
				10th Percentile	173.80	158.00
	Temperature	Min Daily	14.2 °C	90th Percentile	15.2	16.2
				Average	16.7	16.7
				10th Percentile	17.2	18.2
		Average Daily	17.3 °C	90th Percentile	19.0	20.6
				Average	19.0	20.6
				10th Percentile	19.0	20.8
		Max Daily	19.9 °C	90th Percentile	20.9	21.9
				Average	21.4	23.4
				10th Percentile	21.9	23.9
	Wind Speed	Hour Average	6.0 m/s	90th Percentile	7.0	7.0
				Average	5.5	6.0
				10th Percentile	5.0	5.0
		Peak Hourly Maximum	23.2 m/s	90th Percentile	24.2	24.2
				Average	22.7	23.2
				10th Percentile	22.2	22.2
		Gust	45.8 m/s	90th Percentile	46.8	46.8
				Average	45.3	45.8
				10th Percentile	44.8	44.8

© Eskom 2026/Rev 0c

PRINTED VERSIONS OF THIS DOCUMENT ARE NOT CONTROLLED

5.8.10 Management System

The appropriate grading for safety classification in terms of RD-0034 following Eskom's classification procedure (National Nuclear Regulator, 2008) has been determined as Safety Class Level 3, i.e. not important to nuclear safety, and in terms of the procedure, compliance with an ISO 9001 or equivalent system is required. Supporting information can be found in ***Chapter 10*** (Management System).

A quality assurance programme has been followed that includes the minimum meteorological parameters to sample, minimum specifications for meteorological instrumentation and siting criteria, data collection and validation procedures, instrument maintenance procedures, methods of analyses and archiving procedures. (Refer to ***Chapter 10***).

The collection of meteorological data from the monitoring station at the site is done every two weeks. These data are stored on two computer servers (mirrored) in two separate fire-proof strong rooms. Detailed records are kept of the work carried out, calculations made and databases established. These include:

- raw monitoring database;
- processed monitoring database;
- dispersion model input files;
- dispersion model output files;
- dispersion factor database (short- and long-term simulations);
- meteorological instrumentation calibration certificates.

Electronic records are stored in a secure central repository with regular off-site back-ups.

Whereas the monitoring of meteorological parameters can be verified by inspectors, dispersion modelling and further processing of meteorological parameters do not lend themselves to direct verification or tests that can be precisely defined and controlled. Peer review of these evaluations is essential and was done by a suitably qualified and experienced person, independent from those who did the work.

It is stated in *Section 1* of RG-0016 that *"All calculation models and/or evaluation models used in safety analyses are designed, developed, verified and validated, implemented, used and controlled in accordance with recognised nuclear industry standards and/or practices."* The Verification

© Eskom 2026/Rev 0c

PRINTED VERSIONS OF THIS DOCUMENT ARE NOT CONTROLLED

and Validation report (Burger, 2024) was completed with the following objectives:

- to identify, describe and understand the different physical processes being simulated;
- to demonstrate the capabilities and limitations of the mathematical formulations, utilised in the selected software, in simulating the identified physical processes;
- to verify the software input pre-processing and the output post-processing;
- to define and demonstrate the minimum qualifications required to use the software and the models.

In the V&V Report, it was concluded that the US EPA AERMOD atmospheric model satisfy the requirements for simulation atmospheric dispersion from nuclear installation(s) for the purposes of the SSR. The following documentation has been included as appendices to this SSR:

- dispersion model input files (***Appendix 5.8.J*** to ***Appendix 5.8.P***);
- dispersion model output files (***Appendix 5.8.Q*** to ***Appendix 5.8.T***);
- meteorological instrumentation calibration certificates. (***Appendix 5.8.F***).

The RG 011 regulatory compliance matrix is provided in ***Table 5.8.76***, that lists the relevant clauses and the specific sections/regulations referred to and in which sections of this SSR they have been addressed.

© Eskom 2026/Rev 0c

PRINTED VERSIONS OF THIS DOCUMENT ARE NOT CONTROLLED

Table 5.8.76
Regulatory Compliance Matrix

RG 0011 clause	RG 0011 sub clause	Issue	Section where Covered
Assessment of hazards associated with external natural and human-induced events	7.1 General approach for External Events	(2) Adequately investigated with respect to all characteristics that could affect safety in relation to natural and human-induced events	5.8.1, 5.8.5.1
		(3) Hazards associated with external events, which are to be considered in the design of the nuclear facility, must be determined. For an external event (or a combination of events), the parameters and the values of those parameters used to characterise the hazards must be chosen so that they can be used readily in the design of the nuclear facility.	5.8.1, 5.8.6.1.11(a)-(c), 5.8.6.2.1, 5.8.6.2.2, 5.8.11, 5.8.12 (Table 5.8.78, Table 5.8.78)
		(5) Prehistorical, historical and instrumental information and records, as applicable, on the occurrences and severity of those important natural phenomena or human-induced situations/activities should be collected for the region and carefully analysed for reliability, accuracy and completeness	5.8.5, 5.8.6, 5.8.9, Appendix 5.8.A, Appendix 5.8.D, Appendix 5.8.I
		(6) Appropriate methodologies should be adopted for establishing the hazards from important external phenomena	5.8.4 & 5.8.5
		(7) Methodologies used should be the current and state of the art, and should be justified as being compatible with the characteristics of the region.	5.8.4 & 5.8.5, Appendix 5.8.A, V & V Report
		(8) Preferential consideration should be given to applicable probabilistic methodologies	Appendix 5.8.B

© Eskom 2026/Rev 0c

PRINTED VERSIONS OF THIS DOCUMENT ARE NOT CONTROLLED

RG 0011 clause	RG 0011 sub clause	Issue	Section where Covered
		(10) The size of the region, to which a method for establishing the hazards associated with major external phenomena is to be applied, should be large enough to include all features and areas that could be of significance in the determination of the event.	5.8.6.1.1 (a) & (b), 5.8.6.2.1 (b) & (c), 5.8.7, 5.8.10
		(12) If data for a particular type of natural phenomenon are incomplete for the region, then data from other regions having sufficiently similar characteristics should be used, with proper justification, in evaluation of the design basis event.	5.8.6.1.1, 5.8.6.1.2, 5.8.6.1.3, 5.8.6.1.5
	7.2 Natural Events 7.2.2 Meteorological Events	(1) Meteorological and climatological characteristics for the region around the site should be investigated and evaluated to ensure the safety of nuclear facility. Meteorological events/parameters to be considered for evaluation of design bases include:	
		- Wind	5.8.6.1.1, 5.8.6.2.1(a)-(c), 5.8.6.2.2(c)
		- Precipitation	5.8.6.1.3, , 5.8.6.2.1(d), 5.8.6.2.2(a)
		- Storm surge	5.8.6.1.4, 5.8.6.1.2(d)
		- Tropical cyclone	5.8.6.2.1(b)
		- Air temperature (dry bulb and wet bulb)	5.8.6.1.2, 5.8.6.2.2(b)
		- Humidity	5.8.6.1.6
		(2) The following rare meteorological events should also be considered in the evaluation of site characteristics:	
		- Lightning	5.8.6.2.1(f)
		- Tornado	5.8.6.2.1(c)
		- Snow	5.8.6.5.1.5
		- Waterspouts	5.8.6.2.1(c)
		- Dust and sandstorms	5.8.6.11(a)

© Eskom 2026/Rev 0c

PRINTED VERSIONS OF THIS DOCUMENT ARE NOT CONTROLLED

RG 0011 clause	RG 0011 sub clause	Issue	Section where Covered
		- Hail storms	5.8.6.1.5, 5.8.6.2.1(e)
		- Freezing precipitation	5.8.6.1.3
		- Frost	5.8.6.1.3
		- Cloud burst	5.8.6.2.1(d)
		- Other phenomena	5.8.6.2
		(3) Hazards associated with all relevant meteorological phenomena should be identified and evaluated to arrive at the corresponding design basis parameter to ensure the safety of the facilities to be located at the site	5.8.10, 5.8.12 (Table 5.8.78, Table 5.8.78)
		(4) Historical data of the event at and around the site should be utilised for evaluation of the potential of occurrence, frequency and severity of the meteorological event.	5.8.5, 5.8.6, Appendix 5.8.I
		(5) Historical data on persistent high winds during cyclones, tornadoes and storms occurring at and around the region should be used for static loading and wind induced missile generation, while data on short duration bursts of wind should be utilised for studies of dynamic loading. Historical data on circulating wind during tornadoes, if any, occurring at or around the region should also be collected.	5.8.5, 5.8.6.2, Appendix 5.8.I
		(6) Collected data should be used to generate design basis wind speeds taking into account the safety goal defined in PP-0014	5.8.6.2.1(c)
		(7) Site-specific design basis wind speeds should be based on sufficient and reliable data.	5.8.1.1, 5.8.6.2.1(b)-(c)
	7.2 Natural Events 7.2.3 Flooding	4) Suitable meteorological, hydrological and topographical data, including data on relevant bodies	5.8.5, 5.8.6.1, 5.8.6.2, 5.8.9, Appendix 5.8.A

© Eskom 2026/Rev 0c

PRINTED VERSIONS OF THIS DOCUMENT ARE NOT CONTROLLED

RG 0011 clause	RG 0011 sub clause	Issue	Section where Covered
		of water, should be collected. Uncertainty and data adequacy, if any, should be taken into consideration	
8 Assessment of the potential radiological impacts of the nuclear facility	8.3 Transport and Diffusion of Effluents Discharged into the Atmosphere 8.3.1 General Considerations	(1) A meteorological investigation should be carried out to evaluate regional and site-specific meteorological parameters. Data should be collected from appropriate elevations above ground in order to obtain realistic dispersion parameters.	5.8.6.1.1, 5.8.6.1.2, 5.8.6.1.8, 5.8.6.1.9, 5.8.7
		(3) The type and extent of acquired and stored meteorological data should allow for reliable statistical analyses to determine the distribution of radiation exposures	5.8.6.1.1, 5.8.6.1.2, 5.8.6.1.8, 5.8.6.1.9, 5.8.7
		(4) Contamination in the air, on the ground and in water over short and long periods of time should be described in the atmospheric dispersion models, with account taken of diffusion conditions in the region.	5.8.7
		(5) Use of parameters in calculational models should be substantiated as to their appropriateness for use in estimating releases	5.8.7
		6) The atmospheric dispersion and deposition models used must be documented, described in detail and substantiated to allow a review of their accuracy and validity, source configuration, suitability of input parameters, topography, and appropriateness for the site, plant and release characteristics.	5.8.7 & Atmospheric Dispersion Modelling Verification and Validation: Numerical Atmospheric Dispersion Model
	8.3.2 Meteorological considerations	(1) A programme for meteorological investigation should be designed to collect and evaluate data continuously and should provide data for an adequate time period (for at least two full years) that are representative of the site and should continue for the lifetime of the facility. In addition, the data should be	5.8.2, 5.8.5, 5.8.5.6

© Eskom 2026/Rev 0c

PRINTED VERSIONS OF THIS DOCUMENT ARE NOT CONTROLLED

RG 0011 clause	RG 0011 sub clause	Issue	Section where Covered
		compared with data collected after the plant is constructed, but before operation, to determine whether changes are necessary to the design bases or to assumptions made in the calculation model.	
		(2) In collecting meteorological data, care should be taken to prevent local effects from unduly altering the values of the parameters to be measured. It should be ensured that the data collected adequately represent local meteorological conditions	5.8.5.4, 5.8.5.5, Appendix 5.8.A, , Appendix 5.8.D
		(3) In order to provide a description of the meteorological conditions, data on the following should be obtained concurrently:	
		a) Wind vectors (i.e. wind directions and speeds);	5.8.6.1.1
		b) Specific indicators of atmospheric turbulence;	5.8.6.1.9
		c) Precipitation;	5.8.6.1.3
		d) Air temperatures;	5.8.6.1.2
		e) Humidity; and	5.8.6.1.6
		f) Air pressure	5.8.6.1.7
	8.3.3 Instrumentation and measurements	(1) Meteorological equipment should be installed in such a way as to obtain data representing the dispersion conditions at release points. Examination of the terrain around a nuclear facility site is necessary. Topographical features of interest should be considered in the installation of equipment. Instruments should be capable of obtaining data representing the entire profile of the wind, at least up to the height of potential releases.	5.8.5.5, Appendix 5.8.A
		(2) At sites where there is a potential for fogging or icing, due to an increase in atmospheric moisture	5.8.6.1.2, 5.8.6.1.5

© Eskom 2026/Rev 0c

PRINTED VERSIONS OF THIS DOCUMENT ARE NOT CONTROLLED

RG 0011 clause	RG 0011 sub clause	Issue	Section where Covered
		content caused by plant operation, instrumentation should be provided for measuring the dew point (or humidity) on the tower or mast.	
		(3) Equipment should be properly exposed and should be positioned far enough from any obstacles to minimise their effects on measurements. The tower or mast should be sited at approximately the same elevation as finished plant grade and in an area where plant structures will have little or no influence on the meteorological measurements.	5.8.5.5, Appendix 5.8.A
		(4) Meteorological instrumentation and systems should be shielded, maintained, serviced and calibrated on a regular basis in order to mitigate harmful environmental effects such as sun, lightning, ice, sandstorms and corrosive agents and to ensure availability and reliability of data.	5.8.5.3, Appendix 5.8.F
		5) In assessing the accuracy of instrumentation, allowance should be made for errors due to cabling, signal conditioning, recording, solar radiation and the effects of fluctuations in environmental temperature.	5.8.5.4, Appendix 5.8.D, Appendix 5.8.G
		6) Measurements should be made at more than one location where the wind speed or direction varies significantly across the region.	5.8.5.3, Appendix 5.8.A
		7) Measurements should be made at the following elevations in order to obtain wind data continuously: a) At an elevation of 10m in accordance with standards that have been established by the World Meteorological Organization (WMO), for purposes of comparing and correlating wind data from the site with	5.8.5.3

© Eskom 2026/Rev 0c

PRINTED VERSIONS OF THIS DOCUMENT ARE NOT CONTROLLED

RG 0011 clause	RG 0011 sub clause	Issue	Section where Covered
		wind data from the synoptic network of meteorological stations; and	
		b) At the point representing the effective height of discharge.	5.8.5.3, 5.8.5.5, 5.8.7.2 (The design of the nuclear installation has not yet been selected)
		(8) Measurement techniques for recording meteorological data should be in line with the standards published by the national meteorological services. The general tendency is to record average values for a given constant duration, such as 3s gusts, 60s averages or 10min averages (the averaging time is a characteristic of the database).	5.8.4, 5.8.5.6
		(9) The wind vector at different elevations and temperatures should be averaged at least once per hour, while the period of integration for other variables such as solar radiation levels and precipitation levels should be one hour. Wind direction should be averaged as a vector and wind speed as a scalar over the prescribed time period.	5.8.5.6, 5.8.6.1
		(10) The basic reduced data should be compiled into monthly or seasonal and annual joint frequency distributions of wind speed and wind direction by atmospheric stability class. Similar tables of joint frequency distribution should be prepared for each of the other atmospheric stability classes.	5.8.6.1.9
		(11) In developing site-specific diffusion models, sufficient information should be acquired on the space and time distributions of wind and temperature to be able to understand and determine the trajectory of effluents.	5.8.6.1.1, 5.8.6.1.2, 5.8.6.1.8, 5.8.6.1.9, 5.8.7

© Eskom 2026/Rev 0c

PRINTED VERSIONS OF THIS DOCUMENT ARE NOT CONTROLLED

RG 0011 clause	RG 0011 sub clause	Issue	Section where Covered
		(12) a) Fluctuations in wind direction (sigma theta method); b) Air temperature and temperature lapse rate (delta-T method); c) Wind speed and solar radiation levels or sky cover during the daytime, and sky cover or net radiation levels at night-time (insulation method); and d) Wind speed at different heights.	5.8.6.1.9
		(13) Determination of the temperature variation for an atmospheric layer with height between at least two measurement levels should be provided. These levels should include the level at which the wind is measured.	5.8.5, 5.8.6.1.2, 5.8.6.1.9
		(14) The frequency, duration and time of the measurements of temperature variation with height should be concomitant with the wind data.	5.8.5.3
		(15) Precipitation and humidity should be recorded at least hourly.	5.8.5.2, 5.8.5.3, 5.8.6.1.3, 5.8.6.1.6
		(16) A joint frequency distribution of wind direction and wind speed for each stability class (three-dimensional weather statistics) should be provided.	5.8.6.1.9
		(17) The probability of occurrence of different sets of meteorological conditions should be determined during different periods of time over the duration of, for example: An accident, in the first hours of the postulated accident, on the first day, over the first week and over the balance of the duration of the accident	5.8.7

© Eskom 2026/Rev 0c

PRINTED VERSIONS OF THIS DOCUMENT ARE NOT CONTROLLED

RG 0011 clause	RG 0011 sub clause	Issue	Section where Covered
10 nuclear security arrangements during siting	10.4 Security Plan and Measures	(11) Determination of the temperature variation for an atmospheric layer with height between at least two measurement levels should be provided. These levels should include the level at which the wind is measured.	5.8.6.1.2 (Single mast with two temperature probes at 2 m and 8 m, and a wind speed anemometer at 9 m)

© Eskom 2026/Rev 0c

PRINTED VERSIONS OF THIS DOCUMENT ARE NOT CONTROLLED

Information from the Meteorology Section is used in a number of other sections of this SSR. ***Table 5.8.77*** is a summary of the links to different sections that requires meteorological information.

© Eskom 2026/Rev 0c

PRINTED VERSIONS OF THIS DOCUMENT ARE NOT CONTROLLED

Table 5.8.77
Summary of Activities, Links and Quality Requirements

Activity	Links		Quality Requirements
	Inputs	Outputs	
Meteorological Measurement	Desk studies, Additional measurements	***Section 5.9*** (Oceanography and Coastal Engineering) – wind speed, wind direction and barometric pressure ***Section 5.10*** (Hydrology and Hydraulics) – rainfall ***Section 5.11*** (Geohydrology) - recharge and water balance calculations used in the groundwater modelling ***Chapters 6*** (Evaluation of External Events) and ***7*** (Potential Radiological Impact on the Public and the Environment) - external events ***Chapter 8*** – wind speed, stability joint frequency table	Monitoring protocol Calibration certificates Certificate of accreditation for selected laboratories
Modelling	Location and Plant perimeter envelope in ***Chapter 1*** (Introduction) Sea temperature measurements in ***Section 5.9***	***Section 5.11*** – deposition rates for input into the contaminant transport modelling ***Chapter 7*** – air concentration and deposition rates for input into the health risk calculations	Table showing rationale for selection of model code(s). International benchmarking, use and acceptability. Validation and verification of computer software codes used to comply with NNR requirements. Uncertainties and management/incorporation thereof. Sensitivity analysis. Peer Review

5.8.10.1 Maintenance and Service

Proper maintenance of weather station components is required to obtain accurate data. Thus, calibration and inspection of the instruments is done on a bi-annual basis to ensure that the equipment is in good operating

© Eskom 2026/Rev 0c

PRINTED VERSIONS OF THIS DOCUMENT ARE NOT CONTROLLED

condition and measurements are made according to the prescribed standards.

Routine and simple maintenance is accomplished through visual inspection of the weather station. The following preventative maintenance steps are in place to ensure a properly functioning weather station:

- once a month:
  - checking of the solar radiation sensor for level and contamination and clean if necessary;
  - checking of the rain gage funnel for debris and level;
  - visual inspection of the wind sensors and radiation shield;
  - visual inspection of the anemometer at low wind speeds;
  - checking of the filter of the temperature/humidity sensors for contamination;
- bi-annually:
  - calibration of meteorological sensors and their accuracy verified;
  - replacing anemometer bearings;
  - cleaning the radiation shield;
  - replacing sensor cables as required.

In addition, general maintenance of meteorological equipment includes:

- occasional cleaning of the glass on the solar panel;
- checking of the sensor leads and cables for cracking, deterioration, proper routing and strain relief;
- checking of the tower for structural damage, proper alignment and level;
- checking of the equipment quality as part of normal operation;
- checking and control exposure of the instruments regularly;
- check of battery power;
- checking of operational mode of the data logger;
- quality control of all data recorded.

More specific maintenance such as sensor calibration, sensor performance testing and sensor component replacement is done by a skilled technician.

© Eskom 2026/Rev 0c

PRINTED VERSIONS OF THIS DOCUMENT ARE NOT CONTROLLED

The date and time of the calibration, together with the name of the person who performed the calibration, is recorded on the calibration certificate for future reference.

The meteorological system aims to provide a minimum critical data availability of 80 per cent prior to operation, and 99 per cent monthly during operation of the nuclear installation(s).

5.8.10.2 Data collection and storage

Details of the meteorology and corrosion monitoring are provided in the monitoring programme which is detailed in ***Section 5.2***. The monitoring programme for meteorological parameters are based on the requirements contained in Eskom's Meteorological Requirements for Nuclear Installations. Standard 238-52, Cape Town (Eskom, 2022a) and ANSI/ANS-3.11-2015, Determining Meteorological Information at Nuclear Facilities (American National Standard, 2015). As per the two standards, the measurement and storage of meteorological parameters include air temperature (at two heights), wind speed and wind direction, standard deviation of wind speed, precipitation atmospheric pressure and humidity. Additional meteorological parameters in the monitoring programme include solar radiation, lightning and visibility, as well as corrosion.

Responsibility for management and custodianship of documents and data lies with the Eskom Nuclear Sites Project Manager (refer to ***Chapter 10***).

5.8.11 Potential Impact on the Nuclear Installation Design and Operation

External meteorological events could pose hazards that affect very specific nuclear installation systems and are not usually considered in the structural integrity evaluation of the buildings, for example low pressures during extreme wind conditions could affect roof structures, or overpressures that would be obtained from a tornado. Therefore, the following needs to be considered (International Atomic Energy Agency, 2021) in the hazard evaluation and also in the nuclear installation design:

- the impact of wind and lightning on the availability of off-site power;
- the impact of temperature, moisture and lightning on the functionality of safety related equipment, and particularly the instrumentation and control equipment;
- the corrosion potential on the structural integrity of buildings.

Experience has shown (International Atomic Energy Agency, 2021) that the damage caused by lightning could be extensive. It has mainly affected

© Eskom 2026/Rev 0c

PRINTED VERSIONS OF THIS DOCUMENT ARE NOT CONTROLLED

electrical equipment in recorded events, but very often has developed into transformer explosions, serious fire accidents and spurious signals to valves with consequent flooding and loss of off-site power. Special protection from lightning should be designed and implemented, with periodic assessment of a proper earthing system and regular inspections of the insulation of exposed equipment. In general, a comprehensive Faraday cage should be put in place by means of narrow mesh thin steel reinforcing in the outer skin of the building walls. Special care should be taken in the protection of conductors at short distances from each other and/or protruding from the cage protected volume.

Although it was shown that snow is unlikely to occur, if present on the site, it could induce damage to and unavailability of the power supply or the electrical grid. It could also affect ventilation intakes and discharges, structural loading, access by the operator to external safety related facilities and mobility of emergency vehicles.

Consideration should be also given to extreme low temperature that:

- may adversely affect instrumentation and control systems, which may generate spurious signals;
- created moisture condensation in closed rooms, with consequent dropping of water onto electrical equipment causing short circuits and malfunctions;
- may prevent the air ventilation system from working properly;
- may hinder proper operation of diesel generators where the fuel shows separation of paraffin[56];
- may damage the external power supply system and limit the availability of service water.

5.8.12 Conclusions

The site-specific parameters applicable to the Thyspunt site are given in ***Table 5.8.78*** and ***Table 5.8.79.*** The chosen values for the rainfall, wind speed and atmospheric stabilities were based on the time covered by the database at the Thyspunt WS and the Cape St. Francis WS. The prediction of extreme analyses (return periods) was based on the Cape St. Francis

[56] Since diesel fuel is a complex mixture of hydrocarbons, as it cools down in cold weather, it does not freeze at a single temperature. Instead, it turns cloudy as minute wax crystal plates and needles begin to form and eventually thickens like soft jelly. The exact gelling temperature ("wax appearance point" or WAP) can vary depending on the specific composition, the amount of paraffin and additives in the diesel fuel. If cooled further below the WAP, it becomes difficult to pump through the fuel system. In extremely low temperatures it could finally solidify.

© Eskom 2026/Rev 0c

PRINTED VERSIONS OF THIS DOCUMENT ARE NOT CONTROLLED

WS measurements due to the longer length of the observation record for predicting extreme values.

© Eskom 2026/Rev 0c

PRINTED VERSIONS OF THIS DOCUMENT ARE NOT CONTROLLED

Table 5.8.78
Site Specific Parameters Part 1

Meteorological Parameter		Baseline	Climate Change Projections	
			Near-Horizon (2050)	Far Horizon (2100)
Annual Average Wind Speed (m/s) at Thyspunt WS (***on page 5.8-56***)		5.4 ± 0.01	4.9 -0.5+1.5	5.4 -1.0+1.0
Annual Average Wind Speed (m/s) at Cape St Francis WS (***on page 5.8-53***)		6.0± 0.01	5.5 -0.5+1.5	6.0 -1.0+1.0
Hourly Maximum Wind Speed (1) [m/s] (Thyspunt WS 8 m above site ground level) **Return Periods Wind Speed** [m/s] (2) (Cape St Francis WS 10 m above site ground level) (***on page 5.8-165***)	Extreme Observed & Projected Thyspunt WS (***on page 5.8-56***)	19.6 ± 0.0	19.1 -0.5+1.5	19.6 -1.0+1.0
	Extreme Observed & Projected Cape St Francis WS (**on page 5.8-53**)	23.2 ± 0.0	22.7 -0.5+1.5	23.2 -1.0+1.0
	10 Year Return	22.0 ± 1.2	21.4 ± 1.2	22.0 ± 1.2
	100 Year Return	24.7 ± 2.1	24.0 ± 2.1	24.7 ± 2.1
	1 000 Year Return	27.3 ± 3.1	26.6 ± 3.1	27.3 ± 3.1
	10 000 Year Return	29.9 ± 4.1	29.2 ± 4.1	29.9 ± 4.1
	100 000 Year Return	32.6 ± 5.1	31.7 ± 5.1	32.6 ± 5.1
	1 000 000 Year Return	35.2 ± 6.1	34.3 ± 6.1	35.2 ± 6.1
	10 000 000 Year Return	37.9 ± 7.0	36.9 ± 7.0	37.9 ± 7.0
	100 000 000 Year Return	40.5 ± 8.0	39.5 ± 8.0	40.5 ± 8.0
Wind peaks (gusts) (3) [m/s] (Thyspunt WS 8 m above site ground level)	Extreme Observed & Projected Thyspunt WS (***on page 5.8-65***)	32.2 ± 0.0	31.7 -0.5+1.5	32.2 -1.0+1.0
	Extreme Observed & Projected Cape St Francis (***on page 5.8-66***)	45.8± 0.0	45.3 -0.5+1.5	45.8 -1.0+1.0
	10 Year Return	38.1 ± 3.5	37.6 ± 3.5	38.1 ± 3.5

© Eskom 2026/Rev 0c

PRINTED VERSIONS OF THIS DOCUMENT ARE NOT CONTROLLED

Meteorological Parameter		Baseline	Climate Change Projections	
			Near-Horizon (2050)	Far Horizon (2100)
Return Period Gusts [m/s] [2] (Cape St Francis WS 10 m above site ground level) (***on page 5.8-166***)	100 Year Return	44.3 ± 6.2	43.7 ± 6.2	44.3 ± 6.2
	1 000 Year Return	50.2 ± 8.8	49.6 ± 8.8	50.2 ± 8.8
	10 000 Year Return	56.2 ± 11.4	55.5 ± 11.4	56.2 ± 11.4
	100 000 Year Return	62.2 ± 14.1	61.4 ± 14.1	62.2 ± 14.1
	1 000 000 Year Return	68.2 ± 16.7	67.3 ± 16.7	68.2 ± 16.7
	10 000 000 Year Return	74.2 ± 19.3	73.2 ± 19.3	74.2 ± 19.3
	100 000 000 Year Return	80.2 ± 22.0	79.1 ± 22.0	80.2 ± 22.0
Ambient temperature [°C] (Thyspunt WS 2 m above site ground level) **Return Periods Dry Bulb Temperature** [m/s] [4] (Cape St Francis WS 10 m above site ground level) (***on page 5.8-165***)	Average daily maximum dry bulb temperature (***on page 5.8-73***)	20.8 ± 0.1	22.5 0.0+0.0	24.1 -0.04+0.2
	- coincident wet bulb temperature [5]	18.2 ± 0.2	19.4 1.0+1.8	20.1 1.0+2.3
	Average daily maximum wet bulb temperature [5] (***on page 5.8-73***)	16.7 ± 0.1	17.3 0.0+0.5	17.9 0.0+0.9
	Extreme Observed Thyspunt WS (***on page 5.8-74***) & Projected dry-bulb maximum	38.2 ± 0.0	39.7 -0.5+0.5	41.7 -1.5+0.5
	Extreme Observed Cape St Francis WS (***on page 5.8-74***) & Projected dry-bulb maximum	38.5 ± 0.0	40.0 -0.5+0.5	42.0 -1.5+0.5
	10 Year Return	37.0 ± 1.8	42.8 ± 2.9	45.6 ± 3.1
	100 Year Return	42.4 ± 3.1	48.1 ± 4.3	50.9 ± 4.5
	1 000 Year Return	47.7 ± 4.5	53.4 ± 5.7	56.2 ± 5.9
	10 000 Year Return	53.0 ± 5.9	58.7 ± 7.2	61.5 ± 7.4
	100 000 Year Return	58.3 ± 7.4	64.0 ± 8.7	66.9 ± 8.9
	1 000 000 Year Return	63.7 ± 8.9	69.3 ± 10.2	72.2 ± 10.4

© Eskom 2026/Rev 0c

PRINTED VERSIONS OF THIS DOCUMENT ARE NOT CONTROLLED

Meteorological Parameter		Baseline	Climate Change Projections	
			Near-Horizon (2050)	Far Horizon (2100)
	10 000 000 Year Return	69.0 ± 10.4	74.6 ± 11.6	77.5 ± 11.9
	100 000 000 Year Return	74.3 ± 11.9	80.0 ± 13.1	82.8 ± 13.4
	Maximum temperature of 3-hour duration [6] (***on page 5.8-84***)	37.0 Corresponding Wet Bulb Temperature 19.7 ± 1.8	38.7 0.0+0.0	40.3 -0.04+0.2
	Maximum temperature of 6-hour duration [6] (***on page 5.8-84***)	33.1 Corresponding Wet Bulb Temperature 18.8 ± 0.9	34.8 0.0+0.0	36.4 -0.04+0.2
	Maximum temperature of 7-day duration [6] (***on page 5.8-84***)	19.3 Corresponding Wet Bulb Temperature 16.8 ± 0.1	21.0 0.0+0.0	22.6 -0.04+0.2
	Average daily minimum dry bulb temperature (***on page 5.8-73***)	14.4 ± 0.1	16.1 0.0+0.0	17.7 -0.04+0.2
	- coincident wet bulb temperature [5]	11.8 ± 0.1	12.2 -0.1+0.2	12.6 -0.3+0.4
	Average daily minimum wet bulb temperature [5] (***on page 5.8-75***)	12.6 ± 0.1	13.0 0.0+0.3	13.5 0.0+0.6
	Extreme Observed Thyspunt WS (***on page 5.8-74***) & Projected dry-bulb minimum	6.7	9.2 -1.5+0.5	9.2 -0.5+1.5

© Eskom 2026/Rev 0c

PRINTED VERSIONS OF THIS DOCUMENT ARE NOT CONTROLLED

Meteorological Parameter		Baseline	Climate Change Projections	
			Near-Horizon (2050)	Far Horizon (2100)
	Extreme Observed Cape St Francis (***on page 5.8-74***) & Projected dry-bulb minimum	4.9	7.4 -1.5+0.5	7.4 -0.5+1.5
	10 Year Return	5.0 ± 0.7	6.0 ± 1.1	5.7 ± 1.2
	100 Year Return	3.2 ± 1.2	1.6 ± 1.6	3.8 ± 1.7
	1 000 Year Return	1.3 ± 1.7	-0.2 ± 2.1	2.0 ± 2.2
	10 000 Year Return	-0.5 ± 2.2	-2.0 ± 2.6	0.2 ± 2.7
	100 000 Year Return	-2.3 ± 2.7	-3.8 ± 3.1	-1.6 ± 3.2
	1 000 000 Year Return	-4.1 ± 3.2	-5.6 ± 3.6	-3.4 ± 3.7
	10 000 000 Year Return	-5.9 ± 3.7	-7.5 ± 4.1	-5.2 ± 4.2
	100 000 000 Year Return	-7.7 ± 4.2	-9.3 ± 4.7	-7.0 ± 4.7
	Minimum temperature of 3-hour duration [6] (***on page 5.8-84***)	7.2 Corresponding Wet Bulb Temperature 5.4 ± 0.3	8.9 0.0+0.0	10.5 -0.04+0.2
	Minimum temperature of 6-hour duration [6] (***on page 5.8-84***)	7.7 Corresponding Wet Bulb Temperature 6.0 ± 0.2	9.4 0.0+0.0	11.0 -0.04+0.2
	Minimum temperature of 7-day duration [6] (***on page 5.8-84***)	15.5 Corresponding Wet Bulb Temperature 13.3 ± 0.1	17.2 0.0+0.0	18.8 -0.04+0.2

© Eskom 2026/Rev 0c

PRINTED VERSIONS OF THIS DOCUMENT ARE NOT CONTROLLED

Meteorological Parameter		Baseline	Climate Change Projections	
			Near-Horizon (2050)	Far Horizon (2100)
Rainfall [mm] (0.7 m above site ground level)	Average Annual Total Thyspunt WS (***on page 5.8-88***)	774.4	777.5 -22.73+18.76	762.5 -32.33+6.4
	Average Annual Total Cape St Francis WS (***on page 5.8-88***)	619.5	622.6 -22.73+18.76	607.6 -32.33+6.4
	Extreme Annual Total	972.0	975.1 +18.76 -22.73	960.1 -32.33 +6.4
	Annual Re-occurrences (***on page 5.8-150***)*:*			
	10 Year Return	858.7 ± 84.8	861.8 ± 84.8	846.8 ± 84.8
	100 Year Return	1187.9 ± 147.1	1191.0 ± 147.1	1176.0 ± 147.1
	1 000 Year Return	1511.2 ± 212.2	1514.2 ± 212.2	1499.2 ± 212.2
	10 000 Year Return	1833.8 ± 278.4	1836.9 ± 278.4	1821.9 ± 278.4
	100 000 Year Return	2156.4 ± 345.0	2159.5 ± 345.0	2144.5 ± 345.0
	1 000 000 Year Return	2479.0 ± 412.0	2482.1 ± 412.0	2467.0 ± 412.0
	10 000 000 Year Return	2801.6 ± 479.0	2804.7 ± 479.0	2789.6 ± 479.0
	100 000 000 Year Return	3124.2 ± 546.2	3127.2 ± 546.2	3112.2 ± 546.2
	Extreme 24-hour Storm Thyspunt WS (***on page 5.8-88***)	113.5	124.9 -0.0+11.4	Assume same as Near-Horizon
	Extreme 24-hour Storm Cape St Francis WS	157.8	173.8 -0.0+15.8	Assume same as Near-Horizon
	24-Hour Re-occurrences (***on page 5.8-150***)*:*			
	10 Year Return	99.0 ± 20.8	108.9 ± 20.8	99.0 ± 20.8
	100 Year Return	151.4 ± 38.8	166.6 ± 38.8	151.4 ± 38.8
	1 000 Year Return	202.9 ± 56.8	223.2 ± 56.8	202.9 ± 56.8

© Eskom 2026/Rev 0c

PRINTED VERSIONS OF THIS DOCUMENT ARE NOT CONTROLLED

Meteorological Parameter		Baseline	Climate Change Projections	
			Near-Horizon (2050)	Far Horizon (2100)
	10 000 Year Return	254.3 ± 74.9	279.7 ± 74.9	254.3 ± 74.9
	100 000 Year Return	305.6 ± 93.0	336.2 ± 93.0	305.6 ± 93.0
	1 000 000 Year Return	357.0 ± 111.1	392.7 ± 111.1	357.0 ± 111.1
	10 000 000 Year Return	408.4 ± 129.2	449.2 ± 129.2	408.4 ± 129.2
	100 000 000 Year Return	459.7 ± 147.3	505.7 ± 147.3	459.7 ± 147.3
	Extreme 1-hour Storm	51.9	57.1 0.0+5.2	Assume same as Near-Horizon
Mean Sea Level Atmospheric pressure [hPa]	Daily Minimum (***on page 5.8-100***)	999.1 ± 0.2	Not available (7)	Not available (7)
	Daily Maximum (***on page 5.8-100***)	1037.4 ± 0.2	Not available (7)	Not available (7)
	Extreme Lower (Hourly) (***on page 5.8-100***)	994.1 ± 0.2	Not available (7)	Not available (7)
	Average Annual (***on page 5.8-100***)	1016.3 ± 0.2	Not available (7)	Not available (7)
	Extreme Upper (Hourly) (***on page 5.8-100***)	1040.6 ± 0.2	Not available (7)	Not available (7)

Notes:

(1) Thyspunt WS included 7 years of measurements. The maximum wind speeds were on average 20% lower at the Thyspunt WS than the observations at the Cape St Francis WS (highest wind speed 23.2 m/s)

(2) Extreme analyses were completed using the measurements from the Cape St Francis WS since the database included 19 years of data compared to the 7 years of measurements at the Thyspunt WS. These extremes are biased by the 20% on average higher wind speed observations than at the Thyspunt WS and are likely conservative projections.

(3) Thyspunt WS included 7 years of measurements. The maximum wind speeds were on average 20% lower at the Thyspunt WS than the observations at the Cape St Francis WS (highest gust of 45.8 m/s)

(4) Extreme analyses were completed using the measurements from the Cape St Francis WS since the database included 19 years of data compared to the 7 years of measurements at the Thyspunt WS. The maximum dry bulb temperature extremes are slightly different, i.e. 38.2 °C at Thyspunt WS compared to 38.5°C at the Cape St Francis WS. The minimum dry bulb temperature extremes are more significantly different, i.e. 6.7 °C at Thyspunt WS compared to 4.9 °C at the Cape St Francis WS. The lower temperatures at the Cape St Francis WS therefore provides a more conservative estimate of the minimum temperature return periods.

© Eskom 2026/Rev 0c

PRINTED VERSIONS OF THIS DOCUMENT ARE NOT CONTROLLED

Meteorological Parameter	Baseline	Climate Change Projections	
		Near-Horizon (2050)	Far Horizon (2100)
(5) Wet-bulb temperature projections are not part of the primary meteorological variables provided by the climate change model used in the analyses. The projections provided in the table are based on using the daily minimum, average and maximum temperature projected increases and assuming ±25% variation in the corresponding moisture content. (6) Temperatures of 3-hour, 6- hour and 7-day durations assumed projected temperature increases as per the climate change model. (7) Global climate projections from the ARP5 indicate relatively small changes in the projected mean sea-level atmospheric pressure over South Africa (max seasonal increase of 0.5 hPa in summer and reduction of 0.5 hPa in winter for the far horizon).			

© Eskom 2026/Rev 0c

PRINTED VERSIONS OF THIS DOCUMENT ARE NOT CONTROLLED

Table 5.8.79
Site Specific Parameters Part 2

Meteorological Parameter			Value			
Tornadoes	Tornado Probability (EF - Enhanced Fujita Scale)	Based on 116-year database 1905 - 2020 (***on page 5.8-144***)	All[2]	6.8×10^{-6} per year per km²		
			EF0	1.3×10^{-6} per year per km²		
			EF1	2.1×10^{-6} per year per km²		
			EF2	6.6×10^{-7} per year per km²		
			EF3	$<1.0 \times 10^{-8}$ per year per km²		
			EF4	$<1.0 \times 10^{-8}$ per year per km²		
			EF5	$<1.0 \times 10^{-9}$ per year per km²		
		Based on 25-year database 1996 - 2020 [1] (***on page 5.8-144***)	All[2]	3.2×10^{-6} per year per km²		
			EF0	4.0×10^{-5} per year per km²		
			EF1	2.3×10^{-6} per year per km²		
			EF2 [3]	6.6×10^{-7} per year per km²		
			EF3[3]	$<1.0 \times 10^{-8}$ per year per km²		
			EF4[3]	$<1.0 \times 10^{-8}$ per year per km²		
			EF5[3]	$<1.0 \times 10^{-9}$ per year per km²		
	10^{-7} per year wind speed: - maximum wind speed (***on page 5.8-144***) - maximum translational (***on page 5.8-146***) - maximum rotational (***on page 5.8-146***)		75.0 m/s 15.0 m/s 60.0 m/s			
			Lower Quartile	Upper Quartile	Median	Average
	Path Width [m] (*on page 5.8-145*):					
	EF0 tornado (40% to 64% probability)		22.9	68.6	45.7	54.9
	EF1 tornado (36% to 48% probability)		68.6	182.9	91.4	163.8
	EF2 tornado (0% to 4% probability)		137.2	402.3	228.6	344.1
	EF3 tornado (0% to 4% probability)		339.5	1005.8	548.6	736.3
	Path Length [km] (*on page 5.8-145*):					
	EF0 tornado (40% to 64% probability)		0.29	2.7	0.8	2.27
	EF1 tornado (36% to 48% probability)		1.77	9.33	4.4	7.1
	EF2 tornado (0% to 4% probability)		4.53	19.25	10	14.3
	EF3 tornado (0% to 4% probability)		12.38	36.34	23	29.1
	Pressure drop for 10^{-7} per year wind speed (***on page 5.8-146***)		40 hPa			

© Eskom 2026/Rev 0c

PRINTED VERSIONS OF THIS DOCUMENT ARE NOT CONTROLLED

Meteorological Parameter		Value	
	Maximum rate of pressure drop for 10^{-7} per year wind speed (***on page 5.8-146***)	13 hPa/s	
Atmospheric Turbulence (Sigma-Theta Method) (***on page 5.8-107***)	Convective (A)	3.33%	
	Unstable (B)	1.84%	
	Moderately Unstable (C)	4.88%	
	Neutral (D)	40.89%	
	Moderately Stable (E)	46.14%	
	Stable (F)	2.92%	
	Very Stable (G)	0.01%	
Prolonged Inversions ***(on page 5.8-104***)	Likelihood	Annual	30%
		Summer	19%
		Winter	44%
Snowfall (3) (***on page 5.8-98***)	Average	0.0 mm/h	
	Maximum load	0.0 N/m³	
Lightning (***on page 5.8-148***)	Flashes/year/km²	1.0 flash/year/km² (range 0.02 to 1.0)	
	Average strokes per flash	5	
	Maximum strokes per flash	16	
	Average peak current	25 kA	
	Highest peak current	166 kA	
Thunder (***on page 5.8-98***)	Average number of days with thunder	7.2 days/year	
Hail (***on page 5.8-98***)	Average number of days with hail	0.8 days/year	
Frost (***on page 5.8-98***)	Average number of days with frost	0 days/year	
Fog (***on page 5.8-98***)	Average number of days with fog	25.4 days/year (Thyspunt WS) 24.3 days/year (Cape St Francis WS)	
Relative humidity (***on page 5.8-98***)	Summer (relative humidity at 37 ºC, dry bulb)	17.6% (Thyspunt WS) 14.7% (Cape St. Francis WS)	
	Winter (relative humidity at -25 ºC, dry bulb)	78.8% at 6.6 °C (Thyspunt WS) 81.0% at 4.9 °C (Cape St. Francis WS) Assume 100% at -25ºC	
Solar Radiation	Lowest daily total (***on page 5.8-102***)	8.4 MJ/m².day (June)	
	Highest daily total (***on page 5.8-102***)	26.3 MJ/m².day (January)	
	Monthly Total Minimum	84.8 mm (June)	

© Eskom 2026/Rev 0c

PRINTED VERSIONS OF THIS DOCUMENT ARE NOT CONTROLLED

Meteorological Parameter		Value	
Penman-Monteith Evapotranspiration (***on page 5.8-118***)	Monthly Total Minimum	146.1 mm (January)	
Corrosivity (***on page 5.8-130***)	Rate in 1st year	Carbon steel	68.0 (50.6-81.6) µm/year
		Zinc	2.8 (2.2-3.4) µm/year
		Copper	1.8 (1.5;1.9) µm/year
		Aluminium	1.0 (0.7;1.2) µm/year
	Average rate over 20 years	Carbon steel	8.8 to 11.1 µm/year
		Zinc	1.3 to 1.6 µm/year
		Copper	0.4 to 0.5 µm/year
		Aluminium	0.3 to 0.4 µm/year

Notes:

(1) Tornado activity has increased since 1987 within an 80 km radius from the site. Whilst climate change may have contributed to increases in tornado frequencies, it may also simply be that the reporting of tornadoes has increased due to population spread as well as the associated damage to property.

(2) The “All” tornado entry combines all frequencies from EF0 to EF4 in the table.

(3) No tornadoes of strength higher than EF2 were observed during the last 34 years of reporting and therefore assumed the same values as for the long-term analysis.

(4) This reflects current observation; however extreme minimum temperatures (excluding climate change projections) indicate temperatures well below freeze point for water and may result in the occurrence of snow at the site.

© Eskom 2026/Rev 0c

PRINTED VERSIONS OF THIS DOCUMENT ARE NOT CONTROLLED

5.8.13 References

1. Ackerman, S. A. & Cox, S. K., 1989. Surface weather observations of atmospheric dust over the Southwest Summer Monsoon Region. *Meteorology and Atmospheric Physics,* Volume 41, pp. 19-34.
2. Alduchov, O. A. & Eskridge, R. E., 1996. Improved Magnus Form Approximation of Saturation Vapor Pressure. *J. Appl. Meteor.,* Volume 35, pp. 601-609.
3. American National Standard, 2015. *Determining Meteorological Information at Nuclear Facilities, American Nuclear Society, ANSI/ANS-3.11-2015.,* s.l.: American National Standard.
4. AS/NZ, 2021. *Australian/New Zeeland Standard for Structutal Design Actions Part 2: Wind Actions (AZ/NZ1170.2:2021),* s.l.: Jointly Published by Standards Australia International Ltd and Standards New Zeeland.
5. ASCE/SEI_7-10, 2013. *Minimum Design Loads for Buildings and Other Structures,* New York: American Society of Civil Engineers /Structural Engineering Standard.
6. Baddock, M. C. et al., 2014. A visibility and total suspended dust relationship. *Atmospheric Environment,* Volume 89, pp. 329-336.
7. Barry, N. T. & Kuyatt, C. E., 1994. *Guidelines for Evaluating and Expressing the Uncertainty of NIST Measurement Results, NIST Technical Note 1297,* Githersburg: , National Institute of Standards and Technology, United States Department of Commerce Technology Administration.
8. Burger, L., 2019. *Corrosion Monitoring Using ISO 9226 Method at Thyspunt Weather Station: 2008-2013 & 2017-2019 Database Archive,* Cape Town: s.n.
9. Burger, L. W., 2024. *VERIFICATION AND VALIDATION: Numerical Atmospheric Dispersion Model - Thyspunt Site Safety Report Update,* Halfway House: Airshed Planning Professionals.
10. Cadman, R. J. & Peerce, A. R., 1987. *Meteorological Monitoring Along Cape S E Coast during August 1987, TRR/N87/026; Meteorological Monitoring Along Cape S E Coast during September 1987, TRR/N87/026,* Kohannesburg: Eskom.
11. Chepil, W. S. & Woodruff, N. P., 1957. Sedimentary characteristics of dust storms: II. Visibility and dust concentration. *American Journal of Science,* Volume 255, pp. 104-114.

© Eskom 2026/Rev 0c

PRINTED VERSIONS OF THIS DOCUMENT ARE NOT CONTROLLED

12. Cimorelli, A. J. et al., 2004. *AERMOD: Description of Model Formulation, EPA-454/R-03-004,* Research Triangle Park, NC: U.S. Environmental Protection Agency.
13. Clemence, B. S. E., 1992. An Attempt at Estimating Solar Radiation at South African Sites Which Measure Air Temperature Only.. *South African Journal of Plant and Soil,* pp. 9, 40-42.
14. Coppin, P. A., Bradley, E. F. & Finnigan, J. J., 1994. Measurements of Flow Over an Elongated Ridge and Its Thermal Stability Dependence: The Mean Field. *Boundary-Layer Meteorology,* Volume 69, pp. 173-199.
15. CSIR, 2019. *"Climate Change: Detailed projections of future climate change over South Africa." In GreenBook National Overview..* [Online] Available at: https://pta-gis-2-web1.csir.co.za/portal/apps/GBCascade/index.html?appid=b161b2f892194ed5938374fe2192e537 [Accessed 26-29 March 2024].
16. Department of Energy, 2011. *R.927: National Nuclear Regulator Act, 1999 (Act No. 47 OF 1999): Regulations on Licensing of Sites for New Nuclear Installations.* Pretoria: Government Gazette 34735.
17. Elsner, J. B., Jagger, T. H. & Elsner, I. J., 2014. Tornado Intensity Estimated from Damage Path Dimensions. *PLOS One,* 9(9), pp. 1-7.
18. Engelbrecht, F. et al., 2019. *Climate Change Vulnerability Projections at Ultrahigh Spatial Resolutions (8 km) over South Africa, Eskom Confidential Research Report No. RES/RR/15/1780145.,* Johannesburg: Eskom.
19. Eskom, 2014. *Technical Specifications for the Development of Site Safety Reports. NSIP01388. Rev 1.,* Johannesburg: Eskom.
20. Eskom, 2022a. *Meteorological Requirements for Nuclear Installations. Standard 238-52,* Cape Town: Eskom.
21. Eskom, 2022b. *Plant Parameter Envelope for Nuclear Installations, NSIP03179.* Johannesburg: Eskom.
22. Eskom, 2022c. *Technical Specification for Site Safety Reports. Meteorology,* Johannesburg: Eskom.
23. Eskom, 2023a. *Electronic Hourly Average Thyspunt Weather Station Microsoft Database: 2008- 2013 & 2017-2019,* Cape Town, SRK Database Archive, Cape Town: s.n: Eskom.
24. Ette, I. I. I. & Olorode, D. O., 1988. The effects of the Harmattan dust on air conductivity and visibility at Ibadan, Nigeria. *Atmospheric Environment,* Volume 22, pp. 2625-2627.

© Eskom 2026/Rev 0c

PRINTED VERSIONS OF THIS DOCUMENT ARE NOT CONTROLLED

25. Forthofer, J. M., Butler, B. W. & Wagenbrenner, N. S., 2014. A comparison of three approaches for simulating fine-scale winds in support of wildland fire management Part I: Model formulation and accuracy. *Int. J. Wildland Fire,* Volume 23, pp. 969-981.

26. Gifford, F. A., 1961. Uses of Routine Meteorological Observations for Estimating Atmospheric Dispersion. *Nuclear Safety,* Volume 2, pp. 547-51.

27. Gijben, M., 2021. *The South African Lightning Detection Network: MTG LI Mission Advisory Group Meeting, South African Weather Service..* [Online]
Available at: https://www.eumetsat.int/media/47898/The South African Lightning Detection Network.pdf
[Accessed 20 February 2021].

28. Gill, T., 2009. *Initial Steps in the Development of a Comprehensive Lightning Climatology of South Africa.* Johannesburg: Master of Science Thesis, University of the Witwatersrand, School of Geography, Archaeology and Environmental Studies: Climatology Research Group.

29. Goliger, A. M., Milford, R. V., Adam, B. F. & Edwards, M., 1997. *Inkanyamba - Tornadoes in South Africa.* Pretoria: United Litho.

30. Goliger, A. M. & Retief, J. V., 2002. Identification of Zones of Strong Wind Events in South Africa. *Journal of Wind Engineering and Industrial Aerodynamics,* Volume 90, pp. 1227-1235.

31. Greer, I. W., 1996. *Glossary of Weather and Climate with Related Oceanic and Hydrologic Terms..* Boston: American Meteorological Society.

32. Gross, C. J. & Nixon, M., 1993. *Review of Corrosion Data for the Proposed Nuclear Sites on the Eastern, Southern and Western Cape Coasts. Eskom Report No. TRR/S93/091, Project No. 7762M168U/089,* Johannesburg: Section: Materials Technology, Department: Scientific invest.

33. Guo, J. et al., 2022. Damage Mechanism and Modeling of Concrete in Freeze–Thaw Cycles: A Review.. *Buildings 2022,* Volume 12, p. 1317.

34. Hanna, S. R., Egan, B. A., Purdum, J. & Wagler, J., 1999. Evaluation of the ADMS, AERMOD, and ISC3 Dispersion Models with the Optex, Duke Forest, Kincaid, Indianapolis, and Lovett Field Data Sets. *International Journal of Environment and Pollution,* 16(1-6), p. 2001.

35. Herbst, L. & Rautenbach, H., 2015. Climate Change Impacts on Mean Wind Speeds in South Africa. *The Clean Air Journal,* 25(2).

36. Hsu, S. A., 1977. Boundary Layer Meteorological Research in the Coastal Zone,. *Geoscience and Man, H. J. Walker, ed., School of*

© Eskom 2026/Rev 0c

PRINTED VERSIONS OF THIS DOCUMENT ARE NOT CONTROLLED

Geoscience, Louisiana State University, Baton Rouge, LA, Volume 18, pp. 99-111.

37. Intergovernmental Panel on Climate Change, 2012. *Managing the Risks of Extreme Events and Disasters to Advance Climate Change Adaptation. A Special Report of Working Groups I and II of the Intergovernmental Panel on Climate Change ,* Cambridge, UK and New York, USA: Cambridge University Press.
38. Intergovernmental Panel on Climate Change, 2013. *Climate Change 2013: The Physical Science Basis. Contribution of Working Group I to the Fifth Assessment Report of the Intergovernmental Panel on Climate Change,* Cambridge, UK, and New York, NY, USA: Cambridge University Pres.
39. International Atomic Energy Agency, 2001. *Generic Models for Use in Assessing the Impact of Discharge of Radioactive Substances to the Environment. Safety Report Series No. 19.,* Vienna: International Atomic Energy Agency.
40. International Atomic Energy Agency, 2002. *Dispersion of Radioactive Material in Air and Water and Consideration of Population Distribution in Site Evaluation for Nuclear Power Plants. Safety Standards Series, Safety Guide. No.NS-G-3.2,* Vienna: International Atomic Energy Agency.
41. International Atomic Energy Agency, 2011. *Meteorological and Hydrological Hazards in Site Evaluation for Nuclear Installations, Safety Standard Series, Specific Safety Guide No. SSG-18,* Vienna: International Atomic Energy Agency.
42. International Atomic Energy Agency, 2019. *Site Evaluation for Nuclear Installations. Safety Standard Series, Specific Safety Requirements No. SSR-1,* Vienna: International Atomic Energy Agency.
43. International Atomic Energy Agency, 2021. *Design of Nuclear Installations Against External Events Excluding Earthquakes. Safety Standards Series, Specific Safety Guide No. ssg-68,* Vienna: International Atomic Energy Agency.
44. International Organisation for Standardisation, 2012a. *ISO 9223 (2012), Corrosion of Metals and Alloys-Corrosivity of Atmospheres – Guiding Values for the Corrosivity Categories. 2nd Edition,* Geneva: International Organisation for Standardisation.
45. International Organisation for Standardisation, 2012b. *ISO 9224 (2012), Corrosion of Metals and Alloys-Corrosivity of Atmospheres - Guiding Values for the Corrosivity Categories. 2nd Edition.* Geneva: International Organisation for Standardisation.

© Eskom 2026/Rev 0c

PRINTED VERSIONS OF THIS DOCUMENT ARE NOT CONTROLLED

46. International Organisation for Standardisation, 2012c. *ISO 9225 (2012), Corrosion of Metals and Alloys-Corrosivity of Atmospheres - Measurement of Pollution. 2nd Edition,* Geneva: International Organisation for Standardisation.

47. International Organisation of Standardisation, 2012d. *ISO 9226 (2012), Corrosion of Metals and Alloys-Corrosivity of Atmospheres - Determination of Corrosion Rate of Standard Specimens for the Evaluation of Corrosivity. 2nd Edition,* Geneva: International Organisation of Standardisation.

48. International Organisation of Standardisation, 2017. *ISO 17025 (2017), General Requirements for the Competence of Testing and Calibration Laboratories,* Geneva: International Organisation of Standardisation.

49. Johnston, P., 1983. *Variations in Albedo Among Natural and Disturbed South Western Cape Veld Types, Research Report No.46,* Cape Town: School of Environmental Studies, University of Cape Town.

50. Kruger, A. C. & Nxumalo, M. P., 2017. Historical rainfall trends in South Africa: 1921–2015. *Water SA,* 43(2), pp. 285-297.

51. Kruger, A. C. & Nxumalo, M., 2016. Surface Temperature Trends from Homogenized Time Series in South Africa: 1931–2015. *International Journal of Climatology,* 37(5), pp. 2364-2377.

52. Lennard, C. J., Pinto, I. & Nyak, M., 2016. *Investigating Projected Changes in the Nature of Extreme Rainfall Over South Africa During the 21st Century Through an Assessment of Their Associated Synoptic Environments, WRC Report No. 2240/1/15,* Cape Town: Water Reasearch Commission.

53. Lubitz, W. D. & White, B. R., 2007. Wind-tunnel and field investigation of the effect of local wind direction on speed-up over hills. *Journal of Wind Engineering and Industrial Aerodynamics,* Volume 95, pp. 639-661.

54. Malan,, D. J., 1956. The Relation Between the Number of Strokes, Stroke Interval and the Total Duration of Lightning Discharges. . *Geofisica, Pura e Applicalo Milan,* Volume 34, pp. 224-230.

55. Marticorena, B. & Bergametti, G., 1995. Modelling the Atmospheric Dust Cycle: 1. Design of a Soil-Derived Dust Emission Scheme. *Journal of Geophysical Research,* Volume 100, pp. 16415-16430.

56. McBride, C. M., Kruger, A. C. & Dyson, L., 2022. Changes in extreme daily rainfall characteristics in South Africa: 1991-2020. *Weather and Climate Extremes,* Volume 38.

© Eskom 2026/Rev 0c

PRINTED VERSIONS OF THIS DOCUMENT ARE NOT CONTROLLED

57. McDonald, J. & Mehta, K. C., 2006. *A Recommendation for an Enhanced Fujita Scale (EF-Scale)..* Texas: Lubbock, Texas: Wind Science and Engineering Research Center, Texas Tech University.

58. Mzukisi, G. & Mkhwanazi, M., 2010. *South African Weather Service Database* [Interview] 2010.

59. National Nuclear Regulator, 2008. *RD-0034: Quality and Safety Management Requirements for Nuclear Installations. Rev 0,* Centurion: National Nuclear Regulator.

60. National Nuclear Regulator, 2012a. *Consideration of External Events for New Nuclear Installations, Position Paper PP-0014, Rev 0,* Centurion: National Nuclear Regulator.

61. National Nuclear Regulator, 2012b. *Emergency Planning Technical Basis For New Nuclear Installations, Position Paper PP-0015, Rev 0,* Centurion: National Nuclear Regulator.

62. National Nuclear Regulator, 2016a. *Interim Guidance for the Siting of Nuclear Facilities, Regulatory Guide RG-0011 Rev0,* Centurion: National Nuclear Regulator.

63. National Nuclear Regulator, 2016b. *Guidance on the Verification and Validation of Evaluation and Calculation Models used in Safety and Design Analyses, Regulatory Guide RG-0016, Rev 0,* Centurion: National Nuclear Regulator.

64. NDMC, 2021. *Standardized Precipitation Index (SPI), Integrated Drought Management Programme.* [Online] Available at: https://drought.unl.edu/droughtmonitoring/SPI/SPIProgram.aspx

65. Ngo, T. T. & Letchford, C. W., 2007. Experimental study of topographic effects on gust wind speeds. *12th International Conferences on Wind Engineering (ICWE12), Australia,* pp. 1143-1150.

66. Pasquill, F., 1961. The Estimation of the Dispersion of Windborne Materials.. *Meteorological Magazine,* Volume 90.

67. Patterson, E. M. & Gillette, D. A., 1977. Measurements of visibility vs mass of airborne soil particles. *Atmospheric Environment,* Volume 11, pp. 193-196.

68. Peerce, A. R., 1988a. *Meteorological Monitoring Along Cape S E Coast during May 1988, TRR/N88/023; Meteorological Monitoring Along Cape S E Coast during June 1988, TRR/N88/036; Meteorological Monitoring Along Cape S E Coast during July 1988, TRR/N88/035,* Johannesburg: Eskom.

69. Peerce, A. R., 1988b. *Meteorological Monitoring Along Cape S E Coast during August 1988, TRR/N88/040,* Johannesburg: Eskom.

© Eskom 2026/Rev 0c

PRINTED VERSIONS OF THIS DOCUMENT ARE NOT CONTROLLED

70. Penman, H. L., 1948. Natural Evaporation from open Water, Bare and Grass.. *Proc. R. Soc. Lond., Ser. A 193,* , pp. 120-145.

71. Penman, H. L., 1963. *Vegetation and Hydrology. Technical Communication no. 53,* Harpenden, England: Commonwealth Bureau of Soils.

72. Perry, S. G. et al., 2004. AERMOD: A Dispersion Model for Industrial Source Applications. Part II: Model Performance Against 17 Field Study Databases. *Journal of Applied Meteorology,* Volume 44, pp. 694-708.

73. Preston-Whyte, R. A., Diab, R. D. & Tyson, P. D., 1977. Towards an Inversion Climatology of Southern Africa: Part II, Surface Inversions.. *South African Geographical Journal,* pp. 59(1), 45-59.

74. Preston-Whyte, R. A. & Tyson, P. D., 1988. *The Atmosphere and Weather over South Africa..* Cape Town: Oxford University Press.

75. Rakov, V. A., 2007. *Lightning Phenomenology and Parameters Important for Lightning Protection.* Foz do Iguaçu, Brazil, IX International Symposium on Lightning Protection 26-30 November 2007.

76. Rakov, V. A. & Huffines, G. R., 2003. Return Stroke Multiplicity of Negative Cloud-to-Ground Lightning Flashes. *J. App. Meteor.,* Volume 42, pp. 1455-1462.

77. Ramsdell, J. V.,Jr; Rishel, J. P., 2007. *Tornado Climatology of the Contiguous United States, NUREG/CR-4461, Rev 2,* Washington: U.S. Nuclear Regulatory Commission.

78. Riahi, K., Grübler, A. & Nakicenovic, N., 2007. Scenarios of Long-Term Socio-Economic and Environmental Development Under Climate Stabilization. *Technol Forecast Soc Chang,* Volume 74, p. 887–935.

79. SAWS, 1991. *Caelum - A History of Notable Weather Events in South Africa 1550 – 1990,* Pretoria: SA Weather Service Publication.

80. SAWS, 2020. *Trends in Extreme Climate Indices in South Africa: 2019, Document Reference: WCS-CLS-WMO_EXTREME_CLIMATE_INDICES_2019.1, Ver. 01,* Pretoria: South African Weather Services.

81. SAWS, 2024a. *Electronic Hourly Average Cape St Francis Weather Station Microsoft Database: 2004- 2023,* Pretoria: South African Weather Services.

82. SAWS, 2024b. *Annual Rainfall Measurement for Humansdorp 1985 to 2003,* Pretoria: South African Weather Services.

83. SAWS, 2024c. *Rainfall Measurement for Humansdorp 2004 to 2023,* Pretoria: South African Weather Services.

© Eskom 2026/Rev 0c

PRINTED VERSIONS OF THIS DOCUMENT ARE NOT CONTROLLED

84. SAWS, 2024d. *Caelum - A History of Notable Weather Events in South Africa 1991 – 2023,* Pretoria: South African Weathr Services.

85. Schonland, B. F. J., 1956. The Lightning Discharge. *Handbuch, der Physik (Springer - Verlag OHG, Berlin),* Volume 22, pp. 576-628.

86. Schulze, B., 1986. *Climate of South Africa, WB 40..* Pretoria: Weather Bureau, Department of Transport.

87. Schulze, R. E., 1997. *South African Atlas of Agrohydrology and Climatology..* Pietermaritzburg: Department of Agriculture and Engineering, University of Natal.

88. Schulze, R. E., 2011. *A 2011 Perspective on Climate Change and The South African Water Sector, Report TT518/12,* Pietermaritzburg: Water Research Commission..

89. Seidel, D. J., Fu, Q., Randel, W. J. & Reichler, T., 2008. Widening of the Tropical Belt in a Changing Climate. *Nat Geosci.,* Volume 1, pp. 21-24.

90. Shuttleworth, W., 1993. Chapter 4. In: D. Maidment, ed. *Evaporation.* New York: McGraw-Hill, p. pp. 4.1–4.53 .

91. Smithers, J. C. & Schulze, R. E., 2000. *Long Duration Design Rainfall Estimates for South Africa,* Pretoria: Report No. 811/100, Water Research Commission.

92. South African National Standards, 2019. *SANS 10160-3:2019 Basis of Structural Design and Actions for Buildings and Industrial Structures, Part 3: Wind Actions,* Pretoria: South African Bureau of Standards.

93. South African Weather Service, 2017. *A Climate Change Reference Atlas: Based on CMIP5 – CORDEX Downscaling,* Pretoria: South African Weather Service.

94. Stull, R., 1997. *An Introduction to Boundary Layer Meteorology. Kluwer.* Amsterdam: Academic Publishers.

95. Stull, R., 2011. Wet-Bulb Temperature from Relative Humidity and Air Temperature. *American Meteorological Society,* 50(November), pp. 2267-2269.

96. Tim, N., Hünicke, B. & Zorita, E., 2023. Simulated rainfall extremes over southern Africa over the 20th and 21st centuries. *Natural Hazards and Earth System Sciences. [preprint], https://doi.org/10.5194/nhess-2023-147.*

97. Tosen, G. R., Cadman, R. J. & Peerce, A. R., 1987a. *Meteorological Monitoring Along Cape S E Coast during January 1987, TRR/N87/005; Meteorological Monitoring Along Cape S E Coast during March 1987, TRR/N87/011 Meteorological Monitoring Along Cape S E Coast during April 1987, TRR/N87/016,* Johannesburg: Eskom.

© Eskom 2026/Rev 0c

PRINTED VERSIONS OF THIS DOCUMENT ARE NOT CONTROLLED

98. Tosen, G. R., Cadman, R. J. & Peerce, A. R., 1987b. *Meteorological Monitoring Along Cape S E Coast during May 1987, TRR/N87/020; Meteorological Monitoring Along Cape S E Coast during July 1987, TRR/N87/025,* Johannesburge: Eskom.

99. Tyson , P. D., Preston-Whyte, R. A. & Diab, R. D., 1976. Towards an Inversion Climatology of Southern Africa: Part I, Surface Inversions.. *South African Geographical Journal,* Volume 58, pp. 151-163.

100. United States Environmental Protection Agency , 1992. *Fugitive Dust Background Document and Technical Information Document for Best Available Control Measures, EPA-450/2-92-004,* Springfield, VA: U.S. Department of Commerce.

101. United States Environmental Protection Agency, 2000. *Meteorological Monitoring Guidance for Regulatory Modeling Applications. Office of Air Quality Planning & Standards, EPA-454/R-99-005,* Durham: United States Environmental Protection Agency.

102. United States Nuclear Regulatory Commission, 1983. *Atmospheric Dispersion Models for Potential Accident Consequence Assessments at Nuclear Power Plants. Regulatory Guide. 1.145, Rev 1,* Washington DC: United States Nuclear Regulatory Commission.

103. United States Nuclear Regulatory Commission, 2007a. *NUREG-0800, Section 2.3.1 (Regional Climatology), 2.3.2 (Local Meteorology), 2.3.3 (Onsite Meteorological Measurements Programs) and 2.3.4 (Shortterm Dispersion Estimates for Accident Releases) Rev 3,* Washington DC: United States Nuclear Regulatory Commission.

104. United States Nuclear Regulatory Commission, 2007b. *Design Basis Tornado and Tornado Missiles for Nuclear Power Plants. Regulatory Guide. 1.76, Rev 1,* Washington DC: United States Nuclear Regulatory Commission.

105. United States Nuclear Regulatory Commission, 2007c. *Meteorological Monitoring Programs for Nuclear Power Plants, Regulatory Guide. 1.23, Rev 1,* Washington DC: United States Nuclear Regulatory Commission.

106. United States Nuclear Regulatory Commission, 2011. *Design-Basis Hurricane and Hurricane Missiles for Nuclear Power Plants, Regulatory Guide. 1.221, Rev 1.,* Washington DC: United States Nuclear Regulatory Commission.

107. Vamsidhar , V. P., Kumar, A. & Kadiyala, A., 2010. Estimation of Uncertainty in Predicting Ground Level Concentrations from Direct Source Releases in an Urban Area Using the USEPA's AERMOD Model Equations. In: A. Kumar, ed. *Air Quality.* s.l.:Intech.

© Eskom 2026/Rev 0c

PRINTED VERSIONS OF THIS DOCUMENT ARE NOT CONTROLLED

108. Wagner, W. & Pruss, A., 1993. International Equations for the Saturation Properties of Ordinary Water Substance. Revised According to the International Temperature Scale of 1990.. *Journal of Physical and Chemical Reference Data,* 22(No. 3), pp. 783-787.

109. Walder, J. & Hallet , B., 1985. A theoretical model of the fracture of rock during freezing. *Geol Soc Am Bull ,* Volume 96, p. 336–346.

110. Wieranga, J., 1996. Does representative wind information exist?. *Journal of Wind Engineering and Industrial Aerodynamics,* Volume 65, pp. 1-2.

111. WMO, 1987. *The Measurement of Routine Wind Stations: A Review (A.C.M Beljaars).nstruments and Observing Methods,* Geneva: World Meteorological Organization.

112. WMO, 2018. *Guide to Meteorological Instruments and Methods of Observation, (the CIMO Guide) Report No. 8,* Geneva: World Metoerological Organization.

113. World Meteorological Organisation, 2011. *Guide to Climatological Practices, WMO-No. 100,* Geneva: World Meteorological Organisation.

114. World Meteorological Organization, 2012. *Standardized Precipitation Index User Guide, WMO-No. 1090,* Geneva, Switzerlad: World Meteorological Organization.

115. Wright, M. A. & Grab, S. W., 2017. Wind Speed Characteristics and Implications for Wind Power Generation: Cape Regions, South Africa. *South African Journal of Science,* 113(7/8).

116. Yang, T., Nadimpalli, K. & Cechet, R. P., 2014. *Local wind assessment in Australia: computation methodology for wind multipliers, Record 2014/33,* Canberra: Geoscience Australia (http://dx.doi.org/10.11636/Record.2014.033).

© Eskom 2026/Rev 0c

PRINTED VERSIONS OF THIS DOCUMENT ARE NOT CONTROLLED

Appendix 5.8.A: Thyspunt Weather Station Location

As stated in ***Subsection 5.8.2***, the purpose of ***Section 5.8*** of the SSR is to:

1. provide baseline information for site evaluation and this SSR that will be updated over the life cycle of the nuclear installation(s);
2. confirm the suitability of the site through the identification of external meteorological events and potential hazards for the nuclear installation(s);
3. develop the atmospheric structure (including wind and turbulent fields) to enable atmospheric dispersion predictions necessary for the assessment of potential radiological impact to the public and the environment and the evaluation of the feasibility of the emergency planning;
4. define the local air quality with specific reference to corrosion potential.

The purpose has therefore identified the requirements to both (a) determine the local impact that the weather may have on the nuclear installation(s) (points 1, 2 and 4 above) and (b) establish the wind and turbulent fields over a local to regional scale for the purposes of predicting the dispersion of air emissions from the nuclear installation(s) (point 3). For first requirement the aim is therefore to measure the meteorological parameters at a location as close as possible to the proposed installation, whereas the latter requirement needs the measurement of the meteorology (especially wind flow parameters speed, direction, and fluctuation) at both a local and regional scales. The requirement of local measurements with the latter is primarily to assist in establishing the initial dispersion conditions that would be experienced by a release from the nuclear installation(s). The design of the nuclear installation has not yet been selected and in the absence of a selected plant design, Eskom has given priority to completing this SSR for the site using a plant parameter envelope (Eskom, 2022b). Although the heights of release points have not been established, typical release heights may vary from 0 m to about 100 m above ground level (agl).

Valley Flow and Land/Sea Breeze Interactions

The differential heating of slopes can potentially give rise to anabatic (up-valley) flow during the day and katabatic (down-valley) flow during the night. In order to compensate for the valley flow, a return current

© Eskom 2026/Rev 0c

PRINTED VERSIONS OF THIS DOCUMENT ARE NOT CONTROLLED

develops above the near-surface flows known as the 'anti-wind' (***Figure 5.8.A.1***). A third distinct layer then completing the valley circulation is the gradient wind just above the anti-wind (Stull, 1997). Such winds can potentially develop into a down-valley wind during the night since cold descending air accumulates within the valley with the upper slopes remaining warmer. This results in a layer of warm air above cooler air which in turn creates a valley inversion. The warmer air migrates upslope until the colder air completely covers the valley.

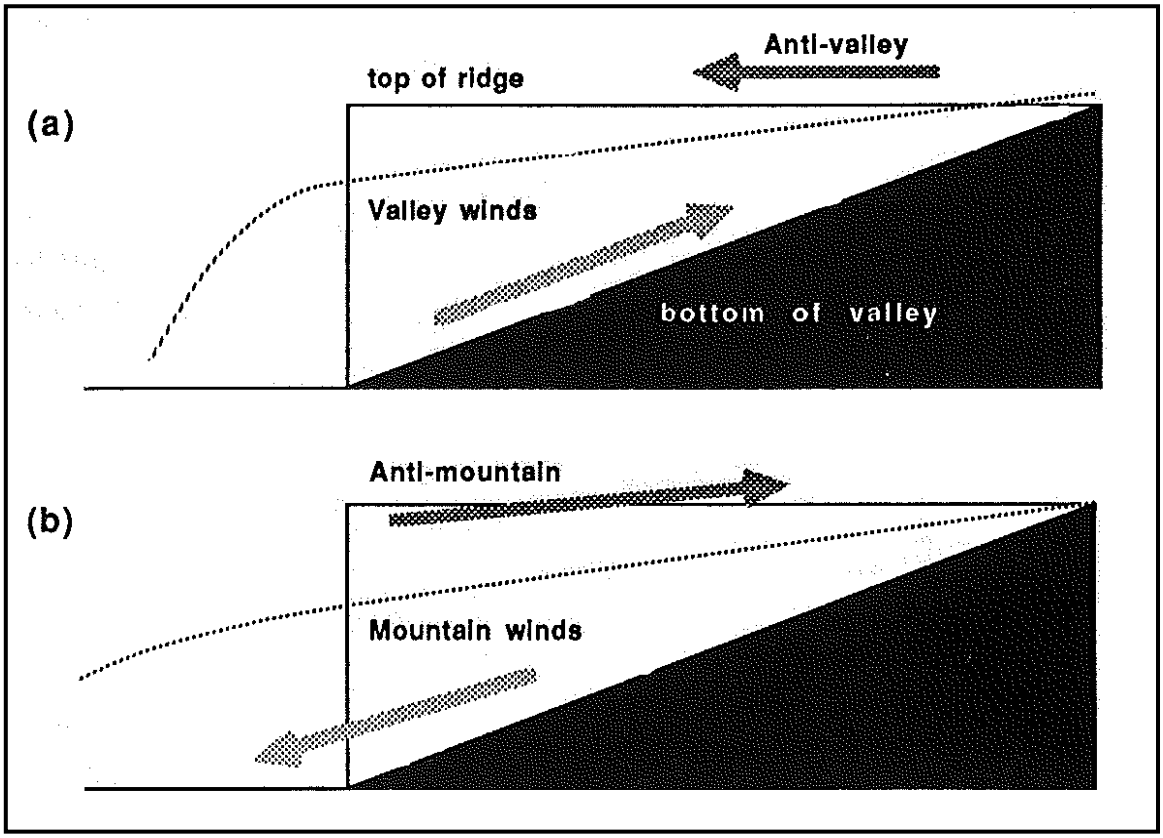


Figure 5.8.A.1
Differential Heating of Slopes (Stull, 1997)

Thus, the valley inversion occurs from the ground upwards, replacing the turbulent mixing layer and resulting in low level stability (Stull, 1997) (***Figure 5.8.A.2***). Therefore, with reference to ***Figure 5.8.A.3***, these conditions may occur as winds flowing down the slopes and following the valley floor towards the coastline, i.e. north-westerly wind flows.

Similarly, during day-time conditions, surface heating of the valley due to incoming solar radiation results in low-level mixing and anabatic flow up the valley sides. The subsiding air in turn heats adiabatically as the valley inversion subsides until a well-mixed atmosphere fills the valley

© Eskom 2026/Rev 0c

PRINTED VERSIONS OF THIS DOCUMENT ARE NOT CONTROLLED

(Stull, 1997). This may potentially also result in winds flowing up the slopes and valley floor, i.e. south-easterly wind flows.

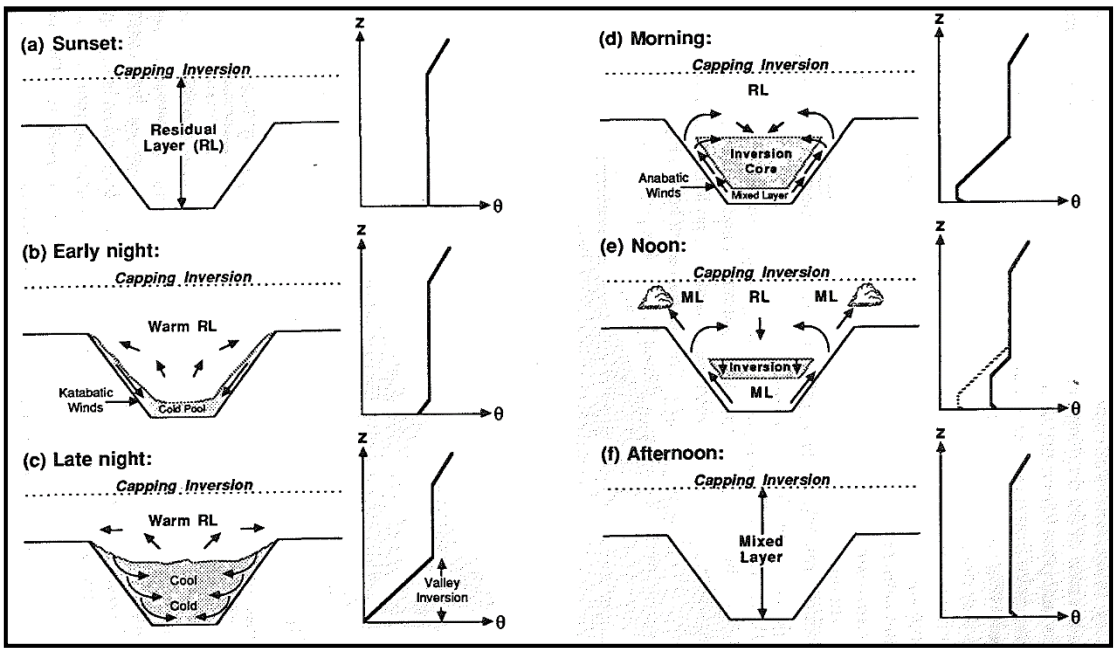


Figure 5.8.A.2
Idealised Evolution of the Cross-Valley Circulations during a Diurnal Cycle (Stull, 1997)

Two profiles were selected at the site (***Figure 5.8.A.3***) for illustration. Topographical Profile 1 and Profile 2 are provided in ***Figure 5.8.A.4*** and ***Figure 5.8.A.5***, respectively. The meteorological station at the site is located at position 'A' in Profile 2. These profiles were selected to illustrate the significance of the valley depths. Both profiles run approximately perpendicular to the valley directions (from west-northwest to east-southeast).

Due to the position of the meteorological station, the meso-scale (large-scale) flow field will not be influenced by mountain and valley flows as the monitor is not located within the valley. However, based on the wind roses, some of the anabatic and katabatic flows were observed (see ***Figures 5.8.3*** to ***5.8.6***). The frequency of northerly and north-westerly winds (katabatic flow) increases during the night-time, whereas the southerly and south-easterly winds (anabatic flow) increase during the daytime. The latter may also be influenced by the land-sea breeze flow patterns.

© Eskom 2026/Rev 0c

PRINTED VERSIONS OF THIS DOCUMENT ARE NOT CONTROLLED

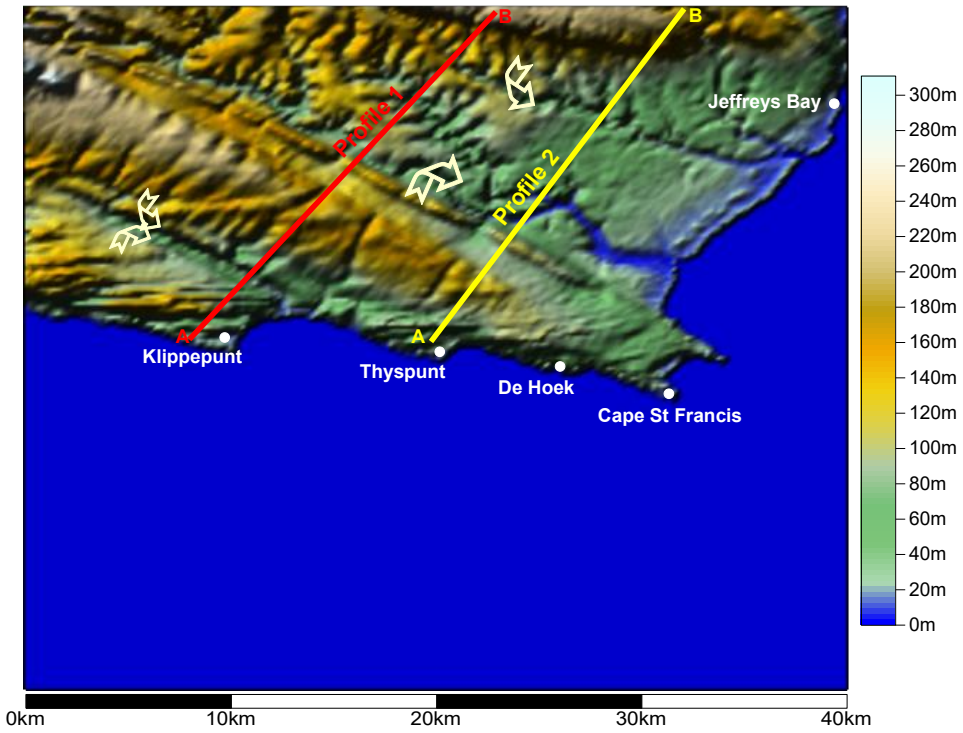


Figure 5.8.A.3
Topographical Profiles Selected Within the Thyspunt Study Area

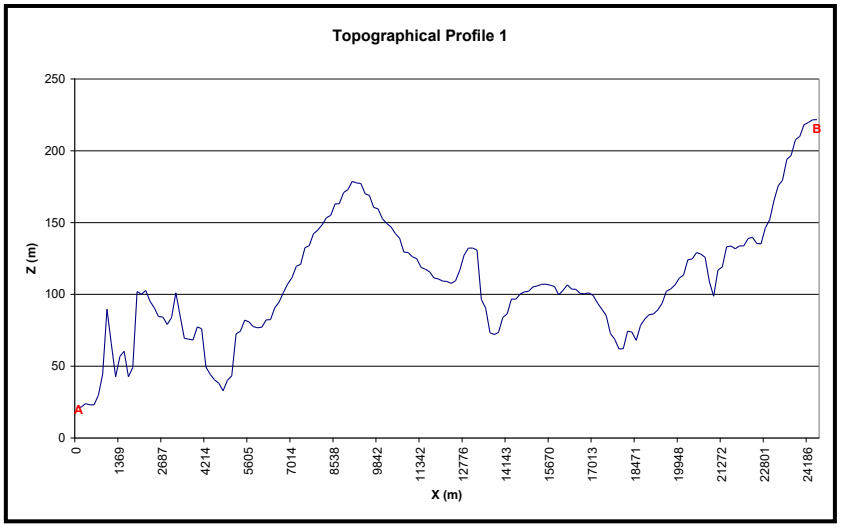


Figure 5.8.A.4
Topographical Profiles 1 (see *Figure 5.8.A.3*)

© Eskom 2026/Rev 0c

PRINTED VERSIONS OF THIS DOCUMENT ARE NOT CONTROLLED

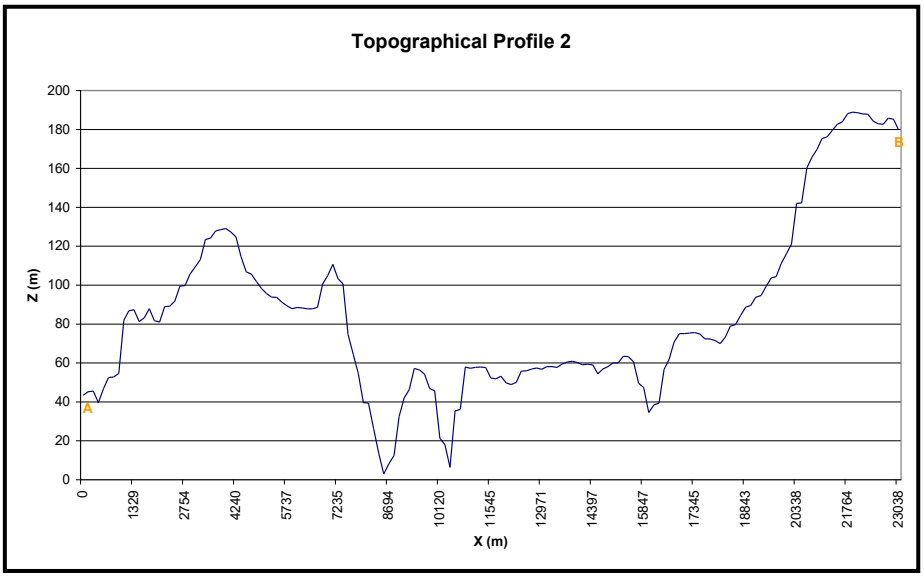


Figure 5.8.A.5
Topographical Profiles 2 (see *Figure 5.8.A.3*)

Impact of Dunes on Wind Field Measurements

Wind speed increases with height above ground level, and this increase typically follows a logarithmic profile in the lowest layer (surface layer, SL) of the atmospheric boundary layer (ABL). The shape of the profile varies according to the local atmospheric stability conditions. So, for instance, under unstable conditions (typically low winds, calm daytime conditions), the wind profile corresponds to plug flow thereby observing a sharp rise in the wind speed at low heights, followed by a fairly constant wind speed with increasing heights. Under stable conditions (typically low winds, calm nighttime conditions), the wind speed increases more gradually with height. Air temperature profiles are similarly logarithmic in the SL.

For the purposes of determining wind loads at different building/structure heights and dispersion of atmospheric releases, direct measurement of meteorological parameters would be ideal. Such measurements can be done using a tall mast with an array of instruments located at increasing heights on the mast, or with sounding devices such as Doppler acoustic sounders (DAS) or atmospheric lidar instruments.

Figure 5.8.A.6 and ***Figure 5.8.A.7*** illustrate the elevation profile through the location of the weather station at Thyspunt. The weather station base is located at an elevation of 51 m amsl, approximately 760 m from the shoreline. The topography from the east to the west is characterised by a gradual rise which reaches a peak of about 70 m amsl at a horizontal distance of about 900 m west of the weather station. Similarly, the

© Eskom 2026/Rev 0c

PRINTED VERSIONS OF THIS DOCUMENT ARE NOT CONTROLLED

topography from south to north is characterised by a rise in the elevation inland from the beach. The elevation reaches about 100 m at a horizontal distance of about 2 km from the shoreline. Whilst there is a gradual rise in elevation from the shoreline to the location of the weather station, the increase in elevation further north only starts at about 700 m from the weather station. The horizontal distance from the weather station to a level half the height below the crest (25.5 m) is estimated to be about 300 m south and 1130 m east. This corresponds to a slope of 8.5 per cent south to north, and 3.1 per cent east to west, respectively. Normally, a slope of less than 10 per cent (ASCE/SEI_7-10, 2013) or more conservatively, 5 per cent (AS/NZ, 2021) would not be regarded significant enough to consider for correction of the wind speed.

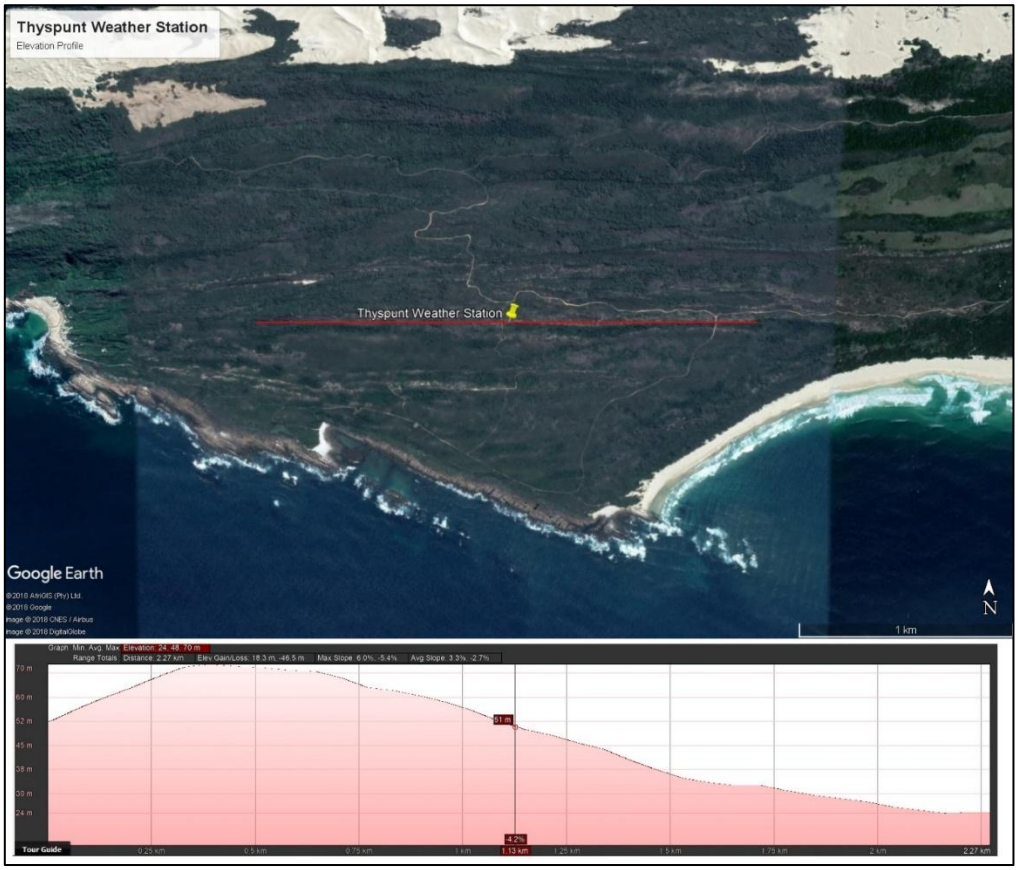


Figure 5.8.A.6
West to East Elevation Profile Through Location of the Thyspunt WS

© Eskom 2026/Rev 0c

PRINTED VERSIONS OF THIS DOCUMENT ARE NOT CONTROLLED

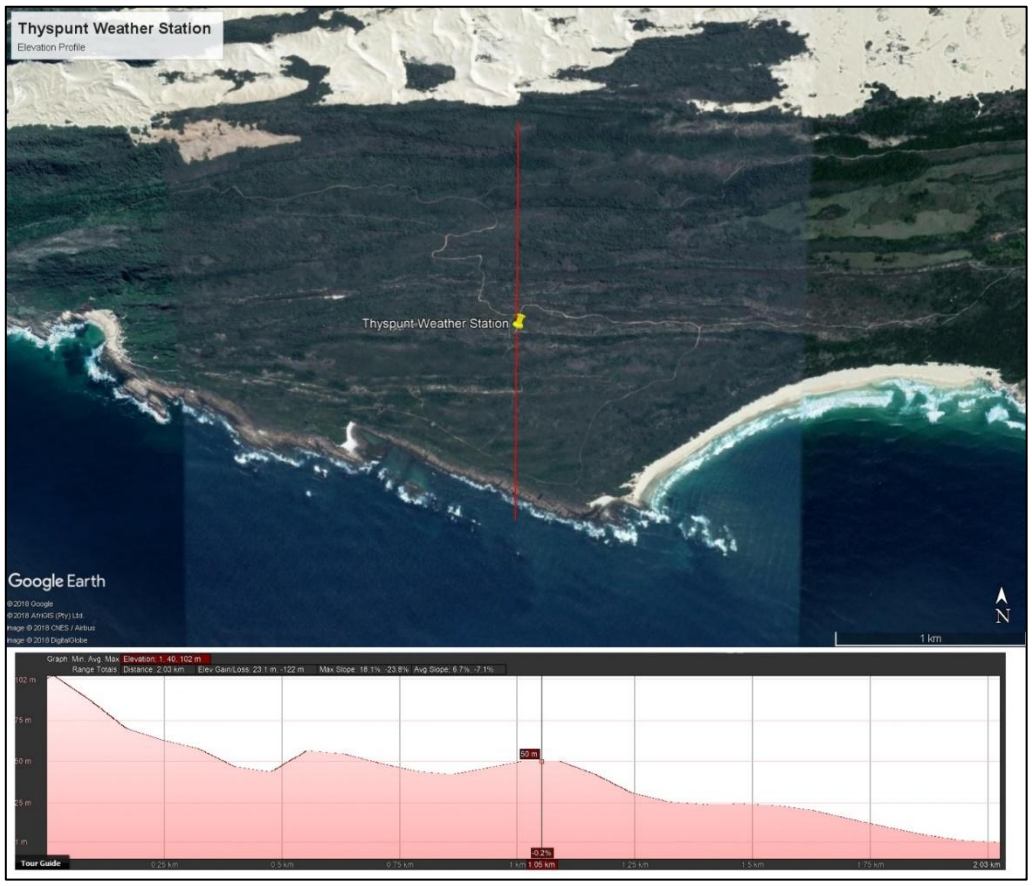


Figure 5.8.A.7
North to South Elevation Profile Through Location of the Thyspunt WS

Surface wind measurements without exposure problems hardly exist. The requirement of open, level terrain is difficult to meet, and most wind stations over land are perturbed by topographic effects or surface cover, or by both (WMO, 1987; Wieranga, 1996). As indicated above, there is potential for the wind flow characteristics to be modified by the presence of differences in elevation at the Thyspunt site.

The World Meteorological Organization (WMO, 2018) provides guidance on various wind speed corrections that can be used to estimate local exposure, including flow distortion (accounts for flow distortion by nearby big objects), non-standard measurement height (accounted for by assuming a logarithmic profile), changes in surface roughness in the study domain and topographic corrections. Topographic correction accounts for terrain height effects around the wind station. The topography correction term (CT) is the ratio of the regionally averaged wind speed (averaged over ridges and valleys typically at 10 m above local terrain) and the wind speed measured at the wind station.

© Eskom 2026/Rev 0c

PRINTED VERSIONS OF THIS DOCUMENT ARE NOT CONTROLLED

In the example of an isolated hill with a station at the top of the hill, CT should be less than 1 to correct for the speed-up induced by the hill, to make the result representative of the area rather than of the hilltop only. CT equals 1 for flat terrain. The (WMO, 2018) further states that for isolated hills and ridges, estimates of CT can be made with the help of simple guidelines. Correction of wind readings for local exposure can be performed only with measurements of reasonable quality at locations that are not too rough (surface roughness lengths, z0 ≤ 0.5 m) and reasonably level. No attempt should be made to correct measurements that have hardly any relation to a regional average. For example, a wind station in a deep valley, where the flow is dominated by katabatic effects, may be important for local forecasts, but cannot be used as a regionally representative wind. In the current application both local and regional requirements exist.

One such guideline is the Australian/New Zeeland Standard for Structural Design Actions Part 2: Wind Actions (AS/NZ, 2021). The standard calculates a hill shape multiplier (M_h) which is equivalent to the topography correction term (C_T) discussed in the WMO (WMO, 2018) document. According to the standard, M_h shall be taken as 1.0 except that for the particular cardinal wind direction in the local topographic zones shown in ***Figure 5.8.A.8*** the value shall be as follows:

(a) for $H/(2L_u) < 0.05$

$$M_h = 0$$

(b) for $0.05 \leq H/(2L_u) < 0.45$

$$M_h = 1 + \left(\frac{H}{3.5(z + L_1)}\right)\left(1 - \frac{|x|}{L_2}\right)$$

where

- H = height of the hill, ridge or escarpment
- L_u = horizontal distance upwind from the crest of the hill, ridge or escarpment to a level half the height below the crest
- x = horizontal distance upwind or downwind of the structure to the crest of the hill, ridge or escarpment
- L_1 = length scale, in metres, to determine the vertical variation of M_h, to be taken as the greater of $0.36\ L_u$ or $0.4\ H$
- L_2 = length scale, in metres, to determine the horizontal variation of M_h, to be taken as $4\ L_1$ upwind for all types, and downwind for hills and ridges, or $10\ L_1$ downwind for escarpments
- z = reference height on the structure above the average local ground level

© Eskom 2026/Rev 0c

PRINTED VERSIONS OF THIS DOCUMENT ARE NOT CONTROLLED

In the current application, the parameters for the two directions (north-south and east-west) are summarised in Table 1. When applying the equations above for Mh, the multiplier varies from 1.0 (900 m to 600 m upwind) to a maximum of 1.07 at the current weather station location and at 10 m agl. In other words, the wind speed measurement observed at the current weather station location is expected to be 7 per cent higher than the conditions at the shoreline. In comparison to the conditions at an elevation of 25 m, which is about 300 m south of the current location, the wind speed difference is calculated to be 5 per cent. Since the slope along the east-west axis is less than 0.045, the standard states that the multiplier is 1.0, i.e. no significant variation in the wind speed. Similarly, the wind speeds at 50 m agl may differ by a maximum of 1 per cent.

Table 5.8.A.1
Hill Shape Multiplier Parameters (AS/NZ, 2021)

Parameter	North-South Direction (Type B Hill)	East-West Direction (Type A Hill)
H	51 m	70 m
L_u	300 m	1130 m
$H/2L_u$	0.085 i.e. equation (b) applies	0.031 i.e. equation (a) applies
x	-900 m to 900 m	-900 m to 900 m
L_1	108 m	406.8 m
L_2	432 m upwind 1080 m downwind	1627.2 m upwind 1080 m downwind
z	10 m	10 m

Ngo and Letchford (Ngo & Letchford, 2007) compared USA, Australian/New Zealand, European and Japanese wind standards and reported that the treatment of topographic effects in the AS/NZS 1170.2 standards was on the whole conservative. For the purpose of wind hazard estimation, it is beneficial to remove the conservatism associated with the topographical multiplier derived from AS/NZS 1170.2 (AS/NZ, 2021). Recommendations by Geoscience Australia (Yang, et al., 2014) suggested that modifications could be made to the topographic multiplier (*Mh*) as follows:

- for essentially flat terrain (flatter than 1 in 20 or outside the local topographic zone), no adjustment to *Mh* is made;
- for topographic features such as shallow hills and escarpments where *Mh* < 1.4 a 5 per cent reduction in the multiplier is adopted;
- for topographic features such as steep hills and escarpments where *Mh* ≥ 1.4 a 10 per cent reduction in the multiplier is adopted.

© Eskom 2026/Rev 0c

PRINTED VERSIONS OF THIS DOCUMENT ARE NOT CONTROLLED

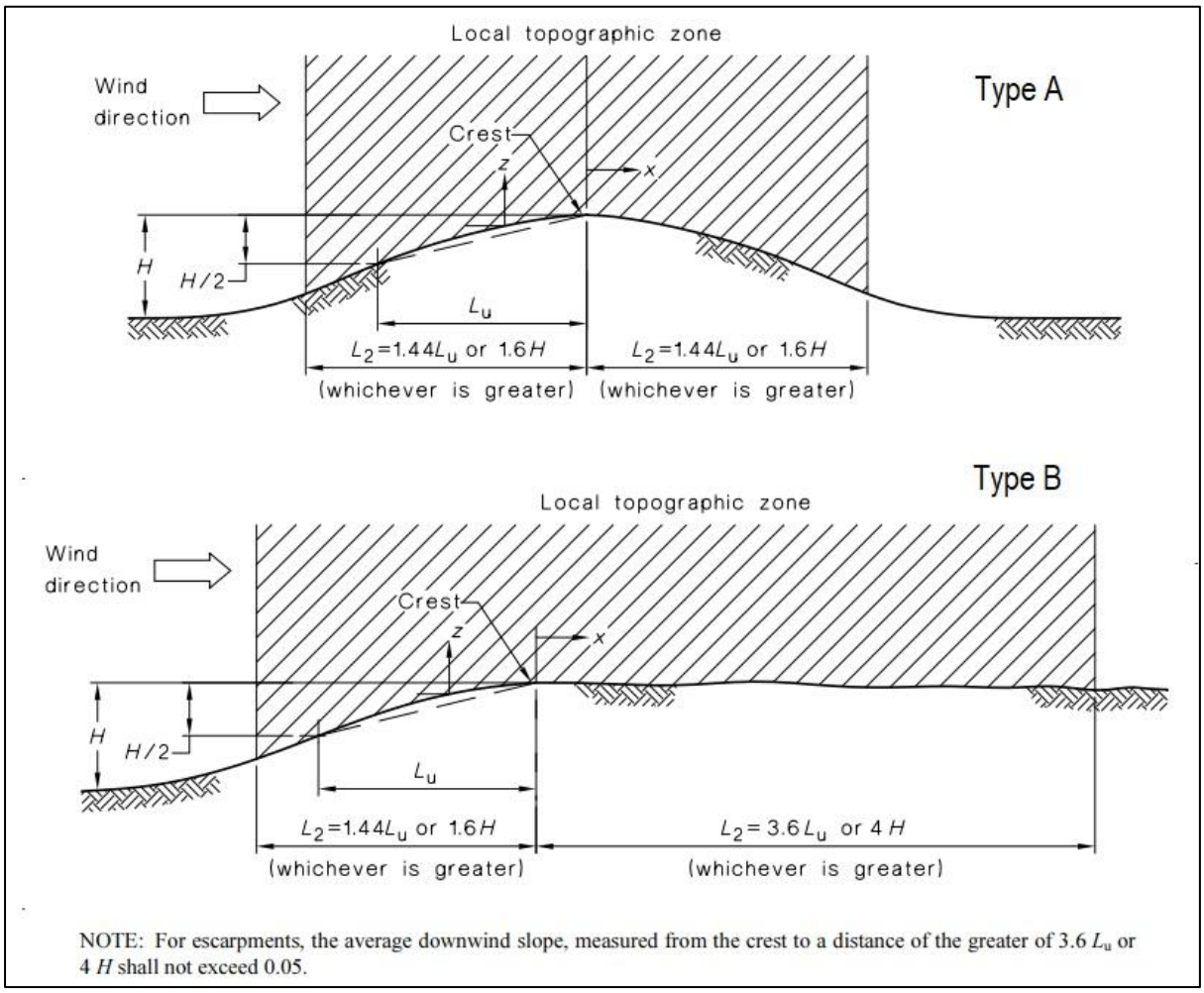


Figure 5.8.A.8
Hills and Ridges for the Calculation of the AS/NZ 1170.2 (AS/NZ, 2021) Standard Hill Shape Multiplier

According to this, the multiplier should be lower by 5 per cent. However, it should also be noted that these correction schemes are limited to the case of a neutrally stable atmosphere. It has been observed that unstable and stable conditions could result in decreased and increased speedups over hills, respectively. With stable conditions this could be up to a factor of about 2 (Coppin, et al., 1994; Lubitz & White, 2007). So, the range of over-estimating the wind speed at a location at a lower elevation towards the shoreline is estimated to be between slightly less than 5 per cent to 10 per cent.

Wind field simulations were performed using the *WindNinja* software package to illustrate and support the preceding discussion. *WindNinja* is a mass-conserving diagnostic wind model developed and maintained by the USFS Missoula Fire Sciences Laboratory (Forthofer, et al., 2014).

© Eskom 2026/Rev 0c

PRINTED VERSIONS OF THIS DOCUMENT ARE NOT CONTROLLED

WindNinja uses a variational calculus technique to minimise the change in an initial wind field while conserving mass locally (within each cell) and globally over the computational domain. The numerical solution is obtained using finite element method (FEM) techniques on a terrain-following mesh consisting of layers of hexahedral cells that grow vertically with height. *WindNinja* also includes a diurnal slope flow parameterization. The *WindNinja* computational domain was constructed from 30 m resolution Shuttle Radar Topography Mission (SRTM) data. Vertical wind speeds were fitted to a logarithmic profile based on the micrometeorological model.

The AS/NZS 1170.2 (AS/NZ, 2021) standard suggested that winds from the east and west may result in insignificant speedups as the wind flows along the dune. To test this, the six Pasquill-Gifford atmospheric stability classes **A** (very unstable) to **F** (very stable) were selected for the wind field simulations using the *WindNinja* package. The results are shown in ***Figure 5.8.A.9*** to ***Figure 5.8.A.14***. Apart from stable atmospheric conditions (**E** and **F**), no significant difference in the wind speed is observed in the modelling domain. With stable conditions, some reduction in wind speeds is noticed at the weather station location and lower towards the seashore compared to the upwind conditions; however, the observations and lower elevation speeds are similar. Identical results were obtained with easterly winds, as shown in ***Figure 5.8.A.15*** to ***Figure 5.8.A.20***.

© Eskom 2026/Rev 0c

PRINTED VERSIONS OF THIS DOCUMENT ARE NOT CONTROLLED

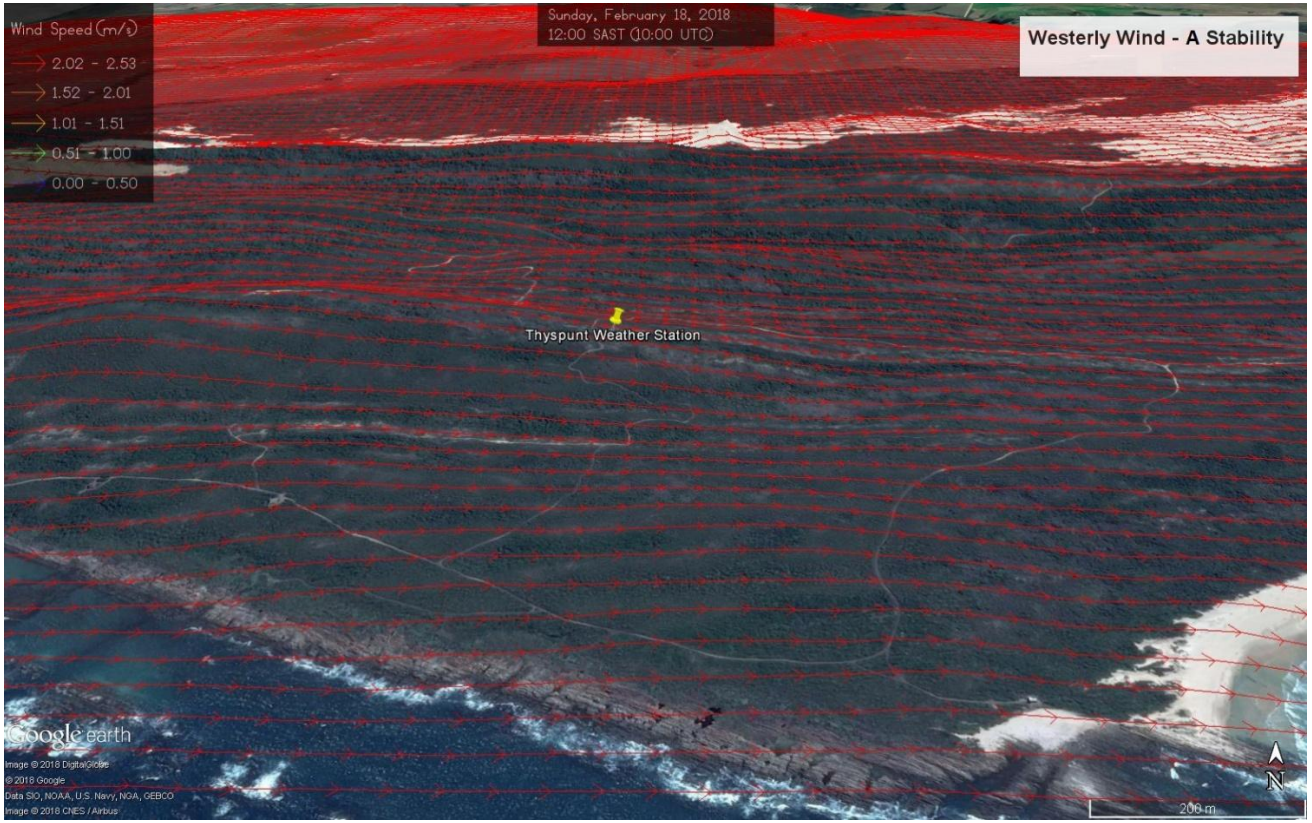


Figure 5.8.A.9
Wind Field Constructed at Thyspunt for a Westerly Wind with Very Unstable Atmospheric Conditions (A stability)

© Eskom 2026/Rev 0c

PRINTED VERSIONS OF THIS DOCUMENT ARE NOT CONTROLLED

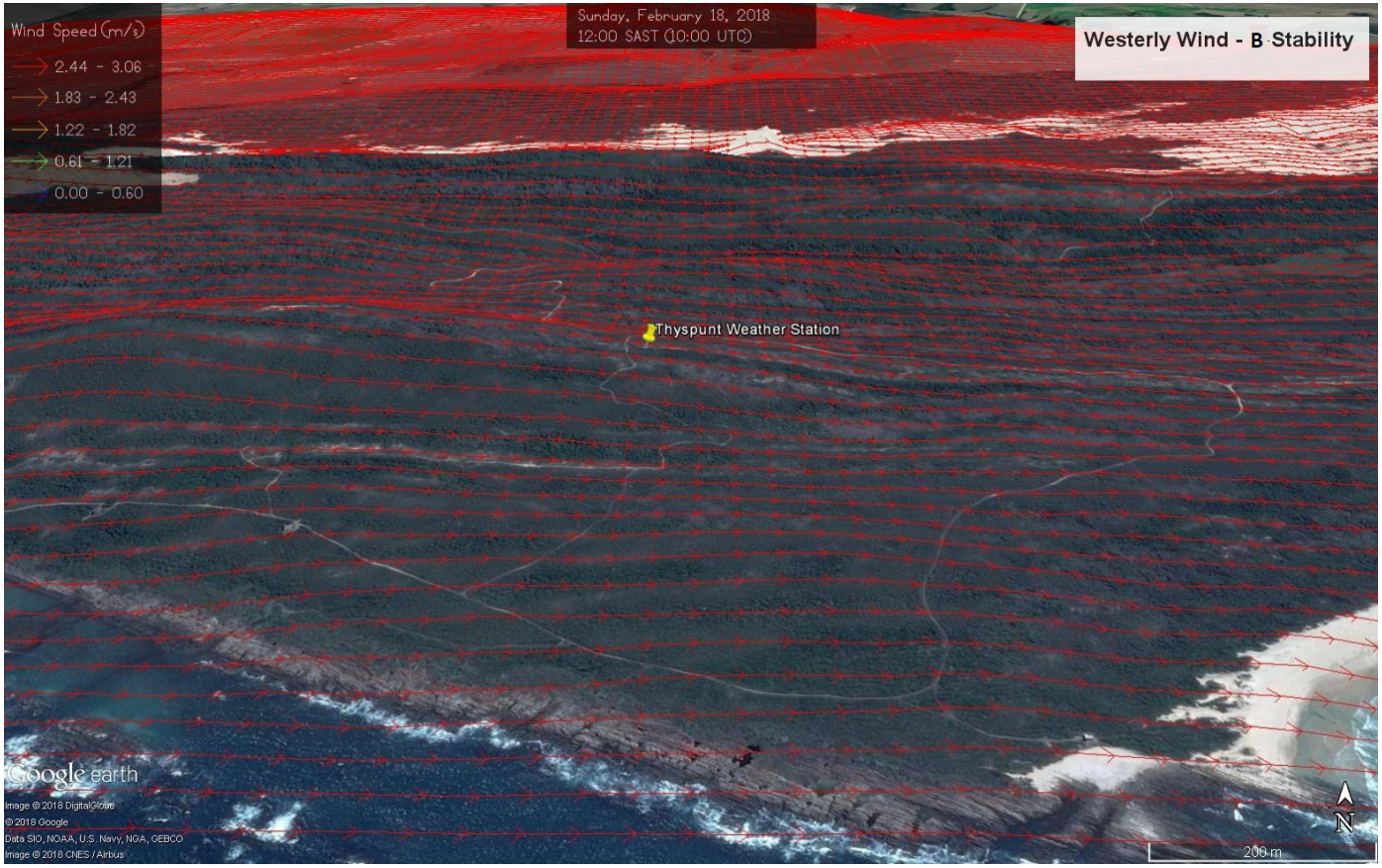


Figure 5.8.A.10
Wind Field Constructed at Thyspunt for a Westerly Wind with Moderately Unstable Atmospheric Conditions (B stability)

© Eskom 2026/Rev 0c

PRINTED VERSIONS OF THIS DOCUMENT ARE NOT CONTROLLED

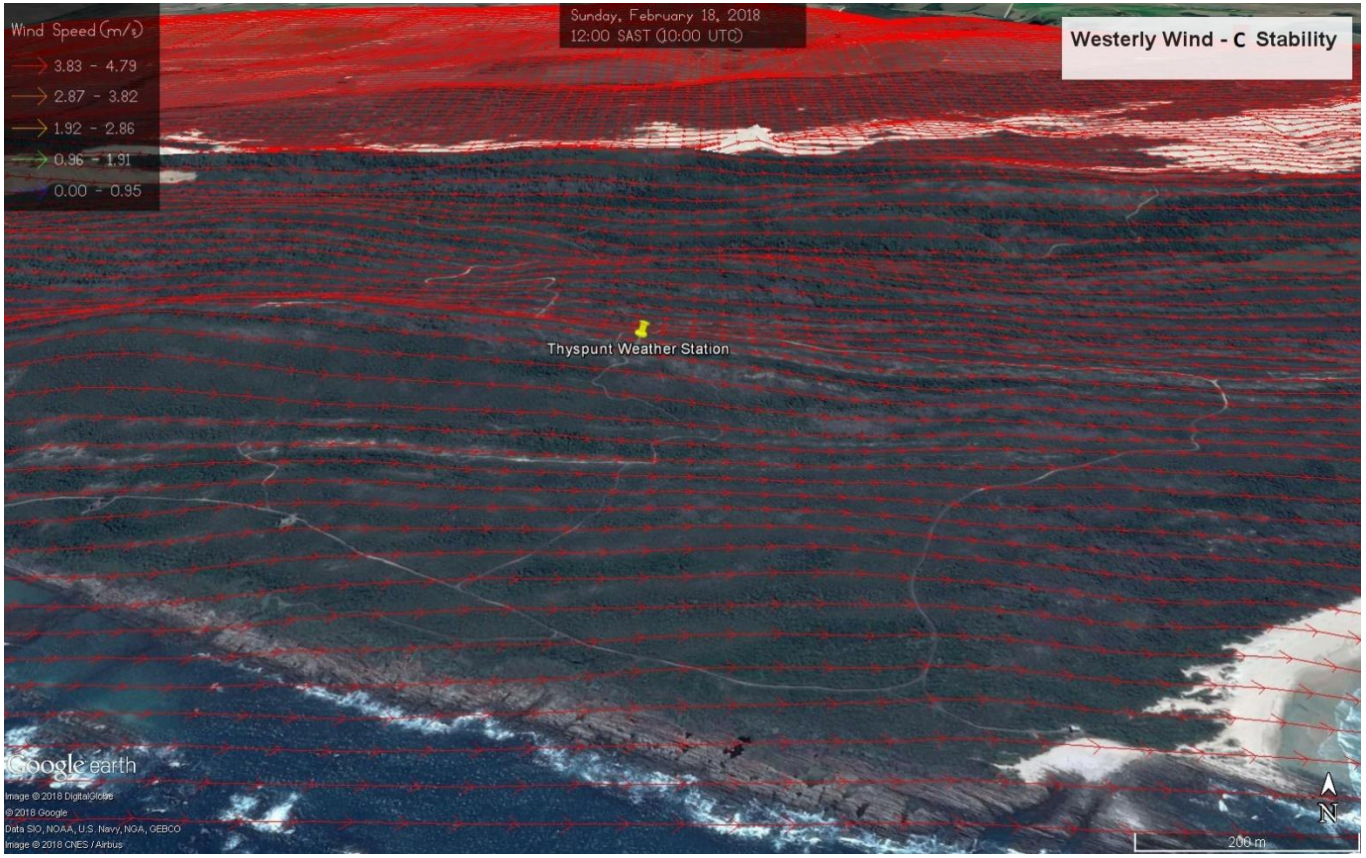


Figure 5.8.A.11
Wind Field Constructed at Thyspunt for a Westerly Wind with Slightly Unstable Atmospheric Conditions (C stability)

© Eskom 2026/Rev 0c

PRINTED VERSIONS OF THIS DOCUMENT ARE NOT CONTROLLED

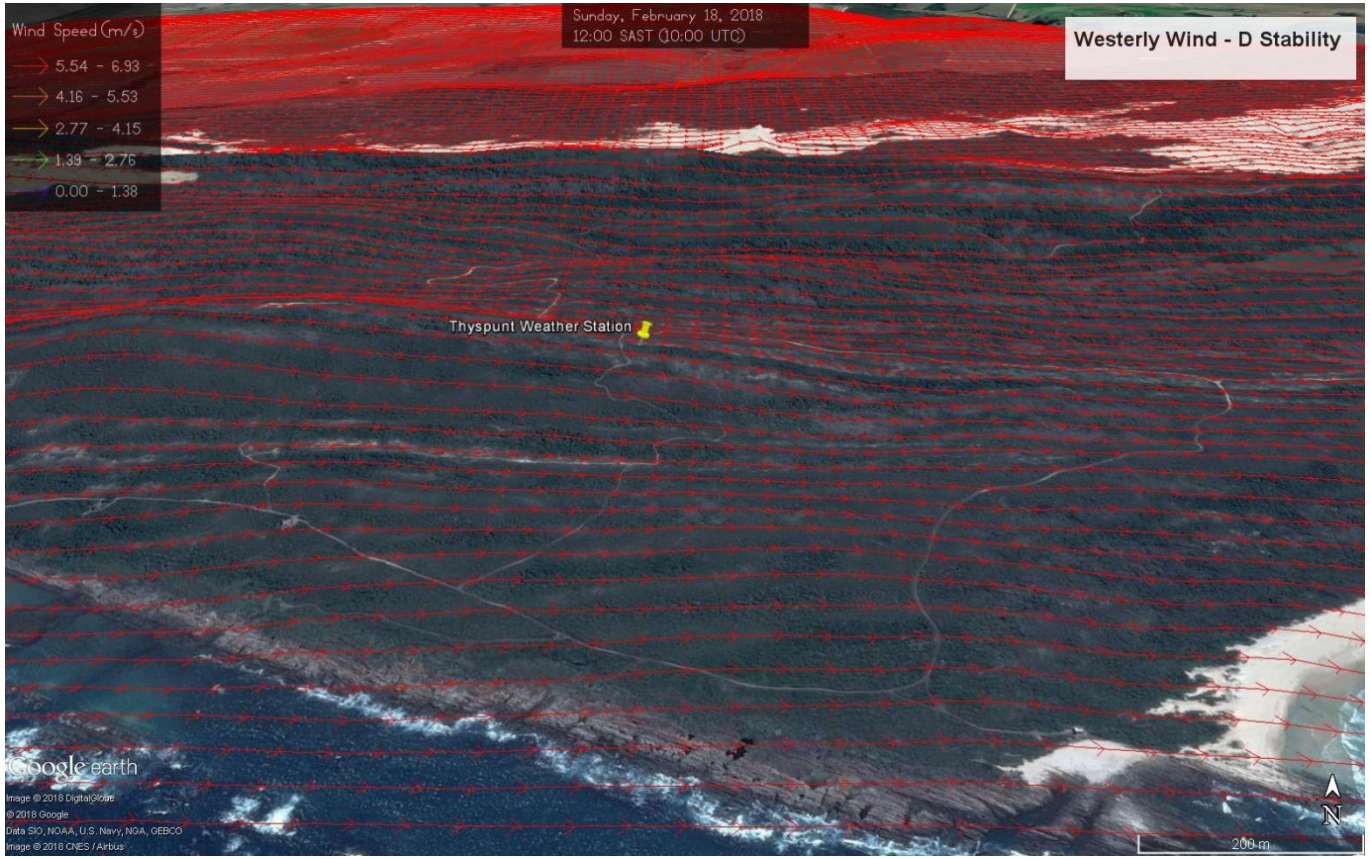


Figure 5.8.A.12
Wind Field Constructed at Thyspunt for a Westerly Wind with Neutral Atmospheric Conditions (D stability)

© Eskom 2026/Rev 0c

PRINTED VERSIONS OF THIS DOCUMENT ARE NOT CONTROLLED

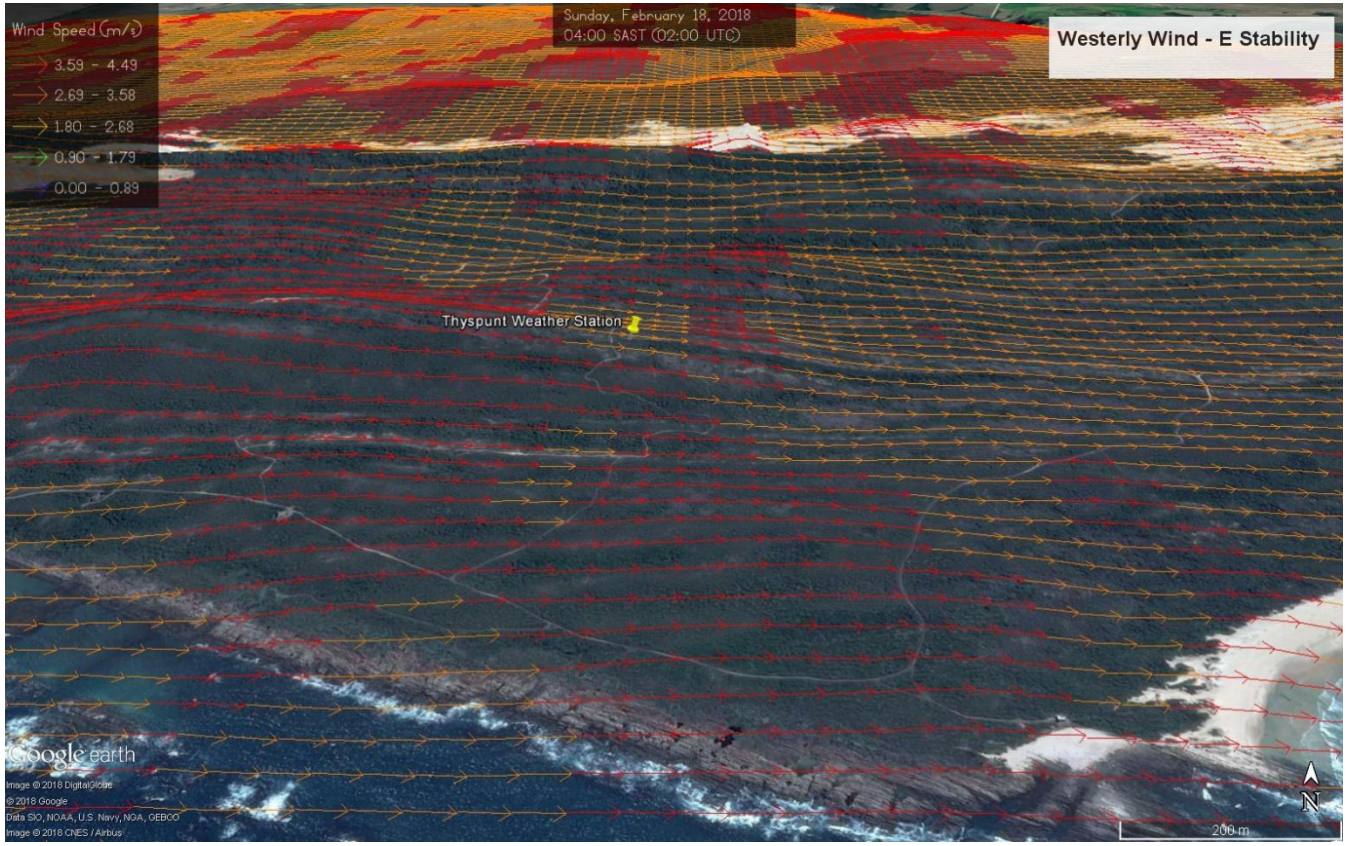


Figure 5.8.A.13
Wind Field Constructed at Thyspunt for a Westerly Wind with Stable Atmospheric Conditions (E stability)

© Eskom 2026/Rev 0c

PRINTED VERSIONS OF THIS DOCUMENT ARE NOT CONTROLLED

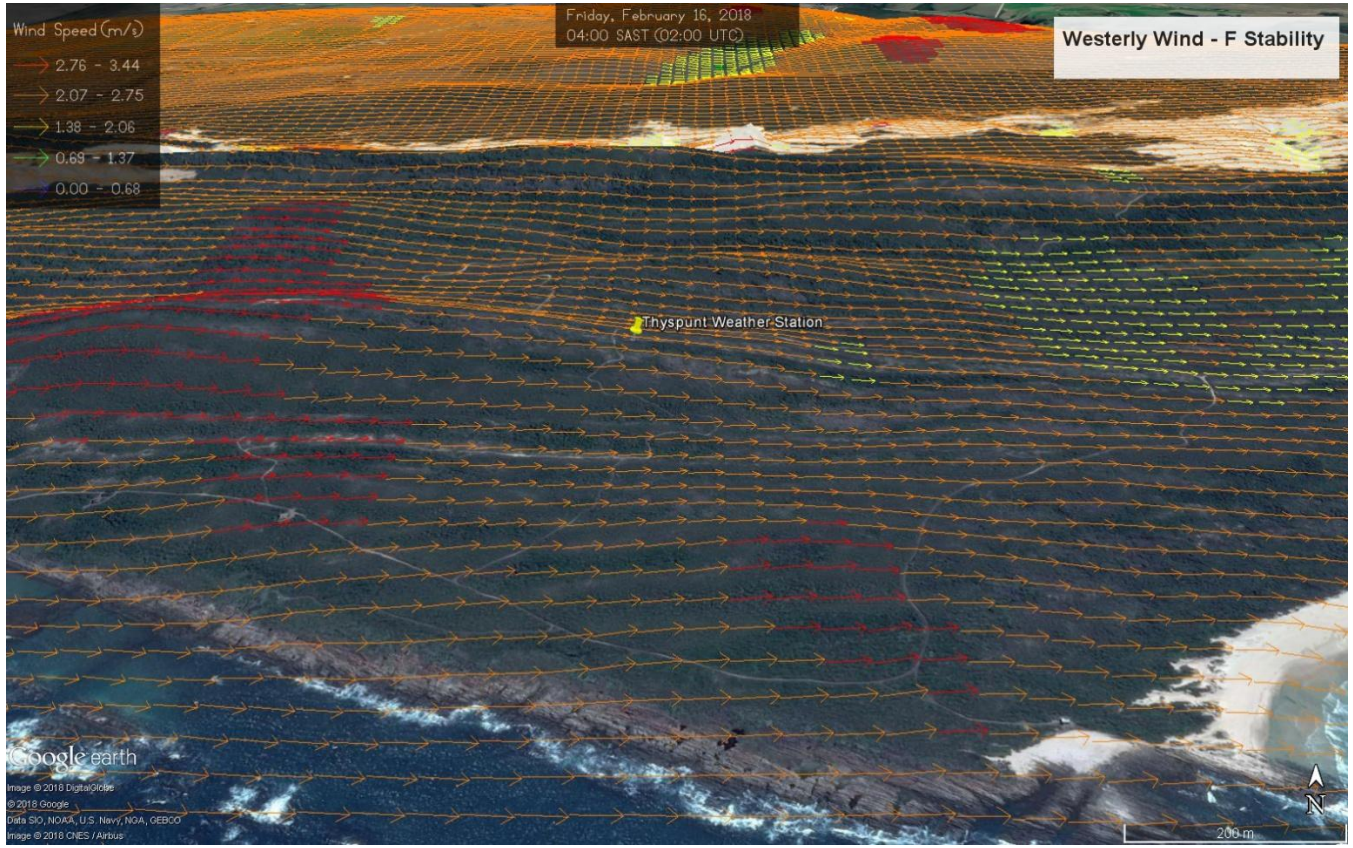


Figure 5.8.A.14
Wind Field Constructed at Thyspunt for a Westerly Wind with Very Stable Atmospheric Conditions (F stability)

© Eskom 2026/Rev 0c

PRINTED VERSIONS OF THIS DOCUMENT ARE NOT CONTROLLED

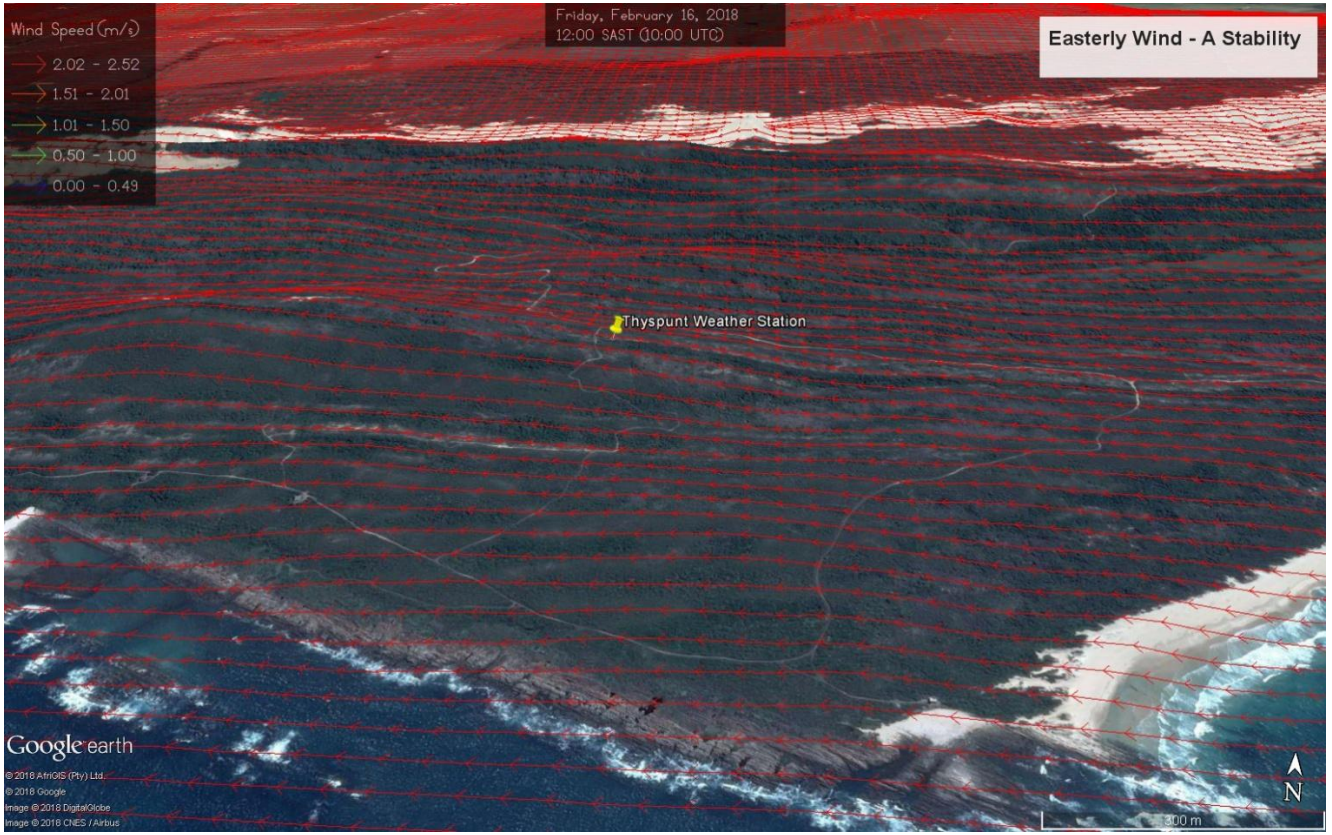


Figure 5.8.A.15
Wind Field Constructed at Thyspunt for an Easterly Wind with Very Unstable Atmospheric Conditions (A stability)

© Eskom 2026/Rev 0c

PRINTED VERSIONS OF THIS DOCUMENT ARE NOT CONTROLLED

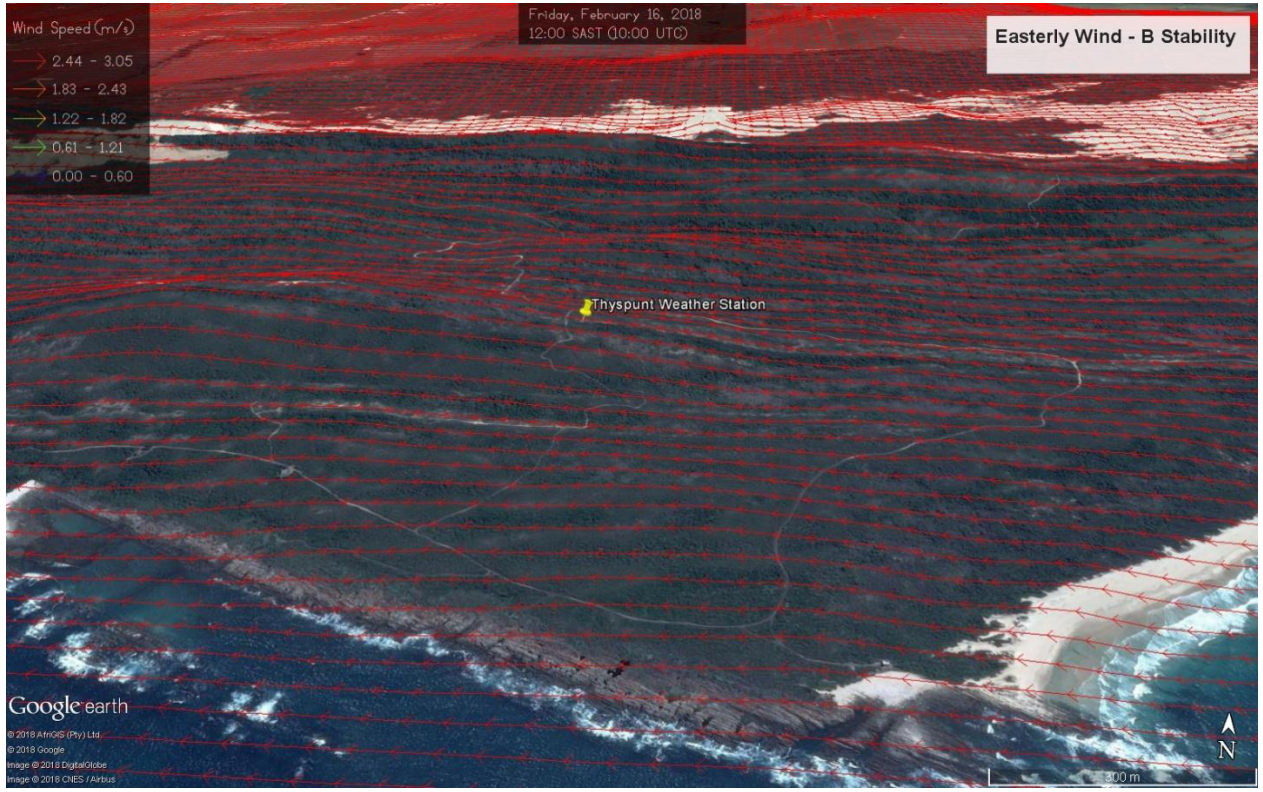


Figure 5.8.A.16
Wind Field Constructed at Thyspunt for an Easterly Wind with Moderately Unstable Atmospheric Conditions (B stability)

© Eskom 2026/Rev 0c

PRINTED VERSIONS OF THIS DOCUMENT ARE NOT CONTROLLED

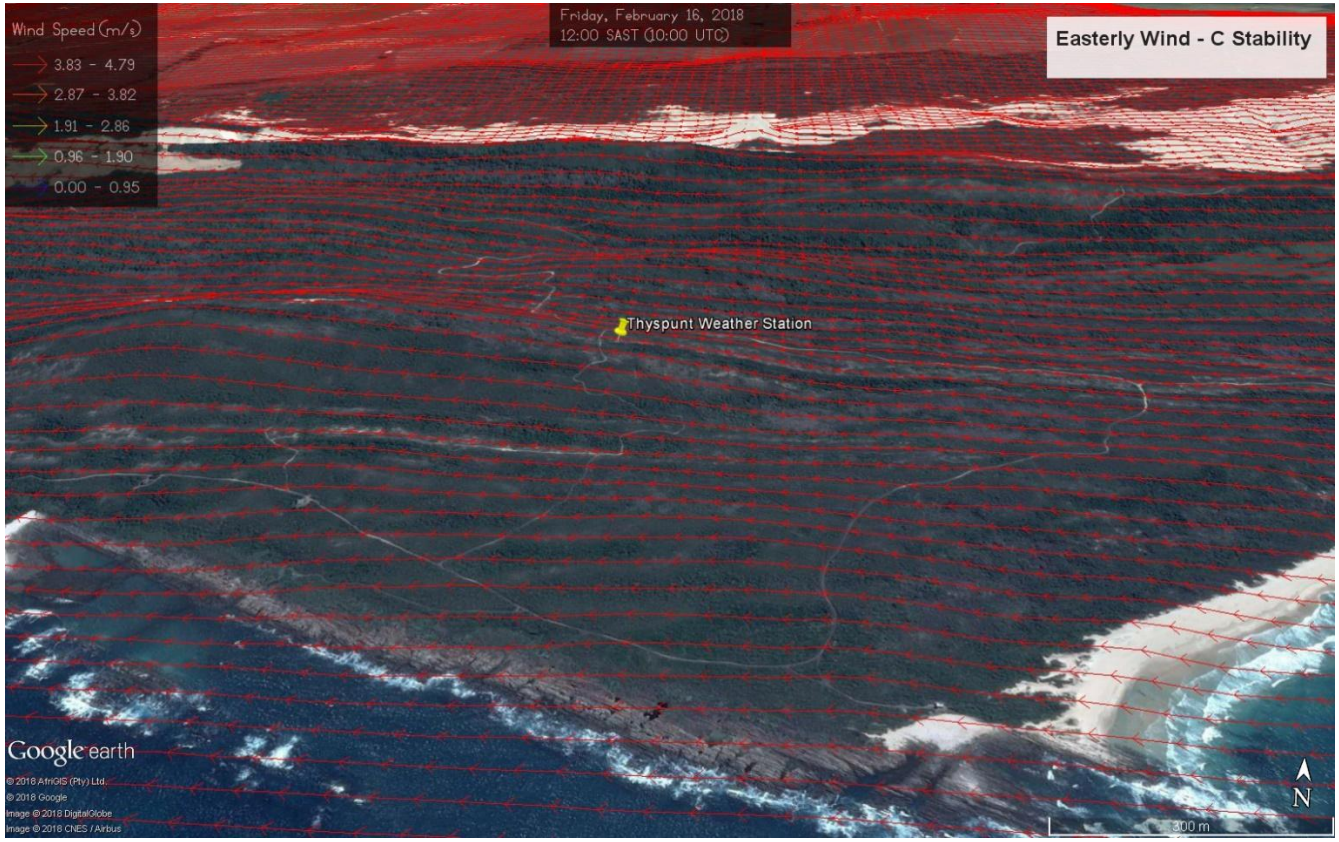


Figure 5.8.A.17
Wind Field Constructed at Thyspunt for an Easterly Wind with Unstable Atmospheric Conditions (C stability)

© Eskom 2026/Rev 0c

PRINTED VERSIONS OF THIS DOCUMENT ARE NOT CONTROLLED

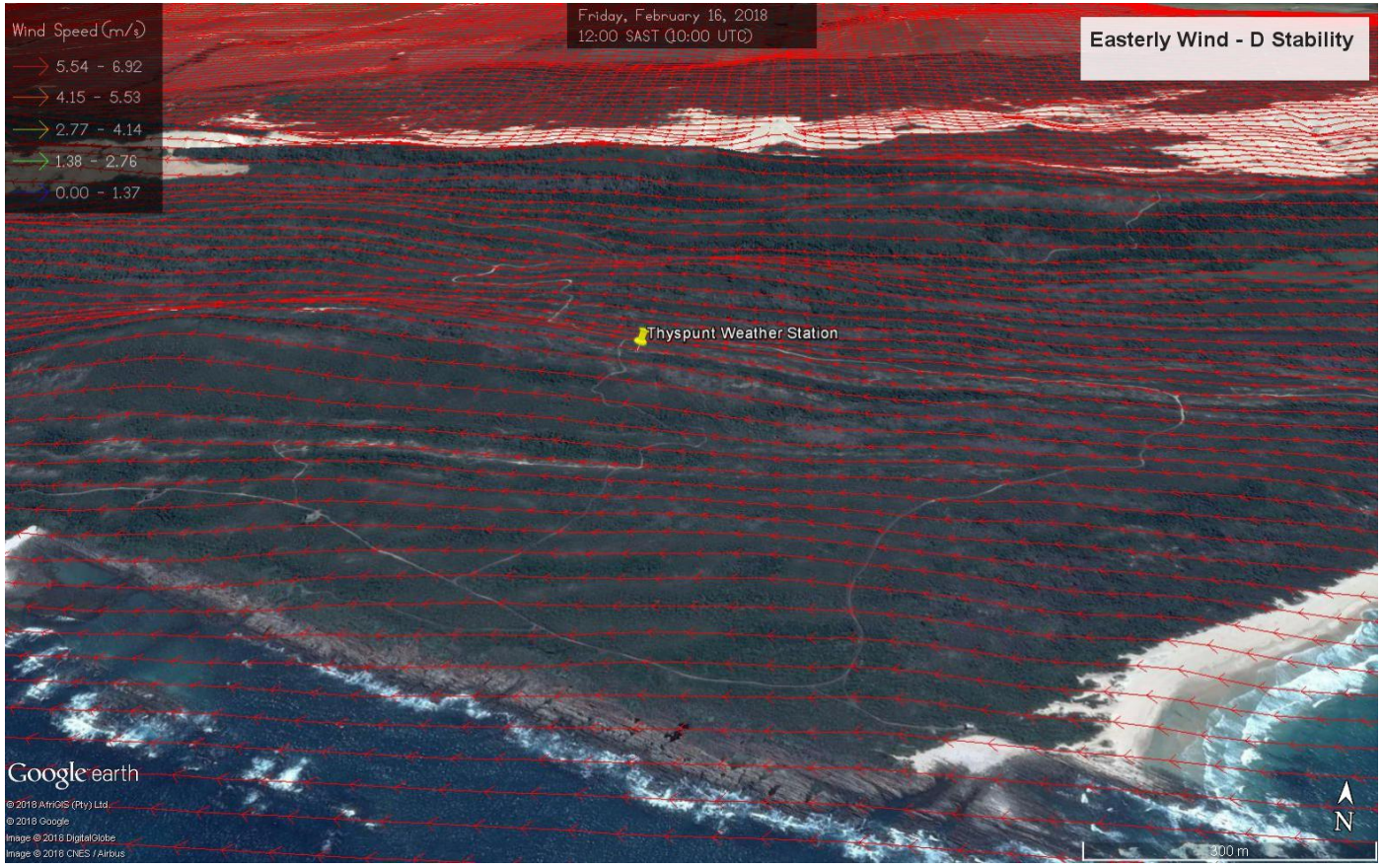


Figure 5.8.A.18
Wind Field Constructed at Thyspunt for an Easterly Wind with Neutral Atmospheric Conditions (D stability)

© Eskom 2026/Rev 0c

PRINTED VERSIONS OF THIS DOCUMENT ARE NOT CONTROLLED

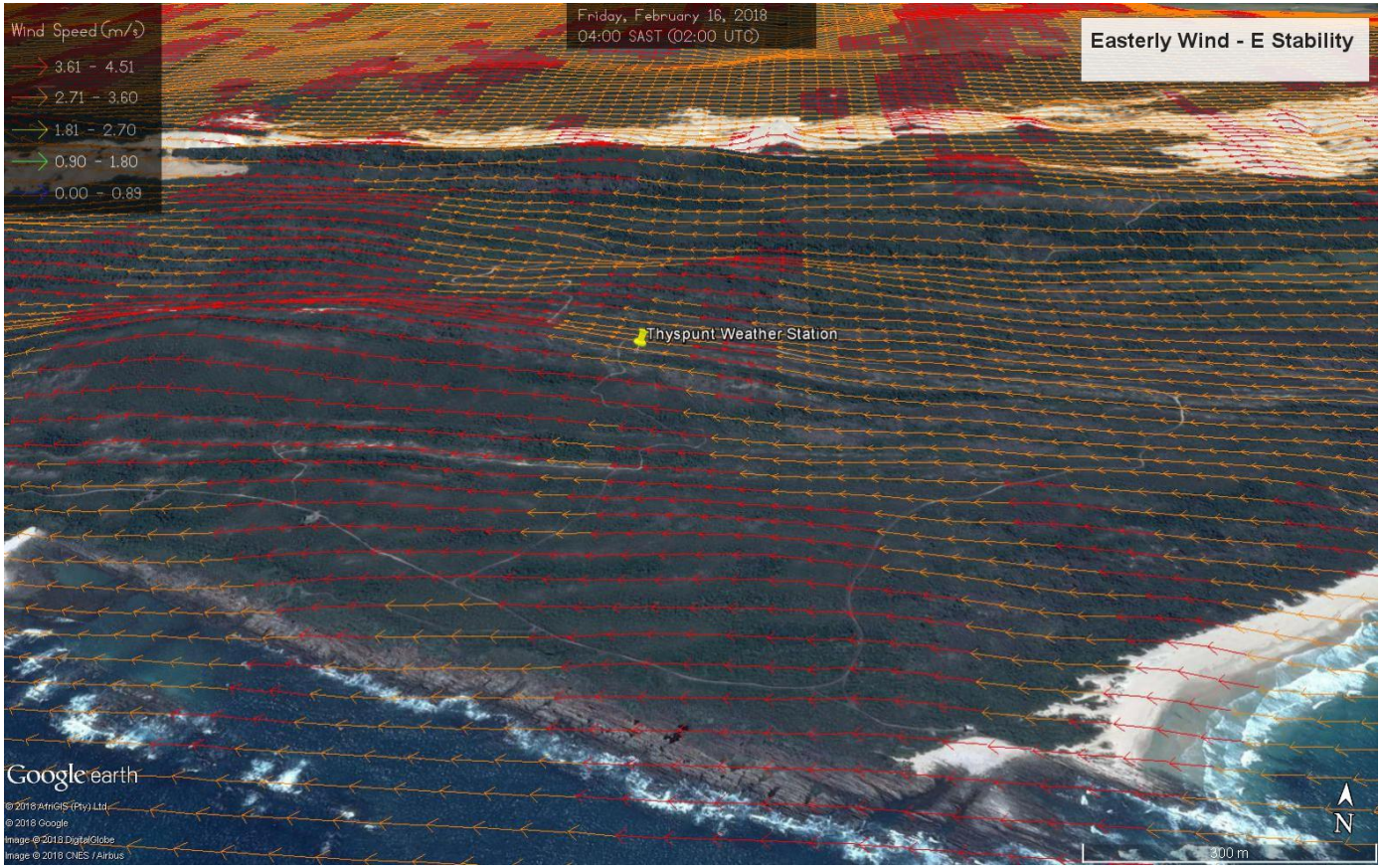


Figure 5.8.A.19
Wind Field Constructed at Thyspunt for an Easterly Wind with Stable Atmospheric Conditions (E stability)

© Eskom 2026/Rev 0c

PRINTED VERSIONS OF THIS DOCUMENT ARE NOT CONTROLLED

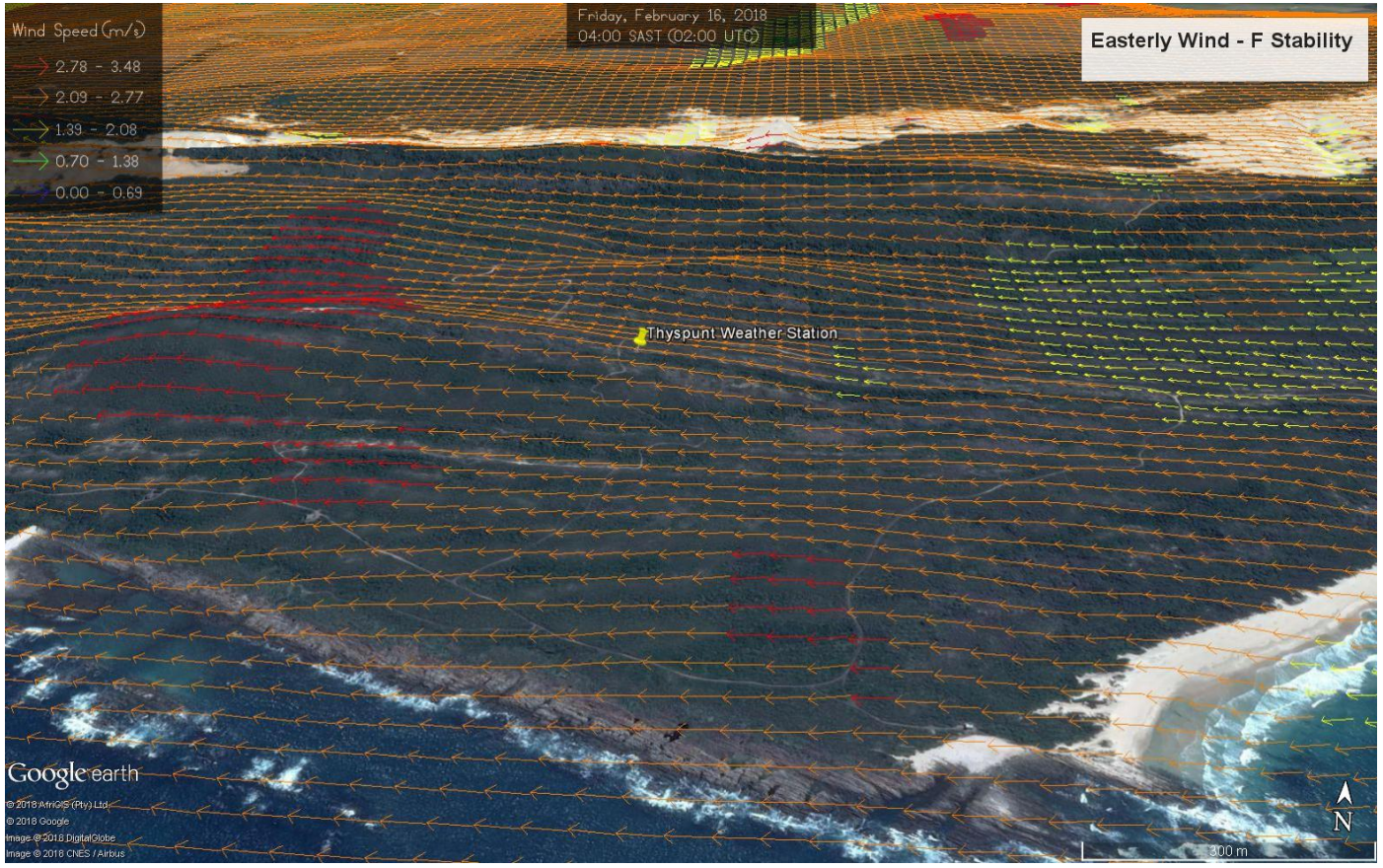


Figure 5.8.A.20
Wind Field Constructed at Thyspunt for an Easterly Wind with Very Stable Atmospheric Conditions (F stability)

© Eskom 2026/Rev 0c

PRINTED VERSIONS OF THIS DOCUMENT ARE NOT CONTROLLED

The *WindNinja* simulation results for southerly winds are shown ***Figure 5.8.A.21*** to ***Figure 5.8.A.26***. The speedup of wind at the weather station is clearly observed during **E** and **F** stabilities, confirming the calculations made using the AS/NZS 1170.2 standard. Similar results were obtained for winds from the north (***Figure 5.8.A.27*** to ***Figure 5.8.A.32***).

Not only do the simulation results collaborate with the AS/NZS 1170.2 standard, but they also illustrate that realistic wind fields can be constructed using well-established numerical methods.

The more recent wind speed and direction observations that were made for the periods 2008-2013 (***Figure 5.8.3***) and 2017-2019 (***Figure 5.8.4***) at both the SAWS weather station at Cape St. Francis (SAWS, 2024a) and the onsite Thyspunt WS (Eskom, 2023a) clearly illustrate the dominance of westerly and easterly wind directions in the wind roses. The difference between day and night-time wind directions are only with respect to variations in the general westerly and easterly sectors, as shown in ***Figure 5.8.5*** and ***Figure 5.8.6***, otherwise it is the same prevalence of westerlies and easterlies.

© Eskom 2026/Rev 0c

PRINTED VERSIONS OF THIS DOCUMENT ARE NOT CONTROLLED

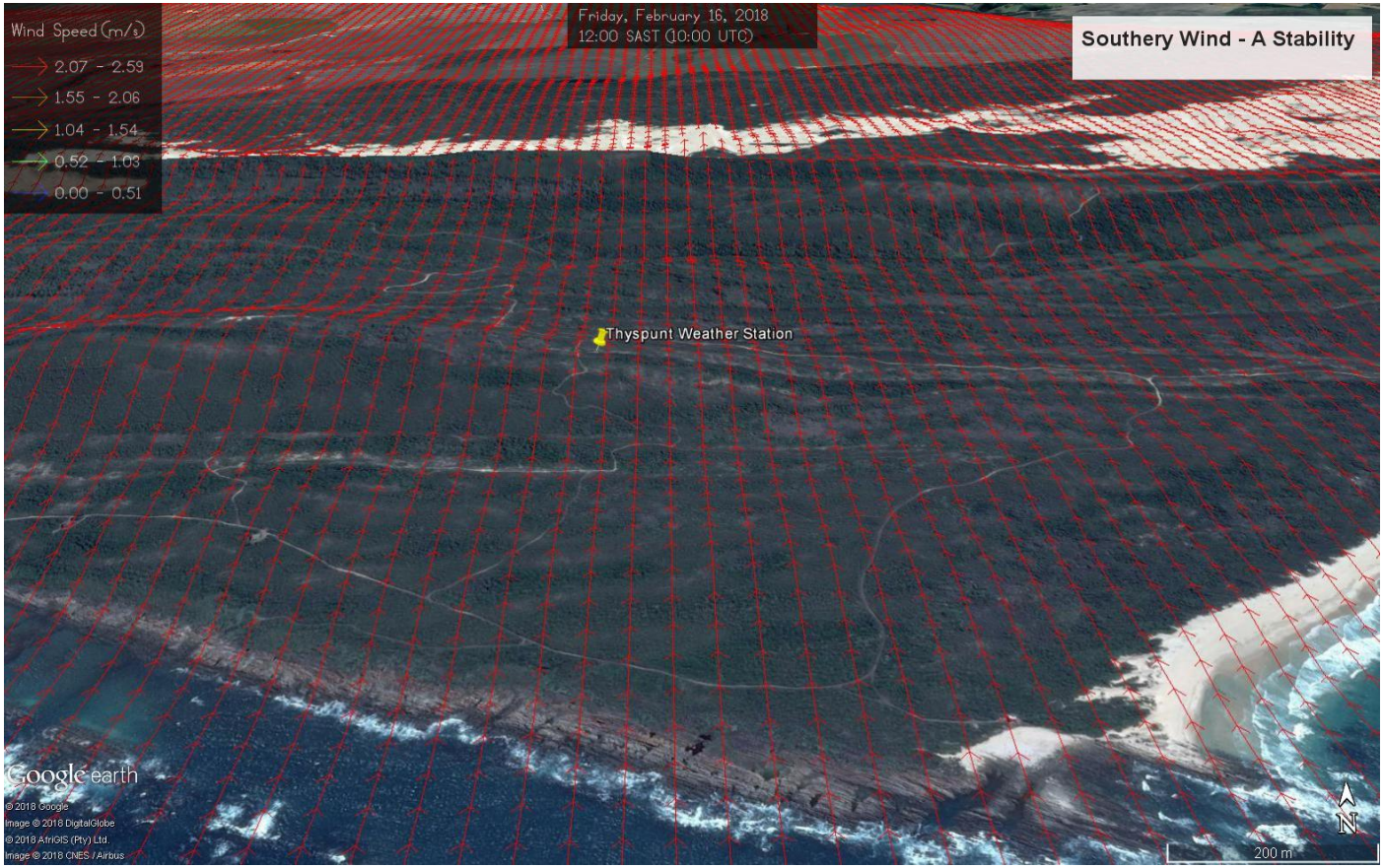


Figure 5.8.A.21
Wind Field Constructed at Thyspunt for a Southerly Wind with Very Unstable Atmospheric Conditions (A stability)

© Eskom 2026/Rev 0c

PRINTED VERSIONS OF THIS DOCUMENT ARE NOT CONTROLLED

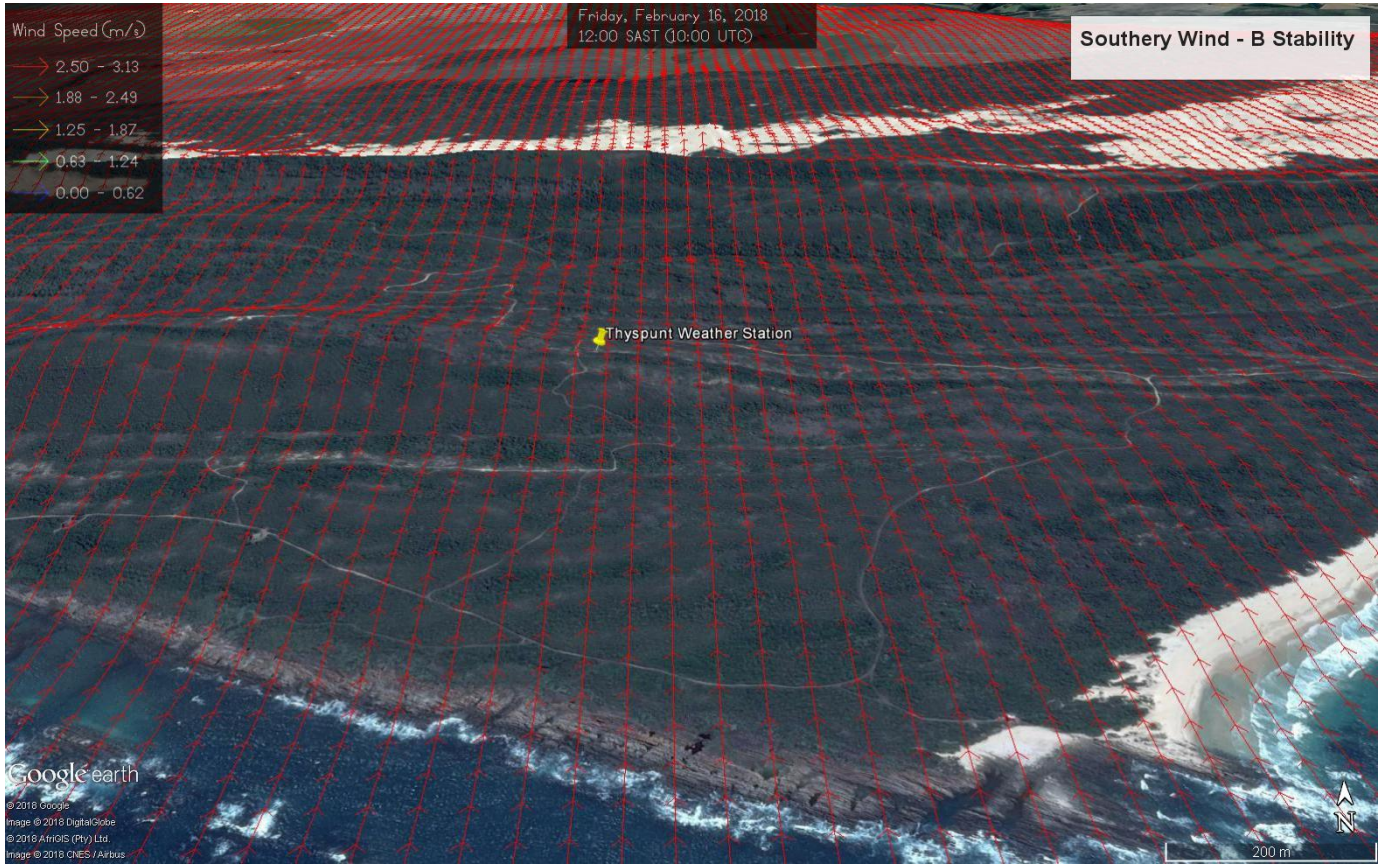


Figure 5.8.A.22
Wind Field Constructed at Thyspunt for a Southerly Wind with Moderately Unstable Atmospheric Conditions (B stability)

© Eskom 2026/Rev 0c

PRINTED VERSIONS OF THIS DOCUMENT ARE NOT CONTROLLED

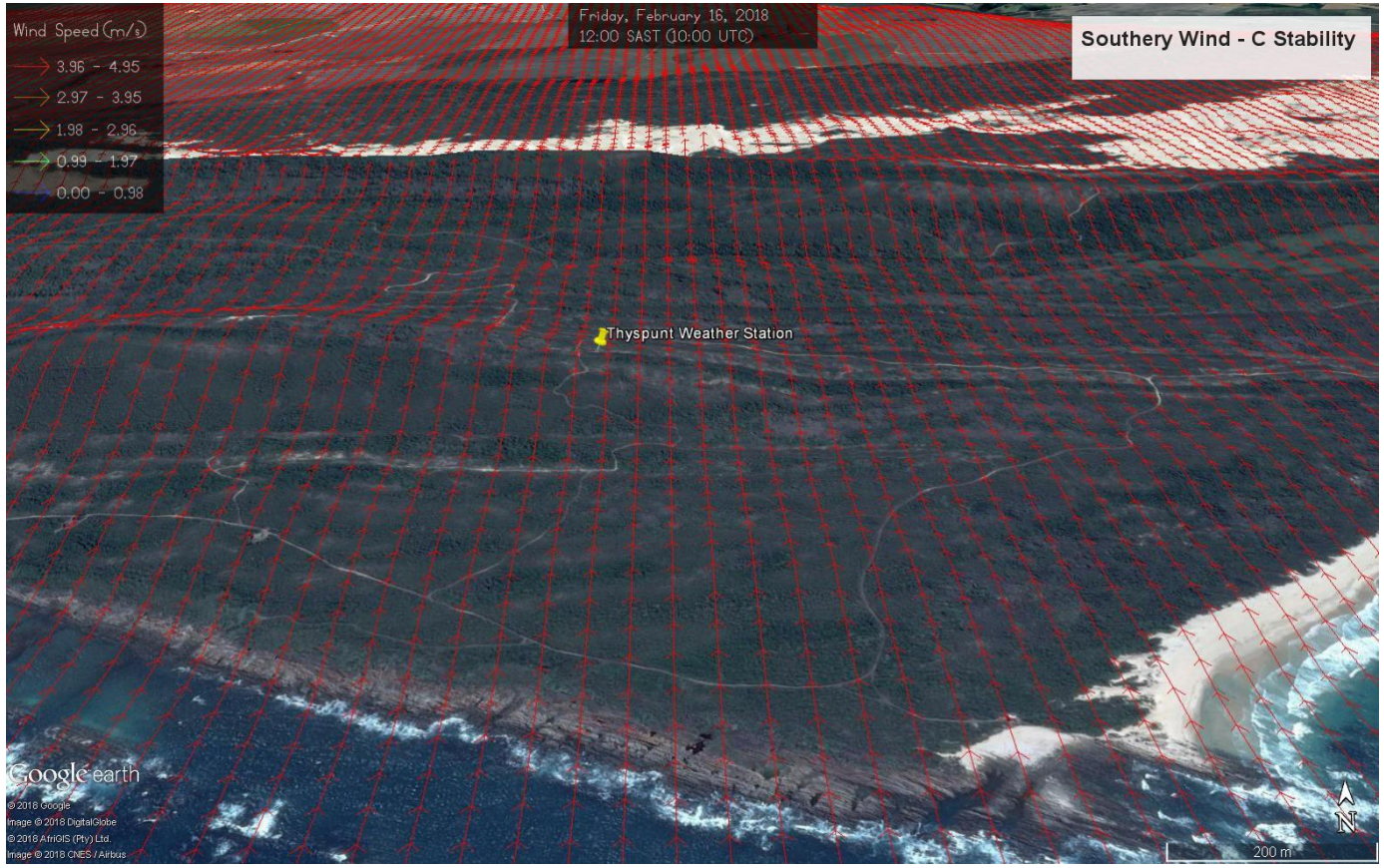


Figure 5.8.A.23
Wind Field Constructed at Thyspunt for a Southerly Wind with Unstable Atmospheric Conditions (C stability)

© Eskom 2026/Rev 0c

PRINTED VERSIONS OF THIS DOCUMENT ARE NOT CONTROLLED

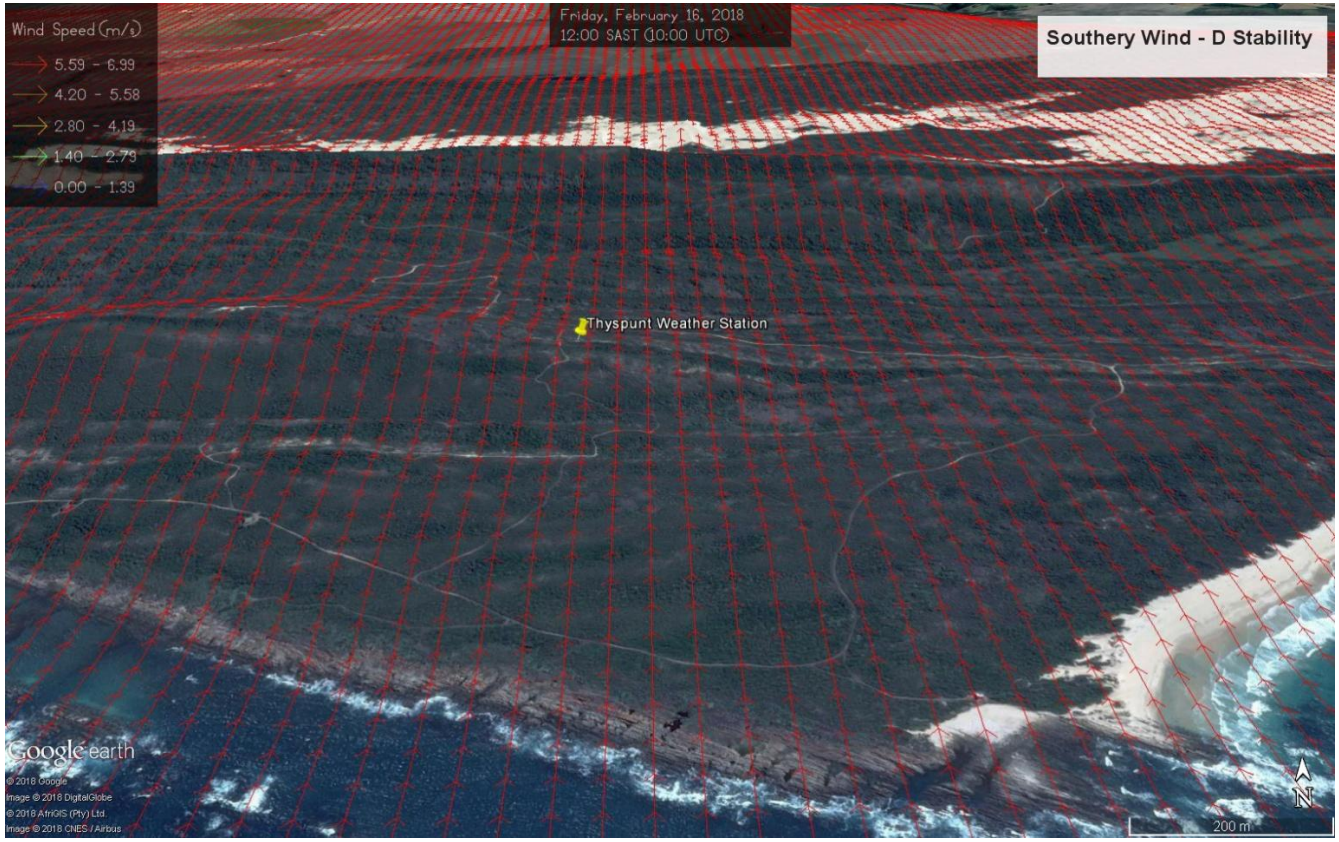


Figure 5.8.A.24
Wind Field Constructed at Thyspunt for a Southerly Wind with Neutral Atmospheric Conditions (D stability)

© Eskom 2026/Rev 0c

PRINTED VERSIONS OF THIS DOCUMENT ARE NOT CONTROLLED

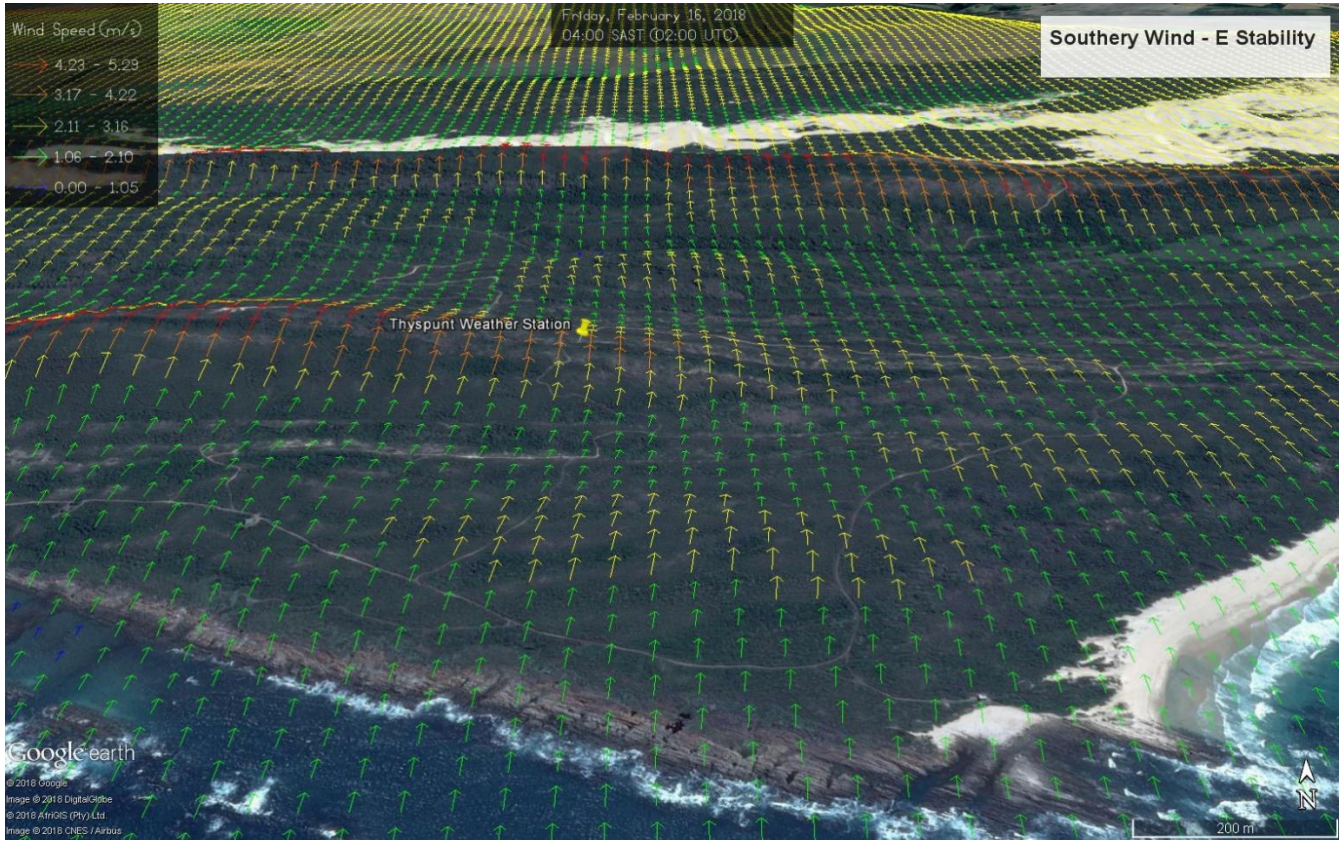


Figure 5.8.A.25
Wind Field Constructed at Thyspunt for a Southerly Wind with Stable Atmospheric Conditions (E stability)

© Eskom 2026/Rev 0c

PRINTED VERSIONS OF THIS DOCUMENT ARE NOT CONTROLLED

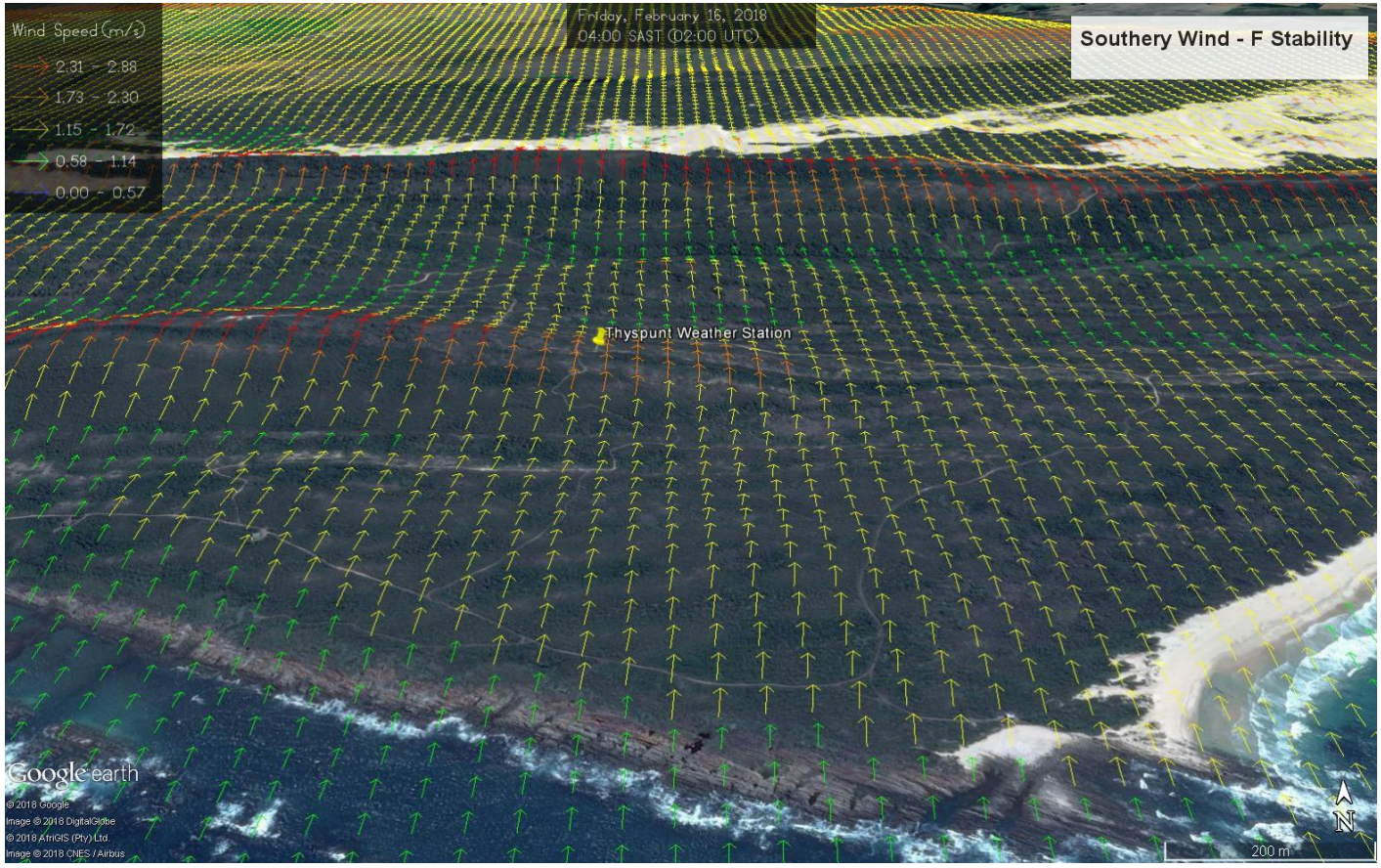


Figure 5.8.A.26
Wind Field Constructed at Thyspunt for a Southerly Wind with Very Stable Atmospheric Conditions (F stability)

© Eskom 2026/Rev 0c

PRINTED VERSIONS OF THIS DOCUMENT ARE NOT CONTROLLED

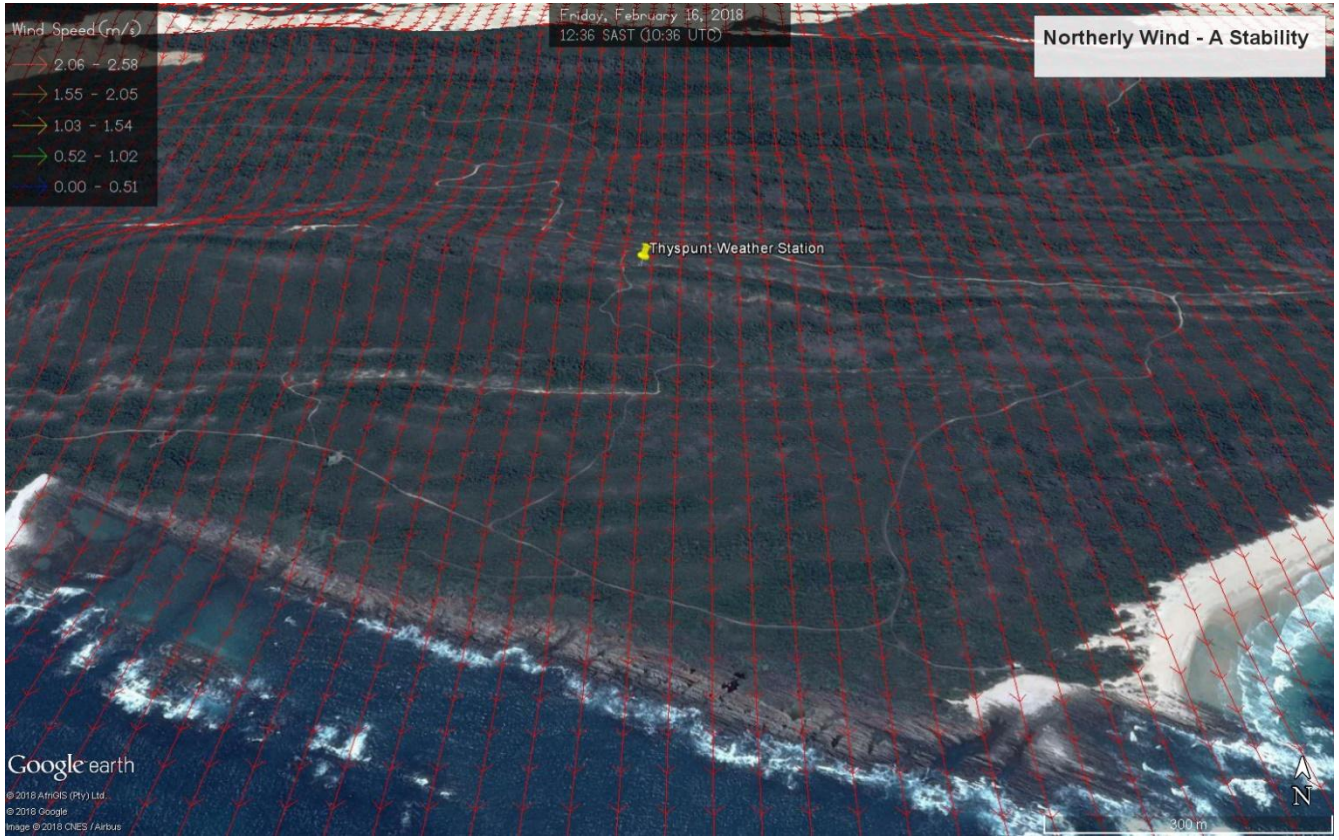


Figure 5.8.A.27
Wind Field Constructed at Thyspunt for a Northerly Wind with Very Unstable Atmospheric Conditions (A stability)

© Eskom 2026/Rev 0c

PRINTED VERSIONS OF THIS DOCUMENT ARE NOT CONTROLLED

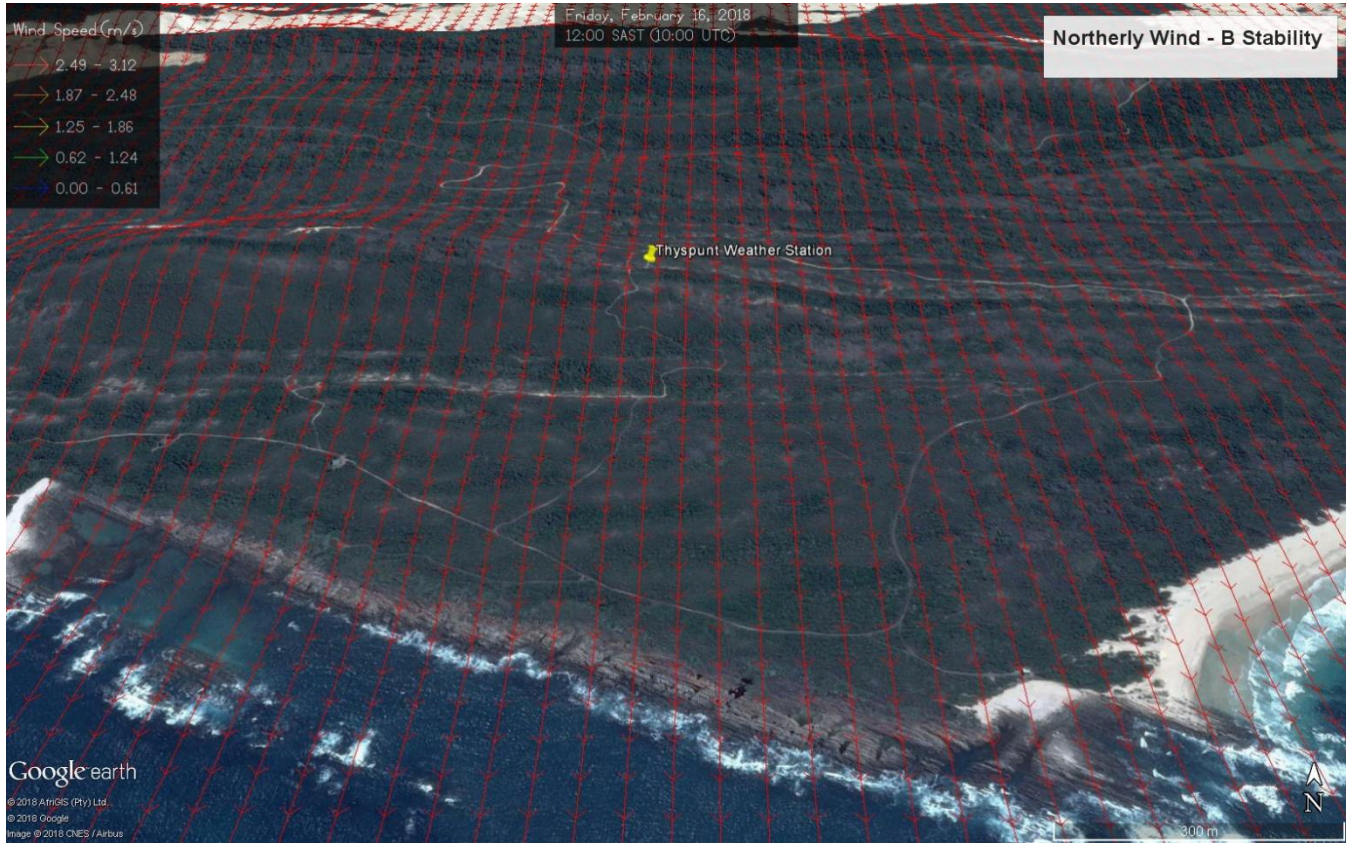


Figure 5.8.A.28
Wind Field Constructed at Thyspunt for a Northerly Wind with Moderately Unstable Atmospheric Conditions (B stability)

© Eskom 2026/Rev 0c

PRINTED VERSIONS OF THIS DOCUMENT ARE NOT CONTROLLED

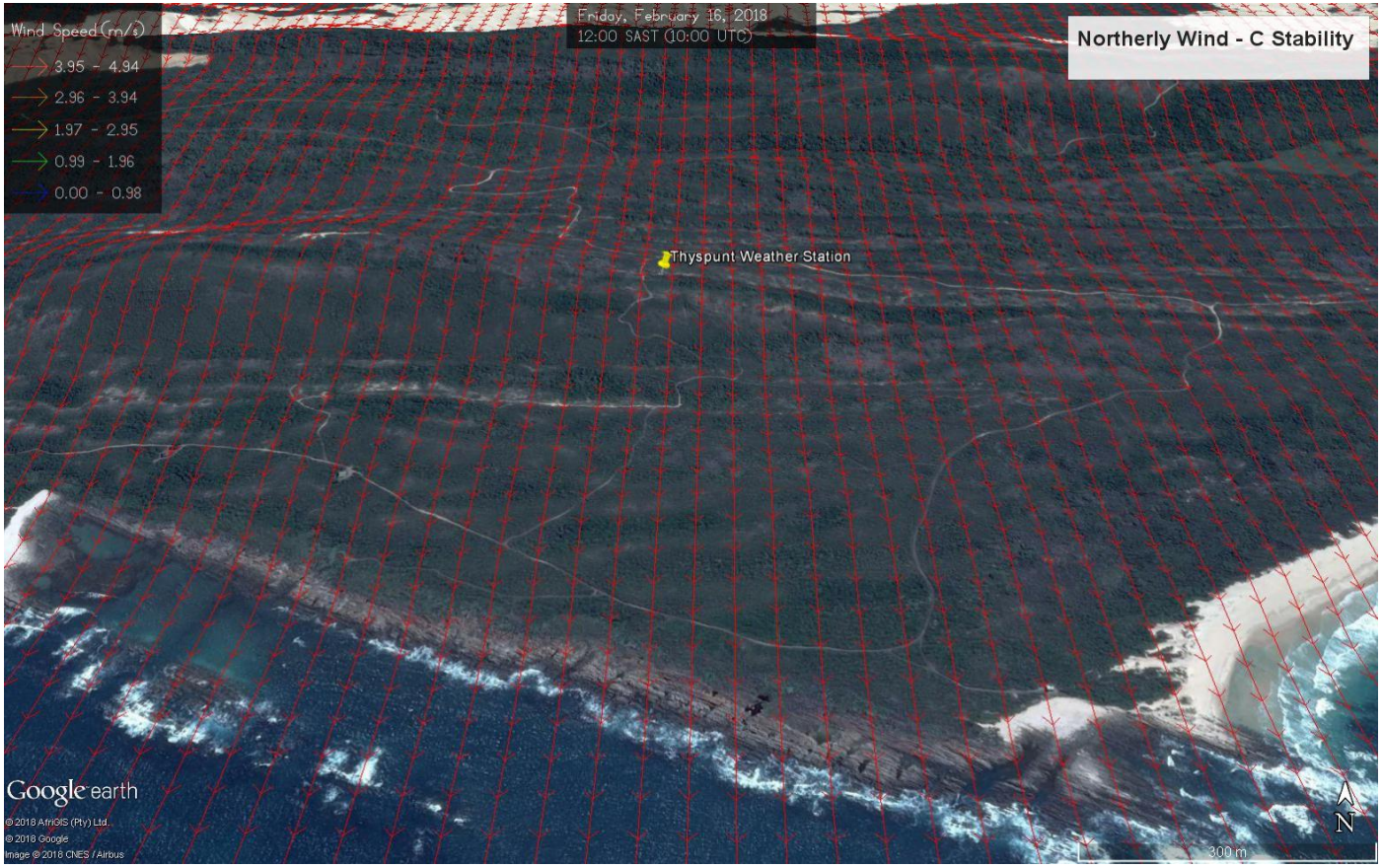


Figure 5.8.A.29
Wind Field Constructed at Thyspunt for a Northerly Wind with Unstable Atmospheric Conditions (C stability)

© Eskom 2026/Rev 0c

PRINTED VERSIONS OF THIS DOCUMENT ARE NOT CONTROLLED

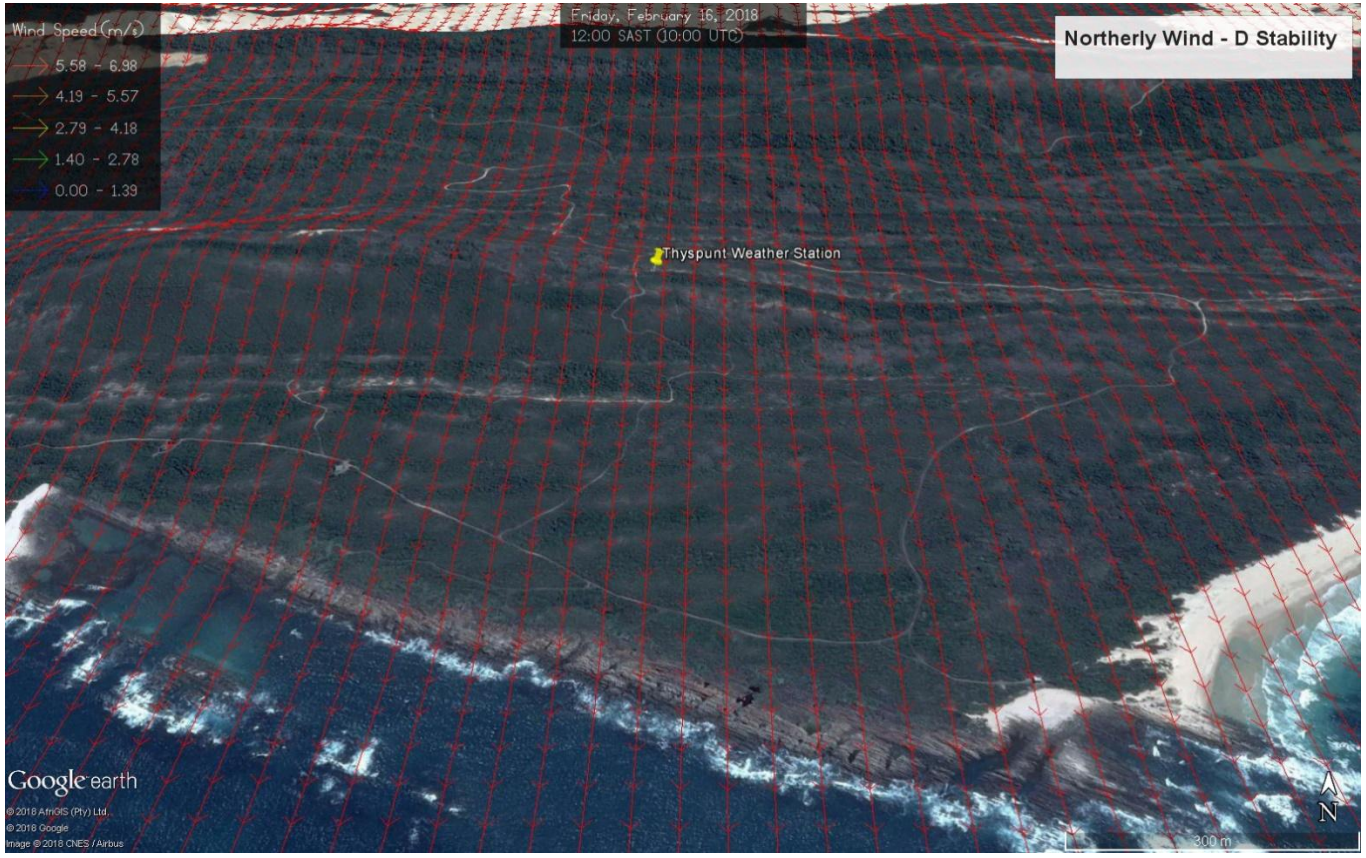


Figure 5.8.A.30
Wind Field Constructed at Thyspunt for a Northerly Wind with Neutral Atmospheric Conditions (D stability)

© Eskom 2026/Rev 0c

PRINTED VERSIONS OF THIS DOCUMENT ARE NOT CONTROLLED

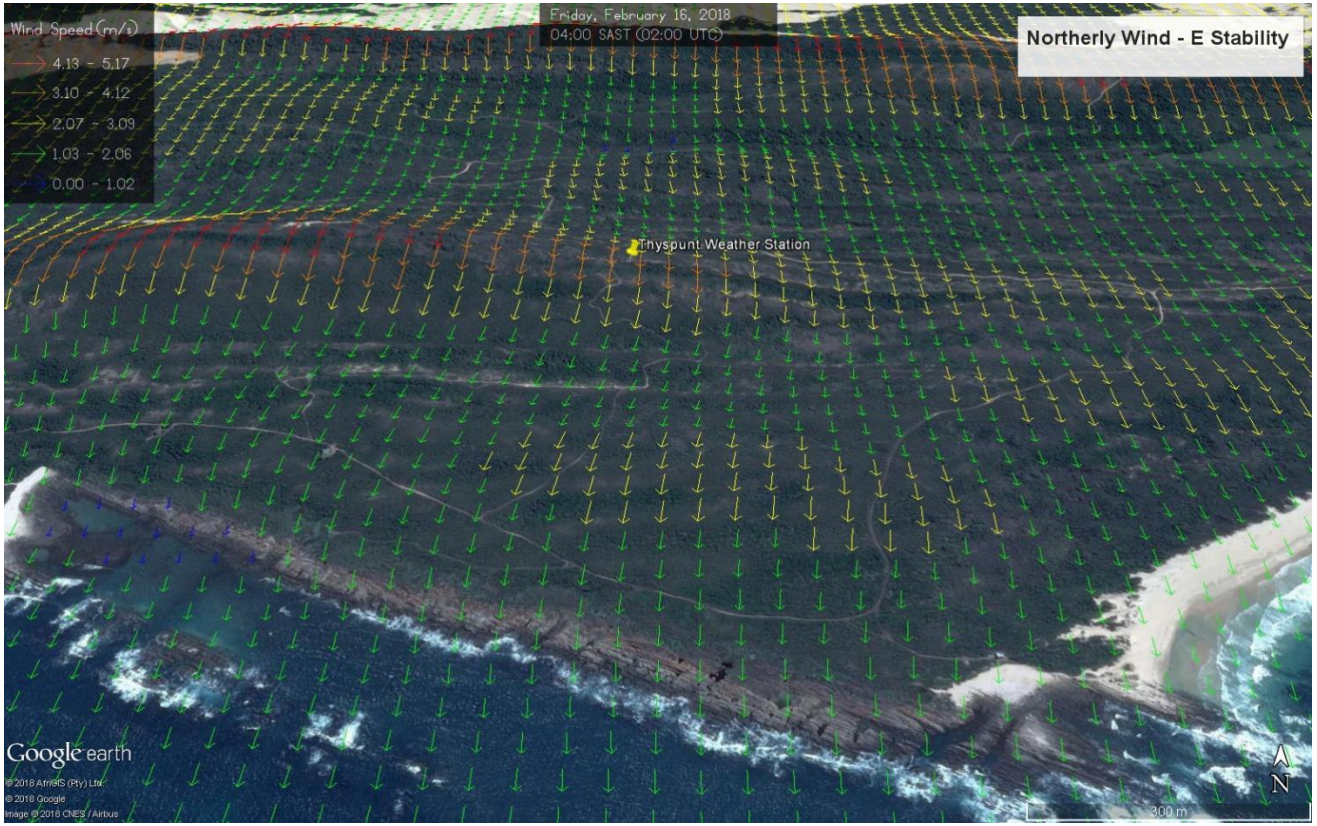


Figure 5.8.A.31
Wind Field Constructed at Thyspunt for a Northerly Wind with Stable Atmospheric Conditions (E stability)

© Eskom 2026/Rev 0c

PRINTED VERSIONS OF THIS DOCUMENT ARE NOT CONTROLLED

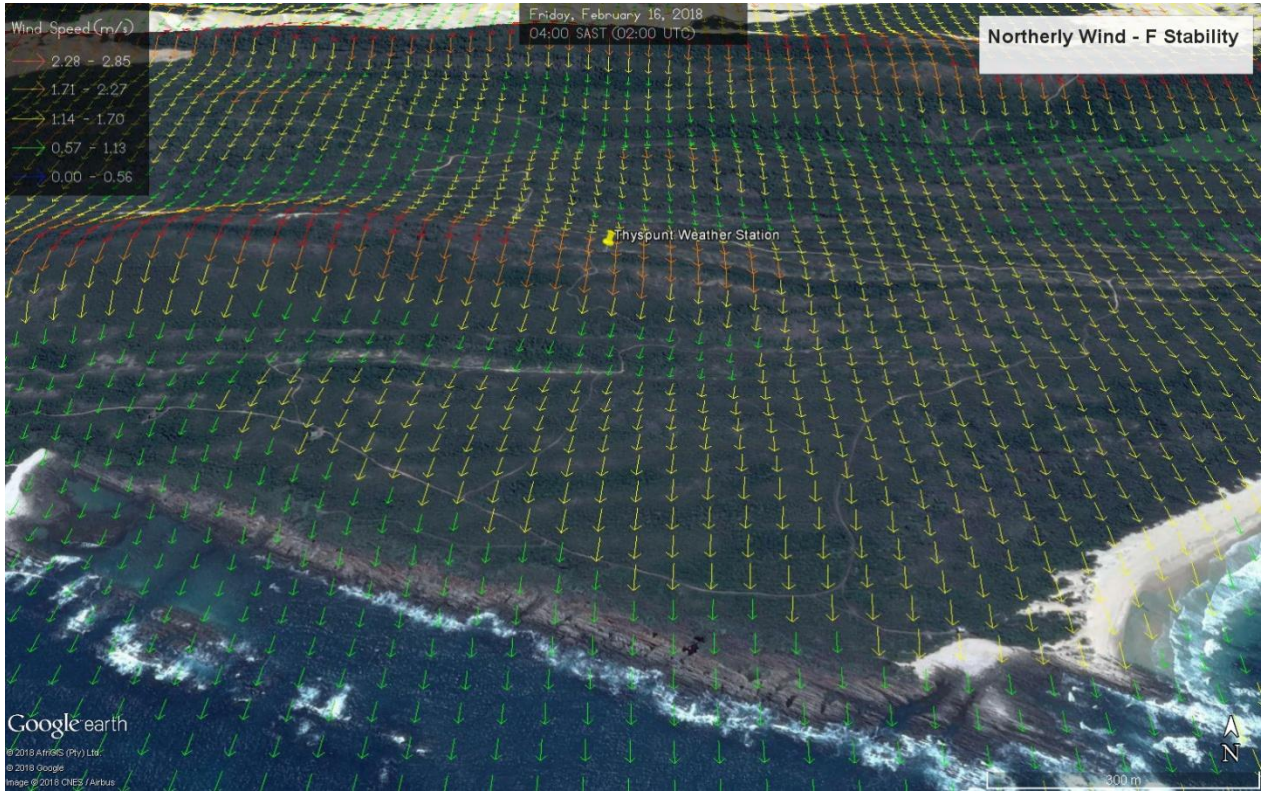


Figure 5.8.A.32
Wind Field Constructed at Thyspunt for a Northerly Wind with Very Stable Atmospheric Conditions (F stability)

© Eskom 2026/Rev 0c

PRINTED VERSIONS OF THIS DOCUMENT ARE NOT CONTROLLED

It is conceivable that there will be differences between wind speed observations made at the current location (which is at an elevation of 51 m) compared with conditions closer to the shoreline. This may be expected when the wind blows from the south or the northern sectors, which occur about 25 per cent of the time. With these wind directions, the current observed wind speeds may be 5 per cent to 10 per cent higher than the winds in the area earmarked for the nuclear installation(s). Since the wind speeds from these directions are generally weak, i.e. average of about 2 m/s from the north and 4 m/s from the south, the average current observations from these directions could be between 0.2 m/s and 0.4 m/s higher than at the lower elevation. These differences were calculated at a height of 10 m agl. At a release point of 50 m or higher, the differences in wind speeds at the two locations would be even less, i.e. 1 per cent.

Given the possibility that the wind speeds may have been slightly overestimated by 5 per cent in magnitude during neutral atmospheric conditions, the fraction of the six atmospheric stability classes may have been incorrectly determined for a location closer to the seashore. The current measurements reflect the actual atmospheric stabilities at the point of measurement. By reducing the wind speeds to extrapolate for conditions at the lower elevation, an approximate reduction of neutral conditions of about 0.8 per cent is estimated.

For the purpose of determining the direct impact that the wind may have on the nuclear installation(s), this would provide a slightly higher estimate of wind speed conditions if located closer to the seashore, and essentially the same if located at the project centroid.

Furthermore, since a relatively long record of weather conditions have already been collected at the current location, it is not recommended to move the weather station; instead, consideration of installing a second station at the lower elevation could be considered if the centroid is moved towards the seashore.

© Eskom 2026/Rev 0c

PRINTED VERSIONS OF THIS DOCUMENT ARE NOT CONTROLLED

Appendix 5.8.B: Distribution of Extreme Values

The extreme rainfall, wind speed and temperature estimates are used to determine critical design which the nuclear installation(s) must withstand during its lifetime. Extreme annual values of meteorological parameters constitute samples of random variables, which may be characterised by specific probability distributions. In principle, the data set should be analysed with probability distribution functions appropriate to the data sets under study. Among these, the generalised extreme value distributions are widely used (International Atomic Energy Agency, 2011): Fisher–Tippett Type I (Gumbel), Type II (Fréchet) and Type III (Weibull).

Extreme meteorological conditions are defined in terms of recurrence periods, e.g. 10-, 100- , …., 100 000 000-year recurrence periods, or equivalently expressed as probabilities of $1x10^{-1}$, $1x10^{-2}$, …., $1x10^{-8}$ per year. So, for example, the 100-year wind speed is defined as the wind speed exceeded on average once in a period of 100 years, or a wind speed with a probability of $1x10^{-2}$ per year.

The Gumbel distribution is suitable to describe the distribution of extreme rainfall (annual totals and 24-hour storm events), wind speed (hourly averages and gusts) and temperatures (minimum and maximum). The classical extreme value theory is based on three asymptotic extreme value distributions. The Generalized Extreme Value (GEV) distribution combines these three distributions into a single mathematical form with the cumulative distribution function:

$$F(x) = \exp\left\{-\exp\left(\frac{x-\xi}{\alpha}\right)\right\} \; F(x) = \exp\left\{-\exp\left(\frac{x-\xi}{\alpha}\right)\right\} \text{ for k} = 0$$

$$F(x) = \exp\left\{-\left[1-k\left(\frac{x-\xi}{\alpha}\right)\right]\right\}^{1/k} \quad \text{for k} \neq 0$$

where k, α and ξ are the shape, scale and location parameter, respectively, and x is the maximum of an epoch.

When $k = 0$, it is the Type I GEV or so-called Gumbel distribution; when $k < 0$, the GEV is called the Type II (or Frechet) distribution, which has a long right tail; when $k > 0$, it is the Type III GEV (a form of the Weibull distribution) and has a short tail. In order to determine whether or not a particular sample came from a population distribution that is Gumbel, Frechet, or Weibull, one may check a probability plot. If such a plot produces points that fall close to a straight line, then the distribution function that the

© Eskom 2026/Rev 0c

PRINTED VERSIONS OF THIS DOCUMENT ARE NOT CONTROLLED

plot is based upon is a reasonable model (International Atomic Energy Agency, 2011). To illustrate, the Gumbel distribution can also be written as:

$$x = \alpha \ln(-\ln[F(x)]) + \xi = \alpha u + \xi$$

So, plotting *x* against *u* gives a straight line. This property enables a visual check to be made of the extent to which a data set fits the Gumbel distribution.

There are a number of different methods available to determine the shape, scale and location parameters from a data set, including:

- Method of Moments;
- Method of L-Moments;
- Method of Maximum Likelihood;
- Gumbel's Fitting Method;
- Method of Least Squares.

In the analysis, all five methods were used. The final selection was based on the method resulting in the best fit to the observed values; identified using the Kolmogorov-Smirnov test. The Kolmogorov–Smirnov test statistic, *D*, quantifies a distance between the GEV distribution function of the sample and the cumulative distribution function of the observation:

$$D = \max \left| F(x_i) - \frac{i-1}{n}, \frac{i}{n} - F(x_i) \right|$$

where $F(x_i)$ is the calculated probability given by the GEV distribution function for an observation x_i, taken from a set of *n* values, ranked from smallest (*i = 0*) to highest (*i = n*), i.e.

$$x_1 < \cdots x_i < \cdots < x_n$$

The null distribution of this statistic is calculated under the null hypothesis that the sample is drawn from the reference distribution (i.e. observations). The null hypothesis, that the GEV distribution function is an appropriate distribution function, is rejected when *D* assumes a large value. For a confidence level of 95 per cent, under the null hypothesis, a distribution function with a *D* larger than $1.36/\sqrt{n}$ would be rejected. For *n = 40*, *D ≤ 0.21*.

© Eskom 2026/Rev 0c

PRINTED VERSIONS OF THIS DOCUMENT ARE NOT CONTROLLED

Extreme Rainfall

The 38-years (1985-2023, missing 2004) of rainfall maxima which were observed at the Cape St. Francis WS are summarised in ***Table 5.8.B.1***. These data were used to fit an appropriate GEV using the five methods listed above. The results from the distribution fit (shape k, scale α, location ξ and Kolmogorov–Smirnov test statistic, D) are summarised in ***Table 5.8.B.2*** (24-hour storm) and ***Table 5.8.B.3*** (annual total rainfall). The tables also include the extremes for return periods 10- to 100 000 000 years. Five methods, i.e. method of moments, method of L-moments, method of maximum likelihood, Gumbel's fitting method and the method of least squares resulted in an acceptable fit for a 95 per cent confidence interval null hypothesis test, with the method of maximum of moments performing the best for the 24-hour storm data and Gumbel's fitting method performing best for the annual rainfall data.

Table 5.8.B.1
Maximum 24-Hour and Annual Total Rainfall (Cape St. Francis WS)

Year	Rainfall [mm]		Year	Rainfall [mm]	
	24-Hour Max	Annual		24-Hour Max	Annual
1985	47.9	553.4	2005	35	457
1986	32	579.3	2006	84	566
1987	57	631.5	2007	158	769
1988	29.2	440.7	2008	70	421
1989	70	495.6	2009	36	419
1990	40	562.4	2010	41	477
1991	36.6	444.1	2011	126	972
1992	89	893.2	2012	61	876
1993	99.5	791.4	2013	53	529
1994	62.5	733.6	2014	38	612
1995	45	703.9	2015	47	645
1996	107.6	935.3	2016	65	535
1997	49.5	652.9	2017	53	318
1998	42.9	657	2018	38	475
1999	103.5	644.1	2019	35	461
2000	50.4	594.9	2020	52	691
2001	40.1	452.9	2021	95	627
2002	66.5	730	2022	48	539
2003	65	739.3	2023	74	915
2004	No data	No data			

These distribution functions are also illustrated in ***Figure 5.8.B.1*** (24-hour storm) and ***Figure 5.8.B.2*** (annual total rainfall).

© Eskom 2026/Rev 0c

PRINTED VERSIONS OF THIS DOCUMENT ARE NOT CONTROLLED

Table 5.8.B.2
Comparison of Methods to Determine Extreme 24-Hour Storms (Cape St. Francis WS)

Return Period	24-Hour Maximum Rainfall [mm]				
	Method of Moments	**Method of L-Moments**	**Method of Maximum Likelihood**	**Gumbel's Fitting Method**	**Method of Least Squares**
10	99.0	98.0	91.5	104.1	101.0
100	151.4	149.1	135.1	162.5	155.6
1000	202.9	199.2	177.9	219.8	209.2
10000	254.3	249.3	220.7	277.0	262.7
100000	305.6	299.3	263.4	334.2	316.1
1000000	357.0	349.4	306.1	391.4	369.6
10000000	408.4	399.4	348.9	448.6	423.1
100000000	459.7	449.5	391.6	505.8	476.6
GEV Parameters					
Shape	0	0	0	0	0
Scale	22.309	21.735	18.561	24.843	23.228
Location	48.791	49.117	49.713	48.189	48.723
Kolmogorov-Smirnov Test:					
D	**0.116**	0.119	0.120	0.130	0.117

© Eskom 2026/Rev 0c

PRINTED VERSIONS OF THIS DOCUMENT ARE NOT CONTROLLED

Table 5.8.B.3
Comparison of Methods to Determine Yearly Total Rainfall (Cape St. Francis WS)

Return Period	24-Hour Maximum Rainfall [mm]				
	Method of Moments	Method of L-Moments	Method of Maximum Likelihood	Gumbel's Fitting Method	Method of Least Squares
10	830.0	841.6	846.2	858.7	842.7
100	1125.6	1153.6	1161.8	1187.9	1152.4
1000	1415.9	1459.9	1471.6	1511.2	1456.5
10000	1705.6	1765.7	1781.0	1833.8	1760.1
100000	1995.3	2071.4	2090.2	2156.4	2063.6
1000000	2285.0	2377.1	2399.5	2479.0	2367.2
10000000	2574.7	2682.9	2708.7	2801.6	2670.7
100000000	2864.4	2988.6	3018.0	3124.2	2974.2
GEV Parameters					
Shape	0	0	0	0	0
Scale	125.810	132.772	134.307	140.097	131.819
Location	546.868	542.822	543.955	543.473	546.023
Kolmogorov-Smirnov Test:					
D	0.088	0.070	0.070	**0.063**	0.078

© Eskom 2026/Rev 0c

PRINTED VERSIONS OF THIS DOCUMENT ARE NOT CONTROLLED

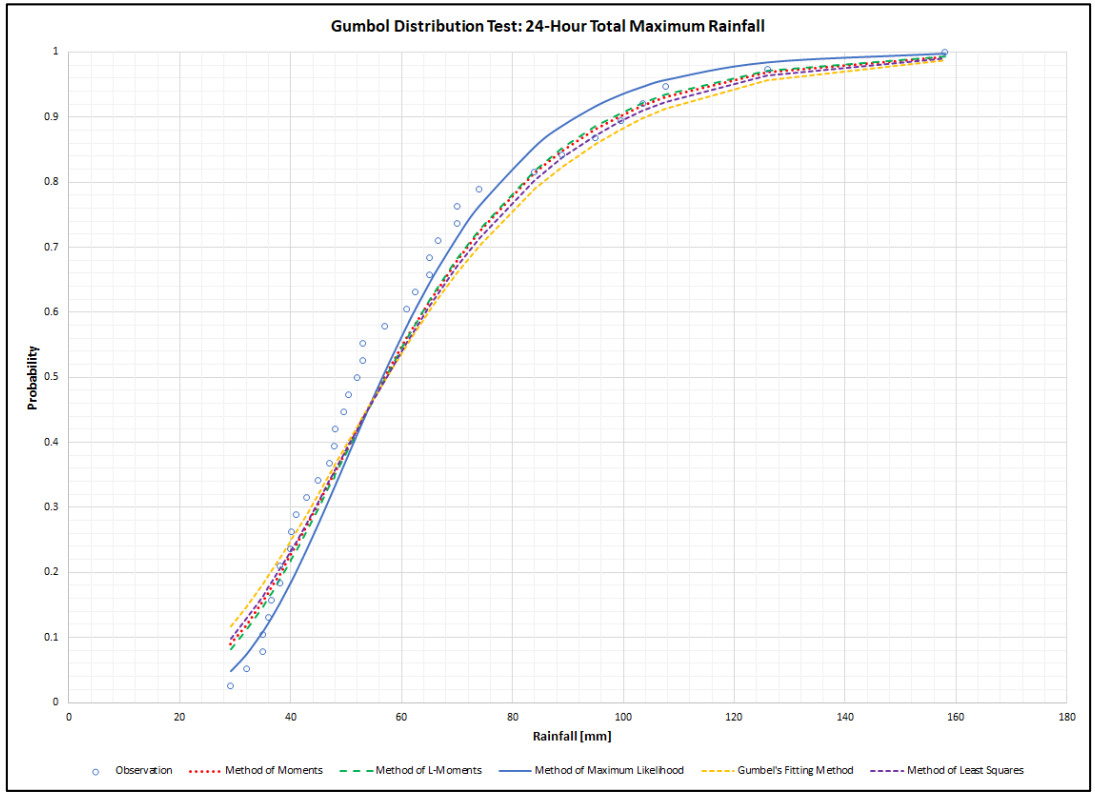


Figure 5.8.B.1
Goodness of Fit Test: Annual Total Rainfall (38-Year Dataset)

© Eskom 2026/Rev 0c

PRINTED VERSIONS OF THIS DOCUMENT ARE NOT CONTROLLED

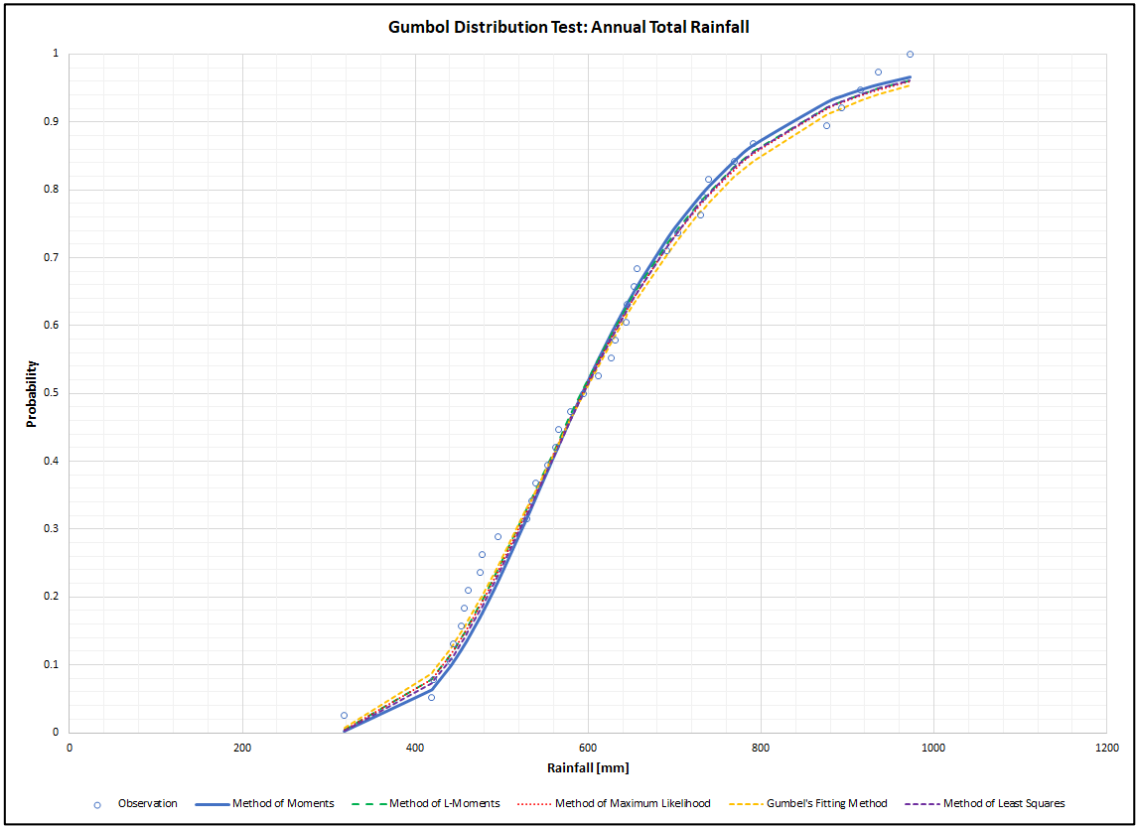


Figure 5.8.B.2

Goodness of Fit Test: Annual Total Rainfall (38-Year Dataset)

© Eskom 2026/Rev 0c

PRINTED VERSIONS OF THIS DOCUMENT ARE NOT CONTROLLED

Caution should be exercised in attempting to fit an extreme value distribution to a data set representing only a few years of records. If extrapolations are carried out over very long periods of time by means of a statistical technique, due regard should be given to the physical limits of the variable of interest (International Atomic Energy Agency, 2011). Care should also be taken in extrapolating to time intervals well beyond the duration of the available records (such as for 'return' periods greater than four times the duration of the sample) (International Atomic Energy Agency, 2011). The extreme values with small probabilities down to the required $1x10^{-8}$ per year (100 000 000-year return period) should recognise that extrapolation to these events carries a significant uncertainty, since they are based on a data set of only 38 years.

Table A-5.8.B.2 is a summary of the estimated extreme rainfall totals and the calculated 95 per cent confidence interval as estimated using the Jackknife sampling method. Jackknife samples are computed by leaving out one observation from the set of observations at a time. Each Jackknife sample is then used to evaluate the average and standard deviation of the estimate. The 95 per cent confidence calculated as 1.96 of the standard error, assuming a normal distribution. These distribution functions are also illustrated in ***Figure 5.8.B.3*** (24-hour storm) and ***Figure 5.8.B.4*** (annual total rainfall) together with the actual observed values.

Table 5.8.B.4
Maximum 24-Hour and Annual Total Rainfall Extremes (Cape St. Francis WS)

Return Period	Rainfall [mm]			
	24-Hour Total Max	95% Confidence Interval	Annual Total	95% Confidence Interval
10	99.0	± 20.8	858.7	± 84.8
100	151.4	± 38.8	1187.9	± 147.1
1000	202.9	± 56.8	1511.2	± 212.2
10000	254.3	± 74.9	1833.8	± 278.4
100000	305.6	± 93.0	2156.4	± 345.0
1000000	357.0	± 111.1	2479.0	± 412.0
10000000	408.4	± 129.2	2801.6	± 479.0
100000000	459.7	± 147.3	3124.2	± 546.2

© Eskom 2026/Rev 0c

PRINTED VERSIONS OF THIS DOCUMENT ARE NOT CONTROLLED

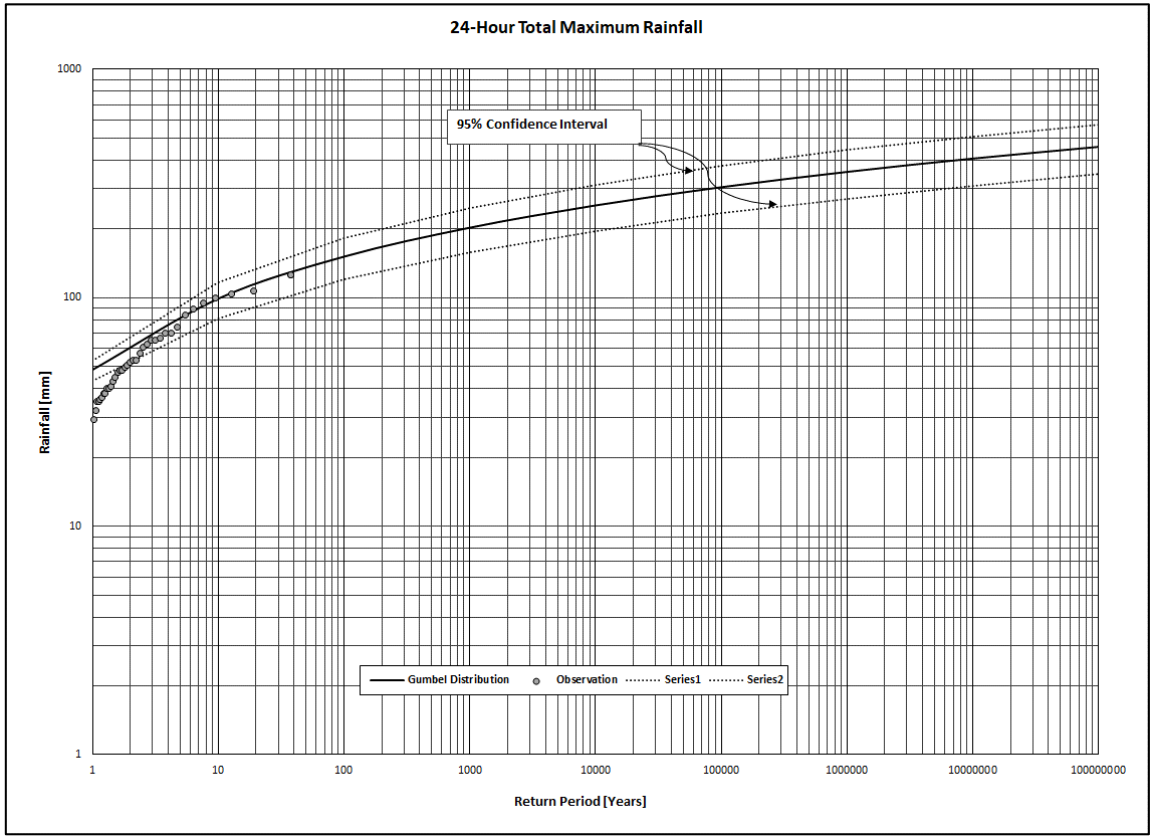


Figure 5.8.B.3

Gumbel Distribution Fit to 24-Hour Storm Events (38-Year Dataset)

© Eskom 2026/Rev 0c

PRINTED VERSIONS OF THIS DOCUMENT ARE NOT CONTROLLED

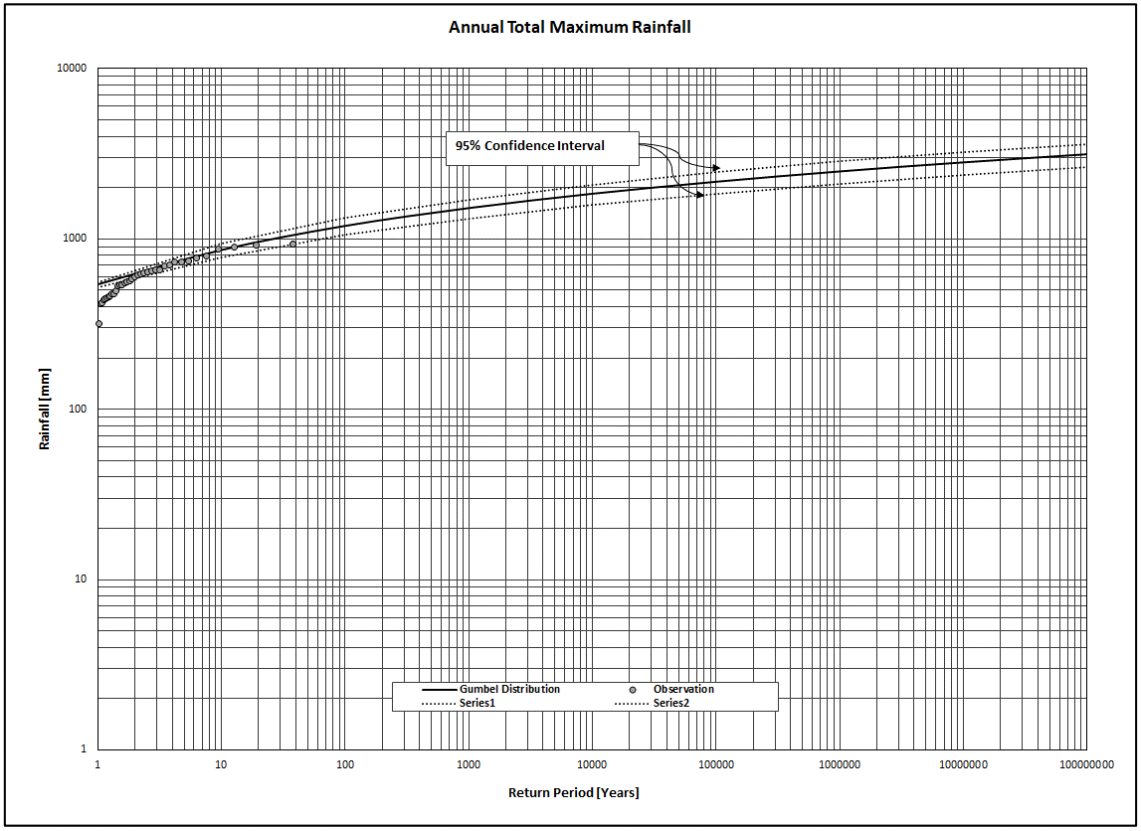


Figure 5.8.B.4

Gumbel Distribution Fit to Annual Total Rainfall (38-Year Dataset)

© Eskom 2026/Rev 0c

PRINTED VERSIONS OF THIS DOCUMENT ARE NOT CONTROLLED

Extreme Temperature

The 19-years (2005-2023) of dry-bulb temperature which were observed at the Cape St. Francis WS are summarised in ***Table 5.8.B.5***. These data were used to fit an appropriate GEV using the five methods discussed in the previous section.

The results from the distribution fit (shape k, scale α, location ξ and Kolmogorov–Smirnov test statistic, D) are summarised in ***Table 5.8.B.6*** (minimum hourly average temperature) and ***Table 5.8.B.7*** (maximum hourly average temperature). The tables include the extremes for return periods 10- to 100 000 000-years using the four of the methods since the method of least squares failed the null hypothesis test. The method of Maximum Likelihood performed the best for the minimum temperatures and method of Moments performed the best for maximum temperatures.

These distribution functions are also illustrated in ***Figure 5.8.B.5*** (minimum hourly average temperature) and ***Figure 5.8.B.6*** (maximum hourly average temperature).

Table 5.8.B.5
Maximum and Minimum Hourly Average Temperature
(Cape St. Francis WS)

Year	Hourly Average Temperature [°C]		Year	Hourly Average Temperature [°C]	
	Minimum	Maximum		Minimum	Annual
2005	5.0	32	2014	6.3	32.1
2006	7.0	28	2015	6.1	34.7
2007	7.1	36.5	2016	5.2	32.3
2008	7.1	37.2	2017	4.9	34.8
2009	7.3	31.6	2018	6.4	37.6
2010	6.7	31.5	2019	5.1	33.1
2011	7.8	28.5	2020	5.5	32.4
2012	6	30.8	2022	7.8	38.5
2013	6.9	34.4	2023	6.1	33.7

© Eskom 2026/Rev 0c

PRINTED VERSIONS OF THIS DOCUMENT ARE NOT CONTROLLED

Table 5.8.B.6
Comparison of Methods to Determine Minimum Hourly Average Dry Bulb Temperature (Cape St. Francis WS)

Return Period	24-Hour Maximum Rainfall [mm]			
	Method of Moments	**Method of L-Moments**	**Method of Maximum Likelihood**	**Gumbel's Fitting Method**
10	5.2	5.1	5.0	4.9
100	3.5	3.3	3.2	2.9
1000	1.9	1.5	1.3	1.0
10000	0.2	-0.3	-0.5	-0.9
100000	-1.4	-2.1	-2.3	-2.9
1000000	-3.0	-3.8	-4.1	-4.8
10000000	-4.7	-5.6	-5.9	-6.7
100000000	-6.3	-7.4	-7.7	-8.7
GEV Parameters				
Shape	0	0	0	0
Scale	0.710	0.769	0.789	0.839
Location	6.773	6.807	6.798	6.801
Kolmogorov-Smirnov Test:				
D	0.110	0.096	**0.088**	0.099

© Eskom 2026/Rev 0c

PRINTED VERSIONS OF THIS DOCUMENT ARE NOT CONTROLLED

Table 5.8.B.7
Comparison of Methods to Determine Maximum Hourly Average Dry Bulb Temperature (Cape St. Francis WS)

Return Period	24-Hour Maximum Rainfall [mm]			
	Method of Moments	**Method of L-Moments**	**Method of Maximum Likelihood**	**Gumbel's Fitting Method**
10	37.0	37.3	37.6	37.8
100	42.4	43.1	43.8	44.2
1000	47.7	48.8	49.9	50.5
10000	53.0	54.5	56.0	56.8
100000	58.3	60.3	62.0	63.1
1000000	63.7	66.0	68.1	69.4
10000000	69.0	71.7	74.2	75.7
100000000	74.3	77.4	80.2	81.9
GEV Parameters				
Shape	0	0	0	0
Scale	0.939	0.950	1.163	1.090
Location	35.137	35.130	35.095	35.679
Kolmogorov-Smirnov Test:				
D	**0.110**	0.129	0.128	0.130

© Eskom 2026/Rev 0c

PRINTED VERSIONS OF THIS DOCUMENT ARE NOT CONTROLLED

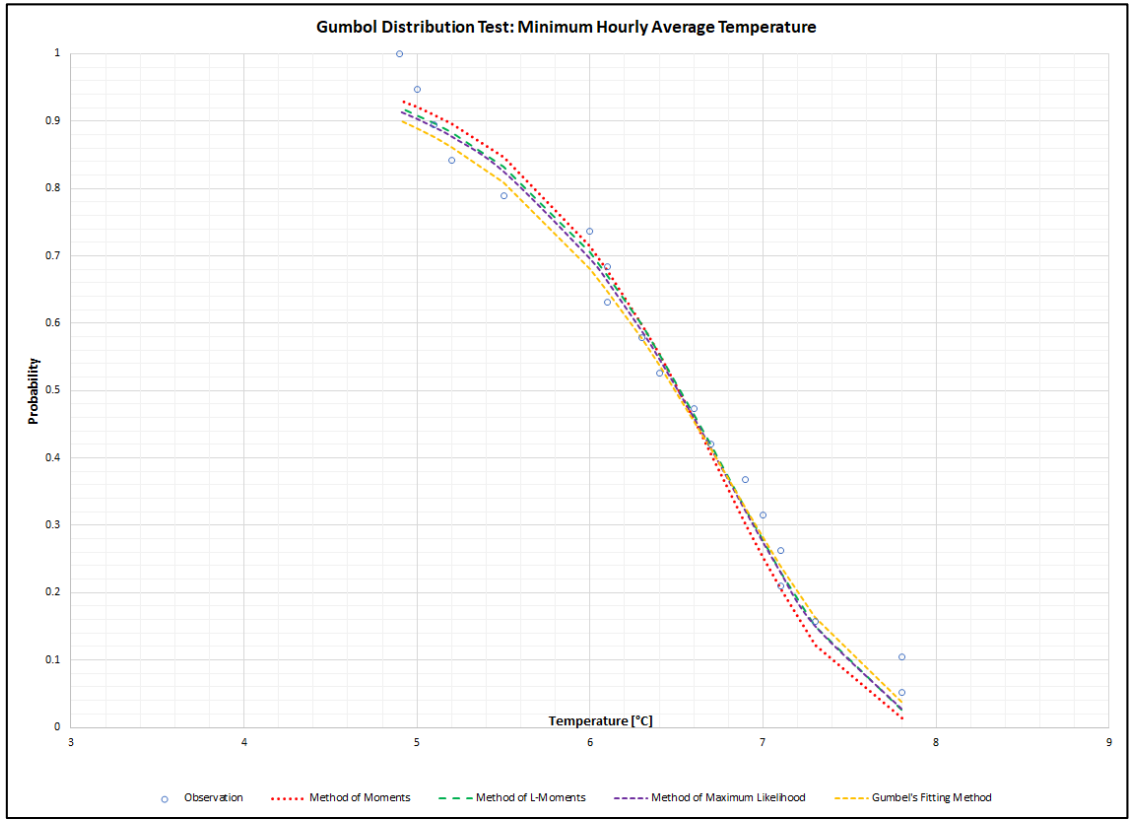


Figure 5.8.B.5
Goodness of Fit Test: Minimum Hourly Average Temperature (19-Year Dataset)

© Eskom 2026/Rev 0c

PRINTED VERSIONS OF THIS DOCUMENT ARE NOT CONTROLLED

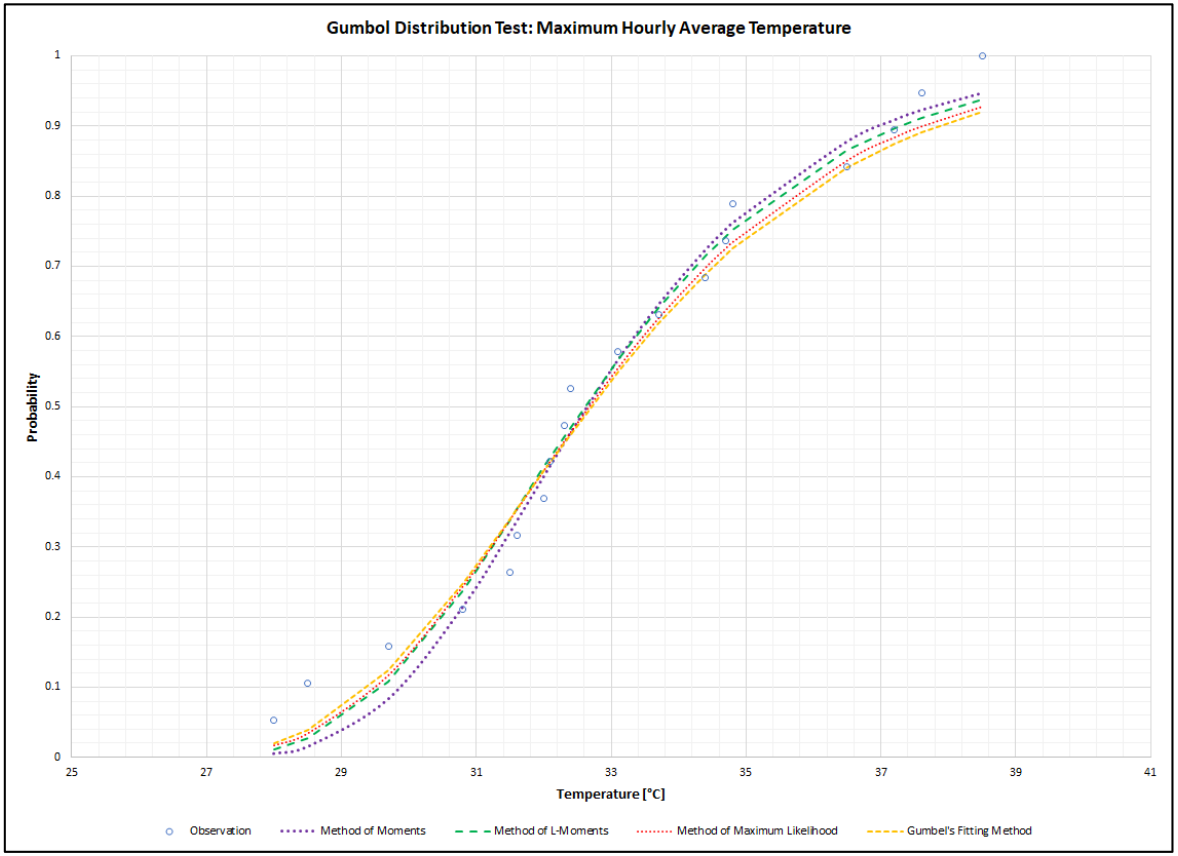


Figure 5.8.B.6

Goodness of Fit Test: Maximum Hourly Average Temperature (19-Year Dataset)

© Eskom 2026/Rev 0c

PRINTED VERSIONS OF THIS DOCUMENT ARE NOT CONTROLLED

Table 5.8.B.8 is a summary of the estimated minimum and maximum temperatures and the calculated 95 per cent confidence interval as estimated using the method of Maximum Likelihood for the minimum temperatures and method of Moments for the maximum temperatures. These distribution functions are also illustrated in ***Figure 5.8.B.7*** (minimum hourly average temperature) and ***Figure 5.8.B.8*** (maximum hourly average temperature) together with the actual observed values.

Since the extreme analyses were based on 19 years of data, caution should be exercised in the use of the projections for very low probabilities.

Table 5.8.B.8
Minimum and Maximum Hourly Average Temperature Extremes (Cape St. Francis WS)

Return Period	Hourly Average Temperature [°C]			
	Minimum	95% Confidence Interval	Maximum	95% Confidence Interval
10	5.0	± 0.7	37.0	± 1.8
100	3.2	± 1.2	42.4	± 3.1
1000	1.3	± 1.7	47.7	± 4.5
10000	-0.5	± 2.2	53.0	± 5.9
100000	-2.3	± 2.7	58.3	± 7.4
1000000	-4.1	± 3.2	63.7	± 8.9
10000000	-5.9	± 3.7	69.0	± 10.4
100000000	-7.7	± 4.2	74.3	± 11.9

© Eskom 2026/Rev 0c

PRINTED VERSIONS OF THIS DOCUMENT ARE NOT CONTROLLED

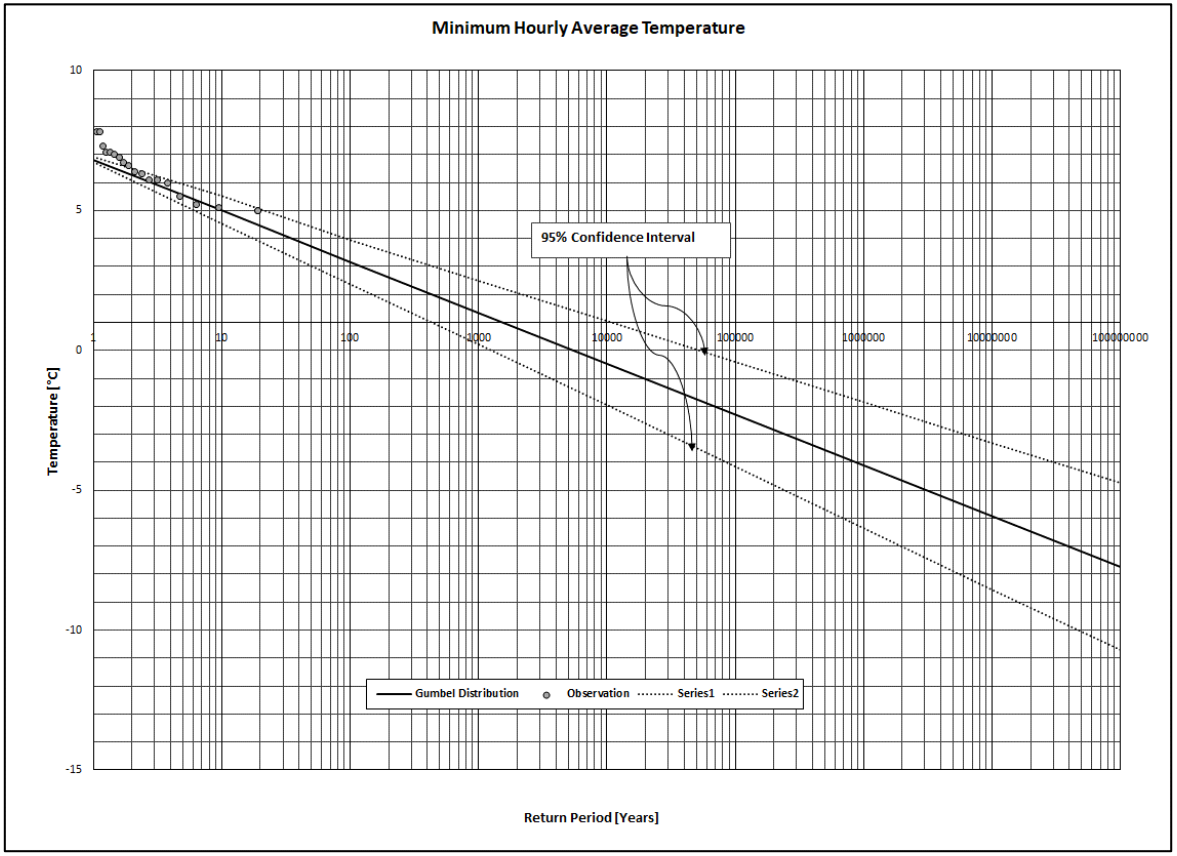


Figure 5.8.B.7

Gumbel Distribution Fit to Minimum Hourly Average Temperature (19-Year Dataset)

© Eskom 2026/Rev 0c

PRINTED VERSIONS OF THIS DOCUMENT ARE NOT CONTROLLED

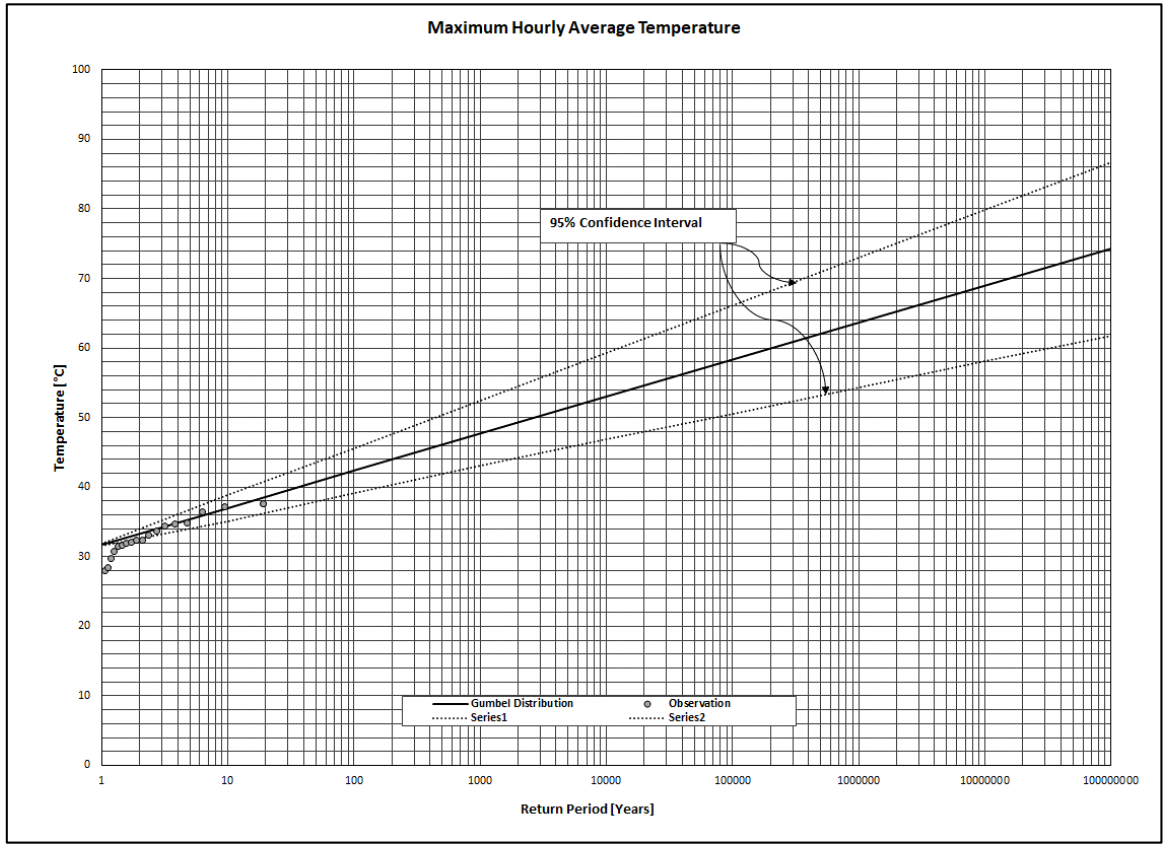


Figure 5.8.B.8

Gumbel Distribution Fit to Maximum Hourly Average Temperature (19-Year Dataset)

© Eskom 2026/Rev 0c

PRINTED VERSIONS OF THIS DOCUMENT ARE NOT CONTROLLED

Extreme Wind Speed

The 19-years (2005-2023) of hourly average wind speed maxima and short duration gusts which were observed at the Cape St. Francis WS are summarised in ***Table 5.8.A.8***. These data were used to fit an appropriate GEV with the results from each of the methods for the distribution fit (shape *k*, scale *α*, location *ξ* and Kolmogorov–Smirnov test statistic, *D*) summarised in ***Table 5.8.B.9*** (maximum hourly averages) and ***Table 5.8.B.10*** (wind gusts). The tables also include the extremes for return periods 10- to 100 000 000 years. The method of L-Moments performed the best for the maximum hourly average wind speed data and the method of Maximum Likelihood performed best for the wind gust data. These distribution functions are also illustrated in ***Figure 5.8.B.9*** (maximum hourly averages) and ***Figure 5.8.B.10*** (wind gusts).

Table 5.8.B.8
Maximum Hourly Average Wind Speeds and Wind Gusts (Cape St. Francis WS)

Year	Wind Speed [m/s]		Year	Wind Speed [m/s]	
	Hourly Average	Gust		Hourly Average	Gust
2005	18.3	No data	2015	19.9	34.5
2006	20.0	No data	2016	18.2	29.8
2007	19.6	31.3	2017	18.9	31.4
2008	21.1	32.0	2018	19.0	38.5
2009	23.2	34.2	2019	20.6	37.9
2010	18.1	35.3	2020	22.8	45.8
2011	19.3	30.5	2021	21.1	31.2
2012	19.4	29.5	2022	19.5	33.1
2013	20.2	34.0	2023	21.2	35.3
2014	20.2	32.6			

© Eskom 2026/Rev 0c

PRINTED VERSIONS OF THIS DOCUMENT ARE NOT CONTROLLED

Table 5.8.B.9
Comparison of Methods to Determine Extreme Hourly Average Wind Speeds (Cape St. Francis WS)

Return Period	Maximum Hourly Average Wind Speed [m/s]				
	Method of Moments	**Method of L-Moments**	**Method of Maximum Likelihood**	**Gumbel's Fitting Method**	**Method of Least Squares**
10	21.9	22.0	21.9	22.3	22.1
100	24.4	24.7	24.4	25.3	24.9
1000	27.0	27.3	27.0	28.3	27.6
10000	29.5	29.9	29.5	31.3	30.3
100000	32.0	32.6	32.0	34.3	33.1
1000000	34.5	35.2	34.6	37.3	35.8
10000000	37.1	37.9	37.1	40.2	38.6
100000000	39.6	40.5	39.6	43.2	41.3
GEV Parameters					
Shape	0	0	0	0	0
Scale	1.096	1.148	1.097	1.296	1.190
Location	19.399	19.369	19.397	19.355	19.385
Kolmogorov-Smirnov Test:					
D	0.092	**0.083**	0.092	0.109	0.090

© Eskom 2026/Rev 0c

PRINTED VERSIONS OF THIS DOCUMENT ARE NOT CONTROLLED

Table 5.8.B.10
Comparison of Methods to Determine Extreme Wind Gusts (Cape St. Francis WS)

Return Period	Wind Gusts [m/s]				
	Method of Moments	**Method of L-Moments**	**Method of Maximum Likelihood**	**Gumbel's Fitting Method**	**Method of Least Squares**
10	39.2	39.0	38.1	40.4	39.6
100	46.5	46.2	44.3	49.2	47.5
1000	53.7	53.2	50.2	57.8	55.2
10000	60.9	60.2	56.2	66.4	62.9
100000	68.1	67.3	62.2	75.1	70.6
1000000	75.3	74.3	68.2	83.7	78.3
10000000	82.5	81.3	74.2	92.3	86.0
100000000	89.7	88.3	80.2	100.9	93.6
GEV Parameters					
Shape	0	0	0	0	0
Scale	3.125	3.048	2.598	3.740	3.339
Location	32.132	32.176	32.302	31.999	32.131
Kolmogorov-Smirnov Test:					
D	0.128	0.125	**0.110**	0.162	0.145

© Eskom 2026/Rev 0c

PRINTED VERSIONS OF THIS DOCUMENT ARE NOT CONTROLLED

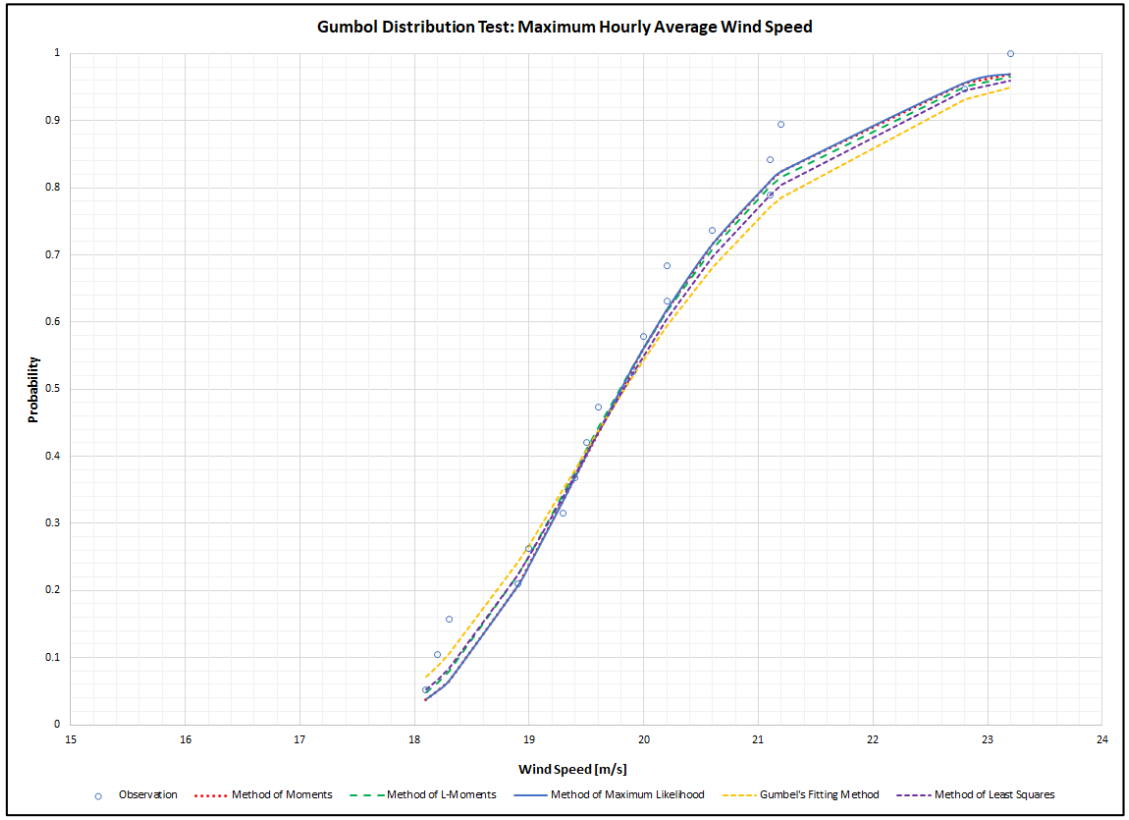


Figure 5.8.B.9
Goodness of Fit Test: Maximum Hourly Average Wind Speed (19-Year Dataset)

© Eskom 2026/Rev 0c

PRINTED VERSIONS OF THIS DOCUMENT ARE NOT CONTROLLED

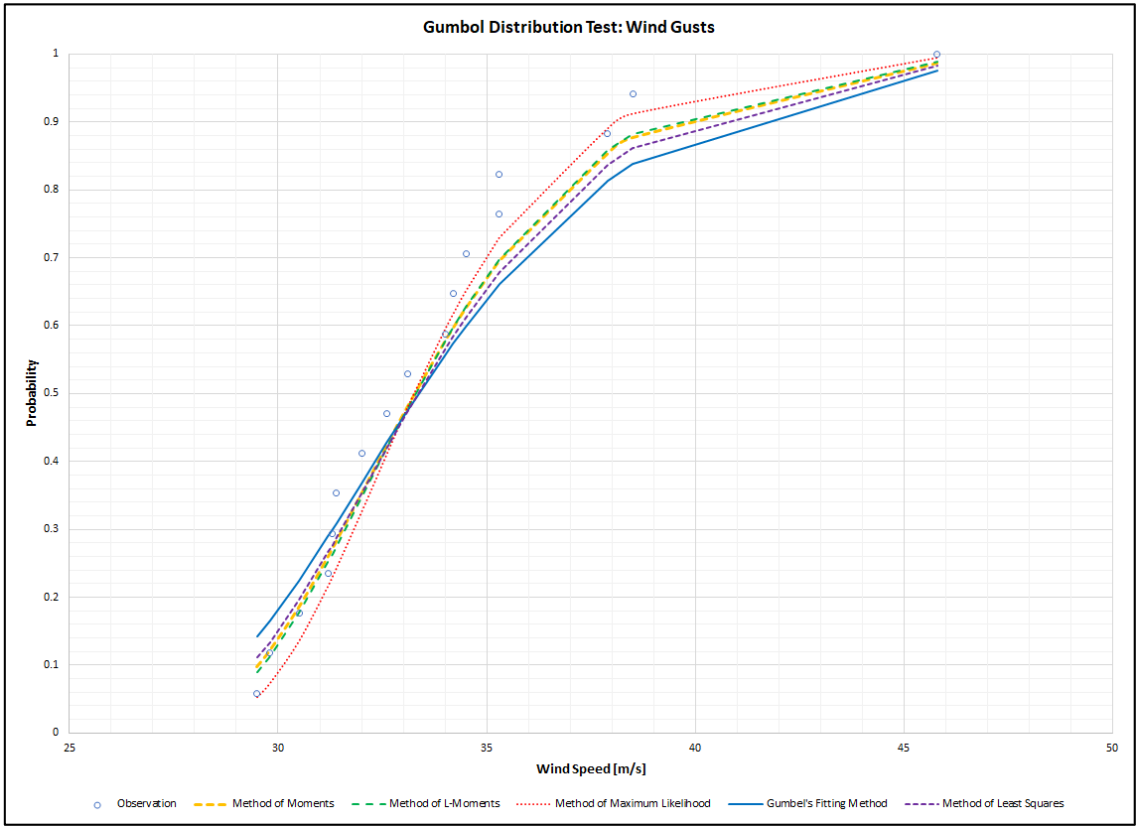


Figure 5.8.B.10

Goodness of Fit Test: Wind Gusts (19-Year Dataset)

© Eskom 2026/Rev 0c

PRINTED VERSIONS OF THIS DOCUMENT ARE NOT CONTROLLED

Table 5.8.B.11 is a summary of the estimated extreme wind speeds using the method of L-Moments for the maximum hourly average wind speed data and the Maximum Likelihood method for the wind gust data. The table also includes the calculated 95 per cent confidence interval as estimated using the Jackknife sampling method. These results are illustrated in ***Figure 5.8.B.11*** (maximum hourly average) and ***Figure 5.8.B.12*** (wind gusts) together with the actual observed values.

Table 5.8.B.11
Maximum Hourly Average Wind Speeds and Wind Gust Extremes (Cape St. Francis WS)

Return Period	Wind Speed [m/s]			
	Hourly Average Wind Speed	95% Confidence Interval	Wind Gust	95% Confidence Interval
10	22.0	± 1.2	38.1	± 3.5
100	24.7	± 2.1	44.3	± 6.2
1000	27.3	± 3.1	50.2	± 8.8
10000	29.9	± 4.1	56.2	± 11.4
100000	32.6	± 5.1	62.2	± 14.1
1000000	35.2	± 6.1	68.2	± 16.7
10000000	37.9	± 7.0	74.2	± 19.3
100000000	40.5	± 8.0	80.2	± 22.0

© Eskom 2026/Rev 0c

PRINTED VERSIONS OF THIS DOCUMENT ARE NOT CONTROLLED

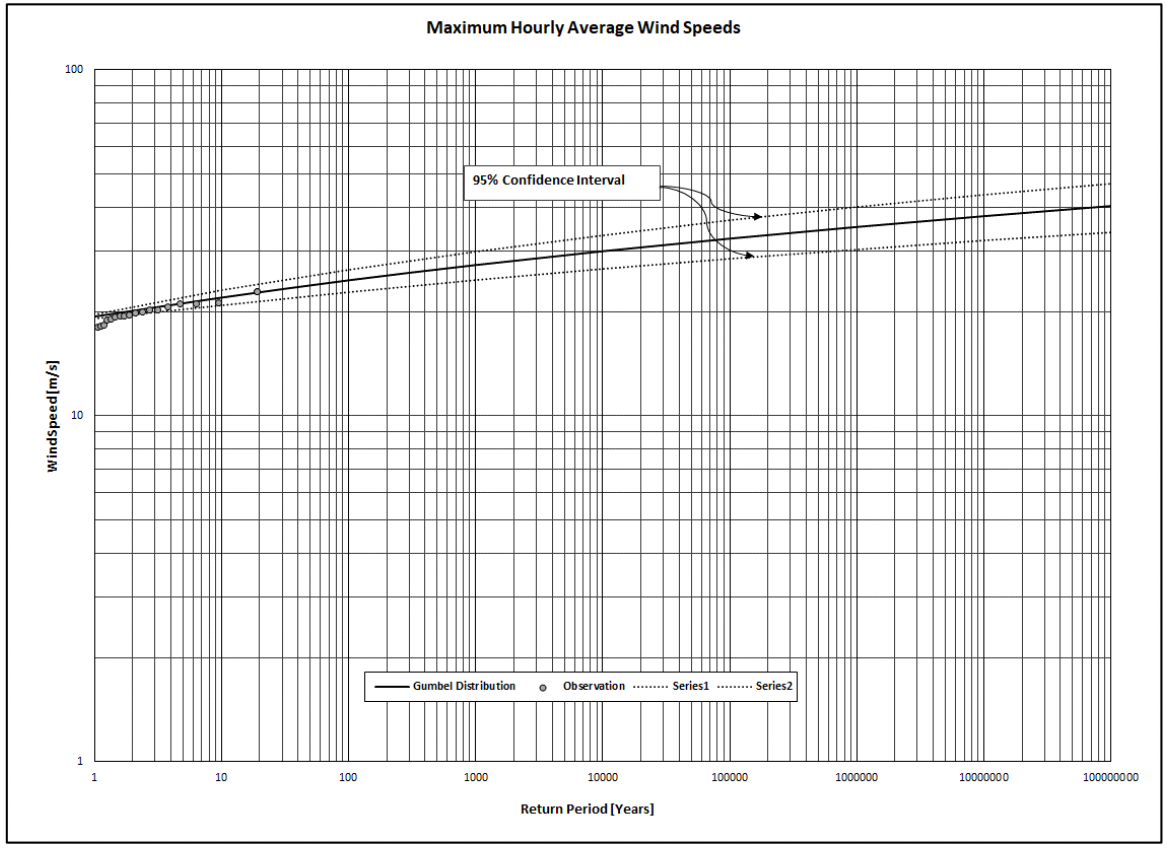


Figure 5.8.B.11

Gumbel Distribution Fit to Maximum Hourly Average Wind Speeds (19-Year Dataset)

© Eskom 2026/Rev 0c

PRINTED VERSIONS OF THIS DOCUMENT ARE NOT CONTROLLED

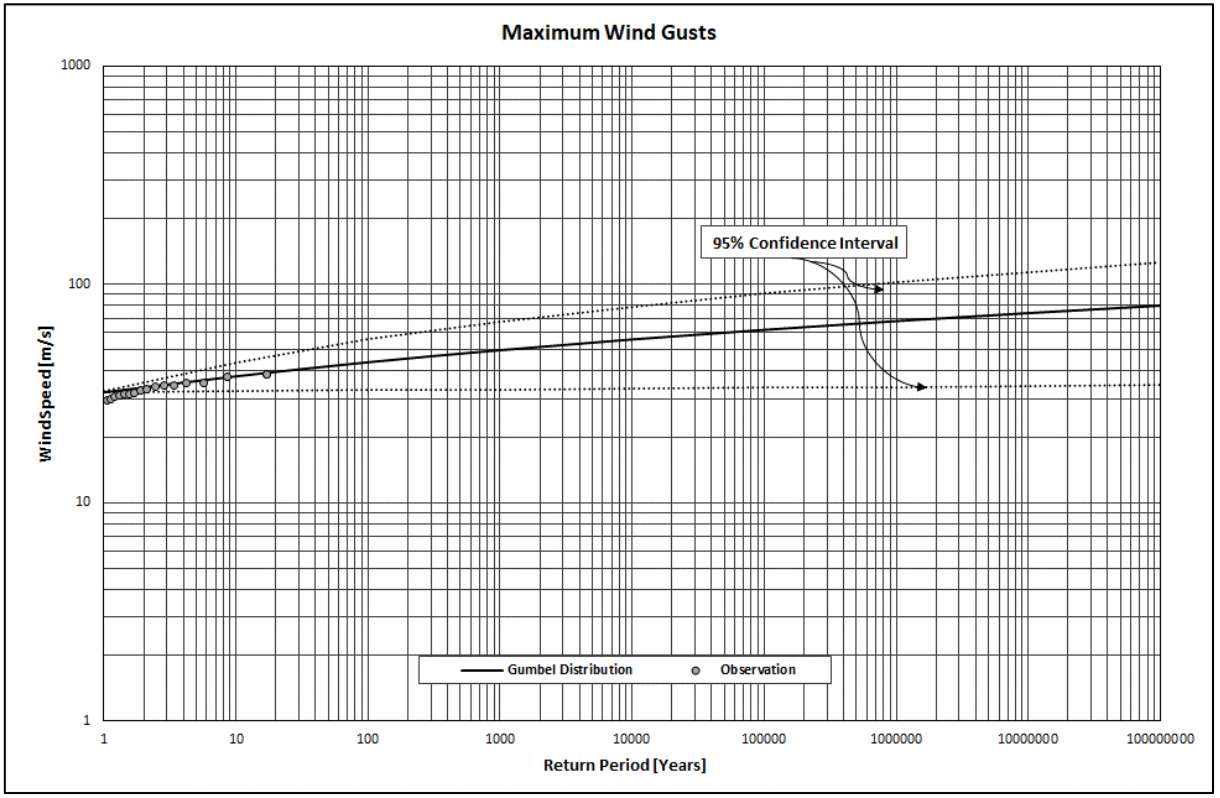


Figure 5.8.B.12

Gumbel Distribution Fit to Wind Gust Events (19-Year Dataset)

© Eskom 2026/Rev 0c

PRINTED VERSIONS OF THIS DOCUMENT ARE NOT CONTROLLED

Appendix 5.8.C: Evapotranspiration Rate Estimation

The classical form for the Penman (Penman, 1948; Penman, 1963) equation to estimate potential evaporation or evapotranspiration is (Shuttleworth, 1993):

$$E_{PEN} = \frac{\Delta}{\Delta + \gamma}\left(\frac{R_n}{\lambda}\right) + \frac{\gamma}{\Delta + \gamma}\left(\frac{6.43 f_u D}{\lambda}\right)$$

where

E_{PEN} = potential, *open water evaporation* or *evapotranspiration* (mm/d)

R_n = net radiation at the surface (MJ/m²/d)

Δ = slope of the saturation vapour pressure curve (kPa/°C) obtained from

$$\Delta = \frac{4098 e_s}{(237.3 + T)^2}$$

with e_s being the saturation vapour pressure at temperature T (°C)

γ = psychrometric coefficient (kPa/°C), given by

$$\gamma = 0.00064734P$$

P = atmospheric pressure (kPa)

λ = 2.45 is latent heat of vaporization (MJ/kg)

D = (e_s - e_a) is the vapour pressure deficit (kPa), where

e_s is the saturation vapour pressure (kPa)

e_a is the actual vapour pressure (kPa)

f_n = wind function: $f_n = a_u + b_u u_2$ where a_u and b_u are wind function coefficients and u_2 is the wind speed at 2 m height (m/s)

For the original Penman (Penman, 1948; Penman, 1963) equation a_u = 1, b_u = 0.537.

© Eskom 2026/Rev 0c

PRINTED VERSIONS OF THIS DOCUMENT ARE NOT CONTROLLED

A slight variation of the Penman equation is the Penman-Monteith equation (Shuttleworth, 1993):

$$E_{PM} = \frac{0.408\Delta(R_n - G) + \gamma \frac{900}{T + 275} u_2 D}{\Delta + \gamma(1 + 0.34u_2)}$$

Where E_{PM} is the *vegetation evaporation* (mm/d), and G is the soil heat flux density (MJ/m²/d). The soil heat flux density is approximately 10 per cent of the net radiation, R_n.

The saturation vapour pressure $e_s(T)$ can be calculated with (Wagner & Pruss, 1993)

$$e_s(T) = 0.6108 exp\left(\frac{17.27T}{273.3 + T}\right)$$

$$e_s(T) = 220640\ exp\left(F_\eta \frac{T_c}{273.15 + T}\right)$$

where

$$F_\eta = -7.85951783\,\eta + 1.84408259\,\eta^{1.5} - 11.7866497\,\eta^3 + 22.6807411\,\eta^{3.5} - 15.9618719\,\eta^4 + 1.80122502\,\eta^{7.5})$$

and

$$\eta = 1 - \frac{273.15 + T}{T_c}$$

where T is the air temperature in °C and T_c the critical temperature of water, 647.096 K.

The actual vapour pressure is obtained from

$$e_a(T) = \frac{RH}{100} e_s(T)$$

where *RH* is the relative humidity in per cent.

The *net radiation* (R_n) is computed as the difference between the incoming *net short wave radiation* (S_n) and the *net long wave radiation* (L_n).

$$R_n = S_n + L_n$$

The incoming net short wave radiation (S_n) is calculated from:

© Eskom 2026/Rev 0c

PRINTED VERSIONS OF THIS DOCUMENT ARE NOT CONTROLLED

$$S_n = (1 - \alpha)S_i$$

where S_i is the *measured incoming solar radiation* (MJ/m².day) at the site and α is reflection coefficient or *albedo*. Albedo indicates the relative amount of solar radiation retained by the earth's surface. Variations in albedo of the earth's land surface are broad. Bare, moist dark soils reflect as little as 0.08, grasslands 0.26 and sandy deserts 0.37 (Johnston, 1983). For open water surfaces a = 0.08 (Shuttleworth, 1993). The albedo for the site varies between 0.097 in January and 0.118 in June based on (Johnston, 1983).

The net long-wave radiation L_n (MJ/m².day) is calculated from:

$$L_n = L_i - L_o$$

where L_i is the *incoming long wave radiation* (MJ/m².day) and L_o is the *outgoing long wave radiation* (MJ/m².day). The net long wave radiation L_n is calculated from (Shuttleworth, 1993):

$$L_n = -f\xi_s\sigma(T_a + 273.15)^4$$

where

f = an adjustment for cloud cover
ξ_s = net emissivity
σ = 4.903x10^{-9} (MJ/m²/K^4/d) is Stephan-Boltzman constant
T_a = average air temperature in °C

The *adjustment for cloud cover f* calculated from the measured incoming solar radiation, S_i and the clear sky radiation S_{si}, is calculated as follows (Shuttleworth, 1993):

$$f = 1.35\frac{S_i}{S_{io}} - 0.35$$

And the *clear sky radiation*

$$S_{i0} = (0.57 + 0.00002Z)S_o$$

where S_o is the *extraterrestrial solar radiation* (MJ/m²/d) and Z is the station elevation above sea level (m).

The *net emissivity* ξ_s is calculated as follows (Shuttleworth, 1993):

$$\xi_s = a_e + b_e\sqrt{e_a(T)}$$

where

a_e = 0.34 (range 0.34 to 0.44)
b_e = -0.14 (range -0.14 to -0.25)

© Eskom 2026/Rev 0c

PRINTED VERSIONS OF THIS DOCUMENT ARE NOT CONTROLLED

The extraterrestrial solar radiation, S_o, is computed from the relative position of the earth to the sun. This is approximated as follows (Shuttleworth, 1993)

$$S_o = \frac{12(60)}{\pi} d_r G_{SC}[(\omega_2 - \omega_1)\sin\varphi\sin\delta + \cos\varphi\cos\delta\,(\sin\omega_2 - \sin\omega_1)]$$

where G_{SC} (= 0.0820 MJ/m²-min) is the solar constant, and the *inverse relative Earth-Sun distance*, d_r is given by

$$d_r = 1 + 0.033\cos\left(\frac{2\pi}{365}J\right)$$

where J is the Julian day (1 = 1 January consecutively counting to 31 December), φ is the longitude (degrees) and δ is the *solar declination* (degrees) given by

$$\delta = asin\left(sin\left(\frac{O_{corr}}{2}\frac{\pi}{180}\right)sin\left(\beta_{app}\frac{\pi}{180}\right)\right)\frac{180}{\pi}$$

with *obliquity correction*, O_{corr}, of the elliptic given by

$$O_{corr} = \epsilon_0 + 0.00256\cos\left((125.04 - 1934.136\,J_C)\frac{\pi}{180}\right)$$

To find the time J_C, measured in Julian centuries from the Epoch J2000, the following equation applies

$$J_C = \frac{J_{ED} - 2451545}{36525}$$

where $J_{ED}$is the Julian Ephemeris Day, obtained from

$$J_{ED} = \frac{t_{Diff} - t_{GMT}}{24} + 2415020.5$$

with the time difference calculate from

$$t_{Diff} = hour\ difference\ (t_{loc} - "01\ January\ 1900\ 00{:}00{:}00")$$

The obliquity correction, $\mathrm{O_{corr}}$, requires the *mean obliquity of the ecliptic*, ϵ_0, or i*nclination of the Earth's axis of rotation*, is the angle between the equator and the ecliptic:

© Eskom 2026/Rev 0c

PRINTED VERSIONS OF THIS DOCUMENT ARE NOT CONTROLLED

$$\epsilon_0 = 23 + \frac{26 + \frac{21.448 - J_C\{46.815 + J_C(0.00059 - 0.001813\,J_C)\}}{60}}{60}$$

The solar declination equation also requires the *Sun's apparent longitude*, β_{app}:

$$\beta_{app} = \beta_{true} - 0.00569 - 0.00478\,sin\left((125.04 - 1934.136\,J_C)\frac{\pi}{180}\right)$$

which in turn requires the *Sun's true longitude*, β_{true}, that may be calculated from:

$$\beta_{true} = \beta_{sun} + E_{ctr}$$

with the *Sun's geometric mean longitude*, β_{sun}, that may be approximated as follows:

$$\beta_{sun} = modulo(280.46646 + J_C(36000.76983 + 0.0003032\,J_C), 360)$$

and the *Sun equation of centre*, E_{ctr}, in minutes which is given by

$$\begin{aligned} E_{ctr} = {} & \left(1.914602 - J_C(0.004817 + 0.000014\,J_C)\right)sin\left(\beta_{sunA}\frac{\pi}{180}\right) \\ & + (0.019993 - 0.000101\,J_C)sin\left(2\beta_{sunA}\frac{\pi}{180}\right) \\ & + sin\left(3J_C\frac{\pi}{180}\right)0.000289 \end{aligned}$$

with the *geometric mean anomaly of the sun*, β_{sunA}, given by

$$\beta_{sunA} = 357.52911 + J_C(15999.05029 - 0.0001537J_C)$$

The angles ω_1 and ω_2 in the equation for the extraterrestrial solar radiation, are the *solar time angle* (radians) at the beginning and end of the calculation period, t_1, computed from

$$\omega_1 = \omega - \frac{\pi t_1}{24}$$

$$\omega_2 = \omega + \frac{\pi t_1}{24}$$

with ω the *solar time angle* (radians) at midpoint of the hourly, or shorter period, t_1 length of the calculation period (hour), e.g., 1 for an hourly period or 0.17 for a 10-minute period, computed from

© Eskom 2026/Rev 0c

PRINTED VERSIONS OF THIS DOCUMENT ARE NOT CONTROLLED

$$\omega = \left(\frac{t_{sunTrue}}{4} + 180\right)\frac{\pi}{180} \qquad for\ \frac{t_{sunTrue}}{4} < 0$$

$$= \left(\frac{t_{sunTrue}}{4} - 180\right)\frac{\pi}{180} \qquad for\ \frac{t_{sunTrue}}{4} \geq 0$$

with the *true solar time*, $t_{sunTrue}$, calculated from

$$t_{sunTrue} = modulus(60\ t_{loc} + E_{time} + sign(t_{GMT})\ 4\beta - 60\ t_{GMT}, 1400)$$

using the *local time* in hours after midnight (i.e., 1 to 24), t_{loc}, and the *equation of time,* E_{time}, in minutes, at any given instance, which is given by

$$E_{time} = 4\left(Y\ sin\left(2\beta_{sun}\frac{\pi}{180}\right) - 2e\ sin\left(\beta_{sunA}\frac{\pi}{180}\right) + 4eY\ sin\left(\beta_{sunA}\frac{\pi}{180}\right) cos\left(2\beta_{sun}\frac{\pi}{180}\right) - 0.5Y^2\ sin\left(4\beta_{sun}\frac{\pi}{180}\right) - 1.2e^2 sin\left(2\beta_{sunA}\frac{\pi}{180}\right)\right)\frac{180}{\pi}$$

with the *eccentricity of the Earth's orbit*, e, calculated from

$$e = 0.016708634 + J_C(0.000042037\ +\ 0.0000001267\ J_C)$$

and the parameter, Y, given by

$$Y = \left[\tan\left(\frac{O_{corr}}{2}\frac{\pi}{180}\right)\right]^2$$

with the with obliquity correction O_{corr} equation as previously provided.

When calculating the solar time angles ω_1 and ω_2 the following limitations apply:

$$if\ \omega_1 < \omega_{sr}\ then\ \omega_1 = \omega_{sr}$$

$$if\ \omega_2 > \omega_{ss}\ then\ \omega_2 = \omega_{ss}$$

where ω_{ss} and ω_{ss} are the *sunrise* and *sunset solar time angles*. These angles are obtained from the *sunrise solar time angle*, HA_{sr},

$$\omega_{sr} = modulo(1440\ t_{noon} - 4\ HA_{sr}, 1440)$$

$$\omega_{ss} = modulo(1440\ t_{noon} + 4\ HA_{sr}, 1440)$$

where the *solar noon*, t_{noon}, is obtained from

© Eskom 2026/Rev 0c

PRINTED VERSIONS OF THIS DOCUMENT ARE NOT CONTROLLED

$$t_{noon} = modulo(720 - 4 - E_{time} + 60\, t_{GMT} + 4\, HA_{sr}, 1440)$$

and the *sunrise solar time angle*, HA_{sr} (degrees) is obtained from

$$HA_{sr} = acos\left(\frac{cos\left(90.833\frac{\pi}{180}\right)}{cos\left(\lambda\frac{\pi}{180}\right)}cos(\delta) - tan\left(\lambda\frac{\pi}{180}\right)tan(\delta)\right)\frac{180}{\pi}$$

with λ being the latitude in degrees.

The most important parameters in the calculation of the solar parameters as discussed above, are given in ***Table 5.8.C.1*** and ***Table 5.8.C.2*** for a 24-hour example. The parameters for evapotranspiration rates are given in ***Table 5.8.C.3*** to ***Table 5.8.C.5*** for the same period.

© Eskom 2026/Rev 0c

PRINTED VERSIONS OF THIS DOCUMENT ARE NOT CONTROLLED

Table 5.8.C.1
Solar Radiation Calculation Parameters(1)

JD	Hour	Julian Century	Geom Mean Long Sun [°]	Geom Mean Anom Sun [°]	Eccent Earth Orbit []	Sun Equation of Ctr [min]	Sun True Longitude [°]	Sun Apparent Longitude [°]	Mean Oblique Ecliptic [°]	Oblique Correction [°]
11	1	0.080	289.851	3246.775	0.017	0.231	290.081	290.078	23.438	23.440
11	2	0.080	289.892	3246.816	0.017	0.232	290.124	290.120	23.438	23.440
11	3	0.080	289.933	3246.857	0.017	0.233	290.166	290.163	23.438	23.440
11	4	0.080	289.974	3246.898	0.017	0.235	290.209	290.205	23.438	23.440
11	5	0.080	290.015	3246.940	0.017	0.236	290.251	290.248	23.438	23.440
11	6	0.080	290.056	3246.981	0.017	0.237	290.293	290.290	23.438	23.440
11	7	0.080	290.097	3247.022	0.017	0.239	290.336	290.333	23.438	23.440
11	8	0.080	290.138	3247.063	0.017	0.240	290.378	290.375	23.438	23.440
11	9	0.080	290.179	3247.104	0.017	0.242	290.421	290.418	23.438	23.440
11	10	0.080	290.220	3247.145	0.017	0.243	290.463	290.460	23.438	23.440
11	11	0.080	290.261	3247.186	0.017	0.244	290.506	290.502	23.438	23.440
11	12	0.080	290.302	3247.227	0.017	0.246	290.548	290.545	23.438	23.440
11	13	0.080	290.343	3247.268	0.017	0.247	290.591	290.587	23.438	23.440
11	14	0.080	290.385	3247.309	0.017	0.249	290.633	290.630	23.438	23.440
11	15	0.080	290.426	3247.350	0.017	0.250	290.676	290.672	23.438	23.440
11	16	0.080	290.467	3247.391	0.017	0.251	290.718	290.715	23.438	23.440
11	17	0.080	290.508	3247.432	0.017	0.253	290.760	290.757	23.438	23.440
11	18	0.080	290.549	3247.473	0.017	0.254	290.803	290.800	23.438	23.440
11	19	0.080	290.590	3247.514	0.017	0.256	290.845	290.842	23.438	23.440
11	20	0.080	290.631	3247.556	0.017	0.257	290.888	290.885	23.438	23.440
11	21	0.080	290.672	3247.597	0.017	0.258	290.930	290.927	23.438	23.440
11	22	0.080	290.713	3247.638	0.017	0.260	290.973	290.969	23.438	23.440
11	23	0.080	290.754	3247.679	0.017	0.261	291.015	291.012	23.438	23.440
11	24	0.080	290.795	3247.720	0.017	0.262	291.058	291.054	23.438	23.440

© Eskom 2026/Rev 0c

PRINTED VERSIONS OF THIS DOCUMENT ARE NOT CONTROLLED

Table 5.8.C.2
Solar Radiation Calculation Parameters(2)

JD	Hour	Sun Declination [°]	Parameter Y	Equation of Time [min]	Hour Angle Sunrise [°]	Solar Noon [min]	Sunrise Time Angle [°]	Sunset Time Angle [°]	Hour Angle [°]	True Solar Time [min]
11	1	-21.939	0.043	-7.491	107.009	0.520	0.223	0.817	-172.164	31.344
11	2	-21.933	0.043	-7.508	107.004	0.520	0.223	0.817	-157.168	91.327
11	3	-21.927	0.043	-7.525	106.998	0.520	0.223	0.817	-142.173	151.310
11	4	-21.920	0.043	-7.542	106.993	0.520	0.223	0.817	-127.177	211.293
11	5	-21.914	0.043	-7.559	106.988	0.520	0.223	0.817	-112.181	271.276
11	6	-21.908	0.043	-7.575	106.983	0.520	0.223	0.817	-97.185	331.260
11	7	-21.901	0.043	-7.592	106.977	0.520	0.223	0.817	-82.189	391.243
11	8	-21.895	0.043	-7.609	106.972	0.520	0.223	0.817	-67.193	451.226
11	9	-21.889	0.043	-7.626	106.967	0.520	0.223	0.817	-52.198	511.209
11	10	-21.882	0.043	-7.642	106.962	0.520	0.223	0.817	-37.202	571.193
11	11	-21.876	0.043	-7.659	106.956	0.520	0.223	0.817	-22.206	631.176
11	12	-21.870	0.043	-7.676	106.951	0.520	0.223	0.817	-7.210	691.159
11	13	-21.863	0.043	-7.692	106.946	0.520	0.223	0.817	7.786	751.143
11	14	-21.857	0.043	-7.709	106.940	0.520	0.223	0.817	22.782	811.126
11	15	-21.850	0.043	-7.726	106.935	0.520	0.223	0.817	37.777	871.109
11	16	-21.844	0.043	-7.742	106.930	0.520	0.223	0.817	52.773	931.093
11	17	-21.837	0.043	-7.759	106.924	0.520	0.223	0.817	67.769	991.076
11	18	-21.831	0.043	-7.775	106.919	0.520	0.223	0.817	82.765	1051.060
11	19	-21.825	0.043	-7.792	106.914	0.520	0.223	0.817	97.761	1111.043
11	20	-21.818	0.043	-7.808	106.908	0.520	0.223	0.817	112.757	1171.027
11	21	-21.812	0.043	-7.825	106.903	0.520	0.223	0.817	127.753	1231.010
11	22	-21.805	0.043	-7.841	106.897	0.520	0.223	0.817	142.748	1290.994
11	23	-21.799	0.043	-7.858	106.892	0.520	0.223	0.817	157.744	1350.977
11	24	-21.792	0.043	-7.874	106.887	0.520	0.223	0.817	172.740	1410.961

© Eskom 2026/Rev 0c

PRINTED VERSIONS OF THIS DOCUMENT ARE NOT CONTROLLED

Table 5.8.C.3
Evapotranspiration Calculation Parameters(1)

JD	Hour	Temperature (°C)	Pressure (kPa)	Relative Humidity (%)	Wind Speed at 10 m (m/s)	Wind Speed at 2 m (m/s)	Solar Radiation (W/m²)	Inverse relative Earth-Sun distance (d_r)	Solar Declination	Hour Angle	w1	w2	Extraterrestrial S_o (MJ/m²-h)
11	1	17.2	100.3	94.3	2.1	1.7	0.000	1.032	-0.383	-172.164	-1.868	-1.868	0.000
11	2	17.2	100.3	88.7	1.8	1.5	0.000	1.032	-0.383	-157.168	-1.868	-1.868	0.000
11	3	17.7	100.2	86.8	1.8	1.5	0.000	1.032	-0.383	-142.173	-1.867	-1.867	0.000
11	4	17.2	100.2	93.9	3.2	2.6	0.000	1.032	-0.383	-127.177	-1.867	-1.867	0.000
11	5	16.8	100.2	96.6	1.7	1.4	0.000	1.032	-0.382	-112.181	-1.867	-1.827	0.000
11	6	17.0	100.1	87.3	1.8	1.5	20.600	1.032	-0.382	-97.185	-1.827	-1.565	0.579
11	7	18.9	100.1	77.1	1.2	1.0	167.000	1.032	-0.382	-82.189	-1.565	-1.304	1.593
11	8	21.8	100.1	70.5	1.1	0.9	381.100	1.032	-0.382	-67.193	-1.304	-1.042	2.571
11	9	25.4	100.0	53.3	1.9	1.6	609.500	1.032	-0.382	-52.198	-1.042	-0.780	3.447
11	10	28.2	100.0	60.3	2.5	2.1	813.000	1.032	-0.382	-37.202	-0.780	-0.518	4.161
11	11	24.4	99.9	70.6	3.4	2.8	969.000	1.032	-0.382	-22.206	-0.518	-0.257	4.663
11	12	22.4	100.0	82.8	4.0	3.3	1065.000	1.032	-0.382	-7.210	-0.257	0.005	4.921
11	13	21.4	100.0	85.5	5.8	4.8	1087.000	1.032	-0.382	7.786	0.005	0.267	4.915
11	14	20.9	99.9	81.4	7.8	6.4	1051.000	1.032	-0.381	22.782	0.267	0.529	4.648
11	15	20.3	99.9	84.7	8.9	7.3	802.000	1.032	-0.381	37.777	0.528	0.790	4.136
11	16	19.6	99.9	89.0	8.0	6.6	500.500	1.032	-0.381	52.773	0.790	1.052	3.415
11	17	19.7	99.9	87.1	7.2	5.9	529.600	1.032	-0.381	67.769	1.052	1.314	2.533
11	18	19.8	100.0	85.4	6.3	5.2	0.000	1.032	-0.381	82.765	1.314	1.575	1.551
11	19	19.6	100.0	96.9	5.8	4.8	0.000	1.032	-0.381	97.761	1.575	1.837	0.536
11	20	19.1	100.2	96.4	6.1	5.0	0.000	1.032	-0.381	112.757	1.837	1.846	0.001
11	21	20.3	100.3	96.5	5.1	4.2	0.000	1.032	-0.381	127.753	1.846	1.846	0.000
11	22	20.4	100.4	99.5	5.3	4.3	0.000	1.032	-0.381	142.748	1.846	1.846	0.000
11	23	20.5	100.4	99.2	4.4	3.6	0.000	1.032	-0.380	157.744	1.846	1.846	0.000
11	24	20.5	100.4	99.8	5.0	4.1	0.000	1.032	-0.380	172.740	1.846	1.846	0.000

© Eskom 2026/Rev 0c

PRINTED VERSIONS OF THIS DOCUMENT ARE NOT CONTROLLED

Table 5.8.C.4
Evapotranspiration Calculation Parameters(2)

JD	Hour	Gamma (Pa/°C)	Saturation Vapour Pressure (Pa)	Actual Vapour Pressure (Pa)	delta (Pa/°C)	Clear sky radiation (R_{so}) (MJ/m²/d)	f-adjustment	Net Emissivity	Net Longwave Radiation (R_L) (W/m²)	Net Radiation (Rn) (W/m²)	Soil Heat Flux (W/m²)
11	1	0.067	1.963	1.851	0.124	0.000	0.000	0.150	0.000	0.000	0.000
11	2	0.067	1.963	1.741	0.124	0.000	0.000	0.155	0.000	0.000	0.000
11	3	0.067	2.026	1.759	0.128	0.000	0.000	0.154	0.000	0.000	0.000
11	4	0.067	1.963	1.843	0.124	0.000	0.000	0.150	0.000	0.000	0.000
11	5	0.067	1.914	1.849	0.121	0.000	0.000	0.150	0.000	0.000	0.000
11	6	0.067	1.938	1.692	0.123	0.435	0.000	0.158	0.000	0.067	0.007
11	7	0.067	2.184	1.684	0.136	1.196	0.328	0.158	-0.077	0.464	0.054
11	8	0.067	2.613	1.842	0.160	1.931	0.609	0.150	-0.141	1.094	0.123
11	9	0.066	3.246	1.730	0.193	2.589	0.794	0.156	-0.201	1.774	0.197
11	10	0.066	3.827	2.308	0.223	3.125	0.915	0.127	-0.196	2.438	0.263
11	11	0.066	3.058	2.159	0.183	3.502	0.995	0.134	-0.214	2.926	0.314
11	12	0.066	2.710	2.244	0.165	3.696	1.000	0.130	-0.203	3.248	0.345
11	13	0.066	2.550	2.180	0.156	3.692	1.000	0.133	-0.205	3.317	0.352
11	14	0.066	2.473	2.013	0.152	3.491	1.000	0.141	-0.216	3.189	0.341
11	15	0.066	2.383	2.018	0.147	3.106	0.905	0.141	-0.193	2.405	0.260
11	16	0.066	2.282	2.031	0.142	2.564	0.599	0.140	-0.126	1.496	0.162
11	17	0.066	2.296	2.000	0.142	1.902	1.000	0.142	-0.213	1.503	0.172
11	18	0.066	2.310	1.973	0.143	1.165	0.000	0.143	0.000	0.000	0.000
11	19	0.066	2.282	2.211	0.142	0.402	0.000	0.132	0.000	0.000	0.000
11	20	0.067	2.212	2.132	0.138	0.000	0.000	0.136	0.000	0.000	0.000
11	21	0.067	2.383	2.300	0.147	0.000	0.000	0.128	0.000	0.000	0.000
11	22	0.067	2.398	2.386	0.148	0.000	0.000	0.124	0.000	0.000	0.000
11	23	0.067	2.413	2.393	0.149	0.000	0.000	0.123	0.000	0.000	0.000
11	24	0.067	2.413	2.408	0.149	0.000	0.000	0.123	0.000	0.000	0.000

© Eskom 2026/Rev 0c

PRINTED VERSIONS OF THIS DOCUMENT ARE NOT CONTROLLED

Table 5.8.C.5
Evapotranspiration Calculation Parameters(3)

JD	Hour	Penman (mm/hr)	Penman-Monteith (mm/hr)
11	1	0.0082	0.0072
11	2	0.0152	0.0125
11	3	0.0180	0.0149
11	4	0.0110	0.0108
11	5	0.0044	0.0036
11	6	0.0346	0.0276
11	7	0.1546	0.1202
11	8	0.3518	0.2806
11	9	0.6164	0.4894
11	10	0.8465	0.6678
11	11	0.9415	0.6952
11	12	0.9848	0.6857
11	13	0.9925	0.6229
11	14	0.9737	0.5617
11	15	0.7374	0.4049
11	16	0.4552	0.2586
11	17	0.4612	0.2724
11	18	0.0441	0.0456
11	19	0.0088	0.0091
11	20	0.0104	0.0108
11	21	0.0092	0.0097
11	22	0.0014	0.0014
11	23	0.0019	0.0020
11	24	0.0005	0.0005

© Eskom 2026/Rev 0c

PRINTED VERSIONS OF THIS DOCUMENT ARE NOT CONTROLLED

Appendix 5.8.D: Instrument Specifications

YOUNG — Model 05305 Wind Monitor-AQ

The Wind Monitor-AQ is a high resolution wind sensor designed specifically for air quality applications. It combines simple, corrosion-resistant construction with low threshold, fast response and excellent fidelity.



The Wind Monitor-AQ meets the requirements of the following regulatory agencies:

U.S. Environmental Protection Agency- Ambient Monitoring Guidelines for Prevention of Significant Deterioration (PSD).

U.S. Nuclear Regulatory Agency- NRC Regulatory Guide 1.23 Meteorological Programs in Support of Nuclear Power Plants.

American Nuclear Society- Standard for Determining Meteorological Information at Power Plants.

Wind speed is sensed by a lightweight, carbon fiber thermoplastic (CFT), helicoid propeller. Propeller rotation produces an AC sine wave voltage signal with frequency directly proportional to wind speed. Slip rings and brushes are not used.

The wind direction sensor is a lightweight vane with performance characteristics that assure excellent fidelity in fluctuating wind conditions. Vane position is sensed by a precision potentiometer. Output is a DC voltage directly proportional to vane angle.

The instrument body is UV stabilized plastic with stainless steel and anodized aluminum fittings. Precision grade, stainless steel ball bearings are used throughout. Transient protection and cable terminations are located in a convenient junction box. The instrument mounts on standard 1 inch pipe.

The Wind Monitor-AQ is available with two additional output signal options. **Model 05305V** offers calibrated 0-1 VDC outputs (0-5 VDC optional), convenient for use with many dataloggers. **Model 05305L** provides a calibrated 4-20 mA current signal for each channel, useful in high noise areas or for long cables (up to several kilometers). Signal conditioning electronics are integrated into the sensor junction box.

Specifications

Range:
Wind speed: 0-50 m/s (112 mph)
Azimuth: 360° mechanical, 355° electrical (5° open)

Accuracy:
Wind speed: ±0.2 m/s (0.4 mph)
Wind direction: ±3 degrees

Threshold:*
Propeller: 0.4 m/s (0.9 mph)
Vane: 0.5 m/s (1.0 mph) at 10° displacement

Dynamic Response:*
Propeller distance constant (63% recovery): 2.1 m (6.9 ft)
Vane delay distance (50% recovery): 1.2 m (3.9 ft)
Damping ratio: 0.45
Damped natural wavelength: 4.9 m (16.1 ft)
Undamped natural wavelength: 4.4 m (14.4 ft)

Signal Output:
Wind speed: magnetically induced AC voltage, 3 pulses per revolution. 1800 rpm (90 Hz) = 9.2 m/s (20.6 mph)
Azimuth: analog DC voltage from conductive plastic potentiometer- resistance 10K Ω, linearity 0.25%, life expectancy- 50 million revolutions

Power Requirement:
Potentiometer excitation: 15 VDC maximum

Dimensions:
Overall height: 38 cm (15.0 in)
Overall length: 65 cm (25.6 in)
Propeller: 20 cm (7.9 in) diameter
Mounting: 34 mm (1.34 in) diameter (standard 1 inch pipe)

Weight:
Sensor weight: 0.7kg (1.5 lbs)
Shipping weight: 2.3 kg (5 lbs)

**Nominal values- determined in accordance with ASTM standard procedures Shielded bearings lubricated with Type LO-1 light General Purpose Instrument Oil.*

MODEL 05305V 0-1 VDC outputs

Power Requirement:
8-24 VDC (5 mA @ 12 VDC)

Operating Temperature:
-50 to 50° C

Output Signals:
0-1.00 VDC full scale
0-5.00 VDC optional

MODEL 05305L 4-20 mA outputs

Power Requirement:
8-30 VDC (40 mA max.)

Operating Temperature:
-50 to 50° C

Output Signals:
4-20 mA full scale

CE *Complies with applicable CE directives.*

Specifications subject to change without notice.

Ordering Information — MODEL

WIND MONITOR-AQ	**05305**
WIND MONITOR-AQ *0-1 VDC OUTPUTS*	**05305V***
WIND MONITOR-AQ *4-20mA OUTPUTS*	**05305L***

** SPECIFY SUFFIX FOR DESIRED WIND SPEED SCALE:*

0-50 M/S	*ADD SUFFIX "M"*
0-100 MPH	*ADD SUFFIX "P"*
0-100 KNOTS	*ADD SUFFIX "N"*
0-200 KM/HR	*ADD SUFFIX "K"*

Copyright © 2001 R.M. Young Company. Printed in U.S.A. 6/01

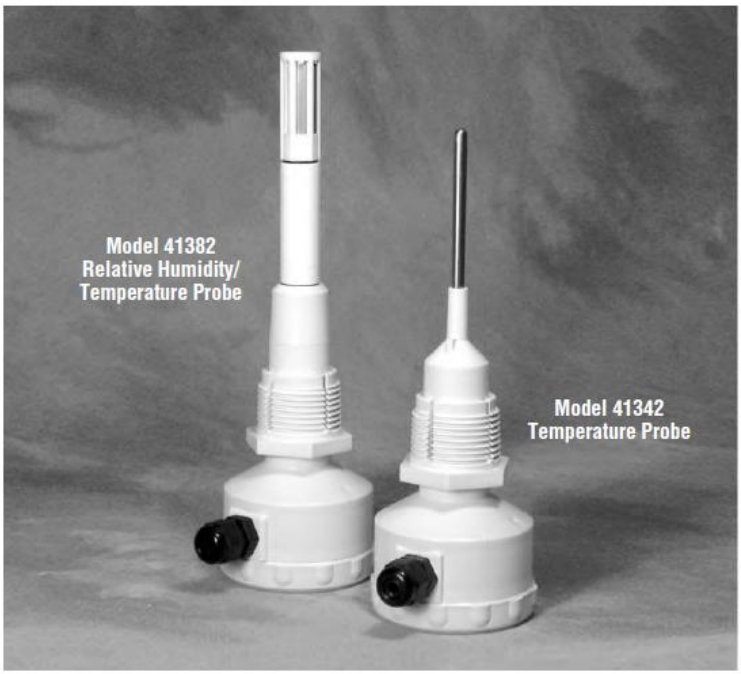
YOUNG
R.M. YOUNG COMPANY
2801 Aero Park Drive
Traverse City, Michigan 49686 USA
TEL: (231) 946-3980 FAX: (231) 946-4772
E-mail: met.sales@youngusa.com
Web Site: www.youngusa.com

© Eskom 2026/Rev 0c

PRINTED VERSIONS OF THIS DOCUMENT ARE NOT CONTROLLED

YOUNG

Model 41382 **Relative Humidity / Temperature Probe**
Model 41342 **Temperature Probe**



The Model 41382 Relative Humidity/Temperature Probe combines a high accuracy, capacitance type humidity sensor and precision Platinum RTD temperature sensor in one probe. This probe offers a choice of 0-1 VDC or 4-20 mA outputs for T and RH. **Model 41342 Temperature Probe** offers accurate temperature-only measurement. Three output options are available: 0-1 VDC, 4-20 mA, and 4 wire RTD. Probes are easily installed in YOUNG naturally ventilated (multi-plate) and aspirated radiation shields. A junction box is provided for cable terminations.

Specifications

Power Required:	**41382**	**41342**
V Option: 10-28 VDC	8 mA	5 mA
L Option: 10-28 VDC	40 mA	20 mA

RELATIVE HUMIDITY: (41382)
Measuring Range: 0-100 %RH
Accuracy at 20 °C: ±2 %RH,
Stability: Better than ±1 %RH per year
Response Time: 10 seconds (without filter)
Sensor Type: Rotronic Hygromer™
Output Signal: V option: 0-1 VDC,
L option: 4-20 mA

TEMPERATURE: (41382, 41342)
Calibrated Measuring Range:
-50 to 50 °C (suffix C)
-50 to 150 °F (suffix F)
Response Time: 10 seconds (without filter)
Accuracy at 0 °C: ±0.3 °C**
±0.1 °C (optional) with NIST traceable calibration
Sensor Type: Platinum RTD
Output Signal: V Option: 0-1 VDC,
L Option: 4-20 mA, 4 wire RTD (41342 only)

Recommended Radiation Shields:
Model 41003P Multi-Plate Radiation Shield
Model 43408P Aspirated Radiation Shield

**Differential measurement recommended with V option.*

Ordering Information	SENSOR CABLE	MODEL
RELATIVE HUMIDITY/TEMP PROBE 4-20 mA output	**18723**	**41382L***
RELATIVE HUMIDITY/TEMP PROBE 0-1 VDC output	**18446**	**41382V***
TEMPERATURE PROBE 4 wire RTD output	**18723**	**41342**
TEMPERATURE PROBE 4-20 mA output	**18641**	**41342L***
TEMPERATURE PROBE 0-1 VDC output	**18443**	**41342V***

**Specify °F or °C*

CE *Complies with applicable CE Directives*

Copyright © 2004 R.M. Young Company. Specifications subject to change without notice. Printed in U.S.A. 10/04

R.M. YOUNG COMPANY
2801 Aero Park Drive
Traverse City, Michigan 49686 USA
TEL: (231) 946-3980 FAX: (231) 946-4772
E-mail: met.sales@youngusa.com
Web Site: www.youngusa.com

© Eskom 2026/Rev 0c

PRINTED VERSIONS OF THIS DOCUMENT ARE NOT CONTROLLED

YOUNG

Model 41003 Multi-Plate Radiation Shield

The Multi-Plate Radiation Shield protects temperature and relative humidity sensors from error-producing solar radiation and precipitation. Compact size and light weight make this shield useful for many applications.



The multiple plates have a unique profile that blocks direct and reflected solar radiation, yet permits easy passage of air. Enlarged top plate and steep edge profile minimize moisture accumulation from precipitation and dew. The plate material is specially formulated for high reflectivity, low thermal conductivity, and maximum weather resistance. The rugged U-bolt mounting clamp attaches easily to any vertical pipe up to 2 inches diameter.

Model 41003 employs a universal clamp-type adapter to securely hold sensors up to 12.5 mm diameter. **Model 41003P** features a special mounting adapter that is custom sized to fit a sensor from 12.5 mm to 26 mm diameter; please specify the sensor diameter when ordering.

The Temperature Probe is a precision Platinum RTD encased in a stainless steel protective sheath.



The sensor assembly is securely mounted in a convenient junction box that fits YOUNG radiation shields. For special applications, the temperature probe is available with various output options. The 4-20 mA current output is useful in high noise, industrial settings or for long cable lengths. The 0-1 VDC option provides a calibrated voltage output signal. Low power circuitry makes it ideal for field studies and remote data-logging applications.

The Relative Humidity/Temperature Probe combines a high-accuracy humidity sensor and temperature sensor into one compact unit. The probe is available with 0-1 VDC or 4-20 mA outputs to satisfy a wide variety of applications.

Ordering Information — MODEL

MULTI-PLATE RADIATION SHIELD **41003**
Includes universal adapter for sensors to 15 mm diameter.

MULTI-PLATE RADIATION SHIELD **41003P**
With custom sensor adapter. Specify diameter from 12.5 mm to 26 mm.

TEMPERATURE PROBE - RTD OUTPUT **41342**
- **4-20 mA OUTPUT*** **41342L***
- **0-1 VDC OUTPUT*** **41342V***

RELATIVE HUMIDITY/TEMPERATURE PROBE:
- **4-20 mA OUTPUT*** **41382L***
- **0-1 VDC OUTPUT*** **41382V***

ACCESSORY JUNCTION BOX *Specify sensor diameter (10 mm max.)* **41390**

Specifications

Sensor Types:
Accommodates temperature and humidity sensors up to 26 mm (1 in) diameter

Radiation Error:
@ 1080 W/m² intensity- Dependent on wind speed
0.4° C (0.7°F) RMS @ 3 m/s (6.7 mph)
0.7° C (1.3°F) RMS @ 2 m/s (4.5 mph)
1.5° C (2.7°F) RMS @ 1 m/s (2.2 mph)

Construction:
UV stabilized white thermoplastic plates
Aluminum mounting bracket, white powder coated
Stainless steel U-bolt clamp

Dimensions:
13 cm (5.1 in) diameter x 26 cm (10.2 in) high
Mounting fits vertical pipe 25-50 mm (1-2 in) diameter

Weight:
Net weight: 0.7 kg (1.5 lb)
Shipping weight: 1.4 kg (3 lb)

MODEL 41342 Platinum Temp. Probe

Sensor Type:
1000 Ω Platinum RTD

Range:
Temperature: ..... -50° C to +50° C (-50° to +150° F)

Accuracy:
±0.3° C at 0° C ..... (standard)
±0.1° C at 0° C ..... (optional)

Available Outputs: (Power Requirement)
4 wire RTD 41342
4-20 mA (12-30 VDC, 20 mA) 41342L
0-1 VDC (8-24 VDC, 5 mA) 41342V

MODEL 41382 Rel. Humidity/Temp. Probe

Sensor Type:
Temperature: ..... 100 Ω Platinum RTD
Humidity: ..... Capacitive Polymer

Range:
Temperature: ..... -50° C to +50° C (-50° to +150° F)
Humidity: ..... 0 to 100% RH

Accuracy:
Temperature: ..... ±0.3° C
Humidity: ..... ±2% RH

Available Outputs: (Power Requirement)
4-20 mA (10-28 VDC, 20 mA) 41382L
0-1 VDC (10-28 VDC, 8 mA) 41382V

SPECIFY TEMPERATURE SCALING:
-50 to +50° C ..... add suffix C
-50 to +150° F ..... add suffix F

R.M. YOUNG COMPANY
2801 Aero Park Drive
Traverse City, Michigan 49686 USA
TEL: (231) 946-3980 FAX: (231) 946-4772
E-mail: met.sales@youngusa.com
Web Site: www.youngusa.com

Copyright © 2006 R.M. Young Company. Specifications subject to change without notice. Printed in U.S.A. 11/06

© Eskom 2026/Rev 0c

PRINTED VERSIONS OF THIS DOCUMENT ARE NOT CONTROLLED

YOUNG Model 52202 Tipping Bucket Rain Gauge

The YOUNG Tipping Bucket Rain Gauge meets the specifications of the World Meteorological Organization (WMO).

The design uses a proven tipping bucket mechanism for simple and effective rainfall measurement. The bucket geometry and material are specially selected for maximum water release, thereby reducing contamination and errors.

Catchment area of 200 cm^2 and measurement resolution of 0.1 mm meet the recommendations of the WMO. Leveling screws and bullseye level are built-in for easy and precise adjustment in the field. Measured precipitation is discharged through a collection tube for verification of total rainfall.

Model 52202 is heated for operation in cold temperatures. An unheated version, 52203, is available for use in moderate climates.

To discourage birds from perching on the funnel rim, accessory bird wire assembly may be attached to the gauge.







Specifications

Size:
18 cm dia. x 30 cm high, (39 cm high with mounting base)

Catchment Area:
200 cm^2

Resolution:
0.1 mm per tip
0.2 mm per tip (optional)

Accuracy:
2% up to 25 mm/hr
3% up to 50 mm/hr

Output:
Magnetic reed switch (N.O.), rating 24VAC/DC 500mA

Operating Temperature:
-20°C to +50°C (heated)

Power:
18 Watts for heater only

Mounting:
Clamp for 1" (1.34" dia.) iron pipe
or 3 bolts on 160mm dia. circle

Other:
Leveling adjustment, thermostatic control for heater, intake screen

Ordering Information — MODEL

TIPPING BUCKET RAIN GAUGE (HEATED)	52202
TIPPING BUCKET RAIN GAUGE (UNHEATED)	52203
BIRD WIRE ASSEMBLY	52250

CE *Complies with applicable CE directives.*
Specifications subject to change without notice.

R.M. YOUNG COMPANY
2801 Aero Park Drive
Traverse City, Michigan 49686 USA
TEL: (231) 946-3980 FAX: (231) 946-4772
E-mail: met.sales@youngusa.com
Web Site: www.youngusa.com

Copyright © 2005 R.M. Young Company. Printed in U.S.A. 8/05

YOUNG

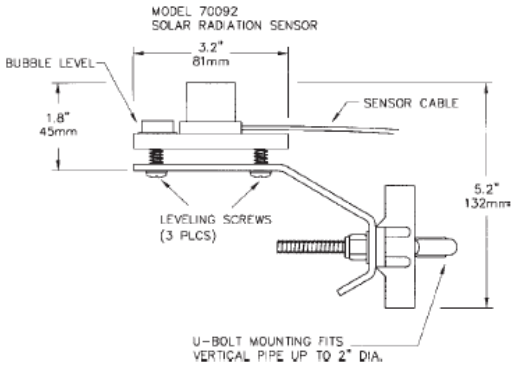
MODEL 70092/70201

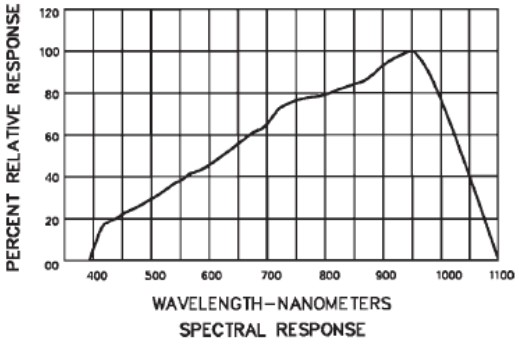
SOLAR RADIATION SENSOR

GENERAL DESCRIPTION: The Model 70092 Solar Radiation Sensor is a low cost pyranometer designed for agricultural, meteorological and hydrological applications. The 70092 features a silicon photovoltaic detector mounted in a fully cosine-corrected head. The pyranometer compares favorably with first class thermopile type pyranometers in clear unobstructed daylight conditions. A convenient offset mounting bracket for attachment to vertical post or tower member is included. For applications requiring greater signal output, MODEL 70201 includes amplifier circuit for full 0-1v signal.

SPECIFICATIONS:

Sensor type:	High stability silicon photovoltaic detector (blue enhanced)
Measurement range:	400-1100 nanometers
Sensitivity:	Typically 80 µA per 1000 W m^{-2}
Linearity:	1% max up to 3000 W m^{-2}
Stability:	<±2% per year
Response time:	10 µS
Signal: 70092	0-8 mV =0-1000 Wm^{-2} typical across 100 W load.
70201	0-1000 mV = 0-1000 Wm^{-2}
Temperature dependence:	0.15% per °C maximum
Cosine Correction:	Cosine corrected up to 80° angle of incidence
Operating temperature:	-20 to +65°C (-4 to 149°F)
Material:	Anodized aluminum housing Acrylic diffuser Aluminum mounting base Powder coated aluminum offset bracket
Weight: 70092	0.5 kg (1.1 lb)
70201	1.0 kg (2.2 lb)
Cable:	3 meters shielded coaxial included





Ordering Information:

Model	Description	Price (US)
70092	Solar Radiation Sensor w/Offset Mounting Bracket	$ 402.00
70201	Solar Radiation Sensor w/ Signal Amplifier (0-1000 mV = 0-1000 Wm^{-2})	$ 782.00

R. M. YOUNG COMPANY - 2801 Aero Park Drive Traverse City Michigan 49686 USA
TEL (231) 946-3980 FAX (231) 946-4772

FEB 01

© Eskom 2026/Rev 0c

PRINTED VERSIONS OF THIS DOCUMENT ARE NOT CONTROLLED

MONITOR SENSORS

LS1 LS2 LS3

µSMART Lightning Strike Sensor

The ***µSMART*** Lightning Strike sensor counts lightning strikes by detecting electrical fields with signal strength greater than the factory set threshold voltage. An early warning of impending lightning activity allows sensitive equipment to be isolated from mains power or the controlled shut down of a plant or dangerous operation.

The sensor ***Monibus*** interface allows the user to modify the sensor operation through the built-in sensor menus. The sensor incorporates a microprocessor to provide accurate, repeatable readings and to allow optional analogue outputs. The robust mechanical design ensures a long operational life.

Mechanical
- Powder coated aluminium body
- Fully sealed
- High durability cable

Specifications

Range:

LS1	1.0 volt/m	3 km
LS2	0.3 volts/m	10 km
LS3	0.1 volts/m	>30 km

Operational: -20°C to +60°C

Output options:
- ***Monibus*** serial data ASCII format
- Voltage 0-1, 0-2.5 volts
- 4-20mA (requires >12Vdc supply)
- Frequency TTL pulse 2-10 Hz

Power Supply: 6-28 Vdc unregulated

Supply current: 1.2 mA active
0.5 mA economy mode

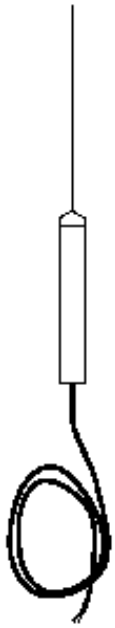
Sensor weight: 250 grams

Dimensions: Overall height – 170 mm x 25 mm Ø

Mounting: 25 mm Ø
dwg no: MSM-06-0038

Cable Details: Standard product has 4m of cable – other cable lengths may be ordered

Warranty: **12 months** – full details can be found in the Monitor Sensors standard warranty document
http://www.monitorsensors.com/docs/std_warranty.pdf



Order codes:

LS1	standard sensor	**LS1-C**	Hi/Low control
LS1-F	TTL pulse		
LS2	standard sensor		
LS2-F	TTL pulse		
LS3	standard sensor		
LS3-F	TTL pulse		

info@monitorsensors.com
ph: 61-7-34909000
fx: 61-7-38897246
www.monitorsensors.com

Monitor Sensors
250 Leitchs Road
PO Box 5692
Brendale QLD 4500
AUSTRALIA

LS brief 00.doc 16/10/06 7:46 AM

YOUNG — Model 73000 Sentry™ Visibility Sensor

The YOUNG Sentry™ Visibility Sensor measures atmospheric visibility (meteorological optical range) by determining the amount of light scattered by particles in the air (smoke, dust, haze, fog, rain, & snow).

Performance in all weather conditions is achieved with an integrated design that keeps all cabling internal to the sensor for complete protection from hazards. The sensor is made from anodized aluminum and rugged, UV-resistant fiberglass enclosures. Based on the proven field experience of the NWS and FAA, the sensor uses a "look down" geometry to reduce window contamination and clogging from blowing snow. The optical windows have continuous duty anti-dew heaters. Optional thermostatically controlled external hood heaters are available for additional protection in extreme environments. All power and signal lines to the Sentry™ are protected with surge and EMI filtering to ensure uninterrupted service for the life of the sensor.

Installation and maintenance are simple with the Sentry™. A sturdy mounting flange located on the bottom of the main enclosure mates with a user-supplied 1-1/2 inch IPS mounting pipe. Power and signal cables are installed through waterproof cable glands on the bottom of the main enclosure to terminal boards for simple but reliable connections.

Calibration of the Sentry™ in the field is as simple as attaching a factory supplied calibration fixture and following a procedure that takes less than 30 minutes.

Ordering Information

73000 Sentry™ Visibility Sensor
73004 Sentry™ Visibility Sensor with Hood Heating

Power – select one:
- **A** AC Power, 200-240 VAC, 50/60 Hz
- **D** DC Power, 10-36 VDC

Signal Output – select one:
- **V** 0-5 VDC (no control relays)
- **W** 0-10 VDC
- **L** 4-20 mA
- **M** 4-20 mA isolated
- **S** RS-232
- **T** RS-422
- **U** RS-485

Control Output – optional
- **C** Single Control Relay (NA w/ output option V)
- **D** Diagnostic Relay
- **E** 2 Control Relays (NA w/ output option V)
- **F** Control Relay and Diagnostic Relay (NA w/ output option V)
- **G** 2 Control Relays, Diagnostic Relay (NA w/ output option V)**

** NOTE: Option G not available with Options S, T or U

EXAMPLE: 73004-DWF – Sentry™ Visibility Sensor with hood heating, DC power, 0-10 VDC output, single control relay and single diagnostic relay

Accessories

73062 Calibration Fixture – recommended
74050 Mounting Bracket – for vertical surfaces including walls, traffic poles and Rohn-type towers
73038 Hood Extensions

Specifications

Visibility Range:	30 m – 16 km
Accuracy:	+/- 10% RMSE
Time Constant:	60 sec
Scatter Angle:	42 deg nominal
Output Options:	0-10 VDC 0-5 VDC 4-20 mA 4-20 mA Isolated RS-232, RS-422 or RS-485
Relay Options:	2 Control 1 Diagnostic
Power: AC Version:	100-240 VAC, 24 VA Nominal 75 VA w/ hood heating
DC Version:	10-36 VDC, 6 VA Nominal 18 VA w/ hood heating
Operating Temperature:	-40 to +60 C
Humidity:	0 to 100% RH
Protection:	IP66 (NEMA-4X)
Weight:	8 kg (18 lb)
Dimensions: (W x H x D)	889 mm x 292 mm x 305 mm 35" x 11.5" x 12"
Mounting:	48 mm (1.9 inch) diameter (standard 1.5 inch IPS pipe)
Optional:	34 mm (1.3 inch) diameter (standard 1 inch IPS pipe)
Construction:	Frame: Anodized Aluminum Enclosures: Fiberglass, UV Resistant
Certifications:	This equipment is in compliance with the essential requirements and other provisions of Low Voltage Directives 73/23/EEC and 89/336/ EEC as amended by Directive 93/68/EEC.



CE Complies with applicable CE directives.

R.M. YOUNG COMPANY
2801 Aero Park Drive
Traverse City, Michigan 49686 USA
TEL: (231) 946-3980 FAX: (231) 946-4772
E-mail: met.sales@youngusa.com
Web Site: www.youngusa.com

Copyright © 2016 R.M. Young Company. Specifications subject to change without notice. Printed in USA. 7/16
Sentry™ is a trademark of the R.M. Young Company

YOUNG Model 61402 Barometric Pressure Sensor

YOUNG Barometric Pressure Sensors combine high accuracy and low power over a wide range of pressures and temperatures.

Now available with SDI-12 output.



Model 61402V provides a calibrated 0-5 VDC analog output. Analog current consumption is less than 4 mA. A special "sleep" mode further reduces current draw to a few µA. RS232 serial output is also available.

Model 61402L features a standard 4-20 mA output or user selectable serial interfaces SDI-12, RS-232, RS-485.

The compact size of the barometer allows easy placement in most standard instrument enclosures. A plug-in connector simplifies wiring.

For outdoor use, an optional **Weatherproof Enclosure** offers a convenient mounting location while the **Pressure Port** helps minimize dynamic pressure errors due to wind.

Specifications

Pressure Range:
500 to 1100 hPa

Operating Temperature:
-40 to +60°C

Digital Accuracy*
0.2 hPa (25°C)
0.3 hPa (-40 to +60°C)

Analog Accuracy**
0.05% of analog pressure range

Analog Temperature Dependence
0.0017% of analog pressure range/ °C (25°C reference)

Long Term Stability:
0.08% FS per year

Update Rate:
1.8 Hz max

Serial Output:
Full duplex RS-232
SDI-12, half duplex RS-485 (61402L only)
1200 to 38400 baud
Polled or continuous
ASCII text, NMEA

Analog Output:
0 to 5000 mV, 0 to 2500 mV (61402V)
4 to 20 mA (61402L)

Resolution:
Serial 0.01 hPa
Analog 0.025% of analog scale

Power:
7 to 30 VDC
61402V – Vout, 3.6 mA
– Sleep mode, 2.7 µA
– RS-232, 7.6 mA
61402L – 4-20 mA, 25 mA max
– RS-232 or RS-485, 8.5 mA
– SDI-12, 1.5 mA

Dimensions:
90 mm (3.6 in) x 60 mm (2.4 in) x 20 mm (0.8 in)

Weight:
44 g (1.5 oz)

* Defined as ±1 standard deviation from NIST traceable pressure reference. Includes non-linearity, hysteresis, repeatability, and calibration uncertainty.

** Defined as ±1 standard deviation from ideal analog output. Total analog output accuracy is the root sum square of digital accuracy, analog accuracy, and analog temperature dependence.

Ordering Information — MODEL

BAROMETRIC PRESSURE SENSOR, 0-5 VDC	61402V
BAROMETRIC PRESSURE SENSOR, 4-20 mA	61402L
WEATHERPROOF ENCLOSURE	61360
PRESSURE PORT WITH OFFSET BRACKET	61002



Weatherproof Enclosure and Pressure Port

CE *Complies with applicable CE directives.*
Specifications subject to change without notice.

R.M. YOUNG COMPANY
2801 Aero Park Drive
Traverse City, Michigan 49686 USA
TEL: (231) 946-3980 FAX: (231) 946-4772
E-mail: met.sales@youngusa.com
Web Site: www.youngusa.com

Copyright © 2021 R.M. Young Company, Printed in U.S.A. 02/21

Appendix 5.8.E: Second Edition of the ISO Corrosion Standard

© Eskom 2026/Rev 0c

PRINTED VERSIONS OF THIS DOCUMENT ARE NOT CONTROLLED

Appendix 5.8.F: Calibration Certificates

© Eskom 2026/Rev 0c

PRINTED VERSIONS OF THIS DOCUMENT ARE NOT CONTROLLED

Appendix 5.8.G: Data Collection and Validation Procedure

Meteorological monitoring data from the automatic weather station at the site are downloaded on a two-weekly basis (or more frequently). This is done remotely with communication via Campbell Scientific Inc Loggernet Software. A cell phone connection allows data retrieval with password protection. Once the site is selected in the software, the telecommunication connection is made and the data are downloaded from the CR1000 Logger. The user may decide to download all or only since the previous download placeholder.

The raw data are copied into a living Excel Spreadsheet ('Met Table (Thyspunt).xls'. The original data text files are kept separately. The data are also duplicated in a similarly living 'validated' Excel Spreadsheet ('Met Table (Thyspunt) Validated.xls' in which a number of data screening tests are done and recorded.

All the meteorological parameters in the 'validated' worksheet are screened, averaged and stored as hourly average parameters according to the criteria given in ***Table 5.8.G.1***. Data values that fail the Range Test, are replaced by a missing parameter ('-9999') placeholder. Each occurrence of a Data Change Test 1 and Data Change Test 2, is manually inspected to see whether an instrument failure occurred; if found to be the case, the value is replaced by the missing parameter '-9999'.

Specific care is taken in rainfall measurements. Originally these measurements were found to observe spurious readings at high wind speeds, i.e. above 9.4 m/s. This was particularly prevalent when the rain gauges were fixed to the 10-metre mast. The rain gauges were subsequently isolated from the mast. Although the interference no longer appears to occur, a check is nevertheless made to see that when rainfall occurs with a relative humidity below 70 per cent, that the wind speed is not above 9 m/s. If this is the situation, the rainfall data are replaced by the missing parameter. The original recordings, the test results and the final, manually changed data are all kept in the 'validated' spreadsheets for reference.

Data values recorded during the bi-annual calibration tests are also removed and replaced with the missing parameter '-9999'. This is noted in the 'validated' spreadsheets.

© Eskom 2026/Rev 0c

PRINTED VERSIONS OF THIS DOCUMENT ARE NOT CONTROLLED

Only the hourly averaged data are provided to the SSR project team. This is generally done every third month. The data are accompanied by the Meteorological Data Checking and Approval Certificate (***Table 5.8.G.2***).

© Eskom 2026/Rev 0c

PRINTED VERSIONS OF THIS DOCUMENT ARE NOT CONTROLLED

Table 5.8.G.1
Recorded Meteorological Data Screening Parameters

Parameter	Range Test				Data Change Test 1				Data Change Test 2			
	Instrument Minimum	Instrument Maximum	Local Minimum	Local Maximum	Minimum or Maximum Change	Delta Value	Duration	Time Unit	Minimum or Maximum Change	Delta Value	Duration	Time Unit
Wind Speed (m/s)	0	60	0	45	Minimum	0.1	6	hours	Minimum	0.5	24	hours
Wind Direction (°)	0	360	0	360	Minimum	0.1	3	hours	Minimum	2	24	hours
Dry Bulb Temperature (°C)	-50	50	-1	41	Maximum	5	2	hours	Minimum	0.2	12	hours
Relative Humidity (%)	0	100	10	100	Minimum	0.1	18	hours	Minimum	1	36	hours
Solar Radiation (W/m²)	0	1400	0	1300	Minimum	10	12	hours	Minimum	100	12	hours
Barometric Pressure (hPa)	900	1100	960	1060	Maximum	6	3	hours	Minimum	1	48	hours
Rainfall (mm)	0	50	0	50	Maximum	50	2	hours	Minimum	0.1	1	month

© Eskom 2026/Rev 0c

PRINTED VERSIONS OF THIS DOCUMENT ARE NOT CONTROLLED

Table 5.8.G.2

Meteorological Data Checking and Approval Certificate

METEOROLOGICAL DATA CHECKING AND APPROVAL CERTIFICATE

Project: *Nuclear-1 Site Safety Reports – Onsite Meteorological Data*

Reference: *02/002*
Date: 8 August 2024

Item #	Reference and Description		Prepared by (Signature & Date)	Checked/Verified (Signature & Date)	Approved for Use (Signature & Date)
	Data Reference	Title			
1	*596224_ESKM_TSSR Validated Met Data May24 to Jul24_20240808.xlsx*	*Thyspunt Onsite 10-Minute Average Validated Meteorological Data: Reporting Period 1 May 2024 – 31 July 2024 Data Report Date: 8 August 2024*	*L Burger* AIRSHED *08/08/2024*	*R von Gruenewaldt* *08/08/2024*	*L Burger* AIRSHED *08/08/2024*

Form RF-02 Rev 0.1

© Eskom 2026/Rev 0c

PRINTED VERSIONS OF THIS DOCUMENT ARE NOT CONTROLLED

Appendix 5.8.H: Particle Size Distribution

MALVERN INSTRUMENTS MASTERSIZER

Result: Analysis Report

Sample Details

Sample ID: 164353
Sample File: JANKON12
Sample Path: C:\SIZERS\DATA\ANNE-MIE\
Sample Notes: NEW10
0.55-6.54M
<1MM

Run Number: 28
Record Number: 70

Measured: 4 Jun 2012 12:36PM
Analysed: 4 Jun 2012 12:36PM
Result Source: Analysed

System Details

Range Lens: 300RF mm
Presentation: 3_SIL01
Analysis Model: Polydisperse
Modifications: None

Beam Length: 2.40 mm
[Particle R.I. = (3.5000, 0.1000); Dispersant R.I. = 1.3300]

Sampler: None

Obscuration: 4.5 %
Residual: 1.638 %

Result Statistics

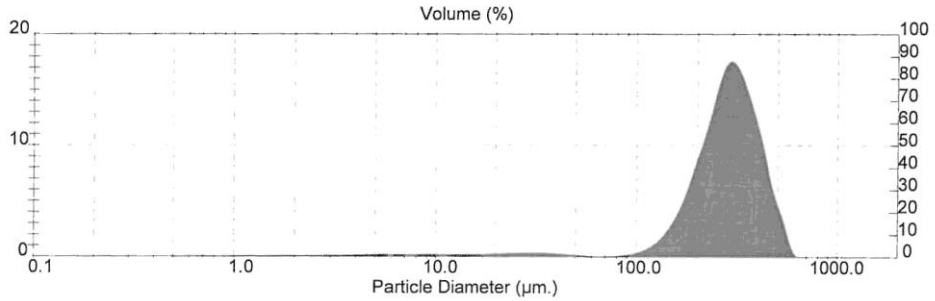
Distribution Type: Volume
Mean Diameters:
D [4, 3] = 283.66 um

Concentration = 0.0356 %Vol
D (v, 0.1) = 153.74 um
D [3, 2] = 63.54 um

Density = 1.000 g / cub. cm
D (v, 0.5) = 283.22 um
Span = 9.668E-01

Specific S.A. = 0.0944 sq. m / g
D (v, 0.9) = 427.54 um
Uniformity = 3.087E-01

Size Low (um)	In %	Size High (um)	Under%	Size Low (um)	In %	Size High (um)	Under%
0.05	0.00	0.06	0.00	6.63	0.23	7.72	2.04
0.06	0.00	0.07	0.00	7.72	0.23	9.00	2.27
0.07	0.00	0.08	0.00	9.00	0.23	10.48	2.50
0.08	0.00	0.09	0.00	10.48	0.22	12.21	2.72
0.09	0.00	0.11	0.00	12.21	0.22	14.22	2.94
0.11	0.00	0.13	0.00	14.22	0.23	16.57	3.17
0.13	0.00	0.15	0.00	16.57	0.26	19.31	3.44
0.15	0.00	0.17	0.00	19.31	0.31	22.49	3.75
0.17	0.00	0.20	0.00	22.49	0.36	26.20	4.10
0.20	0.00	0.23	0.00	26.20	0.39	30.53	4.49
0.23	0.00	0.27	0.00	30.53	0.39	35.56	4.87
0.27	0.00	0.31	0.00	35.56	0.34	41.43	5.22
0.31	0.01	0.36	0.01	41.43	0.26	48.27	5.48
0.36	0.02	0.42	0.03	48.27	0.17	56.23	5.65
0.42	0.03	0.49	0.06	56.23	0.04	65.51	5.69
0.49	0.03	0.58	0.09	65.51	0.04	76.32	5.74
0.58	0.04	0.67	0.13	76.32	0.11	88.91	5.84
0.67	0.05	0.78	0.18	88.91	0.29	103.58	6.14
0.78	0.05	0.91	0.24	103.58	0.71	120.67	6.85
0.91	0.06	1.06	0.30	120.67	1.56	140.58	8.41
1.06	0.06	1.24	0.36	140.58	3.12	163.77	11.53
1.24	0.07	1.44	0.43	163.77	5.73	190.80	17.27
1.44	0.08	1.68	0.51	190.80	9.36	222.28	26.63
1.68	0.09	1.95	0.60	222.28	13.45	258.95	40.08
1.95	0.09	2.28	0.69	258.95	17.24	301.68	57.32
2.28	0.11	2.65	0.80	301.68	16.61	351.46	73.92
2.65	0.12	3.09	0.91	351.46	13.14	409.45	87.06
3.09	0.14	3.60	1.05	409.45	8.39	477.01	95.45
3.60	0.16	4.19	1.21	477.01	4.06	555.71	99.51
4.19	0.18	4.88	1.39	555.71	0.49	647.41	100.00
4.88	0.20	5.69	1.59	647.41	0.00	754.23	100.00
5.69	0.22	6.63	1.81	754.23	0.00	878.67	100.00



Malvern Instruments Ltd.
Malvern, UK
Tel:=+[44] (0)1684-892456 Fax:+[44] (0)1684-892789

Mastersizer S long bed Ver. 2.19
Serial Number: 33544/152

p. 15
04 Jun 12 12:37

© Eskom 2026/Rev 0c

PRINTED VERSIONS OF THIS DOCUMENT ARE NOT CONTROLLED

MALVERN INSTRUMENTS MASTERSIZER

Result: Analysis Report

Sample Details

Sample ID: 164350
Sample File: JANKON12
Sample Path: C:\SIZERS\DATA\ANNE-MIE\
Sample Notes: NEW4
0.03-3.51M
<1MM

Run Number: 24
Record Number: 65

Measured: 4 Jun 2012 11:34AM
Analysed: 4 Jun 2012 11:34AM
Result Source: Analysed

System Details

Range Lens: 300RF mm
Presentation: 3_SIL01
Analysis Model: Polydisperse
Modifications: None

Beam Length: 2.40 mm
[Particle R.I. = (3.5000, 0.1000); Dispersant R.I. = 1.3300]

Sampler: None

Obscuration: 7.3 %
Residual: 1.696 %

Result Statistics

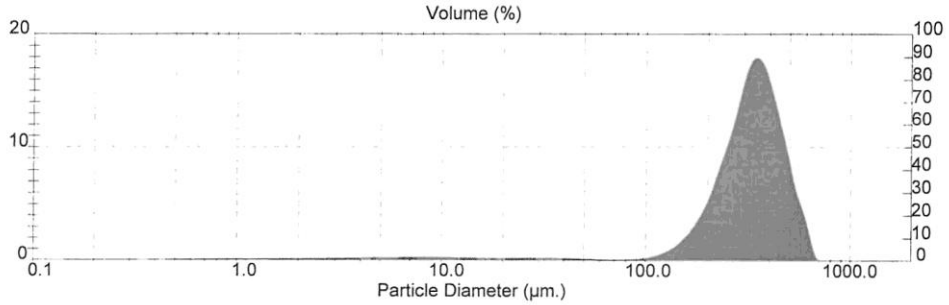
Distribution Type: Volume
Mean Diameters:
D [4, 3] = 324.12 um

Concentration = 0.0470 %Vol
D (v, 0.1) = 171.91 um
D [3, 2] = 52.36 um

Density = 1.000 g / cub. cm
D (v, 0.5) = 326.61 um
Span = 9.664E-01

Specific S.A. = 0.1146 sq. m / g
D (v, 0.9) = 487.54 um
Uniformity = 3.046E-01

Size Low (um)	In %	Size High (um)	Under%	Size Low (um)	In %	Size High (um)	Under%
0.05	0.00	0.06	0.00	6.63	0.27	7.72	2.68
0.06	0.00	0.07	0.00	7.72	0.28	9.00	2.96
0.07	0.00	0.08	0.00	9.00	0.28	10.48	3.23
0.08	0.00	0.09	0.00	10.48	0.26	12.21	3.50
0.09	0.00	0.11	0.00	12.21	0.24	14.22	3.73
0.11	0.00	0.13	0.00	14.22	0.21	16.57	3.95
0.13	0.00	0.15	0.00	16.57	0.20	19.31	4.15
0.15	0.00	0.17	0.00	19.31	0.20	22.49	4.35
0.17	0.00	0.20	0.00	22.49	0.21	26.20	4.56
0.20	0.00	0.23	0.00	26.20	0.23	30.53	4.79
0.23	0.00	0.27	0.00	30.53	0.23	35.56	5.02
0.27	0.00	0.31	0.00	35.56	0.21	41.43	5.23
0.31	0.01	0.36	0.01	41.43	0.18	48.27	5.41
0.36	0.02	0.42	0.04	48.27	0.13	56.23	5.54
0.42	0.04	0.49	0.08	56.23	0.08	65.51	5.62
0.49	0.04	0.58	0.12	65.51	0.05	76.32	5.67
0.58	0.06	0.67	0.18	76.32	0.07	88.91	5.73
0.67	0.08	0.78	0.26	88.91	0.17	103.58	5.90
0.78	0.08	0.91	0.34	103.58	0.42	120.67	6.33
0.91	0.09	1.06	0.42	120.67	0.93	140.58	7.26
1.06	0.10	1.24	0.52	140.58	1.85	163.77	9.11
1.24	0.11	1.44	0.63	163.77	3.42	190.80	12.54
1.44	0.12	1.68	0.75	190.80	5.85	222.28	18.38
1.68	0.13	1.95	0.87	222.28	9.29	258.95	27.68
1.95	0.14	2.28	1.01	258.95	13.48	301.68	41.16
2.28	0.15	2.65	1.16	301.68	17.49	351.46	58.65
2.65	0.16	3.09	1.32	351.46	17.04	409.45	75.69
3.09	0.18	3.60	1.50	409.45	12.87	477.01	88.56
3.60	0.20	4.19	1.69	477.01	7.75	555.71	96.31
4.19	0.22	4.88	1.91	555.71	3.69	647.41	100.00
4.88	0.24	5.69	2.15	647.41	0.00	754.23	100.00
5.69	0.26	6.63	2.40	754.23	0.00	878.67	100.00



Malvern Instruments Ltd.
Malvern, UK
Tel:=+[44] (0)1684-892456 Fax:+[44] (0)1684-892789

Mastersizer S long bed Ver. 2.19
Serial Number: 33544/152

p. 12
04 Jun 12 11:36

© Eskom 2026/Rev 0c

PRINTED VERSIONS OF THIS DOCUMENT ARE NOT CONTROLLED

MALVERN INSTRUMENTS MASTERSIZER

Result: Analysis Report

Sample Details

Sample ID: 164365
Sample File: JANKON12
Sample Path: C:\SIZERS\DATA\ANNE-MIE\
Sample Notes: SAMPLE PIT

<1MM

Run Number: 44
Record Number: 89

Measured: 4 Jun 2012 02:52PM
Analysed: 4 Jun 2012 02:52PM
Result Source: Analysed

System Details

Range Lens: 300RF mm
Presentation: 3_SIL01
Analysis Model: Polydisperse
Modifications: None

Beam Length: 2.40 mm
[Particle R.I. = (3.5000, 0.1000); Dispersant R.I. = 1.3300]

Sampler: None

Obscuration: 8.0 %
Residual: 2.526 %

Result Statistics

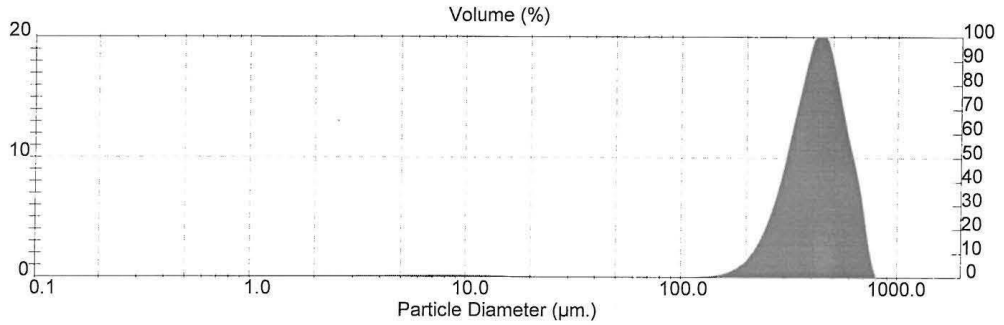
Distribution Type: Volume
Mean Diameters:
D [4, 3] = 424.91 um

Concentration = 0.0802 %Vol
D (v, 0.1) = 268.25 um
D [3, 2] = 81.05 um

Density = 1.000 g / cub. cm
D (v, 0.5) = 423.32 um
Span = 7.917E-01

Specific S.A. = 0.0740 sq. m / g
D (v, 0.9) = 603.38 um
Uniformity = 2.531E-01

Size Low (um)	In %	Size High (um)	Under%	Size Low (um)	In %	Size High (um)	Under%
0.05	0.00	0.06	0.00	6.63	0.16	7.72	1.63
0.06	0.00	0.07	0.00	7.72	0.17	9.00	1.80
0.07	0.00	0.08	0.00	9.00	0.16	10.48	1.96
0.08	0.00	0.09	0.00	10.48	0.15	12.21	2.11
0.09	0.00	0.11	0.00	12.21	0.11	14.22	2.22
0.11	0.00	0.13	0.00	14.22	0.08	16.57	2.30
0.13	0.00	0.15	0.00	16.57	0.05	19.31	2.35
0.15	0.00	0.17	0.00	19.31	0.03	22.49	2.38
0.17	0.00	0.20	0.00	22.49	0.00	26.20	2.38
0.20	0.00	0.23	0.00	26.20	0.00	30.53	2.38
0.23	0.00	0.27	0.00	30.53	0.00	35.56	2.38
0.27	0.00	0.31	0.00	35.56	0.00	41.43	2.38
0.31	0.01	0.36	0.01	41.43	0.00	48.27	2.38
0.36	0.02	0.42	0.03	48.27	0.00	56.23	2.38
0.42	0.03	0.49	0.06	56.23	0.00	65.51	2.38
0.49	0.03	0.58	0.09	65.51	0.00	76.32	2.38
0.58	0.04	0.67	0.13	76.32	0.00	88.91	2.38
0.67	0.05	0.78	0.18	88.91	0.00	103.58	2.38
0.78	0.05	0.91	0.23	103.58	0.02	120.67	2.40
0.91	0.06	1.06	0.29	120.67	0.08	140.58	2.48
1.06	0.06	1.24	0.35	140.58	0.25	163.77	2.72
1.24	0.07	1.44	0.42	163.77	0.68	190.80	3.40
1.44	0.07	1.68	0.49	190.80	1.66	222.28	5.06
1.68	0.08	1.95	0.57	222.28	3.65	258.95	8.71
1.95	0.08	2.28	0.65	258.95	7.17	301.68	15.88
2.28	0.09	2.65	0.74	301.68	12.20	351.46	28.07
2.65	0.09	3.09	0.83	351.46	17.48	409.45	45.56
3.09	0.10	3.60	0.94	409.45	20.64	477.01	66.20
3.60	0.11	4.19	1.05	477.01	17.10	555.71	83.30
4.19	0.12	4.88	1.17	555.71	11.27	647.41	94.57
4.88	0.14	5.69	1.31	647.41	5.43	754.23	100.00
5.69	0.15	6.63	1.46	754.23	0.00	878.67	100.00



Malvern Instruments Ltd.
Malvern, UK
Tel:=+[44] (0)1684-892456 Fax:+[44] (0)1684-892789

Mastersizer S long bed Ver. 2.19
Serial Number: 33544/152

p. 28
04 Jun 12 14:52

© Eskom 2026/Rev 0c

PRINTED VERSIONS OF THIS DOCUMENT ARE NOT CONTROLLED

MALVERN INSTRUMENTS MASTERSIZER

Result: Analysis Report

Sample Details

Sample ID: 164363
Sample File: JANKON12
Sample Path: C:\SIZERS\DATA\ANNE-MIE\
Sample Notes: TB15
0-2M
<1MM

Run Number: 42
Record Number: 87

Measured: 4 Jun 2012 02:40PM
Analysed: 4 Jun 2012 02:40PM
Result Source: Analysed

System Details

Range Lens: 300RF mm
Presentation: 3_SIL01
Analysis Model: Polydisperse
Modifications: None

Beam Length: 2.40 mm
[Particle R.I. = (3.5000, 0.1000); Dispersant R.I. = 1.3300]

Sampler: None

Obscuration: 10.4 %
Residual: 2.747 %

Result Statistics

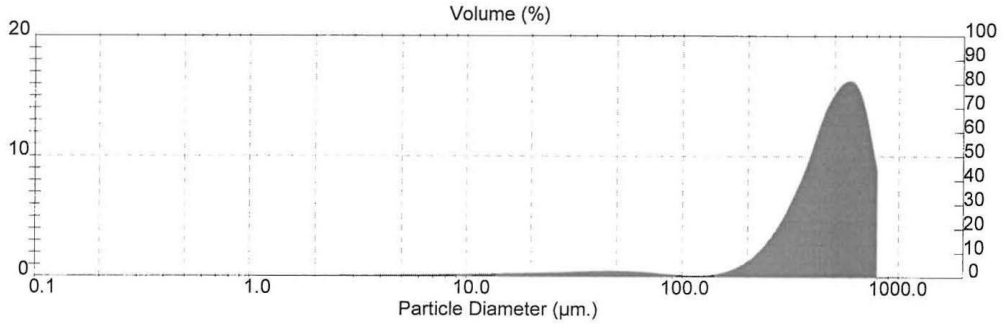
Distribution Type: Volume
Mean Diameters:
D [4, 3] = 482.45 um

Concentration = 0.1204 %Vol
D (v, 0.1) = 224.34 um
D [3, 2] = 89.58 um

Density = 1.000 g / cub. cm
D (v, 0.5) = 495.53 um
Span = 1.033E+00

Specific S.A. = 0.0670 sq. m / g
D (v, 0.9) = 736.01 um
Uniformity = 3.255E-01

Size Low (um)	In %	Size High (um)	Under%	Size Low (um)	In %	Size High (um)	Under%
0.05	0.00	0.06	0.00	6.63	0.16	7.72	1.36
0.06	0.00	0.07	0.00	7.72	0.17	9.00	1.54
0.07	0.00	0.08	0.00	9.00	0.19	10.48	1.73
0.08	0.00	0.09	0.00	10.48	0.22	12.21	1.95
0.09	0.00	0.11	0.00	12.21	0.24	14.22	2.19
0.11	0.00	0.13	0.00	14.22	0.26	16.57	2.45
0.13	0.00	0.15	0.00	16.57	0.29	19.31	2.74
0.15	0.00	0.17	0.00	19.31	0.32	22.49	3.06
0.17	0.00	0.20	0.00	22.49	0.36	26.20	3.42
0.20	0.00	0.23	0.00	26.20	0.40	30.53	3.81
0.23	0.00	0.27	0.00	30.53	0.44	35.56	4.25
0.27	0.00	0.31	0.00	35.56	0.48	41.43	4.73
0.31	0.01	0.36	0.01	41.43	0.50	48.27	5.23
0.36	0.01	0.42	0.02	48.27	0.50	56.23	5.73
0.42	0.02	0.49	0.04	56.23	0.45	65.51	6.19
0.49	0.02	0.58	0.06	65.51	0.38	76.32	6.56
0.58	0.03	0.67	0.09	76.32	0.28	88.91	6.84
0.67	0.03	0.78	0.12	88.91	0.18	103.58	7.02
0.78	0.04	0.91	0.15	103.58	0.12	120.67	7.14
0.91	0.04	1.06	0.19	120.67	0.16	140.58	7.30
1.06	0.05	1.24	0.24	140.58	0.34	163.77	7.64
1.24	0.05	1.44	0.29	163.77	0.75	190.80	8.39
1.44	0.06	1.68	0.34	190.80	1.49	222.28	9.87
1.68	0.06	1.95	0.41	222.28	2.65	258.95	12.53
1.95	0.07	2.28	0.48	258.95	4.36	301.68	16.89
2.28	0.08	2.65	0.55	301.68	6.67	351.46	23.55
2.65	0.08	3.09	0.64	351.46	9.62	409.45	33.17
3.09	0.09	3.60	0.73	409.45	13.13	477.01	46.31
3.60	0.10	4.19	0.83	477.01	15.43	555.71	61.74
4.19	0.11	4.88	0.94	555.71	16.23	647.41	77.96
4.88	0.12	5.69	1.07	647.41	13.88	754.23	91.84
5.69	0.14	6.63	1.21	754.23	8.16	878.67	100.00



Malvern Instruments Ltd.
Malvern, UK
Tel:=+[44] (0)1684-892456 Fax:+[44] (0)1684-892789

Mastersizer S long bed Ver. 2.19
Serial Number: 33544/152

p. 26
04 Jun 12 14:40

© Eskom 2026/Rev 0c

PRINTED VERSIONS OF THIS DOCUMENT ARE NOT CONTROLLED

Appendix 5.8.I: Reportable Meteorological Incidents

Table 5.8.I.1
Summary of Severe Phenomena Recorded in the Region

Event	Location	Year	Consequences
Floods	Port Elizabeth	1867	
Strong Wind	Port Elizabeth	1870	Two Ships Destroyed
Floods	Port Elizabeth	1895	
Strong Wind	Port Elizabeth	1902	20 Ships Destroyed And Great Loss Of Life
Floods	Port Elizabeth	1905	
Floods	Port Elizabeth	1908	River Banks Broke Resulting 7 M Deep Water
Floods	Port Elizabeth	1910	
Strong Wind	Port Elizabeth	1913	Wind Speed Estimated Between 100 And 130 km/h
Floods	Port Elizabeth	1921	
Floods	Port Elizabeth	1922	Shops Flooded And Streets Resembled Rivers
Floods	Port Elizabeth	1926	Streets And Rail tracks Washed Away. Homes And Buildings Flooded.
Floods	Port Elizabeth	1952	Flooded Homes And Houses.
Tornado	Port Elizabeth	1956	Damaged houses Over A Narrow Path
Floods	Port Elizabeth	1961	Significant Property Damage But No Loss Of Life
Floods	Uitenhage	1964	Greatest Cloudburst In Human Memory With Shops And 60 Homes Flooded
Floods	Port Elizabeth	1968	Damage Estimated At R40 Million And 11 People Drowned
Floods	Cape St. Francis	1971	Most Damage Done In Port Elizabeth
Floods	Humansdorp	1971	Most Damage Done In Port Elizabeth
Floods	Port Elizabeth	1971	Most Damage Done In Port Elizabeth
Floods	Humansdorp	1976	Part Of Rail track Washed Away
Floods	Humansdorp	1977	Millions Of Rands Worth Of Damage
Floods	Port Elizabeth	1977	Millions Of Rands Worth Of Damage
Strong Wind	Port Elizabeth	1977	Millions Of Rands Worth Of Damage
Tornado	Port Elizabeth	1978	Relatively Weak Tornado With No Significant Damage Reported
Floods	Uitenhage	1979	
Floods	Port Elizabeth	1979	Homes Flooded And Farmlands Ruined
Floods	Port Elizabeth	1981	Worst Flood Since The 1968 Flood - R50 Million In Damages
Floods	Port Elizabeth	1983	Millions Of Rands Of Damage And Several People Drowned. More Than 1000 People Left Homeless.
Strong Wind	Port Elizabeth	1987	Trees Uprooted And Windows Broken
Strong Wind	Port Elizabeth	1988	Gale-Force Winds Up To 110 km/h Causes Considerable Damage
Strong Wind	Port Elizabeth	1991	Wind Speeds Up To 72 km/h, With A Maximum Gust Reaching 136 km/h. Trees Uprooted And Snapped Off. Roof Of Shopping Centre Ripped Off And Killed 1 Person.

© Eskom 2026/Rev 0c

PRINTED VERSIONS OF THIS DOCUMENT ARE NOT CONTROLLED

Event	Location	Year	Consequences
Strong Wind	Port Elizabeth	1992	Wind Gusted Up To 137 km/h. Roofs Of At Least 30 Building Blown Off. One Person Killed When Wind Caused House To Collapse.
Strong Wind & Hail	Port Elizabeth	1993	Gale-Force Winds Associated With Hail Damaged Houses
Floods	Port Elizabeth	1994	
Strong Wind	Port Elizabeth	1995	Wind Speeds Reached 100 km/h. No Serious Damage Reported
Strong Wind	Port Elizabeth	1995	Wind Gusts Reaching 114 km/h. No Serious Damage Reported
Floods	Cape St. Francis/Port Elizabeth	1995	Trawler Sank In Gal Off Cape St. Francis, But No Lives Were Lost.
Floods	Port Elizabeth	1996	
Floods	Cape St. Francis/Port Elizabeth	1996	Millions Of Rands In Damage To Bridges And Roads. Nine People Dies Near Cape St. Francis When Two Boats Capsized In Heavy Seas.
Lightning/Floods	Port Elizabeth	1997	Caused Power Failures And Killed Two People
Strong Wind	Cape St. Francis	1999	
Tornado	Port Elizabeth	2000	Roofs From At Least 26 Houses Ripped Off, Roads Flooded And Two Men Injured.
Strong Wind	Port Elizabeth	2002	Thousand People Homeless. Severe Damage To Crops
Floods	Port Elizabeth	2004	Extensive Damage To Property
Fire	Humansdorp	2005	9000ha Pine Forest And 15 km^2 Of Farm Land Destroyed
Heavy Rain	Port Elizabeth	2006	Widespread Devastation Leaving Many People Homeless And Causing Major Damage To Infrastructure
Floods	Humansdorp	2006	Recorded 300 mm In 24 Hours
Floods	Port Elizabeth	2006	
Strong Wind	Port Elizabeth	2006	
Very Cold	Port Elizabeth	2007	4 Dead
Lightning	Port Elizabeth	2008	The 60-m fishing boat was hit about 40 nautical miles out to sea. Fisherman rushed to hospital.
Strong Wind	Oyster Bay	2008	Fishing boat sank in heavy seas and gale-force winds off Oyster Bay. Some crew members drowned.
Heavy Rains and Floods	Port Elizabeth	2011	At least 1400 people displaced in Port Elizabeth. Five pupils and three teachers from Uitenhage rescued by helicopter after the bridge collapsed. Two schoolgirls drowned in flood. Three people in Lusikisiki and another one in Keiskammahoek also reported missing.
Heavy Rain	Gamtoos	2011	Heavy rain resulted in the death of two people in Gamtoos River while attempting to cross.
Heavy Rains & Flooding	Cape St. Francis	2012	A bridge on the Cape St. Francis Bay main road washed away.

© Eskom 2026/Rev 0c

PRINTED VERSIONS OF THIS DOCUMENT ARE NOT CONTROLLED

Event	Location	Year	Consequences
Gale Force Winds	St. Francis Bay	2012 11 Nov	Gale-force winds gusting up to 100km/h contributed to the destruction of 75 mostly thatched-roof houses by fire at St. Francis Bay. The estimated cost of the total damage is in the order of R500 million.
Strong Winds	St. Francis Bay	2012 25 Dec	Twenty houses evacuated for safety reasons after three houses in the same street caught alight with strong winds blowing.
Heavy Swells	St. Francis Bay	2014	An 18 m abalone trawler ran aground in big swells on the rocks near the entrance to Port St. Francis harbour.
Heavy Seas and Tidal Waves	Jeffrey's Bay	2014	Rough sea conditions and strong rip currents.
Heavy Rain	Port Elizabeth	2015	Flooding low-lying areas. Evacuating more than 1 000 people from their homes
Strong Winds	Port Elizabeth	2016	Strong winds uprooted trees.
Strong Winds	Humansdorp	2016	Strong gusts affected participating teams in the Sasol Solar Challenge. The canopy of the cockpit of one cars blew off near Humansdorp.
Veld Fires and Strong Winds	Port Elizabeth	2017	
Raw Weather	St. Francis Bay	2017	A chokka boat capsized near St. Francis Bay during raw weather conditions including strong winds, pouring rain and 6-m-high waves.
Gale Force Winds	Jeffrey's Bay	2018	Gusts snapped tent-poles, damaging tents in a caravan park.
Lightning	Oyster Bay	2018	Cows hit by lightning. Only 2 out of 66 did not die instantly.
Heavy Rain	Port Elizabeth	2018	Following torrential rainfall more than 200 people from Missionvale in Port Elizabeth were evacuated. Other areas that were also flooded included Chatty, Bethelsdorp, Malabar and Despatch.
Veld Fires	Tsitsikamma	2018	Residents evacuated due to the veld fires. Low visibility caused by smoke occurred on the N2 freeway between Tsitsikamma and Humansdorp.
Lightning	Jeffrey's Bay	2018	Lightning struck a house in Jeffries Bay, Firefighters managed to stop the blaze.
Storm surge and spring tide	Jeffrey's Bay	2023	The spring tides washed away beaches.
Heavy rain, flood and strong winds	Gqeberha	2023	Heavy rain across Gqeberha which affected over 100 residents that were evacuated from homes. Large areas in Colleen Glen, Greenbushes, Van Stadens and St. Albans were also affected.

© Eskom 2026/Rev 0c

PRINTED VERSIONS OF THIS DOCUMENT ARE NOT CONTROLLED

Appendix 5.8.J to 5.8.T

Data in the following appendices are provided in electronic format:

Appendix 5.8.J: AERMOD Dispersion Model Concentration Input File 5 Km by 5 Km Model Domain

Appendix 5.8.K: AERMOD Dispersion Model Concentration Input File 40 Km by 40 Km Model Domain

Appendix 5.8.L: AERMOD Dispersion Model Deposition Input File 5 Km by 5 Km Model Domain

Appendix 5.8.M: AERMOD Dispersion Model Deposition Input File 40 Km by 40 Km Model Domain

Appendix 5.8.N: AERMET Meteorology Surface Data File

Appendix 5.8.O: AERMET Meteorology Profile File

Appendix 5.8.P: AERMAP Terrain and Land Use File

Appendix 5.8.Q: AERMOD Dispersion Model Concentration Output File 5 Km by 5 Km Model Domain

Appendix 5.8.R: AERMOD Dispersion Model Concentration Output File 40 Km by 40 Km Model Domain

Appendix 5.8.S: AERMOD Dispersion Model Deposition Output File 5 Km by 5 Km Model Domain

Appendix 5.8.T: AERMOD Dispersion Model Deposition Output File 40 Km by 40 Km Model Domain

© Eskom 2026/Rev 0c

PRINTED VERSIONS OF THIS DOCUMENT ARE NOT CONTROLLED